Electrochemical Systems

Fourth Edition

John Newman
Nitash P. Balsara

The Electrochemical Society
Advancing solid state & electrochemical science & technology

WILEY

ELECTROCHEMICAL SYSTEMS

THE ELECTROCHEMICAL SOCIETY SERIES

The Electron Microprobe
Edited by T. D. McKinley, K. F. J. Heinrich, and D. B. Wittry

Chemical Physics of Ionic Solutions
Edited by B. E. Conway and R. G. Barradas

High-Temperature Materials and Technology
Edited by Ivor E. Campbell and Edwin M. Sherwood

Alkaline Storage Batteries
S. Uno Falk and Alvin J. Salkind

The Primary Battery (in Two Volumes)
Volume I
Edited by George W. Heise and N. Corey Cahoon

Volume II
Edited by N. Corey Cahoon and George W. Heise

Zinc-Silver Oxide Batteries
Edited by Arthur Fleischer and J. J. Lander

Lead-Acid Batteries
Hans Bode
Translated by R. J. Brodd and Karl V. Kordesch

Thin Films-Interdiffusion and Reactions
Edited by J. M. Poate, M. N. Tu, and J. W. Mayer

Lithium Battery Technology
Edited by H. V. Venkatasetty

Quality and Reliability Methods for Primary Batteries
P. Bro and S. C. Levy

Techniques for Characterization of Electrodes and Electrochemical Processes
Edited by Ravi Varma and J. R. Selman

Electrochemical Oxygen Technology
Kim Kinoshita

Synthetic Diamond: Emerging CVD Science and Technology
Edited by Karl E. Spear and John P. Dismukes

Corrosion of Stainless Steels, Second Edition
A. John Sedriks

Semiconductor Wafer Bonding: Science and Technology
Q.-Y. Tong and U. Göscle

Fundamentals of Electrochemistry, Second Edition
V. S. Bagotsky

Fundamentals of Electrochemical Deposition, Second Edition
Milan Paunovic and Mordechay Schlesinger

Uhlig's Corrosion Handbook, Third Edition
Edited by R. Winston Revie

Fuel Cells: Problems and Solutions
Vladimir S. Bagotsky

Lithium Batteries: Advanced Technologies and Applications
Edited by B. Scrosati, K. M. Abraham, W. A. van Schalkwijk, and J. Hassoun

Modern Electroplating, Fifth Edition
Edited by Mordechay Schlesinger and Milan Paunovic

Electrochemical Power Sources: Batteries, Fuel Cells, and Supercapacitors
By V. S. Bagotsky, A. M. Skundin, and Y. M. Volfkovic

Molecular Modeling of Corrosion Processes: Scientific Development and Engineering Applications
Edited by C. D. Taylor and P. Marcus

Atmospheric Corrosion, Second Edition
Christofer Leygraf, Inger Odnevall Wallinder, Johan Tidblad, and Thomas Graedel

Electrochemical Impedance Spectroscopy, Second Edition
Mark E. Orazem and Bernard Tribollet

Electrochemical Systems, Fourth Edition
John Newman and Nitash P. Balsara

ELECTROCHEMICAL SYSTEMS

Fourth Edition

JOHN NEWMAN and NITASH P. BALSARA
University of California, Berkeley

WILEY

This edition first published 2021

Edition History
"John Wiley & Sons Inc. (3e, 2004)".

Registered Office
John Wiley & Sons, Inc., 111 River Street, Hoboken, NJ 07030, USA

Editorial Office
111 River Street, Hoboken, NJ 07030, USA

For details of our global editorial offices, customer services, and more information about Wiley products visit us at www.wiley.com.

Wiley also publishes its books in a variety of electronic formats and by print-on-demand. Some content that appears in standard print versions of this book may not be available in other formats.

Library of Congress Cataloging-in-Publication Data
Hardback ISBN: 9781119514602

Central Cover Image: Redrawn from Figure 22.12 by Hee Jeung Oh, with permission from The Electrochemical Society
Cover Image: Courtesy of John Newman, Nitash P. Balsara, and Hee Jeung Oh

Set in 10/12pt NimbusRom by SPi Global, Chennai, India

10 9 8 7 6 5 4 3 2 1

CONTENTS

PREFACE TO THE FOURTH EDITION

Electrochemical systems provide the basis for many technologically important applications, such as batteries and fuel cells, production and refining of metals and chemicals, fabrication of electronic materials and devices, and operation of sensors, including those regulating the air/fuel ratio in automobile engines. The rechargeable lithium-ion battery has emerged as a vital element of the emerging clean-energy landscape. In biological systems, nerve action involves electrochemical processes. While applications continue to evolve, the fundamentals need only minor revision to train and guide people in adapting to new applications. Electrochemical systems involve many simultaneously interacting phenomena, drawn from many aspects of chemistry and physics, and require a disciplined learning process. The book provides a comprehensive coverage of electrochemical theories as they pertain to the understanding of electrochemical systems. It describes the foundations of thermodynamics, chemical kinetics, and transport phenomena including the electric potential and charged species.

This fourth edition incorporates further improvements developed over the years in teaching both graduate and advanced undergraduate students. Chapter 2 has expanded to include cells with polymer electrolytes. Chapter 6 now includes a discussion of equilibration of a charged polymer material and an electrolytic solution (Donnan equilibrium). The discussion of the oxygen electrode in Chapter 8 now includes insight from recent computer simulations. The application of concentrated solution theory to polymer electrolytes is added to Chapters 12 and 14. The number of transport properties describing different systems is now clearly stated. Chapter 15 presents a method for predicting turbulence by means of dissipation. Chapter 15 presents a method for predicting turbulence by means of dissipation. Finally, impedance measurements in electrochemical systems are important because experimental implementation is easy and diagnostic information is obtained without destroying the system. A new chapter on this subject, Chapter 24, is added.

We have much gratitude for the many students and colleagues who have done experiments and calculations that are reported in the book, and to our families for their continual support. We thank Saheli Chakraborty, Youngwoo Choo, Louise Frenck, Michael Galluzzo, Kevin Gao, Lorena Grundy, David Halat, Darby Hickson, Alec Ho, Zach Hoffman, Whitney Loo, Jacqueline Maslyn, Eric McShane, Hee Jeung Oh, Morgan Seidler, Gurmukh Sethi, Deep Shah, Neel Shah, and Irune Villaluenga, who patiently corrected many drafts of this manuscript. NPB thanks JN for the honor of working with him on the fourth edition and for being his mentor for more than a decade.

April 27, 2020

JOHN NEWMAN
Berkeley, California

NITASH P. BALSARA
Berkeley, California

PREFACE TO THE THIRD EDITION

This third edition incorporates various improvements developed over the years in teaching electrochemical engineering to both graduate and advanced undergraduate students. Chapter 1 has been entirely rewritten to include more explanations of basic concepts. Chapters 2, 7, 8, 13, 18, and 22 and Appendix C have been modified, to varying degrees, to improve clarity. Illustrative examples taken from real engineering problems have been added to Chapters 8 (kinetics of the hydrogen electrode), 18 (cathodic protection), and 22 (reaction-zone model and flow-through porous electrodes). Some concepts have been added to Chapters 2 (Pourbaix diagrams and the temperature dependence of the standard cell potential) and 13 (expanded treatment of the thermoelectric cell). The exponential growth of computational power over the past decade, which was made possible in part by advances in electrochemical technologies such as semiconductor processing and copper interconnects, has made numerical simulation of coupled nonlinear problems a routine tool of the electrochemical engineer. In realization of the importance of numerical simulation methods, their discussion in Appendix C has been expanded.

As discussed in the preface to the first edition, the science of electrochemistry is both fascinating and challenging because of the interaction among thermodynamic, kinetic, and transport effects. It is nearly impossible to discuss one concept without referring to its interaction with other concepts. We advise the reader to keep this in mind while reading the book, in order to develop facility with the basic principles as well as a more thorough understanding of the interactions and subtleties.

We have much gratitude for the many graduate students and colleagues who have worked on the examples cited and proofread chapters and for our families for their continual support. KET thanks JN for the honor of working with him on this third edition.

June 1, 2004

JOHN NEWMAN
Berkeley, California

KAREN E. THOMAS-ALYEA
Manchester, Connecticut

PREFACE TO THE SECOND EDITION

A major theme of *Electrochemical Systems* is the simultaneous treatment of many complex, interacting phenomena. The wide acceptance and overall impact of the first edition have been gratifying, and most of its features have been retained in the second edition. New chapters have been added on porous electrodes and semiconductor electrodes. In addition, over 70 new problems are based on actual course examinations.

Immediately after the introduction in Chapter 1, some may prefer to study Chapter 11 on transport in dilute solutions and Chapter 12 on concentrated solutions before entering the complexities of Chapter 2. Chapter 6 provides a less intense, less rigorous approach to the potentials of cells at open circuit. Though the subjects found in Chapters 5, 9, 10, 13, 14, and 15 may not be covered formally in a one-semester course, they provide breadth and a basis for future reference.

The concept of the electric potential is central to the understanding of the electrochemical systems. To aid in comprehension of the difference between the potential of a reference electrode immersed in the solution of interest and the electrostatic potential, the quasi-electrostatic potential, or the cavity potential—since the composition dependence is quite different—Problems 6.16 and Figure 12.1 have been added to the new edition. The reader will also benefit by the understanding of the potential as it is used in semi-conductor electrodes.

June 10, 1991

JOHN NEWMAN
Berkeley, California

PREFACE TO THE FIRST EDITION

Electrochemistry is involved to a significant extent in the present-day industrial economy. Examples are found in primary and secondary batteries and fuel cells; in the production of chlorine, caustic soda, aluminum, and other chemicals; in electroplating, electromachining, and electrorefining; and in corrosion. In addition, electrolytic solutions are encountered in desalting water and in biology. The decreasing relative cost of electric power has stimulated a growing role for electrochemistry. The electrochemical industry in the United States amounts to 1.6 percent of all U.S. manufacturing and is about one third as large as the industrial chemicals industry.[1]

The goal of this book is to treat the behavior of electrochemical systems from a practical point of view. The approach is therefore macroscopic rather than microscopic or molecular. An encyclopedic treatment of many specific systems is, however, not attempted. Instead, the emphasis is placed on fundamentals, so as to provide a basis for the design of new systems or processes as they become economically important.

Thermodynamics, electrode kinetics, and transport phenomena are the three fundamental areas which underlie the treatment, and the attempt is made to illuminate these in the first three parts of the book. These areas are interrelated to a considerable extent, and consequently the choice of the proper sequence of material is a problem. In this circumstance, we have pursued each subject in turn, notwithstanding the necessity of calling upon material which is developed in detail only at a later point. For example, the open-circuit potentials of electrochemical cells belong, logically and historically, with equilibrium thermodynamics, but a complete discussion requires the consideration of the effect of irreversible diffusion processes.

The fascination of electrochemical systems comes in great measure from the complex phenomena which can occur and the diverse disciplines which find application. Consequences of this complexity are the continual rediscovery of old ideas, the persistence of misconceptions among the uninitiated, and the development of involved programs to answer unanswerable or poorly conceived questions. We have tried, then, to follow a straightforward course. Although this tends to be unimaginative, it does provide a basis for effective instruction.

The treatment of these fundamental aspects is followed by a fourth part, on applications, in which thermodynamics, electrode kinetics, and transport phenomena may all enter into the determination of the behavior of electrochemical systems. These four main parts are preceded by an introductory chapter in which are discussed, mostly in a qualitative fashion, some of the pertinent factors which will come

into play later in the book. These concepts are illustrated with rotating cylinders, a system which is moderately simple from the point of view of the distribution of current.

The book is directed toward seniors and graduate students in science and engineering and toward practitioners engaged in the development of electrochemical systems. A background in calculus and classical physical chemistry is assumed.

William H. Smyrl, currently of the University of Minnesota, prepared the first draft of Chapter 2, and Wa-She Wong, formerly at the General Motors Science Center, prepared the first draft of Chapter 5. The author acknowledges with gratitude the support of his research endeavors by the United States Atomic Energy Commission, through the Inorganic Materials Research Division of the Lawrence Berkeley Laboratory, and subsequently by the United States Department of Energy, through the Materials Sciences Division of the Lawrence Berkeley Laboratory.

REFERENCE

1. G. M. Wenglowski, "An Economic Study of the Electrochemical Industry in the United States," in J. O'M. Bockris, ed., *Modern Aspects of Electrochemistry*, no. 4 (London: Butterworths, 1966), pp. 251–306.

December 20, 1972

JOHN NEWMAN
Berkeley, California

CHAPTER 1

INTRODUCTION

Electrochemical techniques are used for the production of aluminum and chlorine, the conversion of energy in batteries and fuel cells, sensors, electroplating, and the protection of metal structures against corrosion, to name just a few prominent applications. While applications such as fuel cells and electroplating may seem quite disparate, in this book we show that a few basic principles form the foundation for the design of all electrochemical processes.

The first practical electrochemical system was the Volta pile, invented by Alexander Volta in 1800. Volta's pile is still used today in batteries for a variety of industrial, medical, and military applications. Volta found that when he made a sandwich of a layer of zinc metal, paper soaked in salt water, and tarnished silver and then connected a wire from the zinc to the silver, he could obtain electricity (see Figure 1.1). What is happening when the wire is connected? Electrons have a chemical preference to be in the silver rather than the zinc, and this chemical preference is manifest as a voltage difference that drives the current. At each electrode, an electrochemical reaction is occurring: zinc reacts with hydroxide ions in solution to form free electrons, zinc oxide, and water, while silver oxide (tarnished silver) reacts with water and electrons to form silver and hydroxide ions. Hydroxide ions travel through the salt solution (the electrolyte) from the silver to the zinc, while electrons travel through the external wire from the zinc to the silver.

We see from this example that many phenomena interact in electrochemical systems. Driving forces for reaction are determined by the thermodynamic properties of the electrodes and electrolyte. The rate of the reaction at the interface in response to this driving force depends on kinetic rate parameters. Finally, mass must be transported through the electrolyte to bring reactants to the interface, and electrons must travel through the electrodes. The total resistance is therefore a combination of the effects of reaction kinetics and mass and electron transfer. Each of these phenomena—thermodynamics, kinetics, and transport—is addressed separately in subsequent chapters. This chapter defines basic terminology and gives an overview of the principal concepts that are derived in subsequent chapters.

Electrochemical Systems, Fourth Edition. John Newman and Nitash P. Balsara.

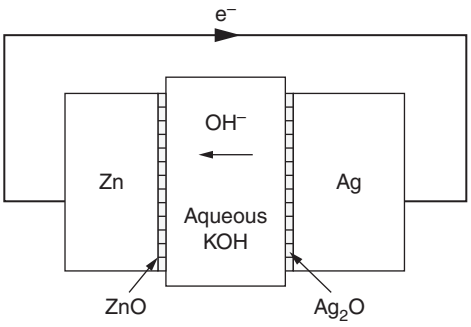

Figure 1.1 Volta's first battery comprised of a sandwich of zinc with its oxide layer, salt solution, and silver with its oxide layer. While the original Volta pile used an electrolyte of NaCl in water, modern batteries use aqueous KOH to increase the conductivity and the concentration of OH^-.

1.1 DEFINITIONS

Every electrochemical system must contain two electrodes separated by an electrolyte and connected via an external electronic conductor. Ions flow through the electrolyte from one electrode to the other, and the circuit is completed by electrons flowing through the external conductor.

An *electrode* is a material in which electrons are the mobile species and therefore can be used to sense (or control) the potential of electrons. It may be a metal or other electronic conductor such as carbon, an alloy or intermetallic compound, one of many transition-metal chalcogenides, or a semiconductor. In particular, in electrochemistry an electrode is considered to be an electronic conductor that carries out an electrochemical reaction or some similar interaction with an adjacent phase. Electronic conductivity generally decreases slightly with increasing temperature and is of the order 10^2 to 10^4 S/cm, where a siemens (S) is an inverse ohm.

An *electrolyte* is a material in which the mobile species are ions and free movement of electrons is blocked. Ionic conductors include molten salts, dissociated salts in solution, and some ionic solids. In an ionic conductor, neutral salts are found to be dissociated into their component ions. The term *species* refers to ions as well as neutral molecular components that do not dissociate. Ionic conductivity generally increases with increasing temperature and is of the order 10^{-4} to 10^{-1} S/cm, although it can be substantially lower.

In addition to these two classes of materials, some materials are *mixed conductors*, in which charge can be transported by both electrons and ions. Mixed conductors are occasionally used in electrodes, for example, in solid-oxide fuel cells.

Thus the key feature of an electrochemical cell is that it contains two electrodes that allow transport of electrons, separated by an electrolyte that allows movement of ions but blocks movement of electrons. To get from one electrode to the other, electrons must travel through an external conducting circuit, doing work or requiring work in the process.

The primary distinction between an electrochemical reaction and a chemical redox reaction is that, in an electrochemical reaction, reduction occurs at one electrode and oxidation occurs at the other, while in a chemical reaction, both reduction and oxidation occur in the same place. This distinction has several implications. In an electrochemical reaction, oxidation is spatially separated from reduction. Thus, the complete redox reaction is broken into two *half-cells*. The rate of these reactions can be controlled by externally applying a potential difference between the electrodes, for example, with an external power supply, a feature absent from the design of chemical reactors. Finally, electrochemical

reactions are always heterogeneous; that is, they always occur at the interface between the electrolyte and an electrode (and possibly a third phase such as a gaseous or insulating reactant).

Even though the half-cell reactions occur at different electrodes, the rates of reaction are coupled by the principles of conservation of charge and *electroneutrality*. As we demonstrate in Section 3.1, a very large force is required to bring about a spatial separation of charge. Therefore, the flow of current is continuous: all of the current that leaves one electrode must enter the other. At the interface between the electrode and the electrolyte, the flow of current is still continuous, but the identity of the charge-carrying species changes from being an electron to being an ion. This change is brought about by a charge-transfer (i.e., electrochemical) reaction. In the electrolyte, electroneutrality requires that there be the same number of equivalents of cations as anions:

$$\sum_i z_i c_i = 0, \tag{1.1}$$

where the sum is over all species i in solution, and c_i and z_i are the concentration and the charge number of species i, respectively. For example, $z_{Zn^{2+}}$ is $+2$, z_{OH^-} is -1, and z_{H_2O} is 0.

Faraday's law relates the rate of reaction to the current. It states that the rate of production of a species is proportional to the current, and the total mass produced is proportional to the amount of charge passed multiplied by the equivalent weight of the species:

$$m_i = -\frac{s_i M_i I t}{nF}, \tag{1.2}$$

where m_i is the mass of species i produced by a reaction in which its *stoichiometric coefficient* is s_i and n electrons are transferred, M_i is the molar mass, F is Faraday's constant, equal to 96,487 C/mol, and the total amount of charge passed is equal to the current I multiplied by time t. The sign of the stoichiometric coefficient is determined by the convention of writing an electrochemical reaction in the form

$$\sum_i s_i M_i^{z_i} \rightleftharpoons n e^-, \tag{1.3}$$

where M_i is the symbol for the chemical formula of species i. For example, for the reaction

$$Zn + 2OH^- \rightleftharpoons ZnO + 2e^- + H_2O, \tag{1.4}$$

s_{ZnO} is -1, s_{OH^-} is 2, and n is 2.

Following historical convention, current is defined as the flow of positive charge. Thus, electrons move in the direction opposite to that of the convention for current flow. *Current density* is the flux of charge, that is, the rate of flow of positive charge per unit area perpendicular to the direction of flow. The behavior of electrochemical systems is determined more by the current density than by the total current, which is the product of the current density and the cross-sectional area. In this text, the symbol i refers to current density unless otherwise specified.

Owing to the historical development of the field of electrochemistry, several terms are in common use. *Polarization* refers to the departure of the potential from equilibrium conditions caused by the passage of current. *Overpotential* refers to the magnitude of this potential drop caused by resistance to the passage of current. Later, we discuss different types of resistances that cause overpotential.

1.2 THERMODYNAMICS AND POTENTIAL

If one places a piece of tarnished silver in a basin of salt water and connects the silver to a piece of zinc, the silver spontaneously will become shiny, and the zinc will dissolve. Why? An electrochemical

reaction is occurring in which silver oxide is reduced to silver metal while zinc metal is oxidized. It is the thermodynamic properties of silver, silver oxide, zinc, and zinc oxide that determine that silver oxide is reduced spontaneously at the expense of zinc (as opposed to reducing zinc oxide at the expense of the silver). These thermodynamic properties are the *electrochemical potentials*. Let us arbitrarily call one half-cell the right electrode and the other the left electrode. The energy change for the reaction is given by the change in Gibbs free energy for each half-cell reaction:

$$\Delta G = \left(\sum_i s_i \mu_i\right)_{\text{right}} - \left(\sum_i s_i \mu_i\right)_{\text{left}}, \tag{1.5}$$

where G is the Gibbs free energy, μ_i is the electrochemical potential of species i, and s_i is the stoichiometric coefficient of species i, as defined by equation 1.3. If ΔG for the reaction with our arbitrary choice of right and left electrodes is negative, then the electrons will want to flow spontaneously from the left electrode to the right electrode. The right electrode is then the more positive electrode, which is the electrode in which the electrons have a lower electrochemical potential. This is equivalent to saying that ΔG is equal to the free energy of the products minus the free energy of the reactants.

Now imagine that instead of connecting the silver directly to the zinc, we connect them via a high-impedance potentiostat, and we adjust the potential across the potentiostat until no current is flowing between the silver and the zinc. (A *potentiostat* is a device that can apply a potential, while a *galvanostat* is a device that can control the applied current. If the potentiostat has a high internal impedance (resistance), then it draws little current in measuring the potential.) The potential at which no current flows is called the *equilibrium* or *open-circuit* potential, denoted by the symbol U. This equilibrium potential is related to the Gibbs free energy by

$$\Delta G = -nFU. \tag{1.6}$$

The equilibrium potential is thus a function of the intrinsic nature of the species present, as well as their concentrations and, to a lesser extent, temperature.

While no net current is flowing at equilibrium, random thermal collisions among reactant and product species still cause reaction to occur, sometimes in the forward direction and sometimes in the backward direction. At equilibrium, the rate of the forward reaction is equal to the rate of the backward reaction. The potential of the electrode at equilibrium is a measure of the electrochemical potential (i.e., energy) of electrons in equilibrium with the reactant and product species. Electrochemical potential is defined in more detail in Chapter 2. In brief, the electrochemical potential can be related to the molality m_i and activity coefficient γ_i, by

$$\mu_i = \mu_i^{\theta} + RT \ln m_i \gamma_i, \tag{1.7}$$

where μ^{θ} is independent of concentration, R is the universal gas constant (8.3143 J/mol·K), and T is temperature in kelvin. If one assumes that all activity coefficients are equal to 1, then equation 1.5 reduces to the Nernst equation

$$U = U^{\theta} - \frac{RT}{nF} \ln\left(\prod_i m_i^{s_i}\right)_{\text{right}} + \frac{RT}{nF} \ln\left(\prod_i m_i^{s_i}\right)_{\text{left}}, \tag{1.8}$$

which relates the equilibrium potential to the concentrations of reactants and products. In many texts, one sees equation 1.8 without the "left" term. It is then implied that one is measuring the potential of the right electrode with respect to some unspecified left electrode.

By connecting an electrode to an external power supply, one can electrically control the electrochemical potential of electrons in the electrode, thereby perturbing the equilibrium and driving a reaction. Applying a negative potential to an electrode increases the energy of electrons. Increasing the electrons' energy above the lowest unoccupied molecular orbital of a species in the adjacent electrolyte will cause reduction of that species (see Figure 1.2). This reduction current (flow of electrons into the electrode and from there into the reactant) is also called a *cathodic* current, and the electrode at which it occurs is called the *cathode*. Conversely, applying a positive potential to an electrode decreases the energy of electrons, causing electrons to be transferred from the reactants to the electrode. The electrode where such an oxidation reaction is occurring is called the *anode*. Thus, applying a positive potential relative to the equilibrium potential of the electrode will drive the reaction in the anodic direction; that is, electrons will be removed from the reactants. Applying a negative potential relative to the equilibrium potential will drive the reaction in the cathodic direction. Anodic currents are defined as positive (flow of positive charges into the solution from the electrode) while cathodic currents are negative. Common examples of cathodic reactions include deposition of a metal from its salt and evolution of H_2 gas, whereas common anodic reactions include corrosion of a metal and evolution of O_2 or Cl_2.

Note that one cannot control the potential of an electrode by itself. Potential must always be controlled relative to another electrode. Similarly, potentials can be measured only relative to some reference state. While it is common in the physics literature to use the potential of an electron in a vacuum as the reference state (see Chapter 3), electrochemists generally use a *reference electrode*, an electrode designed so that its potential is well-defined and reproducible. A potential is well-defined if both reactant and product species are present and the kinetics of the reaction is sufficiently fast that the species are present in their equilibrium concentrations. Since potential is measured with a high-impedance voltmeter, negligible current passes through a reference electrode. Chapter 5 discusses commonly used reference electrodes.

Electrochemical cells can be divided into two categories: *galvanic cells*, which spontaneously produce work, and *electrolytic cells*, which require an input of work to drive the reaction. Galvanic applications include discharge of batteries and fuel cells. Electrolytic applications include charging batteries, electroplating, electrowinning, and electrosynthesis. In a galvanic cell, connecting the positive and negative electrodes causes a driving force for charge transfer that decreases the potential of the positive electrode, driving its reaction in the cathodic direction, and increases the potential of the negative electrode, driving its reaction in the anodic direction. Conversely, in an electrolytic cell, a positive potential (positive with respect to the equilibrium potential of the positive electrode) is applied

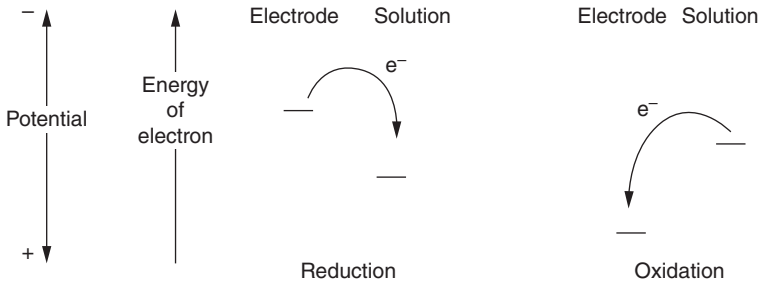

Figure 1.2 Schematic of the relative energy of the electron in reduction and oxidation reactions. During a reduction reaction, electrons are transferred from the electrode to the lowest unoccupied energy level of a reactant species. During oxidation, electrons are transferred from the highest occupied energy level of the reactant to the electrode.

to the positive electrode to force the reaction in the anodic direction, whereas a negative potential is applied to the negative electrode to drive its reaction in the cathodic direction. Thus, the positive electrode is the anode in an electrolytic cell while it is the cathode in a galvanic cell, and the negative electrode is the cathode in an electrolytic cell and the anode in a galvanic cell.

1.3 KINETICS AND RATES OF REACTION

Imagine that we have a system with three electrodes: a zinc negative electrode, a silver positive electrode, and another zinc electrode, all immersed in a beaker of aqueous KOH (see Figure 1.1). We pass current between the negative and positive electrodes. For the moment, let us just focus on one electrode, such as the zinc negative electrode. Since it is our electrode of interest, we call it the *working electrode*, and the other electrode through which current passes is termed the *counterelectrode*. The second zinc electrode will be placed in solution and connected to the working electrode through a high-impedance voltmeter. This second zinc electrode is in equilibrium with the electrolyte since no current is passing through it. We can therefore use this electrode as a reference electrode to probe changes in the potential in the electrolyte relative to the potential of the working electrode.

As mentioned above, a driving force is required to force an electrochemical reaction to occur. Imagine that we place our reference electrode in the solution adjacent to the working electrode. Recall that our working and reference electrodes are of the same material composition. Since no current is flowing at the reference electrode, and a potential has been applied to the working electrode to force current to flow, the difference in potential between the two electrodes must be the driving force for reaction. This driving force is termed the *surface overpotential* and is given the symbol η_s. The rate of reaction often can be related to the surface overpotential by the *Butler–Volmer equation*, which has the form

$$i = i_0 \left[\exp\left(\frac{\alpha_a F}{RT} \eta_s \right) - \exp\left(-\frac{\alpha_c F}{RT} \eta_s \right) \right]. \tag{1.9}$$

A positive η_s produces a positive (anodic) current. The derivation and application of the Butler–Volmer equation, and its limitations, are discussed in Chapter 8. As mentioned above, random thermal collisions cause reactions to occur in both the forward and backward directions. The first term in equation 1.9 is the rate of the anodic direction, while the second term is the rate of the cathodic direction. The difference between these rates gives the net rate of reaction. The parameter i_0 is called the *exchange current density* and is analogous to the rate constant used in chemical kinetics. In a reaction with a high exchange current density, both the forward and backward reactions occur rapidly. The net direction of reaction depends on the sign of the surface overpotential. The exchange current density depends on the concentrations of reactants and products, temperature, and also the nature of the electrode–electrolyte interface and impurities that may contaminate the surface. Each of these factors can change the value of i_0 by several orders of magnitude. i_0 can range from over 1 mA/cm^2 to less than 10^{-7} mA/cm^2. The parameters α_a and α_c, called *apparent transfer coefficients*, are additional kinetic parameters that relate how an applied potential favors one direction of reaction over the other. They usually have values between 0.2 and 2.

A reaction with a large value of i_0 is often called fast or reversible. For a large value of i_0, a large current density can be obtained with a small surface overpotential.

The relationship between current density and surface overpotential is graphed in Figures 1.3 and 1.4. In Figure 1.3, we see that the current density varies linearly with η_s for small values of η_s, and from the semilog graph given in Figure 1.4 we see that the current density varies exponentially with η_s for large values of η_s. The latter observation was made by Tafel in 1905, and Figure 1.4 is termed a

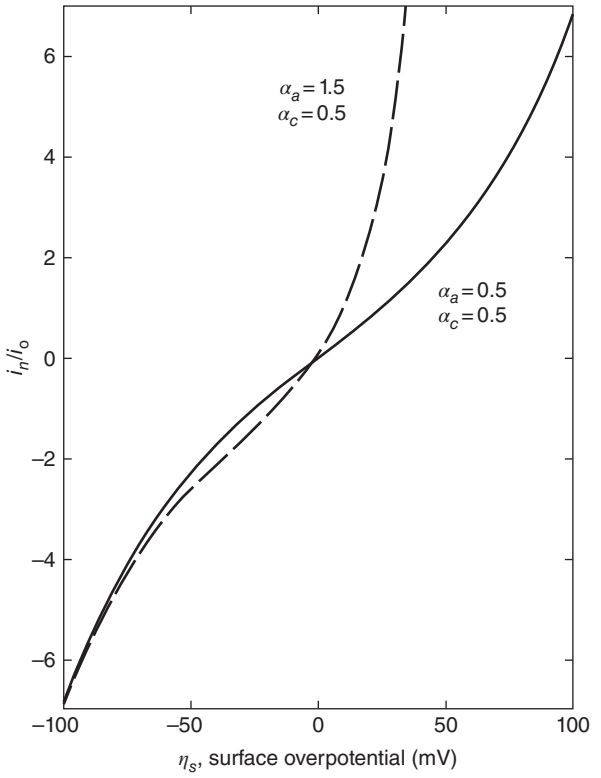

Figure 1.3 Dependence of current density on surface overpotential at 25°C.

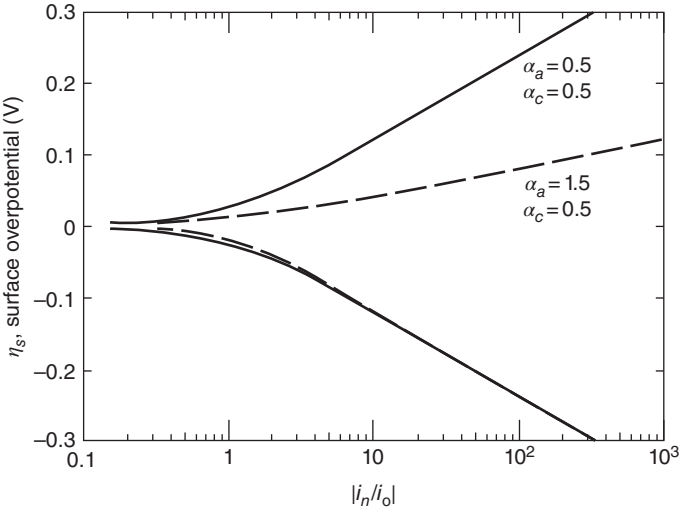

Figure 1.4 Tafel plot of the relationship between current density and surface overpotential at 25°C.

Tafel plot. For large values of the surface overpotential, one of the terms in equation 1.9 is negligible, and the overall rate is given by either

$$i_n = i_0 \exp\left(\frac{\alpha_a F}{RT}\eta_s\right) \quad (\text{for } \alpha_a F\eta_s \gg RT) \tag{1.10}$$

or

$$i_n = -i_0 \exp\left(-\frac{\alpha_c F}{RT}\eta_s\right) \quad (\text{for } \alpha_c F\eta_s \ll -RT). \tag{1.11}$$

The *Tafel slope*, either $2.303RT/\alpha_a F$ or $2.303RT/\alpha_c F$, thus depends on the apparent transfer coefficient.

1.4 TRANSPORT

The previous section describes how applying a potential to an electrode creates a driving force for reaction. In addition, the imposition of a potential difference across an electronic conductor creates a driving force for the flow of electrons. The driving force is the *electric field* **E**, related to the gradient in potential Φ by

$$\mathbf{E} = -\nabla\Phi. \tag{1.12}$$

Ohm's law relates the current density to the gradient in potential by

$$\mathbf{i} = -\sigma\nabla\Phi, \tag{1.13}$$

where σ is the *electronic conductivity*, equal to the inverse of the resistivity.

Similarly, applying an electric field across a solution of ions creates a driving force for ionic current. Current in solution is the net flux of charged species:

$$\mathbf{i} = \sum_i z_i F\mathbf{N}_i, \tag{1.14}$$

where $\mathbf{N}_i$ is the flux density of species i.

While electrons in a conductor flow only in response to an electric field, ions in an electrolyte move in response to an electric field (a process called *migration*) and also in response to concentration gradients (*diffusion*) and bulk fluid motion (*convection*). The net flux of an ion is therefore the sum of the migration, diffusion, and convection terms. In the following pages we look at each term individually. To simplify our discussion, let us consider a solution that contains a single salt in a single solvent, $CuSO_4$ in H_2O. An electrolyte that contains only one solvent and one salt is called a *binary electrolyte*.

To give the reader a quantitative sense of the effect of different transport processes on the performance of an electrochemical system, we give calculations in the following sections for the specific system shown in Figure 1.5. This example consists of two concentric copper cylinders, of inner radius r_i, outer radius r_o, and height H, and with the annulus between filled with electrolyte. Since both cylinders are copper, at rest the open-circuit potential is zero. If we apply a potential between the inner and outer cylinders, copper will dissolve at the positive electrode to form Cu^{2+}, which will be deposited as Cu metal at the negative electrode. This type of process is widely used in industry for the electroplating and electrorefining of metals. While the annulus between concentric cylinders is not a practical geometry for many industrial applications, it is convenient for illustrating the concepts.

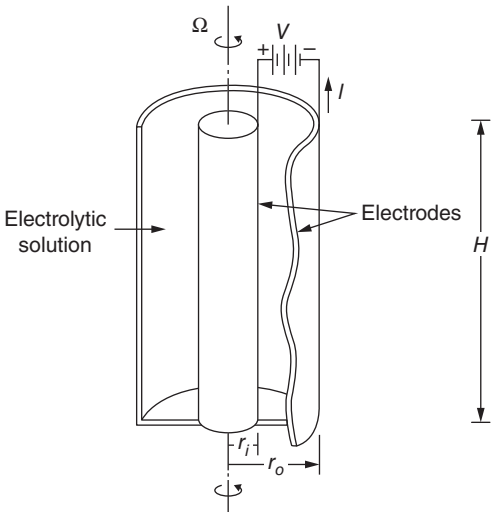

Figure 1.5 Two concentric copper electrodes with the annulus filled with electrolyte. The inner electrode can be rotated.

Migration

Imagine that we place electrodes in the solution and apply an electric field between the electrodes. For the moment, let us imagine that the solution remains at a uniform concentration. We discuss the influence of concentration gradients in the next section. The electric field creates a driving force for the motion of charged species. It drives cations toward the cathode and anions toward the anode, that is, cations move in the direction opposite to the gradient in potential. The velocity of the ion in response to an electric field is its migration velocity, given by

$$v_{i,\text{migration}} = -z_i u_i F \nabla \Phi, \tag{1.15}$$

where Φ is the potential in the solution (a concept that is discussed in detail in Chapters 2, 3, and 6) and u_i, called the *mobility*, is a proportionality factor that relates how fast the ion moves in response to an electric field. It has units of $\text{cm}^2 \cdot \text{mol/J} \cdot \text{s}$.

The *flux density* of a species is equal to its velocity multiplied by its concentration. Thus, the migrational flux density is given by

$$\mathbf{N}_{i,\text{migration}} = -z_i u_i F c_i \nabla \Phi. \tag{1.16}$$

Summing the migrational fluxes according to equation 1.14 for a binary electrolyte, we see that the current density due to migration is given by

$$\mathbf{i} = -F^2(z_+^2 u_+ c_+ + z_-^2 u_- c_-)\nabla \Phi. \tag{1.17}$$

The ionic conductivity κ is defined as

$$\kappa = F^2(z_+^2 u_+ c_+ + z_-^2 u_- c_-). \tag{1.18}$$

Thus, the movement of charged species in a uniform solution under the influence of an electric field is also given by Ohm's law:

$$\mathbf{i} = -\kappa \nabla \Phi. \tag{1.19}$$

We use κ instead of σ to indicate that the mobile charge carriers in electrolytes are ions, as opposed to electrons as in metals.

One can use this expression to obtain the potential profile and total ionic resistance for a cell of a given geometry, for example, our system of concentric cylinders. If the ends are insulators perpendicular to the cylinders, then the current flows only in the radial direction and is uniform in the angular and axial directions. The gradient in equation 1.19 is then simply given by

$$\mathbf{i} = -\kappa \frac{d\Phi}{dr}. \tag{1.20}$$

If a total current I is applied between the two cylinders, then the current density i in solution will vary with radial position by

$$i(r) = \frac{I}{2\pi r H}, \tag{1.21}$$

where H is the height of the cylinder. Substitution of equation 1.21 into equation 1.20 followed by integration gives the potential distribution in solution,

$$\Phi(r) - \Phi(r_i) = -\frac{I}{2\pi H \kappa} \ln \frac{r}{r_i}, \tag{1.22}$$

and the total potential drop between the electrodes is

$$\Phi(r_o) - \Phi(r_i) = -\frac{I}{2\pi H \kappa} \ln \frac{r_o}{r_i}. \tag{1.23}$$

The potential profile in solution is sketched in Figure 1.6. The potential changes more steeply closer to the smaller electrode, and the potential in solution at any given point is easily calculated from equation 1.22. As mentioned above, the *current distribution* on each electrode is uniform (although it is different on the two electrodes, being larger on the smaller electrode). Infinite parallel plates and concentric spheres are two other geometries that have uniform current distributions.

The reader may be familiar with the integrated form of Ohm's law commonly used in the field of electrostatics:

$$\Delta\Phi = IR, \tag{1.24}$$

where R is the total electrical resistance of the system in ohms. For our concentric cylinders we see that

$$R = \frac{\ln(r_o/r_i)}{2\pi H \kappa}. \tag{1.25}$$

For 0.1 M $CuSO_4$ in water, $\kappa = 0.00872$ S/cm. For $H = 10$ cm, $r_o = 3$ cm, and $r_i = 2$ cm, equation 1.25 gives the ohmic resistance of the system to be 0.74 Ω.

This analysis of the total resistance of the solution applies only in the absence of concentration gradients.

Diffusion

The application of an electric field creates a driving force for the motion of all ions in solution by migration. Thus for our system of aqueous copper sulfate, the current is caused by fluxes of both Cu^{2+}

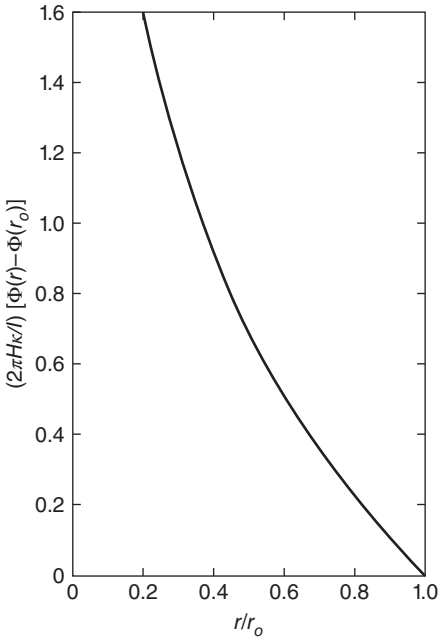

Figure 1.6 Distribution of the potential in solution between cylindrical electrodes.

and SO_4^{2-}, with the cation migrating in the direction opposite to the anion. The *transference number* of an ion is defined as the fraction of the current that is carried by that ion in a solution of uniform composition:

$$t_i = \frac{z_i F N_i}{i}. \tag{1.26}$$

For example, for 0.1 *M* $CuSO_4$ in water at 25°C, $t_{Cu^{2+}} = 0.363$ and $t_{SO_4^{2-}} = 0.637$. However, in our system of copper electrodes, only the Cu^{2+} is reacting at the electrodes. Movement of sulfate ions toward the anode will therefore cause changes in concentration across the solution. In general, if the transference number of the reacting ion is less than unity, then there will be fluxes of the other ions in solution that will cause concentration gradients to form. These concentration gradients drive mass transport by the process of diffusion, which occurs in addition to the process of migration described above. The component of the flux density of a species due to diffusion is

$$\mathbf{N}_{i,\text{diffusion}} = -D_i \nabla c_i, \tag{1.27}$$

where D_i is the diffusion coefficient of species i. In aqueous systems at room temperature, diffusion coefficients are generally of order 10^{-5} cm^2/s.

If the sulfate ion is not reacting electrochemically, how does it carry current? At steady state, of course, it does not. The flux of sulfate in one direction by migration, proportional to its transference number, must be counterbalanced by the flux of sulfate in the opposite direction by diffusion. Thus, concentration gradients will develop until diffusion of sulfate exactly counterbalances migration of sulfate. At steady state,

$$\mathbf{N}_{-,\text{migration}} = -z_- u_- F c_- \nabla\Phi = -\mathbf{N}_{-,\text{diffusion}} = D_- \nabla c_-. \tag{1.28}$$

Before the concentration gradients have reached their steady-state magnitudes, the sulfate ion is effectively carrying current because salt accumulates at the anode side of the cell and decreases at the cathode side of the cell. While migration and diffusion of the sulfate ions oppose each other, migration and diffusion act in the same direction for the cupric ion, which carries all of the current at steady state.

A low transference number means that little of the current is carried by migration of that ion. If the ion is the reacting species, then more diffusion is needed to transport the ion for a lower t_i, and therefore a larger concentration gradient forms.

The magnitude of these concentration gradients is given by a combination of both the transference number and the salt diffusion coefficient, as discussed in Chapters 11 and 12. The salt diffusion coefficient D for a binary electrolyte is an average of the individual ionic diffusivities:

$$D = \frac{z_+ u_+ D_- - z_- u_- D_+}{z_+ u_+ - z_- u_-}. \tag{1.29}$$

For a binary electrolyte, the transference number is related to the mobilities by

$$t_+ = \frac{z_+ u_+}{z_+ u_+ - z_- u_-}. \tag{1.30}$$

The treatment of transport in electrolytic solutions is thus more complicated than the treatment of solutions of neutral molecules. In a solution with a single neutral solute, the magnitude of the concentration gradient depends on only one transport property, the diffusion coefficient. In contrast, transport in a solution of a dissociated salt is determined by a total of three transport properties. The magnitude of the concentration gradient is determined by D and t_+, while κ determines the ohmic resistance.

Convection

Convection is the bulk movement of a fluid. The equations describing fluid velocity and convection are detailed in Chapter 15. The flux density of a species by convection is given by

$$\mathbf{N}_{i,\text{convection}} = c_i \mathbf{v}, \tag{1.31}$$

where $\mathbf{v}$ is the velocity of the bulk fluid. Convection includes natural convection (caused by density gradients) and forced convection (caused by mechanical stirring or a pressure gradient). Convection can be laminar, meaning that the fluid flows in a smooth fashion, or turbulent, in which the motion is chaotic.

Substitution into equation 1.14 for the current gives

$$\mathbf{i}_{\text{convection}} = \sum_i z_i c_i F \mathbf{v}. \tag{1.32}$$

By electroneutrality, $\sum_i z_i c_i = 0$. Therefore, in an electrically neutral solution, bulk convection alone does not cause a net current. However, convection can cause mixing of the solution, and while it alone cannot cause a current, fluid motion can affect concentration profiles and serve as an effective means to bring reactants to the electrode surface.

The net flux density of an ion is given by the combination of equations 1.16, 1.27, and 1.31:

$$\mathbf{N}_i = -z_i u_i F c_i \nabla \Phi - D_i \nabla c_i + c_i \mathbf{v}. \tag{1.33}$$

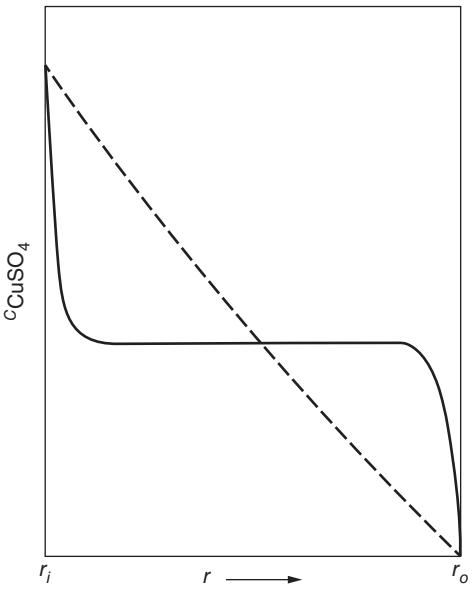

Figure 1.7 Concentration profile in the annular space between the electrodes. The dashed curve refers to the absence of a radial component of velocity. The solid curve refers to the presence of turbulent mixing.

To understand how the different components interact, consider Figure 1.7, which shows the concentration profile between the two copper cylinders at steady state for two cases. The dashed curve shows the case in which there is no convection. The slope of this curve is determined by the transference number, salt diffusion coefficient, and the current density, as mentioned previously. The cation migrates toward the negative electrode (here the outer electrode), and the concentration profile shows that this migration is augmented by diffusion down the concentration gradient. Conversely, migration of the unreacting sulfate ion toward the anode is counterbalanced by diffusion acting in the opposite direction.

If one increases the current density, the slope of the dashed curve in Figure 1.7 increases. At some current density, the concentration of cupric ion at the cathode will reach zero. Experimentally, one observes a large increase in the cell voltage if one tries to increase the current density beyond this value. This current is called the *limiting current* and is the highest current that can be carried by the cupric ion in this solution and geometry. A higher current can be passed only if another reaction, such as hydrogen evolution, starts occurring to carry the extra current.

The concentration profile in solution can be modified by convection. For example, one could flow electrolyte axially through the annulus, causing the concentration to vary with both radial position and distance from the inlet. Conversely, laminar angular flow of the solution in the annulus, such as would be caused by slow rotation of one of the cylinders, would have no impact on the concentration profile since the fluid velocity would be always perpendicular to the concentration gradients.

The solid curve in Figure 1.7 shows the concentration profile for the case when the inner cylinder is rotated at a high speed, causing turbulent convection in the bulk of the solution. At the solid–solution interface, the "no-slip" condition applies, which damps the fluid velocity. Diffusion and migration therefore dominate convection immediately adjacent to the electrodes. The mixing causes the solution to be more or less uniform in all regions except narrow boundary layers adjacent to the electrode surfaces. These boundary regions are called *diffusion layers*. They become thinner as the rate of mixing increases. Because the mixing evens out the concentration in the bulk of the electrolyte, the

concentration gradients can now be steeper in these boundary regions, leading to much higher rates of mass transport than would be possible without the stirring. Thus, stirring increases the limiting current. For example, for the system shown in Figure 1.5 with $r_o = 3$ cm, $r_i = 2$ cm, and 0.1 M aqueous $CuSO_4$, the limiting current given by diffusion and migration in the absence of convection is 0.37 mA/cm^2. If one rotates the inner cylinder at 900 rpm to cause turbulent mixing, the system can carry a much higher limiting current of 79 mA/cm^2.

Convection can occur even in the absence of mechanical stirring. At the cathode, cupric ions are consumed, and the concentration of salt in solution decreases. Conversely, the concentration of salt increases at the anode. Since the density of the electrolyte changes appreciably with salt concentration, these concentration gradients cause density gradients that lead to natural convection. The less dense fluid near the cathode will flow up, and the denser fluid near the anode will flow down. The resulting pattern of streamlines is shown in Figure 1.8. A limiting current, corresponding to a zero concentration of cupric ions along the cathode surface, still can develop in this system. The corresponding current distribution on the cathode now will be nonuniform, tending to be higher near the bottom and decreasing farther up the cathode as the solution becomes depleted while flowing along the electrode surface. The stirring caused by this natural convection increases the limiting current, from a calculated value of 0.37 mA/cm^2 in the case of no convection to 9.1 mA/cm^2 with natural convection.

In the field of electrochemical engineering, we are often concerned with trying to figure out the distribution of the current over the surface of an electrode, how this distribution changes with changes in the size, shape, and material properties of a system, and how changes in the current distribution affect the performance of the system. Often, the engineer seeks to construct the geometry and system parameters in such a way as to ensure a uniform current distribution. For example, one way to avoid the natural convection mentioned above is to use a horizontal, planar cell configuration with the anode on the bottom.

In many applications, such as metal electrodeposition and some instances of analytical electrochemistry, it is common to add a *supporting electrolyte*, which is a salt, acid, or base that increases the conductivity of the solution without participating in any electrode reactions. For example, one might add sulfuric acid to the solution of copper sulfate. Adding sulfuric acid as supporting electrolyte has several interrelated effects on the behavior of the system. First, the conductivity κ is increased, thereby reducing the electric field in solution for a given applied current density. In addition, the

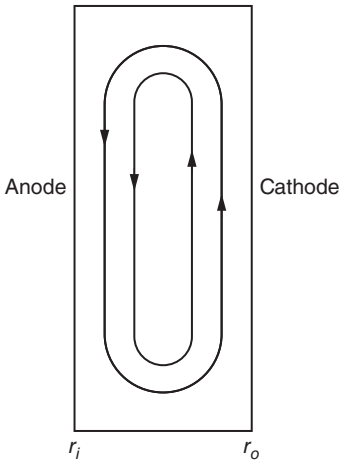

Figure 1.8 Streamlines for free convection in the annular space between two cylindrical electrodes.

transference number of the cupric ion is reduced. These two effects mean that the role of migration in the transport of cupric ion is greatly reduced. The effect of adding supporting electrolyte is thus to reduce the ohmic potential drop in solution and to increase the importance of diffusion in the transport of the reacting ion. Since migration is reduced, a supporting electrolyte has the effect of decreasing the limiting current. For example, adding 1.53 M H_2SO_4 to our 0.1 M solution of $CuSO_4$ will increase the ionic conductivity from 0.00872 to 0.548 S/cm, thus substantially decreasing the ohmic resistance of the system. The resultant decrease in the electric field for a given applied current and lowering of $t_{Cu^{2+}}$ cause a decrease in the limiting current from 79 mA/cm^2 with no supporting electrolyte to 48 mA/cm^2 with supporting electrolyte (with turbulent mixing).

The conductivity of the solution could also have been increased by adding more cupric sulfate. However, in refining a precious metal, it is desirable to maintain the inventory in the system at a low level. Furthermore, the solubility of cupric sulfate is only 1.4 M. To avoid supersaturation at the anode, we might set an upper limit of 0.7 M, at which concentration the conductivity is still only 0.037 S/cm. An excess of supporting electrolyte is usually used in electroanalytical chemistry and in studies of electrode kinetics or of mass transfer, not only because the potential variations in the solution are kept small but also because activity coefficients, transport properties, and even the properties of the interface change little with small changes of the reactant concentration.

The above discussion describes transport under a framework called dilute-solution theory in which migration is considered independently from diffusion. Chapter 12 describes how to unify the treatment of migration and diffusion under the framework of concentrated-solution theory.

1.5 CONCENTRATION OVERPOTENTIAL AND THE DIFFUSION POTENTIAL

Already we have described two sources of resistance: the surface overpotential, which represents the resistance to electrochemical reaction, and the ohmic resistance, which is the resistance to ionic or electronic current. In this section, we discuss how the presence of concentration gradients creates another source of overpotential.

Consider the following scenario shown in Figure 1.9. A solution of 0.1 M $CuSO_4$ is connected to a solution of 0.05 M $CuSO_4$ via a porous glass disk. The disk prevents rapid mixing between the

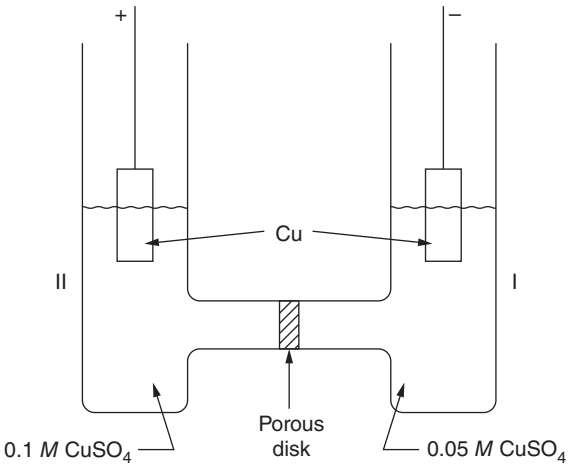

Figure 1.9 Concentration cell.

solutions, but it does allow the flow of current and slow diffusion between the solutions. Into each solution we dip an identical copper electrode.

In Section 1.2, we discuss the dependence of the open-circuit potential on concentration. Thus, from equation 1.8, we can predict that there will be a potential difference between the two electrodes placed in solutions of differing reactant concentrations. Because of the concentration differences, there is a tendency for cupric ions to plate out from the 0.1 M solution and for copper to dissolve into the 0.05 M solution. This manifests itself in a potential difference between the electrodes to prevent the flow of current, the electrode in the more concentrated solution being positive relative to the other electrode. If these electrodes were connected through an external resistor, current would flow through the resistor from the positive to the negative electrode and through the solution from the negative to the positive.

Even if a potential is applied to prevent the flow of current between the electrodes, the situation depicted in Figure 1.9 is not at equilibrium. Diffusion may be restricted by the glass disk, but it will still occur until eventually the two sides of the cell reach the equilibrium condition of equal concentrations. Therefore, the potential difference between the electrodes includes transport properties as well as thermodynamic properties. The meaning of potential in a solution of nonuniform concentration and the calculation of potential differences across nonuniform solutions are treated in detail in Chapters 2 and 12. For the particular case given by Figure 1.9, the potential of the cell is given approximately by

$$\Phi_{\mathrm{I}} - \Phi_{\mathrm{II}} = U_{\mathrm{conc}} = (1 - t_+)\frac{RT}{F} \ln \frac{c_{\mathrm{I}}}{c_{\mathrm{II}}}. \tag{1.34}$$

Notice the difference between this equation and equation 1.8. Equation 1.8 describes how the open-circuit potential depends on the concentrations of reactants and products at equilibrium whereas equation 1.34 includes in addition the diffusion potential caused by the presence of concentration gradients.

If we have a solution with a concentration gradient across it, instead of two solutions separated by a porous disk, the potential between any two points in solution still depends on the concentration differences in a manner described by equation 1.34. This potential difference caused by a concentration gradient can be referred to as a *concentration overpotential*.

Let us consider the concentration overpotentials in our system of concentric copper cylinders. We rotate one cylinder to create turbulent mixing, so that the concentration profile is uniform in the middle of the annulus (see Figure 1.7). This arrangement allows us to isolate the concentration overpotentials at each electrode.

We place three copper reference electrodes in the solution as shown in Figure 1.10. Reference electrode 1 is adjacent to the anode, reference 2 is adjacent to the cathode, and reference 3 is in the middle of the cell where the concentration is uniform. These reference electrodes can sense the potential in a solution carrying current, even though they themselves carry no current. One tries to situate the reference electrodes in such a position that they do not alter conditions significantly from those prevailing in their absence. We can do that here by using very small copper wires.

$\Phi_1 - \Phi_2$ is the potential difference in the solution. It consists of two components, the ohmic potential drop and a concentration overpotential:

$$\Phi_1 - \Phi_2 = U_{\mathrm{conc}} + \int_1^2 \frac{\mathbf{i} \cdot d\mathbf{r}}{\kappa}, \tag{1.35}$$

where we have included κ inside the integral because it may vary with concentration and U_{conc} is given approximately by equation 1.34 (the term concentration overpotential is redefined in equation 1.36).

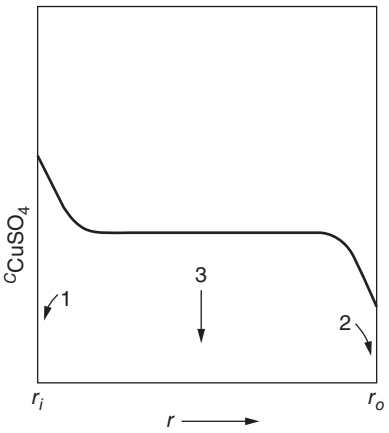

Figure 1.10 Placement of reference electrodes (1, 2, and 3) in the solution between cylindrical electrodes. The concentration profile shown corresponds to turbulent mixing at a current somewhat below the limiting current.

The ohmic portion is proportional to the current and will disappear immediately if the current is interrupted. This provides a means for distinguishing between the two. The total potential difference between the two reference electrodes is measured with the current flowing. The contribution of concentration variations is that value measured just after the current is interrupted but before the concentration distribution can change by diffusion or convection. The difference between these two measurements is the ohmic contribution. (It should be pointed out that—in many geometries—internal current redistribution may occur after the external current is turned off. In these cases, ohmic resistance is still present for some time after the current is interrupted.)

We can use the third reference electrode to separate the concentration overpotential into contributions from the anode and cathode. The concentration overpotential at the anode is then $\Phi_1 - \Phi_3$, and the cathodic concentration overpotential is $\Phi_2 - \Phi_3$, just after the current is interrupted. This decomposition of the concentration overpotential depends on the concept of thin diffusion layers near the electrodes and the existence of a bulk solution where the concentration does not vary significantly. Then the anodic and cathodic concentration overpotentials are independent of the precise location of the third reference electrode, since it is in a region of uniform concentration and there is no current flow.

Alternatively, we can define the concentration overpotential by

$$\eta_c = U_{\text{conc}} + \int_0^{\text{bulk}} \left(\frac{1}{\kappa} - \frac{1}{\kappa_{\text{bulk}}} \right) i_y \, dy, \tag{1.36}$$

where y is the distance from the electrode and bulk represents the solution properties in the uniform region of the annulus. Then $\Phi_1 - \Phi_2 = \eta_c + \Delta\Phi_{\text{ohm}}$, where $\Delta\Phi_{\text{ohm}}$ is the potential difference that would be measured in the hypothetical scenario of the same current distribution but with no concentration gradients. $\Delta\Phi_{\text{ohm}}$ can be calculated using the procedure given in Section 1.4 with constant conductivity. This definition of concentration overpotential means that η_c accounts for all potential changes induced by concentration effects. Figure 1.11 shows how the cathodic overpotential depends on current density for current densities up to the limiting current.

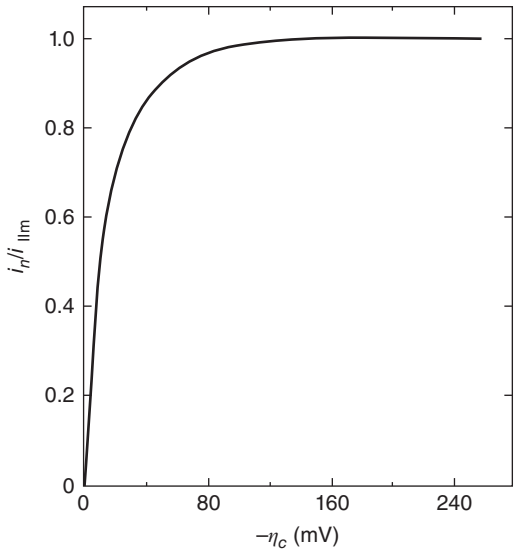

Figure 1.11 Concentration overpotentials at a cathode in 0.1 *M* $CuSO_4$.

1.6 OVERALL CELL POTENTIAL

The potential difference across a cell will depend on all four components described above: the open-circuit potential U, the surface overpotential, the ohmic potential drop, and the concentration overpotential. These potential drops are interrelated, making the calculation of the total potential of the cell more complicated than that given by the ohmic potential drop alone. It is these interrelationships that make electrochemical engineering both a challenging and an interesting field.

The open-circuit potential U represents the maximum work that can be obtained from the system. We use the symbol V to denote the cell potential, which is often called the cell voltage. The cell potential V may differ from the open-circuit potential U, both during and shortly after the passage of current, because the passage of current has induced overpotentials. All of the overpotentials represent dissipative losses. Thus, for a galvanic cell, the actual cell potential during passage of current will always be less than U (the rate of work output of the cell, IV, is less than IU), while for an electrolytic cell the actual cell potential will be greater (the work that one must put into the cell is greater than the reversible work). The cell potential will approach the reversible potential as the current becomes infinitesimally small.

As described in Section 1.3, the potential drop due to kinetic resistance at the anode is $\eta_{s,\,\text{anode}} = \Phi_{\text{anode}} - \Phi_1$, where Φ_{anode} and Φ_1 are measured by electrodes made of the same compounds, and likewise the surface overpotential at the cathode is $\eta_{s,\,\text{cathode}} = \Phi_{\text{cathode}} - \Phi_2$, where Φ_{cathode} and Φ_2 are measured by electrodes made of the same compounds. $\eta_{s,\text{anode}}$ is positive while $\eta_{s,\text{cathode}}$ is negative.

The cell potential is given by

$$\begin{aligned} V &= \Phi_{\text{anode}} - \Phi_{\text{cathode}} \\ &= (\Phi_{\text{anode}} - \Phi_1) + (\Phi_1 - \Phi_2) - (\Phi_{\text{cathode}} - \Phi_2) \\ &= \eta_{s,\text{anode}} + (\eta_{c,\text{anode}} + U + \Delta\Phi_{\text{ohm}} - \eta_{c,\text{cathode}}) - \eta_{s,\text{cathode}}, \end{aligned} \tag{1.37}$$

where each η_s is obtained from an equation of the form of equation 1.9, $\Delta\Phi_{\text{ohm}}$ is given by equation 1.23, calculated using a constant conductivity, and η_c is obtained from equation 1.36, which includes the variation of conductivity with concentration as well as the diffusion potential. For generality, we have included the possibility that the cathode and anode may be made of different metals, such as zinc and silver, respectively. Then we would use a silver electrode for reference 1 and a zinc electrode for reference 2 to measure the surface overpotentials. To isolate the concentration overpotentials, we could use two reference electrodes, for example, a silver and a zinc, placed side by side at position 3. Call $\Phi_{3,a}$ the potential measured by the reference electrode of the same kind as the anode and $\Phi_{3,c}$ that measured by the reference electrode of the same kind as the cathode. $\Phi_{3,a} - \Phi_{3,c}$ is then U, the equilibrium potential difference between the anode and cathode electrodes in a region of uniform concentration. For the case in which all of the electrodes are the same, for example, all copper metal, U is zero. The terms η_c and η_s for the cathode enter with negative signs because of the conventions that have been adopted. Since they are negative, they make a positive contribution to the cell potential of this electrolytic cell. Thus, all of the overpotentials represent resistive losses.

Figure 1.12 indicates what we should expect for the response of the current I to the applied potential V. At low currents, most of the applied potential is consumed by ohmic losses, which increase linearly with the applied current. At low currents the surface overpotential increases linearly with current, and changes with the logarithm of current at moderate currents. As the concentration of reactants at the cathode is depleted near the limiting current, the exchange current density becomes very small and the surface overpotential increases substantially. The concentration polarization at the cathode increases dramatically as the limiting current is approached. At sufficiently large voltages, a second reaction such as hydrogen evolution may occur at the cathode, as indicated by the dashed line on the figure. $\eta_{s,\text{anode}}$ and $\eta_{c,\text{anode}}$ are not shown on the figure because, for this particular cell, they are small. $\eta_{s,\text{anode}}$ is less than $\eta_{s,\text{cathode}}$ because a different value of the apparent transfer coefficient was used (see Figure 1.3). $\eta_{c,\text{anode}}$ is smaller than $\eta_{c,\text{cathode}}$ because the order of magnitude of increase in the logarithm

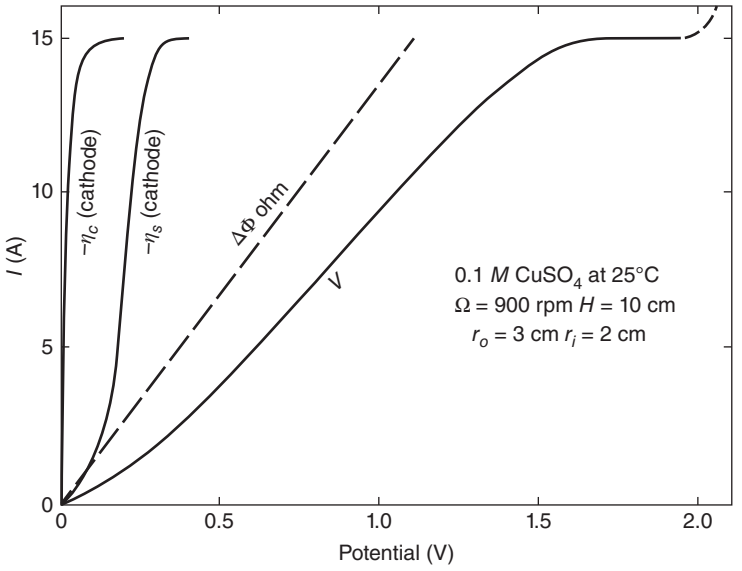

Figure 1.12 The dependence of the cell potential and its component overpotentials on current for concentric cylinders, the inner of which rotates. The overpotentials for the anode are small for this particular system and are not shown.

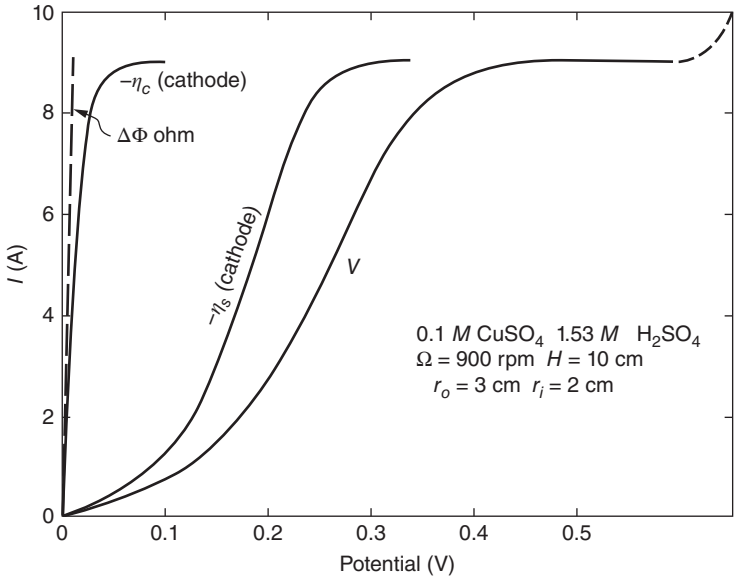

Figure 1.13 Current–potential relations with sulfuric acid added as a supporting electrolyte.

of the concentration of Cu^{2+} at the anode is much less than the order of magnitude of decrease in the logarithm of the concentration at the cathode, where the concentration is driven to zero.

Figure 1.13 shows how the current–potential relationships change when sulfuric acid is added as supporting electrolyte. The ohmic potential drop is reduced relative to Figure 1.12, and the concentration and surface overpotentials now constitute a larger fraction of the applied potential. The magnitude of the limiting current is also reduced.

The *energy efficiency* for a galvanic cell is given by the net work out ($\int IV\,dt$) divided by the reversible work ($\int IU\,dt$), that is, the work that could be obtained if the cell potential were always equal to its equilibrium potential. For an electrolytic cell, the energy efficiency is the reversible work divided by work input required to drive the reaction. One can also speak in terms of current efficiency for cells in which multiple reactions may occur in the same potential range. For example, if a metal's reduction potential is close to that of hydrogen evolution, then one may evolve hydrogen while trying to electrodeposit the metal. *Current efficiency* is the ratio of the charge consumed by the desired reaction to the total charge passed in the cell.

In conclusion, kinetics, thermodynamics, and transport are closely interrelated in electrochemical systems. In Parts A, B, and C, we describe the fundamentals of each in turn. However, it is impossible to discuss each aspect in complete isolation since all three phenomena are interdependent. In Part D, we describe applications that illustrate how to treat the coupled phenomena, and we discuss when simplifying assumptions may be used to reduce the complexity of the analysis of electrochemical systems.

PROBLEMS

1.1 Starting with equation 1.36, derive the following equation for the concentration overpotential in a binary salt solution:

$$\eta_c = \frac{RT}{F}\left[\ln\frac{c_o}{c_b} + t_+\left(1 - \frac{c_o}{c_b}\right)\right].$$

Assume that the concentration profile is linear within the diffusion layer and uniform outside this layer, which can be taken to be of finite thickness. In addition to the relationships expressed in this chapter, it is necessary to use the Nernst–Einstein relation between the mobility and the diffusion coefficient of species *i:*

$$D_i = RTu_i.$$

Use equation 1.18 for the variation of conductivity with concentration. c_o is the concentration at the electrode surface, and c_b is the concentration outside the diffusion layer (see Section 20.2).

NOTATION

c_i	concentration of species i, mol/cm^3
c_b	concentration in bulk solution, mol/cm^3
c_0	concentration at electrode surface, mol/cm^3
D	diffusion coefficient of electrolyte, cm^2/s
D_i	diffusion coefficient of species i, cm^2/s
F	Faraday's constant, 96,487 C/mol
G	Gibbs free energy, J/mol
H	depth of solution, cm
i	current density, A/cm^2
i_n	normal component of the current density, A/cm^2
i_0	exchange current density, A/cm^2
I	total current, A
ℓ	distance, cm
m	molality of species i, mol/kg
n	number of electrons involved in electrode reaction
$\mathbf{N}_i$	flux density of species i, mol/cm^2·s
r	radial position, cm
r_i	radius of inner electrode, cm
r_o	radius of outer electrode, cm
R	resistance, Ω
R	universal gas constant, 8.3143 J/mol·K
s_i	stoichiometric coefficient of species i
t_+	cation transference number
T	absolute temperature, K
u_i	mobility of species i, cm^2·mol/J·s
U	cell potential at open circuit, V
$\mathbf{v}$	fluid velocity, cm/s
$\mathbf{v}_i$	average velocity of species i, cm/s
V	cell potential, V
y	distance from electrode, cm
z_i	charge number of species i
α_a, α_c	anodic and cathodic transfer coefficients
η_c	concentration overpotential, V
η_s	surface overpotential, V
κ	ionic conductivity, S/cm

μ_i	electrochemical potential of species i, J/mol
σ	electronic conductivity, S/cm
Φ	potential, V
$\Delta\Phi_{ohm}$	ohmic potential drop, V
Ω	rotation speed, rad/s

PART A

THERMODYNAMICS OF ELECTROCHEMICAL CELLS

For a discussion of the thermodynamics of electrochemical cells, we first need to introduce free energies, chemical potentials, and activity coefficients. If we restrict ourselves to electrodes in equilibrium with the solution adjacent to them, then the cell potential can be obtained by expressing these phase equilibria in terms of the electrochemical potentials of species present in the electrodes and in the solutions. The condition of phase equilibrium precludes the passage of anything but an infinitesimal current; it also precludes the possibility of the occurrence of spontaneous reactions that require no net current. Under certain conditions it is possible, however, to have more than one reaction simultaneously in equilibrium.

In all but the simplest cells, the expression of the phase equilibria does not lead to an immediately useful result. The solutions adjacent to the two electrodes of a cell usually have different compositions, and in order to preclude spontaneous reactions at the electrodes, it is necessary to prevent the reactants for one electrode from reaching the other. Thus, somewhere between the electrodes there must be a region of nonuniform composition; and in this region, which is referred to as a *liquid junction*, spontaneous diffusion occurs. To treat the potentials of any but the simplest cells, therefore, requires some consideration of the irreversible process of diffusion. The necessary results are carried over from Part C on transport processes in electrolytic solutions.

The treatment of cell potentials follows a certain pattern. The description of phase equilibria allows the cell potential to be expressed in terms of the electrochemical potentials of species in the solutions adjacent to the electrodes. To obtain useful results, these electrochemical potentials must be related to each other, usually by a consideration of the transport process in the junction region.

The concept of the potential is important in electrochemistry, but an understanding of the concept is made difficult by the background that most of us acquire in classical electrostatics. A discussion of the potential and its use in electrochemistry is therefore in order. Many equations in common use can

Electrochemical Systems, Fourth Edition. John Newman and Nitash P. Balsara.

be clarified by this study, and, at the same time, the assumptions inherent in their derivation can be exposed.

The remainder of this part deals with practical and theoretical aspects of electrochemical thermodynamics—in particular, with activity coefficients and reference electrodes.

CHAPTER 2

THERMODYNAMICS IN TERMS OF ELECTROCHEMICAL POTENTIALS

2.1 PHASE EQUILIBRIUM

An electrochemical cell necessarily consists of several phases. These phases must include two electrode metals and an electrolytic solution (three phases); but additional phases, such as a solid salt or a gas, are included in most cells of practical interest. Equilibria between these individual phases (e.g., electrode metal β in equilibrium with the solution δ) characterize an electrochemical cell used for thermodynamic measurements.

The system shown in cell 2.1 is illustrative of the type of cell commonly called a *cell without transference*, which is a cell in which there are no concentration gradients:

$$\begin{array}{c|c|c|c|c|c} \alpha & \beta & \delta & \epsilon & \phi & \alpha' \\ \text{metal} & \text{metal} & \text{electrolytic solution} & \text{solid salt} & \text{metal} & \text{metal.} \end{array} \tag{2.1}$$

The vertical lines denote phase separation. The several phase equilibria that may be attained are:

Phase α in equilibrium with phase β
Phase β in equilibrium with phase δ
Phase δ in equilibrium with phase ϵ
Phase ϵ in equilibrium with phase ϕ
Phase ϕ in equilibrium with phase α'.

Phases α and α' are composed of the same metal but are not necessarily in equilibrium since they may not be at the same electrical potential.

Electrochemical Systems, Fourth Edition. John Newman and Nitash P. Balsara.

If two phases are in equilibrium and if a neutral species A is present in each phase, then the chemical potential of A is the same in the two phases, that is,

$$\mu_A^{\delta} = \mu_A^{\epsilon}. \tag{2.2}$$

Here the subscript A refers to the species, and the superscript refers to the phase. Similar equations hold for other equilibrated species. Indeed, this equation must be obeyed for each species that exists in both neighboring phases before the phases may be said to be in equilibrium.

When two phases are at the same temperature but are not in equilibrium, upon contact there will be transport of material across the phase boundary until the condition described by equation 2.2 is attained. Thus, each of the phases in equilibrium may be considered to be open with respect to those species that can be transported between the phases. It should be pointed out that phase equilibrium as used here does not require that all species be present in each phase or that each species be at the same chemical potential in each phase. For example, if phase α is platinum and phase β is a potassium amalgam, platinum is not present in phase β, and neither potassium nor mercury is present in phase α. It is electrons that are equilibrated between these phases. Similarly, the electrons are presumed to be absent in the solution phase δ. If all species were present in all phases and were equilibrated, then phases α and α' would be in equilibrium, and there would be no electrical potential difference between them.

To repeat, phase equilibrium is taken to be the thermodynamic state in which equation 2.2 applies to those species that are present in both neighboring phases.

In electrochemical systems, there are also equilibria that involve ionic or charged species. Let 1 mol of the neutral species A dissociate into ν_+^A moles of a positively charged species and ν_-^A moles of a negatively charged species. The chemical potential of A can then be expressed as

$$\mu_A^{\alpha} = \nu_+^A \mu_+^{\alpha} + \nu_-^A \mu_-^{\alpha}, \tag{2.3}$$

where μ_+ and μ_- are the electrochemical potentials of the charged species and depend on the temperature, pressure, chemical composition, and electrical state of the phase. We return to these terms in the next section. Since species A is electrically neutral, the coefficients ν_i^A are subject to the restriction

$$\sum_i z_i \nu_i^A = 0, \tag{2.4}$$

where z_i is the charge number of species i and the superscript A refers to the particular neutral species. For example, phosphoric acid (H_3PO_4) is made up of H^+ ions and PO_4^{3-} ions, for which $\nu_+ = 3$, $\nu_- = 1$, $z_+ = 1$, and $z_- = -3$. Copper metal can be regarded as composed of cupric ions and electrons, for which $\nu_+ = 1$, $\nu_- = 2$, $z_+ = 2$, and $z_- = -1$.

Equation 2.2 expresses the condition of phase equilibrium involving neutral species. For the charged species i, the corresponding condition of phase equilibrium between the two phases α and β is

$$\mu_i^{\alpha} = \mu_i^{\beta}. \tag{2.5}$$

If there are several ionic species present in each phase, equation 2.5 must be obeyed for each ionic species present in both phases before phase equilibrium is attained.

Each phase individually will be electrically neutral even though all the ionic species are not present in each phase. Thus, the composition of any phase is determined by specifying the concentrations of all but one of the charged species, the concentration of the remaining species then being given by this condition of electrical neutrality.

Occasionally, it is desirable and convenient to express the condition of equilibrium for an electrode reaction all at once. For the general electrode reaction

$$\sum_i s_i M_i^{z_i} \rightarrow n\mathrm{e}^-, \tag{2.6}$$

this condition is

$$\sum_i s_i \mu_i = n\mu_{\mathrm{e}^-}. \tag{2.7}$$

Here s_i is the stoichiometric coefficient of species i in the electrode reaction and M_i is a symbol for the chemical formula of species i. Superscripts for the appropriate phases in which the species exist should be added.

2.2 CHEMICAL POTENTIAL AND ELECTROCHEMICAL POTENTIAL

The potential of a cell is the difference in electrochemical potential of electrons between the leads connected to the positive and negative electrodes, divided by Faraday's constant. What, then, is electrochemical potential? One can think of it analogously to other types of potentials with which the reader may be familiar, such as gravitational potential. Like a ball rolling down a hill, a species will tend to move from a region where it has a high electrochemical potential to a region where it has a low electrochemical potential. This example raises the question, what factors cause the electrochemical potential of a species to be higher in one region than in another? Electrochemical potential depends on temperature, pressure, composition, and electrical state. We see many examples in our daily lives of the dependence on composition. If one pours sugar into a cup of hot tea and then waits a few minutes, eventually the sugar will diffuse throughout the tea until it has a uniform concentration. This is because the chemical potential of the more concentrated sugar solution is higher than the chemical potential of the less concentrated solution. We speak of the chemical potential of neutral species, μ_A, and of the electrochemical potential of charged species such as ions and electrons, μ_i. The difference between the two is that the energy, or potential, of an electrically charged species is affected by the presence of an electric field, whereas the potential of a neutral species is unaffected by an electric field.

Electrochemical potential is a measure of the energy of the species. Thermodynamics describes macroscopically how the free energy of a species depends on temperature, pressure, composition, and electrical state. Quantum mechanics provides another framework for describing the energy of a species in terms of electron orbitals and energy levels. In quantum mechanical terms, electrochemical potential is defined as the energy level of the electron orbitals in the species that have a 50% probability of occupancy. "Applying a potential" shifts the energy levels, that is, the electrochemical potential, up or down. The quantum mechanical viewpoint will be revisited in Chapter 23 in the context of semiconductors. In contrast to thermodynamics and quantum mechanics, the field of electrostatics ignores chemical interactions and describes an idealized "electric potential" that is the result of moving idealized electric charges from one place to another, ignoring the chemical environment that the electrons experience. This idealization breaks down when one tries to consider electric potential differences between media of different chemical compositions. For example, consider the electrochemical potential difference between electrons in a piece of copper and electrons in a piece of aluminum. Even if both metals are uncharged, there will be an electrochemical potential difference because the chemical environment of copper is different from that of aluminum. What, then, is the electric potential difference? It cannot be measured separately from the chemical potential difference. Therefore, the legitimate measurement to make is the difference in electrochemical potential between

two identical electrodes at the same temperature, pressure, and composition, one electrode connected to the piece of copper metal and the other connected to the piece of aluminum.

However, the electrostatic idealization is not a bad one when considering the electrochemical potential within a given metal. Consider the process of applying a potential difference between two copper spheres, each of mass 38 g (this example is revisited in Section 3.1). Depending on the dielectric medium separating the spheres, transferring about 1×10^{-9} mol of charge from one sphere to the other results in coulombic forces that cause a potential difference of about 2×10^{8} V. However, the 10^{-9} mol has a negligible impact on the chemical composition of the copper. Moreover, all of the charge will reside at the surface of an electronic conductor. Thus, the bulk of the metal is unchanged chemically, but the electrochemical potential of electrons in the metal has been substantially changed by the electric field caused by the charge added to the surface of the metal. Therefore, the idealization of electric potential can be fruitfully used to describe how one can apply a potential to a metal by adding or removing electrons, with little loss of precision from neglecting the chemical effects of the minute change in the concentration of electrons.

However, one should keep in mind that the concept of "electric potential" as used in the field of electrostatics is only an idealized limit of the electrochemical potential in which chemical interactions are ignored. For this reason, the electric potential difference between two phases of different chemical composition is undefined, and one must speak of the cell potential as the difference in the thermodynamic electrochemical potential of electrons between two leads of identical composition, temperature, and pressure. In addition, division of the electrochemical potential into chemical and electrical components is arbitrary. What is meaningful is the electrochemical potential.

Before introducing the definition of μ_i, we should recall the thermodynamic definition of μ_A:

$$\mu_A = \left(\frac{\partial G}{\partial n_A}\right)_{\substack{T,p,n_{B\neq A}}} = \left(\frac{\partial A}{\partial n_A}\right)_{\substack{T,V,n_{B\neq A}}} = \left(\frac{\partial U}{\partial n_A}\right)_{\substack{S,V,n_{B\neq A}}} = \left(\frac{\partial H}{\partial n_A}\right)_{\substack{S,p,n_{B\neq A}}}, \tag{2.8}$$

where G is the Gibbs free energy, A is the Helmholtz free energy, U is the internal energy, H is the enthalpy, S is the entropy, V is the volume, T is the temperature, $n_{B,\,B\neq A}$ is number of moles of all species besides A, and p is the pressure. In making measurements, one always determines a difference in the chemical potential between different thermodynamic states and never the absolute value in a particular state. However, in tabulating data, it is convenient to assign a value to each thermodynamic state. One can do this by arbitrarily assigning the value of the chemical potential in some state and determining the value in other states by comparison to this reference state. For example, the chemical potentials of pure elements at 25°C and 1 bar can be taken to be zero. Once the reference state is clearly specified and the values of the chemical potential in other states are tabulated, one can easily reproduce the experimental results. This will be mentioned again in the treatment of data from electrochemical cells.

One of the characteristics of the chemical potential, developed in thermodynamics, is that the reversible work of transferring a species from one point to another is proportional to the difference in chemical potential between the two points. Guggenheim[1] used this concept to define the electrochemical potential of an ion so that the difference between its values in two phases is defined as the work of transferring reversibly, at constant temperature and constant volume, 1 mol from one phase to the other.* It is a function of temperature, pressure, chemical composition, and electrical state of the phase. It is still necessary to determine how well defined these independent variables are. Consider the following cases where transfer of ions may be involved:

*For condensed phases, a distinction between a constant-volume process and a constant-pressure process is of little practical significance.

1. For constant temperature and pressure and identical chemical composition of phases α and β, the only difference between the two phases will be electrical in nature.
   a. For the transfer of 1 mol of species i from phase β to phase α, the work of transfer is

$$w = \mu_i^\alpha - \mu_i^\beta = z_i F(\Phi^\alpha - \Phi^\beta), \tag{2.9}$$

   where, in the second equation, the difference in electrical state of the two phases can be characterized by the difference in electrical potential of the two phases, as defined by equation 2.9.

   b. For the transfer of ν_1 moles of species 1 and ν_2 moles of species 2 such that

$$\sum_i z_i \nu_i = 0, \tag{2.10}$$

   the work of transfer is zero. Such electrically neutral combinations of ions do not depend on the electrical state of the phase, and we can utilize this fact to examine the potential difference defined above. Since the total work of transfer will be zero for neutral combinations such that equation 2.10 holds, we have

$$w = 0 = \nu_1(\mu_1^\alpha - \mu_1^\beta) + \nu_2(\mu_2^\alpha - \mu_2^\beta). \tag{2.11}$$

   If we take equation 2.9 to apply to the ionic species 1, we can combine equations 2.9 through 2.11 to express the electrochemical potential difference of the ionic species 2 as

$$\begin{aligned} \mu_2^\alpha - \mu_2^\beta &= -\frac{\nu_1}{\nu_2}(\mu_1^\alpha - \mu_1^\beta) = -\frac{z_1\nu_1}{\nu_2}F(\Phi^\alpha - \Phi^\beta) \\ &= z_2 F(\Phi^\alpha - \Phi^\beta). \end{aligned} \tag{2.12}$$

   Therefore, the electric potential difference $\Phi^\alpha - \Phi^\beta$ defined by equation 2.9 does not depend on which charged species, 1 or 2, is used in equation 2.9. In this sense, the electric potential difference is well defined.

2. If the two phases have different chemical composition, but still the same pressure and temperature, the work of transfer of a species from phase β to phase α is still

$$w = \mu_i^\alpha - \mu_i^\beta, \tag{2.13}$$

   but this can no longer be expressed simply in terms of differences of electric potential because the chemical environment of the transferred species will be different in the two phases. The work to transfer neutral species or neutral combinations of species is $w = \mu_A^\alpha - \mu_A^\beta$, which is nonzero if the chemical potential of A is different in the different compositions.

It should be noted that no quantitative characterization or measure of the difference of electrical state of two phases has yet been given when the phases are of different chemical composition. It is possible (and even expedient for some purposes of computation) to define such an electrical variable, but this involves an unavoidable element of arbitrariness and is not essential to a treatment of the thermodynamic phenomena involved. Several possible methods of doing this are discussed in Chapter 3. We prefer to avoid an arbitrary decomposition of μ_i into electrical and chemical components and instead choose to speak in terms of electrochemical potentials.

2.3 DEFINITION OF SOME THERMODYNAMIC FUNCTIONS

We have seen in the previous section that the cell potential is determined by the electrochemical potential of electrons in equilibrium with the components of the electrode and the electrolyte. In Section 2.4, we relate μ_{e^-} to the electrochemical potentials of the cell components. These electrochemical potentials are functions of temperature, pressure, concentration, and electrical state. In this section, we discuss formalisms for describing the dependence of the electrochemical potential on concentration and electrical state.

Before delving into the study of the electrochemical potential of electrolytes in solution, the reader should already be familiar with the concepts of the chemical potentials of pure elements and compounds and their dependence on temperature and pressure, as covered in texts on thermodynamics. Thermodynamics teaches us that there is no absolute value of chemical potential. Rather, any numerical value is only relative to some arbitrary datum. For pure elements and compounds, this arbitrary datum is called the *primary reference state*. The usual convention for the primary reference state is that the chemical potential of pure elements at 298.15 K and 1 bar is zero, although other primary reference states, such as setting the chemical potential to zero at the critical point or the triple point, are sometimes used.

The chemical potential of a species in a mixture depends on the composition of the mixture. To describe this dependence, it is convention to define an "ideal" dependence of μ_i on composition, and then to define a parameter called the activity coefficient to describe the deviation of the actual μ_i from the ideal. The choice of the ideal dependence of μ_i on concentration creates a second arbitrary datum, which is the state at which the activity coefficient is defined to be 1. This state is termed the *secondary reference state*. As is described in this section, the historical convention has been to use different secondary reference states for liquid, gaseous, and solid mixtures.

In this section, the absolute activity, activity coefficient, mean activity coefficient, and osmotic coefficient are introduced. The last two are useful for the tabulation of the composition dependence of the thermodynamic properties of electrolytic solutions but may appear cumbersome in the theoretical treatment of cell potentials.

The absolute activity λ_i of an ionic or a neutral species, used extensively by Guggenheim,[2] is defined by

$$\mu_i = RT \ln \lambda_i. \tag{2.14}$$

It has the advantage of being zero when the species is absent, whereas the chemical potential is equal to minus infinity in such a case. Furthermore, λ_i is dimensionless. It also has the advantage that it can be manipulated like conventional activities but is independent of any secondary reference states that might be adopted for a particular solution or solvent at a particular temperature and pressure.

For solute species in a solution, λ_i is further broken down as follows:

$$\lambda_i = m_i \gamma_i \lambda_i^{\theta}, \tag{2.15}$$

where m_i is the molality, or moles of solute per unit mass of solvent (usually expressed in moles per kilogram of solvent), γ_i is the molal activity coefficient of species i, and λ_i^{θ} is a proportionality constant, independent of composition and electrical state, but characteristic of the solute species and the solvent and dependent on temperature and pressure. For condensed phases, the pressure dependence is frequently ignored.

Other concentration scales can be used, but the activity coefficient and the constant are changed so that λ_i is independent of the concentration scale used. Another concentration scale in common use is molarity, or moles per unit volume of solution (usually expressed in moles per liter, denoted M), and

λ_i is related to this scale by

$$\lambda_i = c_i f_i a_i^{\theta}, \tag{2.16}$$

where c_i is the molarity of species i, f_i is the molar activity coefficient, and a_i^{θ} is a proportionality constant (analogous to λ_i^{θ}). The molality is related to the molarity according to

$$m_i = \frac{c_i}{\rho - \sum_{j\neq 0} c_j M_j} = \frac{c_i}{c_0 M_0}, \tag{2.17}$$

where ρ is the density of the solution (g/cm^3), M_j is the molar mass of species j (g/mol), and where the sum does not include the solvent, denoted by the subscript 0.[†]

The molality is perhaps popular among experimentalists in the physical chemistry of solutions because it can be calculated directly from the masses of the components in the solution, without a separate determination of the density. The concentration on a molar scale is more directly useful in the analysis of transport processes in solutions. Furthermore, the molality is particularly inconvenient if the range of concentrations includes the pure molten salt with no solvent, since the molality is then infinite. However, molar concentrations do not work well in the Gibbs–Duhem equation for multicomponent systems. A mole fraction scale can be used, but then a decision has to be made on how to treat a dissociated electrolyte. The mass fraction has the advantage of depending only on the masses of the components and is also independent of the scale of atomic weights, which has been known to change. However, a mass fraction scale does not allow a simple account of the colligative properties of solutions (freezing-point depression, boiling-point elevation, and vapor-pressure lowering) nor of the properties of dilute solutions of electrolytes. Of these several scales, the molar concentration is the only one that changes with temperature when a particular solution is heated.

The secondary reference states necessary to specify λ_i^{θ} or a_i^{θ} for species in solution are defined by the statement that certain combinations of activity coefficients should approach unity in infinitely dilute solutions; namely,

$$\prod_i (\gamma_i)^{\nu_i} \to 1 \quad \text{as} \quad \sum_{i\neq 0} m_i \to 0 \tag{2.18}$$

and

$$\prod_i (f_i)^{\nu_i} \to 1 \quad \text{as} \quad \sum_{i\neq 0} c_i \to 0 \tag{2.19}$$

for all such combinations of γ_i and f_i where the ν_i's satisfy equation 2.10. In particular, the activity coefficient of any neutral, undissociated species approaches unity as the concentrations of all solutes approach zero. If we take the activity coefficients to be dimensionless, then λ_i^{θ} and a_i^{θ} have the reciprocals of the dimensions of m_i and c_i. In view of the definitions 2.18 and 2.19 of the secondary reference states, λ_i^{θ} and a_i^{θ} are then related by

$$\lambda_i^{\theta} = \rho_0 a_i^{\theta}, \tag{2.20}$$

where ρ_0 is the density of the pure solvent (g/cm^3).

For an ionic species, λ_i depends on the electrical state of the phase. Since λ_i^{θ} and m_i are taken to be independent of the electrical state, we conclude that γ_i is dependent upon this state. A similar statement applies to the activity coefficient f_i. In contrast, Guggenheim takes γ_i to be independent of electrical state and λ_i^{θ} to be dependent upon it. This leaves us with the unsatisfactory situation that γ_i

[†]Consistent units for equation 2.17 would be m_i in mol/g, c_i in mol/cm^3, and ρ in g/cm^3.

should depend on composition at constant electrical state. However, a constant electrical state has not yet been defined for solutions of different composition.

To illustrate further the nature of these activity coefficients, consider a solution of a single electrolyte A that dissociates into ν_+ cations of charge number z_+ and ν_- anions of charge number z_-. (Since only a single electrolyte is involved, the superscript A on ν_+ and ν_- is omitted.) Then the stoichiometric concentration of the electrolyte can be represented as

$$m = \frac{m_+}{\nu_+} = \frac{m_-}{\nu_-} \quad \text{or} \quad c = \frac{c_+}{\nu_+} = \frac{c_-}{\nu_-}. \tag{2.21}$$

The chemical potential of A can then be expressed by equation 2.3 as

$$\mu_A = \nu_+\mu_+ + \nu_-\mu_- = \nu_+ RT \ln(m_+\gamma_+\lambda_+^\theta) + \nu_- RT \ln(m_-\gamma_-\lambda_-^\theta) \tag{2.22}$$

or

$$\mu_A = RT \ln[(m_+\gamma_+\lambda_+^\theta)^{\nu_+}(m_-\gamma_-\lambda_-^\theta)^{\nu_-}]. \tag{2.23}$$

Since A is neutral, equation 2.18 requires that $\gamma_+^{\nu_+}\gamma_-^{\nu_-} \to 1$ as $m \to 0$. Hence, this specification of the secondary reference state allows a certain combination of the λ_i^θ's to be determined:

$$(\lambda_+^\theta)^{\nu_+}(\lambda_-^\theta)^{\nu_-} = \lim_{m\to 0} \frac{e^{\mu_A/RT}}{m_+^{\nu_+} m_-^{\nu_-}}. \tag{2.24}$$

This limiting process then allows the subsequent determination of the combination $\gamma_+^{\nu_+}\gamma_-^{\nu_-}$ at any nonzero value of m by means of equation 2.23. Methods for measuring μ_A are discussed later in this chapter.

By a generalization of these thoughts we come to the following conclusions: Combinations of the form

$$\prod_i (\lambda_i^\theta)^{\nu_i}\gamma_i^{\nu_i}$$

can be determined unambiguously for products whose exponents satisfy the Guggenheim condition

$$\sum_i z_i\nu_i = 0.$$

A choice of the secondary reference state, equation 2.18, thus allows the separate determination of the corresponding products of the forms

$$\prod_i (\lambda_i^\theta)^{\nu_i} \quad \text{and} \quad \prod_i \gamma_i^{\nu_i}.$$

These conclusions follow from the fact that the corresponding combinations of electrochemical potentials and absolute activities

$$\sum_i \nu_i\mu_i \quad \text{and} \quad \prod_i \lambda_i^{\nu_i}$$

are independent of the electrical state for neutral combinations of ions.

On the other hand, differences in μ_i and ratios of λ_i between phases are well defined but depend upon the electrical states of the phases. The absolute values, in a single phase, are not defined because the primary reference state (say, the elements at 25°C and 1 bar) involves no electrical reference state.

Correspondingly, the secondary reference state also involves only neutral combinations of species. Consequently, the λ_i^θ's for ionic species are not uniquely determined, a situation that could be rectified by the arbitrary assignment of the value of λ_i^θ for *one* ionic species in each solvent at each temperature. However, in any application, the equations can be arranged so that only those products of λ_i^θ's (and also γ_i's) corresponding to neutral combinations of ions are ever needed.

Let us return to the solution of a single electrolyte. By convention, the mean activity coefficient γ_{+-} (or $\gamma_\pm$) on the molal scale is defined by

$$\gamma_{+-}^\nu = \gamma_+^{\nu_+}\gamma_-^{\nu_-}, \tag{2.25}$$

where

$$\nu = \nu_+ + \nu_-. \tag{2.26}$$

The discussion above shows that this mean activity coefficient is unambiguously defined and independent of the electrical state of the solution. It is this activity coefficient γ_{+-} that is measured and tabulated for solutions of single electrolytes. Tabulations of chemical thermodynamic properties also usually include $\mu_i^\theta = RT\ln\lambda_i^\theta$ for the ions and

$$\mu_A^\theta = RT\ln\lambda_A^\theta = \nu_+RT\ln\lambda_+^\theta + \nu_-RT\ln\lambda_-^\theta \tag{2.27}$$

for an electrolyte. Combining equations 2.27, 2.25, and 2.22 yields

$$\mu_A = \mu_A^\theta + \nu RT\ln m\gamma_{+-} + RT\ln(\nu_+^{\nu_+}\nu_-^{\nu_-}). \tag{2.28}$$

The thermodynamic properties of solutions of a single electrolyte can, of course, be studied by nonelectrochemical means and without detailed consideration of its state of dissociation into ions. For example, a study of the vapor pressure or the freezing point will yield the variation in the chemical potential μ_A with concentration. It is, in fact, one of the beauties of thermodynamics that it provides a framework to record the macroscopic properties of a system without knowledge of its state of molecular aggregation, as long as the possible molecular species equilibrate rapidly with each other.

If we apply equation 2.15 to the electrolyte A, without regard for its dissociation, we have

$$\mu_A = RT\ln(m\gamma_A\lambda_A^\theta). \tag{2.29}$$

This differs from equation 2.28 principally in the absence of the factor ν. Consequently, γ_A must be different from γ_{+-}, and γ_A must have a concentration dependence considerably different from that of γ_{+-}. Specifically, we have

$$\gamma_A = m^{\nu-1}\gamma_{+-}^\nu(\nu_+^{\nu_+}\nu_-^{\nu_-}). \tag{2.30}$$

Consequently, $\gamma_A \to 0$ as $m \to 0$ for $\nu > 1$, and equation 2.18 cannot be applied to define a secondary reference state for λ_A^θ in equation 2.29. The state of aggregation of the solution at infinite dilution should be used as the secondary reference state for solutes that partially dissociate. This is explored in more detail in Section 4.7. Except for this necessity to choose a different secondary reference state, it is legitimate from a strictly thermodynamic point of view to treat the electrolyte as undissociated, although this is seldom done. By the activity coefficient, we shall thus mean the mean ionic activity coefficient of an electrolyte.

A parallel development can be carried through for the molar scale of concentration. On this scale, the mean activity coefficient of the electrolyte is defined by

$$f_{+-}^\nu = f_+^{\nu_+}f_-^{\nu_-}. \tag{2.31}$$

We then can express the chemical potential of the electrolyte as

$$\mu_A = RT \ln cf_A a_A^{\theta} = RT \ln \lambda_A^{\theta} + \nu RT \ln(cf_{+-}/\rho_0) + RT \ln(\nu_+^{\nu_+} \nu_-^{\nu_-}). \tag{2.32}$$

The mean activity coefficients on the two scales are related by

$$f_{+-} = \frac{\rho_0 \gamma_{+-}}{c_0 M_0}. \tag{2.33}$$

Various examples can be cited to illustrate the consequences of ionic dissociation. Lewis et al.[3] show the effect of considering hydrochloric acid to be dissociated or undissociated by plotting the partial pressure of HCl in equilibrium with the solution against both m and m^2. The partial pressure would be proportional to m for a nonelectrolyte. Because HCl dissociates, the partial pressure is observed to be proportional to m^{ν}. They also plot the freezing-point depressions of acetic acid, a weak acid with a small dissociation constant, indicating that acetic acid behaves as a nonelectrolyte except at very low concentrations. This behavior is also reflected in Figure 2.1, which shows how $1 + d \ln f_A / d \ln c$ varies with the concentration of acetic acid in water. The activity coefficient f_A is defined on a molar scale, analogously with how γ_A is defined on a molal scale. At moderate concentrations, the acetic acid behaves as a nonelectrolyte in that $1 + d \ln f_A / d \ln c$ varies linearly with c at moderate concentrations (up to about 4 M) and in that $1 + d \ln f_A / d \ln c$ appears to approach 1 as c approaches 0. For a dissociated electrolyte, $1 + d \ln f_A / d \ln c$ would be proportional to $\sqrt{c}$ at low concentrations and $1 + d \ln f_A / d \ln c$ would approach ν as c approaches 0. The reason for these differences between electrolytes and nonelectrolytes is explained by the definition of γ_A as given in equation 2.30 (see Section 4.3 for the theory of how γ_{+-} varies with concentration). Although data at very low concentrations are not shown in Figure 2.1, one would expect that acetic acid would behave as an electrolyte when the concentration of acetate ions exceeds that of undissociated acetic acid (which occurs for bulk concentrations below 10^{-5} mol/kg for acetic acid). Thus, $1 + d \ln f_A / d \ln c$ would be expected to shoot up to approach 2 as $c \to 0$.

The activity of the solvent could be expressed by equation 2.15. However, it is more common to relate deviations from ideal behavior to an osmotic coefficient ϕ, defined by

$$\ln \frac{\lambda_0}{\lambda_0^0} = -\phi M_0 \sum_{i \neq 0} m_i, \tag{2.34}$$

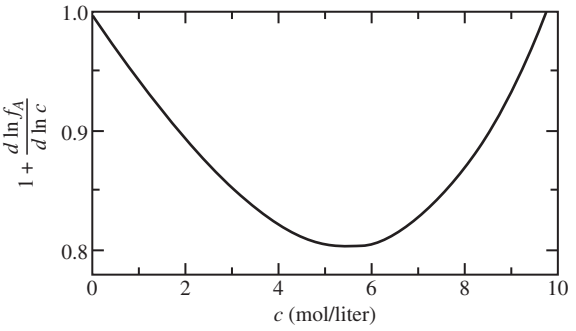

Figure 2.1 Variation of the molar activity coefficient of aqueous acetic acid with concentration. For $1 + d \ln f_{+-} / d \ln c$, divide the ordinate scale by 2. *Source:* Values taken from Vitagliano and Lyons.[4]

where λ_0^0 is the absolute activity of the pure solvent at the same temperature and pressure. For a solution of a single electrolyte, this becomes

$$\ln \frac{\lambda_0}{\lambda_0^0} = -\nu m \phi M_0. \tag{2.35}$$

For a solution of a single electrolyte, the mean molal activity coefficient can be related to the osmotic coefficient by means of the Gibbs–Duhem equation, which, for constant temperature and pressure, reads

$$c_0 d\mu_0 + c d\mu_A = 0. \tag{2.36}$$

Substitution of the relevant equations gives

$$d(m\phi) = m d \ln(m\gamma_{+-}) \tag{2.37}$$

or

$$d[m(\phi - 1)] = m d \ln \gamma_{+-}. \tag{2.38}$$

Integration from $m = 0$ to $m = m$ gives

$$\ln \gamma_{+-} = \int_0^m \frac{\partial [m(\phi - 1)]}{\partial m} \frac{dm}{m}. \tag{2.39}$$

The chemical potential of a gaseous species is expressed as

$$\mu_A = \mu_A^* + RT \ln p_A, \tag{2.40}$$

where p_A is called the fugacity of gas A. The secondary reference state is an ideal gas at 1 bar. This reference state is defined by

$$p_A \to x_A p \quad \text{as} \quad p \to 0, \tag{2.41}$$

where p is the total gas pressure, x_A is the mole fraction of A, and $x_A p$ is the partial pressure of gas A.

For solid solutions, such as alloys, we can represent the chemical potential of component A as

$$\mu_A = \mu_A^0 + RT \ln a_A, \tag{2.42}$$

where the superscript 0 denotes pure A at the same temperature and pressure and where a_A is the relative activity, given by

$$a_A = \frac{\lambda_A}{\lambda_A^0}, \tag{2.43}$$

where λ_A is the absolute activity as in equation 2.14. The secondary reference state is pure A, yielding the requirement that

$$a_A \to 1 \quad \text{as} \quad x_A \to 1. \tag{2.44}$$

2.4 CELL WITH SOLUTION OF UNIFORM CONCENTRATION

The cells discussed in this section are taken to contain a single electrolyte in a solution of uniform concentration throughout the cell. In most textbooks of physical chemistry, electrochemistry, or thermodynamics, a distinction is made between cells *without* transference (no concentration gradients) and cells *with* transference (concentration gradients are present in the electrolytic solution). As we shall see, this division is somewhat subjective, except for the simplest cells. The division rather depends upon whether we are willing to ignore the concentration gradients that do exist.

An example of a cell with the same solution throughout is a cell with two electrodes of the same metal dipping into the same solution of a salt of the metal. To be specific, consider the cell:

$$\overset{\alpha}{\mathrm{Pt}(s)}\left|\overset{\beta}{\mathrm{Cu}(s)}\right|\overset{\delta}{\mathrm{CuSO_4\ in\ H_2O}}\left|\overset{\beta'}{\mathrm{Cu}(s)}\right|\overset{\alpha'}{\mathrm{Pt}(s)}. \tag{2.45}$$

Phase equilibrium among the several phases is described by equation 2.5, for example,

$$\mu_{e^-}^{\alpha} = \mu_{e^-}^{\beta}, \tag{2.46}$$

$$\mu_{Cu^{2+}}^{\beta} = \mu_{Cu^{2+}}^{\delta}. \tag{2.47}$$

Similarly, cupric ions are equilibrated between the solution δ and the electrode β', and electrons are equilibrated between the electrode β' and the platinum lead α'.

The procedure for relating the cell potential to the electrochemical potentials of the components is as follows. First, one draws a schematic of the cell, as shown in equation 2.45. We define the cell potential U to be the potential of the right electrode minus the potential of the left electrode. This is equivalent to saying that the right electrode in our schematic is the working electrode and the left electrode is the reference electrode and is also equivalent to saying that one would measure U in a laboratory by connecting the positive lead of a voltmeter to the right electrode and the negative lead to the left electrode (keeping in mind that depending on how one draws the schematic, i.e., connects the leads of the voltmeter, the voltmeter may read a positive or a negative value).

The cell potential is related to the electrochemical potentials of electrons in the leads by

$$FU = z_{e^-}F(\Phi^{\alpha} - \Phi^{\alpha'}) = \mu_{e^-}^{\alpha} - \mu_{e^-}^{\alpha'}. \tag{2.48}$$

We then write out the reactions at each electrode. In this case, the reaction at both electrodes is

$$\mathrm{Cu} \rightleftharpoons \mathrm{Cu}^{2+} + 2\mathrm{e}^-. \tag{2.49}$$

At equilibrium, these reactions result in a relationship among the electrochemical potentials:

$$\mu_{Cu} = \mu_{Cu^{2+}} + 2\mu_{e^-}. \tag{2.50}$$

Rearranging this equation allows one to obtain μ_{e^-} in terms of the electrochemical potentials of the other components of the cell. One can then substitute these expressions into equation 2.48 to obtain the expression for the cell potential

$$FU = \frac{1}{2}\mu_{Cu}^{\beta} - \frac{1}{2}\mu_{Cu}^{\beta'} - \frac{1}{2}\mu_{Cu^{2+}}^{\delta} + \frac{1}{2}\mu_{Cu^{2+}}^{\delta'}. \tag{2.51}$$

If the electrolyte is uniform across the cell, then $\mu_{Cu^{2+}}^{\delta} = \mu_{Cu^{2+}}^{\delta'}$, and the expression for the cell potential simplifies to

$$FU = \frac{1}{2}\mu_{Cu}^{\beta} - \frac{1}{2}\mu_{Cu}^{\beta'}. \tag{2.52}$$

For this simple cell, the electrodes are identical, and therefore the cell potential is zero. However, there are numerous examples of cells in which the electrodes, while both reacting with the same ion, are of different composition. For example, one could alloy the copper with another metal, resulting in a change in the cell potential. For the present analysis, we require that the alloying metal be inert in the cell, so that it serves only to alter the electrochemical potential of the copper. A cell of this type is

$$\begin{matrix}\alpha & \beta & \delta & \epsilon & \alpha' \\ \mathrm{Pt}(s) & \mathrm{Pb}(s) & \mathrm{PbCl_2\ in\ H_2O} & \mathrm{Pb(Hg)} & \mathrm{Pt}(s)\end{matrix}, \tag{2.53}$$

in which Pb(Hg) is a lead amalgam (alloy with mercury). Following the procedure given above, the cell potential is found to be

$$FU = -F(\Phi^{\alpha} - \Phi^{\alpha'}) = \frac{1}{2}\mu^{\beta}_{\mathrm{Pb}} - \frac{1}{2}\mu^{\epsilon}_{\mathrm{Pb}}. \tag{2.54}$$

This cell provides the means for determining the thermodynamic properties of lead amalgam as a function of the amalgam composition, the most common application for this type of cell.

Another type of cell with a uniform concentration has the form of equation 2.1, if one assumes that the solid salt is insoluble. For example, consider the system

$$\begin{matrix}\alpha & \beta & \delta & \epsilon & \phi & \alpha' \\ \mathrm{Pt}(s) & \mathrm{Li}(s) & \mathrm{LiCl\ in\ DMSO} & \mathrm{TlCl}(s) & \mathrm{Tl(Hg)} & \mathrm{Pt}(s)\end{matrix}, \tag{2.55}$$

where the electrolytic solution is a solution of lithium chloride in the solvent dimethyl sulfoxide (DMSO), TlCl is a salt that is sparingly soluble in DMSO, and Tl(Hg) is a thallium amalgam. By sparingly soluble, we mean that the salt has a very small saturation concentration in the electrolyte. For the present, let us ignore even this small concentration and assume that the electrolyte consists only of LiCl in DMSO. Again, the procedure for obtaining the cell potential is as follows. The cell reactions are given by

$$\mathrm{Li} \rightleftharpoons \mathrm{Li^+} + \mathrm{e^-} \tag{2.56}$$

and

$$\mathrm{Tl} + \mathrm{Cl^-} \rightleftharpoons \mathrm{TlCl} + \mathrm{e^-}. \tag{2.57}$$

Then the electrochemical potentials of the electrons are given by

$$\mu^{\beta}_{\mathrm{Li}} = \mu^{\delta}_{\mathrm{Li^+}} + \mu^{\alpha}_{\mathrm{e^-}} \tag{2.58}$$

and

$$\mu^{\phi}_{\mathrm{Tl}} + \mu^{\delta}_{\mathrm{Cl^-}} = \mu^{\epsilon}_{\mathrm{TlCl}} + \mu^{\alpha'}_{\mathrm{e^-}}. \tag{2.59}$$

The second statement is true because of the conditions of equilibrium among the phases:

$$\mu^{\delta}_{\mathrm{Cl^-}} = \mu^{\epsilon}_{\mathrm{Cl^-}} \quad \text{and} \quad \mu^{\epsilon}_{\mathrm{Tl^+}} = \mu^{\phi}_{\mathrm{Tl^+}}. \tag{2.60}$$

Substituting equations 2.58 and 2.59 into equation 2.48, we find

$$FU = -F(\Phi^{\alpha} - \Phi^{\alpha'}) = \mu^{\beta}_{\mathrm{Li}} - \mu^{\phi}_{\mathrm{Tl}} + \mu^{\epsilon}_{\mathrm{TlCl}} - \mu^{\delta}_{\mathrm{LiCl}}, \tag{2.61}$$

where we have used the identity $\mu_{\mathrm{Li^+}} + \mu_{\mathrm{Cl^-}} = \mu_{\mathrm{LiCl}}$. Thus, the cell potential is related to the thermodynamic properties of neutral species, even though the phase equilibria were expressed in terms

of charged species. This will always be true for cells that can be treated by thermodynamics alone. This type of cell, in which the overall cell reaction includes the electrolyte, can be used to study the thermodynamic properties of the electrolyte.

The above treatment assumes the electrolyte is of uniform composition. However, it is known that there will be thallous chloride in the solution, although the quantity will be small, and the presence of this added electrolyte will change the chemical potential of LiCl in the immediate vicinity of the thallium amalgam–thallous chloride electrode. One cannot allow the thallous chloride to saturate the entire solution because it will react spontaneously with the lithium metal. Thus, there must be a gradient of the concentration of TlCl and of the electrochemical potential of the chloride ion, and one can no longer assume that both electrodes are in contact with the same electrolytic solution. This picture can be represented as

α	β	δ		δ'	ϵ	ϕ	α'
Pt(s)	Li(s)	LiCl in DMSO	transition region	LiCl and TlCl in DMSO	TlCl(s)	Tl(Hg)	Pt(s) .

(2.62)

Here phase δ' differs from phase δ due to the dissolved TlCl, and these are connected by a junction, or transition region, in which the concentration of thallous chloride varies with position.

The equilibria among phases δ', ϵ, and ϕ can now be written:

$$\mu^{\delta'}_{Cl^-} = \mu^{\epsilon}_{Cl^-} \quad \text{and} \quad \mu^{\delta'}_{Tl^+} = \mu^{\epsilon}_{Tl^+} = \mu^{\phi}_{Tl^+}. \tag{2.63}$$

The solution δ' will actually facilitate the equilibrium between the amalgam ϕ and the solid salt ϵ. Instead of equation 2.61, we now obtain

$$FU = \mu^{\beta}_{Li} - \mu^{\phi}_{Tl} + \mu^{\epsilon}_{TlCl} - \mu^{\delta}_{LiCl} + (\mu^{\delta}_{Cl^-} - \mu^{\delta'}_{Cl^-}). \tag{2.64}$$

We see that this equation will be identical with equation 2.61 if we are willing to ignore the difference in electrochemical potential of the chloride ion between the solutions adjacent to the two electrodes. Thermodynamics alone does not provide the means for evaluating this difference since the junction region basically involves the irreversible process of diffusion and must be treated by the laws of transport in electrolytic solutions. For this system, in the absence of current, the gradient of the electrochemical potential of the chloride ion can be expressed in terms of the neutral salts, as discussed in the next section,

$$\nabla\mu_{Cl^-} = t^0_{Li^+}\nabla\mu_{LiCl} + t^0_{Tl^+}\nabla\mu_{TlCl}, \tag{2.65}$$

where t^0_i is the transference number of species i with respect to the solvent velocity. From this equation, we can perceive that the more insoluble the salt (here, TlCl), the smaller the value of $t^0_{Tl^+}$ will be and the more nearly the same the solution will be throughout. Then equation 2.64 can be adequately approximated by equation 2.61.

The purpose of this section has been to illustrate how to apply the phase-equilibrium conditions of Section 2.1 to typical systems that involve an electrolytic solution of uniform composition throughout the cell. For the first two cases examined above (cells 2.45 and 2.53), the thermodynamic properties of the solution do not influence the cell potential. The third example (cell 2.55) can be used to study the thermodynamic properties of the electrolytic solution, although, if the TlCl is soluble, this cell does not belong in this section. The assessment of the errors involved in ignoring the concentration gradients in cells such as cell 2.62 is treated in Section 2.7.

The results of the previous examples can be applied to cells with additional solvent or salt species in solution at a uniform concentration under the following conditions:

1. The additional species changes the thermodynamic properties of the first electrolyte in solution, but it does not react with it to form a precipitate or evolve a gas, and it does not react spontaneously with the electrodes.
2. The additional species does not participate in the phase equilibria except to alter thermodynamic properties in the solution phase.

Such cells would provide information about how the chemical potential of the first salt is affected by the additive.

2.5 TRANSPORT PROCESSES IN JUNCTION REGIONS

The treatment of the open-circuit potentials of electrochemical cells involves first the description of phase equilibria between the electrodes and the solutions or solids adjacent to them (discussed briefly in Section 2.1) followed by a consideration of the junction regions that are likely to exist between the solutions adjacent to the electrodes. We have found, in the previous section, a need to treat such regions.

Equation 2.65 shows that evaluation of the cell potential requires evaluation of the gradient in chemical potential of a species across the electrolyte. To do this, we call upon an equation developed in Part C, transport processes in electrolytic solutions (see Section 12.7):

$$\frac{F}{\kappa}\mathbf{i} = -\sum_i \frac{t_i^0}{z_i}\nabla\mu_i, \tag{2.66}$$

where $\mathbf{i}$ is the current density, κ is the conductivity, t_i^0 is the transference number of species i relative to the velocity of species 0, and $\nabla\mu_i$ is the gradient of the electrochemical potential of species i. This equation is derived from the laws of multicomponent diffusion and can be regarded as an extended form of Ohm's law.

The species 0 whose velocity is used as a reference can be any species in the solution, but it is usually taken to be the solvent, if a solvent is evident. The sum in equation 2.66 includes any neutral species that might be present, and the ratio t_i^0/z_i is not generally zero for a neutral species. However, t_i^0 and t_i^0/z_i are always zero for the reference species, and this is one reason why it is convenient to choose the solvent for this reference.

Equation 2.66 applies, regardless of the number of species, including a solution that contains two or more neutral species. Consider for example the case of a solution of copper sulfate dissolved in a mixture of sucrose and water, with water as a reference. The right side of equation 2.66 will have 3 nonzero terms corresponding the cupric ions, sulfate ions, and sucrose. The term for sucrose is nonzero in spite of the fact that z_i is zero; this is a situation where both the numerator and denominator formally approach zero but the ratio is finite. For the term corresponding to sucrose, it is convenient to replace the term t_i^0/z_i in equation 2.66 by a transport number, τ_i^0. Note that the transport number of a neutral species is also defined relative a reference species. Nothing is gained by defining transport numbers for charged species.

In the treatment of the open-circuit potentials of electrochemical cells, the current density $\mathbf{i}$ is supposed to be zero. However, its presence in equation 2.66 would aid in the assessment of the effects of those small currents that are unavoidable in the actual measurement of cell potentials. In this connection, and to give further insight into equation 2.66, we might note that it reduces to Ohm's law in a medium of uniform composition. Then the variations in the electrochemical potentials can be expressed by equation 2.9, and we have

$$\mathbf{i} = -\kappa\nabla\Phi\sum_i t_i^0 = -\kappa\nabla\Phi, \tag{2.67}$$

the second equality following from the fact that the sum of the transference numbers of all species is equal to one.

To treat junction regions, it is convenient to rewrite equation 2.66 in the form

$$\frac{1}{z_n}\nabla\mu_n = -\frac{F}{\kappa}\mathbf{i} - \sum_i \frac{t_i^0}{z_i}\left(\nabla\mu_i - \frac{z_i}{z_n}\nabla\mu_n\right), \tag{2.68}$$

where species n can be any charged species in the solution. The combinations of electrochemical potentials in parentheses correspond to neutral combinations of species and hence are independent of the electrical state of the solution; these terms depend only on the spatial variation of the chemical composition of the medium (at uniform temperature and pressure). Hence, equation 2.68 permits the assessment of the variation of the electrochemical potential of one charged species in a region of nonuniform composition. In other words, the electrical states of different parts of a phase are related to each other because they are physically connected to each other. In a medium of uniform composition, this amounts to a determination of the ohmic potential drop; in a nonuniform medium, the variation of composition can also be accounted for.

For the solution of lithium chloride and thallous chloride in DMSO, considered in Section 2.4, equation 2.68 becomes equation 2.65 if species n is taken to be the chloride ion and if the current density is zero. In practice, this equation must now be integrated across the junction region for known concentration profiles of TlCl and LiCl.

In this section, only one equation has been presented, one which is roughly equivalent to Ohm's law. It is useful for assessing variations in electrical state across a junction region where the concentration profiles are known. It is not sufficient for the determination of these concentration profiles nor of the current density. These concentration profiles, which may change with time, are determined from the laws of diffusion and the method of forming the junction, topics that are beyond the scope of this section.

2.6 CELL WITH A SINGLE ELECTROLYTE OF VARYING CONCENTRATION

A cell in which the concentration of a single electrolyte varies with location in the cell is the simplest example of a so-called *cell with transference*. An example is

α	β	δ		ϵ	β'	α'
Pt(s)	Li(s)	LiCl in DMSO	transition region	LiCl in DMSO	Li(s)	Pt(s) ,

(2.69)

in which the chemical composition of both platinum leads is identical, as is that of both lithium electrodes. This cell is also sometimes called a *concentration cell*. The concentration of LiCl in the δ phase is different from that in the ϵ phase. The *transition region* is one in which concentration gradients exist, as the concentration varies from that in the δ phase to that in the ϵ phase. This region is sometimes called a *liquid junction*. Diffusion across the transition region will gradually mix the two solutions, but the rate of diffusion can be slowed by using a porous separator or by placing the two solutions in separate compartments joined by a capillary tube (see Figure 1.9).

By means of the conditions of phase equilibrium (equation 2.5) and the definition of the potential difference between phases of identical composition (equation 2.9), the cell potential reduces to

$$FU = -F(\Phi^{\alpha} - \Phi^{\alpha'}) = \mu^{\epsilon}_{\mathrm{Li}^+} - \mu^{\delta}_{\mathrm{Li}^+}. \tag{2.70}$$

One can go no further in treating the cell by reversible thermodynamics since diffusion is present. Equation 2.68 can be applied to evaluate the difference of electrochemical potentials appearing in equation 2.70. If we take the current density to be zero and lithium ions to be species n, equation 2.68 becomes

$$\nabla\mu_{\mathrm{Li}^+} = t^0_{\mathrm{Cl}^-}\nabla\mu_{\mathrm{LiCl}}. \tag{2.71}$$

This can be integrated across the junction region and the results substituted into equation 2.70 to yield

$$FU = \int_\delta^\epsilon t^0_{\mathrm{Cl}^-}\frac{\partial\mu_{\mathrm{LiCl}}}{\partial x}dx. \tag{2.72}$$

In this particular case of a binary electrolyte, both $t^0_{\mathrm{Cl}^-}$ and μ_{LiCl} depend only on the concentration of LiCl, and the integral in equation 2.72 becomes independent of the detailed form of the concentration profile in the junction region:

$$FU = \int_\delta^\epsilon t^0_{\mathrm{Cl}^-}d\mu_{\mathrm{LiCl}} = \int_\delta^\epsilon t^0_{\mathrm{Cl}^-}\frac{d\mu_{\mathrm{LiCl}}}{dm}dm. \tag{2.73}$$

This equation is equivalent to the expressions that appear in most treatments of cells of the type considered here. However, the virtual passage of current used in most derivations has been avoided here because such derivations give the impression that reversible thermodynamics is sufficient to yield the cell potential. The potential difference in equation 2.73 should not be called a *liquid-junction potential*; rather it is the *potential of a cell with a liquid junction*.

Equation 2.73 can be generalized to metals and electrolytes with different charge numbers, with the result

$$FU = \int_\delta^\epsilon \frac{t^0_-}{z_+\nu_+}\frac{d\mu_A}{dm}dm, \tag{2.74}$$

where A denotes the single electrolyte in the solution. The equilibria between the electrodes and the solutions are assumed to involve only cations, and the electrodes are assumed to be identical. This would include the copper sulfate concentration cell in Figure 1.9.

Upon introduction of activity coefficients by means of equation 2.28, equation 2.74 becomes

$$FU = \nu RT\int_\delta^\epsilon \frac{t^0_-}{z_+\nu_+}\left(1 + \frac{d\ln\gamma_{+-}}{d\ln m}\right)d\ln m. \tag{2.75}$$

If the concentration dependence of the transference number is ignored, we have the approximation

$$U = \frac{\nu}{z_+\nu_+}\frac{RT}{F}t^0_-\ln\frac{(m\gamma_{+-})_\epsilon}{(m\gamma_{+-})_\delta} = \frac{\nu}{z_+\nu_+}\frac{RT}{F}t^0_-\ln\frac{(cf_{+-})_\epsilon}{(cf_{+-})_\delta}. \tag{2.76}$$

The latter expression was the basis for the approximation in equation 1.34 for the potential of the copper concentration cell used as an example in Chapter 1.

Finally, one might generalize these results for an arbitrary electrode reaction with a solution of a single electrolyte A. Let the cell be represented as

$$\begin{array}{ccccccc} \alpha & \beta & \delta & & \epsilon & \beta' & \alpha' \\ \mathrm{Pt}(s) & \text{electrode} & \text{solution} & \text{transition region} & \text{solution} & \text{electrode} & \mathrm{Pt}(s) \end{array}, \tag{2.77}$$

where electrode β is identical to electrode β'. If the "electrodes" involve an additional gas phase or sparingly soluble salt, the chemical potentials of these neutral species are taken to be the same on both sides of the cell, and the solubilities are taken to be small enough that the solution can still be regarded as that of the electrolyte alone in the solvent.

A general electrode reaction can be expressed by equation 2.6, which we repeat here:

$$\sum_i s_i M_i^{z_i} \rightarrow n\mathrm{e}^-, \tag{2.78}$$

where s_i is the stoichiometric coefficient of species i and M_i is a symbol for the chemical formula of species i. A generalization of the formulas for phase equilibrium for this reaction is

$$\sum_i s_i \mu_i = n\mu_{\mathrm{e}^-}, \tag{2.79}$$

where superscripts for the appropriate phases in which the species exist should be added. Since the electrode phases have only neutral species, a charge balance based on equation 2.78 yields

$$s_+ z_+ + s_- z_- = -n, \tag{2.80}$$

and we see that the cations and anions of the electrolyte must be responsible for the electrons produced or consumed at the electrodes.

In this case, we choose to treat the cell by means of a reference electrode, perhaps imaginary, of the same kind as the main electrodes and that can be moved, together with its extraneous neutral phases, through the solution in the region between the electrodes. The variation of the potential of this electrode with position is given by the gradient of equation 2.79:

$$s_+ \nabla\mu_+ + s_- \nabla\mu_- + s_0 \nabla\mu_0 = n\nabla\mu_{\mathrm{e}^-} = -nF\nabla\Phi, \tag{2.81}$$

it being presumed that only the properties of the solution vary with position and that the solution contains only solvent, cation, and anion. Equation 2.68 allows us to relate variations of electrochemical potentials of ions to variations of the chemical potential of the electrolyte:

$$\frac{1}{z_+}\nabla\mu_+ = \frac{t_-^0}{z_+\nu_+}\nabla\mu_A. \tag{2.82}$$

The Gibbs–Duhem equation 2.36 allows us to relate the variation of the chemical potential of the solvent to that of the electrolyte:

$$\nabla\mu_0 + M_0 m \nabla\mu_A = 0. \tag{2.83}$$

Combination of equations 2.81 through 2.83 yields

$$F\nabla\Phi = \left(\frac{t_-^0}{z_+\nu_+} - \frac{s_-}{n\nu_-} + \frac{s_0 M_0}{n} m\right)\nabla\mu_A. \tag{2.84}$$

Integration across the junction region gives

$$\begin{aligned} FU = -F(\Phi^{\alpha} - \Phi^{\alpha'}) &= \int_\delta^\epsilon \left(\frac{t_-^0}{z_+\nu_+} - \frac{s_-}{n\nu_-} + \frac{s_0 M_0}{n} m\right)\frac{d\mu_A}{dm} dm \\ &= \nu RT \int_\delta^\epsilon \left(\frac{t_-^0}{z_+\nu_+} - \frac{s_-}{n\nu_-} + \frac{s_0 M_0}{n} m\right)\left(1 + \frac{d\ln\gamma_{+-}}{d\ln m}\right) d\ln m. \end{aligned} \tag{2.85}$$

If t_-^0 is independent of concentration, this becomes

$$FU = \nu RT\left(\frac{t_-^0}{z_+\nu_+} - \frac{s_-}{n\nu_-}\right)\ln\frac{(m\gamma_{+-})_\epsilon}{(m\gamma_{+-})_\delta} + \nu RT\frac{s_0M_0}{n}\int_\delta^\epsilon\left(1 + \frac{d\ln\gamma_{+-}}{d\ln m}\right)dm. \tag{2.86}$$

In the case where the anion and the solvent do not participate in the electrode reaction, equation 2.85 is seen to coincide with equation 2.75.

We have given here, in various degrees of generality, a treatment of concentration cells, where the electrodes are identical but are placed in different solutions of a single electrolyte that are joined by a junction region where the concentration varies. The measured cell potential is found to depend not only on the thermodynamic properties but also on the transport properties of the solutions in the cell. Such cells are useful for determining the activity coefficient if the transference number is known and the transference number if the activity coefficient is known. Both types of determination are common practice.

Let us consider some additional examples. For the cell

$$\overset{\alpha}{\text{Pt}(s), \text{H}_2(g)} \Big| \overset{\epsilon}{\text{HCl in H}_2\text{O}} \Big\{ \text{transition region} \Big\} \overset{\lambda}{\text{HCl in H}_2\text{O}} \Big| \overset{\alpha'}{\text{Pt}(s), \text{H}_2(g)}\,, \tag{2.87}$$

the cell potential is

$$\begin{aligned} FU &= -F(\Phi^\alpha - \Phi^{\alpha'}) = \frac{1}{2}RT\ln\frac{p_{\text{H}_2}^\alpha}{p_{\text{H}_2}^{\alpha'}} - \mu_{\text{H}^+}^\epsilon + \mu_{\text{H}^+}^\lambda \\ &= \frac{1}{2}RT\ln\frac{p_{\text{H}_2}^\alpha}{p_{\text{H}_2}^{\alpha'}} + \int_\epsilon^\lambda t_{\text{Cl}^-}^0 d\mu_{\text{HCl}}. \end{aligned} \tag{2.88}$$

This agrees with equation 2.73 if the partial pressure of hydrogen is the same near the two platinum electrodes.

If the hydrogen electrodes are replaced by silver–silver chloride electrodes, we have the cell

$$\overset{\alpha}{\text{Pt}(s)} \Big| \overset{\beta}{\text{Ag}(s)} \Big| \overset{\delta}{\text{AgCl}(s)} \Big| \overset{\epsilon}{\text{HCl in H}_2\text{O}} \Big\{ \text{transition region} \Big\} \overset{\lambda}{\text{HCl in H}_2\text{O}} \Big| \overset{\delta'}{\text{AgCl}(s)} \Big| \overset{\beta'}{\text{Ag}(s)} \Big| \overset{\alpha'}{\text{Pt}(s)}\,, \tag{2.89}$$

for which the cell potential is

$$FU = -F(\Phi^\alpha - \Phi^{\alpha'}) = \mu_{\text{Cl}^-}^\epsilon - \mu_{\text{Cl}^-}^\lambda = \int_\lambda^\epsilon t_{\text{H}^+}^0 d\mu_{\text{HCl}} \tag{2.90}$$

if the silver electrodes are identical and the solid silver chloride is the same on both sides of the cell. The potential of this cell is opposite in sign to that of the preceding cell and the magnitudes are quite different since $t_{\text{H}^+}^0 \approx 0.82$, whereas $t_{\text{Cl}^-}^0 \approx 0.18$. Equation 2.90 agrees with equation 2.85 if we use the values $s_- = 1$, $s_0 = 0$, and $n = 1$.

Finally, for the cell

$$\begin{array}{c|c|c|c|c|c|c|c|c} \alpha & \beta & \delta & \epsilon & & \lambda & \delta' & \beta' & \alpha' \\ \mathrm{Pt}(s) & \mathrm{Hg}(l) & \mathrm{HgO}(s) & \begin{array}{c}\text{KOH in}\\ \mathrm{H_2O}\end{array} & \begin{array}{c}\text{transition}\\ \text{region}\end{array} & \begin{array}{c}\text{KOH in}\\ \mathrm{H_2O}\end{array} & \mathrm{HgO}(s) & \mathrm{Hg}(l) & \mathrm{Pt}(s) \end{array} \tag{2.91}$$

the reaction at the mercury–mercuric oxide electrodes is

$$\mathrm{Hg} + 2\mathrm{OH}^- \rightarrow \mathrm{HgO} + \mathrm{H_2O} + 2\mathrm{e}^-, \tag{2.92}$$

for which we have

$$n = 2, \quad s_- = 2, \quad s_0 = -1. \tag{2.93}$$

Consequently, the cell potential is given by

$$FU = -F(\Phi^{\alpha} - \Phi^{\alpha'}) = \int_{\lambda}^{\epsilon} \left(t^0_{\mathrm{K}+} + \frac{1}{2} M_0 m \right) d\mu_{\mathrm{KOH}}. \tag{2.94}$$

2.7 CELL WITH TWO ELECTROLYTES, ONE OF NEARLY UNIFORM CONCENTRATION

The purpose of this section is to show an approximate method for calculating the effect of a sparingly soluble salt on the cell potential. By making approximations for the dependence of transference numbers and activity coefficients on concentration, we can relate the potential of the cell to the solubility product for the sparingly soluble salt. An alternative, more straightforward treatment is given in Chapter 6.

The cells of this section have two electrolytes in solution: One of the electrolytes is of nearly uniform concentration throughout, while the concentration of the other varies with position in the cell. An example of this type of cell has been discussed in Section 2.4:

$$\begin{array}{c|c|c|c|c|c|c|c} \alpha & \beta & \delta & & \delta' & \epsilon & \phi & \alpha' \\ \mathrm{Pt}(s) & \mathrm{Li}(s) & \begin{array}{c}\text{LiCl in}\\ \text{DMSO}\end{array} & \begin{array}{c}\text{transition}\\ \text{region}\end{array} & \begin{array}{c}\text{LiCl and TlCl}\\ \text{in DMSO}\end{array} & \mathrm{TlCl}(s) & \mathrm{Tl(Hg)} & \mathrm{Pt}(s)\ , \end{array} \tag{2.95}$$

in which the transition region denotes the region of variable concentration of TlCl. The lithium chloride is of nearly uniform concentration, although its value may be changed slightly near the thallous chloride salt.

The potential of this cell was expressed as

$$FU = \mu^{\beta}_{\mathrm{Li}} - \mu^{\phi}_{\mathrm{Tl}} + \mu^{\epsilon}_{\mathrm{TlCl}} - \mu^{\delta}_{\mathrm{LiCl}} + (\mu^{\delta}_{\mathrm{Cl}^-} - \mu^{\delta'}_{\mathrm{Cl}^-}). \tag{2.96}$$

Just as for the cells of Section 2.6, this expression contains a difference in the electrochemical potential of an ionic species between two points in the solution. In this section, we consider cells for which this term can be regarded as a small error term in an expression that otherwise relates the cell potential to thermodynamic quantities, in contrast to Section 2.6, which described concentration cells for which

the cell potential depended entirely on such a term. The estimation of these errors has been treated by Smyrl and Tobias,[5] whose development we follow here.

Equation 2.65, as repeated below,

$$\nabla\mu_{Cl^-} = t^0_{Li^+}\nabla\mu_{LiCl} + t^0_{Tl^+}\nabla\mu_{TlCl}, \tag{2.97}$$

provides the means for assessing the magnitude of this difference. Thus,

$$\mu^{\delta}_{Cl^-} - \mu^{\delta'}_{Cl^-} = \int_{\delta'}^{\delta}\left(t^0_{Li^+}\frac{d\mu_{LiCl}}{dx} + t^0_{Tl^+}\frac{d\mu_{TlCl}}{dx}\right)dx. \tag{2.98}$$

In contrast to the situation in Section 2.6, this integral cannot be evaluated exactly without knowledge of the detailed concentration profiles in the junction region since the transference numbers and chemical potentials depend on the concentrations of both LiCl and TlCl. Here we only want to assess the magnitude of a term that is usually neglected, and for this purpose we make approximations appropriate to dilute solutions and also take the mobilities of the ions to be equal.

For the transference numbers, these approximations become (see equation 11.9)

$$t^0_{Li^+} = \frac{m_{Li^+}}{2m_{Cl^-}} \quad \text{and} \quad t^0_{Tl^+} = \frac{m_{Tl^+}}{2m_{Cl^-}}. \tag{2.99}$$

From equation 2.23, the variations of the chemical potential of thallous chloride can be expressed as

$$\nabla\mu_{TlCl} = RT\nabla\ln(m_{Tl^+}m_{Cl^-}\gamma^2_{TlCl}), \tag{2.100}$$

and a similar expression applies to the lithium chloride. Substitution of these equations into equation 2.97 gives

$$\nabla\mu_{Cl^-} = RT\nabla\ln m_{Cl^-} + RT\left(\frac{m_{Li^+}}{m_{Cl^-}}\nabla\ln\gamma_{LiCl} + \frac{m_{Tl^+}}{m_{Cl^-}}\nabla\ln\gamma_{TlCl}\right). \tag{2.101}$$

For dilute solutions, the Debye–Hückel limiting law can be used for the activity coefficients (see Section 4.2):

$$\ln\gamma_{LiCl} = \ln\gamma_{TlCl} = -\alpha I^{1/2} = -\alpha m^{1/2}_{Cl^-}, \tag{2.102}$$

where α is the Debye–Hückel constant, equal to 1.176 and 2.57 $kg^{1/2}/mol^{1/2}$ for water and DMSO,[5] respectively, at 25°C. In the Debye–Hückel approximation, the activity coefficients are the same for electrolytes of the same charge type and depend only on the ionic strength I, which here is equal to m_{Cl^-}.

Equation 2.101 now becomes

$$\nabla\mu_{Cl^-} = RT\nabla\ln m_{Cl^-} - \alpha RT\nabla m^{1/2}_{Cl^-}, \tag{2.103}$$

and integration allows us to write equation 2.98 as

$$\mu^{\delta}_{Cl^-} - \mu^{\delta'}_{Cl^-} = -RT\ln\frac{m^{\delta'}_{Cl^-}}{m^{\delta}_{LiCl}} + \alpha RT\left[(m^{\delta'}_{Cl^-})^{1/2} - (m^{\delta}_{LiCl})^{1/2}\right]. \tag{2.104}$$

In order to measure activity coefficients and standard cell potentials by using cells of this type, one makes measurements at low concentrations of LiCl and extrapolates to infinite dilution of this electrolyte, thereby establishing the reference state given by equation 2.18. These measurements at

low concentrations of LiCl are, therefore, the most important thermodynamically and are also the measurements that are most subject to errors from liquid-junctions such as treated here. We can approximate the concentration change from solution δ to δ' as

$$m^{\delta'}_{Cl^-} - m^{\delta}_{LiCl} \approx m^{\delta'}_{Tl^+} = \frac{K_{sp}}{m^{\delta'}_{Cl^-}} \tag{2.105}$$

where K_{sp} is the solubility product of thallous chloride. For the corresponding uncertainty in the measured cell potential to be less than $10\,\mu V$ for $m = 10^{-3}$ mol/kg, the solubility product of the sparingly soluble salt must be less than about 4×10^{-10} (mol/kg)^2.

Another cell of this type, in aqueous solution, is

$$\begin{array}{c|c|c|c|c|c|c} \alpha & \beta & & \delta & \epsilon & \lambda & \alpha' \\ Pt(s), & HCl\ in & transition & HCl\ and\ AgCl & AgCl(s) & Ag(s) & Pt(s)\ , \\ H_2(g) & H_2O & region & in\ H_2O & & & \end{array} \tag{2.106}$$

where solutions β and δ are different primarily because solution δ is saturated with silver chloride. The expression for the cell potential is

$$FU = -F(\Phi^{\alpha} - \Phi^{\alpha'}) = \frac{1}{2}\mu^{\alpha}_{H_2} - \mu^{\beta}_{HCl} - \mu^{\lambda}_{Ag} + \mu^{\epsilon}_{AgCl} + (\mu^{\beta}_{Cl^-} - \mu^{\delta}_{Cl^-}). \tag{2.107}$$

Table 2.1 gives values of $(\mu^{\beta}_{Cl^-} - \mu^{\delta}_{Cl^-})/F$ for $K_{sp} = 10^{-10}$(mol/kg)^2, calculated by a method[6] to be outlined in Section 6.5. Values obtained from equations 2.104 and 2.105 are given for comparison. From Table 2.1, one can see that the effect of the sparingly soluble salt on the cell potential becomes significant when the bulk concentration of the electrolyte is of the same order of magnitude as the square root of the solubility product.

The effect of the sparingly soluble salt on the cell potential, treated above, was ignored for some of the cells in Section 2.6, specifically cells 2.89 and 2.91.

Under the classification of this section, cells with two electrolytes, one of nearly uniform concentration, we could logically include cells with an inert electrolyte of nearly uniform concentration, where

TABLE 2.1 Effect of solubility of silver chloride for decreasing values of bulk HCl concentration

		$(\mu^{\beta}_{Cl^-} - \mu^{\delta}_{Cl^-})/F$ (mV)	
m (mol/kg)	$m^{\delta}_{Cl^-}/m^{\beta}_{Cl^-}$	Calculated	Formula[a]
10^{-4}	1.00961	−0.226	−0.252
5×10^{-5}	1.0392	−0.914	−0.967
2×10^{-5}	1.200	−4.32	−4.82
10^{-5}	1.604	−11.22	−12.34
5×10^{-6}	2.539	−22.16	−24.13
2×10^{-6}	5.499	−40.58	−43.86

[a]From equations 2.104 and 2.105 for $K_{sp} = 10^{-10}$ (mol/kg)^2.

the species that react at the electrodes are present at much smaller concentrations. An example is

$$\begin{array}{c|c|c|c|c|c|c} \alpha & \beta & \delta & \text{transition} & \epsilon & \chi & \alpha' \\ \text{Pt}(s) & \text{Na(Hg)} & \begin{array}{c}\text{NaNO}_3\\ \text{KNO}_3\\ \text{in } \text{H}_2\text{O}\end{array} & \begin{array}{c}\text{region}\\ \text{KNO}_3 \text{ in}\\ \text{H}_2\text{O}\end{array} & \begin{array}{c}\text{AgNO}_3\\ \text{KNO}_3\\ \text{in } \text{H}_2\text{O}\end{array} & \text{Ag}(s) & \text{Pt}(s) \end{array}, \tag{2.108}$$

in which KNO_3 is present throughout the cell at the same, or nearly the same, concentration. The transition region contains concentration gradients of both $NaNO_3$ and $AgNO_3$. The cell potential can be expressed as

$$\begin{aligned} FU &= -F(\Phi^{\alpha} - \Phi^{\alpha'}) \\ &= \mu^{\beta}_{\text{Na}} - \mu^{\delta}_{\text{NaNO}_3} - \mu^{\chi}_{\text{Ag}} + \mu^{\epsilon}_{\text{AgNO}_3} + (\mu^{\delta}_{\text{NO}_3^-} - \mu^{\epsilon}_{\text{NO}_3^-}), \end{aligned} \tag{2.109}$$

on the assumption that KNO_3 is not involved in the phase equilibria at the electrodes, except to alter the chemical potentials of the other electrolytes in the solution.

With the same approximations used above, we can write

$$FU = \mu^{\beta}_{\text{Na}} - \mu^{\chi}_{\text{Ag}} + RT \ln \frac{\lambda^{\theta}_{\text{Ag}^+}}{\lambda^{\theta}_{\text{Na}^+}} + RT \ln \frac{m^{\epsilon}_{\text{Ag}^+}}{m^{\delta}_{\text{Na}^+}} - \alpha RT \left[(m^{\epsilon}_{\text{NO}_3^-})^{1/2} - (m^{\delta}_{\text{NO}_3^-})^{1/2} \right]. \tag{2.110}$$

Variations in the cell potential are thus due primarily to changes in the concentrations of silver and sodium ions. If the ionic strength is reasonably uniform, the last term, related to activity-coefficient corrections, can be ignored. We notice that the ratio $\lambda^{\theta}_{\text{Ag}^+}/\lambda^{\theta}_{\text{Na}^+}$ is uniquely determined according to the considerations of Section 2.3.

When activity coefficients are ignored, equation 2.110 is a form of the so-called Nernst equation, relating cell potentials to the logarithms of ionic concentrations (see equation 1.8). It is frequently written in terms of molar concentrations. The Nernst equation can be used when there is an excess of inert electrolyte of nearly uniform concentration and the reactant species are present at much smaller concentrations. The assessment of the errors involved is considered again in Chapter 6.

We have seen that cell potentials frequently depend upon the transport properties of the electrolytic solutions as well as the thermodynamic properties, and they also depend upon the detailed form of the concentration profiles in the junction region. Under certain conditions, such as those considered in this section, approximations can be introduced so that the cell potential is expressed in terms of thermodynamic properties alone. Whether these approximations are sufficiently accurate depends on the intended application.

2.8 CELL WITH TWO ELECTROLYTES, BOTH OF VARYING CONCENTRATION

Cells of this type may still be divided into two groups according to whether the two electrolytes have an ion in common. A cell with a junction between solutions of $CuSO_4$ and $ZnSO_4$ is an example where there is a common ion; a junction between NaCl and $HClO_4$ is an example where there is not. The former class is discussed first.

Consider the cell

$$\begin{array}{c|c|c|c|c|c|c|c|c} \alpha & \beta & \delta & \epsilon & & \lambda & \delta' & \beta' & \alpha' \\ \mathrm{Pt}(s) & \mathrm{Ag}(s) & \mathrm{AgCl}(s) & \mathrm{HCl\ in\ H_2O} & \text{transition region} & \mathrm{KCl\ in\ H_2O} & \mathrm{AgCl}(s) & \mathrm{Ag}(s) & \mathrm{Pt}(s) \end{array}, \tag{2.111}$$

for which the cell potential is

$$FU = -F(\Phi^{\alpha} - \Phi^{\alpha'}) = \mu^{\epsilon}_{\mathrm{Cl}^-} - \mu^{\lambda}_{\mathrm{Cl}^-}. \tag{2.112}$$

For the present analysis, we ignore the small solubility of AgCl, which was treated in Section 2.7. Integration of equation 2.68 for this case gives

$$\mu^{\epsilon}_{\mathrm{Cl}^-} - \mu^{\lambda}_{\mathrm{Cl}^-} = \int_{\lambda}^{\epsilon} \left(t^0_{\mathrm{H}^+} \frac{\partial \mu_{\mathrm{HCl}}}{\partial x} + t^0_{\mathrm{K}^+} \frac{\partial \mu_{\mathrm{KCl}}}{\partial x} \right) dx. \tag{2.113}$$

Here, as with equation 2.98, and in contrast to equation 2.72, the integral depends on the detailed form of the concentration profiles in the junction region. The evaluation of this integral is considered in Chapter 6 in a manner that is more accurate than that used in Section 2.7.

We should also like to know how to treat the potentials of cells containing two electrolytes of varying concentration but with no common ion. Such a cell is

$$\begin{array}{c|c|c|c|c|c|c} \alpha & \beta & & \delta & \epsilon & \lambda & \alpha' \\ \mathrm{Pt}(s), \mathrm{H_2}(g) & \mathrm{HClO_4\ in\ H_2O} & \text{transition region} & \mathrm{NaCl\ in\ H_2O} & \mathrm{AgCl}(s) & \mathrm{Ag}(s) & \mathrm{Pt}(s) \end{array}. \tag{2.114}$$

The transition region contains the solutions that vary in composition from β to δ. From the conditions of phase equilibria at the electrodes and the definitions of the chemical potentials of neutral species, the cell potential can be written

$$FU = -F(\Phi^{\alpha} - \Phi^{\alpha'}) = \frac{1}{2}\mu^{\alpha}_{\mathrm{H_2}} - \mu^{\lambda}_{\mathrm{Ag}} + \mu^{\epsilon}_{\mathrm{AgCl}} - (\mu^{\beta}_{\mathrm{H}^+} + \mu^{\delta}_{\mathrm{Cl}^-}). \tag{2.115}$$

The cell potential is again related to the thermodynamic properties of electrically neutral components, but a new term has appeared. Instead of the difference of electrochemical potential of a single ion between the two solutions, there is now a combination of electrochemical potentials of two ions. One way to analyze this more complicated situation is to select an intermediate point *I* in the junction where both ions are present. If the concentration profiles are known, equation 2.68 can be used to evaluate the differences $\mu^{\beta}_{H^+} - \mu^{I}_{\mathrm{H}^+}$ and $\mu^{\delta}_{\mathrm{Cl}^-} - \mu^{I}_{\mathrm{Cl}^-}$. The cell potential can then be written

$$FU = \frac{1}{2}\mu^{\alpha}_{\mathrm{H_2}} - \mu^{\lambda}_{\mathrm{Ag}} + \mu^{\epsilon}_{\mathrm{AgCl}} - (\mu^{\beta}_{\mathrm{H}^+} - \mu^{I}_{\mathrm{H}^+}) - (\mu^{\delta}_{\mathrm{Cl}^-} - \mu^{I}_{\mathrm{Cl}^-}) - \mu^{I}_{\mathrm{HCl}}. \tag{2.116}$$

The last term, μ^{I}_{HCl}, can be evaluated if the activity coefficient of HCl is known for the solution of $HClO_4$ and NaCl at the point *I*. The cell potential is, of course, independent of the choice of the location of *I* within the transition region.

Although none of the examples is carried through here, it should be apparent that the potential of such cells can, in principle, be treated. The concentration profiles are determined from the laws of diffusion and the method of forming the junction. The expression for the cell potential will involve the

difference in electrochemical potential of an ion or of two different ions in different solutions, and this difference can be evaluated from equation 2.68, perhaps with the selection of an intermediate point, because the solutions are connected to each other through the junction. The development is brought to fruition in Chapter 6.

2.9 LITHIUM–LITHIUM CELL WITH TWO POLYMER ELECTROLYTES

While we have focused on platinum electrodes and aqueous electrolytes, the concepts described above apply to different kinds of electrolytes such as lithium salts mixed with either cyclic carbonates or polymers. The carbonate-based electrolytes are used in rechargeable lithium-ion batteries while polymer-based electrolytes are being developed for future generations of rechargeable batteries. A popular polymer electrolyte system is a mixture of lithium bis(trifluoromethanesulfonyl)imide (LiTFSI) and poly(ethylene oxide) (PEO).[7, 8] Mixtures of LiTFSI and linear PEO chains in the rubbery state are liquids with long relaxation times; they can thus appear solid-like on short time scales. If the PEO chains are crosslinked, then diffusion of the chains on length scales larger than the distance between crosslinks (typically on the 10-nm length scale) is forbidden, and one obtains a soft solid. Shown below is a cell wherein two LiTFSI/PEO mixtures with different molalities, m_r and m, are brought in contact with each other at constant T and p.

$$\begin{array}{c|c|c|c|c|c|c} \alpha & & \epsilon & & & \lambda & \alpha' \\ \text{Li}(s) & \left|\begin{array}{c}\text{LiTFSI in} \\ \text{PEO}(m_r)\end{array}\right. & \sim & \begin{array}{c}\text{transition} \\ \text{region}\end{array} & \sim & \left|\begin{array}{c}\text{LiTFSI in} \\ \text{PEO}(m)\end{array}\right. & \text{Li}(s)\ . \end{array} \tag{2.117}$$

Such a cell is shown schematically in Figure 2.2a. As soon as the phases ϵ and λ are brought into contact, diffusion of salt across the boundary leads to the development of a transition region. At long times, the concentrations of the electrolytes ϵ and λ will approach each other, and U will be

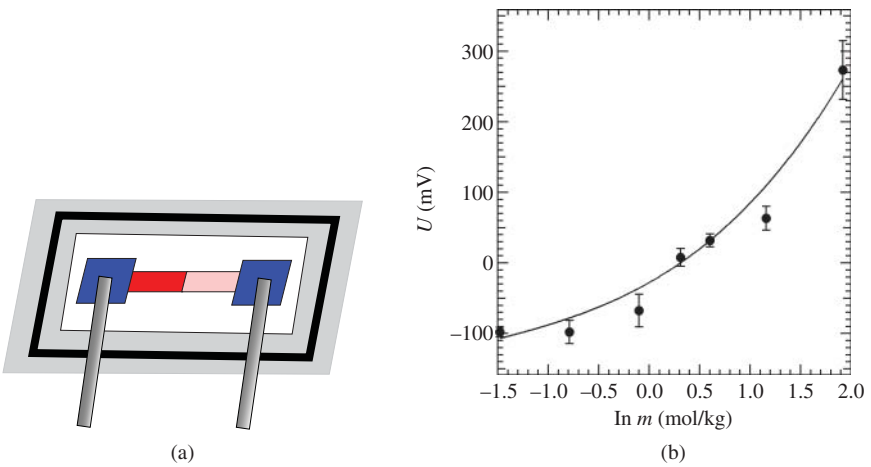

Figure 2.2 (a) Schematic of a concentration cell with two lithium electrodes and a junction between two polymer electrolytes with different salt concentrations (molalities) in contact with each other. (b) Open-circuit potential U, as a function of molality m, of PEO/LiTFSI, with a reference molality of 1.36 mol/kg, measured before diffusion substantially changes the electrolyte concentration at the electrodes.

zero. The time scale on which this equilibrium configuration is obtained will depend on the size of the phases ϵ and λ (diffusion length), the nature of the PEO chains (length and whether or not they are crosslinked), and salt concentration. At early times, the transition region will be confined to the middle of the cell and will not reach either electrode. Under these conditions, the cell potential is given by equation 2.75 applied to univalent salts

$$FU = -F(\Phi^{\alpha} - \Phi^{\alpha'}) = 2RT \int_{m_r}^{m} t_{-}^{0} \left(1 + \frac{d \ln \gamma_{+-}}{d \ln m}\right) d \ln m. \tag{2.118}$$

In the simple case where t_{-}^{0} is a known constant, measurements of U as a function of m, keeping m_r fixed, may be used to determine the dependence of γ_{+-} on the salt concentration. This is often not the case, and the differential form of equation 2.118 must be used to interpret U versus m data:

$$\frac{dU}{d \ln m} = \frac{2RTt_{-}^{0}}{F} \left(1 + \frac{d \ln \gamma_{+-}}{d \ln m}\right), \tag{2.119}$$

where the U data must be augmented by other measurements to enable the determination of the dependences of both γ_{+-} and t_{-}^{0} on salt concentration.[9]

Data obtained from a concentration cell containing PEO (molar mass = 5 kg/mol)/LiTFSI mixtures, with $m_r = 1.36$ mol/kg, are shown in a plot of U versus m in Figure 2.2b.[10, 11] We revisit this data set and additional characterization of this electrolyte in Section 14.3.

2.10 STANDARD CELL POTENTIAL AND ACTIVITY COEFFICIENTS

Uses for Different Types of Cells

We have described four types of cells. The first is of the form of cell 2.45, in which the electrolyte is uniform and the net cell reaction does not involve the electrolyte. The potential of this cell depends on the electrochemical potentials of the components of the electrodes but is independent of the nature or concentration of the electrolyte. Such a cell can be used to obtain thermodynamic data on the electrode materials.

The second is of the form of cell 2.55, in which there is still a uniform electrolyte (assuming the TlCl to be insoluble) but in which the overall cell reaction does involve the electrolyte. For example, for the case of cell 2.55, Li^+ reacts at the left electrode, whereas Cl^- reacts at the right electrode. The potential of this cell depends on the electrochemical potentials both of the electrode materials and of the components of the electrolytic solution. If the thermodynamic properties of the electrode materials are already known, then a cell of this type can be used to measure the chemical potential of the salt in the electrolyte. If nonreactive salts or solvents are mixed into the electrolyte, then this cell can be used to see how the activity coefficient of the reacting salt depends on the presence of other additives in solution.

The third cell is called a concentration cell, and an example is cell 2.69. In a concentration cell, the electrodes are identical, the electrolyte consists of a single salt in a single solvent, and the concentration of the electrolyte is different next to each electrode. The potential of a concentration cell is independent of the nature of the electrodes and depends on the electrochemical potential of the salt in solution and on the transference number. For a binary electrolyte, the cell potential is independent of the shape of the concentration profile across the cell. If the activity coefficient is already known, for example, from cells of type 2.55 or vapor-pressure measurements, then cells of type 2.69 can be used to obtain the transference number. Alternatively, if the transference number is known from moving-boundary or

Hittorf measurements, then the concentration cell can be used to obtain the activity coefficient. The latter procedure is particularly useful in dilute solutions where the transference numbers may be well known and are relatively independent of concentration.

The fourth cell contains two salts nonuniformly distributed across the electrolyte. These cells are less useful for determining thermodynamic properties. The cells discussed in Section 2.7, in which one salt is present in very small concentrations next to one of the electrodes, still will be useful for the determination of thermodynamic properties if the error in the estimation of the transport-related effects can be made sufficiently small. The potential of cells with multicomponent electrolytes with concentration gradients can be computed given knowledge of the composition profile and the dependence of the activity coefficients and transference numbers on composition.

Standard Cell Potential

In general, cell potentials depend on the components of the electrodes and electrolyte, the concentration of those components present in mixtures, and the transference number of the electrolyte (for cells with concentration gradients). Rather than tabulating the cell potential of every pair of electrodes in electrolytes of every possible concentration, it is convention to report the data in two parts, a *standard cell potential*, which is independent of concentration, and an activity coefficient, which describes how μ_i depends on concentration, relative to some idealized dependence.

For example, for the cell 2.55 the potential is expressed as

$$FU = \mu^{\beta}_{\mathrm{Li}} - \mu^{\phi}_{\mathrm{Tl}} + \mu^{\epsilon}_{\mathrm{TlCl}} - \mu^{\delta}_{\mathrm{LiCl}}. \tag{2.120}$$

By means of equation 2.28, this can be written as

$$FU = FU^{\theta} - 2RT \ln(m^{\delta}_{\mathrm{LiCl}} \gamma^{\delta}_{\mathrm{LiCl}}) - RT \ln a^{\phi}_{\mathrm{Tl}}, \tag{2.121}$$

where the relative activity of thallium in the thallium amalgam is given by equation 2.43 and where the standard cell potential is given by

$$FU^{\theta} = \mu^{0}_{\mathrm{Li}} - \mu^{0}_{\mathrm{Tl}} + \mu^{0}_{\mathrm{TlCl}} - RT \ln \lambda^{\theta}_{\mathrm{LiCl}}. \tag{2.122}$$

To measure U^{θ}, one could measure U at some concentration of the electrolyte and of the amalgam. Then U^{θ} can be found from

$$FU^{\theta} = FU + 2RT \ln(m^{\delta}_{\mathrm{LiCl}} \gamma^{\delta}_{\mathrm{LiCl}}) + RT \ln a^{\phi}_{\mathrm{Tl}}, \tag{2.123}$$

if $\gamma_{+-}(m)$ and a_{Tl} are already known. U^{θ} depends only on the temperature, pressure, and the components of the cell. If one has defined the activity coefficients consistently, then U^{θ} will be independent of the concentration of the solution in which U was measured. However, the values of γ_{LiCl} and $\lambda^{\theta}_{\mathrm{LiCl}}$ depend on the choice of secondary reference state, although the product $\gamma_{+-}\lambda^{\theta}_{A}$ is independent of this choice. Since U^{θ} includes λ^{θ}_{A}, then U^{θ} will depend on the choice of secondary reference state, and this choice must be specified when tabulating values of U^{θ}. In addition, since λ^{θ}_{A} has units of inverse molality, U^{θ} will depend on the choice of concentration units. The usual convention is to express λ^{θ}_{A} in kg/mol, and thus m should have units of mol/kg.

Values of the activity coefficient can be obtained experimentally by specifying its value to be 1 at the secondary reference state and then measuring how the chemical potential changes as the concentration is varied from the secondary reference concentration. The reference state used for liquid solutions is expressed by equation 2.18, even though this reference state is difficult to apply experimentally. These

difficulties are associated with the larger relative effect of impurities in dilute solutions, inaccuracies in the determination of the salt concentration at low concentrations, the rapid variation of the activity coefficient with concentration in dilute solutions, and the effect of the solubility of the thallous chloride, which can become significant in dilute solutions. Nevertheless, this reference state is used because no other logical possibility presents itself. It has the advantage that the reference state is essentially the same for all the solute species, and activity-coefficient expressions for multicomponent solutions are thereby simplified.

The method of applying the secondary reference state 2.18 to the cells above is considered again in Chapter 4 after discussion of the behavior of activity coefficients in dilute solutions. One wants to extrapolate to infinite dilution in a way that provides the greatest accuracy.

U^θ and γ_{+-} can also be determined by specifying U^θ and γ_{+-} for a particular thermodynamic state of the system and then determining the value of γ in other states by potential measurements and the use of equation 2.121. Data for μ_A^0 can also be obtained by thermochemical methods, such as by measuring the enthalpy and entropy change upon reaction of elements to form a compound (see Section 2.11).

For the cell 2.114, the cell potential can be written

$$FU = FU^\theta + \frac{1}{2}RT \ln p_{H_2}^\alpha - (\mu_{H^+}^\beta - \mu_{H^+}^I) - (\mu_{Cl^-}^\delta - \mu_{Cl^-}^I) - RT \ln[m_{H^+}^I m_{Cl^-}^I (\gamma_{HCl}^I)^2], \qquad (2.124)$$

where the standard cell potential is

$$FU^\theta = \frac{1}{2}\mu_{H_2}^* - \mu_{Ag}^0 + \mu_{AgCl}^0 - 2RT \ln \lambda_{HCl}^\theta \qquad (2.125)$$

and where p_{H_2} is the fugacity of hydrogen (see equation 2.40). The standard cell potential is a collection of thermodynamic quantities, independent of the concentrations in the cell, and also equal to the standard cell potential of cell 2.106. However, in this case, the nonthermodynamic terms in equation 2.124 are not negligible; they are difficult to evaluate accurately because they require a knowledge of transference numbers and activity coefficients in multicomponent solutions of moderate concentration, as well as a knowledge of how the junction was formed.

As the above example demonstrates, the cells of Section 2.8 are not particularly useful for the precise determination of thermodynamic or transport properties of solutions, or of standard cell potentials. Cell 2.106 will yield the same standard cell potential as cell 2.114 but with less uncertainty. Cells such as those treated in Section 2.8 are encountered in practice, and prediction of their potentials is more a test of our ability to treat junction regions. Tabulated values of standard cell potentials, as well as activity coefficients and transference numbers, do find application in this endeavor.

In compiling the standard cell potentials of many cells, it is desirable to tabulate as few details as possible without being ambiguous. Of n possible electrodes, one can make measurements on $\frac{1}{2}n(n-1)$ different combinations of these electrodes taken two at a time. Only $n-1$ of these combinations are independent, and the others can be obtained by appropriate addition and subtraction of the $n-1$ independent combinations. Hence, one can report the standard cell potentials of $n-1$ possible electrodes against the other possible electrode, and the standard cell potential of other combinations can be obtained from these.

By convention, the hydrogen electrode is used for this reference point. Table 2.2 gives values for selected standard electrode potentials in aqueous electrolytes relative to the hydrogen electrode. To emphasize the thermodynamic nature of these quantities, the explicit expressions in terms of chemical potentials in the secondary reference states are also given. A number of remarks can be made about the entries in Table 2.2.

The sign convention gives the standard potential of the electrode of interest *relative* to the hydrogen electrode; that is, one reports $\Phi_{\text{electrode}} - \Phi_{H_2|H^+}$. The expression for the standard electrode potential involves only those species that are involved in the overall cell reaction. For entry 15, the overall cell reaction is the electrolysis of water and involves no ions at all. The chemical potentials with a superscript 0 denote elements or compounds in the pure state. The values of λ_i^θ depend on the extrapolation to

TABLE 2.2 Selected standard electrode potentials referred to the hydrogen electrode in aqueous solutions at 25°C

	Reaction	$FU^{\theta a}$	U^{θ}(V)
1	$K \rightarrow K^+ + e^-$	$\frac{1}{2}\mu^*_{H_2} - \mu^0_K + RT \ln\left(\lambda^{\theta}_{K^+}/\lambda^{\theta}_{H^+}\right)$	−2.95
2	$Pb + SO_4^{2-} \rightarrow PbSO_4 + 2e^-$	$\frac{1}{2}\left(\mu^*_{H_2} + \mu^0_{PbSO_4} - \mu^0_{Pb}\right) - \frac{1}{2}RT \ln\left[\left(\lambda^{\theta}_{H^+}\right)^2 \lambda^{\theta}_{SO_4^{2-}}\right]$	−0.356
3	$Pb \rightarrow Pb^{2+} + 2e^-$	$\frac{1}{2}\mu^*_{H_2} - \frac{1}{2}\mu^0_{Pb} + \frac{1}{2}RT \ln\left[\lambda^{\theta}_{Pb^{2+}}/\left(\lambda^{\theta}_{H^+}\right)^2\right]$	−0.126
4	$H_2 \rightarrow 2H^+ + 2e^-$	—	0
5	$Hg + 2OH^- \rightarrow HgO + H_2O + 2e^-$	$\frac{1}{2}\left(\mu^*_{H_2} + \mu^0_{HgO} + \mu^0_{H_2O} - \mu^0_{Hg}\right) - RT \ln\left(\lambda^{\theta}_{H^+}\lambda^{\theta}_{OH^-}\right)$	0.098
6	$Cu^+ \rightarrow Cu^{2+} + e^-$	$\frac{1}{2}\mu^*_{H_2} + RT \ln\left[\lambda^{\theta}_{Cu^{2+}}/\left(\lambda^{\theta}_{H^+}\lambda^{\theta}_{Cu^+}\right)\right]$	0.153
7	$Ag + Cl^- \rightarrow AgCl + e^-$	$\frac{1}{2}\mu^*_{H_2} + \mu^0_{AgCl} - \mu^0_{Ag} - RT \ln\left(\lambda^{\theta}_{H^+}\lambda^{\theta}_{Cl^-}\right)$	0.222
8	$Cu \rightarrow Cu^{2+} + 2e^-$	$\frac{1}{2}\mu^*_{H_2} - \frac{1}{2}\mu^0_{Cu} + \frac{1}{2}RT \ln\left[\lambda^{\theta}_{Cu^{2+}}/\left(\lambda^{\theta}_{H^+}\right)^2\right]$	0.337
9	$4OH^- \rightarrow O_2 + 2H_2O + 4e^-$	$\frac{1}{2}\mu^*_{H_2} + \frac{1}{4}\mu^*_{O_2} + \frac{1}{2}\mu^0_{H_2O} - RT \ln\left(\lambda^{\theta}_{H^+}\lambda^{\theta}_{OH^-}\right)$	0.401
10	$Cu \rightarrow Cu^+ + e^-$	$\frac{1}{2}\mu^*_{H_2} - \mu^0_{Cu} + RT \ln\left(\lambda^{\theta}_{Cu^+}/\lambda^{\theta}_{H^+}\right)$	0.521
11	$2I^- \rightarrow I_2(s) + 2e^-$	$\frac{1}{2}\mu^*_{H_2} + \frac{1}{2}\mu^0_{I_2} - RT \ln\left(\lambda^{\theta}_{H^+}\lambda^{\theta}_{I^-}\right)$	0.5355
12	$3I^- \rightarrow I_3^- + 2e^-$	$\frac{1}{2}\mu^*_{H_2} + \frac{1}{2}RT \ln\lambda^{\theta}_{I_3^-} - \frac{3}{2}RT \ln\lambda^{\theta}_{I^-} - RT \ln\lambda^{\theta}_{H^+}$	0.536
13	$Fe^{2+} \rightarrow Fe^{3+} + e^-$	$\frac{1}{2}\mu^*_{H_2} + RT \ln\left[\lambda^{\theta}_{Fe^{3+}}/\left(\lambda^{\theta}_{Fe^{2+}}\lambda^{\theta}_{H^+}\right)\right]$	0.771
14	$Au + 4Cl^- \rightarrow AuCl_4^- + 3e^-$	$\frac{1}{2}\mu^*_{H_2} - \frac{1}{3}\mu^0_{Au} + \frac{1}{3}RT \ln\lambda^{\theta}_{AuCl_4^-} - \frac{4}{3}RT \ln\lambda^{\theta}_{Cl^-} - RT \ln\lambda^{\theta}_{H^+}$	1.00
15	$2H_2O \rightarrow O_2 + 4H^+ + 4e^-$	$\frac{1}{2}\mu^*_{H_2} + \frac{1}{4}\mu^*_{O_2} - \frac{1}{2}\mu^0_{H_2O}$	1.229
16	$2Cl^- \rightarrow Cl_2(g) + 2e^-$	$\frac{1}{2}\mu^*_{H_2} + \frac{1}{2}\mu^*_{Cl_2} - RT \ln\left(\lambda^{\theta}_{H^+}\lambda^{\theta}_{Cl^-}\right)$	1.3595
17	$PbSO_4 + 2H_2O \rightarrow PbO_2 + SO_4^{2-} + 4H^+ + 2e^-$	$\frac{1}{2}\left(\mu^*_{H_2} + \mu^0_{PbO_2} - \mu^0_{PbSO_4}\right) - \mu^0_{H_2O} + \frac{1}{2}RT \ln\left[\left(\lambda^{\theta}_{H^+}\right)^2 \lambda^{\theta}_{SO_4^{2-}}\right]$	1.685

[a] λ_i^{θ} must be expressed in kg/mol. The superscript 0 denotes the pure element or compound at 25°C and 1 atm. The superscript * denotes the chemical potential of gases in an ideal standard state (see Problem 2.14).

TABLE 2.3 Additional standard electrode potentials in aqueous solutions at 25°C

	Reaction	U^θ (V)
1	$Li \rightarrow Li^+ + e^-$	−3.045
2	$Na \rightarrow Na^+ + e^-$	−2.714
3	$Al \rightarrow Al^{3+} + 3e^-$	−1.66
4	$Mn \rightarrow Mn^{2+} + 2e^-$	−1.18
5	$Cr \rightarrow Cr^{2+} + e^-$	−0.91
6[a]	$\frac{1}{2}H_2 + OH^- \rightarrow H_2O + e^-$	−0.828
7	$Zn \rightarrow Zn^{2+} + 2e^-$	−0.763
8	$Cr \rightarrow Cr^{3+} + 3e^-$	−0.74
9	$Fe \rightarrow Fe^{2+} + 2e^-$	−0.440
10	$Cr^{2+} \rightarrow Cr^{3+} + e^-$	−0.41
11	$H_2 \rightarrow 2H^+ + 2e^-$	0
12	$2Hg + 2Cl^- \rightarrow Hg_2Cl_2 + 2e^-$	0.2676
13	$Fe(CN)_6^{4-} \rightarrow Fe(CN)_6^{3-} + e^-$	0.36
14	$2Hg \rightarrow Hg_2^{2+} + 2e^-$	0.789
15	$Ag \rightarrow Ag^+ + e^-$	0.7991
16	$Hg_2^{2+} \rightarrow 2Hg^{2+} + 2e^-$	0.920
17	$2Br^- \rightarrow Br_2(l) + 2e^-$	1.0652
18	$Ag^+ \rightarrow Ag^{2+} + e^-$	1.98
19	$2F^- \rightarrow F_2(g) + 2e^-$	2.87

[a]Represents a hydrogen electrode in a basic medium relative to a hydrogen electrode in an acidic medium. Here

$$FU^\theta = \mu^0_{H_2O} - RT \ln(\lambda^\theta_{H^+}\lambda^\theta_{OH^-}).$$

infinite dilution and therefore depend on the particular solvent involved. Consequently, the table of electrode potentials would be different in a different solvent. Values of λ_i^θ for ions appear only in those combinations that can be unambiguously determined according to the considerations of Section 2.3.

Table 2.3 gives additional values of standard electrode potentials in aqueous solutions at 25°C. Detailed expressions for FU^θ, as given in Table 2.2, are not given here. The reader can reproduce them by reference to the examples in Table 2.2. Latimer[12] prepared the classic tabulation of standard electrode potentials in aqueous solutions. He also discusses how to obtain these by thermochemical calculations as well as by direct measurements on galvanic cells. Tables of chemical thermodynamic data[13] permit rapid evaluation of standard cell potentials.

Standard cell potentials and activity coefficients are tabulated separately. Activity coefficients are characteristic of the solutions and can be measured by nonelectrochemical methods, such as vapor-pressure measurements, or by the cells of Section 2.6, which do not involve standard cell potentials. On the other hand, standard cell potentials are associated with the overall cell reaction, for which all the ionic species in the solution need not be specified. Because of the diverse sources and applications of standard cell potentials and activity coefficients, their separate tabulation is dictated and amounts to the briefest way to collect the results of many experiments on many different systems. Consequently, in an attempt to reproduce the potentials of a particular cell with the use of these separate tabulations, the errors associated with the extrapolation to infinite dilution may not cancel exactly.

Calculation of Cell Potentials

One can use the following procedure to calculate the cell potential based on tables of standard oxidation potentials. First, one chooses one electrode to be the "right" electrode and the other to be the "left"

electrode. For example, let our right electrode be reaction 17 of Table 2.2 and our left electrode be reaction 2. Subtract the potential of the left electrode from that of the right electrode to obtain the cell potential. For our example, this yields $(1.685) - (-0.356) = 2.041$.

If the cell potential as calculated is positive, then we have made the more positive electrode the "right" electrode and the more negative electrode the "left" electrode, and vice versa if the calculated cell potential is negative. Write the positive electrode in the cathodic direction and the negative electrode in the anodic direction. For our example, this is

$$PbO_2 + SO_4^{2-} + 4H^+ + 2e^- \rightarrow PbSO_4 + 2H_2O \tag{2.126}$$

and

$$Pb + SO_4^{2-} \rightarrow PbSO_4 + 2e^-. \tag{2.127}$$

When the positive electrode is connected through an external circuit to the negative electrode, the reactions will occur spontaneously in the directions as written. To get the overall cell reaction, multiply one half-cell reaction so that it involves the same number of electrons as the other, and add the two half-cell reactions. For our example, this yields

$$Pb + PbO_2 + 2H_2SO_4 \rightarrow 2PbSO_4 + 2H_2O. \tag{2.128}$$

The method of Section 2.4 then can be used to write the cell potential in terms of the standard cell potential and concentration-dependent terms. For our example, this is

$$FU = FU^\theta + 3RTm_{H_2SO_4}\phi M_{H_2O} + 3RT\ln(m_{H_2SO_4}\gamma_{H_2SO_4}) + RT\ln 4. \tag{2.129}$$

One can then use tabulated values of γ_{+-} and ϕ to calculate U at different molalities of sulfuric acid. For example, the plot of U as a function of electrolyte concentration given in Figure 12.1 was constructed from the data tabulated in reference [13]. The RT ln 4 term comes in because of the use of γ_{+-} as opposed to γ_A (see equation 2.28).

Another example of how to treat such terms is found in the cell

$$\overset{\alpha}{Pt(s), H_2(g)}\left|\overset{\beta}{H_2SO_4 \text{ in } H_2O}\right|\overset{\delta}{PbSO_4(s)}\left|\overset{\epsilon}{PbO_2(s)}\right|\overset{\alpha'}{Pt(s)}, \tag{2.130}$$

for which the expression for the cell potential is

$$FU = FU^\theta + \frac{1}{2}RT\ln p^\alpha_{H_2} + \frac{3}{2}RT\ln(m^\beta_{H_2SO_4}\gamma^\beta_{H_2SO_4}) - RT\ln a^\beta_{H_2O} + RT\ln 2. \tag{2.131}$$

Use of Cell Potentials to Calculate Equilibrium Constants

The standard cell potential provides data for the sum of the chemical potentials, and thus the products of the absolute activities, of the species involved in the reaction. These data can be used to calculate equilibrium constants. Here, we present three examples of different types of equilibrium constants, such as dissociation constants and solubility products, that can be calculated from the information provided by standard cell potentials.

Entries 9 and 15 of Table 2.2 give

$$\frac{\lambda^\theta_{H^+}\lambda^\theta_{OH^-}}{\lambda^0_{H_2O}} = \exp\left(\frac{1.229 - 0.401}{RT/F}\right) = 10^{14}\frac{kg^2}{mol^2}. \tag{2.132}$$

Since the absolute activities are related at equilibrium by

$$\lambda_{H^+}\lambda_{OH^-} = \lambda_{H_2O}, \tag{2.133}$$

this corresponds to a dissociation constant for water of

$$K_w = \frac{m_{H^+}m_{OH^-}\gamma_{H^+}\gamma_{OH^-}}{a_{H_2O}} = 10^{-14}\ \frac{\text{mol}^2}{\text{kg}^2}. \tag{2.134}$$

Entries 2 and 3 of Table 2.2 yield

$$\frac{\lambda^{\theta}_{Pb^{2+}}\lambda^{\theta}_{SO_4^{2-}}}{\lambda^{0}_{PbSO_4}} = \exp\left(\frac{0.356 - 0.126}{RT/2F}\right) = 6 \times 10^7\ \frac{\text{kg}^2}{\text{mol}^2}. \tag{2.135}$$

Hence, the solubility product of $PbSO_4$ is

$$K_{sp} = m_{Pb^{2+}}m_{SO_4^{2-}}\gamma^2_{PbSO_4} = 1.7 \times 10^{-8}\ \frac{\text{mol}^2}{\text{kg}^2}. \tag{2.136}$$

Entries 6, 8, and 10 of Table 2.2 are not independent. Specifically, two times entry 8 is equal to the sum of entries 6 and 10, both for the numerical values of U^{θ} and for the expressions for FU^{θ}. These entries also describe the equilibrium concentrations of cuprous ions present in the solution of a cupric salt. The cuprous ions can disproportionate according to the reaction

$$2Cu^+ \rightarrow Cu + Cu^{2+}, \tag{2.137}$$

for which the equilibrium condition is

$$\lambda^2_{Cu^+} = \lambda_{Cu}\lambda_{Cu^{2+}}. \tag{2.138}$$

From entries 6 and 10 of Table 2.2,

$$\frac{(\lambda^{\theta}_{Cu^+})^2}{\lambda^{0}_{Cu}\,\lambda^{\theta}_{Cu^{2+}}} = \exp\left(\frac{0.521 - 0.153}{RT/F}\right) = 1.67 \times 10^6\ \frac{\text{kg}}{\text{mol}}. \tag{2.139}$$

Hence the equilibrium constant can be expressed as

$$\frac{m^2_{Cu^+}\gamma^2_{Cu^+}}{m_{Cu^{2+}}\gamma_{Cu^{2+}}} = 0.6 \times 10^{-6}\ \frac{\text{mol}}{\text{kg}}. \tag{2.140}$$

By ignoring the activity coefficients, we estimate the equilibrium concentration of cuprous ions to be 2.4×10^{-4} mol/kg in a 0.1 *M* $CuSO_4$ solution. We see from this example that two or more electrode processes can be simultaneously in equilibrium at the same electrode at the same potential.

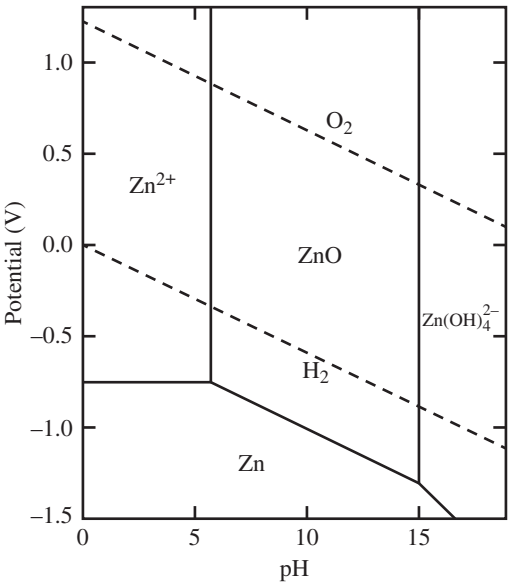

Figure 2.3 Simplified Pourbaix diagram of potential *versus* pH for zinc at 1 mol/kg concentration of Zn^{2+} and $Zn(OH)_4^{2-}$, showing regions of stability of ZnO and $Zn(OH)_4^{2-}$. For reference, the dashed lines for the evolution of oxygen and hydrogen indicate the limits of stability of water.

Multiple Simultaneous Reactions and Pourbaix Diagrams

The occurrence of different reactions at different potentials on the same electrode is often depicted in a plot called a *Pourbaix diagram*. A detailed example of a Pourbaix diagram is given in Section 18.5. Pourbaix diagrams have been constructed for a large number of systems, mostly with aqueous electrolytes.[14] It is customary to include the hydrogen and oxygen reactions on a Pourbaix diagram and to plot the potential of the reactions as a function of the pH of the electrolyte. A Pourbaix diagram shows which species are thermodynamically stable as a function of potential and pH.

Figure 2.3 shows a simplified Pourbaix diagram for the system of a zinc electrode in an aqueous electrolyte, with potentials given relative to the normal hydrogen electrode.[15] Three electrochemical reactions are shown: evolution of oxygen and of hydrogen (dashed lines) and dissolution of zinc (solid horizontal and diagonal segments). All three reactions may occur simultaneously on the same zinc surface. If the potential at the surface of the zinc metal is more positive than the equilibrium potential for a reaction, then that reaction will be driven in the anodic direction; a more negative potential will drive the reaction in the cathodic direction. Thus, O_2 will tend to steal electrons spontaneously from the zinc to form H_2O and Zn^{2+}.

The vertical lines indicate the chemical reactions between Zn^{2+} and H_2O to form $ZnO + 2H^+$ and between ZnO, H_2O, and $2OH^-$ to form $Zn(OH)_4^{2-}$. Thus, from this diagram, one can see that at pH 2, zinc will tend to dissolve to form Zn^{2+}, whereas at pH 10, zinc will react to form a solid coating of ZnO.

2.11 PRESSURE DEPENDENCE OF ACTIVITY COEFFICIENTS

The definition of activity coefficients involves the use of a secondary reference state for the solute, for example, that given by equation 2.18. The value of λ_i^θ depends upon the choice of the secondary reference state in a complementary manner, so that the product $\gamma_i\lambda_i^\theta$ is independent of this choice. If equation 2.18 is to be applied at each temperature and pressure, then λ_i^θ will also depend on temperature and pressure. If, on the other hand, equation 2.18 is applied at each temperature but only at 1 bar, then λ_i^θ depends only on temperature. The mean ionic activity coefficient of neutral combinations of ions will then approach unity at infinite dilution only at this pressure of 1 bar.

The variation of activity coefficients with pressure is determined by the fact that the derivative of the chemical potential with respect to pressure is equal to the partial molar volume:

$$\left(\frac{\partial\mu_A}{\partial p}\right)_{T,m_i} = \left(\frac{\partial V}{\partial n_A}\right)_{\substack{T,p,n_B \\ B\neq A}} = \overline{V}_A. \tag{2.141}$$

We apply this equation only to neutral electrolytes, for which the method of obtaining partial molar volumes from density determinations is given in Appendix A. For an electrolyte,

$$\mu_A = RT\ln[(m_+\lambda_+^\theta)^{\nu_+}(m_-\lambda_-^\theta)^{\nu_-}\gamma_{+-}^{\nu}]. \tag{2.142}$$

If λ_i^θ is taken to be independent of pressure, then equation 2.141 yields

$$\left(\frac{\partial\ln\gamma_{+-}}{\partial p}\right)_{T,m_i} = \frac{\overline{V}_A}{\nu RT} \quad (\lambda_i^\theta \text{ independent of } p). \tag{2.143}$$

For $\overline{V}_A = 27\ \text{cm}^3/\text{mol}$ and a 1–1 electrolyte ($\nu_+ = \nu_- = 1$), the pressure variation of γ_{+-} at 25°C is

$$\frac{\partial\ln\gamma_{+-}}{\partial p} = 5.4\times10^{-4}\ \text{bar}^{-1}. \tag{2.144}$$

Thus, a pressure change of 18 bar is necessary to change γ_{+-} by 1%. This will apply to the value of γ_{+-} at infinite dilution as well.

If, on the other hand, equation 2.18 is applied at each pressure and λ_i^θ depends on pressure, then application of equation 2.141 to equation 2.142 gives

$$\frac{\partial\ln\lambda_+^{\theta\nu_+}\lambda_-^{\theta\nu_-}}{\partial p} + \nu\frac{\partial\ln\gamma_{+-}}{\partial p} = \frac{\overline{V}_A}{RT}. \tag{2.145}$$

Under these conditions, γ_{+-} is independent of pressure at infinite dilution, and consequently

$$\frac{\partial\ln\lambda_+^{\theta\nu_+}\lambda_-^{\theta\nu_-}}{\partial p} = \frac{\overline{V}_A^\theta}{RT}, \tag{2.146}$$

where the superscript θ denotes the value at infinite dilution. At other concentrations, equation 2.145 then becomes

$$\left(\frac{\partial\ln\gamma_{+-}}{\partial p}\right)_{T,m_i} = \frac{\overline{V}_A - \overline{V}_A^\theta}{\nu RT} \quad (\gamma_{+-}\to 1 \text{ at infinite dilution}). \tag{2.147}$$

Since the partial molar volume does not change very much with concentration, the activity coefficient so defined changes even less with pressure than the variation indicated by equation 2.143. For example, if $\overline{V}_A = 32$ at 3 M and 27 cm^3/mol at infinite dilution, then for a 1–1 electrolyte at 25°C,

$$\frac{\partial \ln \gamma_{+-}}{\partial p} = 10^{-4}\ \text{bar}^{-1}, \tag{2.148}$$

and a pressure change of 99 bar is required for a 1% change in γ_{+-}.

From these examples, one can perceive why the pressure dependence of activity coefficients is of little concern.

2.12 TEMPERATURE DEPENDENCE OF CELL POTENTIALS

Many data have been tabulated in the literature that allow calculation of U as a function of temperature. As an example, let us consider the potential of a hydrogen/oxygen fuel cell. The reaction at the positive electrode is reaction 15, and the reaction at the negative electrode is reaction 4 of Table 2.2. Thus, for gaseous reactants and products,

$$U = U^{\theta} + \frac{RT}{4F} \ln\left(\frac{p_{O_2} p_{H_2}^2}{p_{H_2O}^2}\right), \tag{2.149}$$

where

$$FU^{\theta} = \frac{1}{2}\mu_{H_2}^* + \frac{1}{4}\mu_{O_2}^* - \frac{1}{2}\mu_{H_2O}^*. \tag{2.150}$$

From equation 1.6,

$$U = -\frac{\Delta G}{nF} = -\frac{1}{4F}\sum_i s_i \mu_i. \tag{2.151}$$

μ_i^0 and μ_i^* are often tabulated as ΔG_f^o, the Gibbs energy of formation evaluated at the reference state of 1 bar and 298.15 K or an ideal gas at 298.15 K, respectively. From the data in Table 2.4, we can compute U^{θ} to be 1.184 V at 298.15 K.

To calculate how U varies with temperature at constant pressure and composition, we first relate the Gibbs free energy to the enthalpy by the Gibbs–Helmholtz equation,

$$\Delta H = \Delta G - T\Delta S = -T^2 \frac{\partial(\Delta G/T)}{\partial T}. \tag{2.152}$$

Just as the cell potential U is related to ΔG, we can define the enthalpy potential U_H by

$$U_H = -\frac{\Delta H}{nF} = U - T\frac{\partial U}{\partial T}, \tag{2.153}$$

where $\partial U/\partial T$ is related to the entropy of the reaction ΔS by

$$\frac{\partial U}{\partial T} = \frac{\Delta S}{nF}. \tag{2.154}$$

In addition,

$$\frac{\partial(\Delta H)}{\partial T} = \Delta C_p, \tag{2.155}$$

TABLE 2.4 Thermodynamic data for the hydrogen/oxygen fuel cell evaluated at standard reference conditions of 298.15 K and 1 bar for liquid water and the ideal-gas state for gaseous species[a]

	μ_i^* (kJ/mol)	$\widetilde{H}_i^*$ (kJ/mol)	$\widetilde{C}_{p,i}^*$ (J/mol·K)	a_i (J/mol·K)	b_i (J/mol·K^2)	c_i (J·K/mol)	γ_i (J/mol·K^3)
O_2	0.0	0.0	29.355	29.96	4.2×10^{-3}	-1.67×10^{5}	0.0
H_2	0.0	0.0	28.824	27.28	3.3×10^{-3}	0.5×10^{5}	0.0
H_2O (g)	−228.572	−241.818	33.577	30.54	10.3×10^{-3}	0.0	0.0
H_2O (l)	−237.129	−285.830	75.291	75.291	0.0	0.0	0.0

[a] μ_i, $\widetilde{H}_i$, and $\widetilde{C}_{p,i}$ are the Gibbs free energy, enthalpy, and heat capacity per mole of species i for the pure components, respectively.

where ΔC_p is the change in heat capacity between reactants and products, equal to $\sum_i s_i \widetilde{C}_{p,i}$. The temperature dependence of the heat capacity can often be described by an empirical equation of the form

$$\widetilde{C}_{p,i} = a_i + b_i T + \frac{c_i}{T^2} + \gamma_i T^2. \tag{2.156}$$

Thus, we have a strategy for our calculations. Integrate $\Delta C_p/nF$ with respect to temperature to get $-U_H$. Divide by T^2 and integrate again to get U, using the values of U^θ and U_H^θ at some reference temperature T_0 (usually 298.15 K) to obtain the constants of integration. In general, we thus have

$$\Delta H = -nFU_H = \Delta H|_{T_0} + \Delta a(T - T_0) + \Delta b\frac{T^2 - T_0^2}{2} - \Delta c\left(\frac{1}{T} - \frac{1}{T_0}\right) + \Delta\gamma\frac{T^3 - T_0^3}{3}, \tag{2.157}$$

and

$$\Delta G = -nFU = \Delta G\Big|_{T_0}\left(\frac{T}{T_0}\right) + \Delta H\Big|_{T_0}\left(1 - \frac{T}{T_0}\right) + \Delta a\left(T - T_0 - T\ln\frac{T}{T_0}\right)$$
$$-(T - T_0)^2\left(\frac{\Delta b}{2} + \frac{\Delta c}{2TT_0^2}\right) - \frac{\Delta\gamma}{6}(T^3 - 3TT_0^2 + 2T_0^3), \tag{2.158}$$

where $\Delta a = \sum_i s_i a_i$, which for the present example yields $\Delta a = 2a_{H_2O} - 2a_{H_2} - a_{O_2}$, and similarly for Δb, Δc, and $\Delta\gamma$.

The results for the fuel-cell example are shown in Figure 2.4. The data with a liquid water product are physically unrealistic at higher temperatures. The two lines for U cross at 100°C, where the vapor pressure of water equals 1 bar, and the liquid systems would need to be pressurized at higher temperatures.

The rate of heat generation for an isothermal electrochemical system is given by

$$\dot{Q} = I\left(V - U + T\frac{\partial U}{\partial T}\right) = I(V - U_H), \tag{2.159}$$

where I is the current and V is the cell voltage. Thus, a cell operating at $V = U_H$ will have zero heat generation. For this reason, U_H is often called the *thermal neutral potential*. We see that for the case of the hydrogen–oxygen reaction, this situation of $V = U_H$ corresponds to a water electrolyzer rather than a fuel cell—that is, the current would have to flow in the reverse direction. When V is between U and U_H, heat will be absorbed by the system. Whether U_H is higher or lower than U depends on the sign of $\partial U/\partial T$.

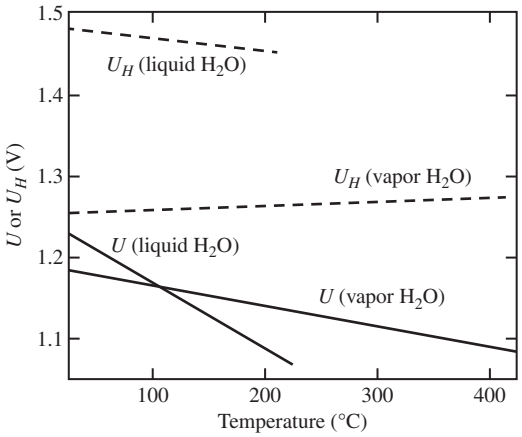

Figure 2.4 Open-circuit potential and enthalpy potential for a hydrogen–oxygen fuel cell, using either liquid or gaseous water as the product, with all pressures at 1 bar.

PROBLEMS

2.1 For theoretical treatments of diffusion, it is sometimes desirable to use a diffusion coefficient $\mathscr{D}$ for which the driving force is based on a gradient of chemical potential. For a solution of a single electrolyte, this is related to the measured value D (based on a concentration driving force) by

$$D = \mathscr{D}(1 + \nu M_0 m)\left(1 + \frac{d \ln \gamma_{+-}}{d \ln m}\right).$$

(a) Show that the factor $1 + d \ln \gamma_{+-}/d \ln m$ is independent of the choice of the secondary reference state and is, therefore, characteristic of the solution at the concentration m. In other words, this factor can be used even for solutions below the freezing point of the pure solvent, where equation 2.18 can be used only by consideration of supercooled liquids.

(b) Show that osmotic coefficients can be used directly for this conversion by deriving the relationship

$$1 + \frac{d \ln \gamma_{+-}}{d \ln m} = \phi + \frac{d\phi}{d \ln m}.$$

(c) Obtain the following relation, where activity coefficients based on molar concentrations are used:

$$D = \mathscr{D} \frac{\dfrac{(1 + \nu M_0 m)}{(1 + M_A m)}\left(1 + \dfrac{d \ln f_{+-}}{d \ln c}\right)}{1 - \dfrac{d \ln \rho}{d \ln c}}.$$

(d) Describe the behavior of $1 + d \ln \gamma_{+-}/d \ln m$ in a concentration range which includes the pure molten salt. What is the behavior of the expression in part (c)?

(e) Express the relationship between $\mathscr{D}$ and D in terms of the activity coefficient γ_A, for which the dissociation of the electrolyte is ignored. On the other hand, for a nonelectrolyte one expects to use the relation

$$D = \mathscr{D}(1 + M_0 m)\left(1 + \frac{d \ln \gamma_A}{d \ln m}\right).$$

Since the two expressions are different and since the measured value D is independent of the state of molecular aggregation, one concludes that $\mathscr{D}$, like γ, is an idealized quantity whose definition depends on whether the solute is to be regarded as dissociated or undissociated.

2.2 Obtain an expression for the potential of the cell

$$\begin{array}{c|c|c|c|c|c} \alpha & \beta & \delta & \epsilon & \phi & \alpha' \\ \mathrm{Pt}(s) & \mathrm{Ni}(s), \mathrm{O_2}(g) & \mathrm{KOH\ in\ H_2O} & \mathrm{HgO}(s) & \mathrm{Hg}(l) & \mathrm{Pt}(s). \end{array}$$

The nickel electrode can be regarded as inert, and the solubility of oxygen and mercuric oxide in the solution can be ignored. Thus, the solution can be regarded to be of uniform concentration. The electrode reactions are

$$\mathrm{O_2} + 4\mathrm{e}^- + 2\mathrm{H_2O} \rightarrow 4\mathrm{OH}^-$$

and

$$\mathrm{Hg} + 2\mathrm{OH}^- \rightarrow \mathrm{HgO} + \mathrm{H_2O} + 2\mathrm{e}^-.$$

Actually, it is difficult to achieve a reversible potential for the oxygen electrode. What is the expression for the standard cell potential, and what is its value?

2.3 Obtain an expression for the potential of the cell

$$\begin{array}{c|c|c|c|c|c} \alpha & \beta & \delta & \epsilon & \phi & \alpha' \\ \mathrm{Pt}(s) & \mathrm{K(Hg)} & \mathrm{KOH\ in\ H_2O} & \mathrm{HgO}(s) & \mathrm{Hg}(l) & \mathrm{Pt}(s). \end{array}$$

The solution can be treated as one of uniform concentration. What is the expression for the standard cell potential, and what is its value? Here, the cell potential depends on the chemical potentials of both the potassium hydroxide and the water in the solution.

2.4 Obtain an expression for the potential of the copper concentration cell in Figure 1.9. What is the standard cell potential? Introduce approximations sufficient to obtain equation 1.34.

2.5 Treat the potential of a copper concentration cell with an excess of sulfuric acid of nearly uniform concentration. What is the standard cell potential? Introduce approximations sufficient to justify the following expression for the concentration overpotential for the rotating cylinder cell with an excess of sulfuric acid as a supporting electrolyte:

$$\eta_c = \frac{RT}{2F} \ln \frac{c^{\epsilon}_{\mathrm{Cu}^{2+}}}{c^{\delta}_{\mathrm{Cu}^{2+}}}.$$

2.6 Obtain an expression for the potential of the cell

$$\begin{array}{c|c|c|c|c|c|c|c} \alpha & \beta & \delta & \epsilon & \phi & \epsilon' & \beta' & \alpha' \\ \mathrm{Pt}(s) & \mathrm{Pb}(s) & \mathrm{PbO_2}(s) & \mathrm{PbSO_4}(s) & \mathrm{H_2SO_4\ in\ H_2O} & \mathrm{PbSO_4}(s) & \mathrm{Pb}(s) & \mathrm{Pt}(s), \end{array}$$

for which the electrode reactions are

$$\mathrm{PbO_2} + \mathrm{SO_4^{2-}} + 4\mathrm{H}^+ + 2\mathrm{e}^- \rightarrow \mathrm{PbSO_4} + 2\mathrm{H_2O}$$

and

$$\mathrm{Pb} + \mathrm{SO_4^{2-}} \rightarrow \mathrm{PbSO_4} + 2\mathrm{e}^-.$$

This is the common lead–acid battery. For the electrode at the left, electrons are equilibrated among phases α, β, and δ, while the lead dioxide protects the lead from contact with the solution. What is the expression for the standard cell potential, and what is its value?

2.7 Treat the potential of the cell

$$\begin{array}{c|c|c\sim\sim c\sim\sim c|c|c} \alpha & \beta & \delta & & \epsilon & \phi & \alpha' \\ \mathrm{Pt}(s) & \mathrm{Cu}(s) & \mathrm{Cu(ClO_4)_2\ in\ H_2O} & \text{transition region} & \mathrm{AgNO_3\ in\ H_2O} & \mathrm{Ag}(s) & \mathrm{Pt}(s)\ . \end{array}$$

What is the expression for the standard cell potential, and what is its value?

2.8 Treat the potential of the cell

$$\begin{array}{c|c\sim\sim c\sim\sim c|c|c} \alpha & \beta & & \delta & \epsilon & \alpha' \\ \mathrm{Pt}(s), \mathrm{H_2}(g) & \mathrm{HCl\ in\ H_2O} & \text{transition region} & \mathrm{KNO_3\ in\ H_2O} & \mathrm{K(Hg)} & \mathrm{Pt}(s)\ . \end{array}$$

What is the expression for the standard cell potential, and what is its value?

2.9 Treat the potential of a cell in which the solution is saturated throughout with a component. Pick one of the cells 2.89 or 2.87 or that of Problem 2.6. What is the expression for the standard cell potential, and what is its value?

2.10 Derive the appropriate form of the Nernst equation for the following cells:

(a) 2.55
(b) 2.62
(c) 2.69
(d) 2.87
(e) 2.89
(f) 2.91
(g) 2.106
(h) 2.111
(i) 2.114
(j) Problem 2.2
(k) Problem 2.3
(l) Problem 2.6
(m) Problem 2.7
(n) Problem 2.8

2.11 Treat the potential of the cell

$$\begin{array}{c|c\sim\sim c\sim\sim c|c|c|c} \alpha & \beta & & \delta & \epsilon & \phi & \alpha' \\ \mathrm{Pt}(s), \mathrm{H_2}(g) & \mathrm{HCl\ in\ H_2O} & \text{transition region} & \mathrm{KOH\ in\ H_2O} & \mathrm{HgO}(s) & \mathrm{Hg}(l) & \mathrm{Pt}(s)\ . \end{array}$$

Here, the electrolytes can react in the junction region to form KCl and H_2O. Assume that the junction region is maintained at a uniform temperature. What is the expression for the standard cell potential, and what is its value?

2.12 Treat the potential of the cell

$$\begin{array}{c|c|c|c|c} \alpha & \delta & \epsilon & \phi & \alpha' \\ \mathrm{Pt}(s), \mathrm{H_2}(g) & \mathrm{KOH\ in\ H_2O} & \mathrm{HgO}(s) & \mathrm{Hg}(l) & \mathrm{Pt}(s), \end{array}$$

where the reaction for the hydrogen electrode in alkaline media is regarded to be

$$2\mathrm{H_2O} + 2\mathrm{e}^- \rightarrow \mathrm{H_2} + 2\mathrm{OH}^-.$$

What is the expression for the standard cell potential, and what is its value?

2.13 From the entries in Tables 2.2 and 2.3, determine the solubility product of silver chloride in water at 25°C.

2.14 In setting up tables of standard electrode potentials, the chemical potentials of gases are referred to the *ideal-gas state* for the secondary reference state. Thus, for hydrogen gas,

$$\mu_{\mathrm{H_2}} = \mu^*_{\mathrm{H_2}} + RT \ln p_{\mathrm{H_2}} = RT \ln p_{\mathrm{H_2}} \lambda^*_{\mathrm{H_2}},$$

where $p_{\mathrm{H_2}}$ is the partial pressure or *fugacity* of hydrogen, expressed in bar. The secondary reference state is defined such that

$$p_{\mathrm{H_2}} \rightarrow x_{\mathrm{H_2}} p \quad \text{as} \quad p \rightarrow 0,$$

where $x_{\mathrm{H_2}}$ is the mole fraction of hydrogen in the gas. Consequently, $\lambda^*_{\mathrm{H_2}}$ is expressed in bar^{-1}, and the value of $\mu^*_{\mathrm{H_2}}$ depends upon this choice of units:

$$\mu^*_{\mathrm{H_2}} = RT \ln \lambda^*_{\mathrm{H_2}}.$$

Show that the fugacity of pure hydrogen gas can be expressed as

$$p_{\mathrm{H_2}} = p \exp\left(\frac{Bp}{RT}\right),$$

where B is the second virial coefficient appearing in the equation of state

$$\frac{pV}{nRT} = 1 + \frac{Bp}{RT}.$$

The second virial coefficient for hydrogen can be expressed as

$$B = 17.42 - 314.7T^{-1} - 211{,}100T^{-2}\ (\mathrm{cm^3/mol}),$$

where T is the temperature (K). Show that the difference between using $\mu^0_{\mathrm{H_2}}$ and $\mu^*_{\mathrm{H_2}}$ in the tables of standard electrode potentials amounts to 7.25 μV in the tabulated values (at 25°C).

2.15 In thiosulfate solutions, silver ions are complexed:

$$Ag^+ + 2S_2O_3^{2-} \rightarrow Ag(S_2O_3)_2^{3-}.$$

The equilibrium constant for this reaction is estimated to be 1.7×10^{13} $(kg/mol)^2$. If the standard electrode potential for the silver electrode (Ag–Ag^+) is 0.7991 V, estimate the standard electrode potential for the deposition of silver from a thiosulfate solution:

$$Ag(S_2O_3)_2^{3-} + e^- \rightarrow Ag + 2S_2O_3^{2-}.$$

Should interference from hydrogen evolution be expected to be more or less of a problem when plating silver from a thiosulfate solution instead of a nitrate solution?

2.16 The following cell is being contemplated for use as an energy-storage system:

α	β	δ		ϵ	β'	α'
$Pt(s)$	$C(s)$	Ti^{3+}, $Ti(OH)_2^{2+}$, HCl in H_2O	transition region	$FeCl_2$, $FeCl_2^+$, HCl in H_2O	$C(s)$	$Pt(s)$.

The electrode reaction and standard electrode potential on the right on charge are

$$FeCl_2 \rightarrow FeCl_2^+ + e^-, \quad U^\theta = 0.6513\,V,$$

and those on the left are

$$Ti(OH)_2^{2+} + 2H^+ + e^- \rightarrow Ti^{3+} + 2H_2O, \quad U^\theta = 0.1\,V.$$

(a) Obtain a complete expression for the cell potential based on chemical and phase equilibria at the electrodes.

(b) Obtain the expression of the Nernst equation for the potential of this cell.

2.17 The battery-development group is evaluating the system:

α	β	δ	β'	ϵ	α'
$Pb(s)$	$PbO(s)$	KOH in H_2O	$PbO(s)$	$PbO_2(s)$	$Pb(s)$.

What open-circuit potential should be expected for the cell? Some thermochemical data at 25°C are as follows:

Compound	μ_i^0 or μ_i^θ (kJ/mol)
Pb (s)	0.0
PbO (s)	−187.89
KOH(θ)	−440.50
H_2O (l)	−237.129
PbO_2 (s)	−217.33

The concentration of KOH has been chosen as 5.7 M, near the conductivity maximum. Information from Chapter 4 may be needed to estimate activity coefficients.

2.18 One idea for a battery is to use a nonaqueous solution of LiCl dissolved in $LiClO_3$ at 150°C. At the negative electrode, lithium goes into solution. At the inert, positive electrode, the chlorate is reduced, and insoluble Li_2O precipitates. A protective, self-healing film is supposed to form on the lithium and prevent the chlorate from reacting there. (If it does not, there is a sharp explosion. This would undoubtedly be very dangerous if significant amounts of reactants were present. Remember that any high-energy, high-power battery is a potential bomb.) Thermochemical data and molar mass of some presumably relevant materials are given in the following table:

	μ_i^0 or μ_i^θ (kJ/mol)	M_i (g/mol)
Li	0.0	6.939
Li^+	0.0	6.939
$LiClO_3$	188.2	72.67
Cl^-	−383.7	17.73
Li_2O	−560.2	29.88

Obtain an expression for the open-circuit potential of this cell. Obtain a numerical value for the standard-cell potential (being sure that you have properly defined the quantity you report). Obtain a numerical value for the theoretical specific energy of this system. Here inert materials such as the solvent, the inert positive, the container, and the current collectors are excluded from the weight in computing this *theoretical* value. Express the specific energy in W-h/kg.

2.19 The electrolyte in a cell has a nearly uniform composition of 2.5 mol/kg of NaCl and 0.2 mol/kg of NaOH. If hydrogen is to be evolved at a left electrode, what minimum cell potential would need to be applied to produce a solution 0.01 mol/kg in chlorate ion at a right electrode? Both electrodes are made of an inert metal. Some thermodynamic data (at 25°C) are given below.

Species	Quantity tabulated	kJ/mol
ClO_3^-	$RT \ln \lambda_i^\theta$	−7.95
Cl^-	$RT \ln \lambda_i^\theta$	−131.228
H^+	$RT \ln \lambda_i^\theta$	0
Na^+	$RT \ln \lambda_i^\theta$	−261.905
OH^-	$RT \ln \lambda_i^\theta$	−157.244
H_2O	μ_0^0	−237.129
O_2	μ_i^*	0
Cl_2	μ_i^*	0
H_2	μ_i^*	0

2.20 Chlorate ions may actually be produced as a by-product of chlorine production by homogeneous reaction of dissolved chlorine with hydroxyl ions.

(a) Give a balanced chemical reaction by which chlorate ions might be produced under these conditions.

(b) Sketch concentration profiles of the relevant species in a diffusion layer near the anode. Assume that the bulk concentration of hydroxyl ions is about 0.001 mol/kg and that the solution near the anode is saturated with chlorine, whose solubility is modest—certainly no larger than 0.001 mol/kg.

(c) From the thermodynamic information given below, estimate the solubility of chlorine in pure water at 25°C.

(d) From the thermodynamic information given below, estimate the equilibrium concentration of chlorate ions if a solution initially 2.5 mol/kg in NaCl and 0.001 mol/kg in NaOH is contacted with Cl_2 maintained at a partial pressure of 1 atm.

Species	Quantity tabulated	kJ/mol
Cl_2	μ_i^*	0
Cl_2	$RT \ln \lambda_i^\theta$	6.94
ClO_3^-	$RT \ln \lambda_i^\theta$	−7.95
OH^-	$RT \ln \lambda_i^\theta$	−157.244
Cl^-	$RT \ln \lambda_i^\theta$	−131.228
Na^+	$RT \ln \lambda_i^\theta$	−261.905
H^+	$RT \ln \lambda_i^\theta$	0
H_2O	μ_i^0	−237.129
Na	μ_i^0	0
O_2	μ_i^*	0
H_2	μ_i^*	0

2.21 A proposed battery has a negative electrode of lithium undergoing dissolution and a positive electrode of MnO_2, which is reduced to Mn_3O_4 according to the reaction

$$3MnO_2 + 4Li^+ + 4e^- \rightleftharpoons Mn_3O_4 + 2Li_2O.$$

Estimate the open-circuit cell potential from the following thermodynamic data at 25°C:

Substance	$\widetilde{H}_i^0$ (kJ/mol)	μ_i^0 (kJ/mol)
MnO_2	−520.03	−465.14
Mn_2O_3	−959.0	−881.1
Mn_3O_4	−1387.8	−1283.2
Li	0	0
Li_2O	−597.94	−561.18

2.22 Lead dioxide, PbO_2, is the active material for the positive electrode of the lead acid battery. This material covers and protects a lead grid, which is used as a current collector. Pb and PbO_2 are both electronic conductors; however, they should be able to react to produce PbO, an ionic

conductor in which O^{2-} ions can be regarded as the charge carrier. Thus, we have an interest in the solid-state electrochemical cell

$$\begin{array}{c|c|c|c|c} \beta & \lambda & \delta & \beta' \\ \mathrm{Pb} & \mathrm{PbO} & \mathrm{PbO_2} & \mathrm{Pb.} \end{array}$$

The reaction at the right electrode is

$$\mathrm{PbO_2} + 2e^- \rightleftharpoons \mathrm{PbO} + O^{2-}.$$

Develop an expression or expressions for the open-circuit potential U of this cell. Obtain a numerical value for U at 25°C on the basis of the following thermochemical data:

Chemical formula	State	$\widetilde{H}_i^0$ (kJ/mol)	μ_i^0 (kJ/mol)	$\widetilde{C}_p^0$ (J/mol·K)
Pb	cr	0	0	26.44
PbO	Yellow	−217.32	−187.89	45.77
PbO_2	cr	−277.4	−217.33	64.64

2.23 A Pourbaix diagram is a plot of electrode potential versus pH. It is used to display thermodynamic information and is helpful in understanding corrosion and other electrochemical processes. It is a form of a phase diagram. The oxygen and hydrogen lines are usually shown to indicate the range of stability of the solvent. The oxygen line extends from 1.229 V at a pH of 0 to 0.401 V at a pH of 14. The hydrogen line extends from 0 V at a pH of 0 to −0.828 at a pH of 14.

Show where to place ranges of stability for Fe^{3+}, Fe^{2+}, and Fe. Also deal with Cu^{2+}, Cu^+, and Cu. Show your reasoning. Deal only with the low pH range, where oxides and hydroxides do not precipitate. The following values of standard electrode potentials may be useful.

Reaction	U^θ (V)
$Cu^+ \rightarrow Cu^{2+} + e^-$	0.153
$Cu \rightarrow Cu^{2+} + 2e^-$	0.337
$Cu \rightarrow Cu^+ + e^-$	0.521
$Fe^{2+} \rightarrow Fe^{3+} + e^-$	0.771
$Fe \rightarrow Fe^{2+} + 2e^-$	−0.440
$Fe \rightarrow Fe^{3+} + 3e^-$	−0.016

NOTATION

a_i	relative activity of species i
a_i^θ	property expressing secondary reference state, liter/mol
A	Helmholtz free energy, J
c	molar concentration of a single electrolyte, mol/liter
c_i	molar concentration of species i, mol/liter

f_i	molar activity coefficient of species i
f_{+-}	mean molar activity coefficient of an electrolyte
F	Faraday's constant, 96,487 C/mol
G	Gibbs free energy, J
H	enthalpy, J
$\mathbf{i}$	current density, A/cm^2
I	ionic strength, mol/kg
K_{sp}	solubility product of sparingly soluble salt, mol^2/kg^2
K_w	dissociation constant for water, mol^2/kg^2
m	molality of a single electrolyte, mol/kg
m_i	molality of species i, mol/kg
M_i	symbol for the chemical formula of species i
M_i	molar mass of species i, g/mol
n	number of electrons involved in electrode reaction
n_i	number of moles of species i, mol
p	pressure, N/cm^2
p_i	fugacity of species i, bar
R	universal gas constant, 8.3143 J/mol·K
s_i	stoichiometric coefficient of species i in an electrode reaction
S	entropy, J/K
t_i^0	transference number of species i with respect to the velocity of species 0
T	absolute temperature, K
U	open-circuit cell potential, V
U	internal energy, J
V	volume, cm^3
$\overline{V}_i$	partial molar volume of species i, cm^3/mol
w	work of transfer, J/mol
z_i	charge number of species i
α	Debye–Hückel constant, (kg/mol)$^{1/2}$
γ_i	molal activity coefficient of species i
γ_{+-}	mean molal activity coefficient of an electrolyte
κ	conductivity, S/cm
λ_i	absolute activity of species i
λ_i^θ	property expressing secondary reference state, kg/mol
μ_i	electrochemical potential of species i, J/mol
ν	number of moles of ions into which a mole of electrolyte dissociates
ν_+, ν_-	numbers of cations and anions into which a mole of electrolyte dissociates
ρ	density, g/cm^3
ρ_0	density of pure solvent, g/cm^3
τ_i^0	transport number of neutral species i with respect to the velocity of the species 0.
ϕ	osmotic coefficient
Φ	electric potential, V

Superscripts

0	pure state
0	relative to velocity of species 0
θ	secondary reference state at infinite dilution
*	ideal-gas secondary reference state

Subscripts

0	solvent
+	cation
−	anion

REFERENCES

1. E. A. Guggenheim, "The Conceptions of Electrical Potential Differences Between Two Phases and the Individual Activities of Ions," *Journal of Physical Chemistry*, *33* (1929), 842–849.
2. E. A. Guggenheim, *Thermodynamics* (Amsterdam: North-Holland, 1959).
3. Gilbert Newton Lewis, Merle Randall, Kenneth S. Pitzer, and Leo Brewer, *Thermodynamics* (New York: McGraw-Hill, 1961), pp. 313 and 300.
4. V. Vitagliano and P. A. Lyons, "Diffusion in Aqueous Acetic Acid Solutions," *Journal of the American Chemical Society*, *78* (1956), 4538–4542.
5. W. H. Smyrl and C. W. Tobias, "The Effect of Diffusion of a Sparingly Soluble Salt on the EMF of a Cell without Transference," *Electrochimica Acta*, *13* (1968), 1581–1589.
6. William H. Smyrl and John Newman, "Potentials of Cells with Liquid Junctions," *Journal of Physical Chemistry*, *72* (1968), 4660–4671.
7. D. E. Fenton, J. M. Parker, and P. V. Wright, "Complexes of Alkali-Metal Ions with Poly(ethylene oxide)," *Polymer*, *14* (1973), 589.
8. S. Lascaud, M. Perrier, A. Vallee, S. Besner, J. Prud'homme, and M. Armand, "Phase Diagrams and Conductivity Behavior of Poly(ethylene oxide)-Molten Salt Rubbery Electrolytes," *Macromolecules*, *27* (1994), 7469–7477.
9. Yanping Ma, Marc Doyle, Thomas F. Fuller, Marca M. Doeff, Lutgard C. De Jonghe, and John Newman, "The Measurement of a Complete Set of Transport Properties for a Concentrated Solid Polymer Electrolyte Solution," *Journal of the Electrochemical Society*, *142* (1995), 1859–1869.
10. Danielle M. Pesko, Ksenia Timachova, Rajashree Bhattacharya, McKenzie C. Smith, Irune Villaluenga, John Newman, and Nitash P. Balsara, "Negative Transference Numbers in Poly(ethylene oxide)-based Electrolytes," *Journal of the Electrochemical Society*, *164* (2017), E3569–E3575. **DOI**: 10.1149/2.0581711jes
11. Irune Villaluenga, Danielle M. Pesko, Ksenia Timachova, Zhange Feng, John Newman, Venkat Srinivasan, and Nitash P. Balsara, "Negative Stefan-Maxwell Diffusion Coefficients and Complete Electrochemical Transport Characterization of Homopolymer and Block Copolymer Electrolytes," *Journal of the Electrochemical Society*, *165* (2018), A2766–A2773. **DOI**: 10.1149/2.0641811jes
12. Wendell M. Latimer, *The Oxidation States of the Elements and Their Potentials in Aqueous Solutions* (Englewood Cliffs, NJ: Prentice-Hall, 1952). Note that Latimer reports $\Phi_{H_2|H^+} - \Phi_{electrode}$, which is opposite to the international sign convention used in this text.
13. Donald W. Wagman, William H. Evans, Vivian B. Parker, Richard H. Schumm, Iva Halow, Sylvia M. Bailey, Kenneth L. Churney, and Ralph L. Nuttall, "The NBS Tables of Chemical Thermodynamic Properties," *Journal of Physical and Chemical Reference Data*, *11* (1982), supplement 2.
14. Marcel Pourbaix, *Atlas of Electrochemical Equilibria in Aqueous Solutions* (Houston: National Association of Corrosion Engineers, 1974).
15. The chemistry of zinc is actually more complicated; several zinc oxide and hydroxide species exist but have been omitted here for clarity. For more details see James McBreen and Elton J. Cairns, "The Zinc Electrode," in Heinz Gerischer and Charles W. Tobias, eds., *Advances in Electrochemistry and Electrochemical Engineering*, Vol. *11* (New York: Wiley, 1978), pp. 273–352.

CHAPTER 3

THE ELECTRIC POTENTIAL

In Chapter 2, we discuss the thermodynamics of electrochemical cells without the introduction of electric potentials except the potential difference between two phases of identical composition, namely the terminals of the cell. Much of the electrochemical literature is written in terms of electrical potentials of various kinds, and it is necessary to set our minds straight on these matters and to investigate how potentials might be used in electrochemistry. Much of the confusion in electrochemistry arises from uncertainty in the use of these concepts.

3.1 THE ELECTROSTATIC POTENTIAL

Electrostatic theory deals with purely electrical forces between bodies and not with any specific chemical forces such as exist between molecules. The systems treated are usually macroscopic bodies separated by a vacuum, and the specific forces are not important. For this reason, the concepts developed in electrostatic theory are not directly applicable to energetic relationships within condensed phases.

The electric force f between two bodies of charges q_1 and q_2, separated by a distance r, is given by Coulomb's law

$$f = \frac{q_1 q_2}{4\pi\epsilon r^2}\,, \tag{3.1}$$

where ϵ is the permittivity of the medium surrounding the bodies. The force is directed along the line joining the bodies and is repulsive if the two charges are of the same sign and attractive if the charges are of opposite sign.

The permittivity ϵ_0 of a vacuum has the value $\epsilon_0 = 8.8542 \times 10^{-14}$ F/cm $= 8.8542 \times 10^{-14}$ C/V·cm. If the bodies are immersed in a dielectric medium composed of polarizable matter, the force between them will be different from that in a vacuum. The ratio ϵ/ϵ_0 is called the relative dielectric constant of the medium. For water, the value of this ratio is 78.303 at 25°C.

Electrochemical Systems, Fourth Edition. John Newman and Nitash P. Balsara.

The force on a body is the sum of the forces exerted on it by all the other bodies in the system. For the development of the theory, it is convenient to define the electric field **E** so that the electric force acting on a charge q is given by

$$\mathbf{f} = q\mathbf{E}. \tag{3.2}$$

The electric field is defined at all points in the medium by supposing that a *test* charge q can be introduced to test the force, and hence the electric field **E** by means of equation 3.2, without disturbing the other charges comprising the system.

In this manner, it is possible to obtain differential equations describing the variation of the electric field. For example, the curl of the electric field is zero:*

$$\nabla \times \mathbf{E} = 0. \tag{3.3}$$

This allows us to introduce the electrostatic potential Φ, so that the electric field can be expressed as the negative gradient of this scalar quantity:

$$\mathbf{E} = -\nabla\Phi. \tag{3.4}$$

This is permissible since the curl of the gradient of any scalar field is zero:

$$\nabla \times \nabla\Phi = 0. \tag{3.5}$$

The variation in the electric field is also related to the charge distribution in the system by Poisson's equation

$$\nabla \cdot (\epsilon\mathbf{E}) = -\nabla \cdot (\epsilon\nabla\Phi) = \rho_{\mathrm{e}}, \tag{3.6}$$

where ρ_e is the electric charge density per unit volume. For a medium of uniform dielectric constant, this is equivalent to the expression of the electrostatic potential in terms of the charges:

$$\Phi(\mathbf{r}) = \sum_i \frac{q_i}{4\pi\epsilon|\mathbf{r} - \mathbf{r}_i|}, \tag{3.7}$$

where the sum includes all the charges in the system.

Equation 3.6 provides a differential equation for the determination of the electrostatic potential in terms of the charge distribution. For a medium of uniform dielectric constant, this becomes

$$\nabla^2\Phi = -\frac{\rho_{\mathrm{e}}}{\epsilon}, \tag{3.8}$$

*Equation 3.3 is an approximate form of one of Maxwell's equations. The full set is

$$\nabla \times \mathbf{H} = \frac{\partial \mathbf{D}}{\partial t} + \mathbf{i},$$
$$\nabla \times \mathbf{E} = -\frac{\partial \mathbf{B}}{\partial t},$$
$$\nabla \cdot \mathbf{D} = \rho_{\mathrm{e}},$$
$$\nabla \cdot \mathbf{B} = 0,$$

where, approximately, $\mathbf{D} = \epsilon\mathbf{E}$ and $\mathbf{B} = \mu\mathbf{H}$. See Ref. [1].

and in a medium with no free charges, it reduces to Laplace's equation

$$\nabla^2\Phi = 0. \tag{3.9}$$

At the interface between two phases, the tangential component of the electric field is continuous. The relationship between the normal components of the electric field in the two phases can be obtained by applying equation 3.6 to a ***pill box*** enclosing a portion of the interface (see Figure 3.1). We include the possibility that the surface charge density at the interface is not zero. By means of the divergence theorem, equation 3.6 can be written in terms of integrals over the surface and the volume of an arbitrary region:

$$\oint \epsilon \mathbf{E} \cdot \mathbf{dS} = \int \rho_e dV. \tag{3.10}$$

This is an expression of Gauss's law, which says that the integral of the outward normal component of $\epsilon\mathbf{E}$ over the surface of a closed region is equal to the charge enclosed. Application of this result to the interface in Figure 3.1 gives the relationship between the normal components of the electric field:

$$\epsilon_1 E_{n1} - \epsilon_2 E_{n2} = \sigma, \tag{3.11}$$

where σ is the charge per unit area at the interface.

A considerable body of electrostatic theory has been developed,[1–3] concerned with the solution of equations 3.8 and 3.9 for a variety of geometries and boundary conditions. We have not discussed the magnetic effects that arise when the electric field varies in time and electric currents are present.

We conclude this section with an example. Consider two metal spheres, each 1 cm in radius and with a distance of 10 cm between their centers (see Figure 3.2). We want to charge each sphere to an average of 10 μC/cm^2 by transporting 125.7 μC or 1.3×10^{-9} mol of electrons from one sphere to the other. The capacity of this system should be about 0.618×10^{-12} F. Hence, we can estimate that the final potential difference between the spheres will be 2.04×10^8 V.

This example shows that large potentials are required to effect a modest separation of electrical charge.

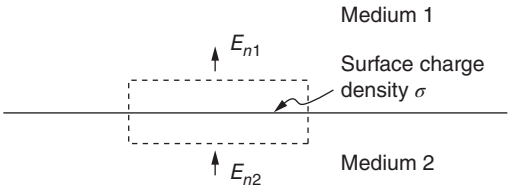

Figure 3.1 Normal components of the electric field at an interface. The interface may have a charge σ per unit area.

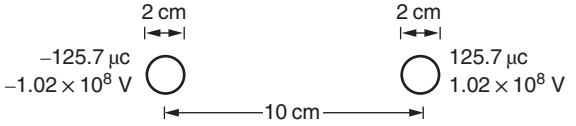

Figure 3.2 Potential difference between two metal spheres for an average surface charge of 10 μC/cm^2.

3.2 INTERMOLECULAR FORCES

The intermolecular potential energy relation for two ions is given an idealized representation in Figure 3.3. The corresponding intermolecular force is shown in Figure 3.4. The noteworthy feature of these interactions is how slowly they go to zero at large distances of separation.

$$\left.\begin{aligned} f &= \frac{q_1 q_2}{4\pi\epsilon r^2} \\ w &= \int_r^\infty f \; dr = \frac{q_1 q_2}{4\pi\epsilon r} \end{aligned}\right\} \quad \text{as} \quad r \to \infty. \tag{3.12}$$

Because they obey the Coulomb force law at large distances, they are called *ions*, to distinguish them from neutral nonpolar molecules or neutral polar molecules, for which the interaction energy is

$$w = \frac{-\text{constant}}{r^6} \quad \text{as} \quad r \to \infty. \tag{3.13}$$

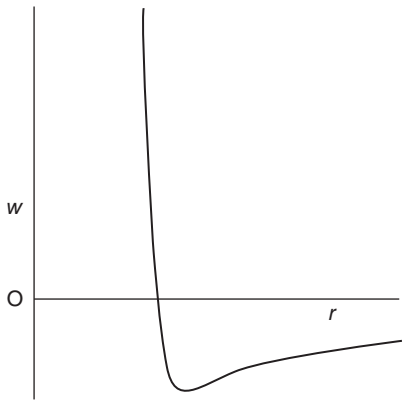

Figure 3.3 Intermolecular potential energy for two ions at a distance r apart.

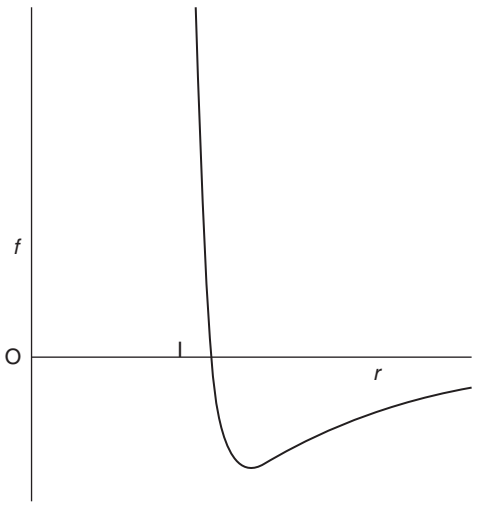

Figure 3.4 Intermolecular force between two ions.

At close distances of approach, the interionic interaction depicted in Figures 3.3 and 3.4 departs from equations 3.12. Since the nature of this deviation at short distances depends on the specific nature of the ions, this deviation is sometimes referred to as the *short-range specific interaction force*. Of course, the decomposition of the single curves of Figures 3.3 and 3.4 into coulombic parts and specific-interaction parts is artificial. It is the intermolecular interaction itself that determines the behavior of ions.

The asymptotic behavior expressed by equations 3.12 is sufficiently common and causes such difficulties as to warrant a special treatment. A large body of knowledge included in electrostatic and electromagnetic theory has been developed to deal with coulombic interactions. This involves, for example, the electrostatic potential given by equation 3.7.

The results and methods of electrostatic theory can be applied most directly to dilute, ionized gases. The restriction to a dilute, ionized gas is useful for two reasons:

1. There is a large fraction of free space, and we can imagine inserting a probe among the ions without actually disturbing them. In a condensed phase, on the other hand, all space is occupied.
2. All the ions are widely separated, so that an ion interacts at close range with no more than one other ion at a time. This close range interaction can be called a *collision*. A nonionized gas can be treated by consideration of binary interactions or binary collisions.[4] In an ionized gas where the inverse square law applies, an ion interacts at all times with all other ions in the system. Some progress can be made by introducing an electric potential that accounts for interactions between distant ions. A binary collision is then an interaction with another ion at small distances where the coulombic force law no longer holds, and this can be treated separately.

Even in this case, however, it remains a fact that the separation of the intermolecular force law into different parts, say, an electric part and a specific chemical part, is without any physical basis. The same difficulty arises in attempts to separate electrochemical potentials, used in Chapter 2, into chemical potentials and electric potentials.

The electrostatic theory can be modified somewhat to handle condensed phases that involve a dilute dispersion of charged particles in an otherwise uniform, dielectric medium. In this case, the electric field due to the charged particles induces dipoles in the dielectric medium or causes a preferential orientation of permanent dipoles. The presence of all these charges induced in the medium can be accounted for by introducing an averaged electric field and an averaged electrostatic potential. The sum in equation 3.7 then extends over the permanently charged particles but not over the charges induced in the dielectric medium. The average of $\mathbf{E}$ and Φ is taken over spatial regions of at least molecular dimensions and accounts for the dipole charges not included in the sum by the use of the permittivity ϵ of the dielectric medium rather than the permittivity ϵ_0 of free space.

This treatment of a condensed phase can be justified only when the charged particles are so far apart that the coulombic interaction applies, just as for a dilute, ionized gas. Also, there should be enough dielectric between charged particles to permit the averaging. Thus, both Φ and ϵ are macroscopic concepts, and it is not meaningful to discuss variations of Φ and ϵ over distances of molecular dimensions. The evaluation of the energy required to move a charged particle from one phase to another requires, in addition, consideration of the energy of interaction with the dielectric solvent and the nature of the charge distribution near the interface.

Although concentrated ionic solutions defy exact treatment on an electrostatic basis, the coulombic inverse square law has many important consequences. For example, the coulombic attraction between charges is so strong that large departures from electrical neutrality are precluded in electrolytic solutions. This conclusion remains valid even though the interionic forces depart from Coulomb's law at small distances.

The electrostatic model of a dilute dispersion of charged particles in a dielectric medium is applied fruitfully in the theory of Debye and Hückel for the activity coefficients of extremely dilute electrolytic solutions. Although the result and the model are applicable only in the limit of infinite dilution, the strong departures from ideal-solution behavior can be clearly attributed to the inverse square law governing the force between ions at large distances. The same model can be applied to determine the consequences of these long-range forces on other properties of the solution, notably the conductivity, at high dilutions.

Long-range forces are also important in electrode reactions. In a nonequilibrium double layer, there can be extremely large forces acting on an ion; and one is led to say that there is a very large gradient of potential in the double layer at an electrode surface even though the rigorous definition of this potential may be difficult.

3.3 OUTER AND INNER POTENTIALS

The *outer* potential, also called the *cavity* or *Volta* potential, is frequently used in electrochemistry. It is defined in terms of the energy required to move a charged particle from a point just outside one phase to a point just outside another phase:

$$w_i = z_i F(\Phi^\beta - \Phi^\alpha). \tag{3.14}$$

In order to avoid the influence of external fields, it is imagined that the charged particle is moved from a macroscopic cavity in one phase to a macroscopic cavity in the other phase (see Figure 3.5), and this is the origin of the term *cavity potential*.

By moving the particle only to a point *outside* each phase, only the long-range forces of charges in that phase are able to act on the test particle; the short-range, specific forces are not encountered. For this reason, the outer potential is independent of the ion type used for the test particle. Differences in outer potentials are measurable since they are differences in the potential of two points in a phase of uniform composition, namely the external medium. However, the accurate measurement of differences in outer potentials is a difficult experimental undertaking. Outer potentials can be used to characterize the electrical state of a phase, but they do not have any direct thermodynamic relevance and require difficult experimental measurements that are not necessary for any thermodynamic discussion.

The *inner* potential, also called the *Galvani* potential, relates to the energy required to move an idealized charged particle to a point *inside* a phase. It is generally conceded that inner potentials are not measurable, and they do not need to occupy our attention further. The difference between the inner potential and the outer potential is called the *surface* potential, another unmeasurable quantity.

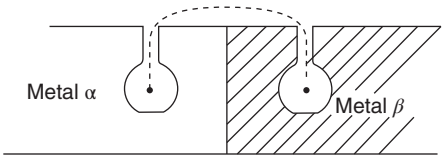

Figure 3.5 Movement of a charged particle from a cavity in one phase to a cavity in another phase. This thought experiment is used to define the Volta potential and the contact potential difference between two metals.

3.4 POTENTIALS OF REFERENCE ELECTRODES

From a practical point of view, the potential that is measured in an electrochemical system in order to assess the electrical state of part of the system is that of a reference electrode. For our present discussion, we mean an electrode that can be inserted directly into the solution at any point. In particular, we exclude reference electrodes that are in a separate vessel and connected to the point in question by a capillary probe, unless the solution in the capillary probe and the auxiliary vessel is of the same composition as the solution at the point where we intend to insert the probe. This restriction is imposed in order to avoid the uncertainties associated with liquid junctions. In practical measurements, this restriction cannot always be observed. Reference electrodes are discussed in more detail in Chapter 5.

A reference electrode should behave reversibly with respect to one of the ions in the solution. The material presented in Chapter 2 shows that the reference electrode will provide, in essence, a measure of the electrochemical potential of that ion. Figure 3.6 shows how Ag–AgCl electrodes might be used to measure the potential difference between two solutions. Equation 2.112 indicates that the measured potential difference is related to the difference in electrochemical potential of chloride ions between the two points α and β:

$$-F(\Phi^{\alpha} - \Phi^{\beta}) = \mu^{\alpha}_{Cl^-} - \mu^{\beta}_{Cl^-}. \tag{3.15}$$

In Figure 3.7, the two reference electrodes are placed in the same vessel. By moving electrode α in the solution, one can investigate the spatial variation of the electrochemical potential of chloride ions even though the concentration of electrolyte is not uniform and a current passes between the two working electrodes.

Reference electrodes provide the most convenient means for assessing the electrical state of an electrolytic solution.

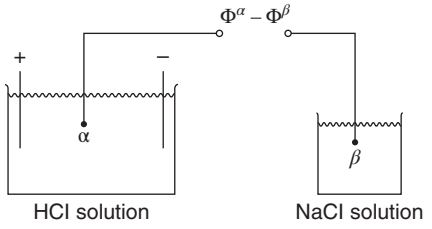

Figure 3.6 Use of reference electrodes to investigate the potential in a solution. Silver–silver chloride reference electrodes are represented by α and β. The vessel on the left also contains two working electrodes.

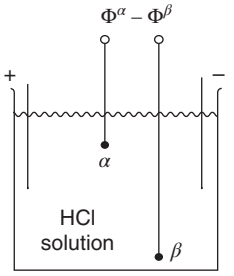

Figure 3.7 Use of reference electrodes to investigate potential variations within a solution.

3.5 THE ELECTRIC POTENTIAL IN THERMODYNAMICS

The potential sought in thermodynamics is one related to the energy required for the *reversible* transfer of ions from one phase to another. This, of course, is the electrochemical potential of an ionic species. The electrostatic potential, aside from the problems involved in its definition in condensed phases, is not directly related to reversible work. Although the electrostatic potential can be avoided in thermodynamics, electrochemical potentials being used in its stead, there does remain a need to characterize the electrical state of a phase.

Frequently, the electrochemical potential of an ionic species is split into an electrical term and a "chemical" term,

$$\mu_i = \mu_i^{\text{chem}} + z_i F\Phi = RT \ln \lambda_i^{\theta} m_i \Gamma_i + z_i F\Phi, \tag{3.16}$$

where Φ is the "electrostatic" potential and Γ_i, is an activity coefficient that now is supposed to be independent of the electrical state of the phase. We should first note that this decomposition is not necessary, since the relevant formulas of thermodynamic significance have already been derived in Chapter 2.

The electrostatic potential Φ could be defined so that it is measurable or unmeasurable. Depending upon how well defined Φ is, so Γ_i is just as well or poorly defined. It is possible to proceed with only a vague concept of the electrostatic potential, as supplied by electrostatic theory, and never bother to define carefully just what is meant. If the analysis is consistent, physically meaningful results can be obtained by recombining poorly defined terms at the end of the analysis.

Any definition of Φ that is chosen should satisfy one condition. It should reduce to the definition 2.9 used for the difference in electric potential between phases of identical composition. Thus, if α and β are phases of identical composition, then

$$\mu_i^{\alpha} - \mu_i^{\beta} = z_i F(\Phi^{\alpha} - \Phi^{\beta}). \tag{3.17}$$

The potential Φ, thus, provides a quantitative measure of the electrical state of one phase relative to a second phase of identical composition. Several possible definitions of Φ satisfy this condition.

The outer potential, which is measurable in principle, can be used for Φ. It has the disadvantages of difficulty of measurement and lack of relevance in thermodynamic calculations. It has the advantage of giving a definite meaning to Φ, and, at the end of the analysis, its definition cancels out so that its value need never be actually measured.

A second possibility is to use the potential of a suitable reference electrode. Since the reference electrode is reversible to an ion in the solution, this is equivalent to using the electrochemical potential of an ion, or $\mu_i/z_i F$. The arbitrariness of this definition is apparent from the need to select a particular reference electrode or ionic species for the definition. This choice has the added disadvantage that μ_i is equal to minus infinity for a solution in which this ionic species is absent. Thus, it does not conform to our usual concept of an electrostatic potential; this is because μ_i relates to reversible work. This choice of the potential does have the advantage of being related to a measurement, with reference electrodes, commonly made in electrochemistry.

A third possibility should occupy our attention here. Select an ionic species n and define the quasi-electrostatic potential Φ as follows:

$$\mu_n = RT \ln c_n + z_n F\Phi. \tag{3.18}$$

Then, the electrochemical potential of any other species can be expressed as

$$\mu_i = RT \ln c_i + z_i F\Phi + RT\left(\ln f_i - \frac{z_i}{z_n} \ln f_n\right) + RT\left(\ln a_i^{\theta} - \frac{z_i}{z_n} \ln a_n^{\theta}\right). \tag{3.19}$$

One should recognize that the combinations of f_i's and a_i^{θ}'s in parentheses are well defined and independent of the electrical state, according to the rules laid down in Section 2.3. At constant temperature, the gradient of the electrochemical potential is then

$$\nabla\mu_i = RT\nabla \ln c_i + z_i F\nabla\Phi + RT\nabla\left(\ln f_i - \frac{z_i}{z_n}\ln f_n\right). \tag{3.20}$$

(In certain applications it will be more natural to use molalities or mole fractions (c_i/c_T; see Section 12.3) in the definition of the quasi-electrostatic potential.)

The arbitrariness of this definition of Φ is again apparent from the need to select a particular ionic species n. This definition of Φ has the advantage of being related unambiguously to the electrochemical potentials and it conforms to our usual concept of an electrostatic potential. It can be used in a solution of vanishing concentration of species n because of the presence of the term $RT \ln c_n$ in equation 3.18.

In the limit of infinitely dilute solutions, the activity-coefficient terms in equations 3.19 and 3.20 disappear due to the choice of the secondary reference state 2.19. In this limit, the definition of Φ becomes independent of the choice of the reference ion n. This forms the basis of what should be termed the *dilute-solution theory* of electrolytic solutions. At the same time, equations 3.19 and 3.20 show how to apply activity-coefficient corrections to dilute-solution theory without the utilization of the activity coefficients of individual ions. In infinitely dilute solutions, the lack of dependence on the ion type n is related to the ability to measure differences in electric potential between phases of identical composition. Such solutions are of essentially the same composition in the sense that an ion in solution is subject only to interactions with the solvent, and even the long-range electrical interactions with other ions are not felt. This concept becomes practically useful in semiconductor electrodes (see Chapter 23).

The introduction of such an electric potential is useful in the calculation of transport processes in electrolytic solutions.[5] Smyrl and Newman use the term *quasi-electrostatic potential* for the potential so defined.

We have discussed here possible ways of using the electric potential in electrochemical thermodynamics. The use of the potential in transport theory is basically the same as its use in thermodynamics. By using electrochemical potentials, it is possible to avoid the electric potential, although its introduction may be useful or convenient. In the kinetics of electrode processes, it is possible to use a Gibbs energy change as a driving force for the reaction. This is equivalent to the use of the surface overpotential defined in Section 1.3.

An electric potential also finds use in microscopic models, such as the Debye–Hückel theory alluded to earlier and developed in the next chapter. Such a potential cannot always be defined with rigor. A clear distinction should always be made between macroscopic theories—such as thermodynamics, transport phenomena, and fluid mechanics—and microscopic theories—such as statistical mechanics and the kinetic theory of gases and liquids. Microscopic theories explain the behavior of, predict the values of, and provide means to correlate macroscopic properties, such as activity coefficients and diffusion coefficients, on the basis of molecular or ionic properties. Quantitative success is seldom achieved without some additional empiricism. The macroscopic theories, on the other hand, provide both the framework for the economical measurement and tabulation of macroscopic properties and the means for using these results to predict the behavior of macroscopic systems.

NOTATION

α_i^{θ}	property expressing secondary reference state, liter/mol
$\mathbf{B}$	magnetic induction, V·s/cm^2
c_i	concentration of species i, mol/liter
$\mathbf{D}$	electric displacement, C/cm^2
$\mathbf{E}$	electric field, V/cm

f	force, J/cm
f_i	molar activity coefficient of species $\boldsymbol{i}$
F	Faraday's constant, 96,487 C/mol
$\mathbf{H}$	magnetic field strength, A/cm
m_i	molality of species i, mol/kg
q	electric charge, C
$\boldsymbol{r}$	distance or position, cm
R	universal gas constant, 8.3143 J/mol·K
S	surface area, cm^2
T	absolute temperature, K
V	volume, cm^3
w	work or interaction energy
$z_{\boldsymbol{i}}$	charge number of species $\boldsymbol{i}$
Γ_i	activity coefficient
ϵ	permittivity, F/cm
ϵ_0	permittivity of free space, 8.8542×10^{-14} F/cm
λ_i^{θ}	property expressing secondary reference state, kg/mol
μ	magnetic permeability, $\Omega \cdot \text{s/cm}$
μ_i	electrochemical potential of species $\boldsymbol{i}$, J/mol
ρ_e	electric charge density, C/cm^3
σ	surface charge density, C/cm^2
Φ	electric potential, V

REFERENCES

1. John David Jackson, *Classical Electrodynamics*, 2nd ed. (New York: Wiley, 1975).
2. James Clerk Maxwell, *A Treatise on Electricity and Magnetism*, Vol. *I* (Oxford: Clarendon Press, 1892).
3. K. J. Binns and P. J. Lawrenson, *Analysis and Computation of Electric and Magnetic Field Problems* (New York: Macmillan, 1963).
4. Sydney Chapman and T. G. Cowling, *The Mathematical Theory of Non-uniform Gases* (Cambridge: University Press, 1939).
5. William H. Smyrl and John Newman, "Potentials of Cells with Liquid Junctions," *Journal of Physical Chemistry*, *72* (1968), 4660–4671.

CHAPTER 4

ACTIVITY COEFFICIENTS

Due to long-range coulombic interactions between ions, the activity coefficients of electrolytes in dilute solutions behave differently from those of nonelectrolytes, as explained by the electrostatic theory of Debye and Hückel. This theory forms the basis for the empirical correlation of activity coefficients over a range of concentration, including the activity coefficients of solutions of several electrolytes.

4.1 IONIC DISTRIBUTIONS IN DILUTE SOLUTIONS

When an electrolyte dissolves in a solvent, it dissociates into cations and anions; this is the source of the electrical conductivity of the solution. This dissociation also manifests itself in the thermodynamic properties of the solution, as discussed in Section 2.3. For example, it leads to the presence of the factor ν in equation 2.28, and it is responsible for the large freezing-point depression and vapor-pressure lowering of solutions of electrolytes.

The distribution of ions is not completely random even in dilute solutions because of the attractive and repulsive electrical forces between ions. Consequently, the thermodynamic properties show further departures from those of nonelectrolytic solutions. Debye and Hückel[1] used an electrostatic model to describe these ionic distributions quantitatively.

Suppose that an ion of valence z_c is at the origin of coordinates. Ions of opposite charge to this *central ion* will be attracted toward the origin, and ions of like sign will be repelled. Random thermal motion of the ions and the solvent molecules tends to counteract this electric effect and promote a random distribution of ions. The balance of these competing effects can be expressed by a Boltzmann distribution of ionic concentrations:

$$c_i = c_{i\infty} \exp\left(-\frac{z_i F \Phi}{RT}\right), \tag{4.1}$$

where $c_{i\infty}$ is the average concentration of species i and Φ is the electrostatic potential established around the central ion. The electrical interaction energy per mole is expressed as $z_i F \Phi$, and other

Electrochemical Systems, Fourth Edition. John Newman and Nitash P. Balsara.

contributions to the interaction energy are ignored. Far from the central ion, the potential Φ approaches zero, and, consequently, c_i approaches $c_{i\infty}$.

The potential Φ results not only from the central ion but also from other ions that are attracted toward or repelled from the origin. Its distribution is governed by Poisson's equation 3.8

$$\nabla^2\Phi = -\frac{\rho_e}{\epsilon} = -\frac{F}{\epsilon}\sum_i z_i c_i. \tag{4.2}$$

In a solution at equilibrium, radial symmetry prevails. In spherical coordinates, with the central ion at the origin, equation 4.2 becomes

$$\frac{1}{r^2}\frac{d}{dr}\left(r^2\frac{d\Phi}{dr}\right) = -\frac{\rho_e}{\epsilon} = -\frac{F}{\epsilon}\sum_i z_i c_{i\infty}\exp\left(-\frac{z_i F\Phi}{RT}\right). \tag{4.3}$$

The centers of other ions are supposed to be precluded from approaching within a distance a of the central ion because of the short-range repulsive forces. Thus equation 4.1 and hence equation 4.3 applies only for $r > a$. The boundary condition at $r = a$ can be found by applying Gauss's law 3.10 to the region within $r = a$:

$$\frac{d\Phi}{dr} = -\frac{z_c e}{4\pi\epsilon a^2} \quad \text{at} \quad r = a. \tag{4.4}$$

This is equivalent to the statement that the charge distribution around the central ion exactly counterbalances the charge on that ion. Thus, integration of equation 4.3 from a to ∞ gives

$$r^2\left.\frac{d\Phi}{dr}\right|_a^\infty = -\int_a^\infty \frac{\rho_e r^2}{\epsilon}\,dr \tag{4.5}$$

$$\int_a^\infty \rho_e 4\pi r^2\,dr = 4\pi\epsilon a^2\left.\frac{d\Phi}{dr}\right|_{r=a} = -z_c e. \tag{4.6}$$

On the left is the integral of the charge density ρ_e over the volume outside $r = a$, and this is equated to the negative of the charge $z_c e$ on the central ion.

Equation 4.3 now describes the potential distribution near the central ion in terms of the known average concentrations $c_{i\infty}$ and other known parameters. To effect a solution, Debye and Hückel approximated the exponential terms in equation 4.3 as though the exponents were small:

$$\exp\left(-\frac{z_i F\Phi}{RT}\right) \approx 1 - \frac{z_i F\Phi}{RT}. \tag{4.7}$$

Equation 4.3 becomes

$$\frac{1}{r^2}\frac{d}{dr}\left(r^2\frac{d\Phi}{dr}\right) = \frac{\Phi}{\lambda^2}, \tag{4.8}$$

where λ is the Debye length given by

$$\lambda = \left(\frac{\epsilon RT}{F^2\sum_i z_i^2 c_{i\infty}}\right)^{1/2}. \tag{4.9}$$

The term involving $\sum_i z_i c_{i\infty}$ is zero because the solution is electrically neutral on the average.

The solution of equation 4.8 satisfying the boundary condition 4.4 and the condition that Φ approaches zero as r approaches infinity is

$$\Phi = \frac{z_c e}{4\pi\epsilon r} \frac{e^{(a-r)/\lambda}}{1 + a/\lambda}. \tag{4.10}$$

The potential due to the central ion alone would be $z_c e/4\pi\epsilon r$. Therefore, equation 4.10 reveals that the other ions attracted toward the origin, being of opposite sign to the central ion, lower the magnitude of the potential and cause it to vanish rapidly at large distances from the central ion. Thus, ions at some distance are shielded from the charge of the central ion by these other ions.

The Debye length λ is an important parameter describing the potential distribution. It has the value $\lambda = 9.6 \times 10^{-8}$ cm $= 0.96$ nm in a 0.1 M aqueous solution of a uni-univalent electrolyte at 25°C. It is inversely proportional to ionic charges and the square root of concentration and directly proportional to the square roots of the permittivity and the absolute temperature. Figure 4.1 shows the distribution of anions and cations near a central cation as calculated from equations 4.1 and 4.10 for a 0.1 M aqueous solution of a uni-univalent electrolyte at 25°C. The shielding ions form an *ion cloud* around the central ion, with a thickness on the order of the Debye length λ.

The parameter a is generally regarded as an average value of the sum of the radii of pairs of hydrated ions. For a solution containing only one kind of anion and one kind of cation, the sum of the radii of a cation and an anion dominates this average since the long-range repulsive forces tend to prevent ions of like sign from interacting at short distances.

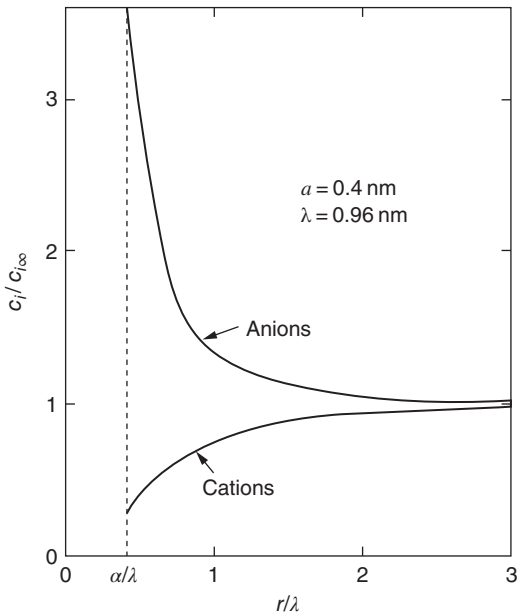

Figure 4.1 Ionic distributions near a central cation, according to the theory of Debye and Hückel, for a 0.1 M aqueous solution of a uni-univalent electrolyte at 25°C.

4.2 ELECTRICAL CONTRIBUTION TO THE FREE ENERGY

For an ideal solution of dissociated ions, the activity coefficient of neutral combinations of ions would be equal to unity. Important departures from ideality result from the coulombic electrical forces between ions. This effect can be assessed by means of the following thought experiment. Start with a given volume of solvent and also a reservoir, which is a large volume of solution containing ions at high dilution. Now imagine that the charge can be removed from the ions, and let this involve an amount of work w_1. The *discharged* ions are now to be transferred reversibly at constant volume from the reservoir to the given volume of solvent. The work involved in this process is the ideal or nonelectrical contribution to the change in the Helmholtz free energy A. The average concentration of a solute species in the new solution is now c_i.

Finally, the ions are to be recharged simultaneously to their appropriate charge levels, an amount of work w_2 being expended in this process. This work w_2 is different from w_1 because the ions are now at a high enough concentration that they shield each other, and the potential distribution around a central ion is given by equation 4.10. The electrical contribution to the Helmholtz free energy is taken to be the difference between these two work terms:

$$A_{\text{el}} = w_2 - w_1. \tag{4.11}$$

It now remains to express this quantitatively.

The work required to bring an element of charge dq from infinity to a distance $r = a$ from a central ion is $\Phi(r = a)\, dq$. Since all the ions are to be charged simultaneously, it is expeditious to let ξ denote the fraction of the final charge carried by any ion at any time during the charging process. Then, the charge on an ion is $z_i e\xi$, and $dq = z_i e\, d\xi$, and ξ varies from 0 to 1 during the charging process. The quantity a/λ in equation 4.10 should be expressed as $\xi a/\lambda$ since λ is inversely proportional to the charge level.

The contribution to $w_2 - w_1$ from charging a central ion of valence z_j is, therefore,

$$\int_0^1 \left[\frac{z_j e\xi}{4\pi\epsilon a} \frac{1}{1 + \xi a/\lambda} - \frac{z_j e\xi}{4\pi\epsilon a} \right] z_j e\, d\xi = -\frac{z_j^2 e^2}{4\pi\epsilon\lambda} \int_0^1 \frac{\xi^2 d\xi}{1 + \xi a/\lambda}. \tag{4.12}$$

The term in brackets is the difference between the potential at $r = a$ for the charging processes corresponding to w_2 and w_1. The electrical contribution to the Helmholtz free energy is now the sum of the contributions from charging the individual ions:

$$A_{\text{el}} = w_2 - w_1 = -\sum_j Ln_j \frac{z_j^2 e^2}{4\pi\epsilon\lambda} \int_0^1 \frac{\xi^2\, d\xi}{1 + \xi a/\lambda}, \tag{4.13}$$

where n_j is the number of moles of species j and L is Avogadro's number. Integration gives

$$A_{\text{el}} = -\frac{Fe}{12\pi\epsilon\lambda} \tau\left(\frac{a}{\lambda}\right) \sum_j z_j^2 n_j, \tag{4.14}$$

where

$$\tau(x) = \frac{3}{x^3}\left[\ln(1 + x) - x + \frac{1}{2}x^2\right]. \tag{4.15}$$

The chemical potential of a species can be obtained by suitable differentiation of the Helmholtz free energy (see equation 2.8):

$$\mu_i = \left(\frac{\partial A}{\partial n_i}\right)_{\substack{T,V,n_j \\ j\neq i}} = \left(\frac{\partial A}{\partial c_i}\right)_{\substack{T,V,c_j \\ j\neq i}} \left(\frac{\partial c_i}{\partial n_i}\right)_{\substack{T,V,n_j \\ j\neq i}} = \frac{1}{V}\left(\frac{\partial A}{\partial c_i}\right)_{\substack{T,V,c_j \\ j\neq i}}. \tag{4.16}$$

From equation 4.14,

$$\frac{A_{\text{el}}}{V} = -\frac{Fe}{12\pi\epsilon\lambda}\tau\left(\frac{a}{\lambda}\right)\sum_j z_j^2 c_j. \tag{4.17}$$

The electrical contribution to the chemical potential, therefore, is

$$\mu_{i,\text{el}} = -\frac{Fe}{12\pi\epsilon}\frac{\tau(a/\lambda)}{\lambda}z_i^2 - \frac{Fe}{12\pi\epsilon}\sum_j z_j^2 c_j \left.\frac{dx\tau(x)}{dx}\right|_{x=a/\lambda}\left(\frac{\partial 1/\lambda}{\partial c_i}\right)_{\substack{T,V,c_j \\ j\neq i}}. \tag{4.18}$$

The second term arises from the fact that λ depends on c_i. It should also be borne in mind that only neutral combinations of these chemical potentials are independent of the electrical state of the phase. Carrying out the differentiation in equation 4.18, we obtain

$$\mu_{i,\text{el}} = -\frac{z_i^2 Fe}{8\pi\epsilon\lambda}\frac{1}{1+a/\lambda}. \tag{4.19}$$

The above method of obtaining the electrical effect on the thermodynamic properties is known as the *Debye charging process*. The electrical contribution to the chemical potential can be arrived at more directly by means of the so-called *Güntelberg charging process*. Equation 4.16 shows that the chemical potential of a species is equal to the reversible work of transferring, at constant temperature and volume, one mole of the species to a large volume of the solution. The electrical contribution to μ_i then comes from charging one ion or a mole of ions in a solution in which all the other ions are *already* charged. The Debye length λ is consequently treated as a constant in this process, and we have

$$\mu_{i,\text{el}} = L\int_0^1 \left[\frac{z_i e\xi}{4\pi\epsilon a}\frac{1}{1+a/\lambda} - \frac{z_i e\xi}{4\pi\epsilon a}\right] z_i e\, d\xi = -\frac{z_i^2 Fe}{8\pi\epsilon\lambda}\frac{1}{1+a/\lambda}. \tag{4.20}$$

This result agrees with equation 4.19.

For dilute solutions, the activity coefficient can now be expressed as

$$\ln f_i = \ln\,\gamma_i = -\frac{z_i^2 Fe}{8\pi\epsilon RT\lambda}\frac{1}{1+a/\lambda}. \tag{4.21}$$

The activity coefficient depends on the composition of the solution through the Debye length λ. Consequently, it is convenient to introduce the molar ionic strength I' of the solution:

$$I' = \frac{1}{2}\sum_i z_i^2 c_i. \tag{4.22}$$

Then, equation 4.21 becomes

$$\ln f_i = \ln\,\gamma_i = -\frac{z_i^2 \alpha'\sqrt{I'}}{1+B'a\sqrt{I'}}, \tag{4.23}$$

where

$$B' = \frac{F}{\sqrt{\epsilon RT/2}}, \tag{4.24}$$

$$\alpha' = \frac{Fe}{8\pi\epsilon RT}B' = \frac{F^2 e\sqrt{2}}{8\pi(\epsilon RT)^{3/2}}. \tag{4.25}$$

In applications, molal concentrations are frequently employed, and the molal ionic strength is defined as

$$I = \frac{1}{2}\sum_i z_i^2 m_i = \frac{I'}{c_0 M_0}. \tag{4.26}$$

In dilute solutions, $c_0 M_0$ is approximately equal to ρ_0, the density of the pure solvent, and one writes $I' = \rho_0 I$. Consequently, in terms of the molal ionic strength, the activity coefficients are given by

$$\ln f_i = \ln \gamma_i = -\frac{z_i^2 \alpha\sqrt{I}}{1 + Ba\sqrt{I}}, \tag{4.27}$$

where

$$\alpha = \alpha'\sqrt{\rho_0} \quad \text{and} \quad B = B'\sqrt{\rho_0}. \tag{4.28}$$

Values of these parameters for aqueous solutions are given in Table 4.1.

The Debye–Hückel limiting law is the limiting form of equation 4.23 or 4.27 as the ionic strength goes to zero.

$$\ln f_i = \ln \gamma_i \to -z_i^2 \alpha'\sqrt{I'} = -z_i^2 \alpha\sqrt{I}. \tag{4.29}$$

This form, which has been verified experimentally, shows that the logarithm of the activity coefficient is proportional to the square root of the ionic strength. This is a stronger concentration dependence than one encounters in solutions of nonelectrolytes. The limiting law is independent of the parameter a. All the quantities entering into α and α' can be measured independently. The nonelectrical contributions to the logarithm of the activity coefficient should be proportional to the concentration or the ionic strength to the first power in dilute solutions. Thus, the limiting law of Debye and Hückel is valid because the effect of long-range electrical forces is so much larger than the effects usually encountered. Other effects are not, however, included in the theory of Debye and Hückel, and its validity is therefore restricted to dilute solutions.

Equation 4.16 gives no direct information on the electrical contribution to the chemical potential of the solvent. However, the Gibbs–Duhem equation can be used for this purpose. For variations at constant temperature and pressure, it reads

$$\sum_i c_i d\mu_i = 0 \tag{4.30}$$

TABLE 4.1 Debye–Hückel parameters for aqueous solutions

T (°C)	0	25	50	75
α', (liter/mol)$^{1/2}$	1.1325	1.1779	1.2374	1.3115
α, (kg/mol)$^{1/2}$	1.1324	1.1762	1.2300	1.2949
B', (liter/mol)$^{1/2}$/nm	3.249	3.291	3.346	3.411
B, (kg/mol)$^{1/2}$/nm	3.248	3.287	3.326	3.368

or

$$-d\mu_0 = M_0 \sum_{i \neq 0} m_i d\mu_i = RTM_0 \sum_{i \neq 0} m_i \, d(\ln \, m_i \gamma_i). \tag{4.31}$$

Substitution of equation 4.27 gives

$$\begin{aligned} -d\mu_0 &= RTM_0 \left[\sum_{i \neq 0} dm_i - 2\alpha I \, d\left(\frac{\sqrt{I}}{1 + Ba\sqrt{I}} \right) \right] \\ &= RTM_0 \left[\sum_{i \neq 0} dm_i - \frac{2\alpha I}{(1 + Ba\sqrt{I})^2} d\sqrt{I} \right]. \end{aligned} \tag{4.32}$$

Integration gives

$$\frac{\mu_0^0 - \mu_0}{RT} = -\ln\left(\frac{\lambda_0}{\lambda_0^0}\right) = M_0 \sum_{i \neq 0} m_i - \frac{2}{3}\alpha M_0 I^{3/2} \sigma(Ba\sqrt{I}), \tag{4.33}$$

where

$$\sigma(x) = \frac{3}{x^3}\left[x - 2\ln(1 + x) - \frac{1}{1 + x} + 1\right]. \tag{4.34}$$

Comparison with equation 2.34 shows that the osmotic coefficient ϕ is

$$\phi = 1 - \frac{\frac{2}{3}\alpha I^{3/2} \sigma(Ba\sqrt{I})}{\sum_{i \neq 0} m_i}. \tag{4.35}$$

Since σ approaches one as the ionic strength approaches zero, $1 - \phi$ is proportional to the square root of the ionic strength in dilute solutions of electrolytes.

4.3 SHORTCOMINGS OF THE DEBYE–HÜCKEL MODEL

The expression of Debye and Hückel for the activity coefficients of ionic solutions is valid only in dilute solutions. This restricted range of validity can be discussed in terms of neglected factors that would be important even in solutions of nonelectrolytes, in terms of the mathematical approximation 4.7, and from the point of view of sound application of the principles of statistical mechanics.

The theory of Debye and Hückel gives specific consideration of only the long-range electrical interactions between ions. Even here, physical properties, such as the dielectric constant, are given values appropriate to the pure solvent. At higher concentrations, ion–solvent interactions and short-range interactions between ions become important. Solvation and association should not be ignored. These effects give contributions to the logarithm of the activity coefficient which are proportional to the solute concentration even in solutions of nonelectrolytes. Consequently, at concentrations where such terms are comparable to the square-root term, the Debye–Hückel theory can no longer adequately describe the thermodynamic properties. Refinement of the electrical contributions is not very useful unless these noncoulombic interactions are also accounted for.

The only significant mathematical approximation introduced by Debye and Hückel is that of equation 4.7. Its validity depends on the magnitude of $z_i F\Phi/RT$ being small compared to unity, and this means that $z_i z_c e F/4\pi\epsilon RTa$ should be small. However, this ratio is larger than unity for uni-univalent electrolytes in water, and the situation becomes worse for higher valence types and for solvents other

than water. Furthermore, this ratio is independent of concentration, and it is not immediately clear that even the Debye–Hückel limiting law is free from error introduced by this approximation.

Fortunately, the Debye–Hückel limiting law can be substantiated by a singular-perturbation treatment of the problem. What enters into equation 4.12 or 4.20 is the potential at $r = a$ due to the *ion cloud*. For extremely dilute solutions, the Debye length becomes very large. This means that most of the ions comprising the ion cloud are at a considerable distance from the central ion, where the potential due to the central ion is greatly reduced and the approximation 4.7 is valid. Consequently, a valid approximation to the concentration distributions is obtained in the region where most of the counterbalancing charge is found; and this, in turn, yields a correct value for the potential at $r = a$ due to the ion cloud. This result is obtained even though there is always a region near the central ion where the approximation 4.7 is not valid.

It is of interest to note that even though the parameter a does not appear in the Debye–Hückel limiting law, no solution of the nonlinearized problem will be found, except with the ion cloud concentrated at the origin, unless a nonzero value for a is assumed.

Equation 4.3 is known as the Poisson–Boltzmann equation, and considerable effort has been devoted to its solution without approximation 4.7 of Debye and Hückel. Gronwall et al.[2] and La Mer et al.[3] obtained series expansions for small values of parameter $z_i z_c eF/4\pi\epsilon RTa$. This is, of course, not the same as a series expansion for small values of the concentration. More recently, Guggenheim[4–7] has reported the results of computer solutions of the Poisson–Boltzmann equation. He concludes that Gronwall's expansions do not give a significant improvement over Debye and Hückel's solution for aqueous solutions of uni-univalent electrolytes and that the terms reported by Gronwall are not sufficient for higher valence types. Guggenheim gives some hope that accurate solutions of the Poisson–Boltzmann equation would give substantial improvement, for higher valence types, over the result of Debye and Hückel at low concentrations where noncoulombic effects are not yet considerable.

Finally, one should note that the theory of Debye and Hückel is not a straightforward application of the principles of statistical mechanics. One may even marvel that the charging process gives a correct electrical contribution to the Helmholtz free energy. The inconsistencies in the model of Debye and Hückel first showed up when refined calculations gave different results for $\mu_{i,\,\mathrm{el}}$ according to the Debye and Güntelberg charging processes. These problems have been discussed clearly by Onsager.[8] The interaction energy which should enter into the Boltzmann factor in equation 4.1 is the *potential of mean force,* the integral of the average force associated with virtual displacements of an ion when all interactions with the solvent and other ions are considered. This is not necessarily equal to $z_i F\Phi$.

An example due to Onsager illustrates this contradiction. Let the potential around a central ion of type j be denoted by Φ_j. The probability of finding an ion of type j within a volume element at the origin is proportional to $c_{j\infty}$. The conditional probability of finding an ion of type i within a volume element at a distance r, when it is known that an ion of type j is at the origin, is, according to the model of Debye and Hückel, proportional to $c_{i\infty} \exp(-z_i F\Phi_j/RT)$. Hence, the probability of finding an ion of type j at a point and an ion of type i at a point at a distance r is proportional to $c_{j\infty} c_{i\infty} \exp(-z_i F\Phi_j/RT)$. However, this probability must be the same, independent of which ion is regarded as the central ion. Thus, we must have

$$c_{j\infty} c_{i\infty} \exp\left(-\frac{z_i F\Phi_j}{RT}\right) = c_{i\infty} c_{j\infty} \exp\left(-\frac{z_j F\Phi_i}{RT}\right), \tag{4.36}$$

where the term on the right is Debye and Hückel's expression for this probability when the ion of type i is regarded as the central ion. Equality of these expressions requires that

$$z_i \Phi_j(r) = z_j \Phi_i(r). \tag{4.37}$$

To complete the demonstration, one needs to show that equation 4.37 is violated for some case where the potentials $\Phi_j(r)$ and $\Phi_i(r)$ are determined by the solution of the Poisson–Boltzmann equation. The simplest case is that of an unsymmetric electrolyte (see Problem 4.1). Equation 4.37 does not happen to be violated for symmetric electrolytes. However, this does not mean that the basic model is free from objection in this case. The Debye and Güntelberg charging processes still give different results for $\mu_{i,\,\mathrm{el}}$.

It is frequently stated erroneously that the model of Debye and Hückel is inconsistent because it violates the principle of superposition of electrostatics. This principle is embodied in Poisson's equation 4.2; the potential due to a given charge distribution will be everywhere doubled if all the charges are doubled but remain in the same positions. Instead, the inconsistency arises from an improper statistical treatment of the problem.

The difficulty pinpointed by Onsager has been overcome by Mayer.[9] He has applied the principles of statistical mechanics to the physical model of Debye and Hückel, namely, hard-sphere ions of diameter a moving in a continuous dielectric fluid. The basic statistical methods, involving cluster integrals, found in Chapter 13 of Mayer and Mayer's book[10] and in the article by McMillan and Mayer,[11] form the starting point for Mayer's work on ionic solutions. Because of the long-range nature of coulombic forces, this extension is not easy, and the cluster method itself is far from simple.

Mayer is able to obtain the Debye–Hückel limiting law without invoking anything comparable to approximation 4.7. He also collects the expressions for the evaluation of the logarithm of the activity coefficient, accurate through terms of order $c^{3/2}$. He recommends evaluation of these terms without expansion for small values of c, although there is no rigorous justification for expecting better accuracy.

For the reasons stated at the beginning of this section, higher order corrections to the activity coefficient cannot be obtained without consideration of noncoulombic effects, and the statistical methods will not be pursued further here. Résibois,[12] states "Disappointingly enough, it must be admitted that the rigorous justification of the D-H theory is the most important progress that has been made by the recent developments in the field of electrolyte theory."

4.4 BINARY SOLUTIONS

In this section, we consider solutions of a single electrolyte that dissociates into ν_+ cations of charge number z_+ and ν_- anions of charge number z_-. The thermodynamic properties of such solutions have been studied extensively; activity and osmotic coefficients are summarized by Lewis and Randall[13] and by Robinson and Stokes.[14]

Since individual ionic activity coefficients can depend on the electrical state of the phase, activity coefficients from equation 4.27 should be combined into the mean molal activity coefficient γ_{+-}:

$$\ln \gamma_{+-} = \frac{z_+ z_- \alpha \sqrt{I}}{1 + Ba\sqrt{I}}. \tag{4.38}$$

From equation 4.35, the corresponding form of the osmotic coefficient is

$$\phi = 1 + \frac{1}{3} z_+ z_- \alpha \sqrt{I} \sigma(Ba\sqrt{I}). \tag{4.39}$$

To account for effects neglected in the theory of Debye and Hückel, additional terms can be added to these expressions:

$$\ln \gamma_{+-} = \frac{z_+ z_- \alpha \sqrt{I}}{1 + Ba\sqrt{I}} + A_2 m + A_3 m^{3/2} + A_4 m^2 + \cdots + A_n m^{n/2} + \cdots, \tag{4.40}$$

$$\phi = 1 + \frac{1}{3} z_+ z_- \alpha \sqrt{I} \sigma(Ba\sqrt{I}) + \frac{1}{2} A_2 m + \frac{3}{5} A_3 m^{3/2} + \frac{2}{3} A_4 m^2 + \cdots + \frac{n}{n+2} A_n m^{n/2} + \cdots, \tag{4.41}$$

where equation 4.41 has been derived from equation 4.40 by means of the Gibbs–Duhem equation 2.38. The values of the As can be determined empirically by fitting equation 4.40 to activity-coefficient data or equation 4.41 to osmotic-coefficient data. Enough terms are carried to ensure a good fit, but no special significance should be attached to the values of the As so obtained.

For many purposes, it is sufficient to drop the terms beyond that in $A_2 m$. Guggenheim[15] then writes A_2 in the form

$$A_2 = \frac{4\nu_+ \nu_-}{\nu_+ + \nu_-} \beta. \tag{4.42}$$

It is further recommended that Ba be given the same value for all electrolytes (say, $Ba = 1$ (kg/mol)$^{1/2}$, which corresponds to $a = 0.304$ nm for aqueous solutions at 25°C). One advantage of this procedure is that for each electrolyte there is now only one adjustable parameter, which can be fit by linear regression.

Equation 4.38 shows that, with the Debye–Hückel expression, the activity coefficient would have the same value for all electrolytes of the same charge type. Departures from this rule must be associated with specific interactions of the ions with the solvent and with each other. The parameter β can, thus, be considered to account for these specific interactions. According to Brønsted's principle of specific interaction of ions,[16] ions of like charge will repel each other to such an extent that their interaction will be nonspecific. This is the basis of the treatment of multicomponent solutions in the next section, and A_2 is expressed by equation 4.42 with a view toward this goal. That treatment also requires that Ba be given the same value for all electrolytes.

Table 4.2 gives values of β for uni-univalent electrolytes at 25°C. Table 4.3 gives values for 2–1 and 1–2 electrolytes.

Pitzer and Brewer[13] use one electrolyte as a reference and treat $\ln(\gamma_{+-}/\gamma_{KCl})$ or $\ln(\gamma_{+-}/\gamma_{CaCl_2})$. In these ratios, the electrical or coulombic effects should largely cancel; and the logarithm of the ratio should be proportional to m in dilute solutions, if the reference electrolyte is of the same valence type as the electrolyte in question. Thus, Pitzer and Brewer use KCl as a reference for 1–1 electrolytes and $CaCl_2$ as a reference for 2–1 and 1–2 electrolytes. Earlier, Lewis and Randall[17] had used a similar comparison to aid in extrapolations to infinite dilution for electrolytes for which data at low concentrations were absent or unreliable. Pitzer and Brewer did not find suitable reference electrolytes of higher valence types for which concordant data were available.

To illustrate the behavior of activity coefficients of electrolytes, Figure 4.2 shows γ_{+-} for HCl and HNO_3. The logarithm of γ_{+-} shows a linear dependence on $\sqrt{m}$ at low concentrations, as predicted by equation 4.38 or 4.40, and the values of γ_{+-} for HCl and HNO_3 approach each other at low concentrations. Hence, the electrical effects tend to cancel in the ratio $\gamma_{HCl}/\gamma_{HNO_3}$, and this ratio shows a linear dependence on m at low concentrations, as indicated by Figure 4.3. The slope of this curve should be proportional to $\beta_{HCl} - \beta_{HNO_3}$.

TABLE 4.2 Values of β (kg/mol) for 1–1 electrolytes at 25°C and for $Ba = 1$ (kg/mol)$^{1/2}$

HCl	0.27	NaOH	0.06	KOH	0.13	RbCl	0.06
HBr	0.33	NaF	0.07	KF	0.13	RbBr	0.05
HI	0.36	NaCl	0.15	KC1	0.10	Rbl	0.04
$HClO_4$	0.30	NaBr	0.17	KBr	0.11	$RbNO_3$	−0.14
HNO_3	0.20[a]	NaI	0.21	KI	0.15	$RbC_2H_3O_2$	0.26
LiOH	−0.21[b]	$NaClO_3$	0.10	$KClO_3$	−0.04	CsOH	0.35
LiCl	0.22	$NaClO_4$	0.13	$KBrO_3$	−0.07	CsCl	0.00
LiBr	0.26	$NaBrO_3$	0.01	KIO_3	−0.07	CsBr	0.00
Lil	0.35	$NaNO_3$	0.04	KNO_3	−0.11	CsI	−0.01
$LiClO_4$	0.34	$NaC_2H_3O_2$	0.23	$KC_2H_3O_2$	0.26	$CsNO_3$	−0.15
$LiNO_3$	0.21	NaCNS	0.20	KCNS	0.09	$CsC_2H_3O_2$	0.28
$LiC_2H_3O_2$	0.18	NaH_2PO_4	−0.06	KH_2PO_4	−0.16	$TlClO_4$	−0.17
NH_4Cl	0.10[b]	NH_4NO_3	−0.10[b]	$AgNO_3$	−0.14	$TlNO_3$	−0.36
						$TlC_2H_2O_2$	−0.04

Source: Guggenheim and Turgeon.[18] Reproduced with permission of The Royal Society of Chemistry.
[a]Derived from Ref. [7].
[b]Derived from Ref. [13].

TABLE 4.3 Values of β and Ba for 2–1 and 1–2 electrolytes at 25°C

	$\sqrt{3}Ba$ (kg/mol)$^{1/2}$	$8\beta/3 \ln 10$ (kg/mol)		$\sqrt{3}Ba$ (kg/mol)$^{1/2}$	$8\beta/3 \ln 10$ (kg/mol)
$MgCl_2$	2.75	0.206	$Mg(NO_3)_2$	2.65	0.208
$CaCl_2$	2.66	0.169	$Ca(NO_3)_2$	2.40	0.052
$SrCl_2$	2.70	0.125	$Sr(NO_3)_2$	2.40	−0.043
$BaCl_2$	2.70	0.066	$Co(NO_3)_2$	2.75	0.148
$MnCl_2$	2.70	0.148	$Cu(NO_3)_2$	2.65	0.122
$FeCl_2$	2.70	0.162	$Zn(NO_3)_2$	2.85	0.172
$CoCl_2$	2.70	0.188	$Cd(NO_3)_2$	2.75	0.104
$NiCl_2$	2.70	0.188	$Mg(ClO_4)_2$	3.25	0.356
$CuCl_2$	2.70	0.084	Li_2SO_4	2.45	−0.065
$MgBr_2$	2.80	0.291	Na_2SO_4	2.20	−0.165
$CaBr_2$	2.80	0.212	K_2SO_4	1.85	−0.087
$SrBr_2$	2.80	0.176	Rb_2SO_4	2.30	−0.148
$BaBr_2$	2.70	0.140	Cs_2SO_4	2.30	−0.113

Source: Guggenheim and Stokes.[19] Reproduced with permission of The Royal Society of Chemistry.

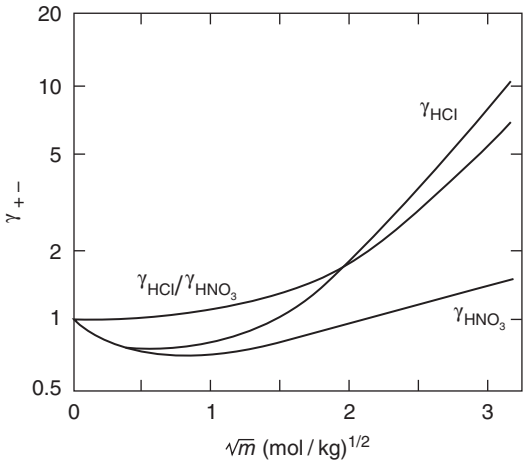

Figure 4.2 Mean molal activity coefficients of HCl (from Ref. [13]) and HNO_3 (from Ref. [23]) and the ratio of the activity coefficients of the two acids.

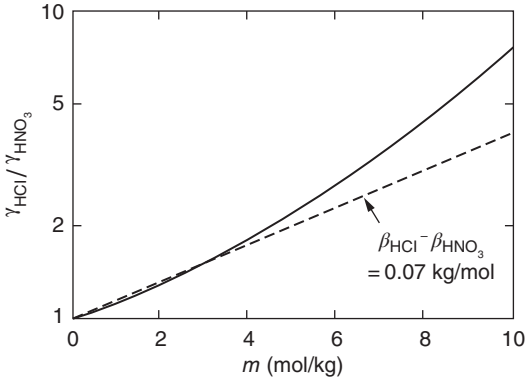

Figure 4.3 Ratio of the activity coefficients of HCl and HNO_3 plotted against the molality.

Robinson and Stokes[14] give a chemical model for hydration and arrive at a two-parameter equation that can be fit to activity-coefficient data.

4.5 MULTICOMPONENT SOLUTIONS

Equations 4.40 and 4.41 express the composition dependence of the activity and osmotic coefficients of a binary solution. The parameters α, Ba, and the As are taken to be constant at a given temperature and pressure; that is, they are independent of the solute concentration. The activity and osmotic coefficients are not independent; equation 4.41 could be derived from equation 4.40 by applying the Gibbs–Duhem relation at constant temperature and pressure. Since the chemical potentials of the components of a mixture are not independent, inconsistencies are most easily avoided by deriving the chemical potentials from an expression for the total free energy. The Gibbs free energy is used instead of the Helmholtz free energy so that chemical potentials can be obtained by differentiation at constant pressure instead of constant volume (see equation 2.8), and the Gibbs–Duhem equation can be more easily applied if the parameters are constant at a given pressure.

For moderately dilute solutions containing several electrolytes, let us express the Gibbs free energy as[21, 22]

$$\frac{G}{RT} = \frac{n_0\mu_0^0}{RT} + \sum_{j\neq 0} n_j[\ln(m_j\lambda_j^\theta) - 1] - \frac{2}{3}\alpha\sqrt{I}\tau(Ba\sqrt{I})\sum_j z_j^2 n_j + \sum_{i\neq 0}\sum_{j\neq 0}\beta_{i,j}n_i m_j, \tag{4.43}$$

where μ_0^0 is the chemical potential of the pure solvent at the same temperature and pressure.

The first two terms on the right in equation 4.43 can be regarded as an *ideal* contribution to the free energy, but it should be realized that this is only a manner of speaking. An ideal contribution should be expressed in terms of mole fractions, particle fractions, volume fractions, or concentrations since the molality approaches infinity as the concentration of the solvent approaches zero. Notice that the combination of λ_j^θ's in the second term is uniquely defined according to the principles of Section 2.3 since the solution as a whole is electrically neutral.

The third term on the right in equation 4.43 represents the electrical contribution expressed by equation 4.14, $Ba\sqrt{I}$ approaching a/λ as the ionic strength approaches zero. Recall that a represents an average value of the sum of the radii of pairs of hydrated ions and that only a single value of a can apply to a given solution.

The last term in equation 4.43 is a first approximation to the effect of specific interactions between pairs of ions, and we take $\beta_{i,j} = \beta_{j,i}$. (This is no loss in generality since $n_i m_j = n_j m_i$.) In accordance with Brønsted's principle of specific interaction of ions, $\beta_{i,j}$ is set equal to zero if $z_i z_j > 0$; that is, for a pair of ions i and j with charges of the same sign.

Molalities and the molal ionic strength I are employed in equation 4.43 because this simplifies the differentiation and facilitates the use of the Gibbs–Duhem equation. Furthermore, Scatchard[22] argues on a theoretical basis that the molal ionic strength is more appropriate for the electrical contribution to the free energy.

Differentiation of equation 4.43 according to equation 2.8 gives, for the chemical potential of the solute species,

$$\frac{\mu_k}{RT} = \ln(m_k \lambda_k^{\theta}) - \frac{z_k^2 \alpha \sqrt{I}}{1 + Ba\sqrt{I}} + 2 \sum_{j \neq 0} \beta_{k,j} m_j \tag{4.44}$$

and, for the chemical potential of the solvent,

$$\frac{\mu_0}{RT} = \frac{\mu_0^0}{RT} - M_0 \sum_{j \neq 0} m_j + \frac{2}{3} \alpha M_0 I^{3/2} \sigma(Ba\sqrt{I}) - M_0 \sum_{i \neq 0} \sum_{j \neq 0} \beta_{i,j} m_i m_j. \tag{4.45}$$

Hence, the solute activity coefficients are

$$\ln \gamma_k = -\frac{z_k^2 \alpha \sqrt{I}}{1 + Ba\sqrt{I}} + 2 \sum_{j \neq 0} \beta_{k,j} m_j, \tag{4.46}$$

and the osmotic coefficient is

$$\phi = 1 - \frac{\frac{2}{3} \alpha I^{3/2} \sigma(Ba\sqrt{I}) - \sum_{i \neq 0} \sum_{j \neq 0} \beta_{i,j} m_i m_j}{\sum_{i \neq 0} m_i}. \tag{4.47}$$

Although equations 4.44 and 4.46 apply to individual ions, the dependence on the electrical state of the phase has not been included. Consequently, these expressions should be used only for electrically neutral combinations of ions, as discussed in Section 2.3.

As a consequence of Brønsted's principle of specific interaction of ions, $\beta_{i,j} = 0$ for a pair of ions of like charge. This means that each β that appears in these equations for multicomponent solutions corresponds to one cation and one anion and can be determined from activity-coefficient or osmotic-coefficient measurements in a binary solution of this electrolyte. Such values are given in Tables 4.2 and 4.3. However, the same value of Ba must be used in fitting the data for the binary solutions. For the systems in Table 4.3, an average value of Ba should be selected, and values of β recomputed from the original data. The same value of Ba should then be used to compute β values for the systems of Table 4.2. The tables of Pitzer and Brewer[13] would be helpful in these calculations, since they give activity coefficients relative to a reference electrolyte, KCl or $CaCl_2$.

The theory presented above is valuable because it allows the thermodynamic properties of multicomponent solutions to be predicted from measurements on binary solutions. For a solution of two electrolytes, the logarithms of the activity coefficients of the electrolytes are predicted to vary

TABLE 4.4 Values of β for ions of like charge

Ions	β (kg/mol)
H^+–Li^+	0.021
H^+–Na^+	0.015
H^+–K^+	−0.010
Li^+–Na^+	0.006
Li^+–K^+	−0.022
$Cl^- - NO_3^-$	0.01

Source: Guggenheim.[7] Reproduced with permission of Oxford University Press.

linearly with the molality of one of the electrolytes when the ionic strength I is maintained constant. Such behavior is commonly observed.

When the above treatment proves to be inadequate, more terms can be added to expression 4.43 for the free energy. For uni-univalent electrolytes, Guggenheim[7, 23] relaxes Brønsted's principle and allows $\beta_{i,j}$ to be different from zero for pairs of ions of like charge. ($\beta_{i,j}$ is still zero for $i = j$.) The new values of β's (see Table 4.4) are not applicable to binary solutions and are somewhat smaller than those for pairs of ions of unlike charge, in partial accord with Brønsted's principle. The modification does not greatly affect the activity coefficients in mixed electrolytes and is perhaps more important in the correlation of enthalpies of mixing.

In addition to the terms in equation 4.43, Scatchard[22, 24] generally carries terms of cubic and higher order in the molalities. Harned and Robinson[25] have reviewed the equilibrium properties of solutions of several electrolytes. They discuss the behavior of activity coefficients corresponding to several representations of the free energy, and they present literature references for those systems where measurements have been made.

4.6 MEASUREMENT OF ACTIVITY COEFFICIENTS

The activity coefficients of electrolytic solutions can be determined by methods applicable to solutions of nonelectrolytes. We mention, in particular, freezing-point measurements, vapor-pressure measurements, and isopiestic methods. Other methods involve the measurement of the potentials of galvanic cells and are peculiar to electrolytic solutions. Robinson and Stokes[14] and Lewis and Randall[13] review these and other methods.

Measurement of freezing-point depressions is useful if the solution can exist in equilibrium with the pure solid solvent. Then, at the freezing point of the solution,

$$\mu_0(T) = \mu_{0,s}(T), \tag{4.48}$$

where $\mu_{0,s}$ denotes the chemical potential of the solid solvent. Next, it is necessary to correct the chemical potentials to a constant temperature (since the data are at the freezing points of the solutions), usually to the temperature T_f of the freezing point of the pure solvent. This is done on the basis of the relation

$$\frac{\partial \mu_i/T}{\partial T} = -\frac{\overline{H}_i}{T^2}, \tag{4.49}$$

where $\overline{H}_i$ is the partial molar enthalpy of component i in the phase in question. Then

$$\frac{\mu_0(T_f)}{T_f} = \frac{\mu_0(T)}{T} - \int_T^{T_f} \frac{\overline{H}_0}{T^2} dT, \tag{4.50}$$

and

$$\frac{\mu_{0,s}(T_f)}{T_f} = \frac{\mu_0^0(T_f)}{T_f} = \frac{\mu_{0,s}(T)}{T} - \int_T^{T_f} \frac{\overline{H}_{0,s}}{T^2} dT, \tag{4.51}$$

where we have noted that at T_f the pure liquid solvent is in equilibrium with the solid solvent. Hence, we have

$$\frac{\mu_0(T_f) - \mu_0^0(T_f)}{T_f} = R \ln \frac{\lambda_0}{\lambda_0^0} = -\phi R M_0 \nu m = -\int_T^{T_f} \frac{\overline{H}_0 - \overline{H}_{0,s}}{T^2} dT. \tag{4.52}$$

The measurements give the freezing points of solutions of molality m. The above calculation then yields the osmotic coefficient for the solution of molality m at the freezing point T_f of the pure solvent. Finally, osmotic coefficients can be converted to activity coefficients by means of the Gibbs–Duhem equation 2.36. Measurements of the freezing-point depressions are an important source of accurate values of activity coefficients of electrolytic solutions, particularly dilute solutions. The calculation procedure was developed by Lewis and Randall[17] and is described in detail by Pitzer and Brewer,[13] including the treatment of the thermal properties of the solution.

Many electrolytes are nonvolatile, and measurement of the vapor pressure yields the chemical potential of the solvent in the solution. This gives directly the osmotic coefficient. Measurement of the absolute vapor pressure is necessary for only one system. Subsequently, only isopiestic measurements for other systems are needed. This amounts to the determination of the solution concentration which has the same vapor pressure as a given solution of the standard system for which the solvent activity is already known. The osmotic coefficients of solutions of many electrolytes have been determined by the isopiestic method, although the accuracy is not adequate below about 0.1 m.

The open-circuit potentials of electrochemical cells are treated extensively in Chapter 2. These provide a means for determining the chemical potential of the solute. Consider cell 2.106:

$$\begin{array}{c|c|c|c|c|c} \alpha & \beta & & \delta & \epsilon & \lambda & \alpha' \\ \mathrm{Pt}(s), \mathrm{H_2}(g) & \mathrm{HCl\ in\ H_2O} & \text{transition region} & \mathrm{HCl\ in\ H_2O} & \mathrm{AgCl}(s) & \mathrm{Ag}(s) & \mathrm{Pt}(s). \end{array} \tag{4.53}$$

If the difference in electrochemical potential of chloride ions between solutions β and δ is ignored, the cell potential can be expressed as (see equation 2.107)

$$FU = -F(\Phi^\alpha - \Phi^{\alpha'}) = FU^\theta + \frac{1}{2} RT \ln p_{\mathrm{H_2}}^\alpha - 2RT \ln(m_{\mathrm{HCl}}^\beta \gamma_{\mathrm{HCl}}^\beta), \tag{4.54}$$

where

$$FU^\theta = \frac{1}{2}\mu_{\mathrm{H_2}}^* - \mu_{\mathrm{Ag}}^0 + \mu_{\mathrm{AgCl}}^0 - 2RT \ln \lambda_{\mathrm{HCl}}^\theta. \tag{4.55}$$

A system should be chosen such that the neglected term $\mu_{\mathrm{Cl^-}}^\beta - \mu_{\mathrm{Cl^-}}^\delta$ is as small as possible. For the present system, where the solubility of silver chloride is low, Table 2.1 shows that the error amounts to less than 0.23 mV for HCl concentrations greater than 10^{-4} m.

Equation 4.54 can be used to calculate γ_{HCl} directly from the measured cell potentials. However, this requires that the standard cell potential U^{θ} be known, and this is determined by definition 2.18 of the secondary reference state. To extrapolate most accurately to infinite dilution, one makes use of the fact that in dilute solutions the activity coefficient behaves like (see equations 4.40 and 4.42)

$$\ln \gamma_{\mathrm{HCl}} = -\frac{\alpha\sqrt{m}}{1+\sqrt{m}} + 2\beta_{\mathrm{HCl}} m, \tag{4.56}$$

where α is the Debye–Hückel constant and is known (see equation 4.28). Consequently, one defines a secondary quantity U' by

$$FU' = FU - \frac{1}{2}RT \ln p^{\alpha}_{\mathrm{H_2}} + 2RT \ln m - \frac{2RT\alpha\sqrt{m}}{1+\sqrt{m}}, \tag{4.57}$$

where m signifies m^{β}_{HCl}. Then, to the extent that equation 4.56 is applicable, U' behaves in dilute solutions like

$$U' = U^{\theta} - \frac{4RT\beta_{\mathrm{HCl}} m}{F}. \tag{4.58}$$

A plot of U' versus m should be linear near $m = 0$. The intercept of this straight line is then U^{θ}, and the slope is $-4RT\beta_{\mathrm{HCl}}/F$. This procedure, which allows the most accurate extrapolation of cell data to infinite dilution, was apparently first used by Schumb et al.[26] Equation 4.54 can now be used to calculate values of γ_{HCl}, which correspond to the secondary reference state 2.18.

For some electrolytes, electrodes reversible to both ions may be impossible to find or difficult to work with. A cell with liquid junction, such as cell 2.91:

$$\begin{array}{c|c|c|c|c|c|c|c|c} \alpha & \beta & \delta & \epsilon & & \lambda & \delta' & \beta' & \alpha' \\ \mathrm{Pt}(s) & \mathrm{Hg}(l) & \mathrm{HgO}(s) & \mathrm{KOH\ in\ H_2O} & \text{transition region} & \mathrm{KOH\ in\ H_2O} & \mathrm{HgO}(s) & \mathrm{Hg}(l) & \mathrm{Pt}(s), \end{array} \tag{4.59}$$

may then be set up with only one type of electrode. The potential of this cell is given by

$$FU = -F(\Phi^{\alpha} - \Phi^{\alpha'}) = \int_{\lambda}^{\epsilon} \left(t^{0}_{\mathrm{K^+}} + \frac{1}{2} M_0 m \right) d\mu_{\mathrm{KOH}}. \tag{4.60}$$

If the transference number $t^{0}_{\mathrm{K^+}}$ is known, measurements of the potential of this cell can be used to study the activity and osmotic coefficients of this electrolytic solution.

For thermodynamic measurements, cells with liquid junction are generally to be avoided. However, when the junction involves solutions of only one electrolyte, the cell potential is independent of the method of forming the junction and can be expressed unambiguously in terms of the thermodynamic and transport properties according to equation 4.60.

4.7 WEAK ELECTROLYTES

Aqueous solutions of sulfuric acid involve the equilibrium between sulfate and bisulfate ions:

$$\mathrm{H^+} + \mathrm{SO_4^{2-}} \rightleftharpoons \mathrm{HSO_4^-}. \tag{4.61}$$

Because the equilibrium is rapid, there are only two independent components, which can be taken to be H_2SO_4 and H_2O. In treating the activity coefficient of the solute, one can consider the solution to be composed of one of the following sets of species:

(a) H_2SO_4 and H_2O
(b) H^+, HSO_4^-, and H_2O
(c) H^+, SO_4^{2-}, and H_2O

In the last two cases, one deals with the mean activity coefficient of hydrogen and bisulfate ions or the mean activity coefficient of hydrogen and sulfate ions.

In Section 2.3, we dealt with the difference between the treatments of the electrolyte as dissociated or without regard for its dissociation. Any one of the above three formulations provides a consistent basis for describing all the relevant thermodynamic properties of the system, although formulations (a) and (b) have the disadvantage that they do not take into account the state of aggregation of the solute at infinite dilution and thus preclude the application of equations 2.18 and 2.19 to define the secondary reference state.

One can attempt to take into explicit account the equilibrium 4.61 by writing

$$\mu_{H^+} + \mu_{SO_4^{2-}} = \mu_{HSO_4^-} \tag{4.62}$$

and defining an equilibrium constant, for example,

$$K = \frac{c^*_{H^+} c^*_{SO_4^{2-}} f^*_{H^+} f^*_{SO_4^{2-}}}{c^*_{HSO_4^-} f^*_{HSO_4^-}} = \frac{a^*_{HSO_4^-}}{a^*_{H^+} a^*_{SO_4^{2-}}}. \tag{4.63}$$

We have put asterisks on these quantities to denote the fact that they refer to a view of the solution as composed of water molecules and hydrogen, bisulfate, and sulfate ions. For example, the concentrations c_i^* are not the stoichiometric concentrations of independent components that can be assessed by ordinary analytical means.

The thermodynamic constant K is independent of concentration. In addition to this constant, we have introduced one extra concentration and one extra activity coefficient. In Problem 4.6, we show how to calculate $K, f^*_{H^+} f^*_{HSO_4^-}$, and $(f^*_{H^+})^2 f^*_{SO_4^{2-}}$, if a microscopic concentration, say $c^*_{HSO_4^-}$, is known as a function of stoichiometric concentration. It should be emphasized, however, that such a procedure is outside the strict bounds of thermodynamics.

In going beyond thermodynamic means to investigate the equilibrium of a weak electrolyte, one could adopt the microscopic model, assume that the activity coefficients of the microscopic species are given by some suitably simple theory (see Section 4.5), and fit the macroscopic thermodynamic quantities to determine the best values of K and any other parameters of the microscopic model. Transport properties also can be used to help determine the values of these parameters.

This approach can be valuable to predict the behavior of macroscopic quantities in the absence of complete data, for example, for the activities of phenolic compounds in water. For sulfuric acid, the data are quite complete, but this approach can give a guide to the correlation of the concentration dependence of the activity coefficient (compare Ref. [14], p. 213).

A second approach is to use, for example, Raman spectra to give independent evidence of the microscopic species concentrations. Then one can obtain a reliable value for K, determine values for the microscopic activity coefficients, and compare these with simple theoretical models, as outlined in Problem 4.6.

The results of Raman spectra measurements are given for sulfuric acid solutions by Young et al.[27] From these results, we can calculate directly the value of

$$K' = \frac{c^*_{H^+} c^*_{SO_4^{2-}}}{c^*_{HSO_4^-}} = \frac{K f^*_{HSO_4^-}}{f^*_{H^+} f^*_{SO_4^{2-}}}. \tag{4.64}$$

This quantity is useful for retrieving the values of the microscopic concentrations from the stoichiometric concentration. We see that K' depends on concentration through the activity coefficients. From the development in the preceding sections, we might expect to be able to correlate K' in terms of the microscopic or "true" ionic strength I_r:

$$I_r = \frac{1}{2} \sum_i z_i^2 c_i^*. \tag{4.65}$$

Such a correlation of Young's data is shown in Figure 4.4, where the experimental points are correlated by the equation

$$\ln \frac{K'}{K} = \frac{5.29\sqrt{I_r}}{1 + 0.56\sqrt{I_r}}, \tag{4.66}$$

where, I_r is expressed in mol/liter. The value of $K = 0.0104$ mol/liter, from Ref. [14], p. 387, is also shown in Figure 4.4. The points on the figure extend to a stoichiometric concentration of sulfuric acid of 2.95 *M*.

Such a correlation can be of value in estimating the microscopic species concentrations in, for example, solutions of copper sulfate and sulfuric acid, where the data are far from complete. The interactions of weak acids and bases involve chemical reactions that can reduce considerably the volatility of the materials. This well known fact is elaborated upon by Edwards et al.[28]

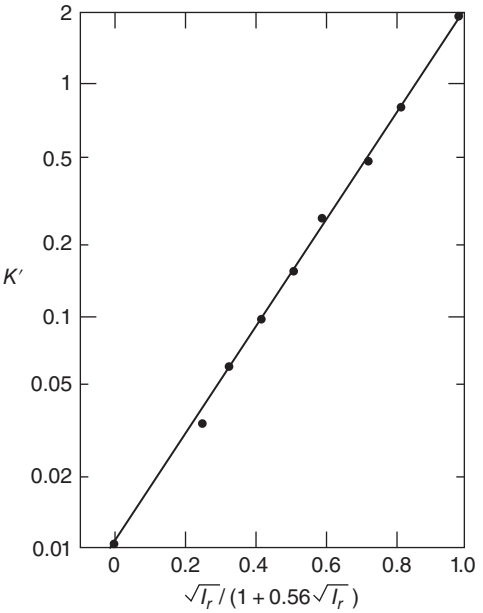

Figure 4.4 Correlation of the second dissociation constant of sulfuric acid with the true ionic strength.

PROBLEMS

4.1 Set up the Poisson–Boltzmann equations for a solution containing cations of charge number z_+ and anions of charge number z_-. Let $x = r/\lambda$; for the cation as the central ion, let $\phi_+ = z_- F\Phi/RT$, and for the anion as the central ion, let $\phi_- = z_+ F\Phi/RT$. Show that $\phi_+ - \phi_-$ satisfies the differential equation

$$\frac{1}{x^2}\frac{d}{dx}\left(x^2\frac{d\phi_+ - \phi_-}{dx}\right) = \frac{z_+}{z_+ - z_-}(e^{-\phi_-} - e^{-z_-\phi_-/z_+}) - \frac{z_-}{z_+ - z_-}(e^{-z_+\phi_+/z_-} - e^{-\phi_+})$$

and the boundary conditions

$$\frac{d\phi_+ - \phi_-}{dx} = 0 \quad \text{at} \quad x = a/\lambda,$$
$$\phi_+ - \phi_- \to 0 \quad \text{as} \quad x \to \infty.$$

The Onsager criterion requires that $\phi_+(x) = \phi_-(x)$ (see equation 4.37). Can this criterion be satisfied exactly when z_+ is not equal to $-z_-$, that is, for a nonsymmetric electrolyte?

4.2 Set up the Poisson–Boltzmann equations as in Problem 4.1. Let $\delta = a/\lambda$ and $S = -z_+ z_- Fe/4\pi\epsilon RTa$ so that the boundary condition at $r = a$ becomes

$$\delta\frac{d\phi_+}{dx} = S \quad \text{at} \quad x = \delta.$$

To justify the Debye–Hückel limiting law, we wish to solve the problem for small values of δ, that is, for small values of the concentration.

(a) Seek a solution by singular-perturbation expansions, letting the inner variable be $\bar{x} = x/\delta$ and the outer variable be $\tilde{x} = x$. (See Ref. [29], for the application of singular-perturbation techniques to a problem of electrochemical interest.) In the inner region, the potential due to the ion cloud is negligible in the first approximation. In the outer region, the potential is small, and the exponential Boltzmann terms can be linearized.

(b) Use the result of part (a) and the Güntelberg charging process to substantiate the limiting law of Debye and Hückel. If possible, obtain the next term in an expansion for small δ.

(c) Repeat part (b) with the Debye charging process.

4.3 In Section 4.2, the Helmholtz free energy was used; in Section 4.5, the Gibbs free energy. For a 0.1 mol/kg solution, calculate the difference between A and G and compare with the electrical contribution to the free energy. Obtain an expression for the difference between the derivative of A with respect to n_i, when the differentiation is carried out at constant volume or constant pressure. Is the determination of the chemical potential of the solvent according to equation 4.31 completely legitimate? Is the derivation of equation 4.41 from equation 4.40 completely rigorous?

4.4 (This is a very difficult problem.) Smyrl and Newman[30] express molar activity coefficients of solute species in essentially the following form (compare equation 4.46):

$$\ln f_i - \frac{z_i}{z_n}\ln f_n = -\frac{\alpha' z_i(z_i - z_n)\sqrt{I'}}{1 + B'a\sqrt{I'}} + 2\sum_{j\neq 0}\left(\beta'_{i,j} - \frac{z_i}{z_n}\beta'_{n,j}\right)c_j,$$

where the sum is over solute species, $\beta'_{i,j} = 0$ for a pair of ions of like charge, and $\beta'_{i,j} = \beta'_{j,i}$.

(a) Is this expression consistent with the thermodynamic requirement that $\partial\mu_i/\partial m_j = \partial\mu_j/\partial m_i$?. (*Hint*: $f_i = 1$ is thermodynamically inconsistent if it is applied to all the species in a multicomponent system.)

(b) Show that

$$2\sum_{j\neq 0}\left(\beta'_{i,j} - \frac{z_i}{z_n}\beta'_{n,j}\right)c_j = 2\sum_{j\neq 0}\left(\beta'_{i,j} - \frac{z_i}{z_n}\beta_{n,j}\right)\frac{c_j}{\rho_0} - \left(1 - \frac{z_i}{z_n}\right)\left(\frac{c_0 M_0}{\rho_0} - 1\right) + O(c^{3/2})$$

if the expression of Smyrl and Newman is to be equivalent to the corresponding one for molal activity coefficients through terms of order c in the solute concentrations. Here, ρ_0 is the density of the pure solvent.

(c) Show for a solution of a single electrolyte that

$$\beta'_{+-} = \frac{\beta_{+-}}{\rho_0} + \frac{\nu\overline{V}_e}{4\nu_+\nu_-},$$

where $\overline{V}_e$ is the partial molar volume of the electrolyte in an infinitely dilute solution. For $\overline{V}_e = 27\ \text{cm}^3/\text{mol}$, compare the value of the correction term with typical values of β_{+-}/ρ_0 for uni-univalent electrolytes from Table 4.2.

4.5 Assume that the Gibbs free energy for a solution of several electrolytes can be expressed as:

$$\frac{G}{RT} = \frac{n_0\mu_0^0}{RT} + \sum_{j\neq 0} n_j[\ln(m_j\lambda_j^\theta) - 1] - \frac{2}{3}\alpha\sqrt{I}\tau(Ba\sqrt{I})\sum_j z_j^2 n_j - \frac{1}{2}\sum_{i\neq 0}\sum_{j\neq 0}\epsilon_{i,j}z_i z_j n_i m_j + \cdots.$$

Here the last terms, involving $\epsilon_{i,j}$ are supposed to account for short-range specific interactions between pairs of solute ions. The factor $z_i z_j$ is included solely for convenience.

(a) Discuss why this expression is sufficiently general without including terms like $\epsilon_{i,0}$ for interaction of species i with the solvent.

(b) Show that, with no loss of generality, we can require that $\epsilon_{i,j} = \epsilon_{j,i}$.

(c) The molalities of the ions are not independent since they satisfy the electroneutrality relation

$$\sum_i z_i m_i = 0.$$

Therefore, since the $\epsilon_{i,j}$'s cannot be determined separately, define

$$\beta_{i,j} = -\frac{1}{4}z_i z_j(2\epsilon_{i,j} - \epsilon_{i,i} - \epsilon_{j,j}),$$

so that $\beta_{i,j} = \beta_{j,i}$ and $\beta_{i,i} = 0$. Show that

$$-\frac{1}{2}\sum_{i\neq 0}\sum_{j\neq 0}\epsilon_{i,j}z_i z_j n_i m_j = \sum_{i\neq 0}\sum_{j\neq 0}\beta_{i,j}n_i m_j.$$

Do you think that the $\beta_{i,j}$ values are subject to experimental determination?

(d) Show that, for a solution of a single electrolyte, the expression for G now reduces to

$$\frac{G}{RT} = \frac{n_0\mu_0^0}{RT} + \sum_{j\neq 0} n_j[\ln(m_j\lambda_j^\theta) - 1] - \frac{2}{3}\alpha\sqrt{I}\tau(Ba\sqrt{I})\sum_j z_j^2 n_j + 2\beta_{+-}M_0 n_0 m_+ m_-.$$

Part (c) reveals why there is no β_{++} or β_{--} for solutions of a single electrolyte.

(e) For mixtures containing cations of the same charge number z_+ and anions of the same charge number z_-, Guggenheim[7] expresses the free energy relative to a reference electrolyte for which $\beta_{+-} = \beta_{+-}^0$. Assume that G^0, a reference free energy, denotes the expression in part (d) with β_{+-} replaced by β_{+-}^0 and with m_+ and m_- having the meaning

$$m_+ = \sum_+ m_i = \nu_+ m \quad \text{and} \quad m_- = \sum_- m_i = \nu_- m,$$

where, m is the total molality of the solution. Show that the *excess* free energy is given by

$$\frac{G - G^0}{RT} = M_0 n_0\left[\sum_{i\neq 0}\sum_{j\neq 0}\beta_{i,j}m_i m_j - 2\beta_{+-}^0 m_+ m_-\right] = (\phi - \phi^0)M_0 n_0 \nu m$$

and that the mean activity coefficient of a cation k and an anion l is

$$\nu \ln\frac{\gamma_{k,l}}{\gamma_{+-}^0} = 2\nu_+\left(\sum_{i\neq 0}\beta_{k,i}m_i - \sum_{i-}\beta_{+-}^0 m_i\right) + 2\nu_-\left(\sum_{i\neq 0}\beta_{l,i}m_i - \sum_{i+}\beta_{+-}^0 m_i\right),$$

where ϕ^0 is the osmotic coefficient and γ_{+-}^0 is the mean molal activity coefficient of the reference electrolyte, both at the molality m.

(f) Let

$$\Delta_{i,j} = \beta_{i,j} - \beta_{+-}^0 \quad \text{if} \quad z_i z_j < 0$$
$$= \beta_{i,j} \quad \text{if} \quad z_i z_j > 0.$$

Show that

$$\frac{G - G^0}{RT} = (\phi - \phi^0)M_0 n_0 \nu m = M_0 n_0 \sum_{i\neq 0}\sum_{j\neq 0}\Delta_{i,j}m_i m_j$$

and

$$\nu \ln \frac{\gamma_{k,l}}{\gamma^0_{+-}} = 2\nu_+ \sum_{i \neq 0} \Delta_{k,i} m_i + 2\nu_- \sum_{i \neq 0} \Delta_{l,i} m_i.$$

Note that β^0_{+-} provides a reference value for $\beta_{i,j}$ for ions with charges of opposite sign, whereas none is available for ions with the same charge.

These exercises indicate that the theory presented in Section 4.5, with $\beta_{i,j}$ not assumed to be zero for ions of opposite charge, is sufficient to account rigorously for the activity coefficients of mixtures of electrolytes through order m.

4.6 For the sulfuric acid solutions considered in Section 4.7,

(a) Express the stoichiometric concentrations of hydrogen and sulfate ions in terms of the microscopic concentrations of hydrogen, bisulfate, and sulfate ions.

(b) Show that the Gibbs–Duhem equation applies to the model system:

$$\sum_i c_i^* d\mu_i = 0$$

at constant temperature and pressure.

(c) Show from equation 4.63 that as the ionic strength approaches zero

$$c^*_{H^+} \to c_{H^+}, \quad c^*_{SO_4^{2-}} \to c_{SO_4^{2-}}, \quad c^*_{HSO_4^-} \to \frac{c_{H^+} c_{SO_4^{2-}}}{K},$$

where K is as yet undetermined. Assume that equation 2.19 applies to the model system.

(d) Apply equation 2.19 and the result of part (c) to show that

$$(a^\theta_{H^+})^2 a^\theta_{SO_4^{2-}} = (a^*_{H^+})^2 a^*_{SO_4^{2-}}.$$

(e) Show from parts (d) and (a) that

$$(f^*_{H^+})^2 f^*_{SO_4^{2-}} = \frac{c^2_{H^+} c_{SO_4^{2-}}}{(c^*_{H^+})^2 c^*_{SO_4^{2-}}} f^3_{H^+,SO_4^{2-}}$$

$$= \frac{c^2_{H^+} c_{SO_4^{2-}} f^3_{H^+,SO_4^{2-}}}{(c_{H^+} - c^*_{HSO_4^-})^2 (c_{SO_4^{2-}} - c^*_{HSO_4^-})},$$

where, $f_{H^+,SO_4^{2-}}$ is the mean molar activity coefficient of hydrogen and sulfate ions and is measurable by thermodynamic means.

(f) If $c^*_{HSO_4^-}$ can measured at one stoichiometric concentration, then we know, from the above result, the value of $(f^*_{H^+})^2 f^*_{SO_4^{2-}}$ at the same concentration. Show that

$$K f^*_{H^+} f^*_{HSO_4^-} = \frac{c^2_{H^{2+}} c_{SO_4^{2-}} f^3_{H^+,SO_4^{2-}}}{(c_{H^+} - c^*_{HSO_4^-}) c^*_{HSO_4^-}}$$

and discuss how to get K and $f^*_{H^+} f^*_{HSO_4^-}$ separately if $c^*_{HSO_4^-}$ is known as a function of stoichiometric concentration.

Note that in this problem we have used only the activity coefficients of neutral combinations of ions, even for the model system.

NOTATION

a	mean diameter of ions, cm
a_i^*	property expressing secondary reference state, for microscopic point of view, liter/mol
A	Helmholtz free energy, J
A_n	coefficients in expression of thermodynamic properties of a solution of a single electrolyte
B	Debye–Hückel parameter, $(kg/mol)^{1/2}/nm$
B'	Debye–Hückel parameter, $(liter/mol)^{1/2}/nm$
c_i	molar concentration of species i, mol/liter
e	electronic charge, 1.60210×10^{-19} C
f_i	molar activity coefficient of species i
F	Faraday's constant, 96,487 C/mol
G	Gibbs function, J
$\overline{H}_i$	partial molar enthalpy of species i, J/mol
I	molal ionic strength, mol/kg
I'	molar ionic strength, mol/liter
I_r	"true" ionic strength, mol/liter
K	dissociation constant, mol/liter
K'	dissociation constant, mol/liter
L	Avogadro's number, 6.0225×10^{23}/mol
m	molality of a single electrolyte, mol/kg
m_i	molality of species i, mol/kg
M_i	molar mass of species i, g/mol
n_i	number of moles of species i, mol
p_i	partial pressure or fugacity of species i, bar
q	charge, C
r	radial position coordinate, cm
R	universal gas constant, 8.3143 J/mol·K
t_i^0	transference number of species i with respect to the velocity of species 0
T	absolute temperature, K
U	open-circuit cell potential, V
U^θ	standard cell potential, V
U'	modified open-circuit potential, V
V	volume, cm^3
w_1, w_2	reversible work of electrical charging, J
z_i	charge number of species i
α	Debye–Hückel constant, $(kg/mol)^{1/2}$
α'	Debye–Hückel constant, $(liter/mol)^{1/2}$
$\beta_{i,j}$	coefficient for ion–ion specific interactions, kg/mol
γ_i	molal activity coefficient of species i
γ_{+-}	mean molal activity coefficient of an electrolyte
ϵ	permittivity, F/cm
λ	Debye length, cm

λ_i	absolute activity of species i
λ_i^{θ}	property expressing secondary reference state, kg/mol
μ_i	chemical or electrochemical potential of species i, J/mol
ν	number of ions into which a molecule of electrolyte dissociates
ν_+, ν_-	numbers of cations and anions into which a molecule of electrolyte dissociates
ξ	fraction of charge
ρ_e	electric charge density, C/cm^3
ρ_0	density of pure solvent, g/cm^3
σ	see equation 4.34
τ	see equation 4.15
ϕ	osmotic coefficient
Φ	electric potential, V

Subscripts

el	electrical
0	solvent
*	from a microscopic point of view
∞	in the bulk solution

REFERENCES

1. P. Debye and E. Hückel, "Zur Theorie der Elektrolyte," *Physikalische Zeitschrift*, *24* (1923), 185–206.
2. T. H. Gronwall, Victor K. La Mer, and Karl Sandved, "Über den Einfluss der sogenannten höheren Glieder in der Debye–Hückelschen Theorie der Lösungen starker Elektrolyte," *Physikalische Zeitschrift*, *29* (1928), 358–393.
3. Victor K. La Mer, T. H. Gronwall, and Lotti J. Greiff. "The Influence of Higher Terms of the Debye–Hückel Theory in the Case of Unsymmetric Valence Type Electrolytes," *Journal of Physical Chemistry*, *35* (1931), 2245–2288.
4. E. A. Guggenheim, "The Accurate Numerical Solution of the Poisson–Boltzmann Equation," *Transactions of the Faraday Society*, *55* (1959), 1714–1724.
5. E. A. Guggenheim, "Activity Coefficients and Osmotic Coefficients of 2:2 Electrolytes," *Transactions of the Faraday Society*, *56* (1960), 1152–1158.
6. E. A. Guggenheim, "Activity Coefficients of 2:1 Electrolytes," *Transactions of the Faraday Society*, *58* (1962), 86–87.
7. E. A. Guggenheim, *Applications of Statistical Mechanics* (Oxford: Clarendon, 1966).
8. Lars Onsager, "Theories of Concentrated Electrolytes," *Chemical Reviews*, *13* (1933), 73–89.
9. Joseph E. Mayer, "The Theory of Ionic Solutions," *Journal of Chemical Physics*, *18* (1950), 1426–1436.
10. Joseph Edward Mayer and Maria Goeppert Mayer, *Statistical Mechanics* (New York: Wiley, 1940).
11. William G, McMillan, Jr., and Joseph E. Mayer, "The Statistical Thermodynamics of Multicomponent Systems," *Journal of Chemical Physics*, *13* (1945), 276–305.
12. Pierre M. V. Résibois, *Electrolyte Theory* (New York: Harper & Row, 1968), p. 29.
13. Gilbert Newton Lewis and Merle Randall, revised by Kenneth S. Pitzer and Leo Brewer, *Thermodynamics* (New York: McGraw-Hill, 1961).
14. R. A. Robinson and R. H. Stokes, *Electrolyte Solutions* (New York: Academic, 1959).
15. E. A. Guggenheim, *Thermodynamics* (Amsterdam: North-Holland, 1959).
16. J. N. Brønsted, "Studies on Solubility. IV. The Principle of the Specific Interaction of Ions," *Journal of the American Chemical Society*, *44* (1922), 877–898.

17. Gilbert N. Lewis and Merle Randall, "The Activity Coefficient of Strong Electrolytes," *Journal of the American Chemical Society*, *43* (1921), 1112–1154.
18. E. A. Guggenheim and J. C. Turgeon, "Specific Interaction of Ions," *Transactions of the Faraday Society*, *51* (1955), 747–761.
19. E. A. Guggenheim and R. H. Stokes, "Activity Coefficients of 2:1 and 1:2 Electrolytes in Aqueous Solution from Isopiestic Data," *Transactions of the Faraday Society*, *54* (1958), 1646–1649.
20. W. A. Roth and K. Scheel, eds., *Landolt–Börnstein Physikalisch-chemische Tabellen*, 5, supplement 3, part 3 (Berlin: Springer, 1936), p. 2145.
21. E. A. Guggenheim, "The Specific Thermodynamic Properties of Aqueous Solutions of Strong Electrolytes," *Philosophical Magazine, Ser. 7*, 19 (1935), 588–643.
22. George Scatchard, "Concentrated Solutions of Strong Electrolytes," *Chemical Reviews*, *79* (1936), 309–327.
23. E. A. Guggenheim, "Mixtures of 1:1 Electrolytes," *Transactions of the Faraday Society*, *62* (1966), 3446–3450.
24. George Scatchard, "Osmotic Coefficients and Activity Coefficients in Mixed Electrolyte Solutions," *Journal of the American Chemical Society*, *83* (1961), 2636–2642.
25. H. S. Harned and R. A. Robinson, *Multicomponent Electrolyte Solutions* (Oxford: Pergamon, 1968).
26. Walter C. Schumb, Miles S. Sherrill, and Sumner B. Sweetser, "The Measurement of the Molal Ferric-Ferrous Electrode Potential," *Journal of the American Chemical Society*, *59* (1937), 2360–2365.
27. T. F. Young, L. F. Maranville, and H. M. Smith, "Raman Spectral Investigations of Ionic Equilibria in Solutions of Strong Electrolytes," in Walter J. Hamer, ed., *The Structure of Electrolytic Solutions* (New York: Wiley, 1959), pp 35–63.
28. Thomas J. Edwards, John Newman, and John Prausnitz, "Thermodynamics of Aqueous Solutions Containing Volatile Weak Electrolytes," *AlChE Journal*, *21* (1975), 248–259.
29. John Newman, "The Polarized Diffuse Double Layer." *Transactions of the Faraday Society*, *61* (1965) 2229–2237.
30. William H. Smyrl and John Newman, "Potentials of Cells with Liquid Junctions." *Journal of Physical Chemistry*, *72* (1968), 4660–4671.

CHAPTER 5

REFERENCE ELECTRODES

In many applications, the ability to assess the potential in the solution is important; this is the primary purpose of reference electrodes. The estimation of potentials across liquid junctions, treated in Chapter 6, is directly related to the use of reference electrodes.

Since the absolute potential of a single electrode cannot be measured, all potential measurements in electrochemical systems are performed with a reference electrode. To obtain meaningful results, the reference electrode should be reversible, and its potential should remain constant during the measurement. Theoretically, any electrode in an equilibrium state can be used as a reference electrode if its thermodynamic properties are known. However, no real electrode is ideal or has a completely reversible equilibrium potential. Since some electrodes are more reversible and easier to reproduce than others, they are more suitable as reference electrodes.

The purpose of this chapter is to discuss how to select a suitable reference electrode. Some important factors that will cause the electrode potential to deviate from the equilibrium potential are discussed, and some reference electrodes that are commonly used in electrochemical measurements are introduced.

The material here follows mainly from the book edited by Ives and Janz.[1] A review on reference electrodes in nonaqueous solvents has been compiled by Butler.[2]

5.1 CRITERIA FOR REFERENCE ELECTRODES

An ideal reference electrode should be reversible and reproducible. In other words, the species that can cross the phase boundary of the reference electrode should exist in equilibrium in both phases of the half-cell, and this equilibrium should not be disturbed during the measurement. Practically, this ideal case is impossible to obtain. One can only select a reference electrode for which the deviation from the ideal case is small enough to suit one's experimental work. In this section, we discuss the causes of deviation of a reference electrode from the ideal case and how to test a reference electrode.

Electrochemical Systems, Fourth Edition. John Newman and Nitash P. Balsara.

Even though a reference electrode is carefully selected so that there is no spontaneous reaction between the electrode and the solution, some irreversible reactions still occur during the measurement. Because all potential detection systems are operated by current, a certain amount of current, even though very small, must be passed through the cell. This current will cause an irreversible reaction to occur at the reference electrode and thus disturbs its equilibrium state. When a current is passed through an electrode, an overpotential representing the deviation from the equilibrium potential is set up and introduces an error in the desired measurement. If the current density is very small, the relation of current density i to the overpotential η_s can be represented by the equation (see equation 1.9 and Section 8.2)

$$i = i_0 \frac{(\alpha_a + \alpha_c)F}{RT} \eta_s, \tag{5.1}$$

where i_0 is the exchange current density. This equation shows that, if a certain amount of current is passed through an electrode, the overpotential decreases as the exchange current density increases. In other words, electrodes with larger exchange current densities are more suitable for reference electrodes. The larger the surface area of a reference electrode, the smaller the current density for a given amount of current, and the smaller the overpotential will be.

A second source of error can arise from liquid junctions. If liquid junctions exist inside the cell, the measured potential will include the liquid-junction potentials. A cell without a liquid junction means that the solution inside the cell is homogeneous. An example is given in equation 2.45. Even in the hydrogen/silver–silver chloride cell 2.106, the solution is not completely homogeneous since the silver ions should not reach the hydrogen electrode. Normally, the liquid-junction potential in this cell can be neglected, although in dilute solutions it becomes appreciable (see Table 2.1).

Other types of cells are even less ideal in this regard. The liquid-junction potentials are established by the activity gradients of species across the cell and can be represented by the integral of equation 6.5. This equation shows that the liquid-junction potential decreases as the difference between the solutions across the junction decreases. Because of the low solubilities of the reactants, the liquid-junction potential of the cell containing the hydrogen electrode, or electrodes of the second kind with a sparingly soluble salt, is small. Therefore, they are more suitable for the purpose of reference electrodes.

For convenience, some cells with liquid junctions are also used for electrochemical measurements. The estimation or minimization of these liquid-junction potentials is treated in Chapter 2 and in more detail in Chapter 6.

As a third source of error, the equilibrium potential of an electrode can be affected by impurities. The impurities inside the electrode can change the electrode activity, or react with the electrolyte, or react with the electrode. The impurities can affect the electrode potential in the following ways:

1. They can react corrosively with the electrode, thus disturbing the equilibrium of the electrode and shifting the potential (see Section 8.7). This is a second reason why the exchange current density for the desired electrode reaction should be high, so that the open-circuit potential is determined by the desired reaction and not by chance impurities. To achieve this high exchange current density, the concentration of the reactant should be much larger than the concentration of impurities.

   Sometimes, the products of the reaction of impurities are insoluble in the solution and deposit on the electrode covering the electrode surface, thus changing the electrode properties. The most common impurity of this kind is oxygen dissolved in the solution. Some electrodes, such as amalgam electrodes, are extremely sensitive to a trace of oxygen dissolved in the solution.

   Some electrodes, such as the hydrogen electrode, need the catalytic action of a metal surface to establish equilibrium. If this catalyst is poisoned by impurities, the equilibrium state of the electrode cannot be attained.

2. The impurities in the solution may change the activity of the reacting species. Some impurities have a strong tendency to form complexes with the reacting species in the solution, thus changing the electrode potential. The electrode potential in nonaqueous solutions can be affected seriously by the presence of even a trace of water.
3. Impurities can change the properties of the electrolyte. Some electrodes are very sensitive to the pH of the solution. Impurities, such as carbon dioxide, in the solution can change the pH of the solution considerably if the solution is near neutral and unbuffered.

5.2 EXPERIMENTAL FACTORS AFFECTING SELECTION OF REFERENCE ELECTRODES

We mentioned in Section 5.1 that, theoretically, an electrode of the second kind with a large exchange current density is suitable as a reference electrode. Experimentally, a good reference electrode should be reproducible, constant in time, and easy to prepare. The reproducibility and stability of an electrode depend on the purity and sometimes on the surface condition of the metal. Discussion of the purification of chemicals is beyond the scope of this book, but the purity of materials is an important consideration. The common methods of treating a metal surface before it is used as an electrode are:

1. Clean and smooth the metal surface mechanically, either by polishing with sandpaper or by scraping.
2. Smooth the metal surface by electrochemical polishing.
3. Clean the electrode surface by prepolarization.

The last method is very effective in removing any oxide layer.

To eliminate all the impurities from the solution and make the metal surface completely reproducible would require a large amount of work. Electrodes that are much less sensitive to impurities and metal surface condition are easier to prepare to obtain the same degree of accuracy and should be chosen as reference electrodes.

There is no definite rule about the selection of reference electrodes. A literature search is the best way to find a suitable reference electrode that has been used in the system of interest. In the literature, usually the method of preparation of the reference electrode is given, as well as its reproducibility and stability. If no suitable reference electrode can be found in the literature, the only way to obtain a good reference electrode is by trial and error. Even if the method of preparation of a reference electrode is given in the literature, the reference electrode should be tested before use; the simplest method is to put several electrodes prepared by the same method into the same solution with a different kind of reference electrode. The potential difference between the identical electrodes is a test of reproducibility; the potential difference between them and the different reference electrode as a function of time is a test of stability. The dependence of the behavior of the electrode on the metal surface can be detected in this way by measuring the potential difference between electrodes prepared by different methods.

Generally, a reference electrode should be selected that is reversible to one of the ions in the solution to avoid liquid junctions. However, such an electrode may be difficult to prepare, or unreproducible, or may not exist. Or the solution in question may be of such complex composition that simultaneous reactions are unavoidable. In such a case, a well-behaved reference electrode in its own solution must be connected to the solution in question by means of a liquid junction. The estimation of the resulting liquid-junction potentials then introduces less uncertainty than the use of an unreliable reference electrode.

5.3 THE HYDROGEN ELECTRODE

Some reference electrodes commonly used in electrochemistry are introduced in this and the following three sections. It is not the purpose of these sections to present a complete process for preparing a reference electrode. These commonly used reference electrodes are used only as examples to show what important factors should be considered in the selection and preparation of reference electrodes. Therefore, the methods of purification of the chemicals and the structure of the cells, which are very important in experimental work, are not included.

The hydrogen electrode is the best reference electrode in aqueous solutions, not only because its potential is universally adopted as the primary standard with which all other electrodes are compared, but also because it is easy to prepare and capable of the highest degree of reproducibility. Another advantage of the hydrogen electrode is that it has a broad field of application. It can be used over large ranges of temperature, pressure, and pH and in many nonaqueous or partly aqueous solutions. The disadvantage of the hydrogen electrode is that its equilibrium depends on the catalytic activity of the metal surface. Thus, its reproducibility and stability are affected by the condition and the aging effect of the metal surface.

The reaction mechanism of the hydrogen electrode is still not clear and free from arguments. However, one can see that, before they can undergo the electrochemical reaction, the hydrogen molecules dissolved in the solution must first dissociate into hydrogen atoms:

$$H_2\ (\text{aq soln}) \rightleftharpoons 2H\ (\text{adsorbed on metal surface}) \rightleftharpoons 2e^- + 2H^+\ (\text{aq soln}). \tag{5.2}$$

Since the dissociation reaction of hydrogen molecules has a very high activation energy comparable to the heat of dissociation (431.8 kJ/mol), the equilibrium can be established only with the aid of a catalyst. Therefore, the metal phase in the hydrogen electrode not only conducts electrons but also acts as a catalyst.

The general requirements for a good metal for the hydrogen electrode are summarized as follows:

1. The metal must be noble and must not itself react or dissolve in the solution.
2. The metal must be a good catalyst for the hydrogen dissociation reaction; that is, the metal can adsorb hydrogen atoms on the surface but will not react with them to form a stable hydride.
3. The metal should not absorb the hydrogen atoms into its crystal lattice, or the equilibrium of the hydrogen electrode will be disturbed.
4. The metal surface should be made by finely divided deposits. Because the catalytic activity of the metal surface is associated with crystal imperfections, the metal surface made by finely divided deposits increases not only the real surface area but also the active catalytic sites.
5. In nonaqueous or partly aqueous solutions, the metal must not promote undesired nonelectrochemical hydrogenation reactions.

Palladium is the best catalyst for the hydrogen dissociation reaction but is not suitable for the hydrogen electrode because a large amount of hydrogen atoms can penetrate into the metal phase; these hydrogen atoms then become inaccessible to the liquid phase, with which they are required to remain in equilibrium. A thin layer of palladium deposited on gold or platinum is satisfactory. Platinized platinum, because of its large surface area, although slightly permeable to hydrogen atoms, is the best metal for the hydrogen electrode. In those cases in which the presence of platinized platinum in the solution will promote some undesirable hydrogenation reactions in nonaqueous or partly aqueous solutions, bright platinum or gold can be used. The surface of bright platinum or gold should be activated by anodic treatment or by chemical treatment with strong oxidizing reagents, such as chromic

acid or aqua regia. Transition metals are also suitable as catalysts for the hydrogen dissociation reaction because of their incompletely filled *d* orbitals.

Some impurities carried by the hydrogen gas are undesirable and should be eliminated. Oxygen will participate in a corrosion reaction on the metal surface. This oxide reacts with the dissolved hydrogen and decreases the concentration of the dissolved hydrogen gas in the neighborhood of the electrode, thus making the potential of the hydrogen electrode shift to the positive side. However, oxygen can activate the catalytic activity of the metal and prolong the life of the electrode. Therefore, a trace of dissolved oxygen in the solution is desirable when a bright platinum or gold electrode is used. Carbon dioxide dissolved in the solution can change the pH of the solution. Other impurities, such as arsenic and sulfur compounds, can act as catalyst poisons and shorten the life of the electrode.

Hydrogen gas directly generated by the electrolytic process is very pure but is unsuitable for hydrogen electrodes because it carries some solution and is not free of oxygen. Pure commercial hydrogen after deoxygenation and passing through a *dust trap* containing potassium hydroxide, which also serves as a carbon dioxide absorbent, is satisfactory. The most common deoxygenation process is to pass the hydrogen gas through a commercial deoxygenating cartridge containing platinum catalysts that are active at room temperature. The other method of deoxygenation is to pass the hydrogen gas through a clean vitreous silica tube containing hot reduced copper (450 to 700°C) or hot palladized or platinum asbestos (200°C).

If rubber tubing is used for the connection, it should be pretreated by boiling in caustic soda solution, thoroughly washed, and then aged for 24 hours in hydrogen gas because sulfur compounds may come from the rubber tubing.

To maintain a constant concentration of the electrolyte, the hydrogen gas should be presaturated with the solvent at the same vapor pressure as that of the electrolytic solution at the same temperature before it enters the cell.

The stability of hydrogen electrodes can be affected by the presence of impurities in three additional ways:

1. The impurities themselves can be reduced by the dissolved hydrogen gas to form soluble products. This will seriously deplete the concentration of the molecular hydrogen in the solution, and the potential of the hydrogen electrode will be displaced positively. Dissolved oxygen gas, CrO_4^{2-}, and Fe^{3+} all fall into this category.
2. Some cations of metals—such as silver, mercury, copper, and lead—can be reduced and deposit as solids, covering the electrode surface and changing the properties of the electrode.
3. Impurities—such as arsenic and sulfur compounds and some organic compounds—can be adsorbed on the active centers of the metal surface and can poison the catalytic activity.

Even in the absence of impurities, the catalytic activity of the metal surface can be destroyed by the *hydrogen poison,* which means that the active centers on the metal surface are *burned out* by the combination reaction of the hydrogen atoms. Since the catalytic activity of the metal surface is associated with crystal imperfections, the active sites are in a higher energy state than the perfect crystal surface. With the help of a large amount of energy delivered by the combination reaction of hydrogen atoms, the active centers can return to the lower energy state (perfect crystal surface) and lose their catalytic activity. An aged or fatigued hydrogen electrode should be reactivated or replatinized before being used again.

In aqueous solutions, the hydrogen electrode can be used in a wide range of pH. It has been used in alkali hydroxide solutions up to a molality of 4 mol/kg and in sulfuric acid solutions up to a molality of 17.5 mol/kg. However, it fails in neutral solutions in the absence of buffers. The hydrogen electrode potential is very sensitive to the pH. In neutral solutions with even a trace of current passed through the cell, the pH of the solution in the neighborhood of the electrode will change considerably.

The pressure of the hydrogen gas can be measured accurately with a barometer. However, in most cell designs, hydrogen gas is bubbled through the solution. Therefore, the effective pressure of the hydrogen gas should be used in potential calculations. For aqueous solutions, the effective pressure can be calculated from the empirical equation:

$$p_{H_2} = p_{bar} - p_{soln} + \frac{0.4h}{13.6}, \tag{5.3}$$

where p_{bar} is the barometric pressure (mmHg), p_{soln} is the vapor pressure of the solution (mmHg), and h is the depth of immersion of the bubbler (mm). Recall that fugacities are to be used in potential calculations (see Problem 2.14).

The hydrogen electrode can also be used in many nonaqueous and partly aqueous solutions, especially alcoholic solutions.

5.4 THE CALOMEL ELECTRODE AND OTHER MERCURY–MERCUROUS SALT ELECTRODES

Mercury is a noble liquid metal, easy to purify, with a completely reproducible surface. Therefore, it is considered to be the best electrode metal. Many mercurous salts have a very low solubility in water and are suitable for the preparation of an electrode of the second kind. However, these advantages of mercury–mercurous salt electrodes are offset by the fact that mercury has two valence states, and all mercurous salts can disproportionate. The calomel electrode (Hg/Hg_2Cl_2) is the most common of all the mercury–mercurous salt electrodes and is used as an example for the discussion in this section.

The calomel electrode was first introduced by Ostwald in 1890. However, no reproducible potential could be obtained, except in saturated KCl solution, and it was rejected for a period of 20 years. In later studies, it was found that many precautions must be taken to obtain a reproducible calomel electrode, as summarized below.

1. *Interaction between the calomel and the mercury surface*. If calomel is added to mercury already covered by solution, no satisfactory reversibility can be obtained. If very finely divided calomel contacts the mercury surface in the dry state, it spreads rapidly, almost violently, over the whole surface and forms a pearly skin. This pearly skin is preserved after solution is added and gives a reproducible electrode. It is suggested that a calomel electrode prepared in this way has a monolayer of calomel molecules covering the mercury surface, with their chlorine atoms covalently bonded to the mercury surface. The calomel molecules act as a two-dimensional gas, free to move along the mercury surface and able to sustain fast exchange equilibria.

   To prepare a reproducible calomel electrode, the very finely divided calomel should first be mixed with mercury to form *calomel–mercury paste*; then this paste is added to the mercury surface in small amounts until the whole surface is covered with *pearly calomel skin*.

   Excess calomel on the mercury surface segregates the solution on the mercury surface from the bulk of the solution. This magnifies the results of any residual nonequilibrium in the system and makes an untidy electrode. The potential is sensitive to movement and is generally unreproducible. A very thin layer of calomel covering the mercury surface is all that is required for a good calomel electrode.

   It was found that the coarse size of calomel particles is not suitable for the calomel electrode. It causes a positive deviation of potential, slow to decay, and leads to erratic behavior. Very finely divided (0.1 to 0.5 μm) calomel particles prepared by the chemical precipitation method are satisfactory. The calomel should be stored in a dark place with exclusion of moisture and air before use.

2. *Wedge effect*. Aqueous solutions can penetrate into the space between the mercury and the glass wall by capillary action, called the *wedge effect*. This will create a large area of thin liquid film contacting the mercury. The properties of this liquid film may not be the same as those in the bulk of the solution. Because of the large area, this thin liquid film can affect the behavior of the electrode seriously.

   The wedge effect can be eliminated by rendering the electrode vessel hydrophobic by treatment with a silicone preparation. Any platinum–glass seal should be avoided. The electric connection is formed by filling a capillary tube with mercury and making electric contact with a removable platinum wire in the remote end.
3. *Dissolved oxygen*. If the solution contains dissolved oxygen, a corrosion reaction will occur:

$$2\mathrm{Hg} + 2\mathrm{HCl} + \frac{1}{2}\mathrm{O_2} \rightarrow \mathrm{Hg_2Cl_2} + \mathrm{H_2O}, \tag{5.4}$$

   shifting the potential positively toward that of the oxygen electrode. In addition, the reaction will result in a gradual change in the properties of the electrolytic solution in the neighborhood of the electrode. This reaction had been known for a long time, but it was thought to be of significant effect only in low concentrations of HCl. Later it was found that this reaction can affect the electrode potential seriously, not only in a high concentration of HCl solution but also in KCl solution.
4. *Disproportionation reaction*. Because of the two valency states of mercury, mercuric ions are produced by a disproportionation reaction. Mercuric ions have a tendency to form complexes. Consequently, two distinct potentials tend to result for the calomel electrode. When a half-cell ($\mathrm{Hg/Hg_2Cl_2/HCl}$) is freshly set up, thermal and other equilibria (diffusion, adsorption, etc.) will be established at a normal rate; and the potential of the cell will level off to a value that is constant within 10 μV over several hours. This is the potential corresponding to the *metastable calomel electrode*. In this case, the solution of the cell is still free from mercuric ions.

   The potential of the *metastable calomel electrode* is not constant. It will increase to a higher value, corresponding to the potential of the *stable calomel electrode,* in which a complete equilibrium among mercury, calomel, and mercuric entities in the solution is established. The difference of the potential between these two calomel electrodes is as much as 0.24 mV at 25°C.

The calomel electrode is best used in acid solution (HCl). The standard potential has been determined over a range of temperatures by a number of workers. Since nearly all potential measurements performed before 1922 were affected by dissolved oxygen, the standard potential of the calomel electrode is not determined without argument because of the limited amount of reliable experimental data.

Due to the disproportionation reaction, two types of calomel electrodes have been distinguished. The *metastable calomel electrode* is satisfactory for isothermal measurements not extending over a long interval of time, applied to the low ranges of concentration and temperature ($c \leq 0.1\ N$; $t \leq 25\ ^\circ\mathrm{C}$). The *stable calomel electrode* is a very sluggish electrode, but its use is obligatory in the higher ranges of concentration and temperature in which, however, its useful life is limited.

The calomel electrode is also commonly used as a standard half-cell of fixed potential. In this case, concentrated neutral KCl solution is used rather than dilute HCl because it is very seldom that the fixed-potential half-cells are required to show a reproducibility better than 0.1 mV and because the disproportionation reaction of the calomel and the oxidation reaction are much slower in concentrated neutral KCl solution.

Among the mercurous salt electrodes, the mercury–mercurous sulfate electrode is second in popularity to the calomel electrode. It is, of course, reversible to sulfate ions. Because mercurous fluoride can be rapidly and completely hydrolyzed in aqueous solution, it is very seldom used as a

reference electrode in aqueous solution. However, it has been used in some nonaqueous solvents, such as liquid hydrogen fluoride.

The behavior of the mercury–mercurous bromide and iodide electrodes is similar to that of the calomel electrode. However, they have two disadvantages compared to the calomel electrode: They are more photosensitive, especially to ultraviolet light; and, while the solubility products decrease markedly in the order from chloride to bromide to iodide, the formation constants of the corresponding complex mercuric halides increase rapidly in the same order and progressively restrict the range of halide concentration in which potential measurements can usefully be made. Therefore, they are used only in special cases. Mercurous phosphate, iodate, and acetate have also been used as the bases of reference electrodes.

5.5 THE MERCURY–MERCURIC OXIDE ELECTRODE

As the calomel electrode is commonly used in acid solutions, so the mercury–mercuric oxide electrode ($Hg/HgO/OH^-$) is commonly used in alkaline solutions. Since mercurous oxide does not exist, there is no disturbing effect due to a variable valence of the mercuric oxide. The formal acidic and basic dissociation constants of mercuric oxide have been estimated to be very small. It is more basic than acidic. Therefore, the usefulness of the mercury–mercuric oxide electrode is confined to alkaline solutions.

The mercury–mercuric oxide electrode has a relatively long life, is stable for several days, and is reproducible to better than ± 0.1 mV. It is easy to prepare; no special precaution is needed if the chemicals are reasonably pure.

The standard potential of the mercury–mercuric oxide electrode has been investigated intensively by many authors. All data agree within 0.4 mV, which indicates that the mercury–mercuric oxide electrode is well behaved.

5.6 SILVER–SILVER HALIDE ELECTRODES

Due to the low solubility of silver halides, silver–silver halide electrodes are electrodes of the second kind. Among them, the most common is the silver–silver chloride electrode [$Ag/AgCl(s)/Cl^-$], which is reversible to the chloride ion. The relationship of its standard electrode potential to that of the silver electrode and the solubility product of silver chloride was treated in Problem 2.13.

The advantages of the silver–silver chloride electrodes are that they are small and compact, can be used in any orientation, and usually do not significantly contaminate any medium into which they are immersed. The disadvantage is that their thermodynamic properties depend on the physical properties of the solid phases, such as mechanical strain and crystal structure, and thus depend on the method of preparation.

There is still no method to prepare a perfect silver–silver halide electrode. Three methods are commonly used in experimental work:

1. *Electrolytic*. Platinum metal is generally used as the electrode base on which a layer of silver is electrodeposited from a solution of $KAg(CN)_2$. After thorough washing, the silver-plated electrode is halidized anodically; in 0.1 *N* HCl solution for a silver chloride electrode and, for silver bromide and silver iodide electrodes, in 0.1 *N* KBr or KI solutions, sometimes made weakly acidic by adding the appropriate acid. About 10% of the silver is halidized. The reproducibility of silver–silver halide electrodes prepared by this method should be within ± 0.02 mV.

2. *Thermal*. The thermal electrodes are prepared by the decomposition of a mixture of silver oxide and silver chlorate, bromate, or iodate, the proportion being approximately 90% silver oxide by weight. Conductance water is added to the mixture to form a smooth paste. A platinum wire spiral is covered with the paste, heated to the decomposition temperature of 650°C, and then slowly cooled to room temperature.

   Silver iodide is sometimes used in the preparation of the silver–silver iodide electrodes (and heated with Ag_2O to 450°C for 10 to 15 minutes), and a mixture of silver oxide and silver perchlorate has also been used in the preparation of silver chloride electrodes.

   The thermal silver–silver halide electrodes are less reliable than the electrolytic or thermal-electrolytic electrodes, probably because the surface condition of the latter types is more reproducible.
3. *Thermal-electrolytic*. By this method, silver is first prepared by decomposing silver oxide and then halidizing by the electrolytic process. The reproducibility of the silver–silver chloride electrode prepared by this method should be within 0.04 mV.

Several less common methods, which we shall not consider here, have also been used in the preparation of silver–silver halide electrodes.

The standard potential of the silver–silver chloride electrode has been thoroughly investigated from the cell

$$H_2 \mid HCl, H_2O \mid AgCl(s) \mid Ag. \tag{5.5}$$

In the temperature range from 0 to 95°C, the results can be expressed as

$$U^\theta = 0.23659 - 4.8564 \times 10^{-4} t - 3.4205 \times 10^{-6} t^2 + 5.869 \times 10^{-9} t^3 \text{ (V)}, \tag{5.6}$$

where t is temperature (°C). The standard potentials of the silver bromide and silver iodide electrodes have also been investigated over a range of temperature, although that of the AgI electrode has been more difficult to establish by direct measurement because of experimental difficulties, such as the oxidation of the HI solution.

Certain impurities, such as iodide and sulfide, can form silver salts with solubilities lower than that of silver chloride or silver bromide and can deposit on the electrode surface, thus changing the electrode potential. Even a trace of bromide in the solution will shift the potential of the silver–silver chloride electrode to the positive side. Oxygen dissolved in the electrolytic solutions can affect the behavior of the silver chloride and bromide electrodes if HCl or HBr is used as the electrolyte by means of the slow oxidation reaction:

$$2Ag + 2HCl + \frac{1}{2}O_2 \rightarrow 2AgCl + H_2O. \tag{5.7}$$

For the silver iodide electrode, a marked oxygen effect is noted in both neutral and acidic solutions.

All silver–silver halide electrodes are subject to the aging effect. The potentials of the older electrodes are slightly positive relative to the new electrodes. This effect is always in the same direction and of the same order of magnitude, about 0.05 mV. The potential of a freshly prepared silver–silver halide electrode increases slowly and will reach a stable value. The period of the aging effect varies from a few minutes to 1 to 20 days. This effect has been attributed to a concentration polarization associated with the electrolytic halidization or the initial immersion of the electrode in the solution being investigated.

Silver–silver halide electrodes are widely used in electrochemical measurements because they are compact and easy to set up. The most important application of the silver–silver chloride electrode is in the investigation of the thermodynamic properties of electrolytes, such as the standard electrode

potential and the activity coefficients. Silver–silver halide electrodes can also be applied in nonaqueous solutions. However, this application is limited by the strong tendency for complex formation of the silver ion, which will greatly increase the solubility of the silver halides. Silver chloride electrodes have important applications in the investigation of the behavior of biological membranes.

5.7 POTENTIALS RELATIVE TO A GIVEN REFERENCE ELECTRODE

Not infrequently one encounters in the literature a set of potentials of various electrodes, in various solutions, referred to a given reference electrode, for example, to a normal calomel electrode in KCl. It is usually noted that these potentials are *corrected for liquid-junction potentials*, whatever that might mean. Let us inquire into what quantity is tabulated, and why such a tabulation might be useful.

Let U' be "the potential of a given electrode relative to a normal calomel electrode in KCl, corrected for liquid-junction potentials." The half-cell of interest is

$$\begin{array}{c|c|c} \delta & \beta & \alpha' \\ \text{solution} & \text{electrode} & \text{Pt(s).} \\ \text{(e.g., 0.1 } N \text{ NaCl)} & \text{(e.g., Hg)} & \end{array} \tag{5.8}$$

If U' is to be a thermodynamic quantity of interest, it must assess the electrical state of electrode β relative to solution δ since these are the only relevant phases.

We should want U' to be a thermodynamic quantity since we should have measured the potential U relative to a well-defined electrode appropriate to the system; for example,

$$\begin{array}{c|c|c|c|c|c} \alpha & \phi & \epsilon & \delta & \beta & \alpha' \\ \text{Pt}(s) & \text{Hg}(l) & \text{Hg}_2\text{Cl}_2(s) & \begin{array}{c}0.1\ N \text{ NaCl} \\ \text{in } \text{H}_2\text{O}\end{array} & \text{Hg}(l) & \text{Pt}(s), \end{array} \tag{5.9}$$

and the introduction of any liquid-junction potential in the conversion to U' would obviate such a useful measurement. The note, *corrected for liquid-junction potentials,* is a further hint that a thermodynamic quantity is intended, although it may also give the erroneous impression that a liquid junction was involved in the measurement.

By these arguments we are led to the conclusion that U' is given by

$$FU' = -\mu_{e^-}^{\beta} - F\Phi^{\delta} + \text{const}, \tag{5.10}$$

where Φ is the quasi-electrostatic potential relative to some ionic species n. (The outer potential Φ might have been intended, but then U' would be a nonthermodynamic quantity.) It seems logical that ion n should be either Cl^- or K^+ since these ions are in the statement of the reference electrode (normal calomel electrode in KCl). The chloride ion is the more likely candidate since the calomel electrode responds to this ion.

In seeking the value of the constant in equation 5.10, we are led next to conclude that U' is the potential of the system

$$\begin{array}{c|c|c|c|c|c} \alpha & \phi & \epsilon & \lambda \quad\quad \delta & \beta & \alpha' \\ \text{Pt}(s) & \text{Hg}(l) & \text{Hg}_2\text{Cl}_2(s) & \begin{array}{l}1\ N \text{ KCl} - - - \text{solution} \\ \text{in } \text{H}_2\text{O}\end{array} & \text{electrode} & \text{Pt}(s). \end{array} \tag{5.11}$$

The dashed line does not denote a junction region. Instead, we make the (perhaps imaginary) requirement that the electrical states of solutions λ and δ are related by

$$\Phi^{\lambda} = \Phi^{\delta}. \tag{5.12}$$

The potential of this system is thus given by

$$\begin{aligned} FU' &= -F(\Phi^{\alpha} - \Phi^{\alpha'}) \\ &= -\mu^{\beta}_{e^-} - F\Phi^{\delta} + \mu^{\phi}_{Hg} - \frac{1}{2}\mu^{\epsilon}_{Hg_2Cl_2} + RT \ln c^{\lambda}_{Cl^-}. \end{aligned} \tag{5.13}$$

Since phases ϕ and ϵ are pure phases, we thus determine that the constant in equation 5.10 is

$$\text{const} = \mu^{0}_{Hg} - \frac{1}{2}\mu^{0}_{Hg_2Cl_2} + RT \ln c^{\lambda}_{Cl^-}, \tag{5.14}$$

where $c^{\lambda}_{Cl^-} = 1$ mol/liter.

Note that the electrode β could be a reversible electrode at equilibrium, an ideally polarizable electrode (see Section 7.1), an irreversible electrode, or an electrode undergoing one or more electrode reactions without affecting the above arguments. Similarly, the solution δ could be of any composition.

Now consider explicitly system 5.9, for which the potential U is given by

$$FU = -\mu^{\beta}_{e^-} + \mu^{\delta}_{Cl^-} + \mu^{0}_{Hg} - \frac{1}{2}\mu^{0}_{Hg_2Cl_2}. \tag{5.15}$$

Hence, the difference is

$$FU - FU' = RT \ln \frac{c^{\delta}_{Cl^-}}{c^{\lambda}_{Cl^-}}. \tag{5.16}$$

The conversion from the measured value of U to the desired value of U' is, thus, very simple in this case.

Now let us take solution δ to be 0.1 N Na_2SO_4 and let us suppose that U is measured relative to a lead–lead sulfate electrode; that is, U is now the potential of the system

$$\begin{array}{c|c|c|c|c|c|c} \alpha & \phi & \epsilon & \delta & \beta & \alpha' \\ Pt(s) & Pb(s) & PbSO_4(s) & \begin{array}{c}0.1\ N\ Na_2SO_4 \\ \text{in } H_2O\end{array} & Hg(l) & Pt(s), \end{array} \tag{5.17}$$

that is,

$$FU = -\mu^{\beta}_{e^-} + \frac{1}{2}\left(\mu^{0}_{Pb} + \mu^{\delta}_{SO_4^{2-}} - \mu^{0}_{PbSO_4}\right). \tag{5.18}$$

The difference between U and U' is now given by

$$\begin{aligned} FU - FU' = &\frac{1}{2}\left(\mu^{0}_{Pb} + \mu^{\delta}_{SO_4^{2-}} - \mu^{0}_{PbSO_4}\right) + F\Phi^{\delta} \\ &- \mu^{0}_{Hg} + \frac{1}{2}\mu^{0}_{Hg_2Cl_2} - RT \ln c^{\lambda}_{Cl^-}. \end{aligned} \tag{5.19}$$

Substitution of equation 3.19 for $\mu^{\delta}_{SO_4^{2-}}$ gives

$$FU - FU' = \frac{1}{2}\left(\mu^0_{Pb} - \mu^0_{PbSO_4} + RT\ \ln\ a^{\theta}_{SO_4^{2-}}\right) - \mu^0_{Hg} + \frac{1}{2}\mu^0_{Hg_2Cl_2} - RT\ \ln a^{\theta}_{Cl^-} + \frac{1}{2}RT\ \ln\ \frac{c^{\delta}_{SO_4^{2-}} f^{\delta}_{SO_4^{2-}}}{\left(c^{\lambda}_{Cl^-} f^{\delta}_{Cl^-}\right)^2}. \tag{5.20}$$

For standard electrode potentials referred to the hydrogen electrode, we have for the lead sulfate electrode (Table 2.2)

$$FU^{\theta}_{PbSO_4} = \frac{1}{2}\left(\mu^*_{H_2} + \mu^0_{PbSO_4} - \mu^0_{Pb}\right) - \frac{1}{2}RT \ln\left[\left(\lambda^{\theta}_{H^+}\right)^2 \lambda^{\theta}_{SO_4^{2-}}\right], \tag{5.21}$$

$$U^{\theta} = -0.356\ \text{V}, \tag{5.22}$$

and for the calomel electrode (Table 2.3)

$$FU^{\theta}_{Hg_2Cl_2} = \frac{1}{2}\left(\mu^*_{H_2} + \mu^0_{Hg_2Cl_2}\right) - \mu^0_{Hg} - RT \ln\left(\lambda^{\theta}_{H^+}\ \lambda^{\theta}_{Cl^-}\right), \tag{5.23}$$

$$U^{\theta} = 0.2676\ \text{V}. \tag{5.24}$$

Since (see equation 2.20)

$$\lambda^{\theta}_i = \rho_0 a^{\theta}_i, \tag{5.25}$$

equation 5.20 becomes

$$FU - FU' = FU^{\theta}_{Hg_2Cl_2} - FU^{\theta}_{PbSO_4} + \frac{1}{2}RT \ln\left[\frac{\rho_0 c^{\delta}_{SO_4^{2-}} f^{\delta}_{SO_4^{2-}}}{(c^{\lambda}_{Cl^-} f^{\delta}_{Cl^-})^2}\right]. \tag{5.26}$$

Because of the conventions that have been adopted in establishing Tables 2.2 and 2.3, ρ_0, the density of the pure solvent, should be expressed in g/cm^3 and the concentrations c_i, should be expressed in mol/liter.

We now need the activity coefficient of sulfate ions relative to chloride ions in the 0.1 N Na_2SO_4 solution δ. It should be emphasized that this is a thermodynamic quantity despite the fact that no chloride ions exist in this solution. Let us use Guggenheim's expression for multicomponent solutions (see Section 4.5) as written on a concentration scale (see Problem 4.4):

$$\ln f_i - \frac{z_i}{z_n} \ln f_n = \frac{\alpha' z_i (z_i - z_n)\sqrt{I'}}{1 + B' a \sqrt{I'}} + 2 \sum_j \left(\beta'_{ij} - \frac{z_i}{z_n}\beta'_{nj}\right) c_j, \tag{5.27}$$

where I' is given by equation 4.22 and α' is given by equation 4.25 or Table 4.1. See Problem 4.4 for the relationship of β' to β. Then

$$\ln \frac{f^{\delta}_{SO_4^{2-}}}{(f^{\delta}_{Cl^-})^2} = -\frac{2\alpha'\sqrt{I'}}{1 + B' a \sqrt{I'}} + 2(\beta'_{Na_2SO_4} - 2\beta'_{NaCl}) c^{\delta}_{Na^+}. \tag{5.28}$$

The calculation of the potential U' from the measured potential U is somewhat complicated in this case, but it introduces no nonthermodynamic concepts.

Finally, suppose that the potential U'' of the cell with liquid junction

$$\begin{array}{c|c|c|c|c|c|c} \alpha & \phi & \epsilon & \kappa & \delta & \beta & \alpha' \\ \mathrm{Pt}(s) & \mathrm{Hg}(l) & \mathrm{Hg_2Cl_2}(s) & 0.1\ N\ \mathrm{KCl} & 0.1\ N\ \mathrm{NaCl} & \mathrm{Hg}(l) & \mathrm{Pt}(s) \\ & & & \text{in } \mathrm{H_2O} & \text{in } \mathrm{H_2O} & & \end{array} \tag{5.29}$$

has been measured. How should we obtain U'? The potential U'' is given by

$$\begin{aligned} FU'' &= -F(\Phi^{\alpha} - \Phi^{\alpha'}) \\ &= -\mu^{\beta}_{e^-} - F\Phi^{\kappa} + \mu^{\phi}_{\mathrm{Hg}} - \frac{1}{2}\mu^{\epsilon}_{\mathrm{Hg_2Cl_2}} + RT\ \ln\ c^{\kappa}_{\mathrm{Cl}^-}. \end{aligned} \tag{5.30}$$

Hence,

$$FU'' - FU' = F(\Phi^{\delta} - \Phi^{\kappa}) + RT\ \ln\ \frac{c^{\kappa}_{\mathrm{Cl}^-}}{c^{\lambda}_{\mathrm{Cl}^-}}. \tag{5.31}$$

Thus, we must obtain an estimate of the liquid-junction potential $\Phi^{\delta} - \Phi^{\kappa}$ between solutions δ and κ, which is beyond the scope of the present chapter. For the last term, $c^{\kappa}_{\mathrm{Cl}^-} = 0.1\ N$ and $c^{\lambda}_{\mathrm{Cl}^-} = 1\ N$.

If solution κ had been a $1\ N$ KCl solution, that is, the left electrode in cell 5.29 were a normal calomel electrode in KCl, then the last term in equation 5.31 would be zero, but we would instead have to estimate $\Phi^{\delta} - \Phi^{\kappa}$ for the junction between $1\ N$ KCl and 0.1 N NaCl.

The result in equation 5.31 can be applied to the case where solution δ is different, say $0.1\ N$ Na_2SO_4. One still has to estimate the liquid-junction potential $\Phi^{\delta} - \Phi^{\kappa}$, referred to the chloride ion.

These examples make it clear that U' represents a thermodynamic quantity. A *correction for liquid-junction potentials* is necessary only if a measurement was made on a cell with liquid junction; and the correction concerns the junction in that cell, which may not involve normal KCl at all. The examples also show that the definition of U' could involve a normal calomel electrode in NaCl without changing the numerical values.

One may well ask why he or she should use potentials relative to a normal calomel electrode in KCl. Why not use a mercury–mercuric oxide electrode for solutions of KOH, a lead–lead sulfate electrode for solutions of Na_2SO_4, and a calomel electrode in NaCl for solutions of NaCl, always letting the electrolyte concentration in the reference electrode be the same as in the solution of interest? In at least two cases, some insight into the physical situation is afforded by the use of one given reference electrode. First, electrocapillary curves coincide on the negative branch plotted against U' (see Figure 7.12), indicating that cations are not specifically adsorbed at a mercury–solution interface. Second, anodic current densities in a metal dissolution reaction are relatively independent of solution composition when plotted against U' but not when plotted against, say, the surface overpotential η_s, which involves a shift of the equilibrium potential with the reactant concentration.

NOTATION

a	mean diameter of ions, cm
a_i^{θ}	property expressing secondary reference state, liter/mol
B'	Debye–Hückel parameter, $(\text{liter/mol})^{1/2}$/nm
c_i	molar concentration of species i, mol/liter
f_i	molar activity coefficient of species i

F	Faraday's constant, 96,487 C/mol
h	depth of immersion of bubbler, mm
i	current density, A/cm^2
i_0	exchange current density, A/cm^2
I'	molar ionic strength, mol/liter
p	pressure, mmHg
p_i	partial pressure or fugacity of species i, mmHg
R	universal gas constant, 8.3143 J/mol·K
T	absolute temperature, K
U	open-circuit cell potential, V
U'	electrode potential relative to a given reference electrode, V
U''	electrode potential measured with a liquid junction present, V
U^θ	standard electrode potential, V
z_i	charge number of species i
α_a, α_c	transfer coefficients
α'	Debye–Hückel constant, (liter/mol)$^{1/2}$
$\beta'_{i,j}$	coefficient for ion–ion specific interactions, liter/mol
η_s	surface overpotential, V
λ_i^θ	property expressing secondary reference state, kg/mol
μ_i	chemical or electrochemical potential of species i, J/mol
ρ_o	density of pure solvent, g/cm^3
Φ	electric potential, V

REFERENCES

1. David J. G. Ives and George J. Janz, eds., *Reference Electrodes* (New York: Academic, 1961).
2. James N. Butler, "Reference Electrodes in Aprotic Organic Solvents," *Advances in Electrochemistry and Electrochemical Engineering*, *7* (1970), 77–175.

CHAPTER 6

POTENTIALS OF CELLS WITH JUNCTIONS

In this chapter, we build on the material developed in Chapter 2, on thermodynamics in terms of electrochemical potentials. Numerical values of cell potentials can now be calculated from standard electrode potentials, ionic concentrations, and methods for estimating activity coefficients and liquid-junction potentials.

Taylor[1] showed clearly that the problems of measuring liquid-junction potentials and individual ionic activity coefficients are inexorably tied up with each other. Also of interest here is the work of MacInnes,[2] Wagner,[3] and Smyrl and Newman.[4]

6.1 NERNST EQUATION

The Nernst equation was defined at the end of Section 2.7. We can state here a more definite procedure for arriving at the appropriate form of the Nernst equation for a particular cell. We use cell 2.114 as an example.

1. Write down the expression for the cell potential using chemical potentials and electrochemical potentials as indicated in Chapter 2. For cell 2.114, this is given by equation 2.115:

$$FU = \frac{1}{2}\mu^{\alpha}_{H_2} - \mu^{\lambda}_{Ag} + \mu^{\epsilon}_{AgCl} - \mu^{\beta}_{H^+} - \mu^{\delta}_{Cl^-}. \tag{6.1}$$

2. Use equation 3.19 to express the electrochemical potentials of ions in solution. For gaseous components, use the fugacity as outlined in Problem 2.14. For the chemical potentials of pure

Electrochemical Systems, Fourth Edition. John Newman and Nitash P. Balsara.

phases, replace the superscript with 0. For alloys, use the expression for the activity, for example, equation 2.43. For equation 2.115, we now have

$$FU = \frac{1}{2}\mu^*_{H_2} - \mu^0_{Ag} + \mu^0_{AgCl} - RT\ln(a^\theta_{H^+}a^\theta_{Cl^-}) + \frac{1}{2}RT\ln p^\alpha_{H_2} - RT\ln(c^\beta_{H^+}c^\delta_{Cl-}) - RT\ln(f^\beta_{H^+}f^\beta_{Cl^-}) + F(\Phi^\delta - \Phi^\beta), \tag{6.2}$$

where the chloride ion has been chosen as species n in using equation 3.19.

3. Identify the standard cell potential, using equation 2.20 where necessary. Equation 6.2 becomes

$$FU = FU^\theta + \frac{1}{2}RT\ln p^\alpha_{H_2} - RT\ln\frac{c^\beta_{H^+}c^\delta_{Cl^-}}{\rho_0^2} - RT\ln(f^\beta_{H^+}f^\beta_{Cl^-}) + F(\Phi^\delta - \Phi^\beta), \tag{6.3}$$

where FU^θ corresponds to entry 7 in Table 2.2.

4. Set all ionic activity coefficients equal to 1, and neglect any difference in quasi-electrostatic potential between points in the solution. Equation 6.3 becomes

$$FU = FU^\theta + \frac{1}{2}RT\ln p^\alpha_{H_2} - RT\ln\frac{c^\beta_{H^+}c^\delta_{Cl^-}}{\rho_0^2}. \tag{6.4}$$

The potential difference $\Phi^\delta - \Phi^\beta$ in equations 6.2 and 6.3 can be called a liquid-junction potential. These quasi-electrostatic potentials are referred to the chloride ion. The ionic activity coefficients always appear in the equation in a manner that compensates for the arbitrary choice of species n. In writing the Nernst equation, both the liquid-junction potential and the ionic activity coefficients are discarded. It would be somewhat inconsistent to retain one but not the other in view of their dependence upon the choice of species n.

The rest of this chapter provides a basis for assessing the error involved in the Nernst equation. We can assert at the outset that we should rather seek other approximations for the cells of Section 2.6, involving a single electrolyte of varying concentration.

6.2 TYPES OF LIQUID JUNCTIONS

The potentials of cells with liquid junctions are assessed, using equation 2.68 to evaluate the variation of the electrochemical potential of an ion in the junction region. As already noted in Chapter 2, the integration of this equation requires a knowledge of the concentration profiles except in the simple case of a two-component solution, an electrolyte and a solvent or two electrolytes with a common ion in a fused salt. Consequently, we discuss first the popular models of liquid junctions.

1. *Free-diffusion junction*. At time zero, the two solutions are brought into contact to form an initially sharp boundary in a long, vertical tube. The solutions are then allowed to diffuse into each other, and the thickness of the region of varying concentration increases with the square root of time. Even if the transport properties are concentration dependent and the activity coefficients are not unity, the potential of a cell containing such a junction should be independent of time.
2. *Restricted-diffusion junction*. The concentration profiles are allowed to reach a steady state by one-dimensional diffusion in the region between $x = 0$ and $x = L$, in the absence of convection. The composition at $x = 0$ is that of one solution and, at $x = L$, that of the other solution. The potential of a cell containing such a junction is independent of L (as well as time). The condition

of no convection is usually not specified (i.e., zero solvent velocity or zero mass-average velocity, etc.).

3. *Continuous-mixture junction*. At all points in the junction, the concentrations (excluding, we suppose, that of the solvent) are assumed to be linear combinations of those of the solutions at the ends of the junction. This assumption obviates the problem of calculating the concentration profiles by the laws of diffusion.
4. *Flowing junction*. In some experiments, the solutions are brought together and allowed to flow side by side for some distance. It is sometimes supposed that observed potentials should approximate those given by a free-diffusion boundary.
5. *Electrode of the second kind*. To these we add the region of varying composition produced when a sparingly soluble salt is brought into contact with a solution containing a common ion. We might use a model similar to the free-diffusion junction if we imagine the salt to be introduced at the bottom of a vertical tube containing the solution. The sparingly soluble salt will then diffuse up the tube, and the concentration at the bottom will be governed by the solubility product.

6.3 FORMULAS FOR LIQUID-JUNCTION POTENTIALS

Substitution of equation 3.19 into equation 2.66 yields (see equation 12.49)

$$F\nabla\Phi = -\frac{F}{\kappa}\mathbf{i} - RT\sum_i \frac{t_i^0}{z_i}\nabla \ln c_i - RT\sum_i \frac{t_i^0}{z_i}\nabla\left(\ln f_i - \frac{z_i}{z_n}\ln f_n\right), \tag{6.5}$$

where Φ is the quasi-electrostatic potential referred to species n. Integration of this equation across the junction region in the absence of current is the basis of the calculation of liquid-junction potentials.

For solutions so dilute that the activity coefficients can be ignored, it becomes immaterial which species is chosen for species n. In these dilute solutions, we can use equation 11.9 to express the transference numbers, with the result that

$$F\nabla\Phi = -\frac{F}{\kappa}\mathbf{i} - RT\frac{\sum_i z_i u_i \nabla c_i}{\sum_j z_j^2 u_j c_j}, \tag{6.6}$$

where u_i is the mobility of species i.

It is now a relatively simple matter to perform the integration for the continuous-mixture junction, where the concentrations are given by

$$c_i = c_i^{\mathrm{II}} + \xi(c_i^{\mathrm{I}} - c_i^{\mathrm{II}}) \tag{6.7}$$

and where ξ varies from 0 in solution II to 1 in solution I. Equation 6.6, in the absence of current, becomes

$$F\nabla\Phi = -RT\frac{A\nabla\xi}{B^{\mathrm{II}} + (B^{\mathrm{I}} - B^{\mathrm{II}})\xi}, \tag{6.8}$$

where

$$A = \sum_i z_i u_i (c_i^{\mathrm{I}} - c_i^{\mathrm{II}}), \quad B^{\mathrm{I}} = \sum_i z_i^2 u_i c_i^{\mathrm{I}}, \quad B^{\mathrm{II}} = \sum_i z_i^2 u_i c_i^{\mathrm{II}}. \tag{6.9}$$

Integration gives

$$\Phi^{\mathrm{I}} - \Phi^{\mathrm{II}} = -\frac{RT}{F}A\frac{\ln(B^{\mathrm{I}}/B^{\mathrm{II}})}{B^{\mathrm{I}} - B^{\mathrm{II}}}. \tag{6.10}$$

This is the Henderson formula[5, 6] for the junction potential of a continuous-mixture junction, valid under the conditions cited in its derivation. Because of its simplicity, it is useful for estimating liquid-junction potentials. The ionic mobilities u_i in A and B can be replaced by the ionic diffusion coefficients D_i (see Table 11.1).

Planck[7, 8] has obtained an implicit expression for the liquid-junction potential for the restricted-diffusion junction for univalent ions where activity coefficients can be ignored. MacInnes[2] has reproduced the derivation of Planck's formula.

The Goldman[9] constant-field equation for liquid-junction potentials is popular among biologists. Although its basis has been justifiably criticized,[10] it predicts values that are in reasonable accord with those obtained by other methods.

6.4 DETERMINATION OF CONCENTRATION PROFILES

The concentration profiles in the junction region are governed by the laws of diffusion in cases 1, 2, and 5 of Section 6.2, the free-diffusion and restricted-diffusion junctions and the electrode of the second kind. The transport laws are developed in Section 11.1 for dilute solutions and in Section 12.1 for concentrated solutions. We treat solutions so dilute that we can neglect the interaction of the diffusing species with the other components except the solvent. The appropriate form of the diffusion law is developed in Section 11.9 (see also Section 12.5 and Ref. [4]). However, the activity coefficients are not assumed to be unity. Instead, Guggenheim's expression for dilute solutions of several electrolytes is used (see Section 4.5 and Problem 4.4).

To determine the concentration profiles in liquid junctions, then, involves solving the diffusion equation 11.72 or 12.29 in conjunction with the first equation of Problem 4.4 and with the material-balance equation 11.3, the electroneutrality equation 11.4, and the condition of zero current.

This problem can be solved numerically for the various models of liquid junction. In the case of restricted diffusion, the equations are already ordinary differential equations. For free diffusion and for an electrode of the second kind, the similarity transformation $Y = y/\sqrt{t}$ reduces the problem to ordinary differential equations. These coupled, nonlinear, ordinary differential equations can be solved readily by the method outlined in Appendix C. The equations can be linearized about a trial solution, producing a series of coupled, linear differential equations. In finite-difference form, these give coupled, tridiagonal matrices that can be solved on a digital computer. The nonlinear problem can then be solved by iteration.

6.5 NUMERICAL RESULTS

We present here calculated[4] values of the liquid-junction potential $\Delta\Phi$ for the several models (Section 6.2) for the junctions between solutions of various compositions. No detailed concentration profiles will be given since the potentials of cells with liquid junctions can be calculated directly from the tabulated values of $\Delta\Phi$, without further reference to the concentration profiles, as indicated in the next section. The tabulation of the values of $\Delta\Phi$, rather than the potentials of complete cells, is convenient because these values relate to the junction itself, whereas more than one combination of electrodes is possible for a given junction. In addition to $\Delta\Phi$, only thermodynamic data are needed to calculate potentials of complete cells, as the entire effect of the transport phenomena is included in $\Delta\Phi$.

The value of $\Delta\Phi$ depends on the choice of the reference ion n. In each case, this is the last ion for a given junction in the tables. For infinitely dilute solutions, $\Delta\Phi$ becomes independent of this choice and, furthermore, depends only on the ratios of concentrations of the ions in the end solutions. Solutions of zero ionic strength ($f_i = 1$) are indicated by an asterisk, but the concentrations are given nonzero values so that these ratios will be clear. These junctions also provide a basis for comparison with more concentrated solutions, to indicate the effect of the activity coefficients.

Table 6.1 gives values of $\Delta\Phi$ for the continuous-mixture, restricted-diffusion, and free-diffusion junctions. Table 6.2 gives values of $\Delta\Phi$ for an electrode of the second kind, where AgCl, with a solubility product* of 10^{-10} (mol/liter)^2, diffuses into hydrochloric acid solutions of various concentrations. For solutions of zero ionic strength, the values of $\Delta\Phi$ for the continuous-mixture and restricted-diffusion

TABLE 6.1 Values of $\Delta\Phi$ for various junctions and various models at 25°C[a]

	mol/liter		$\Phi_1 - \Phi_2$ (mV)		
Ion	Solution 1	Solution 2	Free diffusion	Restricted diffusion	Continuous mixture
H^+	0.2	0.1	—	—	−10.31
Cl^-	0.2	0.1	—	—	−11.43*
K^+	0.2	0.1	—	—	1.861 (2.05)[b]
Cl^-	0.2	0.1	—	—	0.335*
K^+	0	0.01	−33.50	−32.65	−33.75
H^+	0.02	0	−34.67*	−33.80*	−34.95*
Cl^-	0.02	0.01			
K^+	0	0.1	−27.31 (−27.08)[c]	−27.45	−27.47
H^+	0.1	0	(28.25, 18°)[d]	−26.85*	(28.10, 18°)[d]
Cl^-	0.1	0.1	(−28.3)[e] − 26.69*		−26.85*
K^+	0	0.2	−27.92	−28.04	−28.09
H^+	0.2	0	−26.69*	−26.85*	−26.85*
Cl^-	0.2	0.2			
K^+	0	0.2	−22.58	−23.03	−22.31
H+	0.1	0	−20.24*	−20.74*	−19.96*
Cl^-	0.1	0.2			
K^+	0	0.05	−20.70	−21.09	−20.23
H^+	0.02	0	−18.50*	−18.97*	−18.02*
Cl^-	0.02	0.05			
K^+	0	0.1	−18.02	−17.89	−16.84
H^+	0.02	0	−14.05*	−14.12*	−12.90*
Cl^-	0.02	0.1			
K^+	0	0.1	−15.91	−14.99	−14.04
H^+	0.01	0	−10.85*	−10.30*	−9.09*
Cl^-	0.01	0.1			
K^+	0	0.1	−27.24	−27.38	−27.40
H^+	0.09917	0	(−27.98)[f]	−26.77*	−26.76*
Cl^-	0.09917	0.1	−26.60*		
K^+	0	0.1			
H^+	0.09917	0	−27.39	−27.48	−27.55
NO_3^-	0	0.05	−26.53*	−26.62*	−26.70*
Cl^-	0.09917	0.05			
K^+	0.1	0.1	−0.157	−0.157	−0.157
NO_3^-	0.05	0	−0.423*	−0.423*	−0.423*
Cl^-	0.05	0.1			

*The solubility product actually is 1.77×10^{-10} (mol/kg)^2 (see Problem 2.13).

TABLE 6.1 Values of ΔΦ for various junctions and various models at 25°C[a] ***continued***

	mol/liter		$\Phi_1 - \Phi_2$ (mV)		
Ion	Solution 1	Solution 2	Free diffusion	Restricted diffusion	Continuous mixture
Na^+	0.1	0			
H^+	0	0.05	28.58	29.64	28.10
ClO_4^-	0	0.05	26.72*	27.90*	26.22*
Cl^-	0.1	0			
Na^+	0.1	0			
H^+	0	0.1	32.83	33.50	33.50
ClO_4^-	0	0.1	32.35*	33.11*	32.57*
Cl^-	0.1	0			
Na^+	0.2	0			
H^+	0	0.2	33.29	33.88	33.53
ClO_4^-	0	0.2	32.35*	33.11*	32.57*
Cl^-	0.2	0			
Na^+	0.05	0			
H^+	0	0.1	38.77	38.31	39.26
ClO_4^-	0	0.1	39.96*	39.58*	40.48*
Cl^-	0.05	0			
Cu^{2+}	0	0.1			
Ag^+	0.2	0	−6.22*	−6.22*	−6.22*
NO_3^-	0.2	0			
ClO_4^-	0	0.2			

[a] Values for $f_i = 1$ are indicated by an asterisk. The last ion is the reference ion. Experimental values are given in parentheses.
[b] Shedlovsky and MacInnes.[11]
[c] Chloupek et al.[12]
[d] Guggenheim and Unmack.[13]
[e] Grahame and Cummings.[14]
[f] Finkelstein and Verdier.[15]

TABLE 6.2 Values of ΔΦ for a Ag–AgCl electrode in HCl solutions at 25°C[a]

HCl, bulk (mol/liter)	$\Phi_0 - \Phi_\infty$ (mV)	$c^0_{Cl^-}/c^\infty_{Cl^-}$	$(\mu^\infty_{Cl^-} - \mu^0_{Cl^-})/F$ (mV)
10^{-4}	0.0198	1.00961	−0.226
5×10^{-5}	0.0737	1.0392	−0.914
2×10^{-5}	0.359	1.200	−4.32
10^{-5}	0.915	1.604	−11.22
5×10^{-6}	1.780	2.539	−22.16
2×10^{-6}	3.21	5.499	−40.58

[a] Chloride is the reference ion, and β' values are taken to be zero.

junctions agree with the values calculated from the formulas of Henderson and Planck, respectively (see Section 6.3). In Figure 6.1 are presented the results of more extensive calculations on the HCl–KCl junction. Some of the results in Table 6.2 have already been presented in Table 2.1 and discussed in connection with the errors in an electrode of the second kind in very dilute solutions. Table 6.2 shows that only a small part of the error is a "liquid-junction potential."

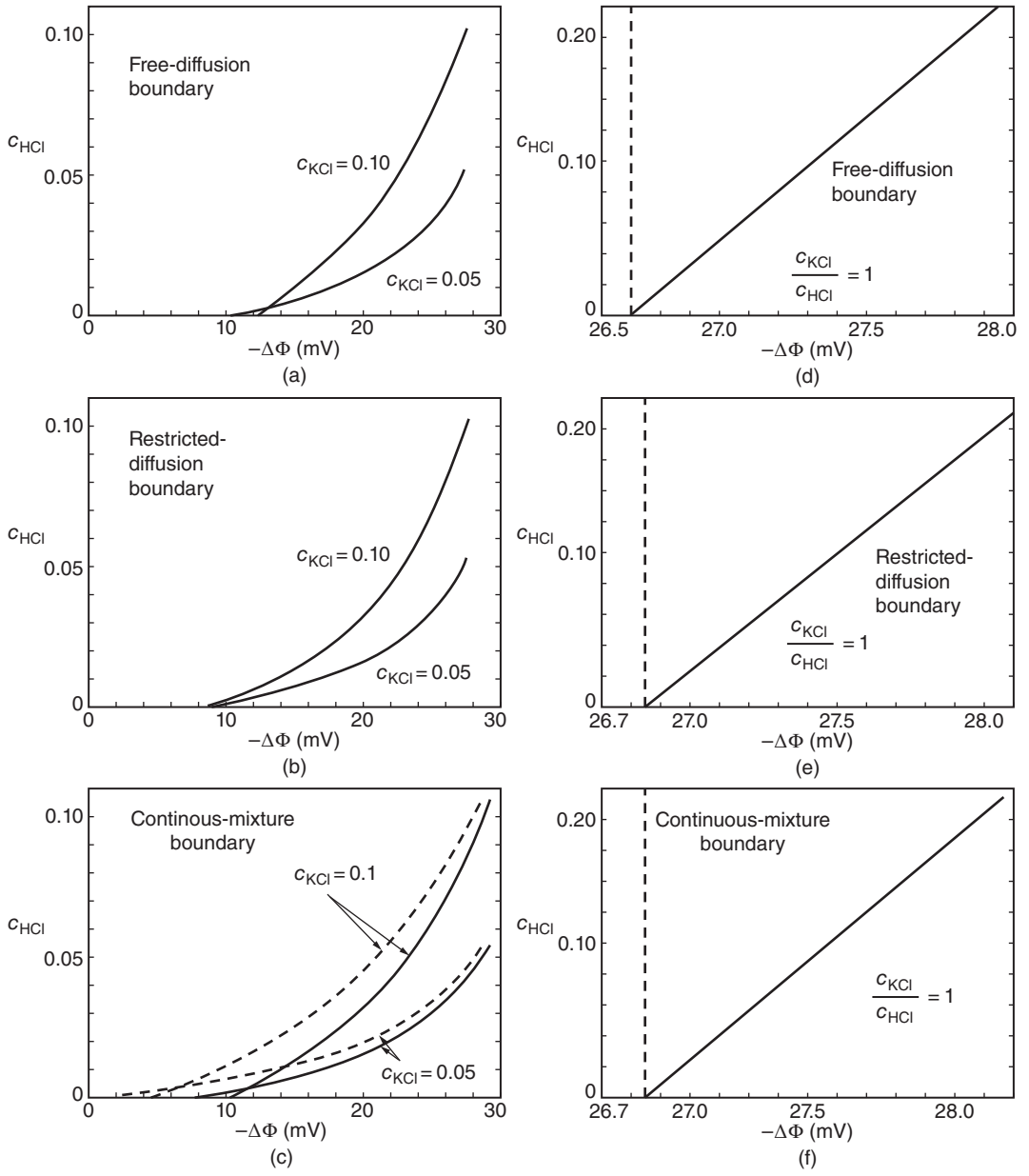

Figure 6.1 Calculated values of $\Delta\Phi$ for free-diffusion, restricted-diffusion, and continuous-mixture boundaries between HCl and KCl. (a–c) graphs are for given concentrations of KCl on one side of the boundary. (d–f) graphs are for a given ratio of concentrations on the two sides of the boundary. The dashed lines represent ideal-solution calculations; the solid lines include activity-coefficient corrections.

The only junction for which our calculations can be compared with other calculations and with experimental results is the 0.1 *M* HCl–0.1 *M* KCl junction. MacInnes and Longsworth[16] have made calculations for this junction of the free-diffusion type and reported a value of 28.19 mV to compare with 27.31 mV of the present study. Spiro[17] has discussed cells with liquid junctions, including salt bridges, for junctions of constant ionic strength across the junction and of the continuous-mixture

type and has included activity-coefficient corrections. For this HCl–KCl junction, Spiro calculated 29.07 mV, and we calculate 27.47 mV. The experimental results are given in Table 6.1. For further discussion of these comparisons, see Ref. [4].

6.6 CELLS WITH LIQUID JUNCTION

Once the concentration profiles are known for a liquid-junction region, it is then possible to calculate the effect of the nonuniform composition on the cell potential. The procedure involves first the treatment of electrode equilibria. This allows the expression of the cell potential in terms of a difference in the electrochemical potential of ions in the solutions adjacent to the two electrodes (see Chapter 2). The evaluation of this difference involves the integration of equation 2.68 across the junction region. Alternatively, one can proceed as in Section 6.1 to obtain an expression involving the liquid-junction potential, which has been evaluated in the course of determining the concentration profiles.

For the cells of Section 2.6, involving a single electrolyte of varying concentration, one should proceed directly with the evaluation of the integral since transference numbers and activity coefficients are usually known accurately for solutions of a single electrolyte and the cell potential does not depend on the method of forming the junction.

For cell 2.114, involving a junction between perchloric acid and a sodium chloride solution, the cell potential was expressed in Section 6.1 as

$$FU = FU^{\theta} + \frac{1}{2}RT \ln p^{\alpha}_{H_2} - RT \ln \frac{c^{\beta}_{H^+} c^{\delta}_{Cl^-}}{\rho_0^2} - RT \ln (f^{\beta}_{H^+} f^{\beta}_{Cl^-}) + F(\Phi^{\delta} - \Phi^{\beta}), \tag{6.11}$$

where FU^{θ} corresponds to entry 7 in Table 2.2 and Φ is referred to the chloride ion. In this case, it is particularly convenient to use the quasi-electrostatic potential since it is no longer necessary to select an intermediate solution in the junction (see equation 2.116). Evaluation of the terms in equation 6.11 for $c^{\beta}_{HClO_4} = 0.05\ M$ and $c^{\delta}_{NaCl} = 0.1\ M$ and a fugacity of hydrogen of 1 bar gives

$$U = 0.222 + 0 + 0.136 + 0.0096 + 0.0281 = 0.396\ \text{V}, \tag{6.12}$$

where the term 0.0281 corresponds to the continuous-mixture junction in Table 6.1.

A salt bridge is often used to separate two electrolytic solutions, and sometimes the stated purpose is "to eliminate liquid-junction potentials." We should now be in a position to evaluate whether this purpose is achieved, if we could define the liquid-junction potential that is supposed to be eliminated. (Recall that the definition in Section 6.1 depends on the choice of the reference species n.)

Such a salt bridge might be

$$\text{HCl (0.1 } M \text{ in } H_2O) \;\big\|\; \text{KCl (0.2 } M \text{ in } H_2O) \;\big\|\; \text{HCl (0.2 } M \text{ in } H_2O). \tag{6.13}$$

It seems clear that the salt bridge does not make the value of μ_{Cl^-} equal in the two hydrochloric acid solutions. The value of $\Delta\Phi$ (referred to the chloride ion) for this combination of junctions is 5.78 mV if the junctions are of the continuous-mixture type. This can be compared with the value $\Delta\Phi = 10.31$ mV for a single, direct junction between 0.1 and 0.2 M HCl solutions.

If the transference numbers of KCl were equal to 0.5 and if departures of activity coefficients from unity could be ignored, the liquid-junction potential of the combination of two junctions of the salt bridge should decrease as the concentration of KCl increases. If one insists on using salt bridges, one might consider as an alternative the series of junctions

$$\text{HCl (0.1 } M \text{ in } H_2O) \;\big|\!\big|\; \text{KCl (0.1 } M \text{ in } H_2O) \;\big|\!\big|\; \text{KCl (0.2 } M \text{ in } H_2O) \;\big|\!\big|\; \text{HCl (0.2 } M \text{ in } H_2O), \tag{6.14}$$

for which $\Delta\Phi = 1.24$ mV and for which the value of $\Delta\Phi$ would approach zero as all the concentrations were reduced in proportion if the transference numbers of KCl were 0.5.

6.7 ERROR IN THE NERNST EQUATION

The approximations made in the Nernst equation are to ignore liquid-junction potentials and to ignore the activity coefficients of ionic species in solution. Table 6.1 gives an idea of the range of magnitude of liquid-junction potentials. In the example treated in equation 6.11, the activity-coefficient term amounts to 10 mV, and the liquid-junction potential amounts to 28 mV.

Before one can decide whether it is more serious to neglect activity coefficients or liquid-junction potentials, one should inquire into the effect of using different species for the reference species n. The effect, of course, cancels if both activity coefficients and liquid-junction potentials are retained. For the junction between solutions δ and ϵ, this difference can be expressed as

$$F(\Phi^{\delta}_{n^*} - \Phi^{\epsilon}_{n^*}) = F(\Phi^{\delta}_{n} - \Phi^{\epsilon}_{n}) + \frac{RT}{z_{n^*}}\left(\ln\frac{f^{\delta}_{n^*}}{f^{\epsilon}_{n^*}} - \frac{z_{n^*}}{z_n}\ln\frac{f^{\delta}_{n}}{f^{\epsilon}_{n}}\right), \tag{6.15}$$

where the species chosen for n is denoted by a subscript on the quasi-electrostatic potential. The activity coefficients can be evaluated by the formalism of Problem 4.4.

For the junction

$$\overset{\epsilon}{0.1\ N\ \text{KCl}} \;\big|\!\big|\; \overset{\delta}{0.1\ N\ \text{HCl}},$$

we have

$$(\Phi^{\delta}_{K^+} - \Phi^{\epsilon}_{K^+}) - (\Phi^{\delta}_{Cl^-} - \Phi^{\epsilon}_{Cl^-}) = 0.87 \text{ mV} \tag{6.16}$$

and

$$(\Phi^{\delta}_{H^+} - \Phi^{\epsilon}_{H^+}) - (\Phi^{\delta}_{K^+} - \Phi^{\epsilon}_{K^+}) = 0. \tag{6.17}$$

For the junction

$$\overset{\epsilon}{0.2\ N\ \text{KCl}} \;\big|\!\big|\; \overset{\delta}{0.1\ N\ \text{HCl}},$$

we have

$$(\Phi^{\delta}_{K^+} - \Phi^{\epsilon}_{K^+}) - (\Phi^{\delta}_{Cl^-} - \Phi^{\epsilon}_{Cl^-}) = 4.01 \text{ mV} \tag{6.18}$$

and

$$(\Phi^{\delta}_{H^+} - \Phi^{\epsilon}_{H^+}) - (\Phi^{\delta}_{K^+} - \Phi^{\epsilon}_{K^+}) = -0.87 \text{ mV}. \tag{6.19}$$

For the junction

$$\overset{\epsilon}{0.1\ N\ \text{KCl}} \;\vdots\; \overset{\delta}{0.05\ N\ \text{KNO}_3,\ 0.05\ N\ \text{KCl}},$$

we have

$$(\Phi^{\delta}_{K^+} - \Phi^{\epsilon}_{K^+}) - (\Phi^{\delta}_{Cl^-} - \Phi^{\epsilon}_{Cl^-}) = -0.54 \text{ mV} \tag{6.20}$$

and

$$(\Phi^{\delta}_{NO_3^-} - \Phi^{\epsilon}_{NO_3^-}) - (\Phi^{\delta}_{Cl^-} - \Phi^{\epsilon}_{Cl^-}) = 0. \tag{6.21}$$

These examples show that liquid-junction potentials can be uncertain by several millivolts, depending on which species is selected for ion n, and this uncertainty can be as large as the magnitude of $\Delta\Phi$ itself in some cases.

Next, let us analyze the cell

$$\begin{array}{c|c|c:c:c|c|c} \alpha & \beta & \delta & & \epsilon & \chi & \alpha' \\ \text{Pt}(s) & \text{Li(Hg)} & \text{LiNO}_3,\ \text{KNO}_3 \text{ in } \text{H}_2\text{O} & \text{transition region } (\text{KNO}_3 \text{ in } \text{H}_2\text{O}) & \text{AgNO}_3,\ \text{KNO}_3 \text{ in } \text{H}_2\text{O} & \text{Ag}(s) & \text{Pt}(s), \end{array} \tag{6.22}$$

in which KNO_3 is present throughout the cell at the same concentration. The transition region contains concentration gradients of both $LiNO_3$ and $AgNO_3$. (Compare with cell 2.108.) The cell potential can be expressed as

$$FU = -F(\Phi^{\alpha} - \Phi^{\alpha'}) = \mu^{\beta}_{Li} - \mu^{\chi}_{Ag} + \mu^{\epsilon}_{Ag^+} - \mu^{\delta}_{Li^+} \tag{6.23}$$

or

$$FU = FU^{\theta} + RT \ln \frac{a^{\beta}_{Li} c^{\epsilon}_{Ag^+}}{c^{\delta}_{Li^+}} + RT \ln \frac{f^{\epsilon}_{Ag^+} f^{\delta}_{K^+}}{f^{\delta}_{Li^+} f^{\epsilon}_{K^+}} + F(\Phi^{\epsilon} - \Phi^{\delta}), \tag{6.24}$$

where Φ is referred to the potassium ion and

$$FU^{\theta} = \mu^{0}_{Li} - \mu^{0}_{Ag} + RT \ln \frac{\lambda^{\theta}_{Ag^+}}{\lambda^{\theta}_{Li^+}} \tag{6.25}$$

and

$$a^{\beta}_{Li} = \frac{\lambda^{\beta}_{Li}}{\lambda^{0}_{Li}}. \tag{6.26}$$

The activity-coefficient term in equation 6.24 can be expressed as

$$\ln \frac{f^{\epsilon}_{Ag^+} f^{\delta}_{K^+}}{f^{\delta}_{Li^+} f^{\epsilon}_{K^+}} = 2(\beta'_{AgNO_3} - \beta'_{KNO_3}) c^{\epsilon}_{NO_3^-} - 2(\beta'_{LiNO_3} - \beta'_{KNO_3}) c^{\delta}_{NO_3^-}. \tag{6.27}$$

Evaluation for $c_{KNO_3} = 0.1\ M$, $c^{\epsilon}_{AgNO_3} = 0.01\ M$, and $c^{\delta}_{LiNO_3} = 0.01\ M$ gives a contribution to U of -2.0 mV from the activity-coefficient term and a contribution of -0.47 mV from the liquid-junction potential. In this case, the Nernst equation is seen to be fairly accurate, the error from the activity coefficients being somewhat larger than the error from the liquid-junction potential.

If we adopt the condition

$$c^{\epsilon}_{Ag^+} = c^{\delta}_{Li^+} \ll c_{K^+}, \tag{6.28}$$

then the expression for the cell potential becomes

$$FU = FU^{\theta} + RT \ln a^{\beta}_{Li} + 2RT(\beta'_{AgNO_3} - \beta'_{LiNO_3})c_{NO_3^-}. \tag{6.29}$$

Thus, the measured cell potential should be a linear function of $c_{NO_3^-}$. As $c_{NO_3^-} \to 0$, the standard cell potential can be determined from the intercept. It would not be necessary to extrapolate to the low concentrations necessary for cells without transference. Thus, a cell with a supporting electrolyte throughout, although it is not useful for determining activity coefficients, can be useful for determining standard cell potentials.

6.8 POTENTIALS ACROSS MEMBRANES

In many cells of interest, a membrane forms all or part of the junction region. Equation 2.66 can still be used to assess variations of electrochemical potentials across the membrane, although there may be some uncertainty about the values of the transference numbers in the region where the chemical potentials vary.

Membranes can belong to four classes. Some are relatively inert, electrically, such as cellulose acetate membranes used to desalt water by reverse osmosis. A porous glass disk could be in this class. Ion-exchange membranes have charged groups bonded to the membrane matrix.[18] Consequently, they tend to exclude co-ion of the same charge as the bound charge. Thus, the transference numbers of anions are small in a cation-exchange resin. Such membranes are used to desalt water by electrodialysis. The third class includes glass, ceramics, and solid electrolytes.[19, 20] A glass membrane in which the transference number for hydrogen ions is one in the region where the chemical potentials vary is used to form an electrode that is, in essence, reversible to the hydrogen ion just like the hydrogen electrode. Such electrodes are used in the measurement of pH since they are more convenient than hydrogen electrodes. Biological membranes[21, 22] constitute an interesting class that has been the subject of extensive investigation to determine how living cells transport material and operate to create nerve impulses.

6.9 CHARGED MEMBRANES IMMERSED IN AN ELECTROLYTIC SOLUTION

Ion-exchange and fuel cell membranes are often polymeric in nature with ions of fixed charge covalently bound to the polymer chains. The simplest manifestation is a physically or chemically crosslinked polymer; the crosslinks prevent the membrane from dissolving when it is immersed in an electrolyte. Such a membrane immersed in an electrolytic solution is shown in Figure 6.2. At equilibrium, thermodynamics dictates the extent to which the membrane (the polymer could be of any shape, e.g., beads) soaks up the solvent and the ions. The electrolytic solution is labeled *s*, and the polymeric membrane phase is labeled *m*. For concreteness, we assume that the bound ions are negatively charged with charge number z^b_-, and the concentration of the bound ions in the equilibrated

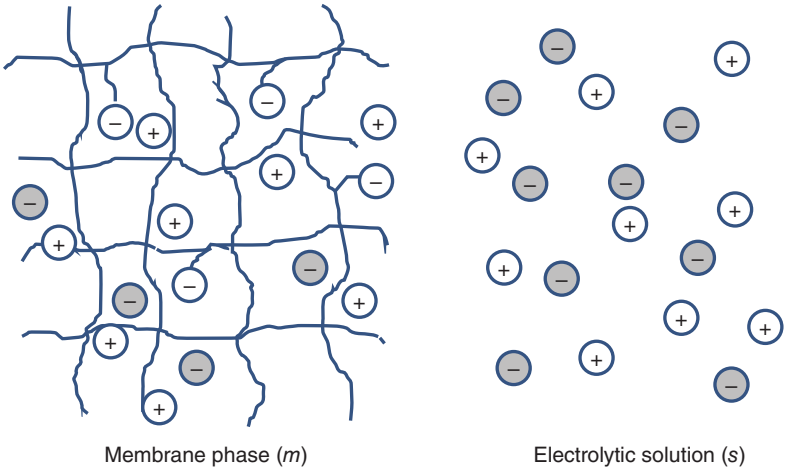

Figure 6.2 Schematic of a charged crosslinked polymer membrane with negative charges covalently bound to the polymer chains in contact with an electrolytic solution. Some of the ions in the electrolytic solution enter the membrane.

membrane is c_-^b. The membrane is electrically neutral, and it contains positively charged counterions with charge number z_+. The electrolytic solution contains positively charged ions that are identical to those in the membrane. If this were not the case, and if the electrolyte is in large excess, ion exchange will occur, and the majority of the ions in both phases will be the same. The negatively charged ions in the solution have a charge number, z_-.

At equilibrium, the chemical potential of each mobile species in the two phases is equal.

$$\mu_i^m = \mu_i^s, \tag{6.30}$$

where i refers to the species (solvent [e.g., water] and the mobile positive and negative ions). For simplicity, we ignore the solvent, and examine only the consequences of ionic equilibria. This is often referred to as the Donnan equilibrium. We take the positive ion to define the quasi-electrostatic potential, Φ^m and Φ^s of both phases. From equation 3.18

$$\mu_+^s = RT \ln c_+ + z_+ F\Phi^s \tag{6.31}$$

and

$$\mu_+^m = RT \ln c_+^m + z_+ F\Phi^m, \tag{6.32}$$

where c_+ is the concentration of positive ions in the solution. For simplicity, the symbols without superscript refer to the solution. Then the electrochemical potential of the mobile negative ion, which is the same ion in both phases, is given by equation 3.19,

$$\mu_-^s = RT \ln c_- + z_- F\Phi^s + RT\left(\ln f_- - \frac{z_-}{z_+}\ln f_+\right) + RT\left(\ln a_-^\theta - \frac{z_-}{z_+}\ln a_+^\theta\right) \tag{6.33}$$

and

$$\mu_-^m = RT \ln c_-^m + z_- F\Phi^m + RT\left(\ln f_-^m - \frac{z_-}{z_+}\ln f_+^m\right) + RT\left(\ln a_-^{\theta,m} - \frac{z_-}{z_+}\ln a_+^{\theta,m}\right), \tag{6.34}$$

where the superscript θ implies the secondary reference state. We use the same secondary reference states to define the chemical potential in both phases.

Equations 6.31 and 6.32 give

$$F(\Phi^s - \Phi^m) = \frac{RT}{z_+} \ln\left(\frac{c_+^m}{c_+}\right). \tag{6.35}$$

The same secondary reference state eliminates the terms involving them when equations 6.33 and 6.34 are substituted into equation 6.30. Equations 6.30, 6.33, and 6.34 then give

$$F(\Phi^s - \Phi^m) = \frac{RT}{z_-} \ln\left(\frac{c_-^m}{c_-}\right) + \frac{RT}{z_-} \ln\left(\frac{f_-^m}{f_-}\right) - \frac{RT}{z_+} \ln\left(\frac{f_+^m}{f_+}\right). \tag{6.36}$$

Elimination of the potential difference between equations 6.35 and 6.36 gives

$$\left(\frac{c_+^m}{c_+}\right)^{\frac{1}{z_+}} \mathcal{F} = \left(\frac{c_-^m}{c_-}\right)^{\frac{1}{z_-}}, \tag{6.37}$$

where

$$\mathcal{F} = \left(\frac{f_+^m}{f_+}\right)^{\frac{1}{z_+}} \left(\frac{f_-^m}{f_-}\right)^{-\frac{1}{z_-}} \tag{6.38}$$

is an electrically neutral combination of activity coefficients in the two phases.

Electroneutrality of the two phases can be expressed as,

$$z_+ c_+ + z_- c_- = 0 \tag{6.39}$$

and

$$z_+ c_+^m + z_- c_-^m + z_-^b c_-^b = 0. \tag{6.40}$$

The ionic species in the solution phase is represented by $(M^{z+})_{\nu_+}(X^{z-})_{\nu_-}$, where

$$z_+ \nu_+ + z_- \nu_- = 0. \tag{6.41}$$

Combination of equations 6.37 and 6.39 through 6.41 yields

$$f_m^{-\frac{1}{\nu_+}} W^{-\frac{\nu_-}{\nu_+}} + W = -Q, \tag{6.42}$$

where f_m is the mean molar activity coefficient of the ions in the membrane divided by that in the solution phase,

$$f_m = \left(\frac{f_+^m}{f_+}\right)^{\nu_+} \left(\frac{f_-^m}{f_-}\right)^{\nu_-}, \tag{6.43}$$

W is the ratio of the coion concentration in the membrane and in the electrolytic solution,

$$W = \frac{c_-^m}{c_-}, \tag{6.44}$$

and Q is the ratio of charge densities in the membrane and in the electrolytic solution concentration.

$$Q = \frac{z_-^b c_-^b}{z_+ c_+}. \tag{6.45}$$

Equation 6.42 is our main result. It enables calculation of the concentration of the coions in the membrane as a function of the charge on the membrane and concentration of the external electrolytic solution. It is interesting that the solution to the problem is given by a relatively simple relationship between three dimensionless quantities. Q is negative, reflecting the fact that our membrane is negatively charged. If we assume $f_m = 1$, that is, the activity coefficients in the membrane and the electrolytic solution are identical (they need not be unity), then one can assume a value for W and calculate the corresponding Q. Results for the cases $\frac{\nu_-}{\nu_+} = \frac{1}{2}, 1,$ and 2 are plotted in Figure 6.3. The concentration of the counterion in the membrane is readily obtained using equation 6.40.

In our discussion thus far, the charge density in the membrane is equal to $Fz_-^b c_-^b$. This is obtained if the membrane is completely ionized. The extent of ionization in polymers is, however, affected by coulombic repulsion along the polymer backbone. In highly charged systems, this repulsion results in partial ionization, that is, a significant number of counterions stay in close proximity to the bound ions. This phenomenon is sometimes called counterion condensation.[23] In this case, c_-^b must be interpreted as the effective charge concentration within the membrane. The dilute charged membrane is similar to semiconducting solids discussed in Chapter 23, where it is assumed that the charged moieties are ionized.

If c_-^b is determined independently, measurement of c_+^m as a function of c_+ (e.g., by titration of the coions in the membrane) yields the activity coefficient in the equilibrated membrane relative to the external solution. Equation 6.42 can be used with experimentally determined values of W as a function of Q to yield f_m. The mean molal activity coefficient of the electrolyte can be calculated if it has been characterized (e.g., Tables 4.1 to 4.3, and Figures 4.2 and 4.3) or measured using the approach described in Section 4.6. It is useful to recall that the secondary reference state for the activity coefficients is generally taken to be an infinitely dilute electrolytic solution.

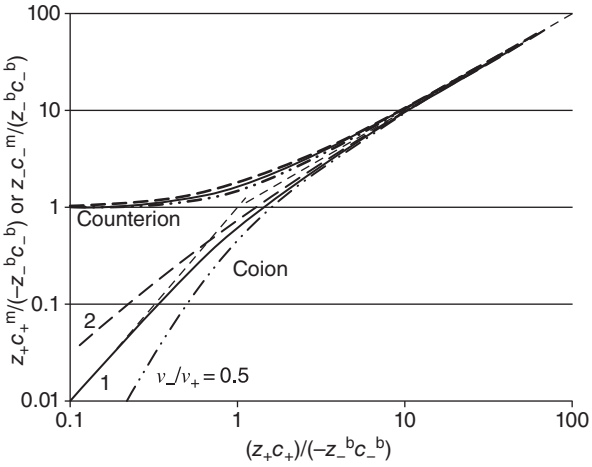

Figure 6.3 Dependence of the coion and counterion concentrations in the membrane on concentration of the electrolytic solution for different values of ν_-/ν_+. Ion concentrations in the membrane are normalized by the charge concentration within the membrane, assumed to be negatively charged. f_m has been taken to be unity.

The potential difference measured between the two equilibrated phases with a reference electrode reversible to one of the mobile ions is zero. It is thus unrelated to the quasi-electrostatic potential difference between the phases, $(\Phi^s - \Phi^m)$, which is clearly nonzero. Measurement of the coion concentration in the membrane in conjunction with equation 6.35 enables measurement of $(\Phi^s - \Phi^m)$.

Finally, membranes with positive bound charges can be treated analogously; the coions will now be positive, and excluded as in Figure 6.3, and the counterions will be negative.

PROBLEMS

6.1 Treat the potential of the cell

α	β			δ	ϵ	α'
Pt(s), $H_2(g)$	HCl in H_2O	transition	region	KNO_3 in H_2O	K(Hg)	Pt(s).

(a) Express the cell potential in terms of chemical potentials and electrochemical potentials of species (except electrons) in the various phases, by means of an equilibrium relationship for each electrode and definitions of chemical potentials of neutral components.

(b) Discuss briefly how to treat the junction region by means of equation 2.66 or 2.68.

(c) What is the expression for the standard cell potential, and what is its value?

(d) Re-express the result of part (a), using the quasi-electrostatic potential. Be sure to specify the reference ion in defining the quasi-electrostatic potential.

(e) State the Nernst equation for this cell.

(f) Solutions β and δ each have 0.1 mol/kg electrolyte concentrations. Obtain a numerical estimate of any activity coefficient combination appearing in the result for part (d). State separately the contribution due to the Debye–Hückel term and that due to terms beyond the Debye–Hückel term.

(g) Would you expect the magnitude of the liquid-junction potential appearing in the result of part (d) to be (choose one): (i) about 2 mV, (ii) about 10 mV, or (iii) about 30 mV?

6.2 Deposition of copper on an electrode of extended surface area is used to remove cupric ions from dilute aqueous waste solutions containing sodium sulfate and sulfuric acid as supporting electrolytes. If the electrode at the stream exit can be maintained at −0.25 V relative to a normal calomel electrode without excessive hydrogen evolution, what is the minimum concentration of copper to which the exit stream can be reduced? Express your answer also in mg/liter. (The molar mass of copper is 63.5 g/mol.) You can use Nernst equations and neglect liquid-junction potentials and activity-coefficient corrections.

6.3 Estimate as accurately as possible the potential of the cell

Fe	2 M $FeCl_2$ in H_2O	Membrane	2 M $FeCl_3$ 0.5 M $FeCl_2$ in H_2O	Inert graphite.

Show all terms you can symbolically. Some parameters may be hard to estimate, but the terms in which they appear may be small. Make the best effort you can to estimate the total cell potential numerically without spending too much time getting accurate parameter values.

6.4 For the cell

α	β	δ	ϵ	≋	λ	ϕ	α'
Pt(s)	Hg(l)	$Hg_2Cl_2(s)$	KCl saturated in H_2O	transition region	Hg ions in 4 M NaCl soln	Hg(l)	Pt(s),

Reaction	FU^θ	U^θ(V)
1. $Hg_2^{2+} \rightarrow 2Hg^{2+} + 2e^-$	$\frac{1}{2}\mu^*_{H_2} - \frac{1}{2}RT\ln\lambda^\theta_{Hg_2^{2+}} + RT\ln\lambda^\theta_{Hg^{2+}}/\lambda^\theta_{H^+}$	0.920
2. $Hg \rightarrow Hg^{2+} + 2e^-$	$\frac{1}{2}\mu^*_{H_2} - \frac{1}{2}\mu^0_{Hg} + \frac{1}{2}RT\ln\lambda^\theta_{Hg^{2+}}/(\lambda^\theta_{H^+})^2$	0.8545
3. $2Hg \rightarrow Hg_2^{2+} + 2e^-$	$\frac{1}{2}\mu^*_{H_2} - \mu^0_{Hg} + \frac{1}{2}RT\ln\lambda^\theta_{Hg_2^{2+}}/(\lambda^\theta_{H^+})^2$	0.789
4. $Hg + 2Cl^- \rightarrow HgCl_2 + 2e^-$	$\frac{1}{2}\mu^*_{H_2} - \frac{1}{2}\mu^0_{Hg} - RT\ln\lambda^\theta_{Cl^-} + \frac{1}{2}RT\ln\lambda^\theta_{HgCl_2}/(\lambda^\theta_{H^+})^2$	0.4768
5. $Hg + 3Cl^- \rightarrow HgCl_3^- + 2e^-$	$\frac{1}{2}\mu^*_{H_2} - \frac{1}{2}\mu^0_{Hg} - \frac{3}{2}RT\ln\lambda^\theta_{Cl^-} + \frac{1}{2}RT\ln\lambda^\theta_{HgCl_3^{2-}}/(\lambda^\theta_{H^+})^2$	0.4434
6. $Hg + 4Cl^- \rightarrow HgCl_4^{2-} + 2e^-$	$\frac{1}{2}\mu^*_{H_2} - \frac{1}{2}\mu^0_{Hg} - 2RT\ln\lambda^\theta_{Cl^-} + \frac{1}{2}RT\ln\lambda^\theta_{HgCl_4^{2-}}/(\lambda^\theta_{H^+})^2$	0.4138
7. $Hg_2^{2+} + 6Cl^- \rightarrow 2HgCl_3^- + 2e^-$	$\frac{1}{2}\mu^*_{H_2} - \frac{1}{2}RT\ln\lambda^\theta_{Hg_2^{2+}}(\lambda^\theta_{H^+})^2 - RT\ln(\lambda^\theta_{Cl^-})^3/\lambda^\theta_{HgCl_3^-}$	0.09787
8. $Hg_2^{2+} + 8Cl^- \rightarrow 2HgCl_4^{2-} + 2e^-$	$\frac{1}{2}\mu^*_{H_2} - \frac{1}{2}RT\ln\lambda^\theta_{Hg_2^{2+}}(\lambda^\theta_{H^+})^2 - RT\ln(\lambda^\theta_{Cl^-})^4/\lambda^\theta_{HgCl_4^{2-}}$	0.03852

the potential of the right electrode is maintained at −0.1 V relative to the left electrode. Estimate numerical values for the total mercury concentration and its distribution among the principal mercury species present if the system is essentially at equilibrium and the standard electrode potentials for a number of mercury species in chloride solution are given in the preceding table. The saturated KCl solution can be taken to be 4.17 M. Ignore activity-coefficient and liquid-junction-potential corrections in your calculations.

6.5 For the cell of Problem 6.4, obtain a numerical estimate of the liquid-junction potential. Again, you may take all activity coefficients to be unity.

6.6 A cell for the production of Cl_2 and NaOH could be represented as follows:

α	β	≋	δ	α'
Pt(s) $H_2(g)$	NaOH in H_2O 2.8 mol/kg	transition region	NaCl in H_2O 3.2 mol/kg	Pt(s) . $Cl_2(g)$

Obtain an expression for the open-circuit cell potential in terms of chemical potentials and electrochemical potentials of specified species in specified phases. Identify an expression for the standard cell potential, and obtain a numerical value for this quantity.

6.7 For the cell of Problem 6.6, obtain the Nernst equation for the open-circuit potential of the cell.

6.8 For the cell of Problem 6.6, estimate a numerical value for the liquid-junction potential. Make sure that your method and assumptions are clear.

6.9 At a point in the transition region of the cell of Problem 6.6, the NaOH molality is 2.5 mol/kg, and the NaCl molality is 0.2 mol/kg. Explain, with formulas, how you would evaluate the relevant activity coefficients of the solutes and the osmotic coefficient of the solvent. Record numerical values for substantially all the parameters you would use in the evaluation. However, you need not actually perform the calculations.

6.10 What would be good reference electrodes to use (not gas electrodes such as Cl_2 or H_2) to probe the potential in the solution on each side of the cell in Problem 6.6?

6.11 A 0.1 mol/kg KOH solution is used to absorb carbon dioxide from an air stream in a packed column. Before the fluid leaves the bottom of the column, essentially all of the KOH is converted to $KHCO_3$. Estimate the electrostatic potential of the liquid at the top of the column relative to the liquid at the bottom. Where did the H come from in the $KHCO_3$? Assume dilute solutions and the absence of current flow. The temperature is 25°C.

6.12 One region of an electrochemical cell contains 0.2 mol/kg HCl in H_2O. A second region contains 0.1 mol/kg HCl in H_2O. The less dense solution is placed above the more dense solution in a vertical tube, and the two solutions are allowed to diffuse into each other. Each solution has immersed within it a silver–silver chloride electrode and a hydrogen electrode—a total of four electrodes (see Figure 6.4). Calculate, to the best of your ability, the activity coefficient $\gamma_{\pm}$ of HCl in each solution. Show your work.

6.13 Treat the potential difference of the two cells each comprised of one hydrogen electrode and one Ag–AgCl electrode in a solution of essentially uniform composition. That is, with reference to Figure 6.4, calculate numerical values for $U_4 - U_2$ and also $U_3 - U_1$.

6.14 Consider the junction between the two solutions (see Figure 6.4).

(a) Would you expect the electrostatic potential to be more positive in the 0.1 mol/kg solution or in the 0.2 mol/kg solution?

(b) Describe qualitatively the mechanism by which this electrostatic difference between the two solutions is established.

(c) Would a different numerical value result for this potential difference if the junction were formed by steady-state diffusion across a porous glass plug instead of by transient diffusion in an unrestricted manner? Explain.

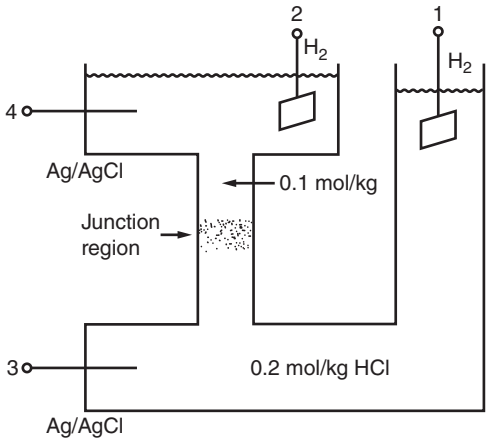

Figure 6.4 Four electrodes in a cell with a liquid junction.

6.15 Treat the potential difference $U_2 - U_1$ between the two hydrogen electrodes in the cell of Problem 6.12. Obtain a numerical value. Summarize the potentials of the four electrodes by giving numerical values for electrodes 2, 3, and 4, all referred to electrode 1. (The result of Problem 6.13 is also needed for this summary.)

6.16 What equation would you try to solve for the concentration profile in the junction region in the cell of Problem 6.12? What numerical value(s) might be appropriate for any physical properties appearing in this equation? (You may need to study Chapter 11 or 17 for this part of the problem.)

After having determined the concentration profile, what equation would you try to solve for the profile of the electrostatic potential in the junction region? What numerical value(s) would you use for any physical properties appearing in this equation? How might you go about determining a distribution of electric charge within the junction region, after having determined both the concentration and potential profile?

NOTATION

a_i relative activity of species i
a_i^θ property expressing secondary reference state, liter/mol
c_i molar concentration of species i, mol/liter
D_i diffusion coefficient of species i, cm^2/s
f_i molar activity coefficient of species i
F Faraday's constant, 96,487 C/mol
i current density, A/cm^2
L thickness of restricted-diffusion junction, cm
p_i partial pressure or fugacity of species i, bar
R universal gas constant, 8.3143 J/mol·K
t_i^0 transference number of species i with respect to the velocity of species 0
T absolute temperature, K
u_i mobility of species i, $cm^2 \cdot mol/J \cdot s$
U open-circuit cell potential, V
U^θ standard cell potential, V
x distance, cm
z_i charge number of species i
κ conductivity, S/cm
λ_i absolute activity of species i
λ_i^θ property expressing secondary reference state, kg/mol
μ_i electrochemical potential of species i, J/mol
ρ_0 density of pure solvent, g/cm^3
Φ electric potential, V

REFERENCES

1. Paul B Taylor. "Electromotive Force of the Cell With Transference and Theory of Interdiffusion of Electrolytes," *Journal of Physical Chemistry*, *31* (1927), 1478–1500.
2. Duncan A MacInnes. *The Principles of Electrochemistry* (New York: Dover, 1961).
3. Carl Wagner, "The Electromotive Force of Galvanic Cells Involving Phases of Locally Variable Composition," *Advances in Electrochemistry and Electrochemical Engineering*, *4* (1966), 1–46.

4. William H. Smyrl and John Newman, "Potentials of Cells with Liquid Junctions," *Journal of Physical Chemistry*, *72* (1968), 4660–4671.
5. P. Henderson, "Zur Thermodynamik der Flüssigkeitsketten," *Zeitschrift für physikalische Chemie*, *59* (1907), 118–127.
6. P. Henderson, "Zur Thermodynamik der Flüssigkeitsketten," *Zeitschrift für physikalische Chemie*, *63* (1908), 325–345.
7. Max Planck, "Ueber die Erregung von Electricität und Wärme in Electrolyten," *Annalen der Physik und Chemie, NF*, *39* (1890), 161–186.
8. Max Planck, "Ueber die Potentialdifferenz Zwischen Zwei Verdünnten Lösungen Binärer Electrolyte," *Annalen der Physik und Chemie, NF*, *40* (1890), 561–576.
9. David E. Goldman, "Potential, Impedance, and Rectification in Membranes," *Journal of General Physiology*, *27* (1943), 37–60.
10. D. Allen Zelman, "An Analysis of the Constant Field Equation," *Journal of Theoretical Biology*, *18* (1968), 396–398.
11. F. Shedlovsky and D. A. MacInnes, *Journal of the American Chemical Society*, *59* (1937), 503.
12. J. B. Chloupek, V. Z. Kanes, and B. A. Danesova, *Collection of Czechoslovak Chemical Communications*, *5* (1933), 469, 527.
13. E. A. Guggenheim and A. Unmack, Kongelige Danske videnskabernes selskab, *Matematisk-Fysiske Meddelelser*, *10* (14) (1931), 1.
14. D. C. Grahame and J. I. Cummings, Office of Naval Research Technical Report 5, 1950.
15. N. P. Finkelstein and E. T. Verdier, "Liquid Junction Potentials at Mixed Electrolyte Salt Bridges" *Transactions of the Faraday Society*, *53* (1957), 1618.
16. D. A. MacInnes and L. G. Longsworth, "The Potentials of Galvanic Cells with Liquid Junctions," *Cold Spring Harbor Symposia on Quantitative Biology*, *4* (1936), 18–25.
17. M. Spiro, "The Calculation of Potentials Across Liquid Junctions of Uniform Ionic Strength," *Electrochimica Acta*, *11* (1966), 569–580.
18. G. J. Hills, "Membrane electrodes," in David J. G. Ives and George J. Janz, eds., *Reference Electrodes* (New York: Academic, 1961), pp. 411–432.
19. R. G. Bates, "The glass electrode," in David J. G. Ives and George J. Janz, eds., *Reference Electrodes* (New York: Academic, 1961), pp. 231–269.
20. George Eisenman, ed., *Glass Electrodes for Hydrogen and Other Cations* (New York: Marcel Dekker, 1967).
21. Kenneth S. Cole, *Membranes, Ions and Impulses* (Berkeley: University of California Press, 1968).
22. J. Walter Woodbury, Stephen H. White, Michael C. Mackey, William L. Hardy, and David B. Chang, "Bioelectrochemistry," in Henry Eyring, ed., *Physical Chemistry, An Advanced Treatise*, Vol. *IXB* (New York: Academic, 1970), pp. 903–983.
23. G. S. Manning, "Limiting Laws and Counterion Condensation in Polyelectrolyte Solutions II. Self-diffusion of the Small Ions," *Journal of Chemical Physics*, *51* (1969), 934–938.

PART B

ELECTRODE KINETICS AND OTHER INTERFACIAL PHENOMENA

The second major area of fundamental electrochemistry necessary in the analysis of electrochemical systems is a knowledge of what goes on at the interface. This part deals with various aspects of this area of electrochemistry, in particular, with models of the structure of the double layer and with the kinetics of electrode processes. Finally, it deals with electrokinetic and electrocapillary phenomena; although these frequently can be ignored in the analysis of electrochemical systems, they are fundamental parts of electrochemistry and colloid chemistry.

Electrochemical Systems, Fourth Edition. John Newman and Nitash P. Balsara.

CHAPTER 7

STRUCTURE OF THE ELECTRIC DOUBLE LAYER

Most of our knowledge of the double layer comes from the study of mercury in contact with electrolytic solutions. The mercury electrode is good for the study of the nature of the double layer because it is a liquid and its surface tension can be measured straightforwardly. As is shown in this chapter, the added observable of surface tension provides insight into the charge at the interface. Mercury is relatively unreactive with aqueous solutions over a fairly wide potential range, which means that no faradaic reactions occur to complicate the study of the capacitive current. Finally, a mercury drop is a highly reproducible surface.

There are two aspects to the study of the double layer, thermodynamics and microscopic models. Thermodynamics provides a sound basis for expressing relationships among potential, surface tension, and the composition of the bulk solution and for determining the surface concentrations of various species at the interface. Microscopic models of the diffuse and the inner parts of the double layer offer an explanation for the behavior of macroscopically measurable quantities, such as the surface tension and the double-layer capacity, and provide a useful picture of the detailed structure of the double layer. By comparing the predictions of a microscopic model with measurements of thermodynamic properties such as capacitance, scientists have gained insight into the structure of the double layer. In many cases, such comparisons show that the double layer may be comprised of multiple adsorbed or oriented layers, and it can be difficult to find a unique model to explain the data. However, the simple models discussed in this chapter, consisting of a diffuse region bordering a charged surface with or without adsorbed ions, have proved to be useful in gaining a qualitative explanation of electrokinetic and colloidal effects, which are discussed in Chapters 9 and 10.

7.1 QUALITATIVE DESCRIPTION OF DOUBLE LAYERS

Why is there a double layer? There is a double layer at an interface, first of all, because some species in the solution may have a preference for being near the solid. Let us suppose that we have a solid–solution

Electrochemical Systems, Fourth Edition. John Newman and Nitash P. Balsara.

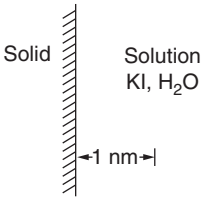

Figure 7.1 Solid–solution interface with no charge in the solid.

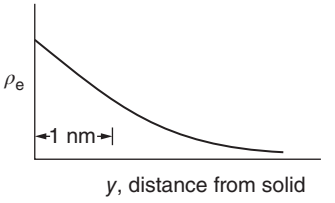

Figure 7.2 Excess electric charge density in the diffuse part of the double layer.

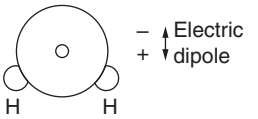

Figure 7.3 Dipole moment in a water molecule.

interface, and let us suppose that there is no charge in the solid itself (see Figure 7.1). If the solution is one of potassium iodide in water, then we might suppose that there is a greater tendency for the iodide ions to get very close to the interface than for the potassium ions. This then forms a double charge layer with a diffuse part in the solution in which there are more potassium ions than iodide ions. The excess of potassium ions in the diffuse part of the double layer balances the excess of iodide ions very close to the interface.

The iodide ions very near the interface can be regarded as bound by covalent (or specific) forces to the solid itself. The excess potassium ions in the solution are prevented from wandering very far from the interface by the electrical force of attraction to the adsorbed iodide ions. Just how far they wander is determined by a balance of the electric force with the thermal agitation, which tries to make ions wander. This distance is characterized by the Debye length (see equation 4.9):

$$\lambda = \sqrt{\frac{\epsilon RT}{2z^2F^2c_\infty}} \tag{7.1}$$

for a single salt of symmetric ionic valences ($z_+ = -z_- = z$). Figure 7.2 shows the electric charge density ρ_e away from the surface of the solid. The Debye length can amount to perhaps 1 nm.

Now consider the interface between a solid (still without charge) and pure water. Suppose that a water molecule looks like that shown in Figure 7.3; that is, it has a nonzero electric dipole moment or, in other words, a separation of charge within the molecule itself. Now even in this simple case, the

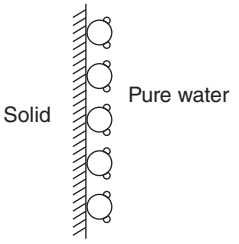

Figure 7.4 Oriented water molecules at an interface with no charge in the solid.

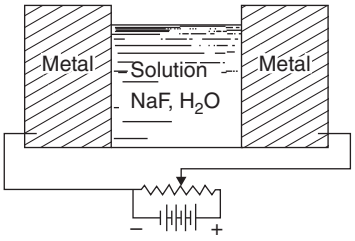

Figure 7.5 Metal–solution interfaces arranged so that the charge on the metal can be varied. Now there is a charge in the metal near the interface with the solution.

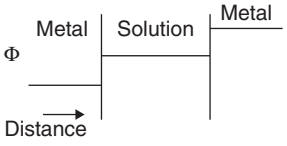

Figure 7.6 Steady potential distribution in a system of ideally polarizable electrodes.

oxygen and the hydrogen may have different tendencies to be close to the solid surface, and the water molecules may orient themselves at the surface. This is also a double charge layer at the interface (see Figure 7.4). In all cases, the interface as a whole, including all the region in which properties vary from one bulk phase to the other, is electrically neutral, as we can easily see in this particular case since the water molecules are themselves neutral.

A second reason for a double layer to form is that we can vary the charge on the metal side of an interface. Imagine now two metal surfaces exposed to a solution (see Figure 7.5). Suppose now that we can apply an appreciable potential difference between these two pieces of metal without there being any appreciable passage of current in the steady state. Where, then, does the potential drop take place? Since it cannot exist in the metal phases or in the solution, due to the absence of an ohmic potential drop, it must occur at the interfaces (see Figure 7.6). Thus, we have a potential jump at the interface that we can vary by means of our external power supply. In this way, we can vary at the same time the charge in the metal at the surface.

The idea that we can vary the charge on the metal side of the surface and also the potential without an electrode reaction occurring is an important one. It perhaps can be only approximated in practice,

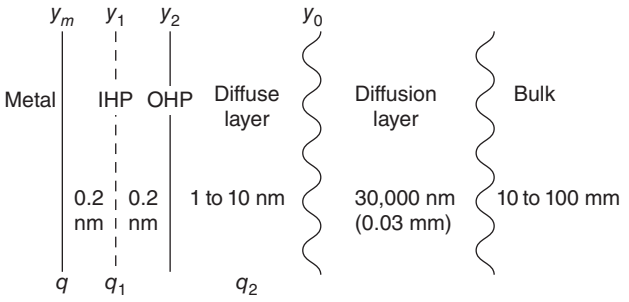

Figure 7.7 Structure of the double layer. The charge on the metal side of the interface is q. Specifically adsorbed ions or molecules are located at the inner Helmholtz plane, while solvated adsorbed ions are located beyond (but not quite at) the outer Helmholtz plane. The diffuse layer is like the bulk of the solution except that it is not electrically neutral, but rather has a net charge q_2. The diffusion layer is electrically neutral but may have a nonuniform salt concentration.

but it can be approximated sufficiently closely for our purposes. Such an electrode system is called an *ideally polarizable electrode*.

A model of the double layer is shown in Figure 7.7, where y_m is the surface of the metal, which is assumed in this chapter to be an impenetrable barrier. A charge on the metal, q, may be present on this surface. The *inner Helmholtz plane* (IHP) is the position of the centers of ions or molecules that are adsorbed at the surface, such as the water molecules shown in Figure 7.4. The *outer Helmholtz plane* (OHP) is the locus of the centers of *solvated* ions at their distance of closest approach to the surface. The solvent molecules prevent the solvated ions from touching the surface directly. The surface charge in the IHP is designated q_1. Next to the OHP is the diffuse layer, a region with a net electrical charge q_2 comprised of solvated anions and cations dispersed in the electrolytic solution. The diffusion layer contains the same electrolytic solution. While the diffusion layer may have a concentration gradient of the salt, it differs from the diffuse layer in that the diffusion layer is electrically neutral. The whole of the interfacial region is electrically neutral:

$$q + q_1 + q_2 = 0. \tag{7.2}$$

The example concluding Section 3.1 is designed to illustrate that extremely large potentials are required to effect any appreciable separation of charge over any appreciable distance. Problem 7.7 also illustrates the magnitude of potential variations in interfacial regions.

If, in Figure 7.5, the two metals are initially uncharged and both are ideally polarizable electrodes, then the application of a current will transfer charge from one metal to the other, leaving them with equal but opposite charges. A current will also flow through the solution, transferring charge from the solution side of one double layer to the solution side of the other double layer so that the charges $q_1 + q_2$ will be equal and opposite in the two double layers. Finally, when a steady state has been attained, the overall system will be electrically neutral, the bulk metal and solution phases will be electrically neutral, and the two interfacial regions will each be electrically neutral. We shall have effected, however, a separation of charge within each double layer over a small distance of perhaps 1 nm, and the charge q or $q_1 + q_2$ on each side of the interface will not be zero.

Let us consider more closely how we may know the charge in the metal side of the surface. For many of these situations, mercury is a useful electrode material, and many concepts derived from this source are applied to solid electrodes. Let us use mercury dropping from the end of a capillary tube into an electrolytic solution (see Figure 7.8). First, consider the situation in which no charge is applied to

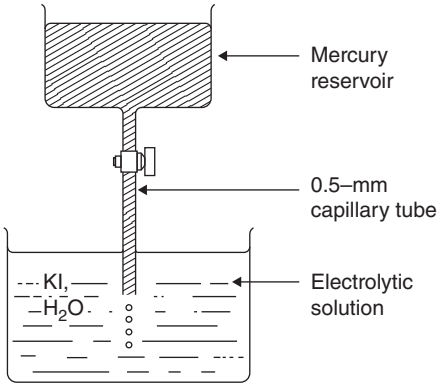

Figure 7.8 Apparatus for determining the point of zero charge on mercury in an electrolytic solution.

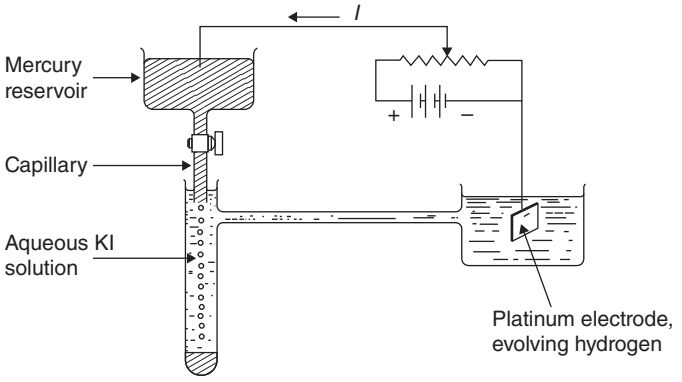

Figure 7.9 Apparatus for charging mercury drops in an electrolytic solution.

the mercury reservoir, and its potential is monitored with respect to a reference electrode, such as the Ag/AgCl electrode shown in Figure 7.11. As the mercury drops fall, they rapidly deplete the mercury reservoir of excess charge so that soon the mercury drops are uncharged, that is, $q = 0$. This potential of the mercury in this condition is called the *point of zero charge*.

If we look at one of these droplets in the course of its fall, we may find that there is a double layer formed as a consequence of the desire of iodide ions to be closer to the mercury surface than the potassium ions. A spherically symmetric shell of adsorbed iodide ions will not induce any redistribution of charge within the mercury drop, since the spherical shell of charge cannot exert any electric forces on charges within the shell. Instead, the adsorbed shell of iodide ions is balanced by an excess of potassium ions in the diffuse part of the double layer (see the first two paragraphs of this section).

Now, imagine that we change the potential of the mercury reservoir, adding a charge at the metal surface (see Figure 7.9). As each drop falls, its surface will carry a small amount of this charge with it. By measuring the current, we can know how much charge is on the surface of each drop. Only the current, the drop size, and the time between drops are important in determining the charge q.

The charge–potential relationships for such a system allow one to define an electric capacity of the double layer, the value of which amounts to about 30 $\mu F/cm^2$, a fairly large value. For a plane plate capacitor with a relative dielectric constant of 78.3, this corresponds to a plate separation of about 2.3 nm and attests to the thinness of the double layer as cited earlier.

In the above discussion, we have distinguished between electrical forces and covalent (or specific) forces. It is really quite difficult to make this distinction precise, even though the concept is useful. The problem has been discussed in Chapter 3. In macroscopic descriptions of interfacial phenomena, reference electrodes should be used to assess the potential of an electrode relative to a solution, but for microscopic models one may resort to the concept of the electrostatic potential.

7.2 GIBBS ADSORPTION ISOTHERM

An interface is the region between two phases, here taken to be homogeneous. There is a transition within the interface from the properties of one phase to those of the other, and the thickness τ of the interface can range from 1 to 10 nm (see Figure 7.10). The thermodynamic treatment of an interface begins generally by considering a system composed of the interface and the two adjacent, homogeneous phases. The extensive properties of the system must be ascribed to these three regions. For example, the number of moles n_i of a species in the system can be written

$$n_i = n_i^{\alpha} + n_i^{\beta} + n_i^{\sigma}. \tag{7.3}$$

Those moles not assigned to the homogeneous phases are assigned to the interface.

The surface concentration Γ_i, is then written as

$$\Gamma_i = \frac{n_i^{\sigma}}{A}, \tag{7.4}$$

where A is the area of the interface, and is usually expressed in mol/cm^2.

One should recognize that there is some ambiguity in the definition of Γ_i because the positions of the surfaces bounding the interface have not been specified. Because the detailed structure of the interface is not subject to direct observation, Gibbs took the thickness of the interface to be zero in his classical thermodynamic treatment of the subject. Then, the position of only one surface needs to be specified. Choose a position $y = y_{\mathrm{I}}$ on Figure 7.10. Then, the definition of the surface concentration can be expressed as

$$\Gamma_i^{\mathrm{I}} = \int_{-\infty}^{y_{\mathrm{I}}} (c_i - c_i^{\alpha})dy + \int_{y_{\mathrm{I}}}^{\infty} (c_i - c_i^{\beta})dy. \tag{7.5}$$

The superscript I is added to Γ_i in this equation to emphasize that the value obtained for Γ_i depends on the position y_{I} chosen for the Gibbs surface. For example, if we choose the position y_{II}, then the surface concentrations Γ_i^{I} and Γ_i^{II} are related by

$$\Gamma_i^{\mathrm{I}} - \Gamma_i^{\mathrm{II}} = (c_i^{\alpha} - c_i^{\beta})(y_{\mathrm{II}} - y_{\mathrm{I}}). \tag{7.6}$$

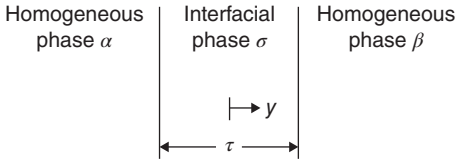

Figure 7.10 Interfacial, nonhomogeneous region of thickness τ between two homogeneous phases.

Thus, an unambiguous value for Γ_i is obtained only if the bulk concentrations of species *i* are identical in the two adjacent, homogeneous phases. This situation prevails, to a fair approximation, in the case of certain organic compounds that may be adsorbed at an air–solution interface but are essentially insoluble in the adjacent phases.

The surface concentration Γ_i as defined above can easily be negative. The ambiguity concerning the choice of the position of the Gibbs surface is usually harmless as long as one is careful to allow for it. The surface concentrations can be fixed by adopting some convention, such as taking Γ_i to be zero for a given reference species, usually the solvent, or taking the mass of the interface to be zero. An alternative is to use quantities, called *Gibbs invariants,* which are independent of the position chosen for the Gibbs surface. For example, the quantity

$$\frac{\Gamma_i}{c_i^\alpha - c_i^\beta} - \frac{\Gamma_j}{c_j^\alpha - c_j^\beta}$$

is such an invariant.

Intensive quantities can be assigned to the interface when these quantities have identical values in the adjacent, homogeneous phases. For example, the temperature and the chemical potentials of equilibrated species have meaning for an interface.

The surface tension σ is a special intensive property of an interface. It depends on the temperature and composition of the adjacent phases. The surface tension has a mechanical meaning in terms of the forces acting at the interface and a thermodynamic meaning in terms of an energy of the surface per unit area. For example, the variation of the Gibbs function for the system considered in the first paragraph of this section is

$$dG = -S\,dT + V\,dp + \sigma\,dA + \sum_i \mu_i\,dn_i. \tag{7.7}$$

Integration at constant temperature, pressure, and composition, while the area and number of moles are allowed to vary from zero to some nonzero values, gives

$$G = \sigma A + \sum_i \mu_i n_i. \tag{7.8}$$

If we also express this as

$$G = G^\sigma + G^\alpha + G^\beta = G^\sigma + \sum_i \mu_i (n_i^\alpha + n_i^\beta), \tag{7.9}$$

we can show that the surface tension is the excess Gibbs free energy of the surface (per unit area)

$$\sigma = \frac{G^\sigma}{A} - \sum_i \mu_i \Gamma_i. \tag{7.10}$$

Incidentally, one can see from equation 7.8 that the surface tension is a Gibbs invariant, independent of the choice of the position of the Gibbs surface.

Differentiation of equation 7.8 and substitution into equation 7.7 gives

$$A\,d\sigma = -S\,dT + V\,dp - \sum_i n_i\,d\mu_i. \tag{7.11}$$

With the Gibbs–Duhem relations for phases α and β, for example,

$$0 = -S^\alpha\, dT + V^\alpha\, dp - \sum_i n_i^\alpha\, d\mu_i, \tag{7.12}$$

we obtain

$$A\, d\sigma = -S^\sigma\, dT + V^\sigma\, dp - \sum_i n_i^\sigma\, d\mu_i \tag{7.13}$$

or

$$d\sigma = -s^\sigma\, dT + \tau\, dp - \sum_i \Gamma_i\, d\mu_i, \tag{7.14}$$

where

$$\begin{aligned} S^\sigma &= As^\sigma = S - S^\alpha - S^\beta, \\ V^\sigma &= A\tau = V - V^\alpha - V^\beta. \end{aligned} \tag{7.15}$$

Equation 7.14 is the surface analogue of the Gibbs–Duhem relation and is known (for $dT = 0$) as the Gibbs adsorption isotherm. By Gibbs convention, the volume assigned to the interface is zero, and τ can be set equal to zero. However, Guggenheim prefers to regard the interface to have a nonzero thickness. In either case, equation 7.14 is applicable, independent of the choice of the position of the surface or surfaces defining the interface.

The Gibbs adsorption equation is useful for determining the surface concentrations Γ_i since accurate direct measurement of Γ_i is usually more difficult than the determination of variations in surface tension and the use of equation 7.14.

In applying the Gibbs adsorption equation, one should remember that it applies to the interface between two phases in equilibrium. Consequently, variations must be carried out with the constraint of this phase equilibrium and the consequent loss of a degree of freedom. For a two-component system, we can take the temperature and one mole fraction as the independent variables. With the Gibbs–Duhem equations for the homogeneous phases, equation 7.14 becomes

$$d\sigma = -\left(s^\sigma - \frac{s^\alpha - s^\beta}{c_1^\alpha - c_1^\beta}\Gamma_1\right)dT - \left(\Gamma_2 - \frac{c_2^\alpha - c_2^\beta}{c_1^\alpha - c_1^\beta}\Gamma_1\right)d\mu_2, \tag{7.16}$$

where s^α and s^β are the entropies per unit volume of phases α and β, respectively. Since

$$d\mu_2 = \left[-\overline{S}_2^\alpha + \overline{V}_2^\alpha\left(\frac{\partial p}{\partial T}\right)_{x_2^\alpha,\mathrm{sat}}\right]dT + \left[\left(\frac{\partial \mu_2}{\partial x_2^\alpha}\right)_{T,p} + \overline{V}_2^\alpha\left(\frac{\partial p}{\partial x_2^\alpha}\right)_{T,\mathrm{sat}}\right]dx_2^\alpha, \tag{7.17}$$

we have finally

$$\begin{aligned} d\sigma = &-\left\{s_{(1)}^\sigma + \Gamma_{2(1)}\left[-\overline{S}_2^\alpha + \overline{V}_2^\alpha\left(\frac{\partial p}{\partial T}\right)_{x_2^\alpha,\mathrm{sat}}\right]\right\}dT \\ &- \Gamma_{2(1)}\left[\left(\frac{\partial \mu_2}{\partial x_2^\alpha}\right)_{T,p} + \overline{V}_2^\alpha\left(\frac{\partial p}{\partial x_2^\alpha}\right)_{T,\mathrm{sat}}\right]dx_2^\alpha, \end{aligned} \tag{7.18}$$

where

$$s^{\sigma}_{(1)} = s^{\sigma} - \frac{s^{\alpha} - s^{\beta}}{c_1^{\alpha} - c_1^{\beta}}\Gamma_1 \quad \text{and} \quad \Gamma_{2(1)} = \Gamma_2 - \frac{c_2^{\alpha} - c_2^{\beta}}{c_1^{\alpha} - c_1^{\beta}}\Gamma_1 \tag{7.19}$$

are the entropy of the interface and the surface concentration of species 2, both evaluated with the Gibbs surface chosen such that $\Gamma_{1(1)} = 0$. We see that a measurement of the variation of the surface tension with x_2^{α} at constant temperature allows us to determine $\Gamma_{2(1)}$. A subsequent measurement of the variation of surface tension with temperature at constant x_2^{α} allows us to determine the surface entropy $s^{\sigma}_{(1)}$.

7.3 THE LIPPMANN EQUATION

We now wish to apply the Gibbs adsorption isotherm to an interface involving an ideally polarizable electrode. We treat the system shown in Figure 7.11. Here the counterelectrode is used to maintain the potential of the mercury, which is measured relative to a silver chloride reference electrode. This latter circuit can be represented by the diagram

$$\begin{array}{c|c|c|c|c|c} \alpha & \beta & \delta & \epsilon & \lambda & \alpha' \\ \mathrm{Pt}(s) & \mathrm{Ag}(s) & \mathrm{AgCl}(s) & \mathrm{KCl\ in\ } \mathrm{H_2O} & \mathrm{Hg}(l) & \mathrm{Pt}(s) \end{array}, \tag{7.20}$$

for which the potential can be expressed by the methods of Chapter 2 as

$$FU = -F(\Phi^{\alpha} - \Phi^{\alpha'}) = \mu_{e^-}^{\alpha} - \mu_{e^-}^{\alpha'} = \mu_{Cl^-}^{\epsilon} - \mu_{e^-}^{\lambda} + \mu_{Ag}^{\beta} - \mu_{AgCl}^{\delta}. \tag{7.21}$$

For variations of the surface tension of the mercury at constant temperature, the Gibbs adsorption isotherm, equation 7.14 becomes

$$d\sigma = -\Gamma_{e^-}\, d\mu_{e^-}^{\lambda} - \Gamma_{K^+}\, d\mu_{K^+}^{\epsilon} - \Gamma_{Cl^-}\, d\mu_{Cl^-}^{\epsilon}. \tag{7.22}$$

We consider the mercury phase λ to be composed of mercury atoms and electrons. The surface concentration of mercury does not appear in equation 7.22 because we take $d\mu_{Hg}^{\lambda} = 0$. The surface

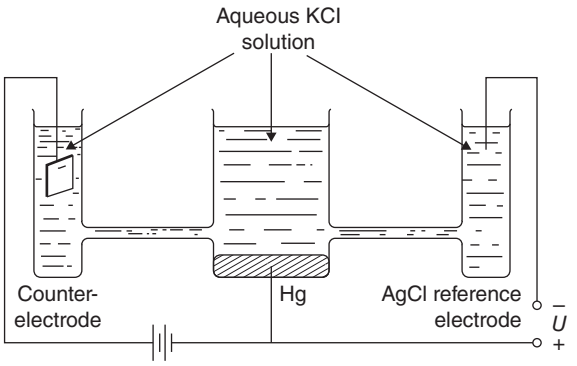

Figure 7.11 System for applying a potential to an ideally polarizable electrode.

concentration of electrons is a Gibbs invariant because the concentration of electrons is zero in the bulk of the homogeneous phases λ and ϵ (see equation 7.6). In fact, Γ_{e^-} is related to the surface charge density q discussed in Section 7.1 for an ideally polarizable electrode:

$$q = -F\Gamma_{e^-}. \tag{7.23}$$

We consider the aqueous phase ϵ to be composed of potassium ions, chloride ions, and water. We choose the Gibbs surface such that $\Gamma_{H_2O} = 0$.

We have emphasized before that the interface as a whole is electrically neutral,

$$\sum_i z_i \Gamma_i = 0. \tag{7.24}$$

If we use equation 7.24 to eliminate Γ_{Cl^-} from equation 7.22 and use equation 7.23 to introduce q, we obtain

$$d\sigma = -\Gamma_{K^+}\, d\mu^{\epsilon}_{KCl} - \frac{q}{F}(d\mu^{\epsilon}_{Cl^-} - d\mu^{\lambda}_{e^-}). \tag{7.25}$$

Finally, equation 7.21 can be used to introduce the potential U:

$$d\sigma = -\Gamma_{K^+}\, d\mu^{\epsilon}_{KCl} - q\, dU. \tag{7.26}$$

This important equation is known as the Lippmann equation. It tells us that, if we measure the variation of the surface tension with composition at constant potential, we can obtain the surface concentration of potassium ions and, if we measure the variation with potential at constant composition, we can obtain the surface charge q. All this can be done on a firm thermodynamic basis without resort to microscopic models of the interface, although the experiments require considerable effort to obtain accurate results. Bear in mind that Γ_{K^+} is relative to the convention that $\Gamma_{H_2O} = 0$.

The above derivation of the Lippmann equation differs from the treatments of reversible electrodes in Chapter 2 in that there are no species that are equilibrated between phases λ and ϵ. Or, if they are equilibrated, they are assumed to be of negligible concentration in one phase or the other. An alternative treatment assumes that there is an impenetrable barrier through which no species, and hence no current, passes. The surface charge q is then the surface charge density on the electrode side of this barrier, and again no species exists on both sides of the barrier in an appreciable concentration. Both developments lead to the Lippmann equation, and the difference in the bases is of little practical consequence.

The double-layer capacity (per unit area) C is the derivative of the double-layer charge q with respect to potential at constant composition:

$$C = \left(\frac{\partial q}{\partial U}\right)_{\mu,T}, \tag{7.27}$$

where the subscript μ denotes constant composition. From equation 7.26 we see that

$$q = -\left(\frac{\partial \sigma}{\partial U}\right)_{\mu,T}. \tag{7.28}$$

Hence,

$$C = -\left(\frac{\partial^2 \sigma}{\partial U^2}\right)_{\mu,T}. \tag{7.29}$$

The double-layer capacity of an ideally polarizable electrode can be measured directly with an alternating current. Because the double layer is thin, it responds rapidly to the alternating current. Consequently, except when the adsorption of long-chain organic compounds is involved, the alternating current capacity does not begin to depart from the static capacity defined by equation 7.27 until a frequency of about 10^6 Hz is reached.

Grahame[1] described an experimental confirmation of the Lippmann equation in which the charge is determined as a function of potential in three independent ways:

1. Differentiation of the surface tension with respect to potential according to equation 7.28.
2. Integration of the double-layer capacity with respect to potential according to equation 7.27. The integration constant must be evaluated to give agreement with the other two methods.
3. Direct measurement of q by means of an apparatus such as that sketched in Figure 7.8.

Note that only the second method can be applied to solid electrodes and that the determination of the point of zero charge, equivalent to the integration constant, is then uncertain.

The above derivation of the Lippmann equation can be modified to apply to a different reference electrode and to multicomponent solutions, including systems involving the adsorption of neutral organic molecules. The application of thermodynamic principles allows a coherent treatment of a variety of data involving the measurement of surface tension, surface charge, and double-layer capacity as functions of temperature, potential, and solution composition. These data can be manipulated by thermodynamic methods to yield derived quantities of interest, such as the surface concentrations. (See Problems 7.2 and 7.3 and references [1, 2].)

The surface tension of mercury in contact with several electrolytic solutions is plotted against potential in Figure 7.12. The potential of zero charge is given in Table 7.1 (at 25°C rather than

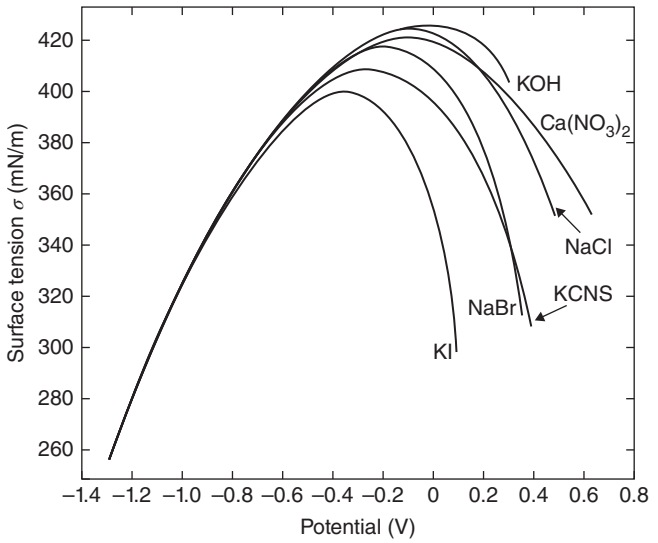

Figure 7.12 Interfacial tension of mercury as a function of potential for several electrolytic solutions at 18°C. Potentials relative to a normal calomel electrode are shifted by 0.48 V. These are referred to as electrocapillary curves because the surface tension is often measured with a capillary electrometer. *Source:* Grahame 1947.[1] Reproduced with permission of The American Chemical Society.

TABLE 7.1 Potential of zero charge for mercury (relative to a normal calomel electrode in KCl) for various electrolytic solutions at 25°C

Electrolyte	c (*M*)	Potential (V)	Electrolyte	c (*M*)	Potential (V)
LiCl	1.0	−0.557	CsCl	1.0	−0.556
	0.1	−0.5592		0.1	−0.5564
NaCl	1.0	−0.557	HCl	0.1	−0.558
	0.1	−0.5591	NH_4Cl	0.1	−0.5587
KCl	1.0	−0.5555	$CaCl_2$	0.1	−0.5586
	0.7	−0.5535	$SrCl_2$	0.1	−0.5588
	0.3	−0.5515	$BaCl_2$	0.1	−0.5587
	0.1	−0.5589	$MnCI_2$	0.1	−0.5589
	0.01	−0.5936	$CoCl_2$	0.1	−0.5585
	0.001	−0.640	$NiCl_2$	0.1	−0.5588
RbCl	0.1	−0.5576	$AlCl_3$	0.1	−0.5585
NaF	1.0	−0.472	$LaCl_3$	0.1	−0.5588
	0.1	−0.474	KCH_3COO	0.1	−0.4884
KF	0.1	−0.4714	$KClO_4$	0.1	−0.5074
$KHCO_3$	0.1	−0.4728	KNO_3	0.1	−0.5166
K_2CO_3	0.05	−0.4734	KBr	0.1	−0.5741
K_2SO_4	0.05	−0.4705	KCNS	0.1	−0.626
KOH	0.1	−0.4767	KI	0.1	−0.732

Source: Grahame et al. 1952.[3] Reproduced with permission of The American Chemical Society. See also reference [4].

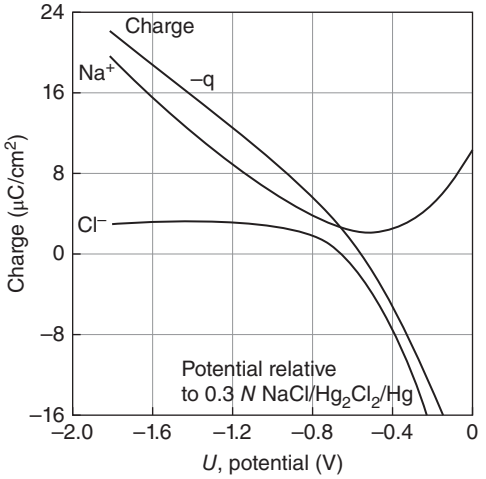

Figure 7.13 Charge and adsorption of sodium and chloride ions at a mercury interface in contact with 0.3 *M* NaCl at 25°C. The surface concentrations of the ions are expressed as $z_i F\Gamma_i$. *Source:* Grahame 1947.[1] Reproduced with permission of The American Chemical Society.

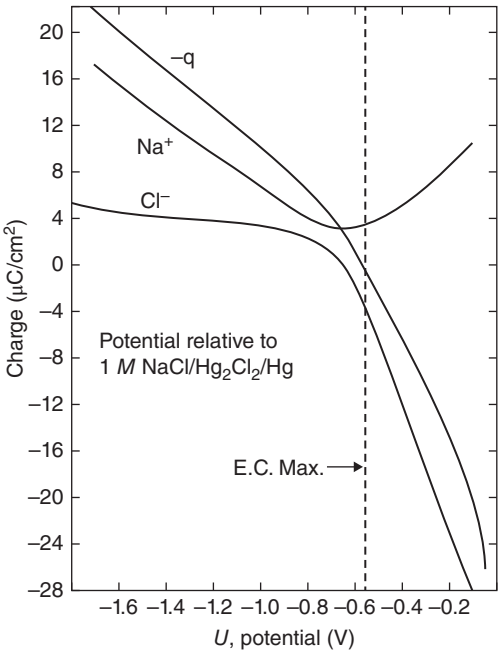

Figure 7.14 Charge and adsorption of sodium and chloride ions at a mercury interface in contact with a 1 *M* NaCl solution at 25°C. The surface concentrations of the ions are expressed as $z_i F\Gamma_i$. *Source:* Grahame 1947.[1] Reproduced with permission of The American Chemical Society.

18°C). From equation 7.28, we see that zero charge corresponds to the maximum on the surface tension curve. Consequently, this point of zero charge is also referred to as the *electrocapillary maximum*. In Figure 7.12, the potentials relative to a normal calomel electrode in KCl have been shifted by +0.48 V in order that the electrocapillary maximum for KOH might appear at about 0 V (see Problem 7.4).

The surface charge and surface concentrations (the latter being expressed as $z_i F\Gamma_i$) are represented in Figures 7.13 and 7.14 for two concentrations of NaCl. Here, the potentials are measured relative to a calomel electrode in the same solution as the ideally polarizable electrode, and no questions of liquid-junction potentials are involved. It is such well-defined potentials that are used in the Lippmann equation 7.26.

Figures 7.15 and 7.16 show the double-layer capacity as a function of potential for NaCl and NaF solutions. More curves of this type can be found in Ref. [1].

7.4 THE DIFFUSE PART OF THE DOUBLE LAYER

The thermodynamics of the double layer was developed for an ideally polarizable electrode in the preceding two sections. Beyond this one must resort to microscopic models. These are discussed qualitatively in Section 7.1.

The diffuse part of the double layer is regarded as part of the electrolytic solution, but here the solution is not electrically neutral. The model used to treat this region is essentially identical to that of Debye and Hückel, used to determine the ionic distributions around a central ion and subsequently

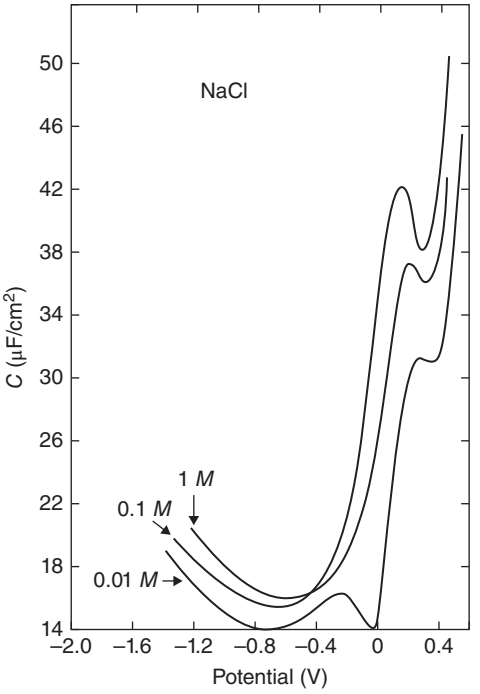

Figure 7.15 Double-layer capacity for mercury in contact with NaCl solutions at 25°C. Potentials are relative to the electrocapillary maximum. *Source:* Grahame 1947.[1] Reproduced with permission of The American Chemical Society.

to calculate the electrical contribution to the activity coefficients (see Sections 4.1 and 4.2). The ionic concentrations in the diffuse part of the double layer are assumed to be related to the potential by the Boltzmann distribution (see equation 4.1)

$$c_i = c_{i\infty} \exp\left(-\frac{z_i F \Phi}{RT}\right), \tag{7.30}$$

and Poisson's equation relates the variation of the potential to the charge density (see equation 4.2). For a planar electrode this becomes

$$\frac{d^2\Phi}{dy^2} = -\frac{F}{\epsilon} \sum_i z_i c_{i\infty} \exp\left(-\frac{z_i F \Phi}{RT}\right), \tag{7.31}$$

where y is the distance from the electrode.

Similar limitations apply to the validity of this model as to that of Debye and Hückel (see Section 4.3). For the planar case, in contrast to the spherical case treated in Section 4.1, one can go further without the introduction of the mathematical approximation of Debye and Hückel (see equation 4.7). We should note again that the derivation of the Lippmann equation in the preceding section did not involve the introduction of any model.

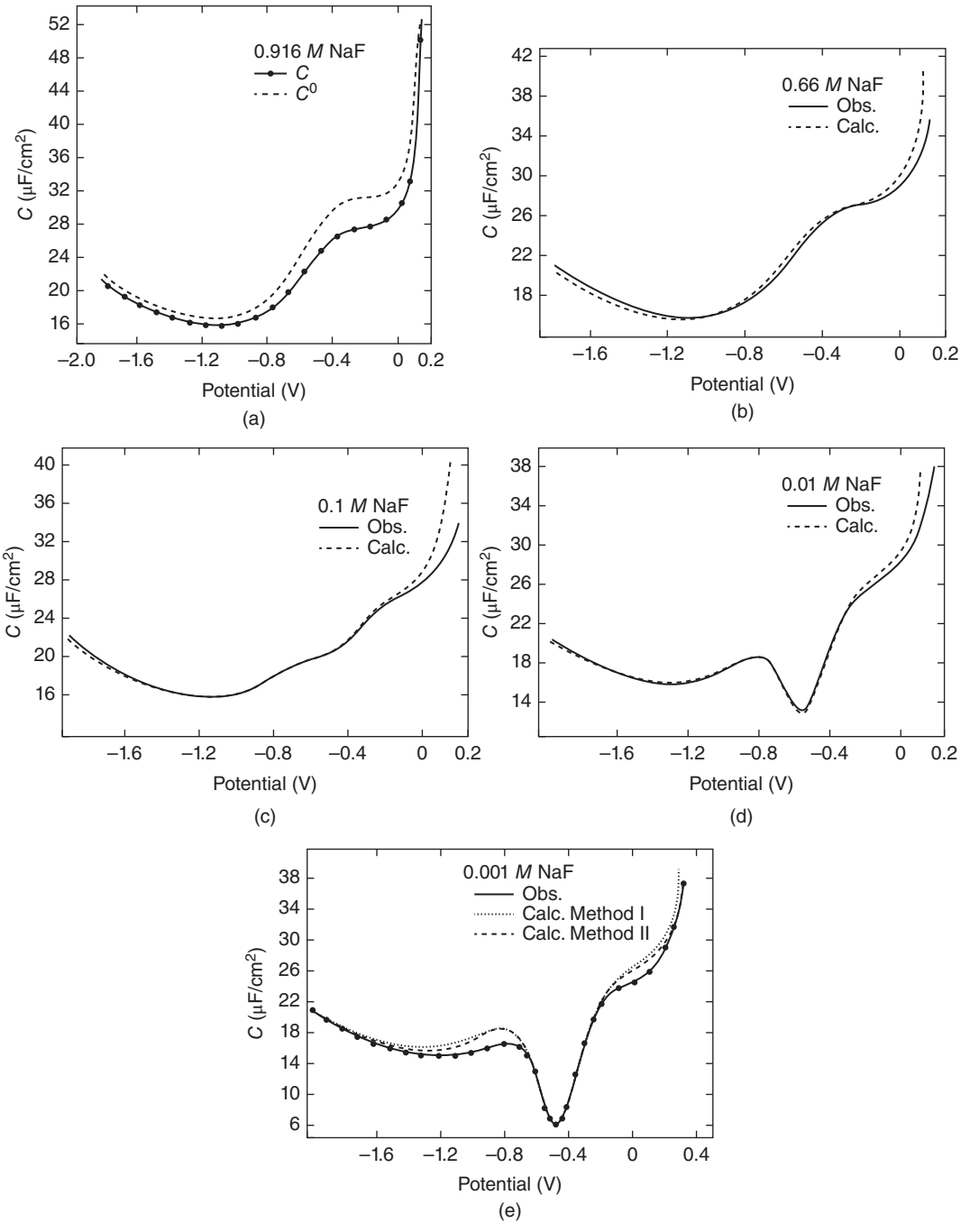

Figure 7.16 Double-layer capacity for mercury in contact with NaF solutions at 25°C. Potentials are relative to the normal calomel electrode. *Source:* Grahame 1954.[5] Reproduced with permission of The American Chemical Society. The calculated capacitance is explained in Section 7.5. At the highest concentration, 0.916 *M* in (a), Grahame has used the measured values C to infer values for C^0, the capacitance across the inner part of the double layer, known as C_{M-2} in Section 7.5. In parts (b–e) of this figure, Grahame has calculated values of C from C^0 and the diffuse-layer theory, using two slightly different methods in the case of the most dilute solution, 0.001 *M* in (e).

The first boundary condition on equation 7.31 is that

$$\Phi \to 0 \quad \text{as} \quad y \to \infty. \tag{7.32}$$

From equation 7.30, we thus see that $c_{i\infty}$ is the concentration of species i approached at large distances from the electrode. Furthermore, since the right side of equation 7.31 is the charge density divided by $-\epsilon$, integration of this equation allows the potential gradient at y_2 to be related to the surface charge density q_2 in the diffuse part of the double layer:

$$\frac{d\Phi}{dy} = \frac{q_2}{\epsilon} \quad \text{at } y = y_2. \tag{7.33}$$

This constitutes the second boundary condition for equation 7.31. Here, y_2 is the position of the inner limit of the diffuse layer, that is, the closest distance to which solvated ions can approach the electrode, the same value being applicable to all ionic species. Note the similarity of y_2 to the parameter a of the theory of Debye and Hückel.

Let us introduce the electric field E:

$$E = -\frac{d\Phi}{dy}. \tag{7.34}$$

The electric field can be determined as a function of the potential by rewriting equation 7.31 as

$$\frac{d^2\Phi}{dy^2} = -\frac{dE}{dy} = -\frac{dE}{d\Phi}\frac{d\Phi}{dy} = E\frac{dE}{d\Phi} = -\frac{F}{\epsilon}\sum_i z_i c_{i\infty} \exp\left(-\frac{z_i F\Phi}{RT}\right). \tag{7.35}$$

Integration gives

$$\frac{1}{2}E^2 = \frac{RT}{\epsilon}\sum_i c_{i\infty}\left[\exp\left(-\frac{z_i F\Phi}{RT}\right) - 1\right], \tag{7.36}$$

the integration constant being evaluated from the fact that as $y \to \infty$, both Φ and E approach zero. The electric field therefore is given in terms of the potential as

$$E = \pm\left\{\frac{2RT}{\epsilon}\sum_i c_{i\infty}\left[\exp\left(-\frac{z_i F\Phi}{RT}\right) - 1\right]\right\}^{1/2}, \tag{7.37}$$

the plus sign being used if Φ is positive and conversely, since E and Φ must be of the same sign.

Without carrying the problem further, we can now relate the charge in the diffuse layer to the potential at y_2 since introduction of condition 7.33 gives

$$q_2 = \mp\left\{2RT\epsilon\sum_i c_{i\infty}\left[\exp\left(-\frac{z_i F\Phi_2}{RT}\right) - 1\right]\right\}^{1/2}, \tag{7.38}$$

where Φ_2 is the potential at y_2. This relationship has important applications in double-layer theory.

The determination of the potential as a function of distance is straightforward in principle, although it can be complicated in practice. Equation 7.34 gives

$$y - y_2 = \int_{\Phi}^{\Phi_2} \frac{d\Phi}{E}, \tag{7.39}$$

where E is given as a function of Φ by equation 7.36.

Although numerical integration of equation 7.39 is necessary in general, the analysis can be completed for the special case where the magnitudes of the ionic charges are all the same, $|z_i| = z$. Let us carry out the development in dimensionless form where

$$x = \frac{y}{\lambda}, \quad \phi = \frac{F\Phi}{RT}, \quad \mathcal{E} = \frac{\lambda FE}{RT}, \quad C_{i\infty} = \frac{2c_{i\infty}}{\sum_j z_j^2 c_{j\infty}}, \tag{7.40}$$

and λ is the Debye length given by equation 4.9. Equations 7.37 and 7.39 become

$$\mathcal{E} = \pm\left[\sum_i C_{i\infty}(e^{-z_i\phi} - 1)\right]^{1/2} \tag{7.41}$$

and

$$x - x_2 = \int_{\phi}^{\phi_2} \frac{d\phi}{\mathcal{E}}. \tag{7.42}$$

For the special case of $|z_i| = z$, we have

$$z\mathcal{E} = \pm(e^{z\phi} - 2 + e^{-z\phi})^{1/2} = 2\sinh\frac{z\phi}{2}. \tag{7.43}$$

Integration of equation 7.42 then gives

$$x - x_2 = \ln\frac{\tanh z\phi_2/4}{\tanh z\phi/4}. \tag{7.44}$$

This result can be rearranged to yield

$$\phi = \frac{2}{z}\ln\frac{1 - Ke^{-x+x_2}}{1 + Ke^{-x+x_2}}, \quad z\mathcal{E} = \frac{-4Ke^{-x+x_2}}{1 - (Ke^{-x+x_2})^2}, \tag{7.45}$$

where K is a dimensionless constant whose value lies between -1 and $+1$ and is related to the potential ϕ_2 and the charge q_2 in the diffuse layer by

$$K = -\tanh\frac{z\phi_2}{4} = \frac{Q_2}{\sqrt{4 + Q_2^2} + 2}, \tag{7.46}$$

where $Q_2 = z\lambda Fq_2/RT\epsilon$.

The double-layer capacity C is defined by equation 7.27. Correspondingly, we define the capacity C_d of the diffuse layer as

$$C_d = -\left(\frac{\partial q_2}{\partial \Phi_2}\right)_{\mu,T}, \tag{7.47}$$

the minus sign being introduced because q_2 is on the opposite side of the double layer from q. With equation 7.38 we have

$$C_d = \frac{\epsilon F}{q_2}\sum_i z_i c_{i\infty}\exp\left(-\frac{z_i F\Phi_2}{RT}\right), \tag{7.48}$$

and for the special case where the magnitudes of the ionic charges are all the same

$$C_d = \frac{\epsilon}{\lambda} \cosh \frac{zF\Phi_2}{2RT}. \tag{7.49}$$

Equation 7.49 indicates that the diffuse-layer capacity is proportional to the square root of the ionic strength because of the composition dependence of the Debye length λ. For aqueous solutions at 25°C and an ionic strength of 0.1 mol/liter, ϵ/λ has a value of about 72 μF/cm^2. There is also a strong dependence on the potential Φ_2. For 1–1 electrolytes at 25°C, the diffuse-layer capacity is about 3.6 times higher when $\Phi_2 = 0.1$ V than when $\Phi_2 = 0$.

7.5 CAPACITY OF THE DOUBLE LAYER IN THE ABSENCE OF SPECIFIC ADSORPTION

The structure of the double layer is discussed qualitatively in Section 7.1, where we indicated that species could be adsorbed by specific forces at the interface. Cations, generally speaking, are not specifically adsorbed, thallous ions being an exception to this rule. Evidence that cations are not specifically adsorbed is given by the fact that the electrocapillary curves of Figure 7.12 coincide on the branch at negative electrode potentials. Anions usually *are* specifically adsorbed, exceptions being fluoride, hydroxyl, and sulfate ions. Evidence that chloride ions are specifically adsorbed can be seen in Figure 7.13, which shows that sodium ions are again adsorbed toward more positive potentials. This is attributed to adsorption of chloride ions in excess of that dictated solely by the charge q on the electrode.

It is simpler to look first at a system involving an electrolyte, such as NaF, where both ions show little or no tendency for specific adsorption. Then we can say that $q_1 = 0$, and, consequently,

$$q_2 = -q; \tag{7.50}$$

that is, the charge in the diffuse layer is given by the charge on the electrode, which can be determined by thermodynamic means. As the subject was developed in Section 7.4, all the properties of the diffuse layer depend solely on the charge q_2. For example, the potential Φ_2 at the inner limit of the diffuse layer is related to q_2 by means of equation 7.38, and the capacity of the diffuse layer C_d is expressed in terms of Φ_2 and q_2 in equation 7.48. In the absence of specific adsorption, the ionic surface concentrations Γ_i must be accounted for by the diffuse layer, and these can also be related to q_2 or Φ_2 (see Problem 7.5). There are thus several ways in which one can test the assumptions that there is no specific adsorption with solutions of NaF and that the diffuse-layer theory is valid.

Grahame[5] looked at the double-layer capacity C. Since

$$U = U - \Phi_2 + \Phi_2, \tag{7.51}$$

we can write

$$\left(\frac{\partial U}{\partial q}\right)_\mu = \left(\frac{\partial (U - \Phi_2)}{\partial q}\right)_\mu + \left(\frac{\partial \Phi_2}{\partial q}\right)_\mu \tag{7.52}$$

or

$$\frac{1}{C} = \frac{1}{C_{M-2}} + \frac{1}{C_{\mathrm{d}}}, \tag{7.53}$$

where C_{M-2} is the capacity of the region between the metal and the plane at $y = y_2$. In obtaining equation 7.53, we have made use of the assumption that $q_2 = -q$, the electroneutrality equation 7.24, and the definition 7.47.

In equation 7.53, we know C by direct measurement, and we know C_d by the assumption of no specific adsorption, as outlined above. Consequently, we can calculate C_{M-2}. Instead, we can make various assumptions about C_{M-2} and make predictions of C using diffuse-layer theory to obtain C_d. The first plausible assumption that C_{M-2} is constant does not work well at all. Grahame therefore made the second plausible assumption that C_{M-2} depends only on q, independent of the bulk concentration. He calculated C_{M-2} as a function of q from equation 7.53 by using data for C for NaF solutions of about 1 M concentration. At these relatively high concentrations, the contribution of C_d in equation 7.53 is small. On the basis of this calculated dependence of C_{M-2} on q, Grahame then made predictions of C for solution concentrations ranging down to 0.001 M (see Figure 7.16). The agreement with experimental values turned out to be quite good, even at the lowest concentration.

In this manner, Grahame has made a substantial case for the relevance of the diffuse-layer theory and the assumption that sodium and fluoride ions are not specifically adsorbed. It remains to explain the charge dependence of C_{M-2}, a problem that appears to require a detailed microscopic theory of the region very close to the mercury surface.

7.6 SPECIFIC ADSORPTION AT AN ELECTRODE–SOLUTION INTERFACE

Specific adsorption refers to the attraction of a species toward the mercury surface by forces that are not purely coulombic in nature. Frequently, anions are specifically adsorbed while cations are not. In this case, Γ_+, which can be obtained by thermodynamic means, can be immediately associated with the surface concentration of cations in the diffuse part of the double layer. The theory in Section 7.4 can then be used to treat the diffuse part of the double layer, all the properties of the diffuse layer being uniquely related by this theory to the surface concentration of cations in that layer. In this manner one can determine the potential Φ_2 at the OHP, the charge q_2 in the diffuse layer, and the surface concentration of anions in the diffuse layer.

From the measured value of Γ_-, one is now in a position to determine the surface concentration of the specifically adsorbed anions. This quantity is subject to chemical interpretation in terms of adsorption isotherms and the energetics of specific adsorption, with either the electrode charge q or the electrode potential as a correlating variable. A lot of work has been done along these lines, and we must refer to the literature for details.[1, 2, 6, 7] Electrocapillary phenomena and effects of the double layer will be encountered again in Chapters 8 to 10.

PROBLEMS

7.1 A weighed amount of NaCl solution (n moles) of mole fraction x^i_{NaCl} is added to a highly porous carbon of area A. After the carbon has settled, the supernatant solution has a different mole fraction, x^f_{NaCl}. The amount of NaCl adsorbed is calculated as $n(x^i_{\mathrm{NaCl}} - x^f_{\mathrm{NaCl}})/A$. What value of Γ_{NaCl} is calculated, that is, relative to what Gibbs convention for the position of the surface?

7.2 From the Lippmann equation 7.26, derive the Maxwell relations

$$\left(\frac{\partial \Gamma_{K^+}}{\partial U}\right)_{\mu} = \left(\frac{\partial q}{\partial \mu}\right)_{U}, \quad \left(\frac{\partial \mu}{\partial U}\right)_{\Gamma_{K^+}} = -\left(\frac{\partial q}{\partial \Gamma_{K^+}}\right)_{U},$$

$$\left(\frac{\partial \Gamma_{K^+}}{\partial q}\right)_{\mu} = -\left(\frac{\partial U}{\partial \mu}\right)_{q}, \quad \left(\frac{\partial \mu}{\partial q}\right)_{\Gamma_{K^+}} = \left(\frac{\partial U}{\partial \Gamma_{K^+}}\right)_{q}.$$

Show that

$$\left(\frac{\partial q}{\partial \mu}\right)_U = -\left(\frac{\partial q}{\partial U}\right)_\mu \left(\frac{\partial U}{\partial \mu}\right)_q = -C\left(\frac{\partial U}{\partial \mu}\right)_q .$$

7.3 Show how to obtain the surface concentration Γ_{K^+} for the mercury, KCl solution interface from measurements of the double-layer capacity as a function of potential and KCl concentration. In addition, the potential and the surface tension at the point of zero charge can be assumed to be known as functions of concentration.

7.4 **(a)** The potential of the point of zero charge for mercury in various electrolytic solutions is given in Table 7.1. This is measured relative to a normal calomel electrode in KCl. On the assumption that this is supposed to be a thermodynamic quantity, for example, not involving the uncertainty of liquid-junction potentials, discuss the merit of the suggestion that, for the interface

$$\begin{array}{c|c} \delta & \beta \\ 0.1\,N\,Na_2SO_4 & Hg(l), \\ \text{in } H_2O & \end{array}$$

the tabulated value represents (or should represent)

$$\frac{-\mu^{\beta}_{e^-} - F\Phi^{\delta} + \mu^0_{Hg} - \frac{1}{2}\mu^0_{Hg_2Cl_2} + RT \ln c^{\lambda}_{Cl^-}}{F},$$

where Φ^{δ} is the quasi-electrostatic potential of phase δ relative to the chloride ion as species n and $c^{\lambda}_{Cl^-}$ is the concentration of the chloride ion in the 1 N KCl solution of the reference electrode (see Section 5.7).

(b) If the potential of zero charge for the interface

$$\begin{array}{c|c} \delta & \beta \\ 0.3\,M\,NaCl & Hg(l) \\ \text{in } H_2O & \end{array}$$

is measured relative to a calomel electrode in the same solution, how should we calculate the potential of zero charge relative to the normal calomel electrode in KCl?

(c) If the potential of zero charge for the interface of part (b) is measured relative to a calomel electrode in 0.3 N KCl in a system involving a liquid junction, how might we estimate the value relative to the normal calomel electrode in KCl, corrected for the liquid junction? Repeat for the case where the experimental reference electrode is in 1 N KCl.

(d) For the interface of part (a), assume that the potential has been measured relative to a lead sulfate electrode in the same solution. Show how to calculate the potential relative to the normal calomel electrode in KCl.

(e) If the potential for the interface of part (a) has been measured relative to a calomel electrode in 0.1 N KCl in a system involving a liquid junction, show how to estimate the value relative to the normal calomel electrode in KCl, corrected for the liquid junction.

(f) How should we modify the values in Table 7.1 in order to obtain tables of potentials of zero charge relative to a hydrogen electrode in 1 M HCl and relative to a hydrogen electrode in 1 M HNO_3? Would these two tables be different? Speculate on what we might mean by "potentials relative to a standard hydrogen electrode."

7.5 Let the surface excess $\Gamma_{i,d}$ of an ionic species in the diffuse layer be defined as

$$\Gamma_{i,d} = \int_{y_2}^{\infty} (c_i - c_{i\infty}) dy$$

(compare equation 7.5). Show, for the special case where the magnitudes of the ionic charges are all the same, $|z_i| = z$, that diffuse-layer theory yields the expression

$$\Gamma_{i,d} = 2\lambda c_{i\infty}(e^{-z_i\phi_2/2} - 1).$$

From this result, show that

$$\left(\frac{\partial \Gamma_{i,d}}{\partial q_2}\right)_{\mu} = \frac{2/F}{1 + e^{z_i\phi_2}} \frac{z_i c_{i\infty}}{\sum_j z_j^2 c_{j\infty}}$$

and that, consequently, in the absence of specific adsorption, the potential U_z of zero charge varies with composition as

$$\frac{dU_z}{d\mu} = \frac{1}{2zF},$$

where U_z is measured relative to a reference electrode reversible to the anion. Note that for repelling potentials $\Gamma_{i,d}$ shows a limiting amount of exclusion from the double layer, $\Gamma_{i,d} \to -2\lambda c_{i\infty}$.

7.6 **(a)** Apply the Debye–Hückel approximation, equation 4.7, to the theory of the diffuse layer, and show that the diffuse-layer capacity is given, in this approximation, by

$$C_d = \frac{\epsilon}{\lambda}.$$

(b) Show from equations 7.37 and 7.39 that asymptotically, as y approaches infinity, the potential and electric field in the diffuse layer are given by

$$\Phi = \lambda A e^{-y/\lambda} \quad \text{and} \quad E = A e^{-y/\lambda},$$

where A is a constant independent of position.

7.7 For a layer of water dipoles oriented perfectly at an interface as sketched in Figure 7.4, estimate the magnitude of the difference in electrostatic potential across the layer. Take the dipole moment of water to be 7.85×10^{-30} C·m, the area per molecule to be 0.16×10^{-18} m^2, and the permittivity to be that of free space. Compare the magnitude of the result with potential differences encountered in electrochemistry, for example, in Table 2.3 or in the figures in this chapter.

7.8 **(a)** For an ideally polarizable electrode in a solution of a single salt in the absence of specific adsorption, show how to calculate C, U, Γ_+, and σ as functions of q and μ if you are given C_{M-2} as a function of q. In addition, the potential and the surface tension at the point of zero charge can be assumed to be known as functions of concentration.

(b) Is all of this last information necessary?

7.9 A porous carbon material acts as an ideally polarizable electrode and has a double-layer capacity of 30 $\mu F/cm^2$ and a surface area of 250 m^2/g. Estimate the electric capacity of a cubic centimeter of electrode packed with this material. The density of the pure solid carbon is 2.25 g/cm^3, its molar mass is 12.00 g/mol, and the porosity (void volume fraction) of the porous material is estimated to be 0.7 as packed. What difference in applied potential is required to effect a change of surface charge density of 10 $\mu C/cm^2$? If this change of surface charge density is accomplished by the adsorption of chloride ions, what surface area, expressed in nm^2, is available to each adsorbed chloride ion?

7.10 **(a)** The following data at 18°C are obtained for the surface tension of mercury in NaCl solutions at the point of zero charge. Estimate the surface concentration of NaCl for a 0.3 *M* NaCl solution at the point of zero charge.

c_{NaCl} (*M*)	σ (mN/m)
0	425
1	422

(b) What convention is used for the position of the Gibbs interface for the result expressed in part (a)?

7.11 A waste solution from washing radiator parts contains 20 mg/liter of Zn^{2+} in a solution mainly made up of 400 mg/liter of NaCl. It is proposed to remove the zinc by electrosorption on a bed of porous carbon electrodes. Alternate layers 1 cm thick are polarized negatively 0.5 V relative to the remaining layers. If the porous carbon has a double-layer capacity of 69 F/cm^3, how many bed volumes of solution can be treated before the bed becomes saturated? Assume that only the divalent zinc ions are involved in the sorption process over a potential change of 0.25 V. The molar mass of zinc is 65.37 g/mol.

7.12 A bulk solution 0.06 *M* in sodium chloride and 0.001 *M* in zinc chloride is subjected to electrosorption on a high-surface-area carbon material. Assume that there is no specific adsorption, and estimate the selectivity of the diffuse layer for zinc ions relative to sodium ions. Assume that the potential at the outer Helmholtz plane (relative to the bulk solution) is so small that the expression for the Boltzmann distribution can be linearized wherever it is encountered.

7.13 The MnO_2 in the cell of Problem 2.21 is estimated to have a surface area of 58 m^2/g. If this material has a double-layer capacity of 50 $\mu F/cm^2$ and can be polarized (i.e., displaced in potential) by 100 mV, how many coulombs can be associated with double-layer charging? How does this compare with the coulombs that can be passed in the discharge reaction? (The molar mass of MnO_2 is 86.93 g/mol.)

NOTATION

A	area, cm^2
c_i	concentration of species i, mol/cm^3
C	double-layer capacity, F/cm^2
C_d	capacity of the diffuse layer, F/cm^2
C_i	dimensionless concentration
C_{M-2}	capacity of region between the metal and the inner limit of the diffuse layer, F/cm^2
E	electric field, V/cm
$\mathcal{E}$	dimensionless electric field

F Faraday's constant, 96,487 C/mol
G Gibbs free energy, J
K see equation 7.46
n_i number of moles of species i, mol
p pressure, N/cm^2
q surface charge density on the metal side of the double layer, C/cm^2
q_1 surface charge density of specifically adsorbed ions, C/cm^2
q_2 surface charge density in the diffuse layer, C/cm^2
Q_2 see equation 7.46
R universal gas constant, 8.3143 J/mol·K
S entropy, J/K
T absolute temperature, K
U electrode potential, V
V volume, cm^3
x y/λ
x_i mole fraction of species i
y distance from surface, cm
y_2 position of inner limit of diffuse layer, cm
z_i charge number of species i
Γ_i surface concentration of species i, mol/cm^2
ϵ permittivity, F/cm
λ Debye length, cm
μ_i electrochemical potential of species i, J/mol
ρ_e electric charge density, C/cm^3
σ surface tension, mN/m
τ thickness of surface, cm
ϕ dimensionless potential
Φ electric potential, V

Superscripts

α, β phases α and β
σ surface

REFERENCES

1. David C Grahame. "The Electrical Double Layer and the Theory of Electrocapillarity," *Chemical Reviews*, *41* (1947), 441–501.
2. Paul Delahay, *Double Layer and Electrode Kinetics* (New York: Interscience, 1965).
3. D. C. Grahame, E. M. Coffin, J. I. Cummings, and M. A. Poth, "The Potential of the Electrocapillary Maximum of Mercury. II," *Journal of the American Chemical Society*, *74* (1952), 1207–1211.
4. Richard S. Perkins and Terrell N. Andersen, "Potentials of Zero Charge of Electrodes," *Modern Aspects of Electrochemistry*, *5* (1969), 203–290.
5. David C. Grahame, "Differential Capacity of Mercury in Aqueous Sodium Fluoride Solutions. I. Effect of Concentration at 25°," *Journal of the American Chemical Society*, *76* (1954), 4819–4823.
6. Roger Parsons, "Equilibrium Properties of Electrified Interphases," *Modern Aspects of Electrochemistry, I* (1954), 103–179.
7. Richard Payne, "The Electrical Double Layer in Nonaqueous Solutions," *Advances in Electrochemistry and Electrochemical Engineering*, *7* (1970), 1–76.

CHAPTER 8

ELECTRODE KINETICS

8.1 HETEROGENEOUS ELECTRODE REACTIONS

Current concepts of double-layer structure are based on information obtained from the mercury electrode in the absence of the passage of a faradaic current, that is, from an ideally polarizable electrode. Now we want to turn to the consideration of charge-transfer or faradaic reactions. In electrochemical systems of practical importance, including corrosion, it is reactions at the electrodes that are of primary importance.

The first thing we want to know about an electrode reaction is its rate. For a single electrode reaction occurring in a steady state, the rate of the reaction is related in a simple manner by Faraday's law to the current density i_n, which is easily measured experimentally. Simultaneous reactions are discussed in Section 8.7. Transient electrode processes involve the double-layer capacity, discussed in Chapter 7 and again in Section 8.4. They may also involve transient changes in the nature of the electrode surface.

The rate of the electrode reaction, characterized by the current density, depends first on the nature and previous treatment of the electrode surface. Second, the rate of reaction depends on the composition of the electrolytic solution adjacent to the electrode, just outside the double layer. This may be different from the composition of the bulk solution because of limited rates of mass transfer, treated in Parts C and D. However, the diffuse part of the double layer is regarded as part of the interface. It is too thin to probe adequately, and the theory of the diffuse layer is a microscopic model rather than a macroscopic theory. The effect of double-layer structure on electrode kinetics is discussed in Section 8.4.

Finally, the rate of the reaction depends on the electrode potential. This electrode potential is characterized by the surface overpotential η_s defined in Section 1.3 as the potential of the working electrode relative to a reference electrode of the same kind placed in the solution adjacent to the surface of the working electrode (just outside the double layer). This is a macroscopically well-defined potential and can be expressed in terms of electrochemical potentials. For the general electrode reaction expressed by equation 2.6, the equilibrium condition 2.7 is

$$\sum_i s_i \mu_i = n\mu_{e^-}. \tag{8.1}$$

Electrochemical Systems, Fourth Edition. John Newman and Nitash P. Balsara.

The surface overpotential η_s expresses the departure from the equilibrium potential and is given by

$$F\eta_s = F(\Phi_{\text{electrode}} - \Phi_{\text{solution}}) = -\mu_{e^-} + \sum_i \frac{s_i}{n}\mu_i. \tag{8.2}$$

The sign can be understood by thinking of μ_{e^-} as related to the potential by $z_i F\Phi = \mu_i$, and remembering that z_i is negative for the electrons. Superscripts for the appropriate phases in which the species exist should be added; in particular, μ_{e^-} is the electrochemical potential of the electrons in the metal of the electrode. This definition of η_s is equivalent to that given in Section 1.3.

As an example, the surface overpotential for a copper electrode undergoing the reaction

$$\text{Cu} \rightleftharpoons \text{Cu}^{2+} + 2\text{e}^- \tag{8.3}$$

is

$$\eta_s = -\frac{2\mu_{e^-} + \mu_{Cu^{2+}} - \mu_{Cu}}{2F}. \tag{8.4}$$

Thus, we can state three definitions of the driving force η_s for electrochemical reactions:

1. The potential of the electrode minus that of a reference electrode of the same kind and located adjacent to the surface. (Perhaps no such electrode exists in a corroding system where spontaneous side reactions occur. Also, it would be desirable if the reference electrode were protected from exposure to current flow, even if its net current is zero.)
2. The potential of the electrode (relative to the solution) minus the value at equilibrium or open-circuit. Conceptually this is what one is trying to achieve, as an idealization.
3. The electrochemical potential of electrons in the electrode compared to electrochemical potentials of other participants in the electrode reaction, according to equation 8.2. This is particularly helpful with modeling because it allows the surface overpotential to be defined in the same manner as other modeling quantities.

All three definitions are equivalent to the extent that they can be applied. In the presence of side reactions or corrosion reactions, the use of a reference electrode and the concept of an open-circuit potential are compromised.

By the above construction, the reaction rate goes to zero at $\eta_s = 0$, for any composition or reaction surface. For analyzing the behavior of electrochemical systems, we seek the macroscopic relationship between the current density and the surface overpotential and the composition adjacent to the electrode surface:

$$i_n = f(\eta_s, c_i). \tag{8.5}$$

Microscopic models may be useful in correlating these results, although they are not essential. Transient electrode processes can also involve the double-layer capacity and possibly hysteresis related to changes in the surface of the electrode.

For sources treating electrode kinetics in general, one should consult Vetter,[1] Delahay,[2] and Bockris and Reddy.[3] Vetter has a wealth of experimental information on specific electrode reactions, and Tanaka and Tamamushi[4] give tables of parameters for a number of reactions.

8.2 DEPENDENCE OF CURRENT DENSITY ON SURFACE OVERPOTENTIAL

We have already indicated in Section 1.3, the simplest type of dependence of the current density on the surface overpotential and composition adjacent to the electrode surface, that given by the Butler–Volmer equation 1.9:

$$i_n = i_0 \left[\exp\left(\frac{\alpha_a F \eta_s}{RT} \right) - \exp\left(\frac{-\alpha_c F \eta_s}{RT} \right) \right], \tag{8.6}$$

and we have indicated that this can be regarded as a result of cathodic and anodic reactions proceeding independently, each with an exponential dependence on the surface overpotential η_s. The exchange current density i_0 then depends on the composition of the solution adjacent to the electrode, as well as the temperature and nature of the electrode surface.

We have also indicated in Section 1.3 the Tafel approximations, equations 1.10 and 1.11 valid for large surface overpotentials. At low surface overpotentials, equation 8.6 can be approximated by a linear expression:

$$i_n = i_0 \frac{(\alpha_a + \alpha_c)F}{RT} \eta_s. \tag{8.7}$$

Another method of plotting equation 8.6 is worth noting. Equation 8.6 can be written

$$i_n = i_0 \left\{ \exp\left[\frac{(\alpha_a + \alpha_c)F}{RT} \eta_s \right] - 1 \right\} \exp\left(-\frac{\alpha_c F}{RT} \eta_s \right) \tag{8.8}$$

or

$$\ln \frac{i_n}{\exp\left(\frac{\alpha_a + \alpha_c}{RT} F \eta_s \right) - 1} = \ln i_0 - \frac{\alpha_c F}{RT} \eta_s. \tag{8.9}$$

If the sum $\alpha_a + \alpha_c$ is known, experimental values of i_n as a function of η_s (at a given composition adjacent to the electrode) yield a straight line when the left side of equation 8.9 is plotted versus η_s. Then, the slope gives the value of α_c, and the intercept gives the value of i_0. As indicated in the next section, there is some reason to expect the sum $\alpha_a + \alpha_c$ to have an integral value.

It should be emphasized again that, for a given composition adjacent to the electrode surface, there are three kinetic parameters in equation 8.6; these are i_0, α_a, and α_c. Experimental data are needed to determine these constants, in those cases where the experimental data can be adequately represented by equation 8.6.

The exchange current density i_0 depends on the composition of the solution adjacent to the electrode surface. Frequently, this dependence can be represented in terms of the concentrations of reactant and product species raised to some power:

$$i_0 = \left(\frac{c_1}{c_1^\infty} \right)^\gamma \left(\frac{c_2}{c_2^\infty} \right)^\delta i_0(c_i^\infty), \tag{8.10}$$

where species 1 and 2 are reactant and product species and $i_0(c_i^\infty)$ is the exchange current density for some conveniently selected values of c_i^∞. The concentrations adjacent to the electrode are denoted by c_i.

Many simple electrode reactions follow equation 8.6, possibly with some allowance for the effect of double-layer structure (see Section 8.4). However, many reactions of technical importance show

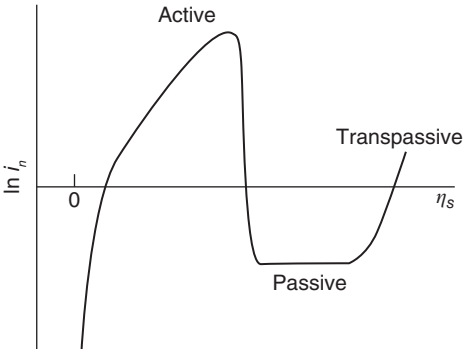

Figure 8.1 Current–potential relation for an electrode exhibiting passivation.

considerably different behavior. Outstanding among these are anodic dissolution processes showing passivation. A typical curve for such a process is shown in Figure 8.1. Here, the reaction rate first increases for increasing overpotential as indicated by equation 8.6. However, for sufficiently large overpotentials, a protective anodic oxide film, which may be very thin, forms on the electrode; and the current density drops to a very low value. Eventually, it may increase again either for the anodic dissolution process or, for an electronically conducting film, for anodic evolution of oxygen on the film. This is called the *transpassive region* of the curve. Such passivation phenomena can be reproducible, with very little time required for the formation or removal of the oxide film. Many ferrous alloys show this passivation phenomenon, with the passive current density and the maximum active current density depending on the composition of the alloy as well as the composition of the solution. Such behavior is important in the analysis of corroding systems.

The oxygen reaction generally is sluggish and not reproducible. On noble metals, oxide films can form, and a considerable hysteresis can be present, so that the reaction rate depends strongly on the previous history of the electrode, as well as on the present values of the overpotentials and the concentrations adjacent to the electrode.

8.3 MODELS FOR ELECTRODE KINETICS

We should like to distinguish between surface reactions that are simple reactions and those that are elementary steps. A simple reaction is the simplest that can be observed by analytical methods; that is, the reactants and products can be determined by macroscopic analysis, but intermediates in the reaction cannot be detected or are quite unstable. A simple reaction may be composed of one or many elementary steps. An elementary step is the elementary, mechanistic process by which a reaction occurs. A stable reactant may thus produce, via one elementary step, an unstable intermediate that immediately enters into reaction in another elementary step.

For example, the copper dissolution and deposition reaction in equation 8.3 can be regarded as being composed of two elementary steps, each of which involves the transfer of an electron:

$$\mathrm{Cu} \rightleftharpoons \mathrm{Cu^+} + \mathrm{e^-} \quad \text{(fast)}, \tag{8.11}$$

$$\mathrm{Cu^+} \rightleftharpoons \mathrm{Cu^{2+}} + \mathrm{e^-} \quad \text{(slow)}. \tag{8.12}$$

According to Mattsson and Bockris,[5] the second step is inherently much slower than the first step. Only in exceptional cases does an elementary step involve the transfer of more than one electron.

The rates of the elementary steps comprising a simple reaction should always be proportional to one another. For example, reaction 8.11 should occur once every time reaction 8.12 occurs. A reaction is much simpler to analyze if it can be treated as a simple reaction because then the rates of the elementary steps are simply related to each other. Whether a reaction should be regarded as a simple reaction or two or more simple reactions depends on just how unstable the active intermediate is, on the limits of detection of our analytical methods, and on the accuracy with which we wish to describe the system.

For the copper reaction, the intermediate cuprous ions are not completely unstable, and they can diffuse away from the electrode where they decompose by the disproportionation reaction

$$2Cu^{+} \rightleftharpoons Cu^{2+} + Cu. \tag{8.13}$$

Furthermore, it makes a difference whether reaction 8.3 proceeds in the anodic or the cathodic direction. In the cathodic direction, the slow reaction 8.12 occurs first and is relatively slow. The cuprous ions thus produced react in reaction 8.11. Thus, the rate of reaction 8.11 is limited by the rate of supply of cuprous ions from reaction 8.12 and is the same as the rate of reaction 8.12. In the anodic direction, the cuprous ions are produced by the relatively fast reaction 8.11. These can either diffuse away from the electrode or react in reaction 8.12. Now the rate of reaction 8.12 is determined in large part by its own kinetic characteristics and may not occur as fast as reaction 8.11, the difference corresponding to the cuprous ions which diffuse away from the electrode.

The rigorous treatment of the anodic process requires the treatment of reactions 8.11 and 8.12 as simultaneous reactions (see Section 8.7) rather than as elementary steps of a simple reaction, and the analysis is complicated by the need to account for the diffusion and convection of cuprous ions, requiring the consideration of transport processes described in Part C. On the other hand, if the cuprous ions were a species adsorbed on the electrode, they could not diffuse away. The coverage of cuprous ions would increase so that reactions 8.11 and 8.12 again occur at the same rate, and reaction 8.3 can be regarded as a simple equation. An example of detailed mechanistic analysis of the hydrogen evolution reaction is covered in a later section.

In our further treatment of the copper reaction, we assume that the cuprous ions do not diffuse away from the electrode, that their concentration reaches a value such that reactions 8.11 and 8.12 occur at the same rate, and that reaction 8.3 can be regarded as a simple reaction.

The distribution of potential in the double layer (see Chapter 7) gives rise to a potential difference between the electrode and the solution, which we shall denote by

$$V = \Phi_{\text{met}} - \Phi_{\text{soln}}, \tag{8.14}$$

where Φ_{met} is the electrostatic potential of the electrode and Φ_{soln} is the electrostatic potential of the solution just *outside* the double layer. This is usually not a well-defined potential; we can take V to be the potential relative to a given electrode (see Section 5.7).

Figure 7.7 illustrates the region near the interface and the greatly different length scales that can be associated with the diffuse layer, the diffusion layer, the bulk, and the reaction sites related to the metal surface and the inner and outer Helmholtz planes. For a reaction transferring an electron from the electrode to a $Fe(CN)_6^{3-}$ ion to form a $Fe(CN)_6^{4-}$ ion, depicted in Figure 8.2, the action occurs in the inner part of the interface, where the $Fe(CN)_6^{3-}$ ion in the outer Helmholtz plane is stripped of its waters of hydration to become adsorbed in the inner Helmholtz plane. With the ion and water molecules remaining relatively stationary, the electron transfer occurs with this configuration. The $Fe(CN)_6^{4-}$ ion can then desorb to the outer Helmholtz plane and become hydrated again. Other mass transfer of ions occurs through the diffuse layer and the diffusion layer. Figure 8.2 also illustrates what is meant by just outside the double layer, a concept that distinguishes between the diffuse layer

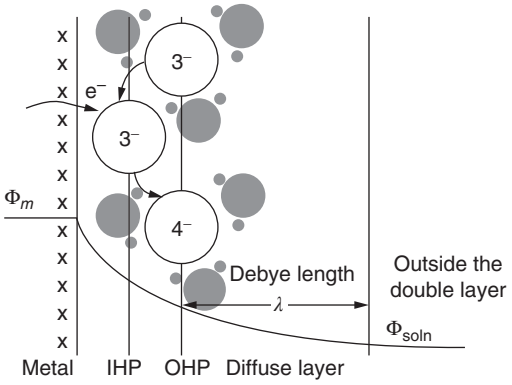

Figure 8.2 A 3-valent ion (ferricyanide) from the outer Helmholtz plane can be adsorbed at the inner Helmholtz plane, where it can react with an electron from the metal electrode. The resulting 4-valent ion (ferrocyanide) is then desorbed.

(which has a nonzero distributed charge density) and the diffusion layer (which is largely electrically neutral).

A Simple Stoichiometry

Let us write a redox reaction as

$$O + n\mathrm{e}^- \rightleftharpoons R, \tag{8.15}$$

where O is the oxidized species and R is the reduced species. If only one reaction is occurring at the electrode, then the current is proportional to the net rate of reaction. The reactions in the cathodic and anodic directions occur simultaneously, each with its own dependence on the surface overpotential and reactant concentrations.

The net rate of reaction r is equal to the difference between the rate of the forward reaction and the rate of the backward reaction, and can be written as

$$r = \frac{i_n}{nF} = k_a c_R \exp\left[\frac{(1-\beta)nF}{RT}V\right] - k_c c_O \exp\left(\frac{-\beta nF}{RT}V\right), \tag{8.16}$$

where k_a and k_c are rate constants for the anodic and cathodic reactions, respectively, and c_R and c_O are the concentrations of the anodic and cathodic reactants, respectively. This implies that the cathodic and anodic reactions are first order in the reactants.

Equation 8.16 for this electrochemical reaction is similar to what one sees in ordinary chemical kinetics, with the additional factor of the dependence of the rates on the potential. The rate constants k_a and k_c would be expected to show an Arrhenius dependence on temperature, and they also depend on the nature of the electrode surface. The k's and the exponential factors together represent Arrhenius rate constants with potential-dependent activation energies.

The *symmetry factor* β represents the fraction of the applied potential V that promotes the cathodic reaction. Similarly, $1-\beta$ is the fraction of the applied potential that promotes the anodic reaction. Frequently, it is assumed that β should have the value $\frac{1}{2}$, although the theoretical justification for this is not completely rigorous.

The meaning of the symmetry factor β is usually illustrated by means of a potential–energy diagram. Figure 8.3 shows two upward opening parabolas describing adiabatic electron transfer at an active

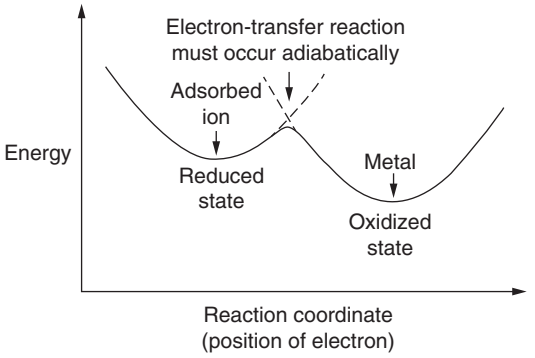

Figure 8.3 Active-intermediate diagram, showing the potential energy of an electrode–ion system as a function of distance of the electron from the ion.

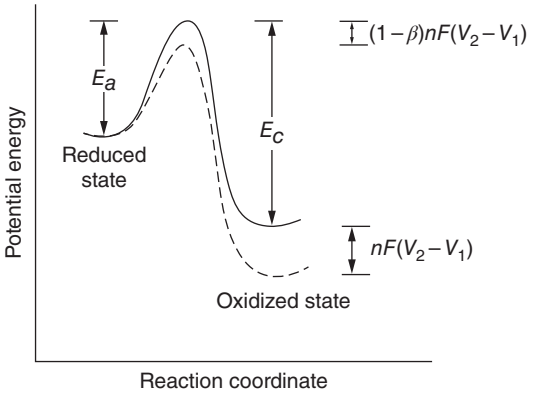

Figure 8.4 Potential–energy diagram for an elementary charge-transfer step. The solid curve is for $V = V_1$. The dashed curve is for $V = V_2$, where V_2 is greater than V_1.

intermediate. The reaction coordinate can be thought of as the position of the electron during the transfer process. In Figure 8.4, the potential–energy curve for an applied potential V_1 is shown by a solid line, the activation energies E_a and E_c in the anodic and cathodic directions, respectively, being indicated on the figure. A change of the applied potential from V_1 to V_2 results in a change of the energy of the reduced state relative to the oxidized state by an amount $nF(V_2 - V_1)$, and this tends to drive the reaction anodically if V_2 is greater than V_1.

If the applied potential is changed from V_1 to V_2, the potential–energy diagram is envisioned to change to the dashed curve. (The zero of potential is not material here; consequently, the reduced state has been sketched at the same energy level. The zero of potential is absorbed into the rate constants k_a and k_c in equation 8.16.) Then, according to Figure 8.4, the activation energy in the cathodic direction increases by $\beta nF(V_2 - V_1)$, and the activation energy in the anodic direction decreases by $(1 - \beta)nF(V_2 - V_1)$:

$$E_{c2} = E_{c1} + \beta nF(V_2 - V_1), \tag{8.17}$$

$$E_{a2} = E_{a1} - (1 - \beta)nF(V_2 - V_1). \tag{8.18}$$

This corresponds to the exponential terms in equation 8.16 and illustrates how β is the fraction of the applied potential that favors the cathodic reaction.

At some value U of the potential difference V between the metal and the solution, the rate of the forward reaction equals the rate of the backward reaction, and the net rate of reaction is zero. Then equation 8.16 becomes

$$k_a c_R \exp\left\{\frac{(1-\beta)nFU}{RT}\right\} = k_c c_O \exp\left\{\frac{-\beta nFU}{RT}\right\}. \tag{8.19}$$

Further rearrangement yields

$$U = \frac{RT}{nF} \ln \frac{k_c c_O}{k_a c_R}, \tag{8.20}$$

a form of the Nernst equation. As discussed in Section 8.1, the potential at which the net rate of reaction is zero is known as the *equilibrium potential*, and the surface overpotential η_s is defined as the difference between the actual potential and the equilibrium potential:

$$\eta_s = V - U. \tag{8.21}$$

Substituting these two equations into equation 8.16 yields

$$\begin{aligned}\frac{i_n}{nF} =& k_a c_R \exp\left[\frac{(1-\beta)nF}{RT}\eta_s + (1-\beta)\ln\frac{k_c c_O}{k_a c_R}\right] \\ &- k_c c_O \exp\left(\frac{-\beta nF}{RT}\eta_s - \beta \ln \frac{k_c c_O}{k_a c_R}\right).\end{aligned} \tag{8.22}$$

With this definition of η_s and the *exchange current density* i_0 defined by

$$i_0 = nF k_a^{\beta} k_c^{1-\beta} c_R^{\beta} c_O^{1-\beta}, \tag{8.23}$$

equation 8.22 can be written

$$i_n = i_0 \left\{\exp\left[\frac{(1-\beta)nF}{RT}\eta_s\right] - \exp\left(-\frac{\beta nF}{RT}\eta_s\right)\right\}. \tag{8.24}$$

This equation is known as the *Butler–Volmer equation*, often seen in the form given in equation 8.6. From equation 8.23, one sees that i_0 depends on the composition of the solution adjacent to the electrode, as well as the temperature and the nature of the electrode surface. Comparison with equation 8.6 shows that for this redox reaction we have $\alpha_a = (1-\beta)n$ and $\alpha_c = \beta n$.

The next section repeats this development for a general stoichiometry. After that, the discussion of the hydrogen evolution reaction shows how α_a and α_c might be related to the β's of the component elementary steps of a simple reaction.

A General Stoichiometry

Consider an elementary step that can be represented by the general equation

$$\sum_i s_i M_i \rightleftharpoons n\mathrm{e}^-. \tag{8.25}$$

The number of electrons transferred n is zero if the elementary step does not involve charge transfer; it is one if charge transfer is involved, multiple electron transfers being unlikely in an elementary step. The rate of the elementary step can then usually be expressed by the equation

$$r = \frac{i_n}{nF} = k_a \exp\left[\frac{(1-\beta)nF}{RT}V\right]\prod_i c_i^{p_i} - k_c \exp\left(-\frac{\beta nF}{RT}V\right)\prod_i c_i^{q_i}. \tag{8.26}$$

If more than one elementary step is involved in the simple reaction, an additional subscript should be added to r, i_n, n, β, k_a, k_c, p_i, q_i, and s_i to distinguish the elementary steps from each other and from the overall reaction.

Just as in equation 8.16, k_a and k_c are rate constants for the anodic and cathodic directions, respectively. Only the reaction stoichiometry has been generalized. The reaction orders for species i in the anodic and cathodic directions are p_i and q_i, respectively.

For a simple reaction involving one elementary step, equation 8.26 yields for the equilibrium potential U

$$\frac{nFU}{RT} = \ln\frac{k_c}{k_a} + \sum_i (q_i - p_i)\ln c_i. \tag{8.27}$$

Comparison with the Nernst equation for this reaction suggests that q_i, p_i, and s_i should be related by

$$q_i - p_i = -s_i. \tag{8.28}$$

In fact, for an elementary step, we presume that the reaction orders are given by the elementary reaction 8.25 itself. If $s_i = 0$, the species is neither a reactant nor a product, and we set p_i and q_i equal to zero. If $s_i > 0$, the species is an anodic reactant, and we set $p_i = s_i$ and $q_i = 0$. If $s_i < 0$, the species is a cathodic reactant, and we set $q_i = -s_i$ and $p_i = 0$.

With definition 8.21 of the surface overpotential, equation 8.26 can be written as equation 8.24, where now the exchange current density i_0 is given by

$$\frac{i_0}{nF} = k_a \exp\left[\frac{(1-\beta)nF}{RT}U\prod_i c_i^{p_i}\right] = k_c \exp\left(-\frac{\beta nF}{RT}U\right)\prod_i c_i^{q_i}. \tag{8.29}$$

Elimination of U by means of equation 8.27 gives

$$i_0 = nFk_c^{1-\beta}k_a^{\beta}\prod_i c_i^{(q_i+\beta s_i)}. \tag{8.30}$$

This gives an explicit dependence of the exchange current density i_0 on the reactant and product concentrations adjacent to the electrode. We see that γ and δ in equation 8.10 correspond to $q_i + \beta s_i$. Because β is a fraction, the power on c_i in equation 8.30 is generally a fraction even though p_i, q_i, and s_i are all integers. This power is positive if the rules following equation 8.28 apply. Thus, the exchange current density increases if either the reactant or product concentration is increased.

An increase in the concentration of an anodic reactant for which $p_i = 1$ leads to a proportionate increase in the anodic term in equation 8.26 at constant V. However, i_0 is related to this term, not at constant V, but at the equilibrium potential. An increase in the concentration of the anodic reactant shifts the equilibrium potential such that the two terms in equation 8.26 remain equal. Thus, both terms in equation 8.26 increase, and the exchange current density i_0 increases, proportional to a fractional power of the anodic concentration. Study of Figure 8.5 may be helpful in understanding how this works.

Simple Reactions with Elementary Steps

For more complex electrode reactions, one needs to write down the reaction mechanism in terms of elementary steps and analyze the kinetics of each step, as has been done here for a single elementary step. For the elementary steps 8.11 and 8.12 of the copper reaction, we write equation 8.26 as

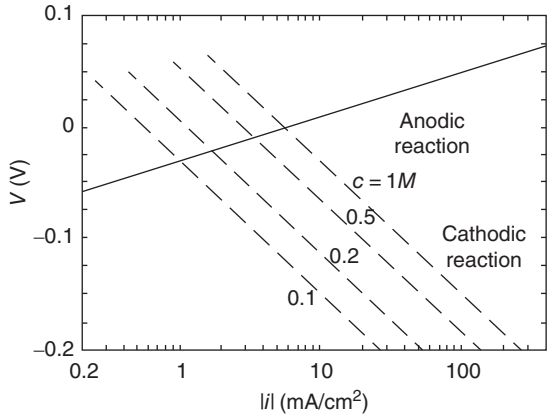

Figure 8.5 Anodic and cathodic contributions to the current density (from equation 8.35 with $\beta_3 = 0.5$) plotted against the potential relative to a copper electrode in 1 M $CuSO_4$ (see Section 5.7).

$$\frac{i_2}{F} = k_{a2} \exp\left[\frac{(1-\beta_2)F}{RT}V\right] - k_{c2} c_{Cu^+} \exp\left(-\frac{\beta_2 F}{RT}V\right) \tag{8.31}$$

and

$$\frac{i_3}{F} = k_{a3} c_{Cu^+} \exp\left[\frac{(1-\beta_3)F}{RT}V\right] - k_{c3} c_{Cu^{2+}} \exp\left(-\frac{\beta_3 F}{RT}V\right). \tag{8.32}$$

Subscripts 2 and 3 have been added corresponding to reactions 8.11 and 8.12. The concentration of the anodic reactant in reaction 8.11, copper, has not been included in equation 8.31 since it is constant. As stated earlier, we assume that reactions 8.11 and 8.12 occur at the same rate. Hence

$$i_n = i_2 + i_3 = 2i_2 = 2i_3. \tag{8.33}$$

Next, we introduce the surface overpotential for the overall reaction (see equation 8.4), not those for reactions 8.11 and 8.12 individually. We also assume that reaction 8.11 is fast and essentially in equilibrium. (For the more general case, see Problem 8.1.) For large values of k_{a2} and k_{c2}, equation 8.31 yields the potential-dependent equilibrium concentration of cuprous ions:

$$c_{Cu^+} = \frac{k_{a2}}{k_{c2}} \exp\left(\frac{FV}{RT}\right). \tag{8.34}$$

Substitution into equation 8.32 gives

$$\frac{i_3}{F} = \frac{i}{2F} = \frac{k_{a3}k_{a2}}{k_{c2}} \exp\left(\frac{(2-\beta_3)F}{RT}V\right) - k_{c3} c_{Cu^{2+}} \exp\left(-\frac{\beta_3 F}{RT}V\right). \tag{8.35}$$

From equation 8.35, the equilibrium potential is

$$U = \frac{RT}{2F} \ln\left(\frac{k_{c3}k_{c2}}{k_{a3}k_{a2}} c_{Cu^{2+}}\right), \tag{8.36}$$

and the exchange-current density is

$$i_0 = 2Fk_{c3}\left(\frac{k_{a3}k_{a2}}{k_{c3}k_{c2}}\right)^{\beta_3/2} c_{Cu^{2+}}^{(2-\beta_3)/2}. \tag{8.37}$$

With the surface overpotential given by equation 8.21, equation 8.35 can now be written in the form of the Butler–Volmer equation 8.6, where

$$\alpha_a = 2 - \beta_3 \tag{8.38}$$

and

$$\alpha_c = \beta_3. \tag{8.39}$$

The concentration dependence of the exchange-current density from equation 8.37 can now be expressed as

$$i_0 = \left(\frac{c_{Cu^{2+}}}{c^{\infty}_{Cu^{2+}}}\right)^{\gamma} i_0(c^{\infty}_{Cu^{2+}}), \tag{8.40}$$

where

$$\gamma = \frac{2 - \beta_3}{2}. \tag{8.41}$$

Mattsson and Bockris[5] studied the copper deposition reaction in 1 *N* sulfuric acid with various concentrations of copper sulfate. The exchange-current density i_0 can depend on the concentration of sulfuric acid and the nature of the electrode surface as well as the cupric ion concentration. Mattsson and Bockris studied surfaces prepared by quenching molten copper in purified helium and surfaces prepared by electrodeposition of copper.

Mattsson and Bockris[5] conclude that reaction 8.11 is inherently fast compared to reaction 8.12. Within the limits of reproducibility, α_a was 1.6 and α_c was 0.5, indicating that the symmetry factor β_3 for reaction 8.12 is equal to 0.5. A value of γ (in equation 8.40) of 0.6 was obtained for the deposited electrodes and a value of 0.3 for the helium-prepared electrode. On the other hand, equation 8.41 gives $\gamma = 0.75$ if $\beta_3 = 0.5$. Our examination of their data suggests a value of 0.42 for γ for the deposited electrodes. For later calculations, we shall use this value for γ and take i_0 equal to 1 mA/cm^2 for a cupric ion concentration of 0.1 mol/l.

The results of Mattsson and Bockris[5] deviate from equation 8.6 at low overpotentials. They attribute this to slow diffusion of adsorbed ions and atoms to and from lattice sites, indicating that this is not a simple charge-transfer process. This, along with standard deviations of 10% or 20% in the exchange-current density values, indicates that electrode kinetics is, in general, neither predictable nor reproducible on solid electrodes.

The anodic and cathodic contributions to the current density according to equation 8.35 are plotted in Figure 8.5 to illustrate the fact that the anodic contribution is independent of cupric ion concentration when plotted against the potential relative to a given reference electrode (see the remarks at the end of Section 5.7). With some approximations, this situation and the appearance of the conventional reaction orders is restored when the total overpotential is used instead of the surface overpotential; see Problem 20.4.

The models discussed in this section provide a basis for the electrode kinetic equation 8.6. However, these models do not have the rigor of a thermodynamic derivation. The expressions in equation 8.26 are not rigorously valid, and in equations 8.27 and 8.20, it was seen that comparison was made to the approximate Nernst equation rather than to the exact thermodynamic expression of the equilibrium

potential. Furthermore, the potential V depends on the choice of the given reference electrode. A different reference electrode would involve, implicitly, different combinations of ionic activity coefficients.

Equation 8.6 involves an unambiguous potential, the surface overpotential, and is thus superior to equations 8.26, from which equation 8.6 can be "derived." In equation 8.6, one can only say that the exchange-current density depends on the composition of the solution. Although not completely rigorous, the models do provide an explicit idea of the composition dependence of the exchange-current density.

The surface overpotential alone is discussed in this chapter. In Chapter 20, the concentration overpotential and the total overpotential are developed. Complex models of elementary steps and reaction sequences are developed further in Section 23.4 in the context of reaction at a semiconductor electrode. As a prelude, the student might explore surface coverages in Problem 8.6 and in the following sections. Models of electrode kinetics are also developed with the goal of making quantitative estimates of rate constants.[6]

Hydrogen Electrode Reaction

Various mechanisms can be constructed from three reactions: the Volmer reaction

$$H_{ad} \rightleftharpoons H^+ + e^-, \tag{8.42}$$

the Heyrovský reaction

$$H_2 \rightleftharpoons H^+ + e^- + H_{ad}, \tag{8.43}$$

and the Tafel reaction

$$2H_{ad} \rightleftharpoons H_2, \tag{8.44}$$

depending upon which reaction, if any, is rate determining, which reaction, if any, is equilibrated, and which reaction, if any, proceeds at a negligible rate. We shall number these reactions 1, 2, and 3 for consistency, and occasionally V, H, and T will stand for Volmer, Heyrovský, and Tafel. It is believed that the oxidation of hydrogen on a platinum catalyst occurs by the Tafel and Volmer steps, with the Tafel reaction being the rate-limiting step. In this section, we use these three steps in hypothetical combinations to provide examples of the methodology for developing an overall rate expression for a reaction involving multiple elementary steps.

The general procedure is to write down rate expressions for the above steps in the reaction mechanism and then to eliminate the surface concentration Γ_{ad} of the intermediate H_{ad} and relate the reaction rates of the steps to the rate of the overall reaction. For an overall rate expression in terms of the surface overpotential, set the rate to zero and identify the open-circuit potential U. This should reduce to a Nernst expression in which only ratios of rate constants occur, in the form of equilibrium constants. Because there can be only one Nernst equation for the overall reaction, independent of the catalytic nature of the electrode surface (Pt or Hg or some other material), this implies relationships among the equilibrium constants for the three individual steps.

Example of the Volmer–Tafel (VT) Mechanism

Here we develop an overall rate expression for the hydrogen electrode reaction proceeding according to the following mechanism. The Tafel reaction 8.44 is relatively rapid and can be treated as equilibrated, while the Volmer reaction 8.42 determines the overall rate. In particular, we show the exponential dependence on the surface overpotential η_s and discuss how the exchange current density is defined.

Solution The rate expression for the Tafel reaction would be

$$r_3 = k_f \Gamma_{\text{ad}}^2 - k_b p_{\text{H}_2} (\Gamma_{\max} - \Gamma_{\text{ad}})^2, \tag{8.45}$$

where $\Gamma_{\max} - \Gamma_{\text{ad}}$ is the surface concentration of unoccupied catalytic sites, which constitute a participant in the electrode reaction. Since this reaction can be treated as equilibrated, we have

$$\frac{\Gamma_{\text{ad}}}{\Gamma_{\max} - \Gamma_{\text{ad}}} = \left(\frac{k_b}{k_f} p_{\text{H}_2} \right)^{1/2} = \sqrt{P}, \tag{8.46}$$

or

$$\Gamma_{\text{ad}} = \frac{\Gamma_{\max} \sqrt{P}}{1 + \sqrt{P}} \quad \text{and} \quad \Gamma_{\max} - \Gamma_{\text{ad}} = \frac{\Gamma_{\max}}{1 + \sqrt{P}}, \tag{8.47}$$

where P, a dimensionless partial pressure of H_2, has been defined by equation 8.46.

The rate expression for the Volmer reaction would be

$$r_1 = k_{a1} \Gamma_{\text{ad}} \exp \left[\frac{(1 - \beta_1) FV}{RT} \right] - k_{c1} (\Gamma_{\max} - \Gamma_{\text{ad}}) c_{\text{H}^+} \exp \left[\frac{-\beta_1 FV}{RT} \right]. \tag{8.48}$$

Substitution of equation 8.47 and recognition of the relationship of i to r_1 give

$$\frac{i_n}{F} = r_1 = \frac{\Gamma_{\max}}{1 + \sqrt{P}} \left[k_{a1} \sqrt{P} e^{(1-\beta_1) FV/RT} - k_{c1} c_{\text{H}^+} e^{-\beta_1 FV/RT} \right]. \tag{8.49}$$

At open circuit, the Nernst equation results

$$U = \frac{RT}{F} \ln \left[\frac{k_{c1} c_{\text{H}^+}}{k_{a1} \sqrt{P}} \right], \tag{8.50}$$

showing the correct dependence on hydrogen partial pressure and on hydrogen ion concentration. This expression is independent of reaction mechanism, and therefore certain combinations of equilibrium constants are related to each other and to the standard cell potential. Thus, U^θ follows the approximate relationships:

$$\frac{FU^\theta}{RT} \sim \ln \left[\frac{k_{c1}}{k_{a1}} \left(\frac{k_f}{k_b} \right)^{1/2} \right] = \ln \left[\frac{k_{c2}}{k_{a2}} \left(\frac{k_b}{k_f} \right)^{1/2} \right]. \tag{8.51}$$

There are three elementary steps in the mechanism, but only two thermodynamically independent reactions and only one overall reaction (which does not mention the adsorbed hydrogen species). Introduction of the surface overpotential $\eta_s = V - U$ into equation 8.49 yields

$$i_n = i_{0V} [e^{(1-\beta_1) F\eta_s/RT} - e^{-\beta_1 F\eta_s/RT}], \tag{8.52}$$

where

$$i_{0V} = \frac{F\Gamma_{\max} (k_{a1} \sqrt{P})^{\beta_1} (k_{c1} c_{\text{H}^+})^{1-\beta_1}}{1 + \sqrt{P}}. \tag{8.53}$$

Equation 8.52 is of the Butler–Volmer form. Different catalytic metals have different values of the equilibrium constant for hydrogen adsorption as well as different rate constants for the components of

the mechanism. Again, the overall thermodynamics is independent of the catalysis. Figure 8.6 shows the current–potential relationship for the hydrogen-evolution reaction on various electrode materials. It is noteworthy that the Tafel slopes are so similar and that the magnitude of the exchange current density varies by so many orders of magnitude.

Equation 8.52 would be nearly identical to the equation for the HT mechanism (see Problem 8.10), if the β values were the same for the two charge-transfer reactions. However, the exchange-current density would have a different dependence on the hydrogen partial pressure in the two cases, but the dependence on the hydrogen ion concentration would then be the same.

The above reaction analysis should be contrasted to what we would get if we had analyzed the overall reaction

$$H_2 \rightleftharpoons 2H^+ + 2e^-, \tag{8.54}$$

as though it were an elementary step. Then we would write

$$\frac{i_n}{2F} = r = k_a p_{H_2} \exp\left(\frac{\alpha_a FV}{RT}\right) - k_c c_{H^+}^2 \exp\left(\frac{-\alpha_c FV}{RT}\right). \tag{8.55}$$

This relation has different reaction orders at constant V from what we derived in the analysis of the reaction mechanism. Furthermore, the sum of α_a and α_c is 2 here but only 1 for equation 8.52.*

Second Example—The HV Mechanism

Now we develop an overall rate expression for the hydrogen reaction proceeding according to a mechanism where the Volmer reaction 8.42 is equilibrated, while the Heyrovský reaction 8.43 is rate determining. In this case, a true Butler–Volmer equation does not result.

Solution Again, we use 1 for the Volmer reaction and 2 for the Heyrovský reaction (the number 3 being reserved for the Tafel reaction). The rates of the relevant two reactions are given by equation 8.48 and

$$r_2 = k_{a2} p_{H_2} (\Gamma_{max} - \Gamma_{ad}) \exp\left(\frac{(1-\beta_2)FV}{RT}\right) - k_{c2} \Gamma_{ad} c_{H^+} \exp\left[\frac{-\beta_2 FV}{RT}\right]. \tag{8.56}$$

Each of these reactions occurs once when the overall reaction of hydrogen oxidation occurs once; hence, $i_n/2F = r_1 = r_2$. Take the first reaction to be virtually equilibrated:

$$\frac{\Gamma_{ad}}{\Gamma_{max} - \Gamma_{ad}} = \frac{k_{c1}}{k_{a1}} c_{H^+} \exp\left(-\frac{FV}{RT}\right) = D, \tag{8.57}$$

which also defines D, a potential-dependent equilibrium constant. We can also solve for both Γ_{ad} and $\Gamma_{max} - \Gamma_{ad}$, which occur in the other kinetic equation 8.56:

$$\Gamma_{ad} = \frac{\Gamma_{max} D}{1+D} \quad \text{and} \quad \Gamma_{max} - \Gamma_{ad} = \frac{\Gamma_{max}}{1+D}. \tag{8.58}$$

*Reaction orders are conventionally defined at constant electrode potential V (relative to a reference electrode of a given kind), not at constant surface overpotential. Figure 8.5 is plotted so that one can see the reaction order.

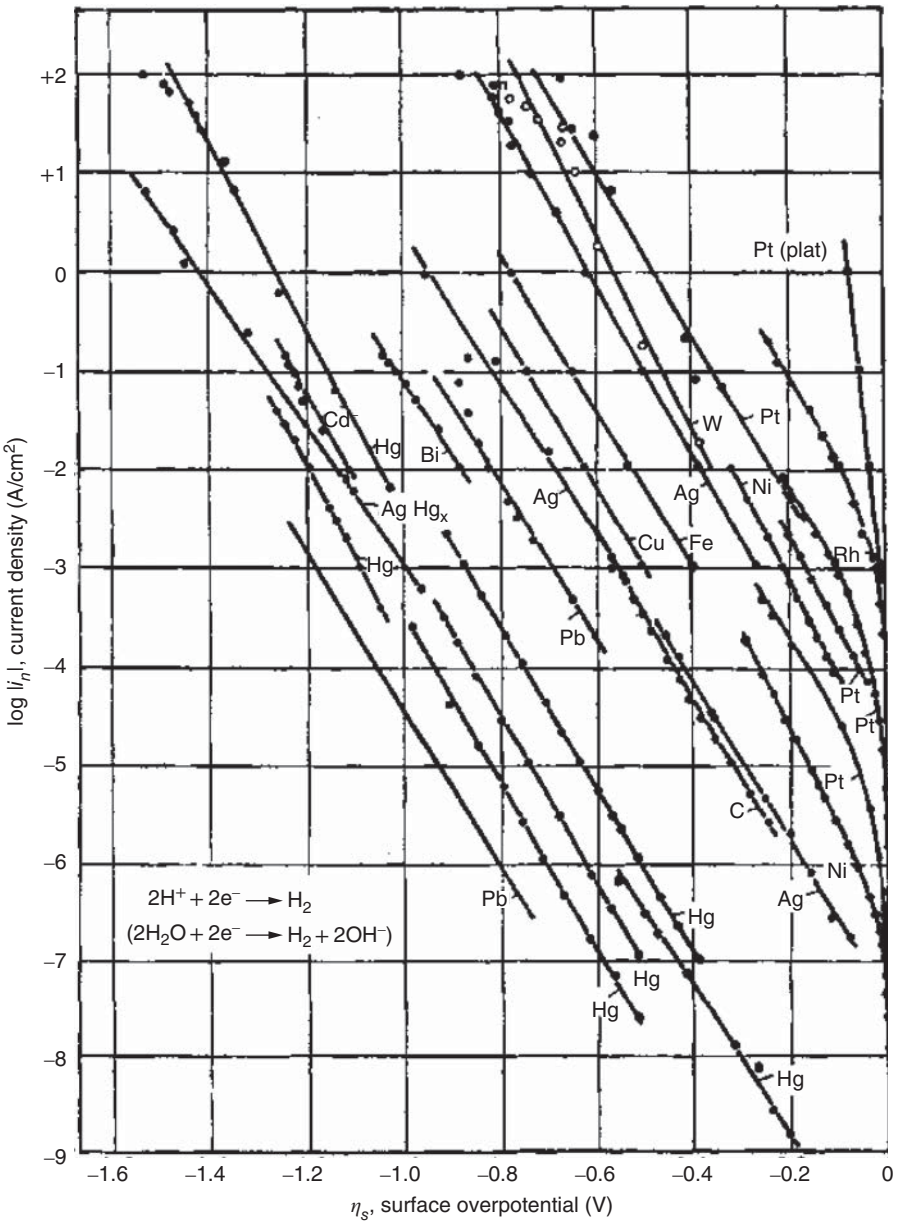

Figure 8.6 Tafel plot of surface overpotential for the hydrogen-evolution reaction on various electrode materials. *Source:* From Vetter 1961.[1] Data from different sources can differ substantially.

Thus, equation 8.56 becomes

$$\frac{i_n}{2F} = \frac{\Gamma_{\max}}{1+D}\left\{k_{a2}p_{H_2}\exp\left[\frac{(1-\beta_2)FV}{RT}\right] - k_{c2}Dc_{H^+}\exp\left[\frac{-\beta_2 FV}{RT}\right]\right\}. \tag{8.59}$$

At open circuit,

$$k_{a2}p_{H_2}\exp\left(\frac{2FU}{RT}\right) = k_{c2}c_{H^+}^2\frac{k_{c1}}{k_{a1}} \tag{8.60}$$

or

$$U = \frac{RT}{2F}\ln\left(\frac{k_{c2}k_{c1}c_{H^+}^2}{k_{a2}k_{a1}p_{H_2}}\right), \tag{8.61}$$

which has the correct concentration and partial-pressure dependence for the Nernst equation. With the surface overpotential η_s, defined by equation 8.21, the rate expression becomes

$$i_n = i_{HV}\frac{\exp\left[\frac{(1-\beta_2)F\eta_s}{RT}\right] - \exp\left(\frac{-(1+\beta_2)F\eta_s}{RT}\right)}{1+\sqrt{P}e^{-F\eta_s/RT}}, \tag{8.62}$$

where

$$i_{HV} = 2F\Gamma_{\max}(k_{a2}p_{H_2})^{(1+\beta_2)/2}\left(\frac{k_{c2}k_{c1}}{k_{a1}}c_{H^+}^2\right)^{(1-\beta_2)/2}. \tag{8.63}$$

The dimensionless partial pressure of H_2, P, is again given by equation 8.46 when equation 8.51 is used to relate the equilibrium constants. Equation 8.62 is not completely in the form of the Butler–Volmer equation since the denominator depends on η_s. The asymptotic forms are given below:

$$i_n = i_{HV}\exp\left[\frac{(1-\beta_2)F\eta_s}{RT}\right] \quad \text{for } \eta_s \gg \frac{RT}{F}, \tag{8.64}$$

and

$$i_n = -\frac{i_{HV}}{\sqrt{P}}\exp\left(\frac{-\beta_2 F\eta_s}{RT}\right) \quad \text{for } \eta_s \ll -\frac{RT}{F}. \tag{8.65}$$

Figure 8.7 shows the complicated current–potential behavior. The true exchange-current density for this case can be taken to be the forward or backward rate in equation 8.62 when $\eta_s = 0$:

$$i_{0H} = \frac{i_{HV}}{1+\sqrt{P}}. \tag{8.66}$$

An alternative would be to use i_{HV} as a term called the exchange-current density, making this look a little bit more like Problem 8.1.

Three Steps Together The above two examples show how to simplify the reaction mechanism by considering one step to be rate determining and another to be equilibrated, with the third step being of negligible importance. This leads to a total of six *mechanisms* that can be created from the three steps.

The above examples also illustrate general principles on the analysis of a reaction mechanism by means of simplifying assumptions:

1. One (or more) of the elementary steps can be taken to be equilibrated (see Problem 8.1).

2. Reaction rate constants come in three sizes:
   (a) Large (which implies that the reaction is equilibrated),
   (b) Small (which implies that the reaction can be ignored),
   (c) Intermediate (which implies that the rate expression must be accounted for and also suggests that this reaction is a candidate for the rate-determining step).
3. The apparent rate-determining step can change with applied potential because some rate constants are effectively potential dependent (see Figure 8.7).
4. The ratio of forward and backward rate constants is always an equilibrium constant and, therefore, is determined by thermodynamics alone. It is better to take this into account explicitly. (The Butler–Volmer equation does this; equilibrium is built into U while i_0 is a kinetic quantity.)
5. A computer can be used to analyze complex reaction sequences. A large number of rate parameters may appear, but points 2a and 2b can eliminate some from real consideration.

When the simplifying assumptions are not considered appropriate, one can treat (particularly with the aid of computers) all of the reaction steps simultaneously, according to their specific rate constants. Without going into great detail, we discuss some general aspects. With three steps, we can focus on two ratios of rate constants. Ratios establishing the relative rates of reactions 1 and 3 and of reactions 2 and 1 are

$$\lambda_1 = \frac{k_{a1}}{k_f \Gamma_{\max}}, \quad \lambda_2 = \frac{k_{c2}}{k_{c1}}. \tag{8.67}$$

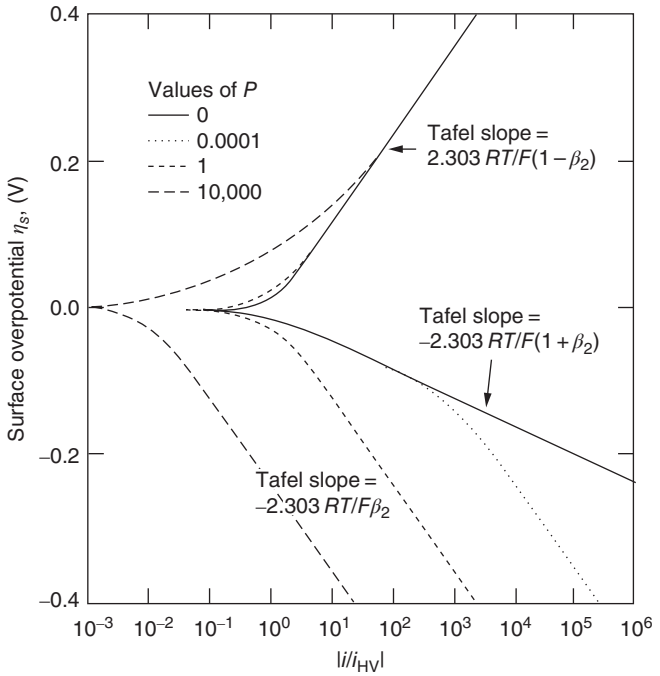

Figure 8.7 Tafel plot of overpotentials for the hydrogen electrode when the Heyrovský reaction ($H^+ + e^- + H_{ad} \rightarrow H_2$) is the rate-determining step and the Volmer reaction is rapid.

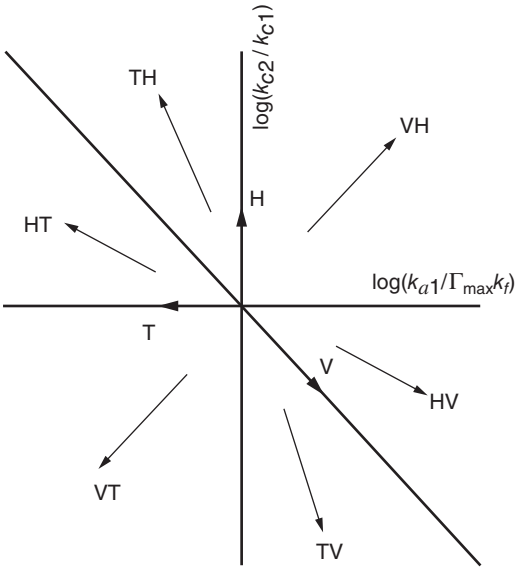

Figure 8.8 Map of the relative rates for the three elementary steps involved in the hydrogen electrode reaction. The three intersecting lines give the directions for increasing rate constants for the Volmer (V), Heyrovský (H), and Tafel (T) reactions. The other arrows indicate where the six limiting cases can be found, the first letter standing for the rate-determining step and the second letter showing the equilibrated step.

This permits us to make a parameter map as in Figure 8.8, using $\log(\lambda_1)$ and $\log(\lambda_2)$ as the coordinate axes.

In Figure 8.8, the three intersecting lines give the directions for increasing rate constants for the Volmer (V), Heyrovský (H), and Tafel (T) reactions. Any particular electrode, such as Pt or Hg, can be represented by a point on this diagram. When all three steps are important, the point would lie relatively close to the origin, where the three lines intersect. When a particular step is equilibrated, its rate constants are relatively large, and the point would be found out along the direction of the arrow for that step. Correspondingly, when the reaction is slow, the point would be located in the opposite direction along this line.

The six simplified mechanisms can be represented by the arrows located between the three intersecting lines representing the steps themselves. For example, the HV mechanism has the Volmer step equilibrated and therefore lies along the arrow direction for the V line. The Tafel step is unimportant, and therefore the HV arrow lies adjacent to the negative arrow direction for the T line. The Heyrovský reaction becomes the rate-determining step; the H line is more or less perpendicular to the arrow for the HV mechanism.

In addition to the rate-constant ratios λ_1 and λ_2, the algebra in treating the reactions simultaneously is simplified with a dimensionless partial pressure of hydrogen and a dimensionless concentration of hydrogen ions:

$$P = \frac{k_b}{k_f} p_{\mathrm{H_2}}, \quad C = \frac{k_{c1}}{k_{a1}} c_{\mathrm{H^+}}. \tag{8.68}$$

Dimensionless potential and overpotential can also be introduced, and the coverage can be made dimensionless with $\Gamma_{\max}$. To proceed, one needs to write expressions for the rates of the three elementary steps (already done in equations 8.45, 8.48, and 8.56 and identify the net current density i_n

in terms of these three rates. A balance on the adsorbed species can be regarded as the governing equation for the surface coverage. These steps have already been carried out for two specific mechanisms, VT and HV. The resulting current–potential curves can be even more complicated than Figure 8.7, because of the greater complexity of considering the three steps simultaneously.

Of the six reaction mechanisms represented by the small arrows in Figure 8.8, two give pure Butler–Volmer equations, namely the VT mechanism (treated in an earlier section) and the HT mechanism. Two show a more complicated behavior because of the potential dependence of rate constants; these are the HV mechanism (treated in the preceding section) and the VH mechanism. The remaining two mechanisms, the TH and the TV mechanisms, show a limiting-current behavior, possibly because the Tafel step is nonelectrochemical. (Note that this is a kinetic limiting current, not a transport limiting current.)

8.4 EFFECT OF DOUBLE-LAYER STRUCTURE

The double-layer structure can have an effect on the overall behavior of the interface, first, by superimposing a capacitive effect on top of the electrode kinetics of the electrode reaction itself. This means that when the potential of the electrode is varied, the current that flows is partly due to charging the double-layer capacity and partly due to a faradaic reaction. The capacity of the double layer in the absence of a faradaic reaction is discussed in Chapter 7.

We might now express the current density i for an electrode of constant area as

$$i = f(\eta_s, c_i) + C\frac{d\eta_s}{dt}, \tag{8.69}$$

where C is the double-layer capacity, η_s is the surface overpotential, c_i is the concentration of species i just outside the double layer, and f is a function describing the kinetics of the electrode reaction (see equation 8.5).

The double layer can behave like a capacitor that is in parallel with the electrode reactions, so that the current passing from the electrode to the solution either can take part in charge-transfer reactions or can contribute to the charge in the double-layer capacitor. It is this capacitive effect that reduces electrode polarization when alternating current is used for conductivity measurements. The double-layer capacity can also depend on the concentrations c_i and the electrode potential V (see Figures 7.15 and 7.16).

Many experiments described in the literature have involved a growing mercury drop, in which the electrode area changes with time. In this case, the last term in equation 8.69 should be replaced by

$$\frac{1}{A}\frac{dq\,A}{dt},$$

where q is the surface charge density on the electrode side of the interface and A is the instantaneous electrode area. (Recall that i is the current density flowing *from* the electrode *into* the solution.)

Equation 8.69 is written for constant concentrations c_i adjacent to the electrode surface. In this case, the equilibrium potential U is constant, and

$$\frac{dV}{dt} = \frac{d\eta_s}{dt}. \tag{8.70}$$

When the concentrations vary, the last term in equation 8.69 should, strictly, be replaced by dq/dt because q depends on c_i as well as V. This complex transient situation has been explored by Appel.[7]

When more than one reaction occurs, the first term in equation 8.69 should be replaced by $f(V, c_i)$, where f now describes the faradaic current due to all the reactions at the electrode potential V (see Section 8.7). The last term can also be replaced by $C\,dV/dt$.

The distinction between the contributions of the charging current and the faradaic current to the overall current density i in equation 8.69 may be subtle since one can measure only the overall current density directly. Ordinarily, one would try to measure f by making observations under steady conditions where the second term in equation 8.69 is zero. With the assumption that f has the same dependence on η_s and c_i for unsteady conditions in the interface, the double-layer capacity can then be measured by superimposing a small alternating potential. The situation with a growing electrode area is even more complex and has been the subject of some discussion in the literature.[8–11]

The second way in which double-layer structure enters into electrode kinetics is in the method of application of the models of Section 8.3 to an elementary step. Long ago, Frumkin[12] proposed that the diffuse part of the double layer should be treated separately from the charge-transfer reaction. Specifically, it was suggested that the concentrations c_i which enter into equation 8.69 should be the concentrations c_i^0 at the inner limit of the diffuse layer and that the potential η_s in the first term in equation 8.69 should be replaced by $\eta_s - \Phi_2$, where Φ_2 is the potential at the inner limit of the diffuse layer (see Figure 8.2).

The value of Φ_2 is to be taken at zero current (to eliminate the ohmic potential drop) but at the same electrode potential V as involved during the passage of current. It has been shown[13–15] that the equilibrium diffuse layer (see Section 7.4) is disturbed to only a minor extent by the passage of current. Thus, Φ_2 is still related to the surface charge density q_2 in the diffuse layer by equation 7.38 (c_i being represented as $c_{i\infty}$ there), and c_i^0 is related to c_i by

$$c_i^0 = c_i \exp\left(-\frac{z_i F \Phi_2}{RT}\right) \tag{8.71}$$

(compare equation 7.30).

It is difficult to know a priori the magnitude of the surface charge density q_2 in the diffuse layer since this is determined in large part by interaction with the rest of the interface (metal surface and inner Helmholtz plane), the whole of which is electrically neutral. It is not the value of q_2 in the same system at equilibrium (zero current); it depends on the electrode potential in a way that is not readily determined during the passage of current. The discussion in Section 23.4 can help to resolve these issues by showing how kinetic rate constants for anodic and cathodic processes contain the information related to charge distributions in the system.

The structure of the diffuse layer is studied best with an ideally polarizable electrode in the absence of a faradaic current and, hence, in the absence of any reacting species. In practice, we investigate the double layer with the nonreactive supporting electrolyte alone. Then, we add a small amount of the reactant and *assume* that q_2 and Φ_2 (at a given electrode potential) are not changed by the small addition or the small current now being passed.

One can also object that the correction is based on the microscopic theory of the diffuse layer and does not have a firm macroscopic basis. For these reasons, we do not expect that the correction can be applied with any certainty to solid electrodes, significant concentrations of reactants, or high ionic strengths. Nevertheless, the Frumkin correction does give an impressive qualitative account of complicated electrode behavior that can be attributed to double-layer structure, as reviewed by Parsons.[16] Reduction of anions or oxidation of cations can lead to particularly interesting double-layer effects because the reacting ion tends to be repelled by the intense electric field in the diffuse double layer, but this must be qualified by consideration of the potential of the point of zero charge relative to the open-circuit potential for the reaction.

8.5 THE OXYGEN ELECTRODE

The oxygen electrode is the most complicated electrode commonly encountered. One reason is that the reaction is so irreversible, that is, the exchange-current density is so low that even traces of impurities can successfully compete with it. Consequently, the reversible, equilibrium oxygen potential could not be successfully observed until impurities had been rigorously excluded.[17]

A second reason for the complicated behavior of the oxygen electrode is that the overall reaction

$$O_2 + 4H^+ + 4e^- \rightleftharpoons 2H_2O \tag{8.72}$$

can be regarded as the result of two simple reactions,

$$O_2 + 2H^+ + 2e^- \rightleftharpoons H_2O_2 \tag{8.73}$$

$$H_2O_2 + 2H^+ + 2e^- \rightleftharpoons 2H_2O, \tag{8.74}$$

in which hydrogen peroxide is a relatively stable and detectable intermediate. This has the consequence that the heterogeneous decomposition of hydrogen peroxide

$$2H_2O_2 \rightleftharpoons 2H_2O + O_2 \tag{8.75}$$

can be regarded as a result of the electrochemical reactions 8.73 and 8.74, the first reaction proceeding anodically and the second reaction proceeding cathodically (the second proceeding as written but with the first proceeding in the opposite direction, so that the electrons cancel in equation 8.75).

Furthermore, the hydrogen peroxide can diffuse away from the electrode at either an anode or a cathode, and depending on the relative rates of reactions 8.73 and 8.74, four or fewer electrons are required to produce or consume a molecule of oxygen. Since reaction 8.73 is generally inherently faster than reaction 8.74, one expects to observe peroxide formation in the cathodic consumption of oxygen, but not in the anodic process. Also, an appreciable time may be needed to get a steady current at a given cathodic potential until a steady bulk concentration of peroxide can build up. Compare Problem 8.1 and the text below equation 8.13.

A third complicating factor for the oxygen electrode is that there is an alternative reaction path involving adsorbed species and not the production of hydrogen peroxide. This leads to a fourth complication. The adsorbed layers can become so thick and are so slow to respond to changes in electrode potential that measurements can easily be carried out at the same potential on surfaces of quite different character. Also, the current for the reaction of these layers can be appreciable compared to the current for the primary reaction.

There are still other complications. Some metals, notably platinum, palladium, and rhodium, can dissolve oxygen to an appreciable extent. This can contribute to a hysteresis and is noted particularly in charging curves. Many metals, even gold, tend to corrode near the oxygen potential. Surface oxides are also responsible for the passivation characteristics of ferrous alloys, so that the reaction rate depends strongly on the previous history of the electrode. This behavior of the oxygen electrode is reviewed by several authors.[18–21]

The mechanism of Rossmeisl et al. [22] for the oxygen electrode involves only heterogeneous reactions, with no intermediate like peroxide leaving the electrode. It involves three adsorbed intermediates, four if you count empty catalyst sites. The reaction mechanism in acid media is

$$^* + H_2O \rightleftharpoons {}^*OH + H^+ + e^-, \tag{8.76}$$

$$^{*}\mathrm{OH} \rightleftharpoons {}^{*}\mathrm{O} + \mathrm{H}^{+} + \mathrm{e}^{-}, \tag{8.77}$$

$$^{*}\mathrm{O} + \mathrm{H_2O} \rightleftharpoons {}^{*}\mathrm{OOH} + \mathrm{H}^{+} + \mathrm{e}^{-}, \tag{8.78}$$

$$^{*}\mathrm{OOH} \rightleftharpoons {}^{*} + \mathrm{O_2} + \mathrm{H}^{+} + \mathrm{e}^{-}, \tag{8.79}$$

where * denotes a site on the catalyst surface, * by itself being an empty site. Water molecules are adsorbed with reactions that emit protons to the solution and electrons to the electrode. There is only one electron involved in each step, and only a few molecular species. With this reaction mechanism, the catalyst is returned to its original state after performing the overall reaction.

The analysis of the mechanism and the derivation of current/potential curves are somewhat similar to those given in Section 8.3 for the hydrogen electrode reaction involving three elementary steps and only one adsorbed species. The Butler–Volmer rate equation is written for each elementary step.

$$r_1 = k_{a1}\Gamma_{*} \exp\left(\frac{(1-\beta_1)F}{RT}V\right) - k_{c1}\Gamma_{*\mathrm{OH}}c_{\mathrm{H}^+} \exp\left(\frac{-\beta_1 F}{RT}V\right), \tag{8.80}$$

$$r_2 = k_{a2}\Gamma_{*\mathrm{OH}} \exp\left(\frac{(1-\beta_2)F}{RT}V\right) - k_{c2}\Gamma_{*\mathrm{O}}c_{\mathrm{H}^+} \exp\left(\frac{-\beta_2 F}{RT}V\right), \tag{8.81}$$

$$r_3 = k_{a3}\Gamma_{*\mathrm{O}} \exp\left(\frac{(1-\beta_3)F}{RT}V\right) - k_{c3}\Gamma_{*\mathrm{OOH}}c_{\mathrm{H}^+} \exp\left(\frac{-\beta_3 F}{RT}V\right), \tag{8.82}$$

$$r_4 = k_{a4}\Gamma_{*\mathrm{OOH}} \exp\left(\frac{(1-\beta_4)F}{RT}V\right) - k_{c4}\Gamma_{*}p_{\mathrm{O_2}}c_{\mathrm{H}^+} \exp\left(\frac{-\beta_4 F}{RT}V\right). \tag{8.83}$$

It is common in reaction analysis in aqueous media to take the activity of water to be unity, and not show it explicitly in the rate equation. It is also common in heterogeneous reaction analysis to divide surface concentrations by the total number of sites per unit area and hence to use fractional coverage.

$$\theta_i = \Gamma_i/\Gamma_{\max}. \tag{8.84}$$

The value of $\Gamma_{\max}$ eventually gets absorbed into rate constants, but one should expect the surface area of a dispersed catalyst to need to be accounted for also.

The unknowns now amount to four reaction rates r_l and four surface concentrations Γ_i. The parameters include four symmetry factors β_l, which are generally taken to be 0.5 for elementary steps, unless a lot of experimental data is available to give better values. There are eight rate constants k_l, but we generally prefer to count four rate constants k_{al} and four thermodynamic equilibrium constants $K_l = k_{al}/k_{cl}$. The thermodynamic constants come from a different (equilibrium) source of information and need to be consistent with each other and with known values for the thermodynamics of the overall reaction (the oxygen electrode reaction in the present case). This is accomplished straightforwardly by assigning a secondary reference thermodynamic quantity to each species, as done in Chapter 2 and carried further in Chapter 23. The adsorption equilibrium constants can be expected to be different on different electrode materials. The situation can be compared with that for the hydrogen electrode (see the latter part of Section 8.3 and particularly Figure 8.6). For this section, and for the chapter generally, the bulk concentrations are taken to be known constants, like c_{H^+} and $p_{\mathrm{O_2}}$. When transport limitations are involved, transport phenomena from Part C need to be treated, although a diffusion-layer thickness is used in Section 8.7. See also Chapters 11 and 17.

Four more equations are needed. These can be expressed as material balances on the adsorbed species and can be written, for a steady process, as

$$\frac{d\Gamma_*}{dt} = 0 = r_4 - r_1, \tag{8.85}$$

$$\frac{d\Gamma_{*\mathrm{OH}}}{dt} = 0 = r_1 - r_2, \tag{8.86}$$

$$\frac{d\Gamma_{*\mathrm{O}}}{dt} = 0 = r_2 - r_3, \tag{8.87}$$

and

$$\frac{d\Gamma_{*\mathrm{OOH}}}{dt} = 0 = r_3 - r_4. \tag{8.88}$$

These equations are redundant, and any one of them should be replaced by the overall site balance

$$\Gamma_* + \Gamma_{*\mathrm{OH}} + \Gamma_{*\mathrm{O}} + \Gamma_{*\mathrm{OOH}} = \Gamma_{\max}. \tag{8.89}$$

A computer is generally helpful in solving the resulting eight simultaneous nonlinear algebraic coupled equations. One wants to use linearization over the nonlinearities to produce an iteration method that converges quadratically, as discussed in Appendix C. Here it is easier because the unknowns do not extend over a spatial domain, as they do in Appendix C, but the method is similar.

After the rates and surface concentrations are obtained, with a series of values of the electrode potential V, the current density is calculated by adding the rates for the four reactions. The number of electrons is the same in all four reactions, and the formula is

$$i_n/F = r_1 + r_2 + r_3 + r_4 = 4r_1. \tag{8.90}$$

The procedure is the same in principle as that used in the latter part of Section 8.3 for the hydrogen electrode reaction.

With experimental data on a catalyst of choice, the parameters listed above would be adjusted to give the best fit of the data. Rossmeisl et al. [22] help by calculating the (potential-dependent) free energy of adsorption of the various surface species by simulating equilibrated species of interest on the surface of several different catalysts. This gives us the equilibrium constants and eliminates the need for them to remain as fitting parameters. These free energies are given in Table 8.1 for three oxides,[22] RuO_2, IrO_2, and TiO_2, and for two metals,[23] Pt and Au. The values for the oxides interest us more because oxides are more likely to be stable at the potential of the oxygen electrode. These values correspond to the open-circuit potential of the O_2 electrode relative to the H_2 electrode (1.229 V).

A valuable lesson is provided by the consideration of the catalysis of a series of reactions that comprise the mechanism of an electrode reaction. It applies both to the present oxygen electrode reaction and to the hydrogen reaction treated in the latter part of Section 8.3. A high-energy (or a low-energy) intermediate leads to very poor kinetics, without even invoking the Butler–Volmer equation. The free energy levels for the intermediates for RuO_2 are plotted in Figure 8.9 as a function of potential. The data at potentials different from the open-circuit potential were also obtained directly from simulations.[22] The reaction path can be considered to be from left to right, since for the mechanism considered here each of the four reactions must occur in sequence, evolving oxygen from left to right and reducing oxygen from right to left. When there is a high-energy intermediate, it constitutes a state which stands in the way of the progression of the reaction, much like the active intermediate shown at the top of the plot of energy versus reaction coordinate in Figure 8.3 or 8.4. With a high-energy intermediate, the left (uphill) reaction becomes the rate-limiting step, and the right

TABLE 8.1 Free energy of surface species at the open-circuit potential of the oxygen electrode ($p_{O_2} = 1$ bar, $c_{H^+} = 1$ mol/L), 1.229 V, with respect to the standard H_2 electrode

State	RuO_2	IrO_2	TiO_2	Pt	Au
*	0	0	0	0	0
*OH	0.08	−0.77	0.965	0.67	0.27
*O	0.23	−0.75	2.09	0.84	0.44
*OOH	0.59	−0.20	1.62	108	105
*With O_2	0	0	0	0	0

Values from Refs. [22, 23] are adjusted slightly to conform to the known value of the standard potential of the oxygen electrode. The unit is eV; multiply by 96.487 to get kJ/mol.

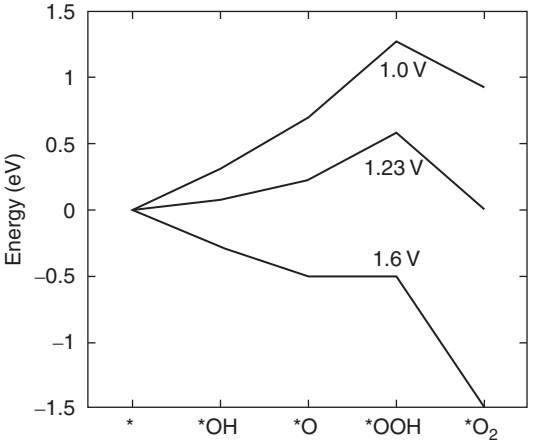

Figure 8.9 The potential-dependent surface free energies of surface species in the oxygen electrode on RuO_2. Adopted from Rossmeisl et al. 2007.[22] Adapted with permission of Elsevier. Potentials are relative to the normal hydrogen electrode. See also Problem 8.13.

reaction becomes the rate-limiting step in the opposite direction. With a low-energy intermediate, the reverse is true; uphill is always more difficult, and energy is not recovered going downhill. The energy landscapes at three different electrode potentials V are plotted in Figure 8.9 to illustrate how the ease or facility of the reaction changes with potential. This can be compared with the dashed line in Figure 8.4.

Figure 8.10 shows current–potential curves for RuO_2. Ruthenium oxide is the best catalyst for oxygen evolution, because the adsorbed intermediates in the sequence lie more on the same energy level with the reactants and the products. Iridium oxide is somewhat worse. Iridium oxide is likely to be preferred in practice because it has a higher degree of stability than ruthenium oxide. Titanium oxide is worse yet. Marshall et al. [24] synthesize and test alloys of RuO_2 and IrO_2 and conclude that the best is that with 40% RuO_2.

Rossmeisl et al. [22] report that for electrode potentials greater than 1.6 V, the adsorption free energies are all going downhill for oxygen evolution and that therefore high rates can be expected. Figure 8.9 shows this decreasing free energy for the curve labeled 1.6 V. Figure 8.10 gives a more complete picture; it shows current densities as functions of electrode potential for both anodic and

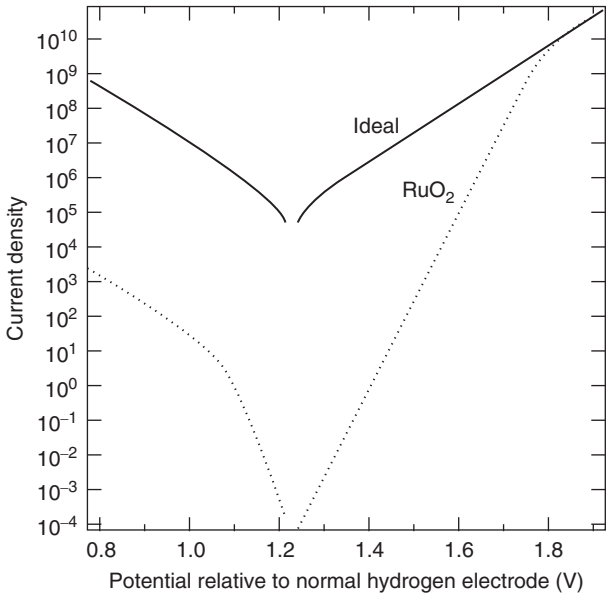

Figure 8.10 Calculated current–potential curves for oxygen reduction and evolution on a Tafel plot. The values for RuO_2 use equilibrium constants slightly modified from those in Ref. [22] (to make the open-circuit potential agree with that in Table 2.2). The ideal system uses unity values for K_1, K_2, K_3, and K_4, thereby giving a fractional coverage of 0.25 for each of the four surface species. This figure is very similar to Figure 8.7, but with the axes rotated by 90°.

cathodic reactions. It also shows that the anodic rate reaches the ideal curve at a potential of about 1.8 V and follows the ideal curve at higher potentials. These curves might be said to be in "arbitrary units;" increase of all the rate constants (k_{a1}, k_{a2}, k_{a3}, and k_{a4}) by an order of magnitude increases all the current densities by the same factor, including those on the ideal curve. For these simulations, the rate constants k_{al} are all given the same value. (The graph changes substantially if the cathodic rate constants k_{cl} are made the same instead of the anodic rate constants. The ideal rate is no longer reached at 1.8 V.) Changing the ratios would change the shape of the curves, and the curve with all the equilibrium constants equal to 1 would no longer be ideal because the four reactions would no longer be equally difficult and the surface coverages would no longer all equal 0.25 away from the open-circuit potential.

This example encapsulates a lesson in catalysis. The better catalysts are those that have free energies of adsorption of intermediates that lie on the path from desired reactant to desired product. Where these energies lie depends on the characteristics of the material. (This is embodied somewhat in Figure 8.8 for the hydrogen electrode, where each catalytic metal shown in Figure 8.6 can be imagined to yield parameters for the three reactions, the Tafel, the Volmer, and the Heyrovský reactions and therefore define a point or dot in Figure 8.8. Reactions which are equilibrated, those which are absent, and those which are rate limiting are defined by the positions of these points in Figure 8.8 and are labeled by the mechanism types.)

The oxygen electrode is discussed extensively in Section 18.5 in connection with an important application, cathodic protection of pipelines and other steel structures.

8.6 METHODS OF MEASUREMENT

One wants to determine the composition and overpotential dependence of the current density in electrode kinetics, that is, to find how f in equation 8.5 depends on c_i and η_s. The electrochemist is interested in elucidating the mechanism of the electrode reaction. The electrochemical engineer is interested in predicting the behavior of practical electrochemical systems. This means that the electrochemist can work with high concentrations of supporting electrolyte on the reproducible surface of liquid mercury in highly purified solutions, whereas the electrochemical engineer needs values of the current density for electrode surfaces and solution compositions (including impurities) that are likely to be encountered.

The electrochemist also wants to study increasingly fast reactions (larger exchange current densities), which becomes increasingly more difficult due to the ohmic potential drop and the concentration variations near the electrode surface. On the other hand, from the point of view of analyzing the overall system behavior, we can assume that the kinetics become unimportant as the electrode reaction becomes too fast to measure conveniently.

For relatively slow reactions, the function f in equation 8.5 can be measured directly under steady conditions by varying the electrode potential and the composition adjacent to the electrode. For faster reactions, there is a preference to use stirred solutions with known hydrodynamic characteristics or to use transient methods. The known hydrodynamic conditions allow us to calculate the composition at the electrode surface, where it may be significantly different from the bulk solution composition (see Sections 17.2, 17.8, and 17.9).

Perhaps the simplest transient procedure is to interrupt the current after a steady condition at the interface has been developed. This may occur before the concentrations have changed appreciably from their initial values, in which case the convection is unimportant. Interrupter methods are useful for deposition and dissolution reactions because they allow the character of the surface to be more carefully controlled, since a smaller charge need be passed.

Interruption of the current is also supposed to eliminate the ohmic potential drop from the measurement, while the surface overpotential is maintained for a while by the charge in the double-layer capacitor. Systems used for interruption (and other transient methods) should have a uniform primary current distribution over the electrode of interest (see Section 18.2), since otherwise the current density in the solution may not be zero everywhere after interruption of the current to the electrode.[25–27]

An ideal geometry in this respect is the sphere, provided that the means of support is constructed so that it does not interfere with the current distribution. Mattsson and Bockris[5] used such a system to study the copper reaction. A growing mercury drop is another common example of this geometry and has the further advantages of a reproducible surface and known hydrodynamic conditions that further promote a uniform rate of mass transfer to the electrode (see Section 17.9).

Rotating cylinders (see Section 17.8) also provide a uniform primary current distribution and uniform, known conditions of mass transfer. With the sphere and cylinder geometries, the ohmic potential drop can be calculated easily, in case interrupter methods are not to be used or one wants a check on the potential change when the current is interrupted.

Microelectrodes in the shape of spheres or disks provide another means to reduce ohmic drop in the solution. Methods of studying electrode kinetics are reviewed in Refs. [1, 28, 29] and include a variety of possibilities among the transient procedures. Mention should be made of the use of a rotating ring–disk system to detect relatively unstable intermediates in the electrode reaction. For example, the presence of hydrogen peroxide produced in carrying out the oxygen reaction on a disk electrode (see Section 8.5) can be quantitatively determined by reacting the hydrogen peroxide back to oxygen on a concentric ring electrode mounted in the same rotating surface as the disk electrode[30, 31] (see Figure 18.22).

8.7 SIMULTANEOUS REACTIONS

We discussed a single electrode reaction, but this idealization is not always achieved. If two or more reactions can occur simultaneously, it is simplest to regard each reaction to occur independently, and the net current density is the sum of the current densities due to the several reactions.[32–35] Under these conditions, the open-circuit potential is not an equilibrium potential corresponding to any of these reactions but is a *mixed* or *corrosion* potential. At open circuit, equilibrium does not prevail; one reaction proceeds anodically and another cathodically, so that the net current density is zero. A potential positive of the equilibrium potential for a reaction will drive the reaction in the anodic direction; a more negative potential will drive the reaction in the cathodic direction. The net rates of the cathodic and anodic reactions must balance by conservation of charge. The mixed potential on a surface will therefore be determined by the kinetics of the reactions. By such a mixed potential, even traces of impurities can obscure the measurement of the equilibrium potential for the oxygen electrode (see Section 8.5).

The same thing occurs in corrosion processes. The anodic process may be dissolution of iron

$$\mathrm{Fe} \rightarrow \mathrm{Fe}^{2+} + 2\mathrm{e}^{-}, \tag{8.91}$$

and the cathodic process may be the reduction of oxygen

$$\mathrm{O}_2 + 4\mathrm{H}^{+} + 4\mathrm{e}^{-} \rightarrow 2\mathrm{H}_2\mathrm{O}, \tag{8.92}$$

the two processes being coupled so that the electrons produced in equation 8.91 are consumed in equation 8.92, leaving a zero net current for the piece of iron. Thus, the rate of corrosion may be determined by the rate of mass transfer of oxygen to the corroding surface. Corrosion in aqueous media is often an electrochemical process.

All corrosion processes do not proceed by simultaneous reactions on the same surface, however. When two dissimilar metals are in contact, an electrochemical cell can easily be established. The anodic dissolution process may occur predominantly on one metal, while the cathodic process of oxygen reduction or hydrogen evolution occurs predominantly on the other metal. In other cases—for example, pitting corrosion—the anodic and cathodic processes may occur on different parts of the same metal. Analysis of these systems requires consideration of the ohmic potential drop and concentration variations in the solution[35, 36] and cannot be confined to the electrochemical reactions at the surface.

Simultaneous reactions are also encountered when, for example, the limiting current for copper deposition is exceeded and hydrogen evolution begins. This is shown in Figures 1.12 and 1.13.

The behavior of passivating metals[35, 36] in corroding systems deserves special mention. For these metals, an increase in the severity of the corrosion environment can lead to passivation and a reduction in the corrosion rate. This can be achieved by making the metal more positive, which is the basis of anodic protection. For the iron–oxygen couple, an increase in stirring, which promotes the rate of oxygen transfer to the surface, can passivate the metal and decrease the corrosion rate.

Let us finally treat the oxygen reduction reaction, regarding equations 8.73 and 8.74 as simultaneous reactions. We shall imagine that a stagnant diffusion layer of thickness δ is adjacent to the metal, and we denote oxygen and hydrogen peroxide as species A and B, respectively. Since reaction 8.73 is inherently faster than reaction 8.74, the hydrogen peroxide produced in the first reaction can diffuse away from the surface instead of reacting in the second reaction. The material balances for oxygen and hydrogen peroxide take the form

$$-\frac{i_2}{2F} = D_A \frac{c_A^{\infty} - c_A^0}{\delta}, \tag{8.93}$$

$$\frac{i_3 - i_2}{2F} = -D_B \frac{c_B^\infty - c_B^0}{\delta}. \tag{8.94}$$

Equation 8.93 represents the rate of diffusion of oxygen to the surface, this oxygen being consumed in reaction 8.73. (Subscripts 2 and 3 denote reactions 8.73 and 8.74, respectively.) Equation 8.94 represents the rate of diffusion of hydrogen peroxide away from the surface, this being equal to the difference between the rates at which it is being produced in reaction 8.73 and consumed in reaction 8.74.

At 25°C in water, the saturation concentration of oxygen is 1.26×10^{-3} mol/liter at a partial pressure of one atmosphere (corrected for the vapor pressure of water but not for the fugacity coefficients in the gas phase), and the diffusion coefficient is 1.9×10^{-5} cm^2/s. Davis et al.,[37] among others, report the saturation concentration and the diffusion coefficient as functions of the concentration of potassium hydroxide.

In acidic or neutral media, let us assume that reactions 8.73 and 8.74 are pseudo first order in oxygen and peroxide and write

$$\frac{i_2}{2F} = k_{a2} c_B^0 \exp\left(\frac{\alpha_{a2} F}{RT} V\right) - k_{c2} c_A^0 \exp\left(-\frac{\alpha_{c2} F}{RT} V\right), \tag{8.95}$$

$$\frac{i_3}{2F} = k_{a3} \exp\left(\frac{\alpha_{a3} F}{RT} V\right) - k_{c3} c_B^0 \exp\left(-\frac{\alpha_{c3} F}{RT} V\right), \tag{8.96}$$

where the k's may now be pH dependent and where the electrode potential V is measured relative to a hydrogen electrode in the same solution (see Section 5.7).

For sufficiently negative potentials, the anodic terms in equations 8.95 and 8.96 are negligible, and this seems particularly appropriate for the relatively irreversible oxygen electrode. In addition, we take $\alpha_{c2} = \alpha_{c3} = 0.5$ and $c_B^\infty = 0$. With these approximations, equations 8.93 to 8.96 can be combined to express the overall current density as

$$-\frac{i_2 + i_3}{2F} \frac{\delta}{c_A^\infty D_A} = \frac{e^{-\phi}}{1 + e^{-\phi}} \left(1 + \frac{1}{1 + K e^{\phi}}\right), \tag{8.97}$$

where

$$\phi = \frac{\alpha_{c2} F V'}{RT}, \tag{8.98}$$

$$V' = V - \frac{RT}{\alpha_{c2} F} \ln \frac{k_{c2} \delta}{D_A}, \tag{8.99}$$

and

$$K = \frac{D_B k_{c2}}{D_A k_{c3}}. \tag{8.100}$$

Equation 8.97 is plotted in Figure 8.11.

Figure 8.11 shows limiting currents for the reduction of oxygen and hydrogen peroxide (compare Figures 1.12 and 1.13). For small values of K, the processes occur simultaneously; for large values of K, the processes become clearly distinguishable. For either very small or very large values of K, the current reaches half of its plateau value when $V = (RT/\alpha_{c2}F) \ln(k_{c2}\delta/D_A)$, thus providing a method of determining k_{c2}. This value of V is known as the *half-wave potential*.

The position of the second wave relative to the first depends on the value of K, that is, on the slowness of reaction 8.74 relative to reaction 8.73. Polarographic curves for the reduction of oxygen on mercury[38, 39] suggest that K has a value of about 3×10^7 for this system. A more exact analysis

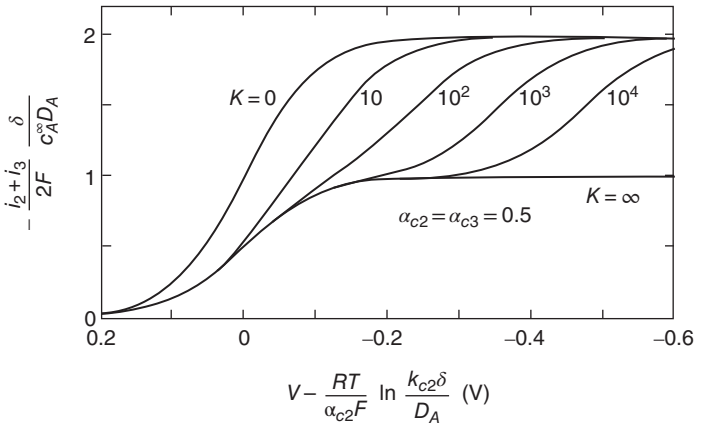

Figure 8.11 Theoretical polarographic curves for the reduction of oxygen, with neglect of the anodic reaction terms. In this, $K = D_B k_{c2}/D_A k_{c3}$.

would include the possibility of α_{c2} and α_{c3} being different from each other and different from 0.5. Also, the anodic term in equation 8.95 should perhaps be included in the analysis.

One can contrast the behavior of cupric ion reduction to oxygen reduction. Since reaction 8.11 is faster than reaction 8.12, cuprous ion reduction should occur simultaneously with reduction of cupric ions to cuprous ions, and only one polarographic wave would be distinguishable. On the other hand, reaction 8.73 is faster than reaction 8.74, and two waves are observed for oxygen reduction.

PROBLEMS

8.1 **(a)** Ignoring the fact that cuprous ions can diffuse away from the electrode, derive the following expression for the dependence of the current density on the surface overpotential for the copper reaction:

$$i = \frac{i_0\left\{\exp\left[\frac{(2-\beta_3)F}{RT}\eta_s\right] - \exp\left(-\frac{\beta_3 F}{RT}\eta_s\right)\right\}}{1 + \frac{k_{a3}}{k_{c2}}\left[\frac{k_{c3}k_{c2}}{k_{a3}k_{a2}}c_{Cu^{2+}}\exp\left(\frac{2F}{RT}\eta_s\right)\right]^{(1+\beta_2-\beta_3)/2}},$$

where η_s is given by equation 8.21, U by equation 8.36, and i_0 by equation 8.37. This equation has been written so as to be directly comparable to equation 8.6.

(b) Show that this expression reduces to equation 8.6 for large cathodic overpotentials. Show that the Tafel slope for large anodic overpotentials is $2.303RT/(1-\beta_2)F$ (see equation 1.10). Reaction 8.11 appears to be rate controlling for large anodic overpotentials, and reaction 8.12 for large cathodic overpotentials. Rationalize this in physical terms.

(c) Show that this expression reduces to equation 8.6 when k_{c2} and $k_{a2}/c_{Cu^{2+}}$ are much larger than k_{c3} and k_{a3}.

8.2 Develop the analog of equation 8.24 with consideration of the Frumkin correction,

$$i = i_0 \exp\left[\frac{F\Phi_2}{RT}\left(\beta n - \sum_i z_i q_i\right)\right]\left\{\exp\left[\frac{(1-\beta)nF}{RT}\eta_s\right] - \exp\left(-\frac{\beta nF}{RT}\eta_s\right)\right\},$$

where the composition dependence of i_0 is given by equation 8.30.

8.3 The standard electrode potential for reaction 8.73 is 0.682 V and that for reaction 8.74 is 1.77 V. Derive the second of these values from the first and entry 15 of Table 2.2. Show that the equilibrium concentration of hydrogen peroxide should be about 3.2×10^{-19} mol/liter for an oxygen partial pressure of 1 bar.

8.4 An electrode exhibiting active–passive kinetics, or passivation, is in a circuit that can maintain its potential at a given value relative to a reference electrode placed near it but at such a distance that there remains a significant resistance between the passivating electrode and the reference electrode.

(a) Sketch on a linear scale the current density of the working electrode versus the potential relative to an imaginary reference electrode adjacent to its surface.

(b) For a fixed value of $V - V_{\text{ref}}$, develop a graphical method of determining the current density at the working electrode, with due allowance for the resistance between the two actual electrodes.

(c) Discuss the possibility of multiple solutions for the current density. What conditions of resistance, potential, and shape of the current–potential relation ensure a single solution, and what conditions permit multiple solutions? Which of these solutions are stable and which unstable? If one cyclically increases and decreases $V - V_{\text{ref}}$ over a large range, what hysteresis will result in the current density?

8.5 An aqueous solution contains 10^{-3} *M* $CuSO_4$ and 1.5 *M* H_2SO_4 and is saturated with H_2 at a partial pressure of 1 bar. A copper disk is rotated in this solution at about 400 rpm, so that the mass-transfer coefficient for copper deposition is 3×10^{-3} cm/s. Copper deposition is interfered with, to some extent, by hydrogen evolution, which, however, does not significantly modify the H^+ concentration near the surface. Calculate and plot the *total* current density versus the electrode potential $V - \Phi_0$ (measured by means of an adjacent reference electrode of a *given* kind, copper in a 0.1 *M* cupric ion solution). The exchange-current density for Cu is 1 mA/cm^2 at a concentration of 0.1 *M*; the transfer coefficients can be taken to be 0.5 and 1.5 in the cathodic and anodic directions, respectively; and the concentration dependence of i_0 is given by $\gamma = 0.75$ (so that the cathodic reaction is first order in cupric concentration at a fixed value of $V - \Phi_0$). The exchange current density for hydrogen evolution is 10^{-7} A/cm^2, with anodic and cathodic transfer coefficients of 0.5.

8.6 Alternating-current impedance techniques are promising as a tool to investigate electrode processes because, by varying the frequency, one can obtain a lot of information and if the amplitude of the applied signal is kept small, the analysis should be tractable because the system should show a linear response. We hope to develop a comprehensive treatment that includes migration, convection, and diffusion in the diffusion layer on a rotating disk and arbitrary numbers of homogeneous and heterogeneous reactions involving an arbitrary number of species. This problem here should focus on the surface coverage and the double-layer capacity, on the assumption that the diffusion layer has already been treated.

It is felt that adsorbed species should be treated in terms of surface excesses Γ_i, and that adsorbed species must compete for a limited number of surface sites that number $\Gamma_{\max}$ (in units of mol/cm^2). The *coverage* of a species then is taken to be $\Gamma_i/\Gamma_{\max}$. It is felt that the double-layer capacity is merely a manifestation of adsorption of these charged species. Develop a model for surface adsorption and electrochemical reaction. Ignore the diffuse layer or regard the boundary of your model to be the outer Helmholtz plane—with the adsorbed species occupying the inner Helmholtz plane. Three electric potentials are involved, Φ_m, Φ_1, and Φ_2, corresponding to the metal, the adsorbed layer, and the outer Helmholtz plane, respectively.

(a) Develop a material balance for the species in the adsorbed layer. The equation in Problem 8.5 might be a helpful starting point.

(b) Put down plausible kinetic equations for adsorption and/or electrochemical reaction. For concreteness, you should deal with the following mechanism for zinc deposition or dissolution:

$$\mathrm{Zn^{2+}}(2) \rightarrow \mathrm{Zn^{2+}}(1),$$
$$\mathrm{Zn^{2+}}(1) + \mathrm{e^-}(m) \rightarrow \mathrm{Zn^{+}}(1),$$
$$\mathrm{Zn^{+}}(1) + \mathrm{e^-}(m) \rightarrow \mathrm{Zn}(1),$$
$$\mathrm{Zn}(1) \rightarrow \mathrm{Zn}(m),$$

where 1, 2, or m in parentheses indicates the position of the entity (in the inner Helmholtz plane, the outer Helmholtz plane, or the metal).

8.7 Assume that the kinetics of the electrochemical reduction of ferricyanide ion to ferrocyanide ion is rapid. Develop an equation for the current density as a function of potential (or vice versa). The potential is that of the working electrode relative to a ferricyanide–ferrocyanide reference electrode placed just outside the *diffusion* layer (not the diffuse part of the double layer). You can neglect the ohmic potential drop, assume an excess of supporting electrolyte, and assume that there is a stagnant diffusion layer of thickness δ adjacent to the working electrode.

8.8 Analyze the kinetics of the reaction sequence in chloride medium:

$$\mathrm{Cu} \rightarrow \mathrm{Cu^+} + \mathrm{e^-} \quad \text{(slow)},$$
$$\mathrm{Cu^+} + 2\mathrm{Cl^-} \rightarrow \mathrm{CuCl_2^-} \quad \text{(fast)}.$$

Compare with the apparent reaction orders obtained when the overall reaction

$$\mathrm{Cu} + 2\mathrm{Cl^-} \rightarrow \mathrm{CuCl_2^-} + \mathrm{e^-}$$

is analyzed as though it were an elementary step. Obtain expressions for the composition dependence of the exchange current density in the two cases.

8.9 Consider the evolution of bromine gas or liquid at a metal anode, occurring via the elementary steps:

$$\mathrm{Br^-} + \mathrm{M} \rightleftharpoons \mathrm{MBr} + \mathrm{e^-}.$$
$$2\mathrm{MBr} \rightarrow 2\mathrm{M} + \mathrm{Br_2}.$$

Assuming that the first reaction is rapid and pseudo-equilibrated and the second is irreversible and rate determining, derive an expression for the current density as a function of electrode potential. Provide expressions for the exchange-current density and the standard electrode potential.

8.10 Develop an overall rate expression for the hydrogen reaction proceeding according to the following mechanism. The Tafel reaction is equilibrated:

$$\mathrm{H_2} \rightleftharpoons 2\mathrm{H_{ad}},$$

and the Heyrovský reaction is rate determining:

$$H_2 \rightarrow H^+ + e^- + H_{ad} \quad \text{(rate-determining step)}.$$

In particular, show the exponential dependence on the surface overpotential η_s and discuss how the exchange-current density might be defined.

8.11 Investigate the behavior of the adsorption equilibrium constants in the latter part of Section 8.5.

(a) Show that, at equilibrium (and at $p_{O_2} = 1$ bar, $c_{H^+} = 1$ mol/L) $k_{al}/k_{cl} \exp(FU/RT) = \Gamma_{l+1}/\Gamma_l = K_l \exp(FU/RT)$, where subscripts 1, 2, 3, and 4 on Γ correspond to *, *OH, *O, and *OOH, respectively. This implies that the equilibrium constants depend on the choice of the reference electrode, as do the rate constants. If the reference electrode is chosen to be of the same kind as the working electrode, the exponential factor will be unity. (For the oxygen electrode, a reference electrode of the same kind is a poor choice in practice because the oxygen electrode has such a low exchange current density.)

(b) Show that $K_1K_2K_3K_4 = 1$ at the equilibrium potential for the oxygen reaction. (The equilibrium constants, defined as $K_l = k_{al}/k_{cl}$, are independent of electrode potential. Do they depend on the choice of the reference electrode?)

(c) Show that at the equilibrium potential the surface coverages are $\theta_1 = 1/(1 + K_1 + K_1K_2 + K_1K_2K_3)$ and $\theta_2 = \theta_1K_1$, $\theta_3 = \theta_2K_2$, $\theta_4 = \theta_3K_3$.

(d) Calculate and report numerical values for the coverage of each surface species in Table 8.1 for RuO_2, IrO_2, and TiO_2. Comment briefly on the results.

(e) Identify candidates for a rate-determining step for both oxidation and reduction for the three oxides. Explain your reasoning.

8.12 For the RuO_2 material, $K_1 = \exp[(0.08 - 0)F/RT]$. Similarly, $K_4 = \exp[(0 - 0.59)F/RT]$, where the numerical values come from Table 8.1. What are the units of K_1 and K_4? Take into account the defining equations 8.80 and 8.83 and the fact that the concentration of protons and the partial pressure of oxygen have units. Similar problems were encountered in Chapter 2, where units could be hidden in secondary reference quantities and something that looks like the exponential of a dimensionless quantity can end up having units. How does this affect the kinetic expressions when applied to a system not at pH = 0 and not at a partial pressure of oxygen of 1? (Answer to the last part: Use the numerical value calculated and let the kinetic equations take care of the dependence on concentration and pressure.)

8.13 For Table 8.1 or Figure 8.9, the numbers of atoms must be the same for products and reactants. In this particular case, one starts with two water molecules and one empty catalytic site. Write down the species and their number for each entry in one column of the table. The same specifics apply to each abscissa species shown in Figure 8.9; these are not free energies of just one adsorbed species.

8.14 Look at the data in Table 8.1 for IrO_2. Are there high- or low-energy intermediates? Calculate θ_i values for the four species at the open-circuit potential. Do you expect IrO_2 or RuO_2 to be the better catalyst for the oxygen electrode?

8.15 Outline a program for treating basic and intermediate solutions by adding to equations 8.76 to 8.79 four more equations with OH^- ions as a reactant instead of H^+ ions as a product. The advantage would be that four more rate constants can be added, thereby permitting treatment of data at various pH, even though the surface coverage (perhaps an oxide) might change.

(a) Write down the four additional kinetic equations. What assumption are you likely to make for the symmetry factors β_l?

(b) What modifications should be made for the site balances?

(c) The surface species are presumed to remain the same. How many additional equilibrium constants are introduced? Discuss in detail how you would obtain these equilibrium constants from those given (as in Table 8.1) for the acid system.

(d) An elaborate experimental program is funded to treat the catalysis of the oxygen electrode at various values of the pH. Suggest a procedure for obtaining the necessary data and treating it so as to be able to predict kinetic behavior in the intermediate pH range. Confine yourself to only one catalyst. (Answer: Determine rate constants k_{al} for acid media from data in acid at pH = 0. Determine rate constants k_{al} for the additional rate equations in a medium at pH = 14. Argue that these extreme pH values can be treated with minimal interaction because the concentration of OH^- ions is very small in the acid solutions and that of H^+ ions is very small in the basic solution (pH = 14).)

8.16 Suppose that we have been treating the RuO_2 system, but that there is reason to believe that the rate constant k_{a3} of the third reaction in the sequence is several orders of magnitude lower than those of the other rate constants. How would this affect the surface concentrations of the several surface species for both anodic and cathodic reactions. You can speak of this as a potential bottleneck. Would any of the four reactions become a candidate for a rate-limiting step? Again, consider both directions, anodic and cathodic.

NOTATION

A	electrode area, cm^2
c_i	concentration of species i, mol/cm^3
C	double-layer capacity, F/cm^2
D_i	diffusion coefficient of species i, cm^2/s
e^-	symbol for the electron
E_a, E_c	activation energies in anodic and cathodic directions, J/mol
f	function in expression of electrode kinetics
F	Faraday's constant, 96,487 C/mol
i_n	current density, A/cm^2
i_0	exchange current density, A/cm^2
k_a, k_c	rate constants in anodic and cathodic directions
M_i	symbol for the chemical formula of species i
n	number of electrons transferred in electrode reaction
p_i	reaction order for anodic reactants
q	surface charge density on the metal side of the double layer, C/cm^2
q_i	reaction order for cathodic reactants
q_2	surface charge density in the diffuse layer, C/cm^2
r	reaction rate, $mol/cm^2 \cdot s$
R	universal gas constant, 8.3143 J/mol·K
s_i	stoichiometric coefficient of species i in electrode reaction
t	time, s
T	absolute temperature, K
U	open-circuit potential, V
V	electrode potential, V
z_i	charge number of species i
α_a, α_c	transfer coefficients

β	symmetry factor
γ, δ	exponents in composition dependence of the exchange current density
δ	thickness of stagnant diffusion layer, cm
η_s	surface overpotential, V
μ_i	electrochemical potential of species *i*, J/mol
Φ	electric potential, V
Φ_2	potential at inner limit of diffuse layer, V

REFERENCES

1. Klaus J. Vetter, *Elektrochemische Kinetik* (Berlin: Springer, 1961) [English edition: *Electrochemical Kinetics* (New York: Academic, 1967)].
2. Paul Delahay, *Double Layer and Electrode Kinetics* (New York: Interscience, 1965).
3. John O'M. Bockris and Amulya K. N. Reddy, *Modern Electrochemistry*, Vol. *2* (New York: Plenum, 1970).
4. N. Tanaku and R. Tamamushi, "Kinetic Parameters of Electrode Reactions," *Electrochimica Acta*, *9* (1964), 963–989.
5. E. Mattsson and J. O'M. Bockris, "Galvanostatic Studies of the Kinetics of Deposition and Dissolution in the Copper + Copper Sulphate System," *Transactions of the Faraday Society*, *55* (1959), 1586–1601.
6. Michael J. Weaver, "Redox Reactions at Metal-Solution Interfaces," in R. G. Compton, ed., *Comprehensive Chemical Kinetics*, Vol. *27*, Electrode Kinetics: Reactions (Amsterdam: Elsevier, 1987), pp. 1–60.
7. Peter Willem Appel, *Electrochemical Systems: Impedance of a Rotating Disk and Mass Transfer in Packed Beds,* Dissertation, University of California, Berkeley, 1976.
8. Paul Delahay, "Double Layer Studies," *Journal of the Electrochemical Society*, *113* (1966), 967–971.
9. Karel Holub, Gino Tessari, and Paul Delahay, "Electrode Impedance without *a Priori* Separation of Double-Layer Charging and Faradaic Process," *Journal of Physical Chemistry*, *71* (1967), 2612–2618.
10. W. D. Weir, "*A Posteriori* Separation of Faradaic and Double-Layer Charging Processes: Analysis of the Transient Equivalent Network for Electrode Reactions," *Journal of Physical Chemistry*, *71* (1967), 3357–3359.
11. Fred C. Anson. "Electrochemistry," *Annual Review of Physical Chemistry*, *19* (1968), 83–110.
12. A. Frumkin, "Wasserstoffüberspannung und Struktur der Doppelschicht," *Zeitschrift für physikalische Chemie 164* (1933), 121–133.
13. V. Levich, "Teoriya neravnovesnogo dvoinogo sloya," *Doklady Akademii Nauk SSSR*, *67* (1949), 309–312.
14. V. G. Levich, "K teorii neravnovesnogo dvoinogo sloya," *Doklady Akademii Nauk SSSR*, *124* (1959), 869–872.
15. John Newman, "The Polarized Diffuse Double Layer," *Transactions of the Faraday Society*, *61* (1965), 2229–2237.
16. Roger Parsons, "The Structure of the Electrical Double Layer and its Influence on the Rates of Electrode Reactions," *Advances in Electrochemistry and Electrochemical Engineering*, *1* (1961), 1–64.
17. J. O'M. Bockris and A. K. M. Shamshul Huq. "The mechanism of the electrolytic evolution of oxygen on platinum," *Proceedings of the Royal Society*, *A237* (1956), 277–296.
18. Klaus J Vetter. *Electrochemical Kinetics* (New York: Academic, 1967), pp. 615–644.
19. J. P. Hoare, "The Oxygen Electrode on Noble Metals," *Advances in Electrochemistry and Electrochemical Engineering*, *6* (1967), 201–288.
20. James P Hoare, *The Electrochemistry of Oxygen* (New York: Interscience, 1968).
21. A Damjanovic, "Mechanistic Analysis of Oxygen Electrode Reactions," in J. O'M. Bockris and B. E. Conway, eds., *Modem Aspects of Electrochemistry*, No. *5* (New York: Plenum, 1969), pp. 369–483.
22. J. Rossmeisl, Z.-W. Qu, H. Zhu, G.-J. Kroes, and J. K. Nørskov, "Electrolysis of water on oxide surfaces," *Journal of Electroanalytical Chemistry*, *607* (2007), 83–89.

23. J. Rossmeisl, A. Logadottir, and J. K. Nørskov,"Electrolysis of water on (oxidized) metal surfaces," *Chemical Physics*, *319* (2005), 178–184.
24. A. T. Marshall, S. Sunde, M. Tsypkin, and R. Tunold, "Performance of a PEM water electrolysis cell using Ir_x Ru_y Ta_z O_2 electrocatalysts for the oxygen evolution electrode," *International Journal of Hydrogen Energy*, *32* (2007), 2320–2324.
25. John Newman, "Ohmic Potential Measured by Interrupter Techniques," *Journal of the Electrochemical Society*, *117* (1970), 507–508.
26. Kemal Nişancioğlu and John Newman, "The Transient Response of a Disk Electrode," *Journal of the Electrochemical Society*, *120* (1973), 1339–1346.
27. Kemal Nişancioğlu and J. Newman, "The Short-Time Response of a Disk Electrode," *Journal of the Electrochemical Society*, *121* (1974), 523–527.
28. John E. B. Randles, "Concentration Polarization and the Study of Electrode Reaction Kinetics," in P. Zuman, ed., *Progress in Polarography*, Vol. *I* (New York: Interscience, 1962), pp. 123–144.
29. Ernest Yeager and Jaroslav Kuta, "Techniques for the Study of Electrode Processes," in Henry Eyring, ed., *Physical Chemistry; An Advanced Treatise, Vol. IXA, Electrochemistry* (New York: Academic, 1970), pp. 345–461.
30. A. N. Frumkin and L. I. Nekrasov, "O kol'tsevom diskovom elektrode," *Doklady Akademii Nauk SSSR*, *126* (1959), 115–118.
31. Yu. B. Ivanov and V. G. Levich, "Izuchenie nestoĭkikh promezhutochnykh produktov elektrodnykh reaktsiĭ s pomoshch'yu vrashchayushchegosya diskovogo elektroda," *Doklady Akademii Nauk SSSR*, *126* (1959), 1029–1032.
32. Carl Wagner and Wilhelm Traud, "Über die Deutung von Korrosionvorgängen durch Überlagerung von elektrochemischen Teilvorgängen und über die Potentialbildung an Mischelektroden," *Zeitschrift für Electrochemie*, *44* (1938), 391–402.
33. M. Stern and A. L. Geary, "Electrochemical Polarization I. A Theoretical Analysis of the Shape of Polarization Curves," *Journal of the Electrochemical Society*, *104* (1957), 56–63.
34. Klaus J Vetter. *Electrochemical Kinetics* (New York: Academic, 1967), pp. 732–747.
35. Mars G. Fontana and Norbert D. Greene, *Corrosion Engineering* (New York: McGraw-Hill, 1967).
36. John Newman, "Mass Transport and Potential Distribution in the Geometries of Localized Corrosion," in Hugh S. Isaacs, ed., *Advances in Localized Corrosion* (Houston: National Association of Corrosion Engineers, 1990), pp. 227–234.
37. R. E. Davis, G. L. Horvath, and C. W. Tobias, "The Solubility and Diffusion Coefficient of Oxygen in Potassium Hydroxide Solutions," *Electrochimica Acta*, *12* (1967), 287–297.
38. I. M. Kolthoff and C. S. Miller, "The Reduction of Oxygen at the Dropping Mercury Electrode," *Journal of the American Chemical Society*, *63* (1941), 1013–1017.
39. R. Brdička and K. Wiesner, "Polarographie Determination of the Rate of the Reaction Between Ferrohem and Hydrogen Peroxide," *Collection of Czechoslovak Chemical Communications*, *12* (1947), 39–63.

CHAPTER 9

ELECTROKINETIC PHENOMENA

This chapter deals with the effects observed when the diffuse double layer and an external electric field interact in relation to a hydrodynamic flow. A tangential electric field can produce a small change in velocity over the very small thickness of the double layer, and a shear stress or velocity gradient at the surface can produce electrical effects.

This subject is important in the study of colloids. It also yields some information on the structure of the electrical double layer at a solid–solution interface, which cannot be studied with the aid of the interfacial tension. The treatment here is incomplete, particularly with regard to experimental results for specific interfaces, and the reader is referred to the literature.[1–3]

9.1 DISCONTINUOUS VELOCITY AT AN INTERFACE

Suppose that we have a planar, solid dielectric in contact with an electrolytic solution and that there is a tangential electric field (see Figure 9.1). A double layer can exist at the surface due to the specific adsorption of ions, and this means that there will be a counterbalancing charge in a diffuse layer. The structure of this diffuse layer is discussed in Section 7.4. The tangential electric field exerts a force on the charge in the diffuse layer. This layer, being part of the solution, is mobile and can be expected to move relative to the solid as a result of the electric field.

The tangential electric field is taken to be uniform throughout the dielectric and the solution. The structure of the double layer will then not be disturbed from that treated in Section 7.4. The resulting motion of the solution will be described by the Navier–Stokes equation 15.10 with the electrical force included (see equation 15.5). This equation is simplified by the fact that the velocity is only in the x direction and depends only on the distance y from the dielectric. In the steady state and with no significant gradient of the dynamic pressure, we have (see equation B.9 in Appendix B)

$$\mu \frac{\partial^2 v_x}{\partial y^2} + \rho_e E_x = 0. \tag{9.1}$$

Electrochemical Systems, Fourth Edition. John Newman and Nitash P. Balsara.

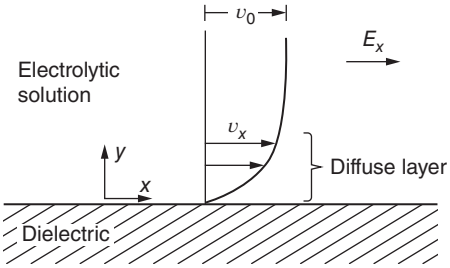

Figure 9.1 Velocity produced by a tangential electric field in the diffuse charge layer. A positive charge in the diffuse layer will produce a negative zeta potential and will result in a positive value of v_0 if E_x is also positive.

Substitution of Poisson's equation 3.8 gives

$$\mu \frac{\partial^2 v_x}{\partial y^2} - \epsilon \frac{\partial^2 \Phi}{\partial y^2} E_x = 0, \tag{9.2}$$

and integration gives

$$\mu \frac{\partial v_x}{\partial y} = \epsilon \frac{\partial \Phi}{\partial y} E_x, \tag{9.3}$$

the integration constant being evaluated from the fact that both $\partial v_x/\partial y$ and $\partial \Phi/\partial y$ are zero outside the diffuse layer. A second integration gives

$$\mu(v_x - v_0) = \epsilon(\Phi - \Phi_\infty)E_x, \tag{9.4}$$

where v_0 is the value of the velocity outside the diffuse layer.

If we take ζ to be the value of $\Phi - \Phi_\infty$ at the plane where $v_x = 0$, equation 9.4 yields

$$v_0 = -\frac{\epsilon \zeta E_x}{\mu}. \tag{9.5}$$

The *zeta potential* ζ can be roughly associated with the potential Φ_2 at the inner limit of the diffuse layer, since this is the plane where we should expect the velocity v_x to become zero. However, we are unlikely to have an independent determination of Φ_2 at a solid–solution interface.

The zeta potential is a property of the dielectric–solution interface and is due to the amount of specific adsorption at that interface. Because μ and ϵ are unlikely to be constant through the diffuse layer, ζ should more be regarded as a macroscopic variable relating the velocity v_0 to the tangential electric field E_x, and its relationship to the potential Φ_2 thereby becomes more remote.

Because of the thinness of the diffuse layer compared to macroscopic dimensions, equation 9.5 can be regarded as a relation between the local slip velocity v_0 and the local tangential field E_t, even though the dielectric–solution interface is not planar, the tangential electric field is not uniform, and the gradient of the dynamic pressure is not zero. We shall attempt to clarify the meaning of this approximation in the context of a straight capillary through a dielectric; and this approximation will be applied to spherical, colloidal particles in the treatment of electrophoretic velocities and sedimentation potentials.

Small metal particles behave much like small dielectric particles if the metal behaves like an ideally polarizable electrode (see Section 7.1). Then, the electric field is essentially zero within the metal, and

the local polarization varies because of the tangential electric field. As long as the polarization does not become so great as to violate the condition of ideal polarizability, equation 9.5 can be applied to relate the local slip velocity v_0 to the local tangential electric field E_t. With metal particles, one has the possibility to vary the charge density on the metal side of the interface.

Levich[4] preferred to replace the zeta potential by the charge density q_2 in the diffuse layer. With the Debye–Hückel approximation we can relate ζ and q_2 by

$$q_2 = -\frac{\epsilon\zeta}{\lambda}, \tag{9.6}$$

(see Problem 7.6) so that equation 9.5 becomes

$$v_0 = \frac{q_2 \lambda E_x}{\mu}. \tag{9.7}$$

A zeta potential can be on the order of 0.1 V. For a relative dielectric constant ϵ/ϵ_0 of 78.3, a viscosity μ of 0.89 mPa s, and an electric field of 10 V/cm, equation 9.5 yields

$$v_0 = -7.8 \times 10^{-3} \text{ cm/s}. \tag{9.8}$$

This is a relatively small value and can be neglected in many applications.

9.2 ELECTRO-OSMOSIS AND THE STREAMING POTENTIAL

Let us consider a capillary of radius r_0 in a dielectric material. The capillary is filled with an electrolytic solution, and there is a uniform electric field in the direction z along the axis of the capillary. However, the electric field is not zero in the radial direction. Instead, Poisson's equation is obeyed in the form

$$\frac{1}{r}\frac{\partial}{\partial r}\left(r\frac{\partial \Phi}{\partial r}\right) = -\frac{\rho_e}{\epsilon}. \tag{9.9}$$

The term $\partial^2\Phi/\partial z^2$ is zero since the axial electric field E_z is constant. The momentum equation (see Chapter 15) can be written

$$-\frac{dp}{dz} + \frac{\mu}{r}\frac{\partial}{\partial r}\left(r\frac{\partial v_z}{\partial r}\right) + E_z\rho_e = 0, \tag{9.10}$$

the electric force $E_z\rho_e$ appearing in the force balance.

Substitution of equation 9.10 into equation 9.9 and integration twice with respect to r, subject to the conditions that $v_z = 0$ at $r = r_0$ and v_z and Φ are finite at $r = 0$, give

$$v_z = E_z\frac{\epsilon}{\mu}(\Phi - \Phi_{r=r_0}) - \frac{dp}{dz}\frac{r_0^2 - r^2}{4\mu}. \tag{9.11}$$

Hence, the volumetric flow rate Q can be expressed as

$$\begin{aligned}\frac{Q}{2\pi} &= \int_0^{r_0} r v_z dr = E_z\frac{\epsilon}{\mu}\int_0^{r_0} r(\Phi - \Phi_{r=r_0})dr - \frac{dp}{dz}\int_0^{r_0} r\frac{r_0^2 - r^2}{4\mu}dr \\ &= -E_z\frac{\epsilon}{2\mu}\int_0^{r_0} r^2\frac{\partial\Phi}{\partial r}dr - \frac{r_0^4}{16\mu}\frac{dp}{dz}.\end{aligned} \tag{9.12}$$

Now, let us turn our attention to the electric current. We express the flux density of a species as (see equation 11.1)

$$N_{iz} = z_i u_i F c_i E_z + c_i v_z. \tag{9.13}$$

The concentrations do not vary in the z direction for a given value of r; hence, there is no diffusion term in equation 9.13. The current density in the solution becomes

$$i_z = F\sum_i z_i N_{iz} = F^2 E_z \sum_i z_i^2 u_i c_i + F v_z \sum_i z_i c_i = \kappa E_z + v_z \rho_e, \tag{9.14}$$

where

$$\kappa = F^2 \sum_i z_i^2 u_i c_i \tag{9.15}$$

is the conductivity (see equation 11.7) and

$$\rho_e = F\sum_i z_i c_i \tag{9.16}$$

is the charge density. The total current I can be expressed as

$$\frac{I}{2\pi} = \int_0^{r_0} r i_z dr = E_z \int_0^{r_0} r\kappa\, dr + \int_0^{r_0} r v_z \rho_e dr. \tag{9.17}$$

Now substitute equation 9.11 for v_z and equation 9.9 for ρ_e.

$$\begin{aligned}\frac{I}{2\pi} &= E_z \int_0^{r_0} r\kappa\, dr - \frac{E_z \epsilon^2}{\mu}\int_0^{r_0} (\Phi - \Phi_{r=r_0})\frac{\partial}{\partial r}\left(r\frac{\partial \Phi}{\partial r}\right) dr \\ &\quad + \epsilon \frac{dp}{dz}\int_0^{r_0} \frac{r_0^2 - r^2}{4\mu}\frac{\partial}{\partial r}\left(r\frac{\partial \Phi}{\partial r}\right) dr \\ &= E_z \int_0^{r_0} r\kappa\, dr + E_z \frac{\epsilon^2}{\mu}\int_0^{r_0} r\left(\frac{\partial \Phi}{\partial r}\right)^2 dr + \frac{dp}{dz}\frac{\epsilon}{2\mu}\int_0^{r_0} r^2 \frac{\partial \Phi}{\partial r} dr.\end{aligned} \tag{9.18}$$

Notice that the coefficient of E_z in equation 9.12 is identical to the coefficient of $-dp/dz$ in equation 9.18. This is an example of the Onsager reciprocal relation.

To obtain explicit expressions for the potential distribution within the capillary, let us use the Debye–Hückel approximation 4.7:

$$c_i = c_i^0 e^{-z_i F\phi/RT} \approx c_i^0\left(1 - \frac{z_i F\phi}{RT}\right), \tag{9.19}$$

where $\phi = \Phi - \Phi_{r=0}$ and c_i^0 is the concentration of species i on the center line of the capillary.

Now equation 9.9 becomes

$$\frac{1}{r}\frac{\partial}{\partial r}\left(r\frac{\partial \phi}{\partial r}\right) = -\frac{F}{\epsilon}\sum_i z_i c_i^0 + \frac{F}{\epsilon}\sum_i z_i^2 c_i^0 \frac{F\phi}{RT} \tag{9.20}$$

or

$$\frac{1}{x}\frac{d}{dx}\left(x\frac{d\psi}{dx}\right) = -\Gamma + \psi, \tag{9.21}$$

where

$$\psi = \frac{F\Phi}{RT}, \quad x = \frac{r}{\lambda}, \quad \Gamma = \frac{\sum_i z_i c_i^0}{\sum_i z_i^2 c_i^0}, \tag{9.22}$$

and

$$\lambda = \left(\frac{\epsilon RT}{F^2 \sum_i z_i^2 c_i^0} \right)^{1/2} \tag{9.23}$$

is the Debye length.

The solution to equation 9.21 is

$$\psi = \Gamma - \Gamma I_0(x), \tag{9.24}$$

where I_0 is the modified Bessel function of the first kind, of order zero. The coefficient of I_0 is evaluated from the condition that $\psi = 0$ at $x = 0$. The other solution, $K_0(x)$, of the homogeneous form of equation 9.21 is unbounded at $x = 0$ and must be discarded.

The approximate expression for the charge density now is

$$\rho_e = F(\Gamma - \psi) \sum_i z_i^2 c_i^0 = \Gamma I_0(x) F \sum_i z_i^2 c_i^0 = \frac{\Gamma I_0(x) \epsilon RT}{F\lambda^2}. \tag{9.25}$$

Note that the charge density on the center line of the capillary is not exactly zero. We should now like to relate the constant Γ to the surface charge density q_2 per unit of circumferential area of the capillary:

$$\int_0^{r_0} 2\pi r \rho_e dr = 2\pi r_0 q_2 \tag{9.26}$$

or

$$\frac{\Gamma \epsilon RT}{F} \int_0^{R_0} x I_0(x) dx = r_0 q_2 \tag{9.27}$$

or

$$\Gamma = \frac{q_2 F \lambda}{\epsilon RT I_1(R_0)}, \tag{9.28}$$

where $R_0 = r_0/\lambda$ and I_1 is the modified Bessel function of the first kind, of order one. Also,

$$\rho_e = \frac{q_2 I_0(x)}{\lambda I_1(R_0)}, \tag{9.29}$$

and

$$\frac{\partial \Phi}{\partial r} = \frac{RT}{\lambda F} \frac{d\psi}{dx} = -\frac{q_2}{\epsilon} \frac{I_1(x)}{I_1(R_0)}. \tag{9.30}$$

We are now in a position to evaluate the integrals in equations 9.12 and 9.18:

$$\begin{aligned} \frac{\epsilon}{2\mu} \int_0^{r_0} r^2 \frac{\partial \Phi}{\partial r} dr &= -\frac{\lambda^3 q_2}{2\mu I_1(R_0)} \int_0^{R_0} x^2 I_1(x) dx \\ &= -\frac{\lambda q_2 r_0^2}{2\mu} \frac{I_2(R_0)}{I_1(R_0)} = -\frac{\lambda q_2 r_0^2}{2\mu} \left[\frac{I_0(R_0)}{I_1(R_0)} - \frac{2}{R_0} \right], \end{aligned} \tag{9.31}$$

$$\int_0^{r_0}\left(\frac{\partial\Phi}{\partial r}\right)^2 r dr = \frac{\lambda^2 q_2^2}{\epsilon^2 I_1^2(R_0)}\int_0^{R_0} I_1^2(x)x\,dx$$

$$= \frac{q_2^2\lambda r_0}{\epsilon^2}\left\{\frac{I_0(R_0)}{I_1(R_0)} - \frac{R_0}{2}\left[\frac{I_0^2(R_0)}{I_1^2(R_0)} - 1\right]\right\}$$

$$= \frac{q_2^2 r_0^2}{2\epsilon^2}\left[1 - \frac{I_0(R_0)I_2(R_0)}{I_1^2(R_0)}\right], \tag{9.32}$$

$$\int_0^{r_0} rc_i dr = \frac{c_i^0 r_0^2}{2}\left\{1 + z_i\frac{q_2\lambda F}{\epsilon RT}\left[\frac{2}{R_0} - \frac{1}{I_1(R_0)}\right]\right\}, \tag{9.33}$$

and

$$\int_0^{r_0} r\kappa\, dr = \frac{r_0^2}{2}\kappa_{\text{avg}}, \tag{9.34}$$

where

$$\kappa_{\text{avg}} = \kappa^0\left\{1 + \frac{q_2\lambda F}{\epsilon RT}\left[\frac{2}{R_0} - \frac{1}{I_1(R_0)}\right]\frac{\sum_i z_i^3 u_i c_i^0}{\sum_i z_i^2 u_i c_i^0}\right\} \tag{9.35}$$

and

$$\kappa^0 = F^2\sum_i z_i^2 u_i c_i^0 \tag{9.36}$$

is the conductivity on the centerline of the capillary.

Equation 9.18 now becomes

$$\frac{I}{\pi r_0^2} = \langle i_z\rangle = E_z\left\{\kappa_{\text{avg}} + \frac{q_2^2}{\mu}\left[1 - \frac{I_0(R_0)I_2(R_0)}{I_1^2(R_0)}\right]\right\} - \frac{dp}{dz}\frac{\lambda q_2}{\mu}\frac{I_2(R_0)}{I_1(R_0)}, \tag{9.37}$$

and equation 9.12 becomes

$$\frac{Q}{\pi r_0^2} = \langle v_z\rangle = E_z\frac{\lambda q_2}{\mu}\frac{I_2(R_0)}{I_1(R_0)} - \frac{r_0^2}{8\mu}\frac{dp}{dz}. \tag{9.38}$$

Figure 9.2 shows the velocity profile in the capillary when there is no pressure drop, $dp/dz = 0$. This can be obtained from equation 9.11, which now becomes

$$v_z = \frac{\lambda q_2 E_z}{\mu I_1(R_0)}[I_0(R_0) - I_0(x)] - \frac{dp}{dz}\frac{r_0^2 - r^2}{4\mu}. \tag{9.39}$$

In the absence of a pressure drop, an axial electric field can induce a flow in the capillary, and this is known as *electro-osmosis*. The average velocity or flow rate is then given by equation 9.38 as

$$\frac{\mu\langle v_z\rangle}{\lambda q_2 E_z} = \frac{I_2(R_0)}{I_1(R_0)} \quad \text{when} \quad \frac{dp}{dz} = 0 \tag{9.40}$$

and is tabulated in Table 9.1 as a function of R_0, the ratio of the radius of the capillary to the Debye length. For large values of R_0, the diffuse layer is relatively thin, and the velocity variation occurs near

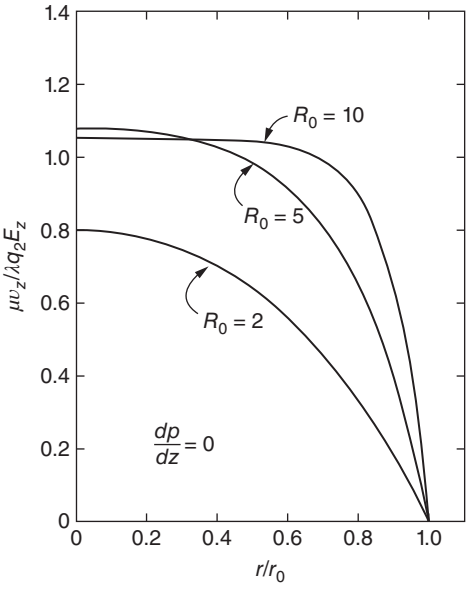

Figure 9.2 Velocity profile in the capillary when there is no pressure drop; this is the case of electro-osmosis.

TABLE 9.1 Dimensionless flow rate $\mu\langle v_z\rangle/\lambda q_2 E_z$ as function of R_0 in the absence of a pressure drop

R_0	$I_2(R_0)/I_1(R_0)$	R_0	$I_2(R_0)/I_1(R_0)$
0	0	10	0.85419
0.1	0.02499	20	0.92599
0.2	0.04992	50	0.97015
0.5	0.12372	100	0.98504
1	0.24019	250	0.99401
2	0.43313	500	0.99700
5	0.71934	∞	1.0

This also corresponds to the dimensionless pressure drop $(dp/dz)r_0^2/8\lambda q_2 E_z$ generated in the absence of net fluid flow or to the dimensionless streaming potential with no net current or to the dimensionless streaming current at zero potential drop (see equations 9.41, 9.42, 9.44, and 9.46).

the wall. This velocity change is given approximately as $\lambda q_2 E_z/\mu$ and is essentially the same as that given by equation 9.7.

The second term on the right in equation 9.39 corresponds to the usual velocity profile induced by a pressure gradient *dp/dz*. The experiment might be constrained by a condition of no net flow, $Q = 0$, rather than no pressure drop. In this case, the axial electric field induces a pressure drop rather than a flow, and this pressure drop is given according to equation 9.38 as

$$\frac{r_0^2}{8\lambda q_2 E_z}\frac{dp}{dz} = \frac{I_2(R_0)}{I_1(R_0)} \quad \text{when} \quad Q = 0, \tag{9.41}$$

also tabulated in Table 9.1. The velocity is not zero throughout the capillary; the second term in equation 9.39 now assumes a magnitude such that the average velocity is zero. The local velocity

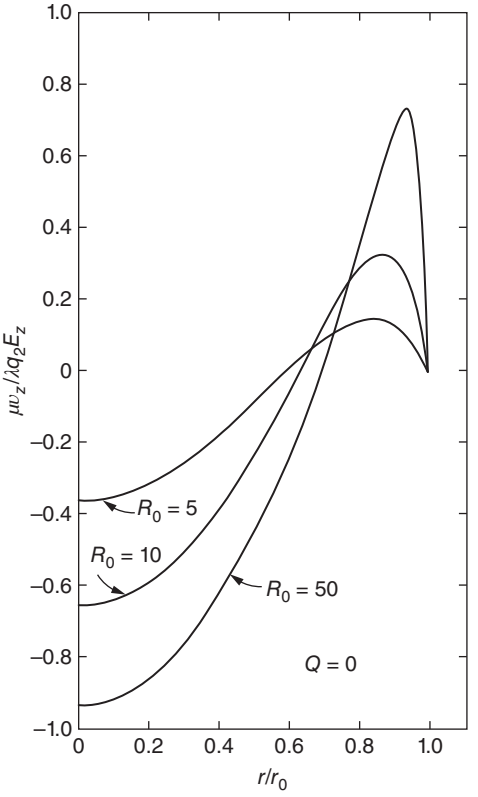

Figure 9.3 Velocity profile in the capillary when there is no net fluid flow.

profile is shown in Figure 9.3. For large values of R_0, there appears to be a velocity discontinuity at the wall of magnitude $v_0 = \lambda q_2 E_z/\mu$, in agreement with equation 9.7. This velocity change actually occurs over the thickness of the diffuse layer, which is now very small compared to the radius of the capillary. Superimposed on this is a parabolic Poiseuille velocity profile given by the last term in equation 9.39.

Equation 9.12 or 9.38 shows how an axial electric field can give rise to fluid flow or a pressure drop, that is, how electrical phenomena can produce fluid mechanical phenomena. On the other hand, equation 9.18 or 9.37 shows how a pressure drop can produce an electric current or a potential drop. Suppose that the electrolytic solution is forced by a pressure drop to flow through the capillary and that the electrical conditions impose a zero net current. Then, the fluid flow generates the so-called *streaming potential*, given by equation 9.37 as

$$\frac{\mu E_2 \kappa_{\text{eff}}}{\lambda q_2 (dp/dz)} = \frac{I_2(R_0)}{I_1(R_0)} \quad \text{with} \quad I = 0, \tag{9.42}$$

where

$$\kappa_{\text{eff}} = \kappa_{\text{avg}} + \frac{q_2^2}{\mu}\left[1 - \frac{I_0(R_0)I_2(R_0)}{I_1^2(R_0)}\right]. \tag{9.43}$$

One may prefer to relate the streaming potential to the flow rate rather than the pressure drop. Elimination of *dp/dz* between equations 9.37 and 9.38 then gives

$$-\frac{\pi r_0^4 E_z \kappa'_{\text{eff}}}{8\lambda q_2 Q} = \frac{I_2(R_0)}{I_1(R_0)} \quad \text{with} \quad I = 0, \tag{9.44}$$

where

$$\kappa'_{\text{eff}} = \kappa_{\text{avg}} + \frac{q_2^2}{\mu}\left[1 - \frac{I_0(R_0)I_2(R_0)}{I_1^2(R_0)} - \frac{8}{R_0^2}\frac{I_2^2(R_0)}{I_1^2(R_0)}\right]. \tag{9.45}$$

If the electrical conditions impose a zero potential drop, for example, by having large reversible electrodes at the ends of the capillary and shorting these electrodes together, then the resulting *streaming current* can be expressed according to equations 9.37 and 9.38 as

$$\frac{-I\mu}{\pi r_0^2 \lambda q_2 (dp/dz)} = \frac{Ir_0^2}{8\lambda q_2 Q} = \frac{I_2(R_0)}{I_1(R_0)} \quad \text{with} \quad E_z = 0. \tag{9.46}$$

The above development shows how a unified treatment can be given to the phenomena of electro-osmosis and the streaming potential. In the former, electrical effects can give rise to fluid flow, and in the latter fluid flow gives rise to electrical effects. In reality, the two are interrelated by equations 9.37 and 9.38, in which there are two driving forces, E_z and *dp/dz*, and two flow quantities, I and Q. However, the electrical effects and the fluid flow phenomena are not separated in these equations.

Let us take an example of pure water in a capillary of radius $r_0 = 20\ \mu\text{m} = 0.002$ cm. We assume the ionic species to be H^+ and OH^- ions with concentrations $c_+^0 = c_-^0 = 10^{-7}$ mol/liter at 25°C. Then the Debye length is $\lambda = 0.96\ \mu\text{m}$, and R_0 is about 20. We take $q_2 = 0.01\ \mu\text{C/cm}^2$, corresponding to a zeta potential of about −138 mV. From these values, we find

$$\frac{q_2 F \lambda}{\epsilon RT} = 5.4, \quad \kappa^0 = 5.5 \times 10^{-8}\ \text{S/cm}, \quad \frac{q_2^2}{\mu\kappa^0} = 2.05,$$

$$\Gamma = 1.3 \times 10^{-7}, \quad \frac{\kappa_{\text{avg}}}{\kappa^0} = 1.15, \quad \frac{\kappa_{\text{eff}}}{\kappa_{\text{avg}}} = 1.089, \quad \frac{\kappa'_{\text{eff}}}{\kappa_{\text{avg}}} = 1.059.$$

Under these conditions, the application of 100 V across the capillary, with no net fluid flow, should generate a pressure difference equivalent to a column of water 7.3 cm high.

Frequently, the diffuse layer is very thin compared to other geometric lengths, and we want to develop an approximate method of analysis that recognizes this fact. For large values of R_0, the diffuse layer is confined to a region close to the wall where the cylindrical geometry is not important. Outside this region, the solution is electrically neutral. We consider first the fluid flow and then the current flow.

For large values of R_0, equation 9.39 reduces to

$$v_z = v_0 - \frac{dp}{dz}\frac{r_0^2 - r^2}{4\mu}, \tag{9.47}$$

where

$$v_0 = \frac{\lambda q_2 E_z}{\mu}. \tag{9.48}$$

Equation 9.47 applies outside the diffuse layer and corresponds to the solution of equation 9.10 with zero charge density and with the boundary condition that $v_z = v_0$ at $r = r_0$. This value of v_0 comes from the treatment of the thin diffuse layer according to Section 9.1.

Thus, one treats the fluid mechanical problem by solving the momentum equation as though the solution were electrically neutral, but with a slip velocity at a solid wall which is related to the tangential component of the electric field by equations 9.48, 9.7, or 9.5. Figures 9.2 and 9.3 show how this situation is approximated more closely as R_0 increases.

Equation 9.47 yields the flow rate as

$$\frac{Q}{\pi r_0^2} = \langle v_z \rangle = E_z \frac{\lambda q_2}{\mu} - \frac{r_0^2}{8\mu} \frac{dp}{dz}, \tag{9.49}$$

which is also obtained from equation 9.38 as R_0 becomes infinite.

The situation for the current relationships is simple at first sight. As R_0 approaches infinity, κ_{avg}, κ_{eff}, and κ'_{eff} all approach κ^0, and equation 9.37 becomes

$$\frac{I}{\pi r_0^2} = \langle i_z \rangle = \kappa^0 E_z - \frac{\lambda q_2}{\mu} \frac{dp}{dz}. \tag{9.50}$$

This yields the correct asymptotic forms for the streaming potential and the streaming current according to equations 9.42, 9.44, and 9.46. Outside the diffuse layer, the solution is taken to be electrically neutral with the conductivity κ^0, and this region obviously contributes the term $\kappa^0 E_Z$ to equation 9.50. The last term must come then from the diffuse layer.

For the purpose of examining the contribution of the diffuse layer, we want to define a surface current density j_s, attributed to the diffuse layer, so that the total current is expressed as

$$I = \pi r_0^2 \kappa^0 E_z + 2\pi r_0 j_s, \tag{9.51}$$

the surface current density being multiplied by the circumference in order to obtain the contribution to the total current. Substitution of equation 9.51 into equation 9.37 yields, in the limit of large R_0,

$$j_s = \kappa_s E_z + \beta \lambda q_2, \tag{9.52}$$

where

$$\kappa_s = \frac{q_2 \lambda^2 F^3}{\epsilon RT} \sum_i z_i^3 u_i c_i^0 + \frac{\lambda q_2^2}{2\mu} \tag{9.53}$$

is the *surface conductivity* and β is the velocity derivative $\partial v_z / \partial y$ just outside the diffuse layer (y being the distance from the surface). In the present case,

$$\beta = -\frac{r_0}{2\mu} \frac{dp}{dz} \tag{9.54}$$

(see equation 9.47).

The terms in equations 9.52 and 9.53 are subject to physical interpretation. The first term on the right in equation 9.53 might be termed the surface excess conductivity, due to the fact that the ionic concentrations within the diffuse layer differ from their bulk values. This quantity can be positive or negative and is zero for a symmetric electrolyte with equal cation and anion mobilities. In the Debye–Hückel approximation (again for a symmetric electrolyte), $c_+ + c_-$ is uniform within the

diffuse layer. Therefore, replacing less mobile ions by more mobile counterions would increase the local conductivity. If this approximation were relaxed, one should expect the ionic strength to increase in the diffuse layer, and this would lead to more positive values of the surface excess conductivity.

The last term in equation 9.53 might be called the surface convective conductivity and is due to the motion of the fluid in the diffuse layer as it is induced by the electric field. Since the induced velocity is proportional to q_2 and the charge density is proportional to q_2, the surface convective conductivity is proportional to the square of q_2 and is always positive.

A shear stress in the fluid near the surface induces further fluid motion in the diffuse layer and leads to an additional convective contribution to the surface current density. This term is written in terms of β in order to refer to a quantity relevant to the local conditions at the interface. In some cases, erosion corrosion may be related to this last term in equation 9.52 because the shear stress may vary over the surface.[5, 6] This causes the surface current density to vary, and if this current cannot be supplied by the bulk solution because of its low conductivity, it can lead to a corrosion reaction at a metal surface.

If the solid surface itself were moving, it would be necessary to include an additional convective term in equation 9.52 when the surface current density includes only the current on the mobile side of the double layer. The interface as a whole remains electrically neutral.

Equations 9.51 and 9.52 lead to the expression

$$\frac{I}{\pi r_0^2} = E_z\left(\kappa^0 + \frac{2\kappa_s}{r_0}\right) - \frac{dp}{dz}\frac{\lambda q_2}{\mu} \tag{9.55}$$

for the total current. Comparison with equation 9.50 shows that the surface conductivity can be neglected for large values of r_0/λ.

Equation 9.52 and equation 9.48 or 9.5 are vector equations relating to the surface current density, the slip velocity at the surface, the tangential electric field, and the shear stress. They can be applied in other geometric situations where the diffuse layer can be taken to be thin compared to other characteristic lengths. In this approximation, the diffuse layer is essentially planar, and these equations could be refined to account for the fact that the planar diffuse layer can be solved without the Debye–Hückel approximation.

9.3 ELECTROPHORESIS

Electrophoresis means the motion of a dielectric particle in an electrolytic solution under the influence of an electric field. The electric field interacts with the diffuse layer to produce a relative motion of the solid and the fluid, as discussed in Section 9.1. This relative motion serves to propel the particle through the fluid. The analysis applies equally well to a metallic particle, if the potential jump across the interface is in a range where the surface is ideally polarizable and the charge in the diffuse layer is essentially uniform over the surface of the particle.

Consider a spherical particle of radius r_0, and let the origin of a spherical coordinate system be fixed in the center of the particle. With this convention, the fluid moves past the particle in a steady manner, and, far from the particle, the z component of the velocity is v_∞. Let the z component of the electric field be E_∞ far from the particle. The objective is to relate v_∞ to E_∞. Gravitational forces are neglected.

Outside the diffuse layer, the solution is electrically neutral, the fluid motion satisfies the Navier–Stokes equation 15.10 and the continuity equation 15.3, and the electric potential satisfies Laplace's equation 11.16. With the assumption that the diffuse layer is thin compared to the radius of the particle, the fluid mechanical equations are to be solved with the boundary conditions that the velocity approaches the uniform velocity at infinity, that the fluid exerts no net force on the particle

including the diffuse layer, and that the slip velocity at the surface matches the tangential electric field according to equation 9.48

$$v_\theta = \frac{\lambda q_2 E_\theta}{\mu} \quad \text{at} \quad r = r_0. \tag{9.56}$$

The potential is to satisfy Laplace's equation subject to the conditions that the electric field approaches the uniform field at infinity and there is a charge balance at the interface

$$\kappa \frac{\partial \Phi}{\partial r} = \nabla_s \cdot \mathbf{j}_s \quad \text{at} \quad r = r_0, \tag{9.57}$$

where $\nabla_s \cdot \mathbf{j}_s$ is the surface divergence of the surface current density.

An exact solution of the Navier–Stokes equation satisfying the condition at infinity and the condition of zero net force on the particle plus the diffuse layer is

$$v_r = \left(1 - \frac{r_0^3}{r^3}\right) v_\infty \cos\theta, \tag{9.58}$$

$$v_\theta = -\left(1 + \frac{r_0^3}{2r^3}\right) v_\infty \sin\theta. \tag{9.59}$$

It is not always realized that this is an exact solution of the Navier–Stokes and continuity equations.

From these results,

$$\beta = \frac{3}{2}\frac{v_\infty}{r_0} \sin\theta, \tag{9.60}$$

and the surface current density from equation 9.52 becomes

$$j_s = \frac{3}{2}\frac{v_\infty \lambda q_2}{r_0}\left(1 - \frac{\kappa_s \mu r_0}{\lambda^2 q_2^2}\right) \sin\theta. \tag{9.61}$$

where E_θ has been eliminated by means of equation 9.56. The surface divergence of the surface current density therefore is

$$\nabla_s \cdot \mathbf{j}_s = \frac{1}{r_0 \sin\theta}\frac{\partial}{\partial\theta}(j_s \sin\theta) = \frac{3 v_\infty \lambda q_2}{r_0^2}\left(1 - \frac{\kappa_s \mu r_0}{\lambda^2 q_2^2}\right) \cos\theta, \tag{9.62}$$

and boundary condition 9.57 becomes

$$\frac{\partial \Phi}{\partial r} = \frac{3 v_\infty \lambda q_2}{r_0^2 \kappa}\left(1 - \frac{\kappa_s \mu r_0}{\lambda^2 q_2^2}\right) \cos\theta. \tag{9.63}$$

The solution of Laplace's equation satisfying condition 9.63 and giving the proper electric field at infinity is

$$\Phi = -\left[r + \left(\frac{1}{2} + A\right)\frac{r_0^3}{r^2}\right] E_\infty \cos\theta, \tag{9.64}$$

where

$$A = \frac{3 v_\infty \lambda q_2}{2 r_0^2 \kappa E_\infty}\left(1 - \frac{\kappa_s \mu r_0}{\lambda^2 q_2^2}\right). \tag{9.65}$$

Equation 9.64 yields the tangential electric field at the surface of the particle:

$$E_\theta = -\left(\frac{3}{2} + A\right) E_\infty \sin\theta. \tag{9.66}$$

Substitution of this result into equation 9.56 yields the final expression for the electrophoretic velocity in terms of the applied field:

$$v_\infty = \frac{\dfrac{E_\infty \lambda q_2}{\mu}}{1 - \dfrac{\lambda^2 q_2^2}{r_0^2 \kappa \mu} + \dfrac{\kappa_s}{\kappa r_0}}. \tag{9.67}$$

The second term in the denominator in equation 9.67 is of order λ^0/r_0^2 and is small compared to the last term, which is of order λ/r_0. Both terms should be negligible compared to the first term, and the electrophoretic velocity can be expressed in terms of the zeta potential as

$$v_\infty = -\frac{E_\infty \epsilon \zeta}{\mu}. \tag{9.68}$$

Recall that v_∞ is the velocity of the fluid with respect to the particle. Therefore, a particle with a positive zeta potential moves in the direction of the electric field.

9.4 SEDIMENTATION POTENTIAL

Small particles will fall through an electrolytic solution in a gravitational field with essentially a Stokes velocity profile. This is not an exact solution of the Navier–Stokes equation; rather, it applies for small values of the Reynolds number $\mathrm{Re} = 2v_\infty r_0/\nu$. If the particle has a positive zeta potential, then the charge in the diffuse layer is negative. The shear stress near the particle will cause a surface current density to flow from the back of the particle to the front. This current must then flow through the bulk of the solution from the front to the back. This means that the potential behind a particle with a positive zeta potential will be negative relative to the potential in front of the particle. A number of particles falling through the solution then establishes an electric field whose magnitude is given by

$$E_z = \frac{\dfrac{-6\pi n v_\infty r_0 \lambda q_2}{\kappa}}{1 + \dfrac{\kappa_s}{\kappa r_0} - 2\dfrac{\lambda^2 q_2^2}{r_0^2 \kappa \mu}}, \tag{9.69}$$

where n is the number of particles per unit volume of the system. E_z is in the direction opposite to the velocity v_∞, of the particles. The same remarks apply to the terms in the denominator of this equation as to those in equation 9.67.

By means of a force balance, the velocity of fall is given as

$$v_\infty = \frac{2(\rho' - \rho) g r_0^2}{9\mu} \frac{1 + \dfrac{\kappa_s}{\kappa r_0} - 2\dfrac{\lambda^2 q_2^2}{r_0^2 \kappa \mu}}{1 + \dfrac{\kappa_s}{\kappa r_0} - \dfrac{\lambda^2 q_2^2}{r_0^2 \kappa \mu}}, \tag{9.70}$$

which differs insignificantly from the velocity for an uncharged particle

$$v_\infty = \frac{2(\rho' - \rho)gr_0^2}{9\mu} \tag{9.71}$$

given by Stokes's law since $\lambda^2 q_2^2 / r_0^2 \kappa\mu$ is of order λ^2 / r_0^2. In equations 9.70 and 9.71, ρ' is the density of the particle, ρ is the density of the electrolytic solution, and g is the magnitude of the gravitational acceleration.

The sedimentation potential is analogous to the streaming potential discussed in Section 9.2. In both cases, the relative motion of a solid and an electrolytic solution gives rise to electrical effects. However, the sedimentation potential is not much studied because it is difficult to obtain an appreciable magnitude experimentally.

By adding shorted reversible electrodes to the system, one could maintain a zero electric field. One should then observe a sedimentation current analogous to the streaming current discussed in Section 9.2.

PROBLEMS

9.1 **(a)** For a diffuse layer, the electrokinetic slip velocity is given by equation 9.5,

$$v_0 = -\frac{\epsilon\zeta E_x}{\mu},$$

equation 9.7 being valid only when the Debye–Hückel approximation is applicable. The second basic electrokinetic equation is equation 9.52. Show that in general this equation should be replaced by

$$j_s = \kappa_s E_x - \epsilon\beta\zeta,$$

where the surface conductivity is

$$\kappa_s = F^2 \sum_i z_i^2 u_i \Gamma_{i,d} + \frac{\epsilon^2}{\mu} \int_0^\zeta E_y d\Phi.$$

Here E_y is given as a function of Φ by equation 7.37, and q_2 can be determined in terms of ζ from equation 7.38.

(b) For a solution of a binary, symmetric electrolyte, q_2 and ζ are related by

$$q_2 = -\frac{2\epsilon RT}{zF\lambda} \sinh \frac{zF\zeta}{2RT}.$$

Show that the expression for the surface conductivity becomes

$$\kappa_s = \frac{\kappa\lambda^2 zFq_2}{\epsilon RT} \left(t_+ - t_- - \tanh \frac{zF\zeta}{4RT} \right) + \frac{\dfrac{\lambda q_2^2}{\mu}}{1 + \sqrt{1 + \left(\dfrac{zF\lambda q_2}{2\epsilon RT} \right)^2}},$$

where κ is the conductivity of the bulk solution and

$$t_+ = 1 - t_- = \frac{u_+}{u_+ + u_-}$$

is the cation transference number.

(c) Show that when the Debye–Hückel approximation is valid, that is, when $zF\zeta/RT \ll 1$, the results in part (b) reduce to equations 9.6 and 9.53. Notice that the surface excess conductivity in part (b) is higher than that in equation 9.53, while the surface convective conductivity is lower.

9.2 Show on the basis of Problem 9.1 that equation 9.55 should be written as

$$\frac{I}{\pi r_0^2} = E_z\left(\kappa^0 + \frac{2\kappa_s}{r_0}\right) + \frac{\epsilon\zeta}{\mu}\frac{dp}{dz}$$

and that consequently, for large values of r_0/λ, the streaming potential (equations 9.42 and 9.44) should be written

$$-\frac{\mu E_z \kappa^0}{\epsilon\zeta\dfrac{dp}{dz}} = \frac{\pi r_0^4 E_z \kappa^0}{8\epsilon\zeta Q} = 1 \quad \text{with} \quad I = 0,$$

and the streaming current (equation 9.46) should be written

$$\frac{I\mu}{\pi r_0^2 \epsilon\zeta\dfrac{dp}{dz}} = \frac{-Ir_0^2}{8\epsilon\zeta Q} = 1 \quad \text{with} \quad E_z = 0.$$

Make the corresponding changes in equation 9.49 and in the expressions for pressure drop at zero flow (equation 9.41) and flow at zero pressure drop (equation 9.40).

9.3 Show on the basis of Problem 9.1 that the electrophoretic velocity, equation 9.67, should be written

$$v_\infty = \frac{-\dfrac{E_\infty \epsilon\zeta}{\mu}}{1 + \dfrac{\kappa_s}{\kappa r_0} - \dfrac{\epsilon^2\zeta^2}{r_0^2\kappa\mu}}$$

or, for practical purposes, as equation 9.68. The sedimentation potential, equation 9.69, should be written

$$E_z = \frac{6\pi n v_\infty r_0 \epsilon\zeta}{\kappa}.$$

These equations are written in the form in the text for easier comparison with the corresponding results in Chapter 10.

9.4 **(a)** Is the normal component of the current density continuous at an interface if the normal component is to be evaluated just outside the interface?

(b) Rationalize or convince yourself of the validity of equation 9.57.

(c) Obtain an estimate of the magnitude of $\nabla_s \cdot \mathbf{j}_s$ from equation 9.62 by using the values $v_\infty = 0.3$ cm/s, $\lambda = 1$ nm, $r_0 = 20\,\mu$m, $\mu = 0.89$ mPa s, $\kappa_s/\lambda = 0.01$ S/cm, and $q_2 = 7\,\mu$C/cm^2.

9.5 Justify the material balance for a species at an interface:

$$\frac{\partial \Gamma_i}{\partial t} + \nabla_s \cdot \mathbf{J}_{is} = N_{iy}^0 - N_{iy}^\infty,$$

where $\mathbf{J}_{is}$ is the surface flux of species i, N_{iy}^0 is the normal component of the flux at the surface, involved in faradaic electrode reactions, and N_{iy}^∞ is the normal component of the flux evaluated just outside the diffuse layer. Use this equation to derive equation 9.57.

NOTATION

c_i	concentration of species i, mol/cm^3
$\mathbf{E}$	electric field, V/cm
E_∞	electric field far from the particle, V/cm
F	Faraday's constant, 96,487 C/mol
g	magnitude of the gravitational acceleration, cm/s^2
$\mathbf{i}$	current density, A/cm^2
I	total current, A
j_s	surface current density, A/cm
n	number of particles per unit volume of the system, cm^{-3}
N_i	flux of species i, mol/cm^2·s
p	pressure, N/cm^2
q_2	surface charge density in the diffuse layer, C/cm^2
Q	volumetric flow rate, cm^3/s
r	radial distance in spherical or cylindrical coordinates, cm
r_0	radius of particle or capillary, cm
R	universal gas constant, 8.3143 J/mol·K
R_0	r_0/λ
Re	$2v_\infty r/\nu$, the Reynolds number
T	absolute temperature, K
u_i	mobility of species i, cm^2·mol/J·s
$\mathbf{v}$	fluid velocity, cm/s
v_0	electrokinetic velocity discontinuity, cm/s
v_∞	velocity far from the particle, cm/s
x	distance along a surface, cm
x	r/λ
y	distance from surface, cm
z	distance along capillary or in direction of particle motion, cm
z_i	charge number of species i
β	velocity derivative outside diffuse layer, s^{-1}
Γ	dimensionless charge density on axis of capillary
ϵ	permittivity, F/cm
ϵ_0	permittivity of free space, 8.8542×10^{-14} F/cm
ζ	zeta potential, V
θ	angle from the axis of particle motion
κ	solution conductivity, S/cm
κ_s	surface conductivity, S
λ	Debye length, cm

μ	viscosity, mPa·s
ν	kinematic viscosity, cm^2/s
ρ	density, g/cm^3
ρ_e	electric charge density, C/cm^3
ϕ	$\Phi - \Phi_{r=0}$
Φ	electric potential, V
ψ	$F\phi/RT$, dimensionless potential

REFERENCES

1. J. Th. G. Overbeek, "Electrokinetic Phenomena," in H. R. Kruyt, ed., *Colloid Science*, Vol. I (Amsterdam: Elsevier, 1952), pp. 194–244.
2. A. J. Rutgers and M. De Smet, "Electrokinetic Researches in Capillary Systems and in Colloidal Solutions," in *Electrochemical Constants*, National Bureau of Standards (U.S.) Circular 524 (1953), pp. 263–279.
3. A. Klinkenberg and J. L. van der Minne, eds., *Electrostatics in the Petroleum Industry* (Amsterdam: Elsevier, 1958).
4. Veniamin G. Levich, *Physicochemical Hydrodynamics*, section 94 (Englewood Cliffs, NJ: Prentice-Hall, 1962).
5. T. R. Beck, D. W. Mahaffey, and J. H. Olsen, "Wear of Small Orifices by Streaming Surrent Driven Corrosion," *Journal of Basic Engineering*, *92* (1970), 782–788.
6. T. R. Beck, D. W. Mahaffey, and J. H. Olsen. "Pitting and Deposits with an Organic Fluid by Electrolysis and by Fluid Flow," *Journal of the Electrochemical Society*, *119* (1972), 155–160.

CHAPTER 10

ELECTROCAPILLARY PHENOMENA

The motion of charged mercury drops in an electrolytic solution can lead to much larger electrophoretic velocities and sedimentation potentials than with solid particles because the drop can develop an internal circulation. The motion of the surface leads to larger surface current densities and hence larger sedimentation potentials. In electrophoresis, the electric force is not applied close to a solid surface, and larger velocities result.

For mercury drops, we can ignore the usual electrokinetic effects since the surface velocity itself is much larger than the electrokinetic velocity discontinuity discussed in Section 9.1. Instead, we treat the mercury drop as an ideally polarizable electrode, where the surface tension varies with the local electrode potential on the drop. These variations of surface tension serve to propel the drop through the solution in the electrophoretic case. They can also affect the velocity of fall in a gravitational field in the sedimentation case.

The mechanism and observations of electrocapillary motion were described by Christiansen[1] in 1903. Frumkin and Levich[2–4] presented a detailed theoretical analysis of the phenomena.

10.1 DYNAMICS OF INTERFACES

The force balance at an interface is treated in Section 15.3. For a spherical drop, equation 15.14 reads

$$\tau'_{r\theta} - \tau_{r\theta} + \frac{1}{r_0}\frac{\partial \sigma}{\partial \theta} = 0, \tag{10.1}$$

where $\tau'_{r\theta}$ is the force in the θ direction exerted on the interface by the fluid within the drop and $-\tau_{r\theta}$ is the force exerted by the fluid outside the drop. The shear stress is related to the velocity derivatives for a Newtonian fluid:

$$\tau_{r\theta} = -\mu\left[r\frac{\partial}{\partial r}\left(\frac{v_\theta}{r}\right) + \frac{1}{r}\frac{\partial v_r}{\partial \theta}\right]. \tag{10.2}$$

Electrochemical Systems, Fourth Edition. John Newman and Nitash P. Balsara.

Surface-tension-driven flows can lead to a variety of interesting phenomena. The surface tension generally depends on the composition of the solution near the interface. In mass-transfer studies, nonuniformities of surface tension can develop, resulting in what is called interfacial turbulence.[5, 6] In the *Marangoni effect*, a nonuniform surface tension arises from differential evaporation of the components of the solution. In the fall of a drop in a solution with surface-active agents, nonuniformities of surface tension can hinder the internal circulation, so that the drop falls like a solid sphere.[7, 8] Similar circumstances can hinder the formation of ripples on a falling liquid film.

In the electrocapillary motion of mercury drops, the surface tension can vary due to the nonuniform potential in the solution. This can produce a motion, like electrophoresis, if there is an applied electric field, or it can hinder the fall of drops in a manner similar to the surface-active agents referred to above. Electrocapillary motion can also lead to some maxima observed in polarographic currents with a dropping mercury electrode.[9, 10]

If proper account is taken of the variation of surface tension at a fluid–fluid interface, the concept of the *surface viscosity* becomes of dubious value.

10.2 ELECTROCAPILLARY MOTION OF MERCURY DROPS

The electrocapillary motion of mercury drops in an external electric field is very similar to the electrophoretic motion of solid particles treated in Section 9.3. The velocity distribution outside the drop is again given by equations 9.58 and 9.59, so that

$$v_\theta = -\frac{3}{2} v_\infty \sin\theta \quad \text{at} \quad r = r_0 \tag{10.3}$$

and

$$\tau_{r\theta} = -\frac{3\mu v_\infty}{r_0} \sin\theta \quad \text{at} \quad r = r_0. \tag{10.4}$$

Since the interface as a whole now moves, the surface current density is

$$j_s = -q v_\theta \quad \text{at} \quad r = r_0, \tag{10.5}$$

with $-q$ being the charge density on the solution side of the double layer. We take q to be essentially constant over the surface of the drop so that the surface divergence is

$$\nabla_s \cdot \mathbf{j}_s = \frac{3q v_\infty}{r_0} \cos\theta. \tag{10.6}$$

For an ideally polarizable drop, the current entering and leaving the surface cannot come from within the drop. Consequently, the current comes from the electrolytic solution, and equation 9.57 applies:

$$\frac{\partial \Phi}{\partial r} = \frac{3q v_\infty}{r_0 \kappa} \cos\theta \text{ at } r = r_0. \tag{10.7}$$

This forms one of the boundary conditions for Laplace's equation, the other being the uniform field far from the drop. Consequently, the potential in the solution outside the drop is again given by equation 9.64, where now

$$A = \frac{3q v_\infty}{2 r_0 \kappa E_\infty}. \tag{10.8}$$

The velocity distribution inside the drop is

$$v'_r = \frac{3}{2}\left(\frac{r^2}{r_0^2} - 1\right) v_\infty \cos\,\theta, \tag{10.9}$$

$$v'_\theta = -\frac{3}{2}\left(2\frac{r^2}{r_0^2} - 1\right) v_\infty \sin\,\theta. \tag{10.10}$$

This is not an exact solution of the Navier–Stokes equation. It is a solution of the approximate form of the equation of motion for creeping flow. Equations 10.9 and 10.10 yield

$$\tau'_{r\theta} = \frac{9}{2}\frac{\mu' v_\infty}{r_0} \sin\,\theta \;\text{ at }\; r = r_0. \tag{10.11}$$

The motion of the surface also creates a surface current density on the metal side of the double layer. However, this current can easily be supplied from within the drop because of the high conductivity of the metal, and the potential in the drop remains uniform. Consequently, the Lippmann equation 7.26 allows the variation in surface tension to be related to the variation of the potential in the solution near the drop:

$$\frac{\partial \sigma}{\partial \theta} = -q\frac{\partial U}{\partial \theta} = q\frac{\partial \Phi}{\partial \theta} \;\text{ at }\; r = r_0. \tag{10.12}$$

With equation 9.64, we have

$$\frac{\partial \sigma}{\partial \theta} = q r_0 E_\infty \left(\frac{3}{2} + A\right) \sin\,\theta. \tag{10.13}$$

Finally, substitution of equations 10.4, 10.8, 10.11, and 10.13 into the force balance equation 10.1 allows us to determine the velocity v_∞ in terms of the electric field E_∞:

$$v_\infty = \frac{-qE_\infty r_0}{2\mu + 3\mu' + \dfrac{q^2}{\kappa}}. \tag{10.14}$$

As in the case of equations 9.67 and 9.68, a positively charged drop moves in the direction of the electric field, v_∞ being the velocity of the fluid with respect to the particle.

Levich[11] cites from the Russian literature examples of the experimental verification of equation 10.14. This can be done with some thoroughness, since it is possible to vary the surface charge on the drop (see Figure 7.9). One notices that the velocity in equation 10.14 can be larger than the usual electrophoretic velocities given by equation 9.67 or 9.68 by a factor of the order of r_0/λ. Again in contrast to equation 9.67, the last term in the denominator of equation 10.14 generally is not negligible, and in media of low conductivity the velocity of electrocapillary motion can be small.

The charge in the double layer is the origin of the electrocapillary motion and gives rise to the numerator in equation 10.14. The tangential electric field produces a variation in surface tension that propels the drop (see equation 10.12). However, if the double layer has too great an ability to carry a surface current compared to the bulk solution, it can reduce the tangential electric field and hence the variation of surface tension around the drop. This will lower the velocity of electrophoretic motion, as represented by the last term in the denominator of equation 10.14.

10.3 SEDIMENTATION POTENTIALS FOR FALLING MERCURY DROPS

Mercury drops falling through an electrolytic solution will establish a sedimentation potential in much the same manner as solid particles, as discussed in Section 9.4. In this case, equation 9.69 is replaced by

$$E_z = \frac{2\pi n v_\infty r_0^2 \dfrac{q\mu}{\kappa}}{\mu + \mu' + \dfrac{q^2}{3\kappa}}, \tag{10.15}$$

where E_z is in the direction opposite to the velocity v_∞ of the particles. The velocity of fall of the drops is now given by

$$v_\infty = \frac{2(\rho' - \rho) g r_0^2}{3\mu} \frac{\mu + \mu' + \dfrac{q^2}{3\kappa}}{2\mu + 3\mu' + \dfrac{q^2}{\kappa}}. \tag{10.16}$$

Now, both the sedimentation potential and the velocity of fall are subject to experimental verification, as presented by Levich.[12] For large values of q^2/κ, the drop falls like a solid particle according to Stokes's law:

$$v_\infty = \frac{2(\rho' - \rho) g r_0^2}{9\mu}. \tag{10.17}$$

The motion of the charge in the double layer then establishes a potential distribution around the drop that determines the variation of surface tension so as to retard strongly the motion of the surface. For a small surface charge, on the other hand, the internal circulation of the drop is not retarded, and it falls with the somewhat larger velocity

$$v_\infty = \frac{2(\rho' - \rho) g r_0^2}{3\mu} \frac{\mu + \mu'}{2\mu + 3\mu'}. \tag{10.18}$$

For a small viscosity μ' of the drop compared to the viscosity μ of the solution, this velocity can be 50% larger than the Stokes velocity.

The sedimentation potential for falling drops is much greater than that given by equation 9.69 for solid particles, by a factor of order r_0/λ. The terms involving q^2/κ in the denominator in equations 10.15 and 10.16 are, in general, not negligible, in contrast to the corresponding terms in equations 9.69 and 9.70.

NOTATION

E_∞	electric field far from the drop, V/cm
g	magnitude of the gravitational acceleration, cm/s^2
j_s	surface current density, A/cm
n	number of drops per unit volume of the system, cm^{-3}
q	surface charge density on the mercury side of the double layer, C/cm^2
r	radial distance from the center of the drop, cm
r_0	radius of the mercury drop, cm
U	electrode potential, V
v_r	velocity in the r direction, cm/s
v_θ	velocity in the θ direction, cm/s
v_∞	velocity far from the drop, cm/s

θ	angle from the axis of drop motion
κ	solution conductivity, S/cm
λ	Debye length, cm
μ	viscosity, mPa·s
ρ	density, g/cm^3
σ	surface tension, mN/m
$\tau_{r\theta}$	shear stress, N/cm^2
Φ	electric potential in the solution, V

Superscript

$'$	in the drop

REFERENCES

1. C. Christiansen, "Kapillarelektrische Bewegungen," *Annalen der Physik, ser. 4*, *12* (1903), 1072–1079.
2. A. Frumkin and B. Levich, "The Motion of Solid and Liquid Metallic Bodies in Solutions of Electrolytes. I," *Acta Physicochimica URSS*, *20* (1945), 769–808.
3. A. Frumkin and B. Levich, "The Motion of Solid and Liquid Metallic Bodies in Solutions of Electrolytes. II. Motion in the Field of Gravity." *Acta Physicochimica URSS*, *2I* (1946), 193–212.
4. V. Levich, "Dvizhenie tverdykh i zhidkikh metallicheskikh chastits v rastvorakh elektrolitov. III. Obshchaya teoriya," *Zhumal Fizicheskoi Khimii*, *21* (1947), 689–701.
5. Thomas K. Sherwood and James C. Wei, "Interfacial Phenomena in Liquid Extraction," *Industrial and Engineering Chemistry*, *49* (1957), 1030–1034.
6. C. V. Sternling and L. E. Scriven, "Interfacial Turbulence: Hydrodynamic Stability and Marangoni Effect," *AIChE Journal*, *5* (1959), 514–523.
7. A. Frumkin and V. Levich, "O vliyanii poverkhnostno-aktivnykh veshchestv na dvizhenie na granitse zhidkikh sred," *Zhurnal Fizicheskoi Khimii*, *21* (1947), 1183–1204.
8. John Newman, "Retardation of falling drops," *Chemical Engineering Science*, *22* (1967), 83–85.
9. A. Frumkin and B. Bruns, "Über Maxima der Polarisationskurven von Quecksilberkathoden," *Acta Physicochimica URSS*, *I* (1934), 232–246.
10. A. Frumkin and V. Levich, "Dvizhenie tverdykh i zhedkikh metallicheskikh chastits v rastvorakh elektrolitov. IV. Maksimumy na krivy tok-napryazhenie kapel' nogo elektroda," *Zhumal Fizicheskoi Khimii*, *21* (1947), 1335–1349.
11. Veniamin G. Levich, *Physiecochemical Hydrodynamics*, Section 10.1 (Englewood Cliffs, NJ: Prentice-Hall, 1962).
12. Ibid., Sections 10.2 and 10.3.

PART C

TRANSPORT PROCESSES IN ELECTROLYTIC SOLUTIONS

Frequently, the rate of an electrochemical process is governed by the transport of a reactant species to the electrode surface by diffusion and convection. In other processes, the ohmic potential drop in the solution is decisive. This part of the book treats the transport processes, *migration* and *diffusion*, in electrolytic solutions from a descriptive point of view. For example, it is recognized that electric conduction is a manifestation of the movement of charged species, but the quantitative characterization of conduction in terms of the molecular properties of the species is not considered vital. Engineering applications do not require values of transport properties predicted from molecular theory if measured values are available.

Basic diffusion laws for dilute solutions are presented in Chapter 11 and are modified for concentrated solutions in Chapter 12. The dilute-solution theory has been applied fruitfully to many electrochemical problems; it is adequate for approximate analysis. It is more or less familiar to all electrochemists. Nevertheless, a careful definition of transport properties requires modifications of that theory except at infinite dilution. Furthermore, there are questions for which the dilute-solution theory promotes circular or incorrect reasoning. A classic example is the question of liquid-junction potentials and individual ionic activity coefficients. Such questions can be clarified or avoided in the theory for concentrated solutions.

One should be aware that the consequences of dilute-solution theory developed in Chapter 11 are subject to qualification or reinterpretation as a result of the theory of concentrated solutions. It is not always indicated in the text whether a particular result has a strong analogy or is of little meaning in the concentrated-solution theory.

Thermal effects and transport properties are developed in Chapters 13 and 14. The fluid mechanics necessary to calculate the convective velocity is introduced in Chapter 15.

Transport equations are given in vector notation for generality and brevity. A short statement of the information needed to comprehend such equations is found in Appendix B.

Electrochemical Systems, Fourth Edition. John Newman and Nitash P. Balsara.

Chapters 11 and 12 are taken largely from J. Newman, "Transport Processes in Electrolytic Solutions," in C. W. Tobias, *Advances in Electrochemistry and Electrochemical Engineering,* Vol. 5;

CHAPTER 11

INFINITELY DILUTE SOLUTIONS

11.1 TRANSPORT LAWS

Mass transfer in an electrolytic solution requires a description of the movement of mobile ionic species, material balances, current flow, electroneutrality, and fluid mechanics. Equations for the first four of these are presented in this section and are elaborated upon in the following sections. The medium we wish to describe consists of a nonionized solvent, ionized electrolytes, and uncharged minor components. This description should be restricted to dilute solutions.

The flux density of each dissolved species is given by

$$\underset{\text{flux}}{\mathbf{N}_i} = \underset{\text{migration}}{-z_i u_i F c_i \nabla \Phi} \underset{\text{diffusion}}{- D_i \nabla c_i} + \underset{\text{convection}}{c_i \mathbf{v}}. \tag{11.1}$$

The flux density $\mathbf{N}_i$ of species i, expressed in mol/cm^2·s, is a vector quantity indicating the direction in which the species is moving and the number of moles going per unit time across a plane of 1 cm^2, oriented perpendicular to the flow of the species. This movement is due first of all to the motion of the fluid with the bulk velocity $\mathbf{v}$. However, the movement of the species can deviate from this average velocity by diffusion if there is a concentration gradient ∇c_i or by migration if there is an electric field $-\nabla\Phi$ and if the species is charged (z_i is the number of proton charges carried by an ion).

The migration term is peculiar to electrochemical systems or systems containing charged species. Here Φ is the electrostatic potential whose gradient is the negative of the electric field. These are not quantities that can be measured easily and directly in a liquid solution. The quantity u_i is called the *mobility* and denotes the average velocity of a species in the solution when acted upon by a force of 1 N/mol, independent of the origin of the force. Thus, $z_i F$ is the charge per mole on a species. Multiplication by the electric field $-\nabla\Phi$ gives the force per mole. Multiplication by the mobility u_i gives the migration velocity, and finally multiplication by the concentration c_i gives the contribution to the net flux density $\mathbf{N}_i$ due to migration in an electric field.

The second and third terms on the right side of equation 11.1 are the usual terms required to describe nonelectrolytic systems. The species will diffuse from regions of high concentration to regions of lower concentration. The three terms on the right in equation 11.1 thus represent three mechanisms of mass

Electrochemical Systems, Fourth Edition. John Newman and Nitash P. Balsara.

transfer: migration of a charged species in an electric field, molecular diffusion due to a concentration gradient, and convection due to the bulk motion of the medium. Equation 11.1 thus serves to define two *transport properties*, the diffusion coefficient D_i and the mobility u_i.

The current in an electrolytic solution is due to the motion of charged particles, and we can easily express this quantitatively:

$$\mathbf{i} = F\sum_i z_i \mathbf{N}_i. \tag{11.2}$$

Here, $\mathbf{i}$ is the current density expressed in amperes per square centimeter, and z_iF is again the charge per mole.

Next we need to state a material balance for a minor component:

$$\underset{\text{accumulation}}{\frac{\partial c_i}{\partial t}} = \underset{\text{net input}}{-\nabla \cdot \mathbf{N}_i} + \underset{\text{production (in homogeneous chemical reactions)}}{R_i}. \tag{11.3}$$

In engineering parlance, accumulation is equal to input minus output plus production. For a differential volume element, accumulation is simply the time rate of change of concentration.

For the net input, it is necessary to compute the net amount of material brought in by the different fluxes on the various faces of the volume element (see Figure 11.1).

The difference in fluxes contributes to accumulation or depletion.

$$\lim_{\Delta x \to 0} \frac{N_{ix}|_x - N_{ix}|_{x+\Delta x}}{\Delta x} = -\frac{\partial N_{ix}}{\partial x}.$$

The Δx in the denominator comes from dividing by the volume of the element.

The production per unit volume R_i involves homogeneous chemical reactions in the bulk of the solution, but not any electrode reactions, which occur at the boundaries of the solution. In electrochemical systems, the reaction is frequently restricted to electrode surfaces, in which case R_i is zero.

Finally, we can say that the solution is electrically neutral.

$$\sum_i z_i c_i = 0. \tag{11.4}$$

Such electroneutrality is observed in all solutions except in a thin double charge layer near electrodes and other boundaries. This double layer may be of the order of 1 to 10 nm in thickness. The phenomena related to the double layer at electrodes can usually be taken into account by the boundary conditions. Hence, it is reasonable to adopt equation 11.4 in a description of the bulk of a solution. The validity of this equation will be considered again in Section 11.8.

These four equations provide a consistent description of transport processes in electrolytic solutions, and their physical significance is worth repeating. The first states that species in the solution can move

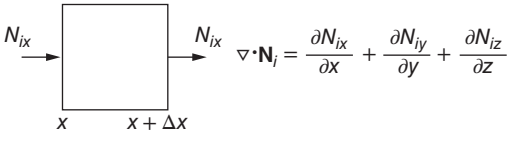

Figure 11.1 Accumulation due to differences in the fluxes at the faces of a volume element.

by migration, diffusion, and convection. The second equation merely says that the flux of a charged species constitutes an electric current. The third is a material balance for a species, and the fourth is the condition of electroneutrality. Although the specific description may be refined, any theory of electrolytic solutions needs to consider these physical phenomena.

Note that in order to solve a mass-transfer problem it is necessary to know the convective velocity **v**. This requires the equations of fluid mechanics, which are discussed in Chapter 15. The analysis of electrochemical systems by means of the above differential equations requires in addition a statement of the geometry of the system and of conditions existing at boundaries of the system. Important among these are the electrode kinetics treated in Part B. Boundary conditions will be discussed as they arise, mostly in Part D (see also equations 11.25 to 11.27).

We can also obtain physical insight by considering the validity of the above four equations. The validity of the electroneutrality equation 11.4 will be discussed separately in Section 11.8, where we come to the conclusion that electroneutrality is an *accurate approximation*. Equations 11.2 and 11.3 can be regarded as expressions of basic physical laws, stating that current is due to the motion of charged particles and that individual species either are conserved or take part in homogeneous chemical reactions. However, the rate processes in the expression of the production rate and the flux density introduce uncertainties. The production rate involves chemical kinetics, for which rate expressions are neither predictable nor general. The flux density has been expressed by equation 11.1, but even this breaks down in concentrated solutions.

It is always possible to write mathematical expressions for the basic physical laws of conservation of mass, energy, and momentum in terms of the fluxes of these quantities, but the difficult part is to find correct expressions for these fluxes in terms of the appropriate driving forces in the system. We are not speaking of the microscopic, theoretical explanation of transport properties, but rather of the macroscopic definition of the appropriate transport properties.

The flux equation 11.1 breaks down, first of all, because migration and diffusion fluxes must be defined with respect to some average velocity of the fluid (**v** in equation 11.1), and the flux relations so defined must be consistent with this choice. We have not been careful to specify the fluid velocity. In a concentrated solution, it is not just the solvent velocity that contributes to the average velocity. This difficulty is avoided here by not applying equation 11.1 to the solvent and by restricting ourselves to dilute solutions where **v** is essentially the same as the velocity of the solvent.

Furthermore, the flux equation 11.1 incorrectly defines the transport properties; in fact, it defines an incorrect number of transport properties. This situation arises because equation 11.1 considers the interaction or friction force of a solute species with the solvent and essentially neglects interactions with the other solutes.

Finally, the driving force for diffusion should be an activity gradient, and activity gradients are identical to concentration gradients only in extremely dilute solutions. However, in a generalization of equation 11.1, one should avoid the use of single ionic activity coefficients, which are not physically measurable. Furthermore, care is needed in the definition of potentials in media of varying composition (see Chapter 3). One concludes that the correct driving force for both diffusion and migration is the gradient of an electrochemical potential (discussed in Chapter 2), and any decomposition of this into ∇c_i and $c_i \nabla \Phi$ is unnecessary.

The multicomponent diffusion equation, presented in Section 12.1, avoids these difficulties. Nevertheless, equation 11.1 is recommended for general use because it is prevalent, both explicitly and implicitly, in the electrochemical literature and because it gives a good account of the physical processes involved without excessive complication. One should remember that it is strictly valid only in dilute solutions.

The remaining sections of this chapter are designed to illustrate further the meaning, the application, and the limitations of the basic transport laws discussed here.

11.2 CONDUCTIVITY, DIFFUSION POTENTIALS, AND TRANSFERENCE NUMBERS

Let us expand the expression for the current density in the solution, equation 11.2, in terms of the species fluxes, equation 11.1:

$$\mathbf{i} = -F^2 \nabla\Phi \sum_i z_i^2 u_i c_i - F \sum_i z_i D_i \nabla c_i + F\mathbf{v} \sum_i z_i c_i. \tag{11.5}$$

By virtue of electroneutrality, the last term on the right is zero, which is equivalent to saying that bulk motion of a fluid with no charge density can contribute nothing to the current density. When there are no concentration variations in the solution, this equation reduces to the common concept of electrolytic conductance:

$$\mathbf{i} = -\kappa \nabla\Phi, \tag{11.6}$$

where

$$\kappa = F^2 \sum_i z_i^2 u_i c_i \tag{11.7}$$

is the conductivity of the solution. This is an expression of Ohm's law, valid for electrolytes in the absence of concentration gradients.

Still with no concentration variations, we can say that the current carried by species j is

$$t_j \mathbf{i} = -F^2 z_j^2 u_j c_j \nabla\Phi = \frac{z_j^2 u_j c_j}{\sum_i z_i^2 u_i c_i} \mathbf{i}, \tag{11.8}$$

where

$$t_j = \frac{z_j^2 u_j c_j}{\sum_i z_i^2 u_i c_i} \tag{11.9}$$

is the fraction of the current carried by species j and is also known as the transference number. In such a case, it is convenient and proper to identify a migration flux density of species i:

$$\mathbf{N}_i^{\text{migr}} = -z_i u_i F c_i \nabla\Phi = \frac{t_i}{z_i F} \mathbf{i}. \tag{11.10}$$

When there are concentration gradients, the current density is not proportional to the electric field, and Ohm's law does not hold. Due to the diffusion current represented by the second term in equation 11.5, the current density could even have a different direction from the electric field. One can turn equation 11.5 around:

$$\nabla\Phi = -\frac{\mathbf{i}}{\kappa} - \frac{F}{\kappa} \sum_i z_i D_i \nabla c_i, \tag{11.11}$$

and say the same thing backwards. Even in the absence of current, there may be a gradient of potential. The second term in this equation gives rise to what is known as the diffusion potential. If all the diffusion coefficients were equal, this would be zero by electroneutrality. In conductivity measurements an alternating current is used so that concentration differences will not build up (and so as to reduce polarization at the electrodes).

The conductivity and the transference number are additional transport properties, defined in equations 11.7 and 11.9 in terms of the ionic mobilities introduced earlier. These transport properties

have relevance in solutions of varying composition, but they do not retain their same physical significance. Ohm's law is valid, and the transference number has the physical meaning of the fraction of current carried by an ionic species only in the absence of concentration gradients.

When there are concentration gradients, one can identify contributions to the species flux density $\mathbf{N}_i$ due to migration, molecular diffusion, and convection, according to equation 11.1. However, the current density in equation 11.5 is composed of portions due to migration and to diffusion, and it is no longer proper to identify the migration flux according to the last expression in equation 11.10, although one finds in the literature such deceptively simple statements as

$$\mathbf{N}_i^{\text{diff}} = \frac{1 - t_i}{z_i F}\mathbf{i}. \tag{11.12}$$

It should be apparent that the transference number and the expression of the migration flux in terms of current density should be used with caution in cases where concentration gradients exist.

11.3 CONSERVATION OF CHARGE

It is a physical law of nature that electric charge is conserved. This fact is already built into the basic transport relations. Multiplication of equation 11.3 by $z_i F$ and addition over species yield

$$\frac{\partial}{\partial t} F \sum_i z_i c_i = -\nabla \cdot F \sum_i z_i \mathbf{N}_i + F \sum_i z_i R_i. \tag{11.13}$$

The last term will be zero as long as all the homogeneous reactions giving rise to the R_i are electrically balanced. Then, the term on the left is the time rate of change of the charge density; the first term on the right is minus the divergence of the current density; and the equation describes conservation of charge. In view of the assumption of electroneutrality, the equation reduces to

$$\nabla \cdot \mathbf{i} = 0. \tag{11.14}$$

In physical terms, our line of reasoning has been that charge is carried by particles of matter and that conservation (or electrically balanced reaction) of these particles implies conservation of charge.

Insertion of equation 11.5 into equation 11.14 yields

$$\nabla \cdot (\kappa \nabla \Phi) + F \sum_i z_i \nabla \cdot (D_i \nabla c_i) = 0. \tag{11.15}$$

In the absence of concentration gradients and with a uniform value of the conductivity κ, this reduces to

$$\nabla^2 \Phi = 0, \tag{11.16}$$

that is, the potential satisfies Laplace's equation in a region of uniform composition.

11.4 THE BINARY ELECTROLYTE

By a binary electrolyte we mean the solution of a single salt composed of one kind of cation and one kind of anion. At times the term has been known to denote a symmetric electrolyte, which dissociates

into equal numbers of anions and cations. Let the positive species be denoted by the subscript + and the negative species by the subscript −. The mobilities and the diffusion coefficients will be assumed to be constant.

Let ν_+ and ν_- be the numbers of cations and anions produced by the dissociation of one molecule of electrolyte. The concentration of the electrolyte is then defined by

$$c = \frac{c_+}{\nu_+} = \frac{c_-}{\nu_-}, \tag{11.17}$$

so that the electroneutrality equation 11.4 is satisfied. Substitution of the flux equation 11.1 into the material balance equation 11.3 with $R_i = 0$ yields equations for each of the ionic species:

$$\frac{\partial c}{\partial t} + \mathbf{v} \cdot \nabla c = z_+ u_+ F \nabla \cdot (c \nabla \Phi) + D_+ \nabla^2 c. \tag{11.18}$$

$$\frac{\partial c}{\partial t} + \mathbf{v} \cdot \nabla c = z_- u_- F \nabla \cdot (c \nabla \Phi) + D_- \nabla^2 c. \tag{11.19}$$

Subtraction gives

$$\left(z_+ u_+ - z_- u_-\right) F \nabla \cdot (c \nabla \Phi) + \left(D_+ - D_-\right) \nabla^2 c = 0. \tag{11.20}$$

This can be used to eliminate the potential from either of equations 11.18 and 11.19, with the result

$$\frac{\partial c}{\partial t} + \mathbf{v} \cdot \nabla c = D \nabla^2 c, \tag{11.21}$$

where

$$D = \frac{z_+ u_+ D_- - z_- u_- D_+}{z_+ u_+ - z_- u_-}. \tag{11.22}$$

Equation 11.21 is called the equation of convective diffusion. This equation or its analogue applies to heat transfer or nonelectrolytic mass transfer, and its solutions have been extensively studied in the literature. Consequently, it is possible to apply many of these results to electrochemical systems with only minor changes in notation. This will be taken up in Part D.

Equation 11.21 shows that in the absence of current a salt, such as copper sulfate in water, will behave like one species because of the requirement of electroneutrality. The observed diffusion coefficient D represents a compromise between the diffusion coefficient of the anion and the cation.[1] If these diffusion coefficients are different, the species will tend to separate, thereby creating a minute charge density that prevents further separation. The charge density creates a nonuniform potential that acts to speed up the ion with the smaller diffusion coefficient and slow down the ion with the larger diffusion coefficient.

But equation 11.21 was derived without assuming that the current density is zero. The interesting and useful conclusion is that the concentration distribution in a solution of a single salt is governed by the same equation as the concentration distribution of a neutral species, even when a current is being passed.

The potential distribution in a solution of a single salt is to be determined from equation 11.20. An integrated form of this equation can be obtained from the expression 11.2 for the current density

$$-\frac{\mathbf{i}}{z_+ \nu_+ F} = (z_+ u_+ - z_- u_-) F c \nabla \Phi + (D_+ - D_-) \nabla c. \tag{11.23}$$

This equation shows directly how the potential gradient is related to the concentration gradient and the difference in diffusion coefficients for the diffusion of a salt in the absence of current:

$$F\nabla\Phi = -\frac{D_+ - D_-}{z_+u_+ - z_-u_-}\nabla \ln c. \tag{11.24}$$

This is the diffusion potential, discussed in connection with equation 11.11, which prevents any substantial separation of charge in a diffusing system. Equation 11.23 is analogous to equation 11.5, while equation 11.20 is analogous to equation 11.14.

In situations where the boundary conditions permit, equation 11.21 can be solved first for the concentration distribution. If the current density distribution is known, the potential distribution can then be readily determined from equation 11.23. If the current density distribution is not known, the potential distribution must be determined from equation 11.20 and the current distribution subsequently from equation 11.23.

However, it is frequently possible to determine the current density distribution at an electrode from the concentration distribution but without the potential distribution. The normal component of the velocity will be zero at the electrode. Let us also assume that only the cation reacts at the electrode, a common situation for a binary electrolyte. Then, the normal components of the cation and anion flux densities at the electrode are

$$N_{+y} = \frac{i_y}{z_+F} = -z_+u_+F\nu_+c\frac{\partial\Phi}{\partial y} - D_+\nu_+\frac{\partial c}{\partial y}, \tag{11.25}$$

and

$$N_{-y} = 0 = -z_-u_-F\nu_-c\frac{\partial\Phi}{\partial y} - D_-\nu_-\frac{\partial c}{\partial y}, \tag{11.26}$$

where y is the distance from the electrode. Elimination of the potential gradient gives

$$\frac{i_y}{z_+\nu_+F} = -\frac{z_-u_-D_+ - z_+u_+D_-}{z_-u_-}\frac{\partial c}{\partial y} = -\frac{D}{1-t_+}\frac{\partial c}{\partial y} \quad \text{at } y = 0. \tag{11.27}$$

Here D is given by equation 11.22, and t_+ is the cation transference number given by equation 11.9, which reduces to

$$t_+ = 1 - t_- = \frac{z_+u_+}{z_+u_+ - z_-u_-} \tag{11.28}$$

for a binary electrolyte. Equation 11.27 shows that the current density is directly related to the concentration derivative at the electrode.

In this discussion, we have treated the diffusion coefficients and mobilities (but not the conductivity) as constants. Usually these quantities depend upon the concentration. However, restriction to a constant-property fluid is common in the literature and has advantages of simplicity and generality. If we relax the assumption of constant properties, equation 11.23 still stands, but equation 11.21 is to be replaced by

$$\frac{\partial c}{\partial t} + \mathbf{v}\cdot\nabla c = \nabla\cdot(D\nabla c) - \frac{\mathbf{i}\cdot\nabla t_+}{z_+\nu_+F}, \tag{11.29}$$

where D is given by equation 11.22 and t_+ by equation 11.28. The first term on the right is the expected generalization of the diffusion term in the convective-diffusion equation for a varying diffusion coefficient.

11.5 SUPPORTING ELECTROLYTE

When the flux equation 11.1 is inserted into the material-balance equation 11.3, one obtains

$$\frac{\partial c_i}{\partial t} + \mathbf{v} \cdot \nabla c_i = z_i F \nabla \cdot (u_i c_i \nabla \Phi) + \nabla \cdot (D_i \nabla c_i) + R_i. \tag{11.30}$$

This also uses the incompressibility of the fluid ($\nabla \cdot \mathbf{v} = 0$). The equation is useful for describing the medium since the flux density has been eliminated, and it could therefore be used to determine the concentration distribution when the velocity and potential distributions are known. Equation 11.1 is still useful for formulating boundary conditions.

For a mass-transfer problem in forced convection, the velocity distribution can be assumed to be known, but usually the potential distribution needs to be determined. This means that equation 11.30 for each ionic species must be solved simultaneously, the electroneutrality equation 11.4 providing the additional relation needed to determine the potential. That is to say, all the equations are coupled through the potential. The problem thus posed is quite complicated.

We have already seen the simplification possible when only two ionic species are present. Then the requirement of electroneutrality allows the potential to be eliminated, and the concentration of the electrolyte satisfies the equation of convective diffusion. A similar simplification applies when migration and reactions in the bulk of the solution can be neglected. Then equation 11.30 becomes

$$\frac{\partial c_i}{\partial t} + \mathbf{v} \cdot \nabla c_i = D_i \nabla^2 c_i, \tag{11.31}$$

for a constant diffusion coefficient. This is again the equation of convective diffusion.

In mass-transfer studies in electrolytic systems, in studies of electrode kinetics, and in some commercial electrochemical cells, a *supporting* or *indifferent* electrolyte is frequently added to increase the conductivity of the solution and thereby reduce the electric field. The mass transfer of minor species then will be primarily due to diffusion and convection, and the effect of migration can be qualitatively dismissed. The concentration distribution is then governed by equation 11.31.

Levich[2] has given a more formal statement of this procedure, one that also allows investigation of the concentration distribution of the major species. Let us develop this for three ionic components, the third of which is present in small amount. We do not consider the possibility of reaction in the bulk of the solution, that is, $R_i = 0$. In the zero approximation, one assumes that the minor constituent is absent and solves for the potential and the concentration of the major species by using the method for binary electrolytes (see Section 11.4). Let this solution be denoted by c_1^0, c_2^0, and Φ^0.

Then we can write

$$\begin{aligned} c_1 &= c_1^0 + c_1^{(1)}, \quad & c_2 &= c_2^0 + c_2^{(1)}, \\ c_3 &= c_3^{(1)}, & \Phi &= \Phi^0 + \Phi^{(1)}. \end{aligned} \tag{11.32}$$

These are substituted into the basic equations; and, in the first approximation, terms of degree greater than one in $c_1^{(1)}$, $c_2^{(1)}$, $c_3^{(1)}$, and $\Phi^{(1)}$ are dropped. The equations for the first approximation are then linear.

In many cases of importance, the minor constituent is the only one taking part in electrode reactions, and the zero solution yields constants for c_1^0, c_2^0, and Φ^0. This applies to mass-transfer studies, where the system is selected so that the behavior of the minor component is of interest. For commercial cells, a loss of current efficiency would result if the supporting electrolyte were to participate in electrode

reactions, hence the name *indifferent* electrolyte. For this case, the equations for the first approximation reduce to

$$\frac{\partial c_3^{(1)}}{\partial t} + \mathbf{v} \cdot \nabla c_3^{(1)} = D_3 \nabla^2 c_3^{(1)}, \tag{11.33}$$

$$\frac{\partial c_1^{(1)}}{\partial t} + \mathbf{v} \cdot \nabla c_1^{(1)} = D_e \nabla^2 c_1^{(1)} + \frac{z_3 u_1 (D_2 - D_3)}{z_1 u_1 - z_2 u_2} \nabla^2 c_3^{(1)}, \tag{11.34}$$

and

$$-\frac{\mathbf{i}}{z_1 F} = (z_1 u_1 - z_2 u_2) F c_1^0 \nabla \Phi^{(1)} + (D_1 - D_2) \nabla c_1^{(1)} + \frac{z_3}{z_1} (D_3 - D_2) \nabla c_3^{(1)}, \tag{11.35}$$

where

$$D_e = \frac{z_1 u_1 D_2 - z_2 u_2 D_1}{z_1 u_1 - z_2 u_2} \tag{11.36}$$

is the diffusion coefficient of the supporting electrolyte. Here c_2 has been eliminated by means of the electroneutrality equation, and the mobilities and diffusion coefficients have been assumed to be constant.

The minor species obeys the equation of convective diffusion with its ionic diffusion coefficient; equation 11.33 is the same as equation 11.31. The supporting electrolyte obeys the equation of convective diffusion with the diffusion coefficient of the salt, but with an additional term of interaction with the minor species. The equations are to be solved in the order given: first, for the concentration of the minor component, second, for the concentration of the supporting electrolyte, and finally, for the potential from equation 11.35. In case the current is not known at this point, one can take the divergence of this equation (see equation 11.14) and solve a second-order differential equation for the potential.

It is not difficult to extend the development to a case where two minor constituents are involved in the electrode reaction but the major species are not involved. An example would be an oxidation–reduction reaction with a supporting electrolyte. Whether the above treatment applies to the reaction of a nonelectrolyte, such as oxygen, will be considered in the problems (see also Section 19.3).

The treatment of a supporting electrolyte can be considered to be the beginning of a perturbation expansion of the problem. The expansion parameter would be a characteristic concentration of the minor species divided by a characteristic concentration of the supporting electrolyte. The procedure is, of course, valid only when this ratio is small. In practice, one is usually content to solve equation 11.33 for the minor component.

The concept of supporting electrolytes raises a number of interesting and paradoxical questions. Some of these are considered in Chapter 19.

11.6 MULTICOMPONENT DIFFUSION BY ELIMINATION OF THE ELECTRIC FIELD

Multicomponent diffusion in nonelectrolytic solutions has been treated in the literature. In concentrated solutions, the diffusing species interact with each other; but in dilute solutions, each species diffuses independently according to its own concentration gradient and diffusion coefficient. However, in a dilute electrolytic solution even in the absence of current, the solute species do not diffuse independently. A diffusion potential will be established, and the diffusing ions will interact with it.

Substitution of equation 11.11 into the flux equation 11.1 yields

$$\mathbf{N}_i = \frac{t_i}{z_i F} \mathbf{i} - D_i \nabla c_i + \mathbf{v} c_i + \frac{t_i}{z_i} \sum_j z_j D_j \nabla c_j. \tag{11.37}$$

To satisfy the condition of electroneutrality, the concentration of an ionic species n can be eliminated:

$$z_n c_n = -\sum_{j \neq n} z_j c_j, \tag{11.38}$$

with the result

$$\mathbf{N}_i = \frac{t_i}{z_i F}\mathbf{i} - D_i \nabla c_i + \mathbf{v} c_i + \frac{t_i}{z_i} \sum_j z_j (D_j - D_n) \nabla c_j. \tag{11.39}$$

These equations for all minor species except species n can be substituted into the appropriate material balances (equation 11.3) to give

$$\frac{\partial c_i}{\partial t} + \mathbf{v} \cdot \nabla c_i = D_i \nabla^2 c_i + R_i - \frac{\mathbf{i} \cdot \nabla t_i}{z_i F} - \sum_j \frac{z_j}{z_i} (D_j - D_n) \nabla \cdot (t_i \nabla c_j). \tag{11.40}$$

Even in the absence of current and homogeneous chemical reactions, diffusion of species in an electrolytic solution is coupled in much the same way as diffusion in concentrated, multicomponent, nonelectrolytic solutions. One may also note that the migration flux density $-z_i u_i F c_i \nabla \Phi$ is not the same as $t_i \mathbf{i} / z_i F$ when there are concentration gradients. This was discussed before in connection with equation 11.10.

11.7 MOBILITIES AND DIFFUSION COEFFICIENTS

We mentioned in Section 11.1 that a single driving force, the gradient of the electrochemical potential of a species, is appropriate for both diffusion and migration. We are thus led to expect that the ionic mobility and diffusion coefficient are related. This relationship is provided by the Nernst–Einstein equation

$$D_i = RTu_i. \tag{11.41}$$

This equation is strictly applicable only at infinite dilution, although its failure is related to the approximate nature of the flux equation 11.1. The quantities D_i and u_i in equation 11.41 are not adequately defined at nonzero concentrations, and further inquiry into the nature of this equation should await the consideration of concentrated electrolytes in Chapter 12.

With the Nernst-Einstein relation, equations 11.7 and 11.41 can be combined to give

$$\kappa = \frac{F^2 z_+ c_+ (z_+ D_+ - z_- D_-)}{RT}, \tag{11.42}$$

and the expression 11.22 for the diffusion coefficient of a binary electrolyte becomes

$$D = \frac{D_+ D_- (z_+ - z_-)}{z_+ D_+ - z_- D_-}. \tag{11.43}$$

One commonly encounters the statement that "a salt bridge used to eliminate liquid-junction potentials should contain a salt with equal cation and anion transference numbers." (Liquid-junction potentials are diffusion potentials that arise when one connects two electrolytic solutions of different composition; see Chapter 6.) This can be interpreted with the aid of the Nernst–Einstein equation. For the solution of a single salt, the transference numbers are nominally independent of concentration (due to electroneutrality) and are given by equation 11.28. With equation 11.41 we have

$$t_+ = \frac{z_+ D_+}{z_+ D_+ - z_- D_-}, \quad t_- = \frac{-z_- D_-}{z_+ D_+ - z_- D_-}. \tag{11.44}$$

TABLE 11.1 Values of equivalent conductances and diffusion coefficients of selected ions at infinite dilution in water at 25°C

Ion	z_i	λ_i^0 (S·cm^2/mol)	$D_i \times 10^5$ (cm^2/s)	Ion	z_i	λ_i^0 (S·cm^2/mol)	$D_i \times 10^5$ (cm^2/s)
H^+	1	349.8	9.312	OH^-	−1	197.6	5.260
Li^+	1	38.69	1.030	Cl^-	−1	76.34	2.032
Na^+	1	50.11	1.334	Br^-	−1	78.3	2.084
K^+	1	73.52	1.957	I^-	−1	76.8	2.044
NH_4^+	1	73.4	1.954	NO_3^-	−1	71.44	1.902
Ag^+	1	61.92	1.648	HCO_3^-	−1	41.5	1.105
Tl^+	1	74.7	1.989	HCO_2^-	−1	54.6	1.454
Mg^{2+}	2	53.06	0.7063	$CH_3CO_2^-$	−1	40.9	1.089
Ca^{2+}	2	59.50	0.7920	SO_4^{2-}	−2	80	1.065
Sr^{2+}	2	59.46	0.7914	$Fe(CN)_6^{3-}$	−3	101	0.896
Ba^{2+}	2	63.64	0.8471	$Fe(CN)_6^{3-}$	−4	111	0.739
Cu^{2+}	2	54	0.72	IO_4^-	−1	54.38	1.448
Zn^{2+}	2	53	0.71	ClO_4^-	−1	67.32	1.792
La^{3+}	3	69.5	0.617	BrO_3^-	−1	55.78	1.485
$Co(NH_3)_6^{3+}$	3	102.3	0.908	HSO_4^-	−1	50	1.33
Fe^{2+}	2	54	0.72	Fe^{3+}	3	68.4	0.61

Equality of the transference numbers, coupled with the Nernst–Einstein equation, implies that the diffusion coefficients are equal for symmetric salts ($z_+ = -z_-$). Then, the concentration can vary without giving rise to diffusion potentials (see equation 11.24 or 11.11). (We still do not have a satisfactory answer to the question of what happens at the junctions of the salt bridge with the two solutions we were trying to connect.)

Alternatively, equation 11.11 can now be written, by means of the Nernst–Einstein relation, as

$$F\nabla\Phi = -\frac{F}{\kappa}\mathbf{i} - RT\sum_i \frac{t_i}{z_i}\nabla \ln c_i. \tag{11.45}$$

Table 11.1 gives an indication of the magnitudes of ionic diffusion coefficients and mobilities. Ionic mobilities are usually not found directly in the literature; instead values of *ionic equivalent conductances* are reported. These are related to ionic mobilities by

$$\lambda_i = |z_i|F^2 u_i. \tag{11.46}$$

Ionic diffusion coefficients can then be calculated with the aid of the Nernst–Einstein relation:

$$D_i = \frac{RT\lambda_i}{|z_i|F^2}. \tag{11.47}$$

Table 11.1 shows that most ionic diffusion coefficients in aqueous solution are about 1 or 2×10^{-5} cm^2/s. Exceptions are hydrogen ions and hydroxyl ions, for which D_i values are 9.3 and 5.3×10^{-5} cm^2/s.

The equivalent conductance Λ of a single salt is the sum of the values for the two ions

$$\Lambda = \lambda_+ + \lambda_- \tag{11.48}$$

and is related to the conductivity of the solution by

$$\Lambda = \frac{\kappa}{z_+ \nu_+ c}. \tag{11.49}$$

The value of Λ will thus be about 100 S·cm^2/mol except for acids and bases. The conductivity of the solution is obtained by multiplying Λ by the equivalent concentration $z_+\nu_+c$, but this should be in mol/cm^3 in order for κ to be in S/cm. Thus, the conductivity of 0.6 M NaCl solution (roughly sea water) will be about 0.04 S/cm when due allowance is made for the concentration dependence of Λ.

The transference number of an ion in a binary salt solution will be

$$t_+ = 1 - t_- = \frac{\lambda_+}{\lambda_+ + \lambda_-} \tag{11.50}$$

and will be close to 0.5 except for acids and bases, where t_+ can be as high as 0.8 or as low as 0.2. For solutions with an excess of inert electrolyte, the transference number of a minor ionic species is proportional to its concentration and inversely proportional to the concentration of the supporting electrolyte and hence will be small.

Ionic equivalent conductances, such as those in Table 11.1, are ordinarily determined by measuring the equivalent conductance Λ and the transference number t_+ for solutions of single salts and extrapolating the values so obtained to infinite dilution. Equations 11.48 and 11.50 then yield λ_+ and λ_-. Good agreement is usually obtained for, say, λ_i for chloride ions determined from solutions of NaCl and separately from solutions of KCl. Diffusion coefficients calculated from equation 11.43 are also in good agreement with values measured at high dilution.

An approximate guide to the temperature dependence of ionic diffusion coefficients is provided by the Stokes–Einstein relationship

$$D_i = \frac{RT}{6\pi\mu R_i}, \tag{11.51}$$

where μ is the viscosity of the solution and R_i is the radius of a hydrated ion. Thus, ionic diffusion coefficients and equivalent conductances can vary by 2 to 3 percent per kelvin. This is a fairly strong temperature dependence. Equation 11.51 can also be used to estimate the concentration dependence of ionic diffusion coefficients.

11.8 ELECTRONEUTRALITY AND LAPLACE'S EQUATION

The electroneutrality equation 11.4 is not a fundamental law of nature. A more nearly correct relationship would be Poisson's equation, which, for a medium of uniform dielectric constant, reads (see equation 3.8)

$$\nabla^2\Phi = -\frac{F}{\epsilon}\sum_i z_i c_i \tag{11.52}$$

and relates the charge density to the Laplacian of the electric potential. The proportionality constant in this equation is Faraday's constant F divided by the permittivity or dielectric constant ϵ. The value of this proportionality constant is quite large (1.392×10^{16} V·cm/mol for a relative dielectric constant of 78.303), so that what, in terms of concentrations, would be a negligible deviation from electroneutrality amounts to a considerable deviation from Laplace's equation for the potential.

Another way of saying the same thing is that F/ϵ is so large that an appreciable separation of charge would require prohibitively large electric forces. Still another way is that the conductivity is

so large that any initial charge density would be neutralized very rapidly or would rapidly flow to the boundaries of the solution (see Problem 11.12).

The equations given in Section 11.1, with appropriately stated boundary conditions, are sufficient to describe transport processes in electrolytic solutions. Therefore, the use of both Poisson's equation and electroneutrality would be inconsistent. The proper thing to do is to *replace* Poisson's equation in the analysis by the electroneutrality condition (11.4) on the basis of the large value of F/ϵ. Thus, electroneutrality does *not* imply Laplace's equation for the potential

$$\nabla^2\Phi = 0; \tag{11.53}$$

this would be inconsistent. Of course, one could retain Poisson's equation and discard the assumption of electroneutrality in the description of electrochemical systems. However, the close adherence of electrolytic solutions to the condition of electroneutrality, as well as the consequent mathematical simplification in the treatment of specific problems, justifies the approach taken here. For the perturbation analysis of phenomena near an electrode with the use of Poisson's equation, see Refs. [3, 4].

Electroneutrality and Laplace's equation are firmly entrenched in electrochemistry, but the assumption of electroneutrality does not imply that Laplace's equation holds for the potential. In many cases, the distribution of potential and current in cells of various configurations is determined from Laplace's equation for the potential and Ohm's law

$$\mathbf{i} = -\kappa\nabla\Phi \tag{11.54}$$

for the current. This procedure is valid when the current is not appreciably limited by mass transfer of reactants to the electrodes. Then the concentrations are fairly constant, and equation 11.54 applies with a fairly constant conductivity. Conservation of charge then yields Laplace's equation for the potential (see equations 11.14 through 11.16). This justification of Laplace's equation is considerably different from the statement that electroneutrality implies Laplace's equation for the potential. The procedure outlined here can be expected to lead to inconsistencies if one subsequently attempts to investigate the detailed behavior of each species in the solution near electrodes.

It should be pointed out that it is not permissible to neglect the charge density in the electrode double layer, since the electric field is indeed very large in this region. This region may be 1 to 10 nm in thickness and is treated in Section 7.4. The double layer can legitimately be regarded as part of the interface and not part of the solution. In extremely dilute solutions, the charge density may also be appreciable compared to the total ionic concentration.

Next we illustrate the validity of the assumption of electroneutrality by means of an example. Let us consider a cell in which a binary electrolyte is used to deposit the cation on the cathode while the anode dissolves and replenishes the solution. Let us further simplify the problem by assuming a steady state with no convection and with variations in only one dimension. This is not supposed to represent a common system; it is merely a test of the electroneutrality assumption. Consider a uniunivalent electrolyte, such as silver nitrate, and use the Nernst–Einstein relation (equation 11.41) throughout.

The procedure is to solve the problem using the electroneutrality equation, and, in the end, the deviation from electroneutrality can be assessed by means of Poisson's equation 11.52. Since the flux of the anion is zero, equation 11.1 yields

$$Fc\frac{d\Phi}{dx} = RT\frac{dc}{dx}. \tag{11.55}$$

Equation 11.23 becomes

$$-\frac{i}{F} = (u_+ + u_-)Fc\frac{d\Phi}{dx} + (D_+ - D_-)\frac{dc}{dx} = 2D_+\frac{dc}{dx}. \tag{11.56}$$

Integration gives the steady-state concentration in terms of the current density,

$$c = c_{\text{avg}} - \frac{i}{2D_+F}\left(x - \frac{1}{2}L\right), \tag{11.57}$$

where c_{avg} is the average concentration in the cell, x is the distance measured from one electrode, and L is the distance between the electrodes.

Now for

$$i = \pm\frac{4D_+Fc_{\text{avg}}}{L} \tag{11.58}$$

the concentration at one electrode will drop to zero, and the *limiting current* is attained. A higher current can be passed only if another electrode reaction occurs. Let us operate at half of the limiting current, so that

$$c = \frac{c_{\text{avg}}}{2}\left(1 + \frac{2x}{L}\right). \tag{11.59}$$

Equation 11.55 gives

$$\frac{d^2\Phi}{dx^2} = -\frac{4RT}{F}\frac{1}{(L+2x)^2}. \tag{11.60}$$

If, at the same time, both electroneutrality and Poisson's equation were exact, this second derivative would be equal to zero, but it is not. Thus, one can see the incompatibility of these relationships.

Let us test the electroneutrality assumption by calculating the charge density and the difference in concentration of anions and cations required to produce this value of $d^2\Phi/dx^2$.

$$\frac{d^2\Phi}{dx^2} = -\frac{4RT}{F}\frac{1}{(L+2x)^2} = -\frac{F}{\epsilon}(c_+ - c_-). \tag{11.61}$$

At 25°C and for a relative dielectric constant of 78.303, $RT/F = 25.692\,\text{mV}$, and $\epsilon RT/F^2 = 1.846 \times 10^{-18}$ mol/cm. For $L = 0.1$ mm and $x = 0.05$ mm, this gives

$$\frac{d^2\Phi}{dx^2} = -256.92\,\text{V/cm}^2 \tag{11.62}$$

and

$$c_+ - c_- = 1.846 \times 10^{-14}\,\text{mol/cm}^3 = 1.846 \times 10^{-11}\,\text{mol/liter}. \tag{11.63}$$

This indicates that the assumption of electroneutrality is very good in electrochemical systems.

11.9 MODERATELY DILUTE SOLUTIONS

When the gradient of the electrochemical potential is used as the driving force for diffusion and migration, the flux density equation 11.1 for an ionic component becomes

$$\mathbf{N}_i = -u_i c_i \nabla\mu_i + c_i\mathbf{v}. \tag{11.64}$$

The driving force per mole is $-\nabla \mu_i$. Multiplication by the mobility u_i gives the velocity for diffusion and migration, and multiplication by the concentration c_i gives the contribution to the net flux $\mathbf{N}_i$. With the use of the Nernst–Einstein relation 11.41, equation 11.64 becomes

$$\mathbf{N}_i = -\frac{D_i c_i}{RT}\nabla \mu_i + c_i \mathbf{v}. \tag{11.65}$$

The use of the electrochemical potential avoids the problem of defining the electric potential in a medium of varying composition. However, substitution of equation 11.64 into the material balance 11.3 yields

$$\frac{\partial c_i}{\partial t} + \mathbf{v} \cdot \nabla c_i = \nabla \cdot (u_i c_i \nabla \mu_i) + R_i. \tag{11.66}$$

Here one does not have a simple equation for the concentration, as in the case of the equation of convective diffusion 11.31, since μ_i depends on the local electrical state as well as the local composition.

One way to proceed is to define an electric potential on the basis of a chosen ionic species n (the *quasi-electrostatic potential*; see equation 3.18):

$$\mu_n = RT \ln c_n + z_n F \Phi. \tag{11.67}$$

Then we can write for the gradient of the electrochemical potential of any species

$$\nabla \mu_i = \nabla \left(\mu_i - \frac{z_i}{z_n}\mu_n \right) + \frac{z_i}{z_n}\nabla \mu_n. \tag{11.68}$$

The term in parentheses now corresponds to a neutral combination of ions and can be expressed as

$$\begin{aligned} \mu_i - \frac{z_i}{z_n}\mu_n &= RT\left[\ln(a_i^\theta c_i f_i) - \frac{z_i}{z_n}\ln(a_n^\theta c_n f_n) \right] \\ &= RT\left(\ln a_i^\theta - \frac{z_i}{z_n}\ln a_n^\theta \right) + RT\left(\ln c_i - \frac{z_i}{z_n}\ln c_n \right) \\ &\quad + RT\left(\ln f_i - \frac{z_i}{z_n}\ln f_n \right). \end{aligned} \tag{11.69}$$

These combinations of $a_i^{\theta\prime}$s and ionic activity coefficients f_i's are well defined according to the considerations of Section 2.3, and there need be no hesitation in their use.

At uniform temperature, equation 11.68 now becomes

$$\nabla \mu_i = RT\nabla \ln c_i + z_i F \nabla \Phi + RT\nabla\left(\ln f_i - \frac{z_i}{z_n}\ln f_n \right), \tag{11.70}$$

and equation 11.65 becomes

$$\mathbf{N}_i = -\frac{z_i D_i F}{RT} c_i \nabla \Phi - D_i \nabla c_i - D_i c_i \nabla\left(\ln f_i - \frac{z_i}{z_n}\ln f_n \right) + c_i \mathbf{v}. \tag{11.71}$$

Let

$$f_{i,n} = \frac{f_i}{f_n^{z_i/z_n}}, \tag{11.72}$$

so that equation 11.71 can be written as

$$\mathbf{N}_i = -\frac{z_i D_i F}{RT} c_i \nabla\Phi - D_i \nabla c_i - D_i c_i \nabla \ln f_{i,n} + c_i \mathbf{v}. \tag{11.73}$$

The electric potential Φ is introduced because we need a means of assessing the electrical state of the solution. Its arbitrariness is indicated by the necessity of choosing a particular ionic species n in equation 11.67. The advantage of this procedure is that the structure of the equations is now essentially the same as that of the dilute-solution theory of Section 11.1. There are flux equations 11.73 and material-balance equations 11.3 for each species, and these correspond to the unknown flux densities $\mathbf{N}_i$ and concentrations c_i. In addition, there is the electroneutrality equation 11.4 corresponding to the unknown potential Φ. Calculation procedures worked out for the dilute-solution theory can still be applied here.

The equations are now more complicated than before because the activity coefficients $f_{i,n}$ relative to species n depend on the local composition of the solution. Here the thermodynamic properties of multicomponent solutions, discussed in Section 4.5, can be applied to express these activity coefficients in terms of the concentrations. This procedure also shows how activity coefficients can be introduced into the dilute-solution theory without using activity coefficients of individual ions. The arbitrariness in the potential Φ and the reference of ionic activities to the species n reflect in a complementary manner the arbitrariness in selecting species n in equation 11.67. However, the potential Φ is well defined, though arbitrary, and can be used to determine relationships of the electrical state at phase boundaries.

At the same time, this procedure illuminates the limitations of the dilute-solution theory. For sufficiently dilute solutions, $f_{i,n} \to 1$ (see equation 2.19). The use of an electric potential Φ in the dilute-solution theory is therefore not vague; which species n is chosen becomes immaterial when the solution is so dilute that $f_{i,n} \to 1$. One also sees that variations in $f_{i,n}$ are neglected in the dilute-solution theory. This theory works fairly well in moderately concentrated solutions, not so much because $f_{i,n}$ is close to 1 as because variations in $f_{i,n}$ can be neglected.

The use of electrochemical potentials and the considerations of activity-coefficient variations might appear to be the most important first correction to dilute-solution theory and have been treated as such in references [5, 6] and in Chapter 6 on the calculation of the potentials of cells with liquid junctions. However, the variation of ionic diffusion coefficients with concentration may be equally important. It should also be recalled that interactions between a diffusing species and species other than the solvent are not included in equation 11.65 or 11.73 and that the fluid velocity $\mathbf{v}$ has not been carefully defined. These are considered in the next chapter.

PROBLEMS

11.1 Write down expressions for the diffusion coefficient D of the electrolyte, the cation transference number t_+, and the conductivity κ for solutions of sulfuric acid when the electrolyte is assumed to dissociate either as

$$H_2SO_4 \rightleftharpoons H^+ + HSO_4^-$$

or as

$$H_2SO_4 \rightleftharpoons 2H^+ + SO_4^{2-}.$$

Make numerical comparisons for these quantities on the basis of the information given in Section 11.7.

11.2 At the negative electrode in a lead–acid battery, the reaction is

$$\mathrm{Pb}(s) + \mathrm{SO_4^{2-}} \rightleftharpoons \mathrm{PbSO_4}(s) + 2\mathrm{e^-}.$$

Regard the solution as a binary electrolyte of $\mathrm{H_2SO_4}$ dissociated into $\mathrm{H^+}$ and $\mathrm{SO_4^{2-}}$ ions and show that the current density at the electrode surface is related to the concentration gradient by

$$\frac{i_y}{z_-\nu_-F} = -\frac{D}{1-t_-}\frac{\partial c}{\partial y} \quad \text{at } y = 0,$$

analogous to equation 11.27. Discuss any difficulties presented by the presence of the solid $\mathrm{PbSO_4}$ at the electrode.

11.3 At the positive electrode in a lead–acid battery, the reaction is

$$\mathrm{PbO_2}(s) + \mathrm{SO_4^{2-}} + 4\mathrm{H^+} + 2\mathrm{e^-} \rightleftharpoons \mathrm{PbSO_4}(s) + 2\mathrm{H_2O}.$$

Regard the solution as a binary electrolyte of $\mathrm{H_2SO_4}$ dissociated into $\mathrm{H^+}$ and $\mathrm{SO_4^{2-}}$ ions, and show that the current density at the electrode surface is related to the concentration gradient by

$$\frac{i_y}{F} = -\frac{2D}{2-t_+}\frac{\partial c}{\partial y} \quad \text{at } y = 0,$$

analogous to equation 11.27. Discuss any difficulties presented by the presence of the solid $\mathrm{PbSO_4}$ at the electrode.

11.4 The treatment of supporting electrolyte in Section 11.5 should be applicable to the reaction of a dissolved, neutral species such as oxygen:

$$\mathrm{O_2} + 2\mathrm{H_2O} + 4\mathrm{e^-} \rightleftharpoons 4\mathrm{OH^-}.$$

Would the concentration of supporting electrolyte change at all near the electrode surface? Equation 11.34 suggests that it would not since $z_3 = 0$ in this case. Sketch the concentration profiles for the various species when the supporting electrolyte is

(a) NaOH

(b) NaCl

(c) HCl

Rationalize the shape of each profile in terms of the net flux density of the species determined by the electrode reaction and the contributions of diffusion, migration, and convection to this flux density. Remember that the condition of electroneutrality must be satisfied.

For NaCl as a supporting electrolyte, there must be two minor species, $\mathrm{O_2}$ and $\mathrm{OH^-}$. For HCl as a supporting electrolyte, it should be convenient to write the electrode reaction as

$$\mathrm{O_2} + 4\mathrm{H^+} + 4\mathrm{e^-} \rightleftharpoons 2\mathrm{H_2O}.$$

11.5 The diffusion coefficients of cupric ions and sulfate ions at infinite dilution are 0.713×10^{-5} and 1.065×10^{-5} cm^2/s, respectively at 25°C. Estimate the transference number of the cupric ion at infinite dilution and compare with the value 0.363 at a concentration of 0.1 M. Note that the Nernst–Einstein equation

$$D_i = RTu_i$$

relates the diffusion coefficient to the mobility.

11.6 The conductivity of aqueous sodium chloride solutions becomes proportional to the concentration such that κ/c approaches 126.45 S·cm^2/mol at infinite dilution and the cation transference number approaches 0.396 at 25°C. Estimate the diffusion coefficient of the salt at infinite dilution.

11.7 Dissolved oxygen at a concentration of 9.5×10^{-4} M is reacted at the limiting current from a 5 M KOH solution where the diffusion coefficient of oxygen is estimated to be 2.3×10^{-5} cm^2/s and that of KOH is about 5×10^{-5} cm^2/s. The diffusion layer near the electrode can be treated as a stagnant region of thickness 50 μm.

(a) Estimate the magnitude of the limiting current density.

(b) Obtain an expression for the concentration profile of potassium ions.

(c) Estimate a numerical value for the concentration of potassium ions adjacent to the surface (outside the diffuse part of the double layer).

(d) Obtain an expression for the concentration profile of hydroxide ions.

11.8 Consider a rotating-disk electrode 1 cm in diameter and rotating at 2000 rpm. It is in a solution of 1.0 M $FeCl_2$ and 1.0 M NaCl. At 25°C, the viscosity of the solution is estimated to be 1.302 mPa·s, and the density is estimated as 1.20 g/cm^3. The limiting ferrous ion diffusion coefficient at zero concentration is found to be 0.72×10^{-5} cm^2/s, where μ is 0.89 mPa·s.

(a) Calculate the limiting current assuming that there is no hydrogen evolution.

(b) What is the value of the thickness of a Nernst stagnant diffusion layer that approximates the mass-transfer characteristics of the rotating disk?

(c) Calculate the value of the Debye length corresponding to the bulk solution.

11.9 Estimate the electrical conductivity of pure water.

11.10 Because Li reacts readily with water, the solvent in the cell of Problem 2.21 is propylene carbonate. The electrolyte is LiCl. Sketch the concentration profiles of the ions in the gap between the two electrodes, and discuss these profiles in terms of the net flux, the diffusive flux, and the migration flux. You may assume that a steady state exists within this gap.

11.11 When the current flow is interrupted in the cell of Problem 11.10, the concentration profile continues to exist for some time and may then relax over a period of some seconds to minutes. To assess to what extent potential losses can be associated with different phenomena involved in the cell, a second, lithium reference electrode is used, and it is desired to estimate the potential of the following cell:

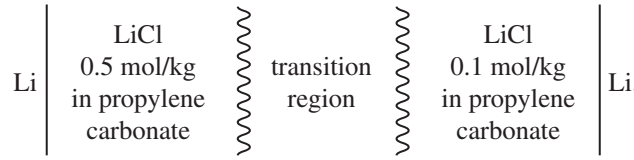

Assume that the Li^+ ion is half as mobile as the chloride ion, and use the Debye–Hückel expression for the activity coefficient with an ion-size parameter of $a = 0.3$ nm, a permittivity ϵ equal to $63\epsilon_0$, and $\rho_0 = 1.203$ g/cm^3.

11.12 Suppose that an electric charge distribution is established initially in a conducting medium. Determine a time constant for the flow of this charge to the boundaries of the medium. Assume that Ohm's law is obeyed with a constant conductivity κ. Obtain a numerical value for the time constant if $\kappa = 0.01$ S/cm and $\epsilon/\epsilon_0 = 79$.

NOTATION

a_i^{θ}	property expressing secondary reference state, liter/mol
c	molar concentration of a single electrolyte, mol/cm^3
c_i	concentration of species i, mol/cm^3
D	diffusion coefficient of electrolyte, cm^2/s
D_i	diffusion coefficient of species i, cm^2/s
f_i	molar activity coefficient of species i
$f_{i.n}$	molar activity coefficient of species i relative to the ionic species n
F	Faraday's constant, 96,487 C/mol
$\mathbf{i}$	current density, A/cm^2
L	distance between electrodes, cm
$\mathbf{N}_i$	flux of species i, mol/cm^2·s
R	universal gas constant, 8.3143 J/mol·K
R_i	rate of homogeneous production of species i, mol/cm^3·s
t	time, s
t_i	transference number of species i
T	absolute temperature, K
u_i	mobility of species i, cm^2·mol/J·s
$\mathbf{v}$	fluid velocity, cm/s
z_i	charge number of species i
ϵ	permittivity, F/cm
ϵ_0	permittivity of free space, 8.8542×10^{-14} F/cm
κ	conductivity, S/cm
λ_i	ionic equivalent conductance, S·cm^2/mol
Λ	equivalent conductance of binary electrolyte, S·cm^2/mol
μ	viscosity, mPa·s
μ_i	electrochemical potential of species i, J/mol
ν_+, ν_-	numbers of cations and anions into which a molecule of electrolyte dissociates
Φ	electric potential, V

REFERENCES

1. W. Nernst, "Zur Kinetik der in Lösung befindlichen Körper'" *Zeitschrift für physikalische Chemie 2* (1888), 613–637.
2. V. Levich, "The Theory of Concentration Polarization," *Acta Physicochimica URSS*, *17* (1942), 257–307.
3. John Newman, "The Polarized Diffuse Double Layer," *Transactions of the Faraday Society*, *61* (1965), 2229–2237.
4. William H. Smyrl and John Newman, "Double Layer Structure at the Limiting Current," *Transactions of the Faraday Society*, *63* (1967), 207–216.
5. William H. Smyrl and John Newman, "Potentials of Cells with Liquid Junctions," *Journal of Physical Chemistry*, *72* (1968), 4660–4671.
6. John Newman and Limin Hsueh, "Currents Limited by Gas Solubility," *Industrial and Engineering Chemistry Fundamentals*, *9* (1970), 677–679.

CHAPTER 12

CONCENTRATED SOLUTIONS

Although the use of the material of Chapter 11 has been quite successful in the analysis of electrochemical problems, in this chapter we want to develop a description of transport processes that is more generally valid.

12.1 TRANSPORT LAWS

Mass transfer in electrolytic solutions requires a description of the movement of mobile ionic species (equation 11.1 or 11.65), material balances (equation 11.3), current flow (equation 11.2), electroneutrality (equation 11.4), and fluid mechanics (see Chapter 15). The equations for material balances, current flow, and electroneutrality given in Section 11.1 remain valid for concentrated solutions, but the flux equation requires modification.

The flux equations treated earlier fail even in ternary solutions of nonelectrolytes since in such solutions there are two independent concentration gradients and the diffusion flux of each species can be affected by both concentration gradients.

To avoid the difficulties mentioned in Section 11.1, equation 11.1 can be replaced by the multicomponent diffusion equation

$$c_i \nabla \mu_i = \sum_j K_{ij}(\mathbf{v}_j - \mathbf{v}_i) = RT \sum_j \frac{c_i c_j}{c_T \mathscr{D}_{ij}}(\mathbf{v}_j - \mathbf{v}_i), \tag{12.1}$$

where μ_i is the *electro*chemical potential of species i and K_{ij} are friction coefficients or interaction coefficients, $\mathbf{v}_i$ is the velocity of species i, an average velocity for the species but not the velocity of individual molecules. Thus, the flux density of species i is $\mathbf{N}_i = c_i \mathbf{v}_i$. The total concentration is

$$c_T = \sum_i c_i, \tag{12.2}$$

Electrochemical Systems, Fourth Edition. John Newman and Nitash P. Balsara.

where the sum includes the solvent. $\mathscr{D}_{ij}$ is a *diffusion coefficient* describing the interaction of species i and j. These diffusion coefficients are, for the moment, simply parameters that can replace the drag coefficients K_{ij}.

$$K_{ij} = \frac{RTc_i c_j}{c_T \mathscr{D}_{ij}}. \tag{12.3}$$

The term $-c_i \nabla \mu_i$ in equation 12.1 can be regarded as a driving force per unit volume acting on species i and causing it to move with respect to the surrounding fluid. The force per unit volume exerted by species j on species i as a result of their relative motion has been expressed as $K_{ij}(\mathbf{v}_j - \mathbf{v}_i)$, that is, proportional to the difference in velocity of the two species. By Newton's third law of motion (action equals reaction), we find that $K_{ij} = K_{ji}$ or

$$\mathscr{D}_{ij} = \mathscr{D}_{ji}. \tag{12.4}$$

Equation 12.1 thus expresses the balance between the driving force and the total drag exerted by the other species.

The number of independent equations with the form of equation 12.1 is one less than the number of species. Addition of equation 12.1 over i gives

$$\sum_i c_i \nabla \mu_i = \sum_i \sum_j K_{ij}(\mathbf{v}_j - \mathbf{v}_i). \tag{12.5}$$

The left side is zero by the Gibbs–Duhem relation (at constant temperature and pressure), and the right side is zero since $K_{ij} = K_{ji}$.

Equation 12.1 avoids the difficulties with the flux equation 11.1 mentioned in Section 11.1. The gradient of the electrochemical potential has been used as the driving force for diffusion and migration, as in Section 11.9. This resolves the question of the electric potential and the activity coefficients of individual ions. The use of the velocity difference $\mathbf{v}_j - \mathbf{v}_i$ in equation 12.1 avoids or postpones the question of the reference or average velocity on which diffusion and migration fluxes are based. The multicomponent diffusion equation is more general than equation 11.1 because it relates the driving force to a linear combination of resistances instead of just to one resistance, that with the solvent. The number of transport properties $\mathscr{D}_{ij}$ defined by equation 12.1 is $\frac{1}{2}n(n-1)$, where n is the number of species present, since $\mathscr{D}_{ij} = \mathscr{D}_{ji}$ and $\mathscr{D}_{ii}$ is not defined. This is different from the number of transport properties u_i and D_i defined by equation 11.1, whether or not the Nernst–Einstein relation 11.41 is used. Thus, for three species (e.g., two ions and a solvent), there are three transport properties defined by equation 12.1; and for four species (e.g., three ions and a solvent), there are six transport properties.

Equation 12.1 is similar to the Stefan–Maxwell equation (see Ref. [1], p. 570) and is equivalent to one developed by Onsager (equation 14, p. 245, in Ref. [2]). The Stefan–Maxwell equations apply to diffusion in dilute gas mixtures and express the driving force as a mole fraction gradient or a gradient of partial pressure instead of the gradient of the electrochemical potential. Equation 12.4 is equivalent to the Onsager reciprocal relation. The reciprocals of the $\mathscr{D}_{ij}$'s can be regarded as friction coefficients similar to those used by Laity[3, 4] and Klemm[5, 6] to describe transport in ionic solutions and melts. Burgers[7] has also used this concept to treat the conductivity of ionized gases, and Lightfoot et al.[8] have applied equation 12.1 to liquid solutions. Truesdell[9] has discussed the validity of the arguments that $K_{ij} = K_{ji}$ (see also Lamm[10]). The modification of equation 12.1 for use in nonisothermal media is indicated in Section 13.1.

12.2 THE BINARY ELECTROLYTE

Equation 12.1 expresses the driving forces in terms of the species velocities $\mathbf{v}_i$ or the species fluxes $c_i\mathbf{v}_i$. For use in the material-balance equation 11.3, it is necessary to invert the set of equations 12.1 so as to express the species flux densities in terms of the driving forces. Since these are linear, algebraic equations, the inversion is straightforward but lengthy. The general procedure is indicated in Section 12.7.

For a binary electrolytic solution composed of anions, cations, and solvent, equation 12.1 yields two independent equations:

$$c_+\nabla\mu_+ = K_{0+}(\mathbf{v}_0 - \mathbf{v}_+) + K_{+-}(\mathbf{v}_- - \mathbf{v}_+), \tag{12.6}$$

$$c_-\nabla\mu_- = K_{0-}(\mathbf{v}_0 - \mathbf{v}_-) + K_{+-}(\mathbf{v}_+ - \mathbf{v}_-). \tag{12.7}$$

These equations can be rearranged, with introduction of the current density from equation 11.2, to read

$$\mathbf{N}_+ = c_+\mathbf{v}_+ = -\frac{\nu_+\mathscr{D}}{\nu RT}\frac{c_T}{c_0}c\nabla\mu_e + \frac{\mathbf{i}t_+^0}{z_+F} + c_+\mathbf{v}_0, \tag{12.8}$$

$$\mathbf{N}_- = c_-\mathbf{v}_- = -\frac{\nu_-\mathscr{D}}{\nu RT}\frac{c_T}{c_0}c\nabla\mu_e + \frac{\mathbf{i}t_-^0}{z_-F} + c_-\mathbf{v}_0, \tag{12.9}$$

where $\nu = \nu_+ + \nu_-$ (see Section 11.4) and $\mu_e = \nu_+\mu_+ + \nu_-\mu_- = \nu RT\ln(cf_{+-}a_{+-}^{\theta})$. Here f_{+-} is the mean molar activity coefficient of the electrolyte (see equation 2.32). The diffusion coefficient of the electrolyte, based on a thermodynamic driving force, is

$$\mathscr{D} = \frac{\mathscr{D}_{0+}\mathscr{D}_{0-}(z_+ - z_-)}{z_+\mathscr{D}_{0+} - z_-\mathscr{D}_{0-}}. \tag{12.10}$$

The transference numbers (with respect to the solvent velocity) are

$$t_+^0 = 1 - t_-^0 = \frac{z_+\mathscr{D}_{0+}}{z_+\mathscr{D}_{0+} - z_-\mathscr{D}_{0-}}. \tag{12.11}$$

The driving force for diffusion used in equations 12.8 and 12.9 is the gradient of the chemical potential μ_e of the electrolyte in the solution. This chemical potential is readily measurable, and no reference to individual ionic activity coefficients is necessary. The diffusion coefficient D of the salt that is usually measured is based on a gradient of the concentration and is related to $\mathscr{D}$ by[11, 12]

$$D = \mathscr{D}\frac{c_T}{c_0}\left(1 + \frac{d\ln\gamma_{+-}}{d\ln m}\right), \tag{12.12}$$

where γ_{+-} is the mean molal activity coefficient and m is the molality (moles of electrolyte per kilogram of solvent). The gradient of chemical potential can be expressed in terms of the gradient of concentration:

$$\frac{\mathscr{D}}{\nu RT}\frac{c_T}{c_0}c\nabla\mu_e = D\left(1 - \frac{d\ln c_0}{d\ln c}\right)\nabla c. \tag{12.13}$$

Insertion of equations 12.8 and 12.13 into the material-balance equation 11.3 yields

$$\frac{\partial c}{\partial t} + \nabla \cdot (c\mathbf{v}_0) = \nabla \cdot \left[D \left(1 - \frac{d \ln c_0}{d \ln c} \right) \nabla c \right] - \frac{\mathbf{i} \cdot \nabla t_+^0}{z_+ \nu_+ F}, \tag{12.14}$$

which bears a strong resemblance to equation 11.29. The second term is different because we have not assumed that $\nabla \cdot \mathbf{v}_0 = 0$.

12.3 REFERENCE VELOCITIES

Diffusion might be defined as a motion of the various components relative to the bulk fluid motion as a result of nonuniform thermodynamic potentials. To avoid ambiguity, a velocity characteristic of the bulk motion must be clearly specified, and the diffusion velocities must be referred to this velocity.

In Section 12.2 and, in particular, in equations 12.8 and 12.9, the solvent velocity has been chosen as the reference velocity. Two other possible reference velocities are the mass-average velocity **v** and the molar-average velocity **v*** defined by

$$\mathbf{v} = \frac{1}{\rho} \sum_i \rho_i \mathbf{v}_i \quad \text{and} \quad \mathbf{v}^* = \frac{1}{c_T} \sum_i c_i \mathbf{v}_i, \tag{12.15}$$

where ρ_i is the mass of species i per unit volume ($\rho_i = M_i c_i$). The choice of which reference velocity to use is arbitrary, and the distinction is less important in sufficiently dilute solutions since the three velocities become the same.

In particular situations, one reference velocity may be more advantageous than another. The solvent velocity becomes less significant in concentrated mixtures and becomes quite inconvenient in a pure fused salt. The mass-average velocity is useful because the fluid mechanical equations (see Chapter 15) are invariably written in terms of **v**. On the other hand, the average velocity is not always determined from momentum considerations, but perhaps from pure stoichiometry (e.g., in some porous electrodes). In such a case, the molar-average velocity might be more convenient. Furthermore, chemists more commonly work in molar units than in mass units.

For a binary electrolytic solution, the material-balance equation 12.14 can be written in the equivalent forms

$$c_T \left(\frac{\partial x_e}{\partial t} + \mathbf{v}^* \cdot \nabla x_e \right) = \nabla \cdot (c_T D \nabla x_e) - \frac{\mathbf{i} \cdot \nabla t_+^*}{z_+ \nu_+ F}, \tag{12.16}$$

and

$$\rho \left(\frac{\partial \omega_e}{\partial t} + \mathbf{v} \cdot \nabla \omega_e \right) = \nabla \cdot (\rho D \nabla \omega_e) - \frac{M_e \mathbf{i} \cdot \nabla t_+}{z_+ \nu_+ F}, \tag{12.17}$$

where $M_e = \nu_+ M_+ + \nu_- M_-$ is the molar mass of the electrolyte, $x_e = c/c_T$ is the mole fraction of the salt (see the remarks below equation 2.17), $\omega_e = (\rho_+ + \rho_-)/\rho$ is the mass fraction of the salt, $t_+^* = (c_- + c_0 t_+^0)/c_T$ is the cation transference number with respect to the molar-average velocity, and $t_+ = (\rho_- + \rho_0 t_+^0)/\rho$ is the cation transference number with respect to the mass-average velocity. Equation 12.16 involves the molar-average velocity, and equation 12.17 involves the mass-average velocity. These equations can be compared with the corresponding forms for binary solutions of nonelectrolytes (see Ref. [1], p. 584).

The cation flux density referred to the molar-average velocity is

$$\mathbf{N}_+ = -\nu_+ c_T D \nabla x_e + \frac{\mathbf{i} t_+^*}{z_+ F} + c_+ \mathbf{v}^*, \tag{12.18}$$

and the cation flux density referred to the mass-average velocity is

$$\mathbf{N}_+ = -\nu_+ \frac{\rho D}{M_e} \nabla \omega_e + \frac{\mathbf{i} t_+}{z_+ F} + c_+ \mathbf{v}. \tag{12.19}$$

Similar equations apply to the anion.

Equations 12.17 and 12.19 have been applied to mass transfer to a rotating-disk electrode from a binary electrolytic solution in Ref. [13].

The corresponding equations for use with the volume-average velocity were developed by Newman and Chapman.[12] The situation with three ionic species is almost as simple as that for two ions and a solvent. Pollard and Newman[14] treated such molten salt systems with a derivation paralleling that in Sections 12.1 through 12.5.

12.4 THE POTENTIAL

Now we want to introduce a *potential in the solution* for use as a driving force for the current. Various candidates for this role were discussed in Section 3.5. We restrict ourselves here to a binary electrolyte.

To assure that the potential introduced can be measured, let us first use the potential Φ of a suitable reference electrode at a point in the solution measured with respect to a similar reference electrode at a fixed point in the solution. By this we mean an actual electrode, not a reference half-cell connected to the point in question by a capillary tube filled with an electrolytic solution. The electrode equilibrium must, of course, involve the anions or the cations and possibly the solvent. This electrode reaction can be written, in general, as

$$s_- M_-^{z-} + s_+ M_+^{z+} + s_0 M_0 \rightleftharpoons n\mathrm{e}^-, \tag{12.20}$$

where M_i is a symbol representing the chemical formula of species i and s_i is the stoichiometric coefficient of species i.

In a practical experimental situation, one may want to replace the reference electrode by a reference half-cell. The additional diffusion potential thus introduced can be calculated exactly for a reference half-cell such as Hg–HgO in a KOH solution if the external electrolyte is also KOH but not if it is KCl (see Chapters 2 and 6).

Application of thermodynamic principles to a reference electrode following equation 12.20 yields

$$s_- \nabla \mu_- + s_+ \nabla \mu_+ + s_0 \nabla \mu_0 = -nF \nabla \Phi. \tag{12.21}$$

This equation can be rearranged so as to replace the electrochemical potentials by the current density and the chemical potential of the electrolyte. Equations 12.8 and 12.9 can be substituted into equation 12.1 to yield

$$\frac{1}{z_-} \nabla \mu_- = -\frac{F}{\kappa} \mathbf{i} - \frac{t_+^0}{z_+ \nu_+} \nabla \mu_e, \tag{12.22}$$

where κ is the conductivity of the solution whose reciprocal is given by

$$\frac{1}{\kappa} = \frac{-RT}{c_T z_+ z_- F^2} \left(\frac{1}{\mathscr{D}_{+-}} + \frac{c_0 t_-^0}{c_+ \mathscr{D}_{0-}} \right). \tag{12.23}$$

Equation 12.22 can be compared with equation 2.68.

From equation 12.21, $\nabla\mu_0$ can be eliminated by means of the Gibbs–Duhem equation, and the terms with the gradients of the electrochemical potentials of the ions can be combined to give

$$s_+\nabla\mu_+ + s_-\nabla\mu_- = \frac{s_+}{\nu_+}\nabla\mu_e - \frac{n}{z_-}\nabla\mu_-, \tag{12.24}$$

since

$$s_+z_+ + s_-z_- = -n. \tag{12.25}$$

Equation 12.21 becomes

$$-F\nabla\Phi = \left(\frac{s_+}{n\nu_+} - \frac{s_0c}{nc_0}\right)\nabla\mu_e - \frac{1}{z_-}\nabla\mu_-. \tag{12.26}$$

Finally, $\nabla\mu_-$ is eliminated by means of equation 12.22 to yield the desired relation

$$\mathbf{i} = -\kappa\nabla\Phi - \frac{\kappa}{F}\left(\frac{s_+}{n\nu_+} + \frac{t_+^0}{z_+\nu_+} - \frac{s_0c}{nc_0}\right)\nabla\mu_e. \tag{12.27}$$

This result is analogous to equation 11.23, but the potential used here is considerably different from the electrostatic potential used earlier. The new definition avoids the questionable concepts regarding potentials in the solution. When the composition is uniform, the two potentials are similar; but the reference electrode potential retains a clearly defined physical significance even in the presence of concentration gradients. Equation 12.27 can be compared directly with equation 2.84.

Another way to avoid the questionable concepts regarding potentials in the solution is to use the quasi-electrostatic potential. In a more general context, this leads eventually to equation 12.67 and will not be pursued further here.

Figure 12.1 shows potentials of three electrodes as a function of the molality of aqueous sulfuric acid solutions at 25°C, in the absence of a flow of current. Vertical distances at a given composition represent open-circuit potential differences among these electrodes calculated according to the methods of Section 2.4, that is, for cells having essentially uniform composition of the solution. Potential differences on a given curve between two points of different composition represent open-circuit potential differences calculated according to the methods of Section 2.6, that is, for cells having identical electrodes but different compositions of a single electrolyte. Recall that such junctions have potential differences independent of the method of forming the junction but do depend on transport properties as well as the composition dependence of the activity coefficient. Potential differences between points on different curves at different compositions still represent meaningful values independent of the composition profile in the junction. (Compare Problems 6.12 through 6.16.)

In probing the solution in different parts of a lead–acid cell one could imagine Φ to be measured with any one of the three reference electrodes. Notice the opposite composition dependence of the PbO_2 electrode. The quasi-electrostatic potential, if we calculated and plotted it, would be expected to have a much smaller composition dependence and to depend only slightly on the choice of the reference ion n (see Section 6.7). In practical applications (see Chapter 22), it may be convenient to imagine use of the Pb reference electrode to probe the solution in the porous Pb negative electrode of the cell and to imagine use of the PbO_2 reference electrode to probe the solution in the porous PbO_2 positive electrode of the cell. The overall electrode potentials might be measured relative to a

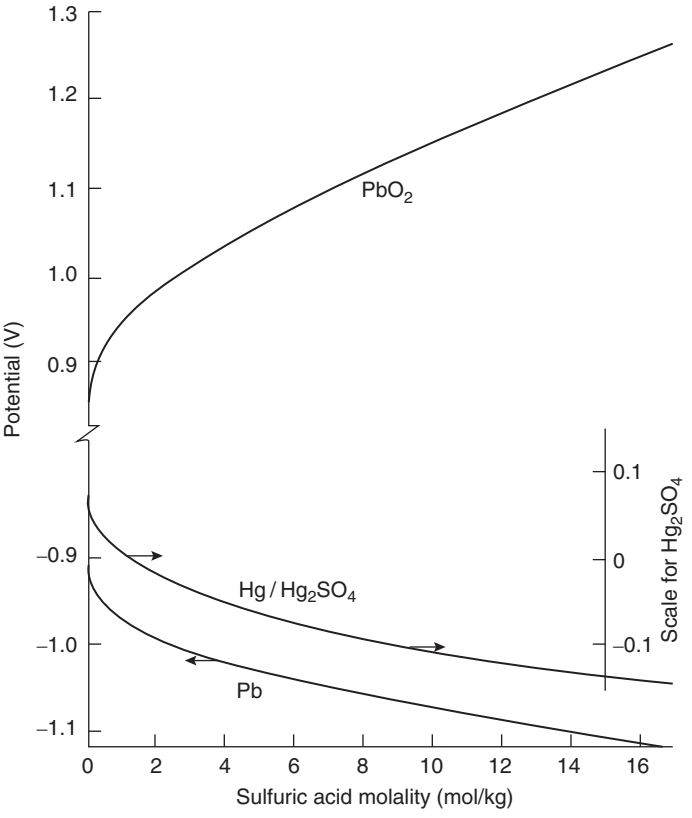

Figure 12.1 Potentials of Pb, PbO_2, and Hg/Hg_2SO_4 electrodes versus the molality of sulfuric acid, plotted in such a way that vertical distances give the potenial differences between electrodes even if the composition is different.

separate Hg/Hg_2SO_4 reference electrode located outside the cell in a vessel of fixed composition (like the 1 mol/kg reference used for the figure).

The analysis of a system with a binary electrolyte can proceed expeditiously with Φ as defined in this section (measured with a reference electrode immersed in the system) because the composition profile in a junction always has the same effect, as shown in Figure 12.1, and potentials measured between points of different composition have clear meaning. Use of a reference electrode with a different electrolyte would only introduce complications and uncertainties. However, it must be emphasized that this potential Φ and the quasi-electrostatic potential have different qualities and behavior.

The sodium/sulfur battery system permits a diagram similar to Figure 12.1 to be constructed. The electrolyte is a sodium polysulfide melt of variable composition. The "sulfur" electrode can involve reaction of different polysulfide species S_y^{2-} on an inert electrode such as carbon or molybdenum. The "sodium" electrode can consist of molten sodium separated from the polysulfide melt by a sodium-ion-conducting membrane, such as β''-Al_2O_3 or certain glasses. The open-circuit potential difference between points of different polysulfide compositions will be substantially less if measured with sodium electrodes rather than sulfur electrodes.

12.5 CONNECTION WITH DILUTE-SOLUTION THEORY

The dilute-solution theory presented in Chapter 11 has many useful facets that are only slightly modified by the more complete theory for concentrated solutions. Consequently, it is important to see how the two theories are related. Let us apply equation 12.1 to one of the minor species in a dilute solution. Then $c_i \ll c_0$, and only one of the terms on the right is important:

$$c_i \nabla \mu_i = \frac{RTc_0}{c_T \mathscr{D}_{0i}} (c_i \mathbf{v}_0 - c_i \mathbf{v}_i). \tag{12.28}$$

Furthermore, the total concentration c_T is approximately equal to the solvent concentration c_0, and equation 12.28 can be rewritten as

$$\mathbf{N}_i = -\frac{\mathscr{D}_{0i}}{RT} c_i \nabla \mu_i + c_i \mathbf{v}_0. \tag{12.29}$$

Equation 12.29 is only slightly different from equation 11.1. The driving forces for diffusion and migration are both included in the gradient of the electrochemical potential in equation 12.29, and we see that the applicability of the Nernst–Einstein equation 11.41 is thus implicit in this equation. The further development of equation 12.29 is carried out in Section 11.9.

The $\mathscr{D}_{0i}$ correspond to the D_i of the dilute-solution theory, but the interactions of the minor components with each other are not explicitly accounted for in the dilute-solution theory. A different number of transport properties is defined in the two cases.

We have seen that the validity of the Nernst–Einstein relation rests primarily on the fact that the driving force for both migration and diffusion is the gradient of the electrochemical potential, and the decomposition of this into a concentration term and an electrostatic-potential term is without basic physical significance. The Nernst–Einstein relation does not really fail in concentrated solutions; rather, additional composition-dependent transport parameters besides the $\mathscr{D}_{0i}$ become necessary to describe the processes. It is not sufficient to allow the D_i and u_i to become concentration dependent, even though one might be willing to relax the Nernst–Einstein relation.

We gain additional insight into the validity of the Nernst–Einstein relation from the Debye–Hückel theory of interionic attraction (see Section 4.1) and the theory of the diffuse layer at an interface (see Section 7.4). These both describe equilibrium situations where the ionic fluxes and the convective velocity are zero. Under these conditions, and with the Nernst–Einstein relation, equation 11.1 becomes

$$\mathbf{N}_i = -\frac{z_i D_i F}{RT} c_i \nabla \Phi - D_i \nabla c_i = 0. \tag{12.30}$$

Integration gives the Boltzmann distribution for the ionic concentrations:

$$c_i = c_{i\infty} \exp\left(-\frac{z_i F \Phi}{RT}\right) \tag{12.31}$$

(see equations 4.1 and 7.30). The use of the Nernst–Einstein relation was necessary for the transport properties to cancel in going from the transport equation 12.30 to the thermodynamic Boltzmann distribution.

Table 12.1 shows, for binary electrolytes, a comparison of the results of the theories for dilute solutions and concentrated solutions. To bring out the similarity, the Nernst–Einstein relation 11.41 has been used in the expression of the transport properties from Section 11.4. The three transport properties $\mathscr{D}_{0+}$, $\mathscr{D}_{0-}$, and $\mathscr{D}_{+-}$ of the theory for concentrated solutions can be calculated as functions of concentration from three independent measurements of D, κ, and t_+^0 (see Section 14.2).

TABLE 12.1 Comparison of results for binary electrolytes

Dilute-solution theory	Concentrated solutions
Equation 11.1	Equation 12.1
Equation 11.29	Equation 12.14
Equation 11.23	Equation 12.27
$D = \dfrac{D_+D_-(z_+ - z_-)}{z_+D_+ - z_-D_-}$	$\mathscr{D} = \dfrac{\mathscr{D}_{0+}\mathscr{D}_{0-}(z_+ - z_-)}{z_+\mathscr{D}_{0+} - z_-\mathscr{D}_{0-}}$
$t_+ = \dfrac{z_+D_+}{z_+D_+ - z_-D_-}$	$t_+^0 = \dfrac{z_+\mathscr{D}_{0+}}{z_+\mathscr{D}_{0+} - z_-\mathscr{D}_{0-}}$
$\dfrac{1}{\kappa} = \dfrac{-RT}{c_0z_+z_-F^2}\left(\dfrac{c_0t_-}{c_+D_-}\right)$	$\dfrac{1}{\kappa} = \dfrac{-RT}{c_Tz_+z_-F^2}\left(\dfrac{1}{\mathscr{D}_{+-}} + \dfrac{c_0t_-^0}{c_+\mathscr{D}_{0-}}\right)$

12.6 EXAMPLE CALCULATION USING CONCENTRATED SOLUTION THEORY

We revisit a problem introduced in Section 11.8 where a binary electrolyte is placed in a cell where the cation dissolves into the electrolyte at the anode and is deposited at the cathode under an applied potential. There, dilute solution theory is used to derive the relationship between current and applied potential and the salt concentration in the cell as a function of position and transport parameters. We now examine these relationships using concentrated solution theory.

We take the potential at the cathode to be zero, the anode is located at $x = 0$, and surface overpotentials are taken to be zero at the two electrodes. The current is applied at $t = 0$ in the x direction across a symmetric cell containing a salt $(M^{z+})_{\upsilon_+}(X^{z-})_{\upsilon_-}$ with electrodes of the pure metal M. The applied external potential creates gradients in the solution in both the potential Φ and salt concentration c. The reference electrode used to measure the potential at any location in the solution is a special case of equation 12.20:

$$-\mathrm{M}^{z+} + \mathrm{M}_{(s)} \rightleftharpoons n\mathrm{e}^-. \tag{12.32}$$

Our model is one-dimensional, and thus current density and flux can be treated as scalars. The relationship between electric current density i and potential Φ is given by equation 12.27, which simplifies in cases where the solvent and the anion do not participate in the reference-electrode reaction to

$$i = -\kappa\frac{d\Phi}{dz} - \frac{\kappa}{F}\left(-\frac{1}{n\nu_+} + \frac{t_+^0}{z_+\nu_+}\right)\frac{d\mu_e}{dx}. \tag{12.33}$$

Since the electrolyte is electrically neutral, μ_e depends only on local concentration, independent of Φ. Charge balance implies that $z_+ = n$. Equation 12.33 applies to the steady state wherein both terms on the right contribute and to the initial state wherein the second term on the right is zero because the solution is initially uniform in concentration. Thus, the initial current at $t = 0$ is

$$i_0 = -\kappa\frac{d\Phi}{dx}, \tag{12.34}$$

and the anode potential Φ_A is

$$\Phi_A = \frac{i_0L}{\kappa}, \tag{12.35}$$

where L is the distance between the electrodes.

The anion flux through the solution, N_-, is related to the current density as given below (equation 12.9)

$$N_- = -\frac{\mathscr{D} c_T c \upsilon_-}{RTc_0 \nu} \frac{d\mu_e}{dx} + \frac{it_-^0}{z_- F}, \tag{12.36}$$

where $\mathscr{D}$ is the diffusion coefficient of the electrolyte based on a thermodynamic driving force, ν is the total number of moles of ions produced by dissociation of the salt ($\nu = \nu_+ + \nu_-$), c_0 is the solvent concentration, c is salt concentration (mol/cm^3), and c_T is the total solution concentration ($c_T = c_0 + \nu c$). At steady state, the anion flux is zero for all x. Equation 12.36 then yields an expression in terms of the steady-state current, i_{ss}:

$$\frac{d\mu_e}{dx} = i_{ss} \frac{t_-^0}{Fz_-} \frac{RTc_0 \nu}{\mathscr{D} c_T c \nu_-}. \tag{12.37}$$

Combining equations 12.37 and 12.12, we get

$$\frac{d\mu_e}{dx} = \frac{\upsilon RT}{m} \left(1 + \frac{d \ln \gamma_\pm}{d \ln m}\right) \frac{dm}{dx} = i_{ss} \frac{t_-^0}{Fz_-} \frac{RTc_0 \nu}{\mathscr{D} c_T c \nu_-}. \tag{12.38}$$

Combining equations 12.38 and 12.12, we get

$$\frac{dm}{dx} = \frac{i_{ss}}{FM_0 z_- \nu_-} \frac{t_-^0}{Dc_0}. \tag{12.39}$$

Collecting the molality-dependent terms and integration gives an implicit formula for the concentration profile, $m(x)$,

$$\int_{m(x=0)}^{m(x)} \frac{D(m)c_0(m)}{t_-^0(m)}\, dm = \frac{i_{ss}}{FM_0 z_- \nu_-} x \tag{12.40}$$

for given $m(x = 0)$ and i_{ss}. In an experiment one controls the average salt molality of the electrolyte, which is obtained by integrating $m(x)$ from $x = 0$ to $x = L$. The spatial dependence of the molar salt concentration, $c(x)$, can then be readily obtained from $m(x)$ using equation 2.17. Let

$$\mathrm{Ne} = a \frac{\kappa RT (t_-^0)^2}{F^2 \mathscr{D} c} \quad \frac{c_0}{c_T} = a \frac{\kappa RT (t_-^0)^2}{F^2 Dc} \left(1 + \frac{d \ln \gamma_\pm}{d \ln m}\right), \tag{12.41}$$

where the parameter a is related to the stoichiometry of the salt,

$$a = \frac{\nu}{(\nu_+ z_+)^2}. \tag{12.42}$$

Thus, at steady-state, equation 12.33 becomes,

$$i_{ss} = -\kappa \frac{d\Phi}{dx} - i_{ss} \mathrm{Ne}. \tag{12.43}$$

Equation 12.43 can be integrated to obtain the spatial dependence of potential,[15]

$$\Phi(x) - \Phi(x = L) = \Phi(x) = -i_{ss} \int_{m(x=L)}^{m(x)} \frac{1 + \mathrm{Ne}(m)}{\kappa(m)} \left(\frac{dm}{dx}\right)^{-1} dm \tag{12.44}$$

where dm/dx determined above is used.

If the concentration dependence of transport parameters is unimportant, then equations 12.40 and 12.17 can be used to obtain a linear relationship between c and x,

$$c(x) - c(x=0) = \frac{i_{ss} t_-^0}{FDz_-\nu_-} x, \tag{12.45}$$

which reduces to equation 11.56 for univalent salts. Equation 12.45 applies to dilute electrolytes or concentrated electrolytes with small applied potentials. In this limit,

$$\frac{d\Phi}{dx} = -\frac{\Phi_A}{L}, \tag{12.46}$$

which, when combined with equation 12.43, yields

$$\frac{Li_{ss}}{\Phi_A} = \frac{\kappa}{1+\mathrm{Ne}}. \tag{12.47}$$

Here, it is assumed that the concentration gradient in the cell is small and thus the concentration dependence of Ne can be ignored. Equations 12.35 and 12.47 then give

$$\frac{i_{ss}}{i_0} = \frac{1}{1+\mathrm{Ne}}. \tag{12.48}$$

Measurement of i_{ss}/i_0 or i_{ss} versus Φ_A at small applied potentials enables determination of Ne, which, in turn, may be used to determine t_-^0, if κ, D, and $d\ln\gamma_\pm/d\ln m$ are known from independent experiments. In the dilute limit, expressions given in Table 12.1 can be used to simplify equations 12.41 and 12.48 to give

$$\frac{i_{ss}}{i_0} = t_{+,\mathrm{id}}, \tag{12.49}$$

where we have used the fact that the activity coefficient is independent of concentration in this limit. This equation has been used as an approximate method for measuring the transference number of binary electrolytes.[16]

We return to steady ionic current in Chapter 14 to discuss measurement of transport properties, κ, D, and t_-^0, and their implication on concentration profiles under applied electric fields. Included in Chapter 14 is a discussion of how the concentration dependence of transport and thermodynamic properties affects ion transport.

12.7 MULTICOMPONENT TRANSPORT

Equation 12.1 expresses the driving forces in terms of the species velocities $\mathbf{v}_i$ or the species flux densities $c_i\mathbf{v}_i$. For use in the material-balance equation 11.3, it is necessary to invert the set of equations 12.1 so as to express the species fluxes in terms of the driving forces. This is carried out in the present section (see references [17 to 19]).

It should first be noted that there are only $n-1$ independent velocity differences and $n-1$ independent gradients of electrochemical potentials in a solution with n species (see equation 12.5). Therefore, equation 12.1 can be expressed as

$$c_i\nabla\mu_i = \sum_j M_{ij}(\mathbf{v}_j - \mathbf{v}_0), \tag{12.50}$$

where $\mathbf{v}_0$ is the velocity of any one of the species and where

$$\begin{aligned} M_{ij} &= K_{ij}, \quad i \neq j \\ &= K_{ij} - \sum_k K_{ik}, \quad i = j. \end{aligned} \tag{12.51}$$

It further follows that $M_{ij} = M_{ji}$. Bearing in mind that there are $n-1$ independent equations of the form of equation 12.50, one can invert this equation to read

$$\mathbf{v}_j - \mathbf{v}_0 = -\sum_{k\neq 0} L^0_{jk} c_k \nabla \mu_k, \quad j \neq 0, \tag{12.52}$$

where the matrix $\mathbf{L}^0$ is the negative of the inverse of the submatrix $\mathbf{M}^0$,

$$\mathbf{L}^0 = -(\mathbf{M}^0)^{-1}, \tag{12.53}$$

and where the submatrix $\mathbf{M}^0$ is obtained from the matrix $\mathbf{M}$ by deleting the row and the column corresponding to the species 0. The inverse matrix $\mathbf{L}^0$ is also symmetric, that is,

$$L^0_{ij} = L^0_{ji}. \tag{12.54}$$

Certain combinations of the L^0_{ij}'s are related to measurable transport properties and have particular significance in the treatment of cells with liquid junctions (see Section 12.8). The current density is related to the fluxes of ionic species by equation 11.2, which can be rewritten as

$$\mathbf{i} = F\sum_i z_i c_i \mathbf{v}_i = F\sum_i z_i c_i (\mathbf{v}_i - \mathbf{v}_0), \tag{12.55}$$

the equivalence of the last two expressions being assured by the electroneutrality of the solution. Substitution of equation 12.52 yields

$$\mathbf{i} = -F\sum_{i\neq 0} z_i c_i \sum_{k\neq 0} L^0_{ik} c_k \nabla \mu_k. \tag{12.56}$$

In a solution of uniform composition,

$$\nabla \mu_k = z_k F \nabla \Phi, \tag{12.57}$$

where $\nabla\Phi$ is the gradient of the electric potential. Equation 12.56 becomes in this case

$$\mathbf{i} = -F^2 \nabla\Phi \sum_{i\neq 0} z_i c_i \sum_{k\neq 0} L^0_{ik} z_k c_k. \tag{12.58}$$

Comparison with Ohm's law (see equation 11.6), also applicable to a solution of uniform composition,

$$\mathbf{i} = -\kappa \ \nabla\Phi, \tag{12.59}$$

allows us to identify the conductivity

$$\kappa = F^2 \sum_{i\neq 0}\sum_{k\neq 0} L^0_{ik} z_i c_i z_k c_k. \tag{12.60}$$

Although the L^0_{ik}'s depend upon the reference velocity chosen, the conductivity κ is invariant with respect to this choice.

Next we can identify the transference numbers. Again, for a solution of uniform composition, equation 12.57 is valid, and equation 12.52 becomes

$$\mathbf{v}_j - \mathbf{v}_0 = -F\nabla\Phi \sum_{k\neq 0} L^0_{jk} z_k c_k. \tag{12.61}$$

For this case of uniform composition, the species flux density is related to the current density and the transference number by the expression

$$t^0_j \mathbf{i} = z_j F c_j (\mathbf{v}_j - \mathbf{v}_0) = -t^0_j \kappa \nabla\Phi. \tag{12.62}$$

Comparison of equations 12.61 and 12.62 shows that the transference number t^0_j of species j with respect to the velocity of species 0 is given by

$$t^0_j = \frac{z_j c_j F^2}{\kappa} \sum_{k\neq 0} L^0_{jk} z_k c_k. \tag{12.63}$$

It is to be noted that the transference number has been defined as the fraction of the current carried by an ion in a solution of uniform composition. In a solution in which there are concentration gradients, the transference number is still a transport property related to the L^0_{ij}'s by equation 12.63, but it no longer represents the fraction of current carried by an ion. (Compare with the remarks at the end of Section 11.2.) A different choice of the reference species will change the L_{ij}'s, and hence the transference numbers with respect to the velocities of different reference species will be different (see Problem 12.2).

Comparison of equation 12.63 with equation 12.60 or of equation 12.62 with equation 12.55 shows that the transference numbers sum to unity:

$$\sum_i t^0_i = 1. \tag{12.64}$$

One could go on to describe diffusion of electrolytes in terms of the inverted transport equations. However, this becomes cumbersome, and the symmetry of the coefficients becomes obscured if one tries to eliminate the special place occupied by the species 0 in the inversion process. One of the primary purposes of the present section is to lead to the development of equation 12.66 in the next section. This equation was used as the basis to treat irreversible diffusion effects in electrochemical cells in Chapters 2 and 6.

In general, the $\frac{1}{2}n(n-1)$ coefficients $\mathscr{D}_{ij}$ yield one conductivity and $n-2$ transference numbers or ratios t^0_i/z_i in the inverted formulation. The remainder of the coefficients generate diffusion coefficients for neutral combinations of species. For example, for a solution containing a solvent and K^+, Na^+, and Cl^- ions, there is one conductivity, two independent transference numbers, and three diffusion coefficients required to describe diffusion of NaCl and KCl in the solvent. These six transport properties correspond to, and are derivable from, the six coefficients $\mathscr{D}_{ij}$ for the system.

The inversion of the multicomponent diffusion equation can be carried out on a digital computer, in the course of solving a problem of interest.[20, 21] Such computer programs can deal with one-dimensional systems characterized by an arbitrary number of homogeneous and heterogeneous reactions, transients, fluid flow, and multicomponent diffusion with composition or temperature-dependent physical properties. Interesting applications include membranes and molten salts. In Refs. [13] and [20], the velocity profile is computed at the same time with proper account for the variation of viscosity and density with position. In reference [20], the temperature in this gaseous system varied from 1200°C on the surface to 20°C in the bulk. Section C.6 has an example of solving a problem in multicomponent diffusion with migration. Often data on physical properties

are not available in the detail needed for multicomponent diffusion—in contrast to binary electrolytes or gas systems—and reasonable estimates must be made or certain key properties regarded as fitting parameters to be adjusted in the comparison of theory and experiment.

12.8 LIQUID-JUNCTION POTENTIALS

It is shown in Chapter 2 that many electrochemical cells involve junction regions where the composition is nonuniform and diffusion therefore occurs. The evaluation of the open-circuit potentials of these cells, and, in particular, the evaluation of the variation of the electrochemical potentials of ions in such junctions, requires consideration of these transport processes.

Equation 12.56 is applicable even in a nonuniform solution, and it can now be rewritten in terms of the conductivity and the transference numbers. Inversion of the order of summation in equation 12.56 gives

$$\mathbf{i} = -F \sum_{i \neq 0} c_i \nabla \mu_i \sum_{k \neq 0} L^0_{ki} z_k c_k, \tag{12.65}$$

where we have also relabeled the subscripts. Since $L^0_{ik} = L^0_{ki}$, substitution of equation 12.63 into equation 12.65 yields

$$\frac{F}{\kappa}\mathbf{i} = -\sum_i \frac{t^0_i}{z_i} \nabla \mu_i. \tag{12.66}$$

As already noted in Section 12.7, a different choice of the reference species will change the transference numbers, but it is apparent from the derivation that equation 12.66 still applies. However, equation 12.63 shows that the ratio t^0_j/z_j is not zero even for a neutral species. While the reference velocity can be chosen arbitrarily to be that of any one of the species, charged or uncharged, it is usually taken to be the velocity of the solvent. In this case there is no problem if there are no other neutral components, since the ratio t^0_i/z_i, is always zero for the reference species.

It is shown in Problem 12.7 that equation 12.66 also has the same form if other reference velocities, such as the mass-average velocity or the molar-average velocity, are used. Again, care should be exercised since the ratio t_i/z_i is then not zero for neutral species.

Equation 12.66 is quite useful in the calculation of the potential of cells with liquid junctions. It was presented and discussed in Section 2.5, and it was applied to the problem of liquid junctions in Chapters 2 and 6. In the cases of interest, the current density is supposed to be zero, but equation 12.66 also allows one to estimate the effect of the passage of small amounts of current. Equation 12.66 is generally useful only if the concentration profiles in the liquid junction are known. These are determined not from equation 12.66 but from the laws of diffusion (equation 12.1 or 12.52) and the method of forming the junction.

Substitution of equation 3.19 into equation 12.66 gives

$$\begin{aligned} F\nabla\Phi = &-\frac{F}{\kappa}\mathbf{i} - RT\sum_i \frac{t^0_i}{z_i}\nabla \ln c_i \\ &- RT\sum_i \frac{t^0_i}{z_i}\nabla\left(\ln f_i - \frac{z_i}{z_n}\ln f_n\right), \end{aligned} \tag{12.67}$$

where Φ is the quasi-electrostatic potential referred to species n. This equation, which was used in Chapter 6, can be compared with equation 11.44 or equation 11.11 and provides an additional

connection with the dilute-solution theory. It also suggests the validity of the Nernst–Einstein relation (see Section 12.5), since this relation was necessary in the derivation of equation 11.44.

PROBLEMS

12.1 Derive equations 12.8 and 12.9 from equations 12.1, 12.2, 11.2, and 12.3.

12.2 Let the transference number t_i, of a species with respect to the velocity $\mathbf{v}$ be defined by the equation

$$t_i\mathbf{i} = z_i F c_i(\mathbf{v}_i - \mathbf{v})$$

for a solution of uniform composition. This equation says that the flux of species i relative to the velocity $\mathbf{v}$ accounts for the fraction t_i, of the current density.

(a) Let t_i' be the transference number of species i relative to the velocity $\mathbf{v}'$. Show that the transference numbers of two species i and j relative to the velocities $\mathbf{v}$ and $\mathbf{v}'$ are related by

$$\frac{t_i' - t_i}{z_i c_i} = \frac{t_j' - t_j}{z_j c_j}.$$

(b) For a binary electrolyte, show that

$$\frac{t_0^+}{z_0} = -\frac{c_0 t_+^0}{z_+ c_+},$$

thus demonstrating that the ratio t_i/z_i is not always zero for a neutral species. Here t_0^+ is the transference number of the solvent relative to the cation velocity.

(c) Show for a binary electrolytic solution that

$$\mathbf{v} - \mathbf{v}_0 = \frac{1}{\rho}\left[-\frac{M_e \mathscr{D}}{\nu RT}\frac{c_T}{c_0} c \nabla \mu_e + \frac{\mathbf{i}}{F}\left(\frac{M_+ t_+^0}{z_+} + \frac{M_- t_-^0}{z_-}\right)\right],$$

where $\mathbf{v}$ is the mass-average velocity, and derive the relation between t_+ and t_+^0 given below equation 12.17.

(d) In a similar manner, derive the relation between t_+^* and t_+^0 given below equation 12.17.

12.3 Derive equation 2.75 from equation 12.27.

12.4 Derive equation 12.27 from equation 12.49, bearing in mind that Φ represents different quantities in the two equations.

12.5 For a binary electrolytic solution,

(a) State the form of the matrices $\mathbf{M}$ and $\mathbf{M}^0$.

(b) Invert $\mathbf{M}^0$ to obtain $\mathbf{L}^0$.

(c) By substitution of the result from part (b) into equations 12.60 and 12.62, verify equation 12.11 for the transference number and equation 12.23 for the conductivity.

(d) By substitution of the result from part (b) into equation 12.52 and elimination of the electrochemical potential of individual ions by means of equation 2.58, derive the expressions 12.8 and 12.9 for the fluxes of the ions.

12.6 Apply the development of Section 12.7 to a four-component system, 0, +, −, and 3. Take species 3 to be charged. In subsequent applications, one can set $z_3 = 0$ in order to treat mixed solvents or membranes. One can set c_0 equal to zero to treat fused salts.

12.7 Use the result of Problem 12.2(a) to show that t_i^0 in equation 12.66 can be replaced by the transference numbers relative to any reference velocity; that is, show that

$$\sum_i \frac{t_i}{z_i} \nabla \mu_i = \sum_i \frac{t_i'}{z_i} \nabla \mu_i.$$

12.8 Calculate the magnitude of a diffusion velocity $D_i \nabla \ln c_i$, and a migration velocity $z_i u_i F \nabla \Phi$ and compare with the magnitude of a typical convective velocity.

12.9 Derive equation 12.17 from equation 12.14 using also the continuity equation

$$\frac{\partial \rho}{\partial t} + \nabla \cdot (\rho \mathbf{v}) = 0$$

(see equation 15.2) and the expression for $\mathbf{v} - \mathbf{v}_0$ in Problem 12.2(c).

12.10 Show that $1 - d \ln c_0 / d \ln c$ appearing in equation 12.13 can also be written as

$$\frac{\rho}{c_0 M_0} \left(1 - \frac{d \ln \rho}{d \ln c} \right) = \frac{1}{c_0 \overline{V}_0}.$$

Appendix A may be helpful here. (See also Problem 2.1.)

12.11 Develop the generalized form of Ohm's law for a concentrated binary electrolyte using the quasi-electrostatic potential rather than the potential of a reference electrode. You may use the shorthand notation of $f_{i,n}$, where $f_{i,n}$ is defined by

$$\ln f_{i,n} = \ln f_i - \frac{z_i}{z_n} \ln f_n,$$

but bear in mind that some simplicity might accrue because there are only two types of ions. Does anything special happen when $\mathscr{D}_{0+} = \mathscr{D}_{0-}$, for which dilute-solution theory suggests the absence of a diffusion potential?

12.12 On the basis of Figure 12.1, estimate the potential difference on interruption of the current in a lead–acid cell when the PbO_2 electrode finds itself at $m_2 = 2$ mol/kg and the Pb electrode finds itself at $m_1 = 4$ mol/kg. Estimate the difference between the quasi-electrostatic potential in a 5 mol/kg solution of H_2SO_4 and the value in a 1 mol/kg solution.

NOTATION

a	parameter related to the stoichiometry of the salt
a_{+-}^{θ}	property expressing secondary reference state, liter/mol
c	molar concentration of a single electrolyte, mol/cm^3
c_i	concentration of species i, mol/cm^3
c_T	total solution concentration, mol/cm^3
D	measured diffusion coefficient of electrolyte, cm^2/s
D_i	diffusion coefficient of species i, cm^2/s

$\mathscr{D}$	diffusion coefficient of electrolyte, based on a thermodynamic driving force, cm^2/s
$\mathscr{D}_{ij}$	diffusion coefficient for interaction of species i and j, cm^2/s
f_{+-}	mean molar activity coefficient of an electrolyte
F	Faraday's constant, 96,487 C/mol
$\mathbf{i}$	current density, A/cm^2
i_{ss}	the steady-state current
i_0	the initial current
K_{ij}	friction coefficient for interaction of species i and j, $J \cdot s/cm^5$
L	distance between electrodes
L^0_{ij}	inverted transport coefficient, $cm^5/J \cdot s$
m	molality of a single electrolyte, mol/kg
M_e	molar mass of electrolyte, g/mol
M_i	symbol for the chemical formula of species i
M_i	molar mass of species i, g/mol
M_{ij}	modified friction coefficient, $J \cdot s/cm^5$
n	number of electrons involved in electrode reaction
n	number of species present in solution
Ne	Newman number
N_i	flux of species i, $mol/cm^2 s$
R	universal gas constant, 8.3143 J/mol·K
s_i	stoichiometric coefficient of species i in electrode reaction
t	time, s
$t_{+,\mathrm{id}}$	ratio of i_{ss} to i_0
t_i	transference number of species i with respect to the mass-average velocity
t_i^0	transference number of species i with respect to the velocity of species 0
t_i^*	transference number of species i with respect to the molar-average velocity
T	absolute temperature, K
u_i	mobility of species i, $cm^2 \cdot mol/J \cdot s$
$\mathbf{v}$	mass-average velocity, cm/s
v_i	velocity of species i, cm/s
$\mathbf{v}^*$	molar-average velocity, cm/s
x_e	mole fraction of electrolyte $= c/c_T$
z_i	charge number of species i
γ_{+-}	mean molal activity coefficient of an electrolyte
κ	conductivity, S/cm
μ_e	chemical potential of an electrolyte, J/mol
μ_i	electrochemical potential of species i, J/mol
ν	number of moles of ions into which a mole of electrolyte dissociates
ν_+, ν_-	numbers of cations and anions into which a molecule of electrolyte dissociates
ρ	density, g/cm^3
ρ_i	mass of species i per unit volume, g/cm^3
Φ	electric potential, V
Φ_A	anode potential
ω_e	mass fraction of electrolyte

Subscript

0	species 0, generally the solvent

REFERENCES

1. R. Byron Bird, Warren E Stewart, and Edwin N. Lightfoot. *Transport Phenomena*, 2 (New York: Wiley, 2002).
2. Lars Onsager, "Theories and Problems of Liquid Diffusion," *Annals of the New York Academy of Sciences*, *46* (1945), 241–265.
3. Richard W. Laity, "General Approach to the Study of Electrical Conductance and Its Relation to Mass Transport Phenomena," *Journal of Chemical Physics*, *30* (1959), 682–691.
4. Richard W. Laity, "An Application of Irreversible Thermodynamics to the Study of Diffusion," *Journal of Physical Chemistry*, *63* (1959), 80–83.
5. Alfred Klemm, "Thermodynamik der Transportvorgänge in Ionengemischen und ihre Anwendung auf isotopenhaltige Salze und Metalle," *Zeitschrift für Naturforschung*, *8a* (1953), 397–400.
6. A. Klemm, "Zur Phanomenologie der isothermen Diffusion in Elektrolyten," *Zeitschrift fur Naturforschung*, *17a* (1962), 805–807.
7. J. M. Burgers, "Some Problems of Magneto-Gasdynamics," in Sydney Goldstein, ed., *Lectures on Fluid Mechanics* (London: Interscience, 1960), pp. 271–299.
8. E. N. Lightfoot, E. L. Cussler, Jr., and R. L. Rettig, "Applicability of the Stefan-Maxwell Equations to Multicomponent Diffusion in Liquids," *AIChE Journal*, *8*(1962), 708–710.
9. C. Truesdell, "Mechanical Basis of Diffusion," *Journal of Chemical Physics*, *37* (1962), 2336–2344.
10. Ole Lamm, "Studies in the Kinematics of Isothermal Diffusion: A Macro-Dynamical Theory of Multicomponent Fluid Diffusion," in I. Prigogine, ed., *Advances in Chemical Physics*, Vol. *6* (New York, Wiley, 1964), pp. 291–313.
11. John Newman, Douglas Bennion, and Charles W. Tobias, "Mass Transfer in Concentrated Binary Electrolytes," *Berichte der Bunsengesellschaft für physikalische Chemie*, *69* (1965), 608-612. [For corrections see ibid., *70* (1966), 493.]
12. John Newman and Thomas W. Chapman, "Restricted Diffusion in Binary Solutions," *AIChE Journal*, *19* (1973), 343–348.
13. J. Newman and L. Hsueh, "The Effect of Variable Transport Properties on Mass Transfer to a Rotating Disk," *Electrochimica Acta*, *12* (1967), 417–427.
14. Richard Pollard and John Newman, "Transport Equations for a Mixture of Two Binary Molten Salts in a Porous Electrode," *Journal of the Electrochemical Society*, *126* (1979), 1713–1717.
15. N. P. Balsara and J. Newman, "Relationship between Steady-State Current in Symmetric Cells and Transference Number of Electrolytes Comprising Univalent and Multivalent Ions," *Journal of The Electrochemical Society*, *162* (2015), A2720–A2722.
16. P. G. Bruce and C. A. Vincent, "Steady-State Current Flow in Solid Binary Electrolyte Cells", *Journal of Electroanalytical Chemistry*, *255* (1987), 1–17.
17. Richard J. Bearman, "The Onsager Thermodynamics of Galvanic Cells with Liquid-Liquid Junctions," *Journal of Chemical Physics*, *22* (1954), 585–587.
18. Richard J. Bearman and John G. Kirkwood, "Statistical Mechanics of Transport Processes. XI. Equations of Transport in Multicomponent Systems," *Journal of Chemical Physics*, *28* (1958), 136–145.
19. William H. Smyrl and John Newman, "Potentials of Cells with Liquid Junctions," *Journal of Physical Chemistry*, *72* (1968), 4660–4671.
20. Richard Pollard and John Newman, "Silicon Deposition on a Rotating Disk," *Journal of the Electrochemical Society*, *127* (1980), 744–752.
21. Bernard Tribollet and John Newman, "Impedance Model for a Concentrated Solution: Application to the Electrodissolution of Copper in Chloride Solutions," *Journal of the Electrochemical Society*, *131* (1984), 2780–2785.

CHAPTER 13

THERMAL EFFECTS

Electrochemical systems have a complicated interplay of mass-transfer and chemical reactions, as described in previous chapters. But situations are seldom isothermal. Heat is generated and carried out of the system, and temperatures are also modified by evaporation, condensation, and precipitation. In this chapter, we need to describe how mass transfer is modified in a nonuniform temperature field and then discuss the basic relationship for heat transfer in regions of complex chemical composition. The combined set of gradients and of heat- and mass-transfer rates is coupled so that heat transfer influences mass transfer, and vice versa, within a given phase. Interphase mass transfer can also generate heat in a way that is particularly important in electrochemical systems. In Section 13.3, reversible and irreversible heat generation is addressed to show how it depends on current and surface overpotential. Section 13.4 treats some aspects of quantifying the electrical state in these complex systems, a function served by reference electrodes in isothermal systems. This section also shows an alternative and perhaps easier method of calculating heat generation at an interface without using a calorimeter. This entails measuring the open-circuit potentials of electrodes as a function of the temperature of individual electrodes, allowing us to pinpoint at which electrode the heat is being generated. A similar measurement of the temperature dependence of the open-circuit potential for a whole cell permits the reversible heat generation in a complete cell to be related to the entropy change for the cell reaction.

Hirschfelder et al.[1] have given a complete and rigorous description of the governing transport laws. Our purpose here is to show how these equations apply also to electrochemical systems if we treat μ_i as the electrochemical potential for an ionic species (instead of the chemical potential). Agar[2] and Denbigh[3] give readable accounts of irreversible thermodynamics that find application here.

Electrochemical Systems, Fourth Edition. John Newman and Nitash P. Balsara.

13.1 THERMAL DIFFUSION

The multicomponent diffusion equation 12.1 relates the driving force for diffusion to resistive forces due to the relative motion of the species. The generalization for cases where there are simultaneously gradients of temperature and pressure would be[1]

$$c_i\left(\nabla\mu_i + \bar{S}_i\nabla T - \frac{M_i}{\rho}\nabla p\right) - RT\sum_j \frac{c_i c_j}{c_T\mathscr{D}_{ij}}\left(\frac{D_j^T}{\rho_j} - \frac{D_i^T}{\rho_i}\right)\nabla \ln T$$
$$= RT\sum_j \frac{c_i c_j}{c_T\mathscr{D}_{ij}}(\mathbf{v}_j - \mathbf{v}_i), \tag{13.1}$$

where $\bar{S}_i$ and D_i^T are the partial molar entropy and the *thermal diffusion coefficient* of species i. The first modification is that the driving force for diffusion and migration is now written according to the first term of this equation. These driving forces now sum to zero even when the temperature and pressure vary. Furthermore, they describe properly equilibrium in a gravitational or centrifugal field (see Problem 13.1). Also, $\nabla\mu_i$ by itself is meaningless if $\nabla T \neq 0$ because primary reference states for entropy do not then cancel.

The second modification is the inclusion of thermal diffusion, represented by the terms in $\nabla \ln T$ in equation 13.1. The gradient of the temperature is a new driving force in the system, in addition to the $n-1$ driving forces $c_i[\nabla\mu_i + \bar{S}_i\nabla T - (M_i/\rho)\nabla p]$, which will be written for brevity occasionally as $\mathbf{d}_i$. The gradient of pressure is not really an independent driving force for heat and mass transfer; rather, it is a driving force for fluid flow, as discussed in Chapter 15. The temperature gradient can contribute to mass transport, as shown in equation 13.1. This process is called thermal diffusion, also known as the *Soret effect*, whereby a temperature gradient maintained across a solution can lead to a variation in composition. The converse process, called the *Dufour effect*, is mentioned in the next section. Thermal diffusion is not, however, usually important in industrial systems. The thermal diffusion coefficients D_i^T are additional transport properties, of which only $n-1$ are independent since they always appear as differences as in equation 13.1. It would make more sense to call D_i^T/ρ_i the thermal diffusion coefficient since this quantity has the units of cm^2/s and $D_A^T/\rho_A - D_B^T/\rho_B$ is approximately constant for a binary solution. Therefore, we define a redundant set of coefficients

$$A_j^i = \frac{D_j^T}{\rho_j} - \frac{D_i^T}{\rho_i} \tag{13.2}$$

so as to achieve an economy of notation and so that A_j^i has the units of cm^2/s.

For a binary electrolyte, we can combine equation 13.1 to yield

$$\mathbf{N}_+ = -\frac{\nu_+\mathscr{D}}{\nu RT}\frac{c_T}{c_0}c\left(\nabla\mu_e + \bar{S}_e\nabla T - \frac{M_e}{\rho}\nabla p\right) + \frac{\mathbf{i}t_+^0}{z_+F} + c_+\mathbf{v}_0 + c_+\mathscr{D}\sigma\nabla T. \tag{13.3}$$

This is a generalization of equation 12.8, $\mathscr{D}$ and t_+^0 being defined by equations 12.10 and 12.11, and σ, called the *Soret coefficient*, is

$$\sigma = \frac{1}{\mathscr{D}T}(t_-^0 A_0^+ + t_+^0 A_0^-). \tag{13.4}$$

With a mass-fraction driving force and a mass-average reference velocity, equation 12.19 now becomes

$$\mathbf{N}_+ = -\nu_+\frac{\rho D}{M_e}\nabla\omega_e + \frac{\mathbf{i}t_+}{z_+F} + c_+\mathbf{v} - \frac{\nu_+\mathscr{D}c_T c}{\nu}\frac{M_0}{RT\rho}\left(\overline{V}_e - \frac{M_e}{\rho}\right)\nabla p + c_+\omega_0\sigma\mathscr{D}\nabla T, \tag{13.5}$$

where D is given by equation 12.12 and t_+ is given below equation 12.17. Consequently, the differential material balance 12.17 is replaced by

$$\rho\left(\frac{\partial\omega_e}{\partial t} + \mathbf{v}\cdot\nabla\omega_e\right) = \nabla\cdot(\rho D\nabla\omega_e) - \frac{M_e\mathbf{i}\cdot\nabla t_+}{z_+\nu_+F} + \frac{M_0}{\nu}\nabla\cdot\left[\mathscr{D}c_T\omega_e\left(\overline{V}_e - \frac{M_e}{\rho}\right)\frac{\nabla p}{RT}\right] - \nabla\cdot(\omega_e\omega_0\rho\mathscr{D}\sigma\nabla T). \tag{13.6}$$

Consideration of entropy production and the second law of thermodynamics shows that σ is governed by the inequality

$$\sigma^2 \le \frac{c_T k'}{\nu c_0 c\mathscr{D}RT^2}, \tag{13.7}$$

where k' is the thermal conductivity (see Section 13.2). Thus, σ can be either positive or negative, depending on whether the solvent or the electrolyte migrates toward the hot wall under the influence of thermal diffusion.

By following the development in Sections 12.6 and 12.7, we can invert equation 13.1 and then derive the result

$$\mathbf{i} = -\frac{\kappa}{F}\sum_i \frac{t_i^0}{z_i}\left(\nabla\mu_i + \overline{S}_i\nabla T - \frac{M_i}{\rho}\nabla p\right) - F\sum_i z_i c_i A_i^0\nabla\ln T, \tag{13.8}$$

where the transference numbers t_i^0 and the conductivity κ are given by equations 12.63 and 12.60, respectively.

For a binary electrolyte, this equation becomes

$$\mathbf{i} = -\frac{\kappa t_+^0}{z_+\nu_+F}\left(\nabla\mu_e + \overline{S}_e\nabla T - \frac{M_e}{\rho}\nabla p\right) - z_+\nu_+FcA_+^-\nabla\ln T - \frac{\kappa}{z_-F}\left(\nabla\mu_- + \overline{S}_-\nabla T - \frac{M_-}{\rho}\nabla p\right). \tag{13.9}$$

The total derivative of μ_e is

$$\nabla\mu_e = \left(\frac{\partial\mu_e}{\partial m}\right)_{T,p}\nabla m + \left(\frac{\partial\mu_e}{\partial T}\right)_{m,p}\nabla T + \left(\frac{\partial\mu_e}{\partial p}\right)_{m,T}\nabla p = \nu RT\left(1 + \frac{\partial\ln\gamma_\pm}{\partial\ln m}\right)_{T,p}\frac{\nabla m}{m} - \overline{S}_e\nabla T + \overline{V}_e\ \nabla p, \tag{13.10}$$

and, therefore, the first term in parentheses in equation 13.9 could also be written as

$$\nabla\mu_e + \overline{S}_e\nabla T - \frac{M_e}{\rho}\nabla p = \frac{\nu RT}{\omega_e\omega_0}\left(1 + \frac{\partial \ln\gamma_\pm}{\partial \ln m}\right)_{T,p}\nabla\omega_e + \left(\overline{V}_e - \frac{M_e}{\rho}\right)\nabla p. \tag{13.11}$$

Note that a different combination of thermal diffusion coefficients occurs in equation 13.9 from that which occurs in equations 13.3, 13.4, and 13.6. In equation 13.9, the $A_+^-\nabla \ln T$ term is new and shows how a temperature gradient influences current flow directly. Thus, we see that the fluxes of heat, mass, and charge are all interrelated at some level.

It is even more difficult to define an electric potential in a solution of varying temperature than in one of varying composition. Even with reference electrodes, thermoelectric effects between the electrode leads and the potential-measuring device must be taken into account (see Section 13.4 and Newman[4]). Equation 13.9 is the analogue of equation 11.23 or 12.27 representing conduction effects, or the generalization of Ohm's law. For the present, we shall let $\nabla\mu_- + \overline{S}_-\nabla T - (M_-/\rho)\nabla p$ represent the effect of a spatial variation of the electrical state of the solution.

Tyrrell[5] has summarized some measurements of Soret coefficients in electrolytic solutions. The value of σ is about 2 to 5×10^{-3} K^{-1}.

13.2 HEAT GENERATION, CONSERVATION, AND TRANSFER

Electrolytic solutions are described by the same basic equations as nonelectrolytic solutions, caution being used to regard the chemical potential μ_i as the electrochemical potential if it applies to an ionic species. The first law of thermodynamics is used to deduce a differential energy balance, which includes the kinetic energy of the flowing fluid. The momentum equation 15.4 is used to subtract this mechanical energy, yielding a thermal energy balance. By means of the appropriate thermodynamic relationships for mixtures, this can be put into the form[6]

$$\rho\hat{C}_p\left(\frac{\partial T}{\partial t} + \mathbf{v}\cdot\nabla T\right) + \left(\frac{\partial \ln\rho}{\partial \ln T}\right)_{p,\omega_i}\left(\frac{\partial p}{\partial t} + \mathbf{v}\cdot\nabla p\right)$$
$$= -\nabla\cdot\mathbf{q} - \boldsymbol{\tau}:\nabla\mathbf{v} + \sum_i \overline{H}_i(\nabla\cdot\mathbf{J}_i - R_i). \tag{13.12}$$

The last term on the right represents thermal effects due to diffusion, migration, and chemical reaction. Here, $\mathbf{J}_i$ is the flux density of species i relative to the mass-average velocity:

$$\mathbf{J}_i = \mathbf{N}_i - c_i\mathbf{v}. \tag{13.13}$$

The second and third terms on the right and the last term on the left represent irreversible and reversible conversion of mechanical energy into thermal energy, $\boldsymbol{\tau}$ being the stress (see Section 15.2). The term $-\boldsymbol{\tau}:\nabla\mathbf{v}$ is referred to as the viscous dissipation.

The heat flux $\mathbf{q}$ can be expressed as

$$\mathbf{q} = \sum_i \overline{H}_i\mathbf{J}_i - k\nabla T + \mathbf{q}^{(x)}, \tag{13.14}$$

the three terms being, respectively, heat carried by the interdiffusion of the species, heat transfer by conduction with the thermal conductivity k, and the Dufour energy flux density given by

$$\mathbf{q}^{(x)} = -\sum_i \frac{D_i^T}{\rho_i}c_i\left(\nabla\mu_i + \overline{S}_i\nabla T - \frac{M_i}{\rho}\nabla p\right). \tag{13.15}$$

The Dufour effect is the converse of thermal diffusion, treated in Section 13.1, and accounts for the balance of the heat induced by interdiffusion. The thermal diffusion coefficients D_i^T are the same as those introduced in the preceding section. Again, the Dufour effect is not usually important in industrial systems. Substitution of equation 13.14 into equation 13.12 yields

$$\rho\hat{C}_p\left(\frac{\partial T}{\partial t}+\mathbf{v}\cdot\nabla T\right)+\left(\frac{\partial \ln\rho}{\partial \ln T}\right)_{p,\omega_i}\left(\frac{\partial p}{\partial t}+\mathbf{v}\cdot\nabla p\right)$$
$$=\nabla\cdot(k\nabla T)-\nabla\cdot\mathbf{q}^{(x)}-\sum_i \mathbf{J}_i\cdot\nabla\overline{H}_i-\boldsymbol{\tau}:\nabla\mathbf{v}-\sum_i \overline{H}_i R_i. \tag{13.16}$$

The thermal effect due to diffusion and migration now appears in a modified form.

For water at 20°C, $\partial \ln\rho/\partial T = -0.207\times10^{-3}\ \mathrm{K}^{-1}$. Since $\hat{C}_p = 4.1819\ \mathrm{J/g\cdot K}$, a change in pressure of 1 bar in the last term on the left in equation 13.16 corresponds to a temperature change of only 0.00145 K in the first term. Consequently, the pressure term in equation 13.16 is usually negligible for condensed phases. More generally, the pressure changes in a system would be calculated by solving the fluid mechanics (Chapter 15).

For a binary electrolyte, the heat flux can be expressed as

$$-k\nabla T+\mathbf{q}^{(x)}=-k'\nabla T+\mathscr{D}T\sigma\mathbf{d}_e+\frac{z_+c_+F}{\kappa}A_+^-\mathbf{i}. \tag{13.17}$$

Here the current density has been introduced from equation 13.9 to avoid using the potential in the solution. This also means that a somewhat different thermal conductivity is measured if no current is ever allowed to pass through the solution:

$$k'=k-\frac{(z_+\nu_+Fc)^2}{\kappa T}(A_-^+)^2. \tag{13.18}$$

If we go a step farther and require that all species fluxes be zero, then we have

$$\mathbf{q}=-k''\nabla T, \tag{13.19}$$

where

$$k''=k'-\frac{\mathscr{D}Rc_0c}{c_T}T^2\sigma^2. \tag{13.20}$$

Thus, a measurement of the heat flux yields the thermal conductivity k'' rather than k' if no special attention is given to the fact that the composition varies within the system and the system is allowed to reach steady state with respect to thermal diffusion. A separate measurement of the Soret coefficient is necessary to yield k'. Evidently caution needs to be used in reporting or using thermal conductivities in the literature. However, the differences among k, k', and k'' are generally small (see Problem 13.11). A multicomponent version of k'' is given later in equation 13.26. In summary, k applies when $\mathbf{d}_i = 0$, k' applies when $\mathbf{i} = 0$, and k'' is evidently the thermal conductivity that would naturally be measured if mass-transfer rates were zero in an experiment, a situation that can be realized more easily than trying to maintain all $\mathbf{d}_i$ equal to zero. (The second law of thermodynamics shows that k'' is never negative; cf. equation 13.7.)

An important difference between electrical and nonelectrical systems is the conversion of electrical energy to thermal energy, called Joule heating, due to the passage of electric current. This arises from the first term in the heat-flux equation 13.14. For example, the current density $\mathbf{i}$ can be related to the

flux densities, $\mathbf{i} = F\sum_i z_i \mathbf{J}_i$, and in a solution of uniform temperature, pressure, and composition, the partial molar enthalpy is related to the electrochemical potential and hence to the electric potential

$$\nabla \overline{H}_i = \nabla \mu_i = z_i F \nabla \Phi, \tag{13.21}$$

as used in this sense already in Section 2.2. Consequently,

$$-\nabla \cdot \sum_i \overline{H}_i \mathbf{J}_i = -\sum_i \mathbf{J}_i \cdot \nabla \overline{H}_i = -\mathbf{i} \cdot \nabla \Phi = \frac{\mathbf{i} \cdot \mathbf{i}}{\kappa}. \tag{13.22}$$

Thus, we conclude that the first term in equation 13.14 is by no means negligible and that the third term on the right in equation 13.16 can be associated in part with Joule heating.

For a constant value of k' or for constant values of ρ and $\hat{C}_p$, it is appropriate to define a thermal diffusivity as $k'/\rho\hat{C}_p$. The thermal energy balance 13.16 then resembles the equation of convective diffusion 11.21 but with source terms for generation of heat by Joule heating, viscous dissipation, and chemical reaction. For water at 20°C, the value of the thermal diffusivity is 1.43×10^{-3} cm^2/s, about 100 times larger than diffusion coefficients encountered in aqueous solutions.

13.3 HEAT GENERATION AT AN INTERFACE

Let us make an energy balance on an interface where a single electrode reaction

$$\sum_i s_i M_i^{z_i} \rightarrow 0 \tag{13.23}$$

is occurring at a steady state (thereby excluding the storage of energy in a charged electric double layer, see Chapter 7).* The total energy flux density must then be continuous:

$$\Delta \left[\left(\frac{1}{2}\rho v^2 + \rho \hat{U} + p \right) v_y + q_y \right] = 0, \tag{13.24}$$

where y is the distance from the electrode into the solution and v_y is measured relative to the interface.

One can use equation 13.1 to replace driving forces $\mathbf{d}_i$ with flux densities $\mathbf{N}_i$ in the thermal-flux-density equations 13.14 and 13.15. After substantial algebraic manipulation,[4] this can be rearranged into the convenient or canonical form

$$\mathbf{q} = \sum_i \overline{H}_i \mathbf{J}_i - k'' \nabla T - RT \sum_i \mathbf{N}_i \sum_j \frac{c_j A_j^i}{c_T \mathscr{D}_{ij}}, \tag{13.25}$$

where

$$k'' = k - \frac{R}{2} \sum_i \sum_j \frac{c_i c_j}{c_T \mathscr{D}_{ij}} (A_j^i)^2. \tag{13.26}$$

With neglect of the kinetic energy and the use of the relationship $\overline{H}_i = \mu_i + T\overline{S}_i$, the energy balance 13.24 becomes

$$-k'' \frac{\partial T}{\partial y} + k_{\mathrm{I}}'' \frac{\partial T_{\mathrm{I}}}{\partial y} = i_y \eta_s + i_y \Pi, \tag{13.27}$$

*We follow the methodology of Section 23.4, whereby electrons are not always mentioned explicitly but are lumped into the sum. Equations 13.23 and 13.28 are thus different from what we are used to.

where I denotes the electrode phase,

$$\eta_s = \frac{1}{nF}\sum_i s_i \mu_i \tag{13.28}$$

is the surface overpotential (8.2 or 23.42) for the electrochemical reaction, and

$$\Pi = \frac{T}{nF}\sum_i s_i \bar{S}_i - \frac{RT}{nF}\left(\sum_i s_i \sum_j \frac{c_j A_j^i}{c_T \mathscr{D}_{ij}}\right)_{\text{soln}} - \frac{RT}{nF}\left(\sum_i s_i \sum_j \frac{c_j A_j^i}{c_T \mathscr{D}_{ij}}\right)_{\text{I}} \tag{13.29}$$

is the *Peltier coefficient*. In this way, $i_y \eta_S$ represents irreversible heat generation at the interface, and $i_y \Pi$ is reversible heat generation. Π has two distinctly different kinds of terms. The sum of partial molar entropies, even though it includes electrically charged species on either side of the interface, represents the major contribution to the reversible heat generation at an interface and predominately quantifies how much heat is generated at each electrode in a cell. The terms in thermal diffusion coefficients represent a correction that would be zero if the Dufour energy were negligible. This is written as two separate terms to remind us that the sums over j include only species in the phase that s_i represents.

The term *Seebeck coefficient*, or possibly galvanic Seebeck coefficient, is sometimes used for $-\Pi/T$.

For a whole electrochemical cell, the reversible heat effects at the two electrodes subtract to yield a quantity that is frequently measured. Then $Q_{\text{rev}} = I(\Pi_{\text{neg}} - \Pi_{\text{pos}})$, where Q_{rev} is the heat generated in the cell and I is the current at the negative (or left) electrode, taken to be positive for an anodic current at that electrode. For example, for cell 2.106, involving a silver–silver chloride electrode and a hydrogen electrode, the reversible heat generated is

$$Q_{\text{rev}} = \frac{IT}{F}\left(\bar{S}^{\beta}_{\text{HCl}} + \bar{S}^{\lambda}_{\text{Ag}} - \frac{1}{2}\bar{S}^{\alpha}_{\text{H}_2} - \bar{S}^{\varepsilon}_{\text{AgCl}}\right), \tag{13.30}$$

the quantity in parentheses being the entropy change for the overall cell reaction:

$$\frac{1}{2}\text{H}_2 + \text{AgCl} \rightleftharpoons \text{Ag} + \text{HCl}. \tag{13.31}$$

Here we have ignored the difference between phases β and δ. The entropy change for the overall cell reaction can be obtained from the temperature coefficient of the reversible cell potential (see equation 2.107):

$$\bar{S}^{\beta}_{\text{HCl}} + \bar{S}^{\lambda}_{\text{Ag}} - \frac{1}{2}\bar{S}^{\alpha}_{\text{H}_2} - \bar{S}^{\varepsilon}_{\text{AgCl}} = F\left(\frac{\partial U}{\partial T}\right)_p, \tag{13.32}$$

so that equation 13.30 becomes

$$Q_{\text{rev}} = IT\left(\frac{\partial U}{\partial T}\right)_p, \tag{13.33}$$

U being the potential at the positive (or right) electrode, relative to the negative (or left) electrode. It should be noted that the reversible heat for an electrochemical cell is not related to the enthalpy change for the reaction but to the entropy change. The enthalpy change is appropriate for pressure–volume systems but not to electrical systems. (Similarly, the Peltier heat can be related to the change of potential when the temperature of one electrode is changed. This allows us to attribute the heat generation locally, to one electrode or the other. See the next section.)

Some texts use a quantity called the heat of transfer, Q_i^*, instead of thermal diffusion coefficients, A_j^i. For a binary electrolyte, one can state the relationship, based on Denbigh,[3] pp. 78 ff, as

$$Q_+^* = -\frac{z_+ z_- \nu_+ \nu_- F^2 c}{\nu_+ \kappa} A_+^- - \frac{\nu R T^2 c_0 t_-^0}{\nu_+ c_T}\sigma. \tag{13.34}$$

A symmetric form applies for Q_-^*. Diffusion of the electrolyte in the absence of current flow might be expected to involve the quantity

$$Q_e^* = \nu_+ Q_+^* + \nu_- Q_-^* = -\frac{\nu R T^2 c_0}{c_T}\sigma, \tag{13.35}$$

without the appearance of the term A_+^-.

A suitable multicomponent form for Q_i^* is

$$Q_i^* = -RT \sum_j \frac{c_j A_j^i}{c_T \mathscr{D}_{ij}}, \tag{13.36}$$

a form suggested by equation 13.25.

13.4 THERMOGALVANIC CELLS

Calculation of the heat generation at an interface requires knowledge of Π. In this section, we describe how to use experimental data to calculate Π_i for each electrode in a cell. This permits us to specify at which electrode the reversible heat is being generated.

Figure 13.1 shows a simple thermogalvanic cell where an aqueous solution of copper sulfate is confined between two horizontal copper electrodes, the upper of which is maintained at a higher temperature than the lower. What will be the potential difference measured between the two copper wires, which are brought to the same temperature at the potentiometer? In this experiment we consider the steady state (after Soret diffusion has occurred) in the absence of current so that all the species fluxes are zero. In addition, we neglect the pressure variation induced by the gravitational field.

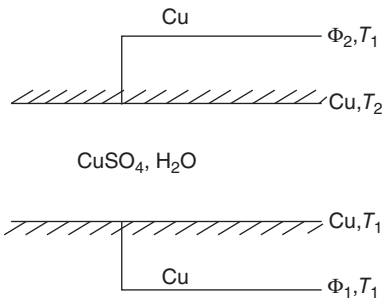

Figure 13.1 Thermogalvanic cell.

In this situation, equation 13.3 or 13.5 reduces to

$$\nabla \mu_e + \bar{S}_e \nabla T = \frac{\nu c_0 R T \sigma}{c_T} \nabla T \tag{13.37}$$

or

$$\nabla \ln m = \frac{\nabla \omega_e}{\omega_e \omega_0} = \frac{\mathscr{D}\sigma}{D}\nabla T = \frac{c_0 \sigma \nabla T}{c_T\left(1 + \dfrac{\partial \ln \gamma_\pm}{\partial \ln m}\right)_{T,p}}, \tag{13.38}$$

where the coefficient of ∇T in the last expression is called the practical Soret coefficient. These equations thus describe how the variation in the solution composition is related to the Soret coefficient σ or how the Soret coefficient can be determined by measuring this variation in composition. Equation 13.1 becomes

$$\nabla \mu_+ = -\bar{S}_+ \nabla T + R\left(\frac{c_0 A_0^+}{c_T \mathscr{D}_{0+}} + \frac{c_- A_-^+}{c_T \mathscr{D}_{+-}}\right)\nabla T \tag{13.39}$$

or

$$\frac{\nabla \mu_+}{z_+ F} = \left(\frac{R c_0 T \sigma \mathscr{D}}{z_+ F c_T \mathscr{D}_{0+}} + \xi_+\right)\nabla T, \tag{13.40}$$

where

$$\xi_+ = \frac{z_+ c_+ F}{\kappa T} A_-^+ - \frac{\bar{S}_+}{z_+ F} \tag{13.41}$$

and might be called a thermoelectric coefficient (see Problem 13.2). Equation 13.40 is used to assess the variation of the electrical state within the solution. We generalize the analysis to include different reactions at the electrodes but still restrict it to a binary electrolyte. Thus, it can apply not only to the $CuSO_4$ thermocell but also to a hydrogen/oxygen fuel cell or to the hydrogen/silver–silver chloride cell 2.106.

Just as in Chapter 2, we can write

$$FU = F(\Phi_2 - \Phi_1) = \mu_{e^-}^{(1)}(T_1) - \mu_{e^-}^{(2)}(T_1). \tag{13.42}$$

Since the lower lead in Figure 13.1 is isothermal, there is no variation of $\mu_{e^-}^{(1)}$, but for the upper lead (see Problem 13.2)

$$\mu_{e^-}(T_2) - \mu_{e^-}(T_1) = F\int_{T_1}^{T_2} \xi_{\text{lead}}\, dT, \tag{13.43}$$

where

$$\xi_{\text{lead}} = \frac{1}{F}\left[-\bar{S}_{e^-} + \frac{R c_+ A_+^-}{c_T \mathscr{D}_{+-}}\right]_{\text{lead}}. \tag{13.44}$$

Substituting successively into the equation for FU, we have

$$\begin{aligned} FU &= \mu_{e^-}^{(1)}(T_1) - \mu_{e^-}^{(2)}(T_2) + F\int_{T_1}^{T_2} \xi_{\text{lead}}^{(2)}\, dT \\ &= \sum_{i \neq e^-}\left(\frac{s_{i,1}}{n_1} - \frac{s_{i,2}}{n_2}\right)\mu_i(T_1) + \sum_{i \neq e^-}\frac{s_{i,2}}{n_2}[\mu_i(T_1) - \mu_i(T_2)] + F\int_{T_1}^{T_2} \xi_{\text{lead}}^{(2)}\, dT. \end{aligned} \tag{13.45}$$

The first term we recognize as $FU_{2,1}(T_1)$, the open-circuit potential of an isothermal cell at T_1.

Next we have to evaluate the differences between μ_i at the two temperatures, which generally requires integration of a form like equation 13.39 or 13.40 across the solution from one temperature

to the other. However, extraneous phases such as Ag, H_2, and AgCl in cell 2.106 are not solution components and require only integration of the molar entropy. Hence we have

$$\begin{aligned} FU &= FU_{2,1}(T_1) + \sum_{i \neq e^-} \frac{s_{i,2}}{n_2} \int_{T_1}^{T_2} \frac{d\mu_i}{dT}\, dT + F \int_{T_1}^{T_2} \xi_{\text{lead}}^{(2)}\, dT \\ &= FU_{2,1}(T_1) - \sum_{i \neq e^-} \frac{s_{i,2}}{n_2} \int_{T_1}^{T_2} \overline{S}_i\, dT - \int_{T_1}^{T_2} \left[\frac{s_{+,2}}{n_2} Q_+^* + \frac{s_{-,2}}{n_2} Q_-^* + \frac{s_{0,2}}{n_2} Q_0^* \right] \frac{dT}{T} \\ &\quad + F \int_{T_1}^{T_2} \xi_{\text{lead}}^{(2)}\, dT. \end{aligned} \tag{13.46}$$

Forms of Q_+^*, Q_-^*, and Q_0^* can be found in equation 13.34 and in Problem 13.12. We now have, after a little algebra,

$$\begin{aligned} FU = FU_{2,1}(T_1) &- \sum_{i \neq e^-} \frac{s_{i,2}}{n_2} \int_{T_1}^{T_2} \overline{S}_i\, dT + \int_{T_1}^{T_2} \frac{z_+ \nu_+ F^2 c A_+^-}{\kappa T}\, dT \\ &+ \int_{T_1}^{T_2} \frac{\nu R T^2}{c_T} \sigma \left(\frac{c_0 t_-^0}{\nu_+} \frac{s_{+,2}}{n_2} + \frac{c_0 t_+^0}{\nu_-} \frac{s_{-,2}}{n_2} - \frac{c s_{0,2}}{n_2} \right) \frac{dT}{T} + F \int_{T_1}^{T_2} \xi_{\text{lead}}^{(2)}\, dT. \end{aligned} \tag{13.47}$$

Comparison with equation 13.29 shows that the open-circuit potential is

$$U = U_{2,1}(T_1) - \int_{T_1}^{T_2} \frac{\Pi_2}{T} dT. \tag{13.48}$$

By modifying the derivation appropriately, this can also be written as

$$U = U_{2,1}(T_2) - \int_{T_1}^{T_2} \frac{\Pi_1}{T} dT. \tag{13.49}$$

Hence,

$$\left(\frac{\partial U}{\partial T_1} \right)_{T_2} = \frac{\Pi_1}{T_1} \tag{13.50}$$

and

$$\left(\frac{\partial U}{\partial T_2} \right)_{T_1} = -\frac{\Pi_2}{T_2}. \tag{13.51}$$

A side problem is that $\Pi_1 - \Pi_2 \neq -T\Delta S/nF$, but instead there is an extra term involving σ for a lead–acid cell (see Ref. [4]) and possibly for cell 2.106, but not for the $CuSO_4$ system or for the hydrogen/oxygen fuel cell.

13.5 CONCLUDING STATEMENTS

The differential energy balance 13.16 is the basis for calculating the temperature profile across an electrochemical cell. Heat conduction can carry thermal energy in or out or through the cell, and Joule heating represents an irreversible source of thermal energy. The energy flux equations are given in

Section 13.2. Reversible and irreversible heat sources at an electrode boundary are in equation 13.27. Standard heat-transfer boundary conditions of conduction, convection, and/or radiation apply at the periphery of the cell. In many cases, the electrochemical cell is thermally thin, so that temperature gradients within the cell are not important, but one needs to calculate the temperature rise within the cell, as heat is generated and carried out of the cell. In that case, the simplified energy balance in equation 22.19 can be used, where I is positive on discharge (or when anodic at the negative electrode). Measuring $\partial U/\partial T$ separately for each electrode, with respect to a second electrode at a fixed temperature, yields the Peltier heat (see equation 13.50), which forms the basis for splitting the reversible heat between the two electrodes. The simplified energy balance (22.19) does not include heats of mixing; these heat effects observed on relaxation after the current is interrupted are discussed in more detail in studies on a general energy balance (Bernardi et al.[7] and Thomas and Newman[8]). $U - T\,\partial U/\partial T$ is the thermoneutral potential or enthalpy potential; when V is less than $U - T\,\partial U/\partial T$ and I is positive, heat is exothermic, and the temperature will increase.

PROBLEMS

13.1 **(a)** Show that, for gravitational equilibrium in a region of uniform temperature, the variation of the chemical potential of a species is given by

$$\nabla \mu_i = \frac{M_i}{\rho} \nabla p.$$

Do this by consideration of a reversible process of removing a mole of the species at one point in the field, moving it against the force of gravity, and reintroducing it at another point. If possible, avoid assuming that the gravitational field is uniform.

Consideration of the process gives some justification for the expression for the driving force for diffusion, $c_i[\nabla \mu_i + \overline{S}_i \nabla T - (M_i/\rho)\nabla p]$, since this driving force should reduce to zero in such an equilibrium situation.

(b) Consider whether this relation correctly describes the equilibrium distributions of concentration in a centrifuge.

(c) The molar mass of NaCl is 58.44 g/mol, and that of H_2O is 18.015. If sea water is 0.5 M in NaCl and 55 M in H_2O at the surface, would the equilibrium concentrations of both H_2O and NaCl be higher at a depth of 2000 m?

13.2 **(a)** A thermocouple consists of metal I and metal II, one junction being at temperature T and the other junction being at temperature T_R, at which temperature the measurement of potential is made. With no current being passed, show that the potential difference measured (see Figure 13.2) is

$$\Phi_{\mathrm{II}} - \Phi_{\mathrm{I}} = \int_{T_R}^{T} (\xi_{\mathrm{II}} - \xi_{\mathrm{I}})\, dT,$$

where, for each metal,

$$\xi = \left(\frac{D_-^{\mathrm{T}}}{\rho_-} - \frac{D_+^{\mathrm{T}}}{\rho_+} \right) \frac{z_- c_- F}{\kappa T} + \frac{\overline{S}_-}{z_- F},$$

the metals being regarded as composed of electrons and metal ions. The electrons are equilibrated between the two metals at the temperature T. This problem gives some insight into what quantity ξ can be determined from the properties of the thermocouple.

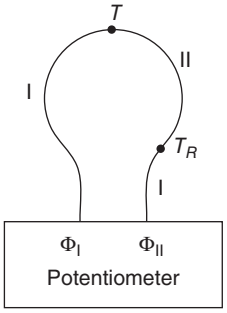

Figure 13.2 Thermocouple.

(b) For given sizes of the wires, what current would be passed through the thermocouple when the ends are shorted together?

(c) It is desired to study the potential of a concentration cell in liquid ammonia at 223 K:

$$\mathrm{Cu}\,\Big|_{283}^{\mathrm{W}}\,\Big|\,\mathrm{Pb}\,\Big|_{223}^{\mathrm{NaSCN},\ \mathrm{NH_3},\ \mathrm{Pb^{2+}}}\,\Big|\,\text{transition region}\,\Big|\,\mathrm{NaSCN},\ \mathrm{NH_3},\ \mathrm{Pb^{2+}}\,\Big|_{223}^{\mathrm{Pb}}\,\Big|\,\mathrm{W}\,\Big|_{293}^{\mathrm{Cu}}.$$

The tungsten rods coming from the cell make contact with copper wires, but through inadvertence these contacts are made at slightly different temperatures, 283 and 293 K. Show that the error introduced into the measurement of the cell potential at 223 K is

$$\Delta\Phi = \int_{283}^{293} (\xi_{\mathrm{W}} - \xi_{\mathrm{Cu}})dT.$$

13.3 Treat again the open-circuit potential of the thermogalvanic cell where it is assumed that a temperature distribution is established rapidly so that the composition of the solution remains equal to the initial (uniform) composition. Note that this might be a natural assumption for the thermocouple system in Problem 13.1, where one of the leads is an alloy.

13.4 Another thermogalvanic cell with different electrode reactions might be

$$|_{T_1}\mathrm{Pb}|_{T_1}\mathrm{PbSO_4}|_{T_1}\mathrm{H_2SO_4, H_2O}|_{T_2}\mathrm{PbSO_4}|_{T_2}\mathrm{PbO_2}|_{T_2}\mathrm{Pb}|_{T_1}.$$

The end leads are held at the same temperature, T_1, to permit an unambiguous definition of the potential. The two half-cells are at different temperatures, as shown. Temperature gradients exist across the H_2SO_4 solution and one of the Pb leads. Obtain an expression for the thermal-galvanic potential, and compare this with expressions you obtain for the Peltier coefficient and the thermogalvanic coefficient.

13.5 How would the potential of the cell in Problem 13.4 change if the Pb lead were replaced by a Cu lead, with another Cu lead also being added to the Pb lead on the other side of the cell?

13.6 Repeat the task of Problem 13.4, but with the hydrogen/silver–silver chloride cell 2.97. Write out Π for each electrode of cell 2.97 and show that the thermal diffusion terms cancel to yield Q_{rev} according to equation 13.30.

13.7 Take σ and $A_{\pm}^{+}$ to be two properties of a binary electrolytic solution. Show that any other combination of D_i^T, such as A_{+}^{0}, can be expressed as a linear combination of these two.

13.8 Obtain a concentration profile of a binary solution at steady state with respect to the Soret effect. Use equation 13.38 with the approximation $\mathscr{D} = D$.

13.9 For the copper sulfate solution of Section 13.4, show that equation 13.40 is replaced by $\nabla\mu_{+}/z_{+}F = \xi_{+}\,\nabla T$, if the solution composition (m) is uniform. Also obtain a revised form for equation 13.47 for this situation.

13.10 Estimate the magnitude of the correction term in equation 13.20. Compare this with the magnitude of the thermal conductivity of water at 20°C (0.60 W/m · K).

13.11 Show that $\sum_i c_i Q_i^* = 0$.

13.12 For a binary electrolyte, show that $Q_0^* = vcRT^2\sigma/c_T$.

NOTATION

A_j^i	modified thermal diffusion coefficient, cm^2/s
c	molar concentration of a single electrolyte, mol/cm^3
c_i	concentration of species i, mol/cm^3
c_T	total solution concentration, mol/cm^3
$\hat{C}_p$	heat capacity at constant pressure, J/g · K
D	measured diffusion coefficient of electrolyte, cm^2/s
D_i^T	thermal diffusion coefficient of species i, g/cm·s
$\mathscr{D}$	diffusion coefficient of electrolyte, based on a thermodynamic driving force, cm^2/s
$\mathscr{D}_{ij}$	diffusion coefficient for interaction of species i and j, cm^2/s
e^-	symbol for the electron
F	Faraday's constant, 96,487 C/mol
$\overline{H}_i$	partial molar enthalpy of species i, J/mol
$\mathbf{i}$	current density, A/cm^2
I	cell current, A
$\mathbf{J}_i$	molar flux density of species i relative to the mass-average velocity, $mol/cm^2 \cdot s$
k	thermal conductivity, J/cm · s · K
k'	thermal conductivity, J/cm · s · K
k''	thermal conductivity, J/cm · s · K
m	molality of a single electrolyte, mol/kg
M_i	symbol for the chemical formula of species i
M_i	molar mass of species i, g/mol
n	number of electrons involved in electrode reaction
n	number of species present in the solution
$\mathbf{N}_i$	flux density of species i, $mol/cm^2 \cdot s$
p	pressure, N/cm^2
$\mathbf{q}$	heat-flux density, $J/cm^2 \cdot s$
$\mathbf{q}^{(x)}$	Dufour energy flux density, $J/cm^2 \cdot s$
$\mathbf{q}'$	conduction and Dufour energy flux density, $J/cm^2 \cdot s$
Q_{rev}	reversible heat-transfer rate, J/s
Q_i^*	heat of transfer of species i, J/mol
R	universal gas constant, 8.3143 J/mol · K

R_i rate of homogeneous production of species i, mol/cm$^3 \cdot$ s
s_i stoichiometric coefficient of species i in electrode reaction
$\overline{S}_i$ partial molar entropy of species i, J/mol $\cdot$ K
t time, s
t_i transference number of species i with respect to the mass-average velocity
t_i^0 transference number of species i with respect to the velocity of species 0
T absolute temperature, K
U reversible cell potential, V
$\hat{U}$ internal energy per unit mass, J/g
$\mathbf{v}$ mass-average velocity, cm/s
$\mathbf{v}_i$ velocity of species i, cm/s
$\overline{V}_i$ partial molar volume of species i, cm^3/mol
y distance from electrode, cm
z_i charge number of species i
γ_{+-} mean molal activity coefficient of an electrolyte
η_s surface overpotential, V
κ conductivity, S/cm
μ_e chemical potential of an electrolyte, J/mol
μ_i electrochemical potential of species i, J/mol
ν number of moles of ions into which a mole of electrolyte dissociates
ν_+,ν_- numbers of cations and anions into which a molecule of electrolyte dissociates
ξ thermoelectric coefficient, V/K
Π Peltier coefficient, V
ρ density, g/cm^3
ρ_i mass of species i per unit volume, g/cm^3
σ Soret coefficient, K^{-1}
τ stress, N/cm^2
Φ electric potential, V
ω_i mass fraction of species i

Subscripts

e electrolyte
0 solvent

REFERENCES

1. Joseph O. Hirschfelder, Charles F. Curtiss, and R. Byron Bird, *Molecular Theory of Gases and Liquids* (New York: Wiley, 1954), p. 718.
2. J. N. Agar, "Thermogalvanic Cells," in Paul Delahay, ed., *Advances in Electrochemistry and Electrochemical Engineering* (New York: Interscience, 1963), pp. 31–121.
3. K. G. Denbigh, *The Thermodynamics of the Steady State* (London: Methuen, 1951).
4. John Newman, "Thermoelectric Effects in Electrochemical Systems," *Industrial and Engineering Chemistry Research*, *34* (1995), 3208–3216.
5. H. J. V Tyrrell. "Thermal-Diffusion Phenomena in Electrolytes and the Constants Involved," in *Electrochemical Constants*, National Bureau of Standards (U. S.) Circular 524 (1953), pp. 119–129.

6. R. Byron Bird, Warren E. Stewart, and Edwin N. Lightfoot, *Transport Phenomena* (New York: Wiley, 2002), 2nd edition (equation F, Table 19.2-4).
7. D. Bernardi, E. Pawlikowski, and J. Newman, "A General Energy Balance for Battery Systems," *Journal of the Electrochemical Society*, *132* (1985), 5–12.
8. Karen E. Thomas and John Newman, 'Thermal Modeling of Porous Insertion Electrodes," *Journal of the Electrochemical Society*, *150* (2003), A176–A192.

CHAPTER 14

TRANSPORT PROPERTIES

14.1 INFINITELY DILUTE SOLUTIONS

In infinitely dilute solutions, there is one diffusion coefficient D_i for each solute species. This transport property describes interaction between this species and the solvent. The properties of aqueous solutions were reviewed in Section 11.7, where it was indicated that the mobility u_i is related to the diffusion coefficient by the Nernst–Einstein relation 11.41.

14.2 SOLUTIONS OF A SINGLE SALT

Sections 12.2 and 12.4 indicate that the solutions of a single salt are characterized by three transport properties: the conductivity κ, the diffusion coefficient D, and the transference number t_+^0. These can be measured as functions of the concentration as well as the temperature, as reviewed by Robinson and Stokes.[1] The conductivity is commonly measured in terms of the alternating current resistance between two electrodes placed in the solution. The Hittorf method of measuring transference numbers involves the determination of the concentration changes near the anode and the cathode when a current is passed. The moving-boundary method, generally regarded as being more accurate than the Hittorf method, measures the rate of movement of the boundary between, say, solutions of NH_4NO_3 and $AgNO_3$ when a current is passed through that boundary.[2] Diffusion coefficients can be measured by following the concentration changes across a porous glass diaphragm. Also, accurate results can be obtained by measuring optically the concentration changes that take place when two solutions of different concentration are placed in contact with each other. This can be done either at very short times, in which case the initial boundary should be sharp, or at very long times[3] with the diffusion taking place in a restricted space about 7 cm high.

Over the years, a surprisingly large amount of data has been taken on the transport properties of solutions of single salts. Landolt–Börnstein[4] is a good source of conductivity data, and Kaimakov and Varshavskaya[5] have searched the literature for transference numbers. Robinson and Stokes[1] have compiled data on diffusion coefficients and activity coefficients, and Chapman and Newman[6] have collected data for a number of systems.

Electrochemical Systems, Fourth Edition. John Newman and Nitash P. Balsara.

The conductivity, diffusion coefficient, and transference number represent three quite different transport properties. We might hope to find a more unified treatment by dealing with the equivalent transport coefficients $\mathscr{D}_{0+}$, $\mathscr{D}_{0-}$, and $\mathscr{D}_{+-}$ defined by equation 12.1. These can be obtained from the measured values of κ, D, and t_+^0 by solving equations 12.10, 12.11, and 12.23:

$$\mathscr{D}_{0-} = \frac{z_+}{z_+ - z_-}\frac{\mathscr{D}}{t_+^0}, \tag{14.1}$$

$$\mathscr{D}_{0+} = \frac{-z_-}{z_+ - z_-}\frac{\mathscr{D}}{1 - t_+^0}, \tag{14.2}$$

$$\frac{1}{\mathscr{D}_{+-}} = \frac{z_+ z_- c_T F^2}{RT\kappa} - \frac{z_+ - z_-}{z_+ \nu_+}\frac{c_0 t_+^0 t_-^0}{c\mathscr{D}}. \tag{14.3}$$

We see that first we need to determine $\mathscr{D}$ from D according to equation 12.12:

$$D = \mathscr{D}\frac{c_T}{c_0}\left(1 + \frac{d\ln\gamma_{+-}}{d\ln m}\right), \tag{14.4}$$

which requires a knowledge of the activity coefficient (see Problem 2.1).

These are more than 30 binary systems[3] with sufficient data to justify calculating values of $\mathscr{D}_{ij}$. Figure 14.1 shows the multicomponent diffusion coefficients of KCl in water at 25°C. We may note that the coefficients for interactions of the ions with the solvent are reasonably constant, while that for ion–ion interactions shows roughly a square-root-of-concentration dependence characteristic of the Debye–Hückel–Onsager theory of ionic interactions in dilute solutions.

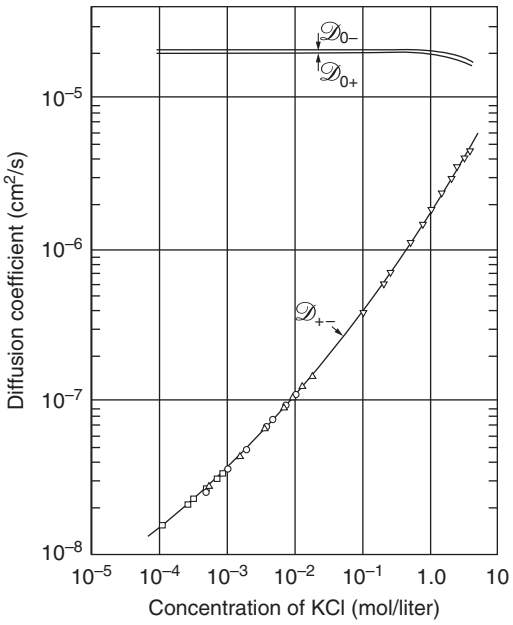

Figure 14.1 Multicomponent diffusion coefficients of KC1–H_2O at 25°C.

On this basis, we define a function G:

$$G = \frac{z_+\mathscr{D}_{0+} - z_-\mathscr{D}_{0-}}{\mathscr{D}_{+-}} \frac{\sqrt{c}}{c_0} \frac{1+\sqrt{q}}{z_+^2 z_-^2 q} \left(\frac{z_+\nu_+}{z_+ - z_-} \right)^{1/2} T^{3/2}, \tag{14.5}$$

where

$$q = \frac{-z_+z_-}{z_+ - z_-} \frac{\lambda_+^0 + \lambda_-^0}{z_+\lambda_+^0 - z_-\lambda_-^0}, \tag{14.6}$$

and λ_i^0 is the ionic equivalent conductance at infinite dilution. The quantity G is essentially $\sqrt{c}/\mathscr{D}_{+-}$, the other factors being based on the theory for dilute solutions. Figure 14.2 shows some calculated G values for several chloride systems. For electrostatic ionic interactions, with neglect of electrophoresis, the limiting value for dilute solutions would be about 2860. We see that this value appears to be more characteristic of concentrated solutions.

Figure 14.3 shows $\mathscr{D}_{0-}$ values for several chloride solutions and accentuates the concentration dependence relative to the logarithmic scale used in Figure 14.1. The behavior definitely depends on the nature of the counterion. We might think that multiplication by a viscosity factor would help (see equation 11.51). The reader can judge from Figure 14.4.

Figures 14.5 and 14.6 show the dependence on temperature. To a first approximation, the temperature dependence is given by the temperature dependence of the limiting value $\mathscr{D}_{0i}^0$ as c approaches zero.

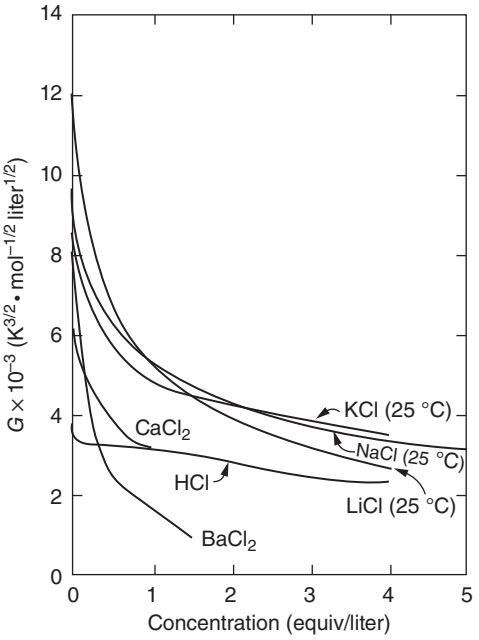

Figure 14.2 Empirical function G for various systems.

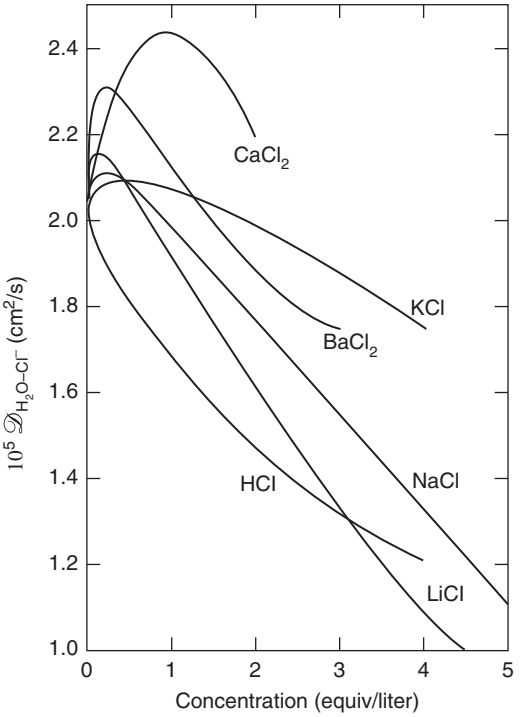

Figure 14.3 Diffusion coefficient of chloride ion in various aqueous solutions at 25°C.

14.3 MIXTURES OF POLYMERS AND SALTS

Salts dissolve in polymers such as poly(ethylene oxide) (PEO), as discussed in Section 2.9.[7, 8] One can either mix the salt with a PEO homopolymer to get a homogeneous mixture that is analogous to classical electrolytes or one could mix the salt with a block copolymer. A diblock copolymer is a molecule wherein two chemically dissimilar chains are covalently bonded to each other. Polymers are usually immiscible in each other. The presence of the covalent bond restricts the phase separation to molecular length scales. An example of a block copolymer is a polystyrene-*block*-poly(ethylene oxide) (SEO) copolymer.[9] If the molar masses of the polystyrene (PS) and PEO blocks are roughly equal, one obtains alternating PS-rich and PEO-rich lamellae. Mixing salt into such copolymers results in salt-free PS-rich lamellae that are nonconducting but mechanically rigid, and salt-containing PEO-rich lamellae. Ion transport is facilitated by soft polymers such as PEO. In SEO-based electrolytes, the PS-rich domains provide mechanical rigidity while the PEO-rich lamellae provide avenues for ion transport. Schematics of homopolymer and block copolymer electrolytes are shown in Figure 14.7. Also shown in the figure is an electron micrograph of a block copolymer electrolyte.

Sections 12.2 and 12.4 are applicable to these mixtures, and they are also characterized by a thermodynamic factor and three transport properties, κ, D, and t_+^0. We first discuss characterization of homogeneous electrolytes comprising mixtures of PEO (molar mass = 5 kg/mol) and lithium bis(trifluoromethanesulfonyl) imide (LiTFSI). This is followed by a discussion of characterization of composite electrolytes such as SEO mixed with LiTFSI. The dependence of κ and D on m is shown in Figure 14.8a and b. The thermodynamic factor and t_+^0 are measured using a combination of experiments.[10, 11] One of these experiments comprises placing an electrolyte film between two lithium

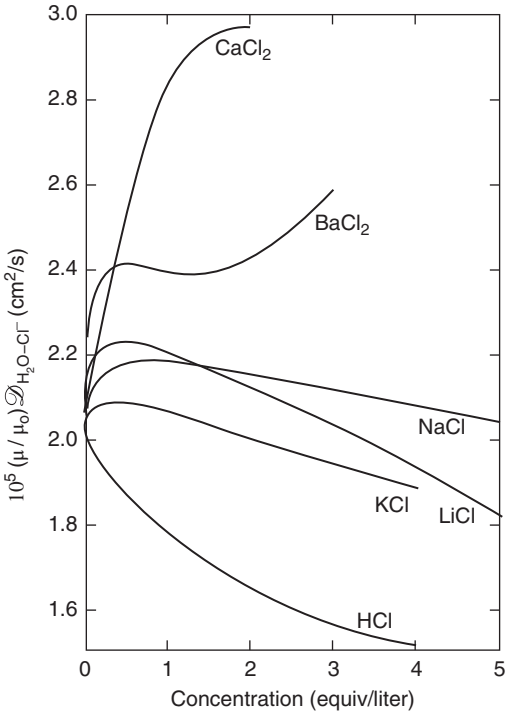

Figure 14.4 Diffusion coefficient of chloride ion with a viscosity factor.

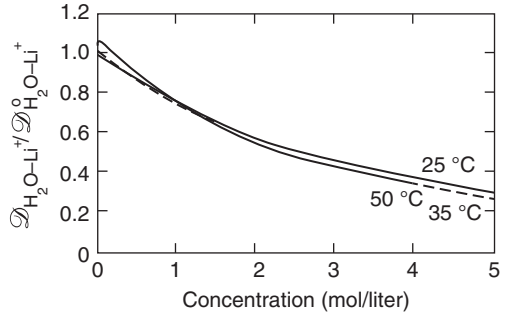

Figure 14.5 Lithium ion diffusion coefficient in lithium chloride solutions at various temperatures.

foils, applying small constant potential, Φ_{ss}, across the foils and measuring the time dependence of the current density. The current density data can be used to determine $t_{+,\mathrm{id}}$, the approximate transference number based on the assumption of an ideal, dilute electrolyte, using equation 12.49. The measured dependence of t_+^0, D, $t_{+,\mathrm{id}}$, and U on m (U versus m data are shown in Figure 2.2) can be used to determine the transference number using the following equation,

$$t_+^0 = 1 + \left(\frac{1}{t_{+,\mathrm{id}}} - 1\right)\frac{z_+\nu_+ FDc}{\kappa}\left(\frac{d\ln m}{dU}\right). \tag{14.7}$$

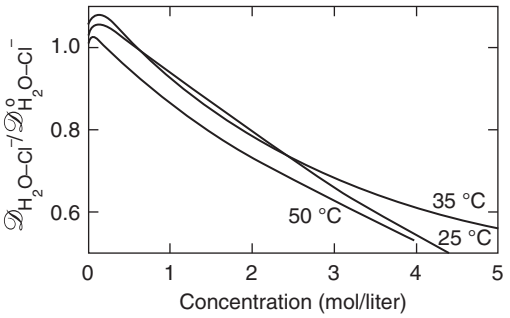

Figure 14.6 Chloride ion diffusion coefficient in lithium chloride solutions at various temperatures.

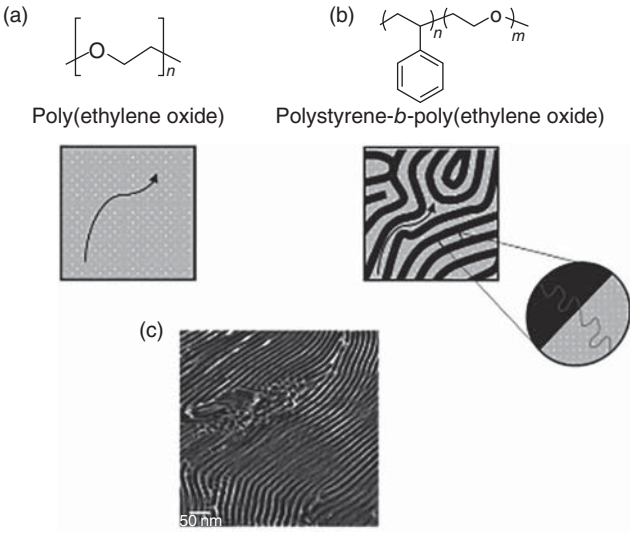

Figure 14.7 Chemical formulae and schematic depictions of (a) homopolymer and (b) block copolymer electrolytes. The arrows in (a) and (b) represent one of the possible pathways for salt diffusion in the homopolymer and block copolymer electrolytes, respectively. In the block copolymer, diffusion is limited to the bright phase. (c) An electron micrograph of a block copolymer electrolyte: polystyrene-*b*-poly(ethylene oxide) with a lithium salt. The conducting domains appear bright in the micrograph.

Equation 14.7 is derived by combining equations 2.119, 12.41, 12.48, and 12.49. Properties of the mixture are shown in Figure 14.8. The dependence of $t_{+,\mathrm{id}}$ and t_+^0 on m is shown in Figure 14.8c. There is a marked difference between t_+^0 and $t_{+,\mathrm{id}}$, indicating that the assumption of ideality does not apply to PEO/LiTFSI mixtures. The dependence of t_+^0 on m is characterized by two maxima separated by a sharp minimum; t_+^0 is even negative in the vicinity of the minimum. In contrast, the dependence of $t_{+,\mathrm{id}}$ on m is characterized by one shallow minimum with no negative values.

Knowledge of t_+^0 enables determination of the thermodynamic factor with the equation

$$\left(1+\frac{d\ln\gamma_{\pm}}{d\ln m}\right)=-\frac{F}{2RT(1-t_+^0)}\left(\frac{dU}{d\ln m}\right), \tag{14.8}$$

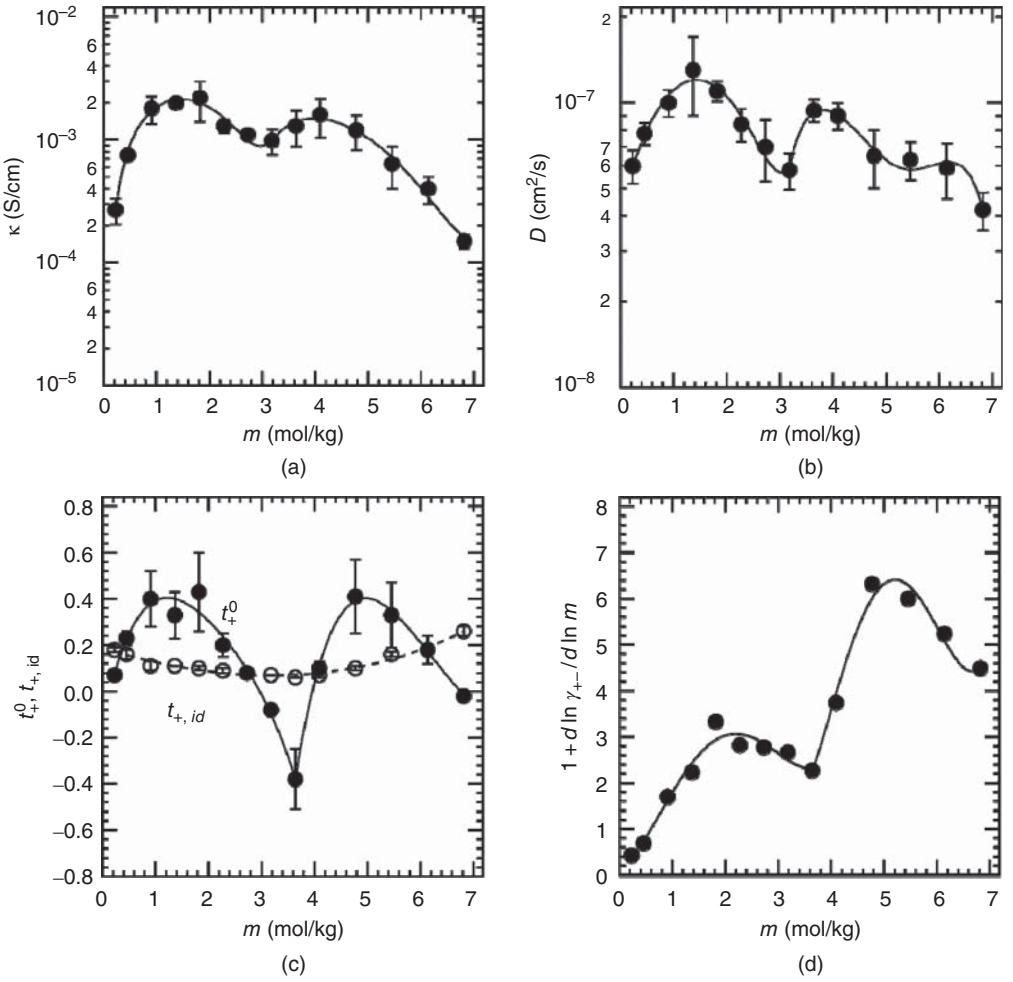

Figure 14.8 Complete characterization of ion transport in a polymer electrolyte (PEO/LiTFSI) at 90°C. (a) Conductivity, κ; (b) salt diffusion coefficient, D; (c) cation transference number, t_+^0; and (d) the thermodynamic factor as a function of molality, m. The approximate transference number based on the assumption of an ideal electrolyte, $t_{+,id}$, is also shown in (c).

which is obtained by rewriting equation 2.119. Figure 14.8d is a plot of the thermodynamic factor versus m. The fact that the thermodynamic factor of PEO/LiTFSI mixtures deviates from unity is another indication that the system is nonideal.

The Stefan–Maxwell diffusion coefficients, $\mathscr{D}_{ij}$, of PEO/LiTFSI can be calculated from the data in Figure 14.8 using equations 14.1 through 14.4, and the results are given in Figure 14.9. The data in this figure should be contrasted with the $\mathscr{D}_{ij}$ versus concentration curves for KCl/water solutions shown in Figure 14.1. The simplest of the PEO/LiTFSI Stefan–Maxwell diffusion coefficients, $\mathscr{D}_{0+}$ is a decaying function of salt concentration (or molality). This is qualitatively similar to the dependence of $\mathscr{D}_{0+}$ on salt concentration of KCl/water mixtures. The plots of $\mathscr{D}_{0-}$ and $\mathscr{D}_{+-}$ versus m of PEO/LiTFSI are qualitatively different from the corresponding plots of KCl/water mixtures. In particular, there are concentration ranges over which the diffusion coefficients are negative, separated from a range

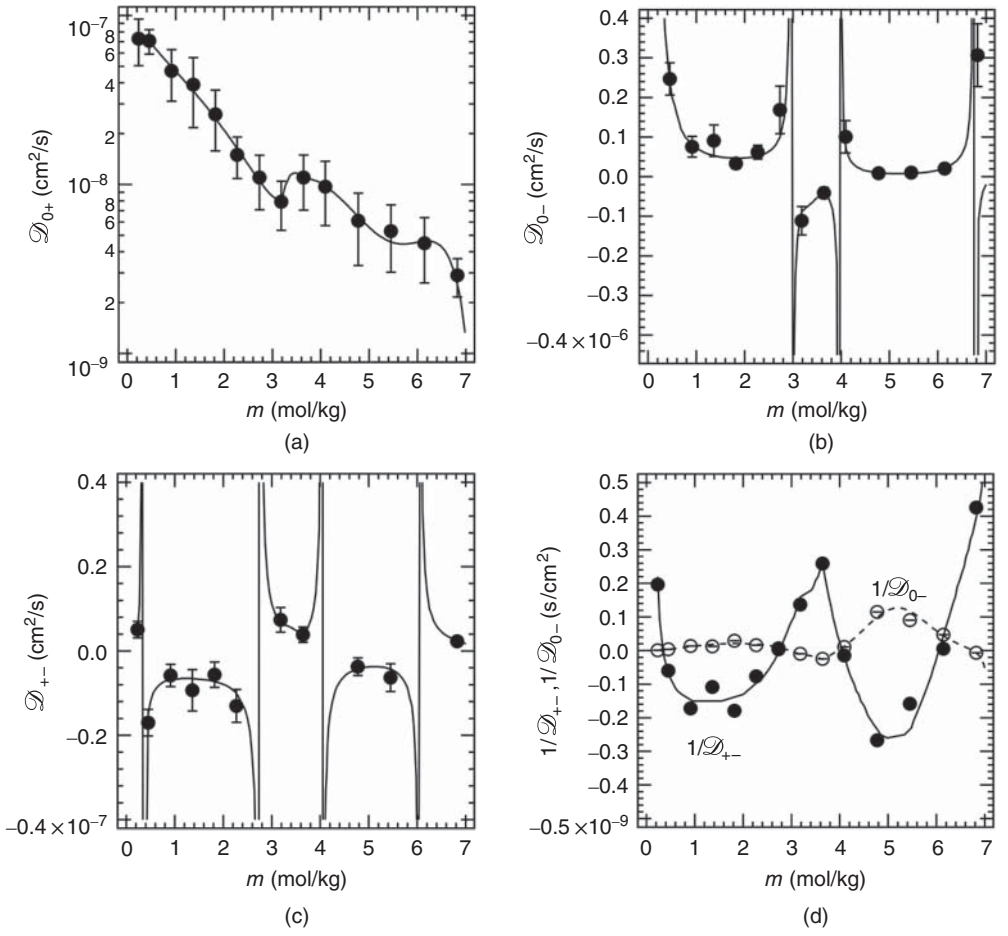

Figure 14.9 (a–c) Stefan–Maxwell diffusion coefficients of PEO/LiTFSI electrolytes as a function of molality. (d) Reciprocal of the Stefan–Maxwell diffusion coefficients in (b) and (c) as a function of molality.

where the diffusion coefficients are positive. The singularities are poles: $\mathscr{D}_{0-}$ approaches $+\infty$ as t_+^0 approaches 0 from one side, and $\mathscr{D}_{0-}$ approaches $-\infty$ as t_+^0 approaches 0 from the other side. For example, $\mathscr{D}_{0-}$ swings from $+\infty$ to $-\infty$ as salt concentration changes from $m = (2.967 - \delta)$ to $(2.967 + \delta)$ mol/kg, where δ is infinitesimally small. Similar swings are seen in $\mathscr{D}_{+-}$. Singularities in $\mathscr{D}_{ij}$ occur when the denominators of equations 14.1 to 14.3 approach zero. In the vicinity of singularities, when a particular $\mathscr{D}_{ij}$ is large, transport is governed by the other relevant Stefan–Maxwell diffusion coefficients; $\mathscr{D}_{ij}$ appear in the denominator of the right side of equation 12.1. For example, in the vicinity of $m = 2.73$ mol/kg where $\mathscr{D}_{0-}$ approaches either $+\infty$ or $-\infty$, the flux of the anion is entirely determined by the magnitude and sign of $\mathscr{D}_{+-}$. In Figure 14.9d, we plot $1/\mathscr{D}_{0-}$ and $1/\mathscr{D}_{+-}$ versus m for PEO/LiTFSI. These plots are significantly simpler than plots of $\mathscr{D}_{0-}$ and $\mathscr{D}_{+-}$ versus m (Figure 14.9b and c). In cases where poles are obtained in $\mathscr{D}_{ij}$ versus salt concentration plots, it is preferable to change the ordinate to $1/\mathscr{D}_{ij}$. Thus, in Figure 14.9d, the plotted quantities pass through zero only when t_+^0 passes through zero in Figure 14.8.

The inescapable physical implication of negative transference numbers is that LiTFSI does not dissociate only into Li^+ and $TFSI^-$ ions that migrate independently under the influence of the applied

electric field. When t_+^0 is negative, it implies that when a field is applied to an electrolyte with uniform composition, both the Li^+ and $TFSI^-$ are driven to the positive electrode. This, in turn, may imply the presence of a multitude of charged clusters in the electrolyte. If, for example, there are three species in solution, Li^+, $TFSI^-$, and $[Li(TFSI)_2]^-$, then a negative transference number would arise if the dominant mobile species are $TFSI^-$ and $[Li(TFSI)_2]^-$ (the Li^+ ions are not as mobile due to specific interactions between the ions and ether oxygens in the PEO). The Stefan–Maxwell diffusion coefficient $\mathscr{D}_{ij}$ quantifies the frictional interactions between all manifestations of species i and j in the electrolyte, including free ions and clusters. A powerful attribute of the Stefan–Maxwell formalism is that it averages over the interactions in the entire solution, regardless of the nature of the associations that underlie the averaged behavior. A limitation of the Stefan–Maxwell formalism is that it does not provide direct information on the nature of the associations that underlie the measured averages. For example, the negative transference numbers in these electrolytes may arise due to the presence of $[Li(TFSI)_2]^-$ or $[Li_2(TFSI)_3]^-$ or some other negatively charged cluster. Such information must be provided by other independent experiments (e.g., spectroscopic experiments like Raman or nuclear magnetic resonance (NMR)). (Compare Section 4.7.)

Measurement of κ, D, t_+^0, and the thermodynamic factor of electrolytes enables predictions of the kind shown in Figures 14.10 through 14.12 (taken from Ref. [12]). Consider the passage of a steady current density i_{ss} through a PEO/LiTFSI electrolyte of a given average molality (m_{av}) and thickness L, placed between two lithium electrodes. This scenario is discussed in Section 12.6. The salt concentration profile, $m(x)$, in the electrolyte can be calculated using equation 12.40 since $D(m)$, $t_-^0(m)$, and $c_0(m)$ are known. Similarly, the potential profile, $\Phi(x)$, in the electrolyte can be calculated using equation 12.44 since $\mathrm{Ne}(m)$ and $\kappa(m)$ are known. It is important to note that this potential is not the electrostatic potential. It is the potential of an electrode at open-circuit relative to a similar electrode at a fixed point in the electrolyte, as discussed in Sections 3.4 (see Figure 3.7) and 12.4. The same reaction, $Li_{(s)} \rightleftharpoons Li^+ + e^-$, occurs on both electrodes. Results for salt concentration and potential profiles obtained for selected m_{av} values as a function of increasing i_{ss} are shown in Figures 14.10 and 14.11. At low current densities, the variation of salt concentration is small, and the transport properties are nearly constant. It is therefore not surprising that the concentration and potential profiles are linear at $i_{ss}L = 0.001$ mA/cm. In this case, the results are similar to the simple model described in Section 11.8. Deviations from linearity can be seen at the intermediate current density ($i_{ss}L = 0.01$ mA/cm). At high current density ($i_{ss}L = 0.04$ mA/cm), the profiles are highly nonlinear. The steep molality and potential gradients seen in Figures 14.10c and 14.11c occur in the range $m = 3$ to 4 mol/kg, where t_+^0 is negative and $\mathscr{D}_{0-}$ exhibits singularities.

The potential difference, Φ_{ss}, required to maintain a steady dc current i_{ss} across an electrolyte of thickness L can readily be measured for PEO/LiTFSI electrolytes using a potentiostat. Ordinarily Φ_{ss}/L is taken to be the potential gradient. Figure 14.11 shows that this is true only in the small-current limit ($i_{ss}L = 0.001$ mA/cm). At higher current densities, the potential gradient in the electrolyte deviates significantly from Φ_{ss}/L, as seen in Figure 14.11b and c. The dependence of the driving force for current, Φ_{ss}/L, in 500-μm thick PEO/LiTFSI electrolytes as a function of the average electrolyte molality m_{av} is shown in Figure 14.12 (molality is dependent on position under an electric field). The dashed curve in Figure 14.12 compares experimental data and theoretical predictions (e.g., Figure 14.11). It is evident that the nonmonotonic dependence of Φ_{ss}/L on salt concentration seen in experiments is approximately consistent with theoretical predictions. The agreement should be better if the curves in Figure 14.8 more accurately represented the actual data.

Many practical applications use composite electrolytes. In lithium-ion and lead-acid batteries, the electrolyte is contained within a porous nonconducting film that separates the two electrodes. The separator/electrolyte system is one example of a composite electrolyte. Here conduction occurs exclusively through one of the phases of the composite. Hydrated Nafion, the electrolyte used in the hydrogen fuel cell, is also a composite electrolyte. Here the proton transport occurs exclusively in

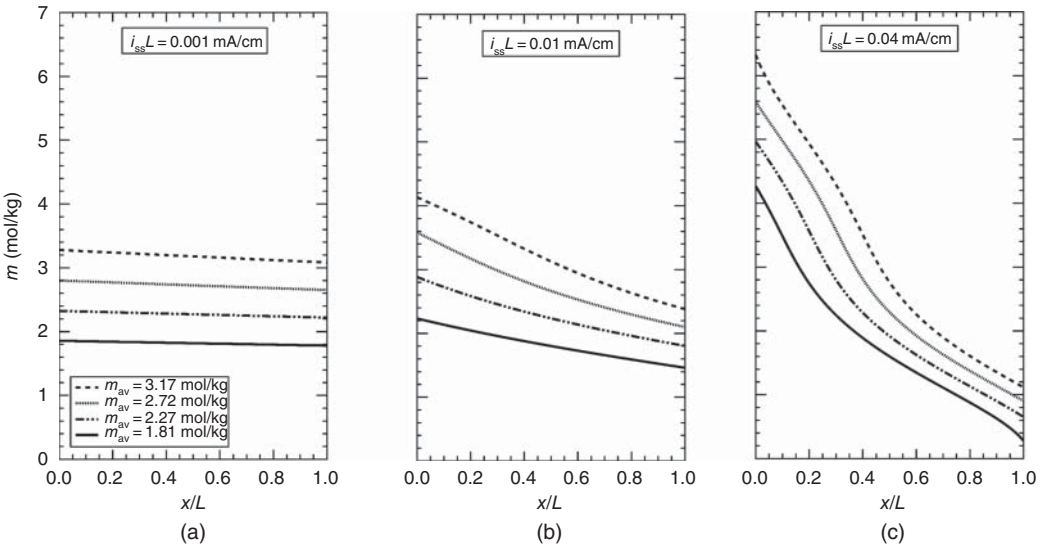

Figure 14.10 Concentration profiles in PEO/LiTFSI electrolytes predicted using characterization data shown in Figure 14.8. Curves depend on the product of steady-state current density (i_{ss}) and electrode separation (L), given at the top of parts a–c. Same scale applies to all figures.

the hydrated channels that form by self-assembly in a tetrafluoroethylene matrix. The SEO/LiTFSI electrolyte shown in Figure 14.7 is a similar composite wherein conduction occurs exclusively through the PEO-rich lamellae. If the composite has only one conductive phase, then it can be completely characterized by the same parameters discussed in Section 14.2. Treatment of transport through composites dates back to Maxwell[13] and Brugeman[14] as discussed in Chapter 22.

A schematic of a composite block copolymer electrolyte is shown in Figure 14.13a. In this case, a useful starting point is a model by Sax and Ottino.[15] In this model, the conductivity of the composite, κ, is given by

$$\kappa(m) = \frac{\varepsilon\kappa_0(m)}{\tau}, \tag{14.9}$$

where ε is the volume fraction of the conducting phase, τ is a tortuosity factor, and κ_0 is the conductivity of the pure conducting phase. There are many ways to define salt concentration in a composite electrolyte. In this treatment, m for a composite electrolyte refers to the salt concentration in the conducting phase (not the "superficial" salt concentration based on the volume of the entire electrolyte). For the example in Figure 14.13a, the pure conducting phase is PEO/LiTFSI with a salt molality m. The model assumes that the presence of the nonconducting phase does not alter the properties of the electrolyte. Effects such as changes in salt distribution at the boundary between the two phases are ignored. Both ε and τ are assumed to be independent of salt concentration.

The importance of both ε and τ can be appreciated by considering transport through a single coherently ordered grain, shown in Figure 14.13b. The conductivity through the single grain is equal to $\varepsilon\kappa_0$ in the direction parallel to the lamellae, since one must account for the presence of the insulating domains. The conductivity perpendicular to the lamella is zero. In order to model the composite pictured in Figure 14.13a, however, one must account for the tortuous paths that the ions must take to travel from one electrode to the other, which we do by introducing the tortuosity τ. For randomly oriented lamellae,[9, 16] $\tau = 3/2$. For many other morphologies, τ is a function of ε.[13, 14] This is discussed in Chapter 22.

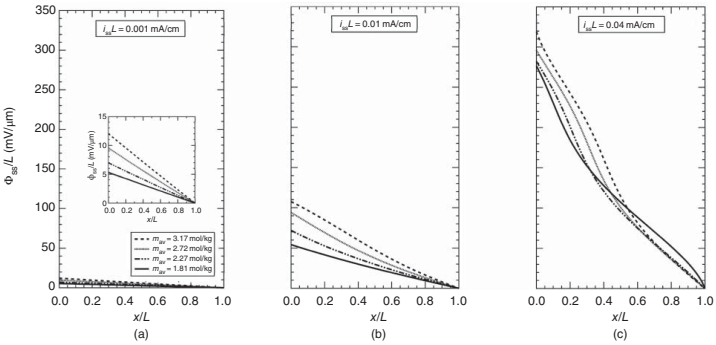

Figure 14.11 Potential profiles in PEO/LiTFSI electrolytes predicted using characterization data shown in Figure 14.8. Curves depend on the product of steady-state current density (i_{ss}) and electrode separation (L), given at the top of parts a–c. Same scale applies to all figures. The inset in (a) shows curves on an expanded scale for clarity.

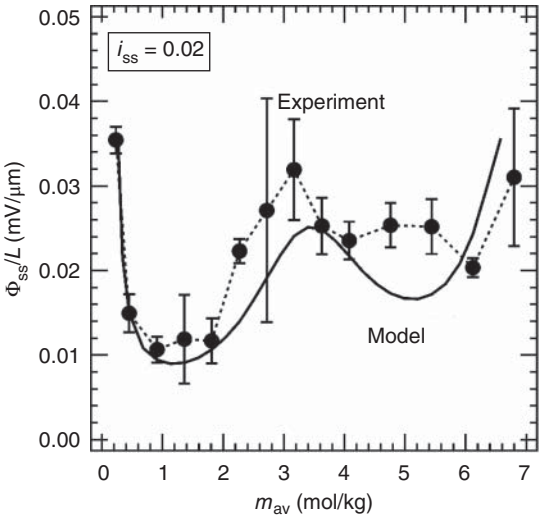

Figure 14.12 Characteristics of lithium-polymer-lithium cells with $L = 500$ μm (thickness of the polymer electrolyte) for a constant steady-state current, $i_{ss} = 0.02\,\text{mA/cm}^2$. The cell potential, ϕ_{ss}, normalized by L, is plotted as a function of average molality, m_{av}. The circles represent experimental measurements. The solid curve represents theoretical predictions based on the characterization data in Figure 14.8 and equations 12.40 and 12.44.

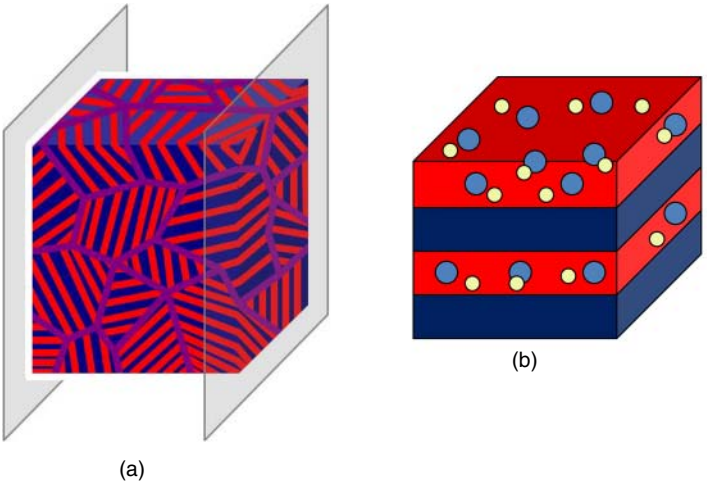

Figure 14.13 (a) Schematic of a composite electrolyte with a lamellar morphology with many randomly oriented grains sandwiched between two electrodes. (b) Schematic of a grain showing the salt localized in one of the lamellae.

Consider a relaxation experiment in the grain in Figure 14.13b, wherein a salt concentration gradient is created by applying a field and is allowed to relax by turning the field off. The diffusion coefficient, D, characterizing this relaxation process is equal to that obtained in the pure conducting phase. In other words, D is independent of ε. This is consistent with experiments on block copolymer electrolytes.[17] However, the salt diffusion through a sample comprising multiple grains (Figure 14.13a) must depend

on τ. The relationship of the salt diffusion coefficient D in the composite to the salt diffusion coefficient D_0 of the conducting phase, is thus given by:[16]

$$D(m) = \frac{D_0(m)}{\tau}. \tag{14.10}$$

This constitutes the definition of the effective diffusion coefficient D in a composite.

The transference number is a measure of the mobility of one ion relative to the other. Since the effect of ε and τ on the motion of both ions is similar, t_+^0 in the composite electrolyte is identical to that in the pure electrolyte, $t_{+,0}^0$.

$$t_+^0(m) = t_{+,0}^0(m). \tag{14.11}$$

The open-circuit potential U of a cell containing a composite electrolyte is affected only by the concentration of ions in the conducting domains next to the electrodes (see Chapter 6). Thus, U of a composite electrolyte with molality m is identical to that in the pure electrolyte with the same molality. Therefore, if one were to characterize a composite electrolyte by measuring κ, D, $t_{+,id}$, and U as functions of m, then the transference number of the composite must be calculated using a slight modification of equation 14.7,

$$t_+^0 = 1 + \left(\frac{1}{t_{+,\mathrm{id}}} - 1\right) \frac{z_+ \nu_+ FDc\varepsilon}{\kappa} \left(\frac{d \ln m}{dU}\right), \tag{14.12}$$

while 14.8 applies without change. The parameter ε enters equation 14.12 because of the dependence of κ and D on ε. Note that the parameters in equation 14.12 correspond to the composite. Measurement of κ, D, t_+^0, and the thermodynamic factor of composite electrolytes enables predictions of the kind shown in Figures 14.10 to 14.12.

The treatment above is for a composite containing a concentrated electrolyte. For dilute electrolytes, equation 11.49 can be used to relate conductivity to ion diffusivities. If a dilute electrolyte were contained within a composite, then the analogous expression would be:

$$\kappa = \frac{F^2 z_+ c_+ \varepsilon (z_+ D_+ - z_- D_-)}{RT}, \tag{14.13}$$

where κ, D_+, and D_- refer to the conductivity and ion diffusion coefficients in the composite.

14.4 TYPES OF TRANSPORT PROPERTIES AND THEIR NUMBER

Complete characterization of a multicomponent solution with respect to its transport properties is an ambitious project because there are so many of them and they vary in a complex fashion with composition and temperature. Let us make sure that we can, at least, count them.

We characterize a solution by its number n_C of thermodynamically independent components. This means that the detailed speciation is not considered. In transport phenomena we follow the same guidelines, although some speciation may be involved if we consider homogeneous chemical reactions.

Even though we do not consider detailed speciation, we generally regard an electrolytic solution to have one more species than the number of thermodynamically independent components. Electroneutrality constrains the latter. For example, a binary electrolytic solution contains anions, cations, and solvent.

The number of transport properties is determined by the number of species. Without considering thermal effects, we have $\frac{1}{2}n(n-1)$ transport properties of the type $\mathscr{D}_{ij}$ for mass transfer, where

TABLE 14.1 Transport properties and their number[a]

n_C	n	Example	M	MD	ME	T	TS	TE	Total
1	1	Diamond	0	0	0	1	0	0	1
1	2	Cu wire	1	0	1	1	0	1	3
2	2	Sucrose, H_2O	1	1	0	1	1	0	3
2	3	H_2SO_4, H_2O	3	1	2	1	1	1	6
3	3	Ethanol, sucrose, H_2O	3	3	0	1	2	0	6
3	4	$CuSO_4$, H_2SO_4, H_2O	6	3	3	1	2	1	10

[a] $M = \frac{1}{2}n(n-1)$, mass transport; MD $= \frac{1}{2}n_C(n_C-1)$, chemical diffusion; ME $= n_C$ if $n > n_C$, electrolytic transport; $T = 1$, thermal conductivity; TS $= n_C - 1$, Soret-type coefficient; TE $= 1$ if $n > n_C$, thermoelectric coefficient. *Source:* Newman.[18]

n is the number of species. For practical purposes we can split these into $\frac{1}{2}n_C(n_C-1)$ transport properties that characterize interdiffusion of chemical components even in the absence of an electric current. For an electrolytic solution there are an additional n_C transport properties that characterize electrolytic conduction; these can be thought of as one electrical conductivity κ and $n_C - 1$ independent transference numbers t_i^0 relative to a suitable reference velocity. Since $n = n_C + 1$, the total number of mass-transport properties is $\frac{1}{2}n_C(n_C-1) + n_C = \frac{1}{2}n(n-1)$.

The addition of thermal effects adds n thermal transport properties. There is one thermal conductivity k and $n-1$ independent thermal diffusion coefficients D_i^T. Of the latter, $n_C - 1$ are of the Soret type and describe steady-state concentration variations. For an electrolytic solution there is also one of the thermoelectric type, and this can be measured only by difference with another electrically conducting material.

Table 14.1 gives examples of systems with various numbers of components and species as well as the number and classification of transport properties. These represent materials of increasing complexity, adding one more species with each line and alternating between electrically neutral materials and electrically conducting materials. For the second entry, in addition to a copper wire, one should mention a molten salt like NaCl or a pure ionic liquid. In these three cases, there is no interdiffusion. The cation transference number of molten NaCl is either unity or zero, depending on whether the anion or the cation velocity is used as the reference. It carries no significance. Some controversy was involved here in the past because people claimed to be able to measure the transference number of a single molten salt, when they were really measuring a transference number relative to another medium, such as a fritted disk. For the fourth entry in Table 14.1, a sulfuric acid solution, another example is a molten mixture of two salts or ionic liquids with a common ion, such as a mixture of NaCl and KCl.[19]

14.5 INTEGRAL DIFFUSION COEFFICIENTS FOR MASS TRANSFER

In practice, we are often interested in mass transfer to an electrode from a multicomponent solution, such as deposition of copper from a solution of copper sulfate and sulfuric acid. However, all the transport properties of such a solution may not be known. What solution property can we measure that will allow us to predict accurately the behavior of the system?

Usually the process will obey approximately the equation of convective diffusion 11.31 with an effective diffusion coefficient that we desire to predict. This will be called an *integral diffusion coefficient* because it represents an average over the behavior and properties encountered in the diffusion

layer near an electrode. The thesis is suggested that this diffusion coefficient should be measured in a system with similar hydrodynamic conditions. For example, an integral diffusion coefficient measured with a rotating disk electrode (see Section 17.2) should be applicable to mass transfer in an annulus or pipe (see Section 17.4). This integral diffusion coefficient is different from the integral diffusion coefficient measured with a diaphragm cell.[20] Similarly, the integral diffusion coefficient measured in transient mass transfer to an electrode at the end of a stagnant diffusion cell should be applicable to a growing mercury drop (see Section 17.9). These latter diffusion coefficients are called *polarographic diffusion coefficients*.

The validity of the use of an integral diffusion coefficient is influenced by the following effects: the value of the Schmidt number ν/D_i, the nonzero interfacial velocity, the effect of ionic migration, and the variations of transport properties with composition. Each effect has been treated individually by several workers, mostly in nonelectrolytic systems.

The treatment of mass transfer is simplified at the high Schmidt numbers that prevail in electrolytic solutions (see Sections 17.5 and 17.6). The correction for the fact that the Schmidt number is not infinite can differ among several hydrodynamic situations; the correction is usually no more than a few percent. The high value of the Schmidt number allows justification for assuming that the other effects are properly accounted for.

The effect of nonzero interfacial velocity due to the high mass-transfer rate can also be expressed as a correction factor to the mass-transfer coefficient in the absence of an interfacial velocity. This correction factor depends on the mass-flux ratio and, in the limit of large Schmidt numbers, has been shown to be the same for arbitrary, two-dimensional boundary layers[21] and for the rotating disk.[20]

Similarly, the effect of ionic migration in the diffusion layer can also be expressed as a correction factor for the mass-transfer rate in the absence of migration[22] (see also Chapter 19). For large Schmidt numbers, one correction factor has been shown to apply to arbitrary two-dimensional and axisymmetric diffusion layers,[23] including the rotating disk, and another to the transient processes of a growing mercury drop and an electrode at the end of a stagnant diffusion cell.[22]

Acrivos[24] has shown that in the limit of high Schmidt numbers one effective diffusion coefficient should apply to mass transfer at the limiting rate from a given solution for arbitrary boundary layer flows, even though the physical properties vary with composition in the diffusion layer.

These considerations lead us to conclude that one effective or integral diffusion coefficient should describe mass transfer at the limiting current from a given solution for arbitrary two-dimensional and axisymmetric diffusion layers in laminar forced convection. This integral diffusion coefficient will depend upon the bulk composition of the solution. Somewhat different integral diffusion coefficients may apply to free convection, turbulent flow, or the transient processes cited above. However, these diffusion coefficients should be closer to each other than to the value obtained with a diaphragm cell, which is a completely different situation from mass transfer to an electrode with the flow of current.

Two electrode reactions have proved to be particularly popular for experimental mass-transfer studies. These are deposition of copper,

$$Cu^{2+} + 2e^- \rightarrow Cu, \tag{14.14}$$

from solutions of copper sulfate and sulfuric acid and the reduction of ferricyanide ions,

$$Fe(CN)_6^{3-} + e^- \rightarrow Fe(CN)_6^{4-}, \tag{14.15}$$

from solutions using NaOH, KOH, or KNO_3 as a supporting electrolyte. Selman[25] has analyzed the available literature on integral diffusion coefficients for these solutions.

PROBLEM

14.1 The simplest ternary ionic solution is one containing a single electrolyte, one of whose ions is present in two isotopic forms. An example would be a sodium chloride solution containing stable sodium ions and radioactive sodium ions. We assume that these ions are identical except that the radioactive ions are tagged. Let the solvent be denoted by 0, the cations by 1 and 2, and the anion by 3. There are six transport properties for this system, $\mathscr{D}_{01}$, $\mathscr{D}_{02}$, $\mathscr{D}_{03}$, $\mathscr{D}_{12}$, $\mathscr{D}_{13}$, and $\mathscr{D}_{23}$. On the assumption that there is no isotope effect, five of these can be predicted from the values of $\mathscr{D}_{0+}$, $\mathscr{D}_{0-}$, and $\mathscr{D}_{+-}$ of the binary untagged solutions, while the last can be obtained from the value of the *self-diffusion coefficient* D_* describing the diffusion of tagged electrolyte in a solution whose total electrolyte concentration is uniform. This gives a way of getting at the concentration dependence of $\mathscr{D}_{12}$ related to interactions of ions of the same charge, something that cannot be ascertained from binary solutions of a single salt. In the following, assume that

$$f_1^{\nu+} f_3^{\nu-} = f_2^{\nu+} f_3^{\nu-} = f_{+-}^{\nu}.$$

(a) Show that $\mathscr{D}_{01}$, $\mathscr{D}_{02}$, $\mathscr{D}_{03}$, $\mathscr{D}_{12}$, and $\mathscr{D}_{13}$ are given by

$$\mathscr{D}_{13} = \mathscr{D}_{23} = \mathscr{D}_{+-},\ \mathscr{D}_{01} = \mathscr{D}_{02} = \mathscr{D}_{0+}, \text{and } \mathscr{D}_{03} = \mathscr{D}_{0-},$$

where $\mathscr{D}_{+-}$, $\mathscr{D}_{0+}$, and $\mathscr{D}_{0-}$ are to be evaluated at the total electrolyte concentration, $c = (c_1 + c_2)/\nu_+$.

(b) Show that $\mathscr{D}_{12}$ can be obtained from measured values of D_* according to the relation

$$\mathscr{D}_{12} = \frac{c_+}{c_T/D_* - c_0/\mathscr{D}_{0+} - c_-/\mathscr{D}_{+-}}.$$

(c) Show that as the total electrolyte concentration approaches zero, D_* approaches $\mathscr{D}_{0+}$.

NOTATION

c	concentration of a single electrolyte, mol/cm^3
c_0	concentration of solvent, mol/cm^3
c_T	total solution concentration, mol/cm^3
D	measured diffusion coefficient of electrolyte, cm^2/s
D_i	diffusion coefficient of species i, cm^2/s
$\mathscr{D}$	diffusion coefficient of electrolyte, based on a thermodynamic driving force, cm^2/s
$\mathscr{D}_{ij}$	diffusion coefficient for interaction of species i and j, cm^2/s
F	Faraday's constant, 96,487 C/mol
G	function related to $\mathscr{D}_{+-}$, K$^{3/2}$·(liter/mol)$^{1/2}$
m	molality of a single electrolyte, mol/kg
q	see equation 14.6
R	universal gas constant, 8.3143 J/mol·K
t_i^0	transference number of species i relative to the solvent velocity
T	absolute temperature, K
u_i	mobility of species i, cm^2·mol/J·s
z_i	charge number of species i
γ_{+-}	mean molal activity coefficient of an electrolyte

κ	conductivity, S/cm
λ_i^0	equivalent ionic conductance of species i at infinite dilution, S·cm^2/mol
μ	viscosity, mPa·s
ν	kinematic viscosity, cm^2/s
ν_+	number of cations into which a molecule of electrolyte dissociates

REFERENCES

1. R. A. Robinson and R. H. Stokes, *Electrolyte Solutions* (London: Butterworths, 1965).
2. Paul Milios and John Newman, "Moving Boundary Measurement of Transference Numbers," *Journal of Physical Chemistry*, *73* (1969), 298–303.
3. Thomas W. Chapman, *The Transport Properties of Concentrated Electrolytic Solutions*, dissertation, University of California, Berkeley, November 1967 (UCRL-17768).
4. A. Eucken, ed., *Landolt-Börnstein, Zahlenwerte und Funktionen aus Physik, Chemie, Astronomie, Geophysik und Technik,* 6th ed., Vol. 2, part 7 (Berlin: Springer, 1960).
5. E. A. Kaimakov and N. L. Varshavskaya, "Measurement of Transport Numbers in Aqueous Solutions of Electrolytes," *Uspekhi Khimii*, *35* (1966), 201–288.
6. Thomas W. Chapman and John Newman, *A Compilation of Selected Thermodynamic and Transport Properties of Binary Electrolytes in Aqueous Solution*, Lawrence Radiation Laboratory, University of California, Berkeley, May 1968 (UCRL-17767).
7. D. E. Fenton, J. M. Parker, and P. V. Wright, "Complexes of Alkali-Metal Ions with Poly(Ethylene Oxide)," *Polymer*, *14* (1973), 589.
8. S. Lascaud, M. Perrier, A. Vallee, S. Besner, J. Prud'homme, and M. Armand, "Phase Diagrams and Conductivity Behavior of Poly(Ethylene Oxide)-Molten Salt Rubbery Electrolytes," *Macromolecules*, *27* (1994), 7469–7477.
9. Mohit Singh, Omolola Odusanya, Gregg M. Wilmes, Hany B. Eitouni, Enrique D. Gomez, Amish J. Patel, Vincent L. Chen, Moon Jeong Park, Panagiota Fragouli, Hermis Iatrou, Nikos Hadjichristidis, David Cookson, and Nitash P. Balsara, "Effect of Molecular Weight on the Mechanical and Electrical Properties of Block Copolymer Electrolytes", *Macromolecules*, *40* (2007), 4578–4585.
10. Yanping Ma, Marc Doyle, Thomas F. Fuller, Marca M. Doeff, Lutgard C. De Jonghe, and John Newman, "The Measurement of a Complete Set of Transport Properties for a Concentrated Solid Polymer Electrolyte Solution," *Journal of the Electrochemical Society*, *142* (1995), 1859–1869.
11. Danielle M. Pesko, Ksenia Timachova, Rajashree Bhattacharya, Mackensie C. Smith, Irune Villaluenga, John Newman, and Nitash P. Balsara, "Negative Transference Numbers in Poly(Ethylene Oxide)-based Electrolytes," *Journal of the Electrochemical Society*, *164* (2017), E3569–E3575.
12. Danielle M. Pesko, Zhange Feng, Simar Sawhney, John Newman, Venkat Srinivasan, and Nitash P. Balsara, "Comparing Cycling Characteristics of Symmetric Lithium-Polymer-Lithium Cells with Theoretical Predictions," *Journal of the Electrochemical Society*, *165* (2018), A3014–A3021.
13. James Clerk Maxwell, *A Treatise on Electricity and Magnetism*, 3rd ed., vol. l (Oxford: Clarendon, 1904), pp. 435–449.
14. D. A. G. Bruggeman, "Berechnung verschiedener physikalischer Konstanten von heterogenen Substanzen. I. Dielektrizitatskonstanten und Leitfiihigkeiten derMischkorper aus isotropen Substanzen," *Annalen der Physik,* ser. 5, *24* (1935), 636–664.
15. J. Sax and J. M. Ottino, "Modeling of Transport of Small Molecules in Polymer Blends: Application of Effective Medium Theory," *Polymer Science and Engineering*, *23* (1983), 165–176.
16. Irune Villaluenga, Danielle M. Pesko, Ksenia Timachova, Zhange Feng, John Newman, Venkat Srinivasan, and Nitash P. Balsara, "Negative Stefan-Maxwell Diffusion Coefficients and Complete Electrochemical Transport Characterization of Homopolymer and Block Copolymer Electrolytes," *Journal of the Electrochemical Society*, *165* (2018), A2766–A2773.

17. Scott A. Mullin, Gregory M. Stone, Ashoutosh Panday, and Nitash P. Balsara, "Salt Diffusion Coefficients in Block Copolymer Electrolytes," *Journal of the Electrochemical Society*, *158* (2011), A619–A627.
18. J. Newman, "Thermoelectric Effects in Electrochemical Systems," *I&EC Research*, *34* (1995) 3208–3216.
19. R. Pollard and J. Newman, "Transport Equations for a Mixture of Two Binary Molten Salts in a Porous Electrode," *Journal of the Electrochemical Society*, *126* (1979), 1713–1717.
20. J. Newman and L. Hsueh, "The Effect of Variable Transport Properties on Mass Transfer to a Rotating Disk," *Electrochimica Acta*, *12* (1967), 417–427.
21. Andreas Acrivos, "The asymptotic form of the laminar boundary-layer mass-transfer rate for large interfacial velocities," *Journal of Fluid Mechanics*, *12* (1962), 337–357.
22. John Newman, "The Effect of Ionic Migration on Limiting Currents," *Industrial and Engineering Chemistry Fundamentals*, *5* (1966), 525–529.
23. John Newman, "The Effect of Migration in Laminar Diffusion Layers," *International Journal of Heat and Mass Transfer*, *10* (1967), 983–997.
24. Andreas Acrivos, "Solution of the Laminar Boundary Layer Energy Equation at High Prandtl Numbers," *The Physics of Fluids*, *3* (1960), 657–658.
25. Jan Robert Selman, *Measurement and Interpretation of Limiting Currents*, dissertation, University of California, Berkeley, June 1971 (UCRL-20557).

CHAPTER 15

FLUID MECHANICS

Since diffusion and migration fluxes are expressed relative to an average velocity of the fluid, mass-transfer calculations require a previous or a simultaneous determination of the velocity. In many systems, the velocity distribution is governed by momentum considerations. The mechanical behavior of fluids is briefly described in this chapter. For more details, one should consult the literature.[1, 2] The velocity profiles for various specific systems will be taken as a basis for determining mass-transfer rates in Part D.

15.1 MASS AND MOMENTUM BALANCES

The mass-average velocity is defined as

$$\mathbf{v} = \frac{1}{\rho} \sum_i c_i M_i \mathbf{v}_i, \tag{15.1}$$

where $c_i \mathbf{v}_i$ is the molar flux density of species i, M_i is the molar mass, and ρ is the density of the medium. The mass-average velocity is useful in fluid mechanics because $\rho \mathbf{v}$ is both the mass-flux density and the momentum density in the fluid. The law of conservation of mass can be expressed in a differential form as

$$\frac{\partial \rho}{\partial t} = -\nabla \cdot (\rho \mathbf{v}). \tag{15.2}$$

This equation can be obtained from the species material balance, equation 11.3, by multiplying that equation by the molar mass M_i and summing over species. When the density is constant in space and time, equation 15.2 reduces to

$$\nabla \cdot \mathbf{v} = 0. \tag{15.3}$$

This is frequently an adequate approximation for dilute liquid solutions.

Electrochemical Systems, Fourth Edition. John Newman and Nitash P. Balsara.

The law of conservation of momentum can be expressed in a differential form as

$$\frac{\partial \rho \mathbf{v}}{\partial t} + \nabla \cdot (\rho \mathbf{v}\mathbf{v}) = \rho \left(\frac{\partial \mathbf{v}}{\partial t} + \mathbf{v} \cdot \nabla \mathbf{v} \right) = -\nabla p - \nabla \cdot \boldsymbol{\tau} + \rho \mathbf{g}, \tag{15.4}$$

where p is the thermodynamic pressure, $\boldsymbol{\tau}$ is the stress tensor, and $\mathbf{g}$ is the acceleration due to gravity. This equation is an expression of Newton's second law of motion; the rate of change of momentum of a fluid element is equal to the force applied. Here, the forces are the pressure gradient, the stress in the fluid, and the force of gravity. The divergence of the stress appears because one needs the net force—the difference between the forces on opposite sides of the fluid element (compare Figure 11.1). The stress tensor will be considered in the following section.

Other forces could be included in the momentum balance. If the fluid is not electrically neutral, we should add to the right side of equation 15.4 the electrical force

$$\rho_e \mathbf{E} = \epsilon (\nabla \cdot \mathbf{E}) \mathbf{E} = \epsilon (\nabla^2 \Phi) \nabla \Phi. \tag{15.5}$$

This term is usually omitted because electrolytic solutions are electrically neutral to a very good approximation. However, this conclusion was arrived at on the basis of the large magnitude of electrical forces, and it is not immediately obvious that the electrical force can be omitted from the momentum balance. This question will be reconsidered in Section 15.5. In some electrochemical systems, the magnetic force

$$\mathbf{i} \times \mathbf{B}$$

should also be included on the right side of equation 15.4. Here, $\mathbf{i}$ is the current density within the solution, and $\mathbf{B}$ is the magnetic induction ($\mathrm{Wb/m^2}$). The magnetic field may itself be due to the flow of current in the system.

For a fluid of constant density, it may be advantageous to define the dynamic pressure $\mathcal{P}$ by

$$\nabla \mathcal{P} = \nabla p - \rho \mathbf{g}. \tag{15.6}$$

Essentially, this equation subtracts the hydrostatic pressure from the thermodynamic pressure to yield the dynamic pressure, changes in which are directly related to the fluid motion.

15.2 STRESS IN A NEWTONIAN FLUID

The stress $\boldsymbol{\tau}$ is related to velocity gradients within the fluid. For Newtonian fluids, which include most electrolytic solutions, the appropriate expression is

$$\boldsymbol{\tau} = -\mu [\nabla \mathbf{v} + (\nabla \mathbf{v})^*] + \frac{2}{3} \mu \mathbf{I} \nabla \cdot \mathbf{v}, \tag{15.7}$$

where $\mathbf{I}$ is the unit tensor and μ is the viscosity, a transport property that depends on temperature, pressure, and composition. A basic physical law requires the stress to be symmetric; this is assured by the presence in equation 15.7 of the transpose $(\nabla \mathbf{v})^*$ of the velocity gradient.

To be specific, a diagonal element of the stress looks like

$$\tau_{xx} = -2\mu \frac{\partial v_x}{\partial x} + \frac{2}{3} \mu \nabla \cdot \mathbf{v}, \tag{15.8}$$

while an off-diagonal element looks like

$$\tau_{xy} = \tau_{yx} = -\mu\left(\frac{\partial v_x}{\partial y} + \frac{\partial v_y}{\partial x}\right). \tag{15.9}$$

For a fluid of constant density and viscosity, substitution of equation 15.7 into equation 15.4 yields

$$\frac{\partial \mathbf{v}}{\partial t} + \mathbf{v}\cdot\nabla\mathbf{v} = -\frac{1}{\rho}\nabla p + \nu\nabla^2\mathbf{v} + \mathbf{g}, \tag{15.10}$$

where $\nu = \mu/\rho$ is the *kinematic viscosity* of the fluid. This equation, known as the Navier–Stokes equation, is written out in rectangular coordinates in Appendix B and in cylindrical coordinates in Section 15.4.

15.3 BOUNDARY CONDITIONS

On solid surfaces the velocity **v** is zero, or, more generally, the velocity is continuous at an interface. An exception to this was encountered in electrokinetic phenomena (see Section 9.1), where the discontinuity in velocity was related to the tangential electric field. However, this was after taking account of the behavior of the diffuse double layer, and in the details of the analysis the velocity was continuous. Electrokinetic phenomena do not need to be considered in all processes.

For a fluid–fluid interface, the velocity at the surface may not be known in advance, and then the relationship between the shear stress in the two phases must be considered. If the interface is of negligible mass (see remark below equation 7.6), the forces at the interface must balance. In the simplest case, this means that the tangential (shear) stress is continuous.

Let the two phases be denoted by superscripts α and β, and let the force per unit area exerted by these phases on the interface be $\mathbf{f}^\alpha$ and $\mathbf{f}^\beta$, respectively. These forces **f** are the product of the stress $\boldsymbol{\tau}$ with the unit normal vector of the interface:

$$\mathbf{f}^\alpha = \mathbf{n}\cdot\boldsymbol{\tau}^\alpha + \mathbf{n}p^\alpha \tag{15.11}$$

and

$$\mathbf{f}^\beta = -\mathbf{n}\cdot\boldsymbol{\tau}^\beta - \mathbf{n}p^\beta, \tag{15.12}$$

where **n** points into phase β. (The stress $\boldsymbol{\tau}$ is expressed in various coordinate systems in Ref. [2].)

Figure 15.1 shows a surface element lying in the plane of the paper. A force balance in the x direction yields

$$(f_x^\alpha + f_x^\beta)\Delta x\,\Delta z + \Delta z(\sigma|_{x+\Delta x} - \sigma|_x) = 0, \tag{15.13}$$

where σ is the interfacial tension (mN/m). If we divide by $\Delta x\,\Delta z$ and let Δx approach zero, we obtain

$$f_x^\alpha + f_x^\beta + \frac{\partial\sigma}{\partial x} = 0. \tag{15.14}$$

A similar equation applies in the z direction. Together, we have

$$\mathbf{f}_s^\alpha + \mathbf{f}_s^\beta + \nabla_s\sigma = 0, \tag{15.15}$$

where $\mathbf{f}_s^\alpha$ and $\mathbf{f}_s^\beta$ denote the components of $\mathbf{f}^\alpha$ and $\mathbf{f}^\beta$ lying in the surface and ∇_s denotes the surface gradient.

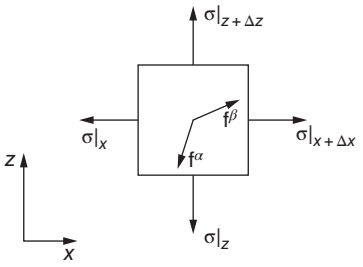

Figure 15.1 Tangential forces on an interfacial element lying in the x, z plane. *Source*: Newman.[3] Copyright 1967. Reprinted with permission from John Wiley & Sons, Inc.

The tangential parts of the forces $\mathbf{f}^{\alpha}$ and $\mathbf{f}^{\beta}$ are viscous in nature, and, if the interfacial tension is independent of position in the surface, equation 15.15 says that the tangential viscous stress is continuous.

For the normal component of the force balance we have

$$f_n^{\alpha} + f_n^{\beta} = \sigma\left(\frac{1}{r_1} + \frac{1}{r_2}\right), \tag{15.16}$$

where r_1 and r_2 are the principal radii of curvature of the surface. The normal components f_n^{α} and f_n^{β} include the thermodynamic pressure p as well as the normal viscous stress. The appropriate signs on the radii of curvature in equation 15.16 would be such that the pressure inside a drop or bubble is greater than the pressure outside.

These elements of surface dynamics enter into the treatment of electrocapillary phenomena (see Chapter 10).

Only the gradient of the pressure appears in equation 15.4 or 15.10. Consequently, it is sometimes possible to solve a problem in terms of this gradient without ever requiring the pressure itself. Then it is sufficient to specify the pressure at only one point.

15.4 FLUID FLOW TO A ROTATING DISK

The rotating-disk electrode is very popular in electrochemical studies, partly because the hydrodynamic conditions are well known and partly because the experimental setup is small and simple. The rotating disk is also one of the few systems for which a nontrivial solution of the equations of fluid mechanics is possible.

We consider the steady flow of an incompressible fluid caused by the rotation of a large disk about an axis through its center. For this purpose we use cylindrical coordinates r, θ, and z, where z is the perpendicular distance from the disk and r is the radial distance from the axis of rotation. The velocity on the surface of the disk is

$$v_r = 0, \quad v_z = 0, \quad v_\theta = r\Omega. \tag{15.17}$$

The last condition expresses the fact that the rotating disk drags the adjacent fluid with it at an angular velocity Ω (rad/s).

Because of the rotation, there is a centrifugal effect that tends to throw the fluid out in a radial direction. This will result in a radial component of the velocity which is zero at the surface, has a maximum value near the surface, and then goes to zero again at greater distances from the disk. In

order to replace the liquid flowing out in the radial direction, it is necessary to have a z component of the velocity, which brings fluid toward the disk from far away. This gives us a qualitative picture of the flow field in which none of the velocity components is zero.

In cylindrical coordinates, the equation of continuity 15.3 is[2]

$$\frac{1}{r}\frac{\partial}{\partial r}(rv_r) + \frac{1}{r}\frac{\partial v_\theta}{\partial \theta} + \frac{\partial v_z}{\partial z} = 0, \tag{15.18}$$

and the components of the equation of motion 15.10 are[2]
(r component)

$$\begin{aligned}\frac{\partial v_r}{\partial t} + v_r\frac{\partial v_r}{\partial r} + \frac{v_\theta}{r}\frac{\partial v_r}{\partial \theta} - \frac{v_\theta^2}{r} + v_z\frac{\partial v_r}{\partial z} \\ = -\frac{1}{\rho}\frac{\partial \mathcal{P}}{\partial r} + \nu\left[\frac{\partial}{\partial r}\left(\frac{1}{r}\frac{\partial}{\partial r}(rv_r)\right) + \frac{1}{r^2}\frac{\partial^2 v_r}{\partial \theta^2} - \frac{2}{r^2}\frac{\partial v_\theta}{\partial \theta} + \frac{\partial^2 v_r}{\partial z^2}\right],\end{aligned} \tag{15.19}$$

(θ component)

$$\begin{aligned}\frac{\partial v_\theta}{\partial t} + v_r\frac{\partial v_\theta}{\partial r} + \frac{v_\theta}{r}\frac{\partial v_\theta}{\partial \theta} + \frac{v_r v_\theta}{r} + v_z\frac{\partial v_\theta}{\partial z} \\ = -\frac{1}{\rho}\frac{\partial \mathcal{P}}{\partial \theta} + \nu\left[\frac{\partial}{\partial r}\left(\frac{1}{r}\frac{\partial}{\partial r}(rv_\theta)\right) + \frac{1}{r^2}\frac{\partial^2 v_\theta}{\partial \theta^2} + \frac{2}{r^2}\frac{\partial v_r}{\partial \theta} + \frac{\partial^2 v_\theta}{\partial z^2}\right],\end{aligned} \tag{15.20}$$

(z component)

$$\begin{aligned}\frac{\partial v_z}{\partial t} + v_r\frac{\partial v_z}{\partial r} + \frac{v_\theta}{r}\frac{\partial v_z}{\partial \theta} + v_z\frac{\partial v_z}{\partial z} \\ = -\frac{1}{\rho}\frac{\partial \mathcal{P}}{\partial z} + \nu\left[\frac{1}{r}\frac{\partial}{\partial r}\left(r\frac{\partial v_z}{\partial r}\right) + \frac{1}{r^2}\frac{\partial^2 v_z}{\partial \theta^2} + \frac{\partial^2 v_z}{\partial z^2}\right],\end{aligned} \tag{15.21}$$

where we have used the dynamic pressure $\mathcal{P}$ introduced in equation 15.6. In our problem with axial symmetry and steady flow, the derivatives with respect to t and θ are zero in these equations.

In 1921, von Kármán[4] suggested that these partial differential equations could be reduced to ordinary differential equations by seeking a solution of the form

$$v_\theta = rg(z), \quad v_r = rf(z), \quad v_z = h(z), \quad \mathcal{P} = \mathcal{P}(z), \tag{15.22}$$

which is a separation of variables. If these expressions are substituted into equations 15.18 to 15.21, one obtains

$$\begin{aligned} 2f + h' &= 0, \\ f^2 - g^2 + hf' &= \nu f'', \\ 2fg + hg' &= \nu g'', \\ \rho hh' + \mathcal{P}' &= \mu h'', \end{aligned} \tag{15.23}$$

where the primes denote differentiation with respect to z.

The boundary conditions are

$$h = f = 0, \quad g = \Omega \quad \text{at} \quad z = 0.$$
$$f = g = 0 \quad \text{at} \quad z = \infty. \tag{15.24}$$

In addition, the value of $\mathcal{P}$ needs to be specified at one point.

The von Kármán transformation is successful in reducing the problem to ordinary differential equations. It should be noted, however, that this solution does not take into account the fact that the radius of the disk might be finite. In practice, these edge effects can frequently be neglected, and the resulting solution is quite useful.[5]

The remaining parameters, ν, ρ, Ω, can be eliminated by introducing a dimensionless distance, dimensionless velocities, and a dimensionless pressure as follows:

$$\zeta = z\sqrt{\frac{\Omega}{\nu}}, \quad \mathcal{P} = \mu\Omega P, \quad v_\theta = r\Omega G,$$
$$v_r = r\Omega F, \quad v_z = \sqrt{\nu\Omega}H. \tag{15.25}$$

The differential equations 15.23 become

$$\begin{aligned} 2F + H' &= 0, \\ F^2 - G^2 + HF' &= F'', \\ 2FG + HG' &= G'', \\ HH' + P' &= H'', \end{aligned} \tag{15.26}$$

where the primes now denote differentiation with respect to ζ. The boundary conditions are

$$H = F = 0, \quad G = 1 \quad \text{at} \quad \zeta = 0.$$
$$F = G = 0 \quad \text{at} \quad \zeta = \infty. \tag{15.27}$$

Since these equations are nonlinear, it seems necessary to obtain the solution numerically. Cochran[6] originally solved these equations by forming series expansions for small values of ζ and for large values of ζ and then adjusting the unknown coefficients in the series until agreement between the two sets of series was obtained at an intermediate value of ζ. However, it is fairly simple to solve coupled, nonlinear, ordinary differential equations by direct numerical techniques (see Appendix C). The solution to equations 15.26 subject to conditions 15.27 is shown in Figure 15.2. After the velocity profiles have been determined, the pressure can be obtained by integrating the last of equations 15.26:

$$P = P(0) + H' - \frac{1}{2}H^2. \tag{15.28}$$

The normal component v_z of the velocity will be important for the calculation of rates of mass transfer to the rotating disk (see Section 17.2). For small distances from the disk, the dimensionless velocity can be expressed as a power series:

$$H = -a\zeta^2 + \frac{1}{3}\zeta^3 + \frac{b}{6}\zeta^4 + \cdots, \tag{15.29}$$

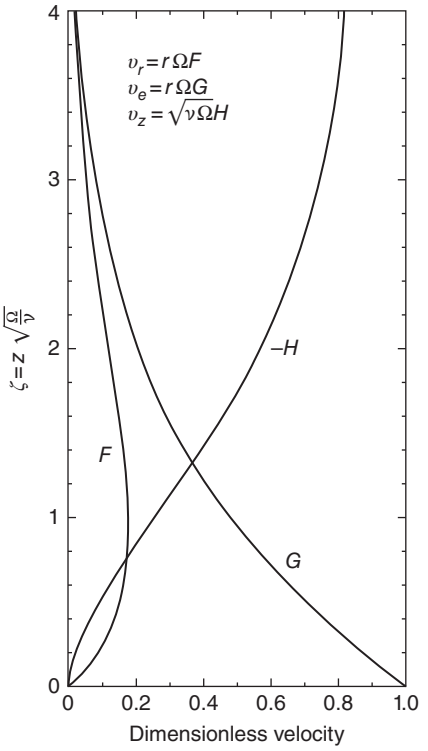

Figure 15.2 Velocity profiles for a rotating disk.

with the coefficients[6, 7]

$$a = 0.51023 \quad \text{and} \quad b = -0.616. \tag{15.30}$$

On the other hand, for large distances from the disk, the dimensionless velocity can be expressed as

$$H = -\alpha + \frac{2A}{\alpha} e^{-\alpha\zeta} + \cdots, \tag{15.31}$$

where

$$\alpha = 0.88447 \quad \text{and} \quad A = 0.934. \tag{15.32}$$

The fact that the normal component of the velocity v_z depends only on the normal distance z and not on the radial distance r is another reason for the popularity of the rotating-disk electrode among electrochemists.

The flow in the boundary layer remains laminar for a Reynolds number, $\mathrm{Re} = r^2\Omega/\nu$, up to about 2×10^5. For larger radial distances, the flow becomes turbulent.

15.5 MAGNITUDE OF ELECTRICAL FORCES

Let us now include the electrical force, equation 15.5, in the momentum balance, equation 15.4. For a rotating disk we might at first imagine that **E** lies in the z direction because of the uniform accessibility

of the surface (see Section 17.2). Then

$$\epsilon(\nabla \cdot \mathbf{E})E_z = \frac{1}{2}\epsilon\frac{dE_z^2}{dz}. \tag{15.33}$$

This enters only into the z component of the equation of motion; that is, the last of equations 15.26 becomes

$$\begin{aligned}\frac{dP}{d\zeta} &= \frac{d^2H}{d\zeta^2} - H\frac{dH}{d\zeta} + \frac{1}{2}\frac{\epsilon}{\mu\Omega}\frac{dE_z^2}{d\zeta} \\ &= \frac{d}{d\zeta}\left(\frac{dH}{d\zeta} - \frac{1}{2}H^2 + \frac{1}{2}\frac{\epsilon}{\mu\Omega}E_z^2\right).\end{aligned} \tag{15.34}$$

For $\Omega = 300$ rpm, $\epsilon = 78.3\epsilon_0$, and $\mu = 0.8903$ mPa·s, $\sqrt{\mu\Omega/\epsilon} = 63.5$ V/cm. This gives us a basis for evaluating the relative importance of electrical forces since, for example, H^2 is of order unity. With $i = 0.1$ A/cm^2 and $\kappa = 0.01$ S/cm, we can expect electric fields of the order of $i/\kappa = 10$ V/cm. If the variation in the field were small compared to $\sqrt{\mu\Omega/\epsilon}$, we could neglect the electrical force altogether.

From equation 11.5, we can express the electric field as

$$\mathbf{E} = \frac{\mathbf{i}}{\kappa} + \frac{F}{\kappa}\sum_i z_i D_i \nabla c_i, \tag{15.35}$$

and hence the electric charge density is

$$\frac{\rho_e}{\epsilon} = -\left(\mathbf{i} + F\sum_i z_i D_i \nabla c_i\right)\cdot\frac{\nabla\kappa}{\kappa^2} + \frac{F}{\kappa}\sum_i z_i D_i \nabla^2 c_i. \tag{15.36}$$

From these equations, we can make several observations. The electric charge density is different from zero only in the thin diffusion layers near electrodes, since it is only in these regions that the concentrations and conductivity vary. The charge density here is still small (see Section 11.8) since ϵ is small, but outside these regions it is identically zero. The electric effect will also be largest with a binary electrolyte since, with a supporting electrolyte, κ will be large compared to the variations in κ.

Furthermore, equation 15.35 shows that in the diffusion layers, where ρ_e is different from zero, $\mathbf{E}$ lies mainly in the direction perpendicular to the electrode. This means that the electric force enters most dominantly into the normal component of the equation of motion, where it affects the pressure distribution without altering the velocity distribution. This effect is relatively unimportant since it is the velocity profiles that determine the mass-transfer rates. This we can see clearly in the case of the rotating disk where, as formulated above, the entire electrical effect can be absorbed into the variation of the dynamic pressure $\mathcal{P}$, and the velocity profiles are not affected at all.

Any part of $\rho_e\mathbf{E}$ that can be expressed as the gradient of some quantity can, in general, be absorbed into $\mathcal{P}$. This is the part of $\rho_e\mathbf{E}$ whose curl is zero.

$$\nabla \times \rho_e\mathbf{E} = \rho_e\nabla\times\mathbf{E} + (\nabla\rho_e)\times\mathbf{E} = (\nabla\rho_e)\times\mathbf{E}. \tag{15.37}$$

The curl of $\mathbf{E}$ is zero since $\mathbf{E}$ is minus the gradient of the potential (see entry 5b of Table B.1). In this manner, we arrive at the conclusion that it is the quantity in equation 15.37 that affects the velocity profiles. As observed above, ρ_e is nonzero only in the diffusion layers, and here we can expect that $\mathbf{E}$ and $\nabla\rho_e$ are nearly parallel to each other so that their cross product is small. This reinforces the

conclusion that the electrical force will have most of its effect on the pressure and less effect on the velocity.

Furthermore, the diffusion layer is much thinner than the hydrodynamic boundary layer at high Schmidt numbers. Here the viscous forces are important, and the electric force might be expected to have less effect on the velocity profile if exerted here than if exerted farther from the wall. On the other hand, the velocities are much smaller here and are important in determining the mass-transfer rate. Consequently, the effect could still be important.

The way to ascertain the effect of the electrical force on the velocity profiles, while excluding the effect on the dynamic pressure, is to take the curl of the equation of motion 15.10. This eliminates the pressure. We assume that the von Kármán transformation 15.25 is still valid and examine the magnitude of the neglected electrical force. Taking the curl of the equation of motion now yields

$$2FG + H\frac{\partial G}{\partial \zeta} = \frac{\partial^2 G}{\partial \zeta^2}, \tag{15.38}$$

$$\frac{d}{d\zeta}\left(F^2 - G^2 + H\frac{dF}{d\zeta} - \frac{d^2F}{d\zeta^2}\right) r\Omega^2 = \frac{E_r}{\rho}\frac{\partial \rho_e}{\partial \zeta} - \frac{E_z}{\rho}\sqrt{\frac{\nu}{\Omega}}\frac{\partial \rho_e}{\partial r}, \tag{15.39}$$

and the continuity equation 15.3 becomes

$$2F + \frac{dH}{d\zeta} = 0. \tag{15.40}$$

The term on the right in equation 15.39 comes from the cross product of $\nabla\rho_e$ and $\mathbf{E}$ (see equation 15.37). As observed before, E_r should be much less than E_z and $\partial\rho_e/\partial r$ should be much less than $\partial\rho_e/\partial z$. This makes it difficult to assess the magnitude of these terms. In order to continue the analysis, let us take ρ_e to be independent of r and take E_r to be independent of ζ in the diffusion layer and given by

$$E_r = A\frac{ir}{\kappa_\infty r_0}, \tag{15.41}$$

where A is approximately equal to 0.73. This is an approximation to the radial dependence of the tangential electric field just outside the diffusion layer when a uniform current density i prevails over the surface of a disk electrode embedded in an insulating plane (see Figure 18.8). The importance of the tangential electric field here finds analogy in the electrokinetic phenomena treated in Chapter 9.

Equation 15.39 can now be integrated to read

$$F^2 - G^2 + H\frac{dF}{d\zeta} = \frac{d^2F}{d\zeta^2} + \frac{Ai\rho_e}{\rho\kappa_\infty r_0\Omega^2}, \tag{15.42}$$

the integration constant being zero since F, G, and ρ_e approach zero as ζ approaches infinity.

For a binary electrolyte, equation 15.36 becomes

$$\frac{\rho_e}{\epsilon} = -\frac{\mathbf{i}\cdot\nabla c}{z_+\nu_+\Lambda c^2} + \frac{RT}{F}\left(\frac{t_+}{z_+} + \frac{t_-}{z_-}\right)\nabla^2 \ln c, \tag{15.43}$$

where Λ is the equivalent conductance (see equation 11.48) and is taken to be constant. We can take the solution of the equation of convective diffusion 11.21 to be

$$c = c_0 + \frac{c_\infty - c_0}{\Gamma(4/3)}\int_0^\xi e^{-x^3}dx, \tag{15.44}$$

where

$$\xi = \left(\frac{a\nu}{3D}\right)^{1/3}\zeta \tag{15.45}$$

and a is given by equation 15.30. This is the appropriate form of equation 17.10 for high Schmidt numbers ν/D, c_0 and c_∞ being the concentrations at the electrode surface and in the bulk solution, respectively. We shall restrict ourselves to a metal deposition reaction where the current density is given by equation 11.27.

With these assumptions, the last term in equation 15.42 becomes

$$\frac{Ai\rho_e}{\rho\kappa_\infty r_0\Omega^2} = \frac{Ai\epsilon}{r_0\kappa_\infty\mu\Omega}\frac{RT}{-z_+z_-F}\left(\frac{a\nu}{3D}\right)^{2/3}\left[\frac{c_\infty - c_0}{c\Gamma(4/3)}\right]^2 e^{-\xi^3}$$
$$\times\left\{z_+ - (z_+t_- + z_-t_+)\left[1 + e^{-\xi^3} + 3\xi^2\frac{c\Gamma(4/3)}{c_\infty - c_0}\right]\right\}. \tag{15.46}$$

The coefficient in this expression can be estimated to be

$$\frac{Ai\epsilon}{r_0\kappa_\infty\mu\Omega}\frac{RT}{F}\left(\frac{a\nu}{3D}\right)^{2/3} = 0.0057, \tag{15.47}$$

where we have used, in addition to the values below equation 15.34, $r_0 = 0.25$ cm for the electrode radius and $\mathrm{Sc} = \nu/D = 1000$ for the Schmidt number.

The factor $(a\nu/3D)^{2/3}$ in equation 15.46 or 15.47 accounts for the fact that the electrical force is applied only within the diffusion layer, which is much thinner than the hydrodynamic boundary layer. The coefficient in equation 15.47 suggests that the neglected electrical force is only 0.6 percent as large as the terms that were retained in equation 15.42 when it was solved in Section 15.4 (the retained term G^2 being equal to 1 at $\zeta = 0$). The factor involving $(c_\infty - c_0)/c$ in equation 15.46 indicates that the electrical effect becomes relatively more important near the limiting current since c then becomes zero at the electrode. (This remark does not, of course, apply when a supporting electrolyte is present.)

15.6 TURBULENT FLOW

Turbulent flow is characterized by rapid and apparently random fluctuations of velocity, pressure, and concentration about their average values. One usually is interested in these fluctuations only in a statistical sense. Consequently, a first step in the study of turbulent flow usually involves an average of the equations presumed to describe the flow. This yields differential equations for certain average quantities, but with the involvement of higher order averages. This procedure thus does not lead to any straightforward means of calculating any average quantities. The problem has a strong analogue in the kinetic theory of gases, where one is not interested in the details of the random motion of the molecules, but only in certain average, measurable quantities.

There are many situations for which a simple, laminar solution of the equation of motion 15.10 can be found, but the actual flow is observed to be turbulent. This has led people to investigate the stability of the laminar flow; if the flow is disturbed by an infinitesimal amount, will the disturbance grow in time or distance or will the disturbance die away and leave the laminar flow? This analysis usually proceeds by linearizing the problem about the basic laminar solution. Sometimes the results agree with experimentally observed conditions of transition to turbulence or a more complex laminar flow, as in the case of Taylor vortices in the flow between rotating cylinders (see Section 17.8); but sometimes there is a considerable discrepancy, as in the case of Poiseuille flow in a pipe.

Mean values in turbulent flow can be defined by a time average, for example,

$$\overline{v}_z = \frac{1}{t_0}\int_t^{t+t_0} v_z \, dt. \tag{15.48}$$

The time t_0 over which the average is taken should be long compared to the period of the fluctuations, which might be estimated as 0.01 s.

In laminar flow, the stress is given by Newton's law of viscosity, equation 15.7. However, in turbulent flow there is an additional mechanism of momentum transfer. The random fluctuations of velocity tend to carry momentum toward regions of lower momentum. Thus, the total mean stress or momentum flux is the sum of a viscous stress and a turbulent momentum flux:

$$\overline{\boldsymbol{\tau}} = \overline{\boldsymbol{\tau}}^{(l)} + \overline{\boldsymbol{\tau}}^{(t)}, \tag{15.49}$$

where the viscous momentum flux $\overline{\boldsymbol{\tau}}^{(l)}$ is given by the time average of equation 15.7 and the turbulent momentum flux $\overline{\boldsymbol{\tau}}^{(t)}$ will be derived later in this section.

Far from a solid wall, momentum transfer by the turbulent mechanism predominates. However, near a solid wall the turbulent fluctuations are damped, and viscous momentum transfer predominates, so that the shear stress at the wall is still given by

$$\tau_0 = -\mu \left.\frac{\partial \overline{v}_z}{\partial r}\right|_{r=R} \tag{15.50}$$

for flow in a pipe of radius R. It seems reasonable that the turbulent fluctuations should be damped near the wall since the fluid cannot penetrate the wall.

The origin of the turbulent momentum flux is revealed by taking the time average of the equation of motion 15.4

$$\frac{\partial \rho \mathbf{v}}{\partial t} = -\nabla \cdot (\rho \mathbf{v}\mathbf{v}) - \nabla p - \nabla \cdot \boldsymbol{\tau}^{(l)} + \rho \mathbf{g}. \tag{15.51}$$

Here $\boldsymbol{\tau}^{(l)}$ denotes the same stress tensor that had previously been called $\boldsymbol{\tau}$ and is given by equation 15.7 for Newtonian fluids.

The deviation of a flow quantity from its time average is defined as follows for the velocity and pressure:

$$\begin{aligned} \mathbf{v} &= \overline{\mathbf{v}} + \mathbf{v}'. \\ p &= \overline{p} + p'. \end{aligned} \tag{15.52}$$

We call $\mathbf{v}'$ the velocity fluctuation or the fluctuating part of the velocity. Several rules of time averaging follow simply from definition 15.48. The time average of a sum is equal to the sum of the time averages:

$$\overline{A + B} = \overline{A} + \overline{B}.$$

The time average of a derivative is equal to the derivative of the time average: $\overline{d\overline{A}/dx} = d\overline{A}/dx$. In general, the time average of a nonlinear term gives more than one term. For example, $\overline{AB} = \overline{A}\,\overline{B} + \overline{A'B'}$. Of course, the time average of a fluctuation is zero, $\overline{A'} = 0$.

In this discussion, the fluid is assumed to have constant properties (ρ, μ, etc.) since, even with this assumption, the turbulent-flow problem remains intractable and since incompressible fluids do exhibit turbulent flow. In fact, a compressible, laminar boundary layer may be more stable than

an incompressible one. With this assumption, the time average of the equation of motion 15.51 yields

$$\frac{\partial \rho \overline{\mathbf{v}}}{\partial t} = -\nabla \cdot (\rho \overline{\mathbf{v}}\,\overline{\mathbf{v}}) - \nabla \overline{p} - \nabla \cdot (\overline{\boldsymbol{\tau}}^{(l)} + \rho \overline{\mathbf{v}'\mathbf{v}'}) + \rho \mathbf{g}. \tag{15.53}$$

The time-averaged continuity equation 15.3 is

$$\nabla \cdot \overline{\mathbf{v}} = 0. \tag{15.54}$$

The mean viscous stress is given by the time average of equation 15.7:

$$\overline{\boldsymbol{\tau}}^{(l)} = -\mu[\nabla \overline{\mathbf{v}} + (\nabla \overline{\mathbf{v}})^*]. \tag{15.55}$$

These equations are the same as the equations before averaging, except for the appearance of the term $-\nabla \cdot (\rho \overline{\mathbf{v}'\mathbf{v}'})$ in the equation of motion 15.53. If we identify the turbulent momentum flux as

$$\overline{\boldsymbol{\tau}}^{(t)} = \rho \overline{\mathbf{v}'\mathbf{v}'} \tag{15.56}$$

and write the total mean stress according to equation 15.49, then the equation of motion becomes

$$\frac{\partial \rho \overline{\mathbf{v}}}{\partial t} = -\nabla \cdot (\rho \overline{\mathbf{v}}\,\overline{\mathbf{v}}) - \nabla \overline{p} - \nabla \cdot \overline{\boldsymbol{\tau}} + \rho \mathbf{g} \tag{15.57}$$

and bears a strong resemblance to the equation before averaging.

These maneuvers illustrate the origin of the turbulent momentum flux, or so-called *Reynolds stress*, given by equation 15.56. The turbulent mechanism of momentum transfer is somewhat similar to the molecular mechanism in gases; one is due to random motion of molecules, and the other is due to random motion of larger, coherent aggregations of molecules.

The averaging process provides no reliable route to the prediction of the Reynolds stress. In the absence of a fundamental theory, many people have written empirical expressions for $\overline{\boldsymbol{\tau}}^{(t)}$ with various degrees of success. It should, perhaps, be emphasized that there is no simple relationship between turbulent stress and velocity derivatives, as there is for the viscous stress in a Newtonian fluid, where μ is a state property depending only on temperature, pressure, and composition.

Many practical problems of turbulence involve the region near a solid wall since this is, in a sense, the origin of the turbulence and because it is in this region that we want to calculate shear stresses and rates of mass transfer. Experimental data have been studied extensively in order to draw some generalization about the behavior near the wall of the turbulent transport terms, these being the higher-order averages, such as the Reynolds stress, resulting from the averaging of the equations of motion and convective diffusion. This generalization takes the form of a universal law of velocity distribution near the wall, and the results can also be expressed in terms of the eddy viscosity and the eddy kinematic viscosity—coefficients relating the turbulent transport terms to gradients of velocity. These coefficients are strong functions of the distance from the wall and, thus, are not fundamental fluid properties. This type of information is frequently deduced from studies of fully developed pipe flow or certain simple boundary layers.

In studying turbulent flow near the wall, it is found that a correlation called the *universal velocity profile* results if the mean tangential velocity is plotted against the distance from the wall as shown in Figure 15.3. This describes fully developed turbulent flow near a smooth wall and applies both to pipe flow and to turbulent boundary layers. The information is correlated by means of the shear stress τ_0 at the wall:

$$v^+ = \frac{\overline{v}_x}{v_*}, \quad y^+ = \frac{y v_*}{\nu}, \quad v_* = \sqrt{\frac{\tau_0}{\rho}}. \tag{15.58}$$

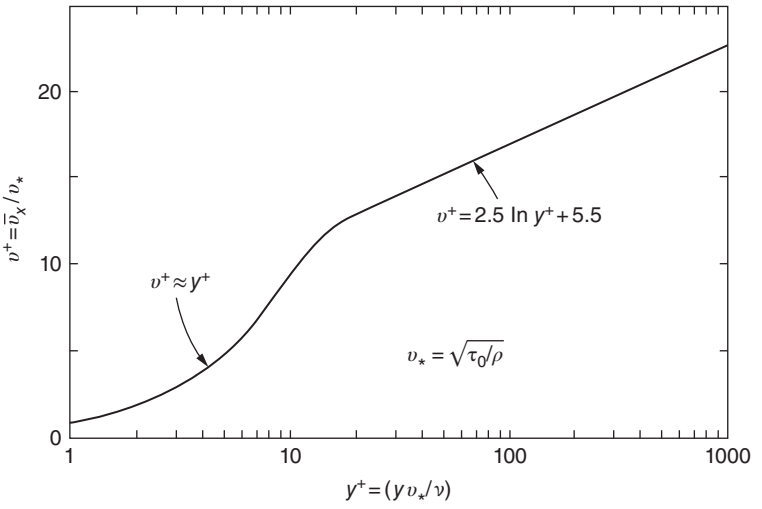

Figure 15.3 Universal velocity profile for fully developed turbulent flow.

Note that away from the wall the mean velocity depends linearly on the logarithm of the distance, while near the wall it increases linearly with the distance. The essential features of the curve are represented by the rough approximations

$$v^+ \approx y^+ \quad \text{for} \quad y^+ < 20 \tag{15.59}$$

and

$$v^+ \approx 2.5 \ln y^+ + 5.5 \quad \text{for} \quad y^+ > 20. \tag{15.60}$$

In the logarithmic region,

$$\bar{v}_x = 2.5\sqrt{\frac{\tau_0}{\rho}} \ln y + \left(2.5 \ln \frac{\sqrt{\tau_0/\rho}}{\nu} + 5.5\right)\sqrt{\frac{\tau_0}{\rho}}. \tag{15.61}$$

Here, the term with the y dependence of the velocity profile is independent of the viscosity; the viscosity of the fluid enters only into the additive constant.

From the data summarized in Figure 15.3, it should be apparent that the Reynolds stress depends strongly on the distance from the wall. A common way to express this is to introduce an *eddy viscosity* $\mu^{(t)}$ by the relation

$$\bar{\tau}_{xy}^{(t)} = -\mu^{(t)} \frac{\partial \bar{v}_x}{\partial y}. \tag{15.62}$$

The empirical results for $\bar{\tau}_{xy}^{(t)}$ are then expressed in terms of the eddy viscosity. Since the turbulent shear flow near a wall should not be expected to be isotropic, other components of the Reynolds stress probably require different values of the eddy viscosity, even at the same distance from the wall.

The universal velocity profile of Figure 15.3 probably applies only to a region near the wall where the shear stress is essentially constant but not to the region near the center of a pipe, say, where the stress goes to zero. If we assume that the shear stress is constant over the region where the universal

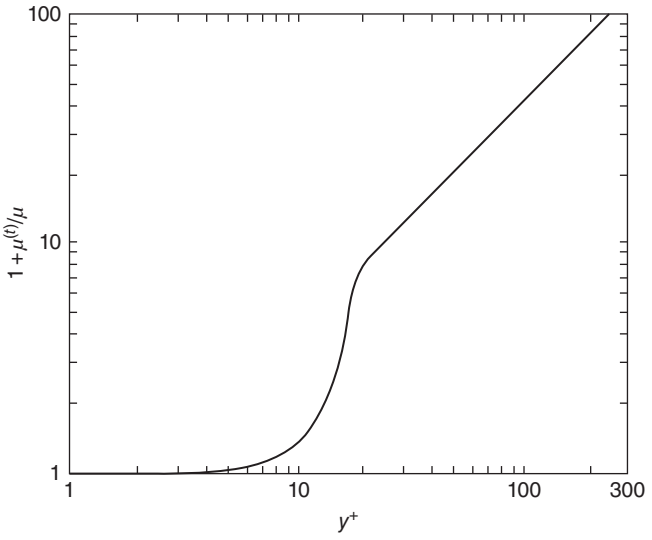

Figure 15.4 Representation of the eddy viscosity as a "universal" function of the distance from the wall.

velocity profile is applicable, then we can obtain an idea of the variation of $\mu^{(t)}$ with distance from the wall.

$$\overline{\tau}_{xy} \approx -\tau_0 = -(\mu + \mu^{(t)})\frac{\partial \overline{v}_x}{\partial y} = -\frac{\mu + \mu^{(t)}}{\mu}\tau_0 \frac{\partial v^+}{\partial y^+}$$

or

$$1 = \left[1 + \frac{\mu^{(t)}}{\mu}\right]\frac{\partial v^+}{dy^+}. \tag{15.63}$$

This result shows that the ratio $\mu^{(t)}/\mu$ should also be a universal function of the wall variable y^+. Figure 15.4 is obtained by differentiation of the universal velocity profile of Figure 15.3. It is not possible to obtain accurate values near the wall by this method because in this region $\mu^{(t)} \ll \mu$. However, this problem should not be of immediate concern since it is the sum $\mu + \mu^{(t)}$ that enters into problems of fluid mechanics.

The universal velocity profile is one of the few generalizations possible in turbulent shear flow, and it is widely applied in the analysis of problems for which experimental observations are not available. Thus, it is the basis of a semi-empirical theory of turbulent flow that can be applied to the hydrodynamics of turbulent boundary layers, mass transfer in turbulent boundary layers, and the beginning of a mass-transfer section in fully developed pipe flow.

15.7 MASS TRANSFER IN TURBULENT FLOW

For the consideration of mass transfer in turbulent flow, one can average the equation of convective diffusion 11.31. The nonlinear term $\mathbf{v}\cdot\nabla c_i$ again yields a new term in the averaged equation:

$$\frac{\partial \overline{c}_i}{\partial t} + \overline{\mathbf{v}} \cdot \nabla \overline{c}_i = D_i \nabla^2 \overline{c}_i - \nabla \cdot \overline{\mathbf{J}}_i^{(t)}, \tag{15.64}$$

where

$$\overline{\mathbf{J}}_i^{(t)} = \overline{\mathbf{v}' c_i'} \tag{15.65}$$

represents the mean turbulent mass flux due to the fluctuations of the concentration and the velocity about their mean values.

Next, one might address the problem of estimating mass-transfer rates in turbulent flow, but with the use of as little additional information as possible. One usually starts with the assumption that the eddy diffusivity $D^{(t)}$, defined by the relation

$$\bar{\mathbf{J}}_{iy}^{(t)} = \overline{c_i' v_y'} = -D^{(t)} \frac{\partial \bar{c}_i}{\partial y}, \tag{15.66}$$

is related to or equal to the eddy kinematic viscosity

$$D^{(t)} = \nu^{(t)} = \frac{\mu^{(t)}}{\rho}, \tag{15.67}$$

although such a simple relation is disputed. This is based on the idea that transfer of momentum and mass is similar, whether it is by a molecular or by a turbulent mechanism. Thus, Figure 15.4 can be used to get information about the variation of the eddy diffusivity in fully developed, turbulent flow near a wall. As stated earlier, $\nu^{(t)}$ is much smaller than ν very close to the wall, and Figure 15.4 gives no information about it. But for mass transfer at large Schmidt numbers, it is necessary to know $D^{(t)}$ closer to the wall. Thus, even if $\nu^{(t)} = D^{(t)}$, we can have at some distance $D^{(t)} \gg D_i$ even where $\nu^{(t)} \ll \nu$ if $\mathrm{Sc} = \nu/D_i$ is large.

Thus, much of our information about $D^{(t)}$ and possibly $\nu^{(t)}$ near the wall comes from mass-transfer experiments. Actually it probably results more from fitting average mass-transfer rates at the wall than from examination in detail of actual concentration profiles. If, for mass transfer in a pipe, we measure the rate by means of the Stanton number

$$\mathrm{St} = \frac{D_i}{\langle \bar{v}_z \rangle \Delta c_i} \left. \frac{\partial \bar{c}_i}{\partial r} \right|_{r=R}, \tag{15.68}$$

then the dependence of the Stanton number on the Schmidt number at large Schmidt numbers is determined by the variation of the eddy diffusivity close to the wall as follows:

$D^{(t)}$ near the wall	St for large Sc
$D(t) \propto y^2$	$\mathrm{St} \propto \mathrm{Sc}^{-1/2}$
y^3	$\mathrm{Sc}^{-2/3}$
y^4	$\mathrm{Sc}^{-3/4}$

It is easy to show that $\nu^{(t)}$ must go to zero as y^3 or a higher power of y but cannot vary as y^2. If v_x' and v_y' are expanded in power series near the wall, then v_x' is proportional to y and, by the continuity equation, v_y' is proportional to y^2. Hence $\bar{\tau}_{xy}^{(t)} = \overline{\rho v_x' v_y'}$ is proportional to y^3, and the same must be true of $\nu^{(t)}$. A controversy between y^3 and y^4 remains. Levich[8] had $D^{(t)}$ proportional to y^3 but later[9] changed this to y^4. Murphee[10] preceded Levich by a decade and favored a y^3 dependence.

Sherwood[11] has reviewed the attempts at describing $D^{(t)}$. The goal of such work is to determine how the eddy diffusivity depends on distance from the wall, that is, to relate $D^{(t)}/\nu$ to y^+, the dimensionless distance from the wall. This is based on the universal velocity profile and on information gleaned from mass-transfer experiments. Following Wasan et al.,[12] we write

$$\begin{aligned} v^+ &= y^+ - A_1 (y^+)^4 + A_2 (y^+)^5 \quad \text{for} \quad y^+ \leq 20, \\ v^+ &= 2.5 \ln y^+ + 5.5 \quad \text{for} \quad y^+ \geq 20. \end{aligned} \tag{15.69}$$

The constants A_1 and A_2 are selected so that v^+ and its derivative are continuous at $y^+ = 20$:

$$A_1 = 1.0972 \times 10^{-4} \quad \text{and} \quad A_2 = 3.295 \times 10^{-6}. \tag{15.70}$$

The corresponding expressions for the eddy diffusivity are

$$\frac{D^{(t)}}{\nu} = \frac{4A_1(y^+)^3 - 5A_2(y^+)^4}{1 - 4A_1(y^+)^3 + 5A_2(y^+)^4} \quad \text{for} \quad y^+ \leq 20,$$
$$\frac{D^{(t)}}{\nu} = \frac{y^+}{2.5} - 1 \quad \text{for} \quad y^+ \geq 20. \tag{15.71}$$

The concept of the universal velocity profile and the variation of eddy diffusivity with distance from the wall as given in Figure 15.5 form the basis of a semiempirical theory widely used to calculate mass-transfer rates in turbulent boundary layers, near the beginning of a mass-transfer section in a pipe, and for similar problems (see, e.g., Ref. [13]).

15.8 DISSIPATION THEOREM FOR TURBULENT PIPE FLOW

It is proposed[14] that certain local statistical turbulent quantities, such as the Reynolds stress, the eddy viscosity, the turbulent energy, and the volumetric dissipation are related to each other. We need to find the relationships from experimental observations.

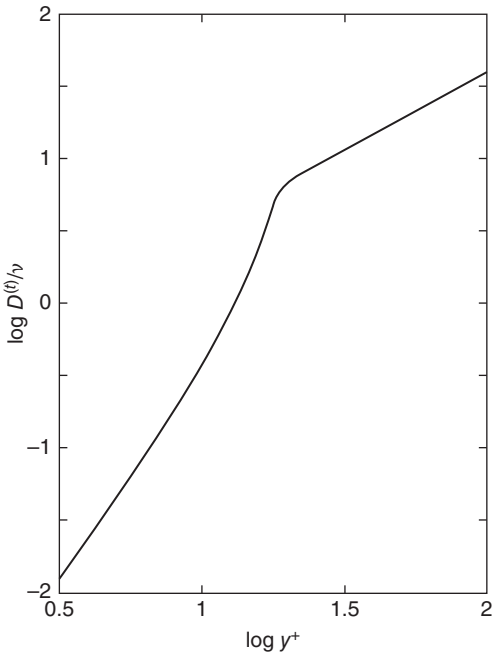

Figure 15.5 Variation of the eddy diffusivity near a wall for fully developed turbulent flow.

The volumetric dissipation $\mathcal{D}_V$ is appealing in this regard because it can be related to the eddy viscosity and because it is directly related to the losses in a system, such as the torque on rotating cylinders and the pressure drop in pipe flow. $\mathcal{D}_V$ is defined as

$$\mathcal{D}_V = -\boldsymbol{\tau} : \nabla \mathbf{v}, \tag{15.72}$$

and it generally describes conversion of mechanical energy into thermal energy. With few approximations, it can be written as

$$\mathcal{D}_V \approx -\overline{\boldsymbol{\tau}} : \nabla \overline{\mathbf{v}} = \tau^2/(\mu + \mu^{(t)}) = (\mu + \mu^{(t)})(\nabla \overline{\mathbf{v}})^2. \tag{15.73}$$

This provides one relationship between $\mathcal{D}_V$ and $\nu^{(t)}$.

It is postulated[14] that $\mathcal{D}_V$ obeys an equation such as

$$\frac{\partial \mathcal{D}_V}{\partial t} + \mathbf{v} \cdot \nabla \mathcal{D}_V = \nabla \cdot [(\nu + \nu^{(t)}) \nabla \mathcal{D}_V] - \text{Decay}, \tag{15.74}$$

that is, the rate of change of $\mathcal{D}_V$ at a point is related to convection, diffusion with a diffusion coefficient of $\nu + \nu^{(t)}$, and decay as turbulence disappears eventually if left alone. A possible form for the Decay is

$$\text{Decay} = k(\mathcal{D}_V^2 + \epsilon \mathcal{D}_V), \tag{15.75}$$

saying that at high values of dissipation the decay is quadratic but at low levels the decay becomes linear in $\mathcal{D}_V$. k and ϵ are constants.

Equation 15.74 does not have a solid basis, and one needs to study several systems experimentally to establish empirical coefficients and even modify forms where necessary. Several systems are appealing because of their simplicity and a wealth of available information on both friction and mass transfer. These systems include steady rotation of disks and cylinders, flow in pipes, and flow along a semiinfinite flat plate in a uniform stream at zero incidence. All these systems are operated at steady state, but two of them involve flow developing along a flat plate or a rotating disk.

Nikuradse[15] gives us detailed experimental distributions of eddy viscosity in pipe flow at 16 Reynolds numbers from 4000 to 3.2×10^6. These show a limiting form at very high Reynolds numbers. Figure 15.6 shows data points for the four lowest Reynolds numbers as well as the limiting profile for high Reynolds numbers as a dashed curve. At low Reynolds numbers, the data lie somewhat above the limit curve, but they approach the limit curve as Re increases. To bring out this behavior, $\nu^{(t)}/\nu$ is divided by R^+, an independent parameter depending on the shear stress at the wall.

$$R^+ = \frac{R}{\nu}\sqrt{\frac{\tau_0}{\rho}}, \tag{15.76}$$

where R is the inner radius of the pipe and τ_0 is the shear stress at the wall. In this geometry the stress τ decreases linearly from $\tau = \tau_0$ at $r = R$ to $\tau = 0$ at $r = 0$.

One can calculate the velocity profile and most flow properties from knowledge of $\nu^{(t)}$ by means of the equations in Section 15.6, from the momentum equation 15.57 and the continuity equation 15.54 and suitable boundary conditions. The friction factor f can be calculated from the formula[16]

$$\sqrt{\frac{2}{f}} = R^+ \int_0^1 \frac{\xi^3 d\xi}{1 + R^+ M(\xi)}, \tag{15.77}$$

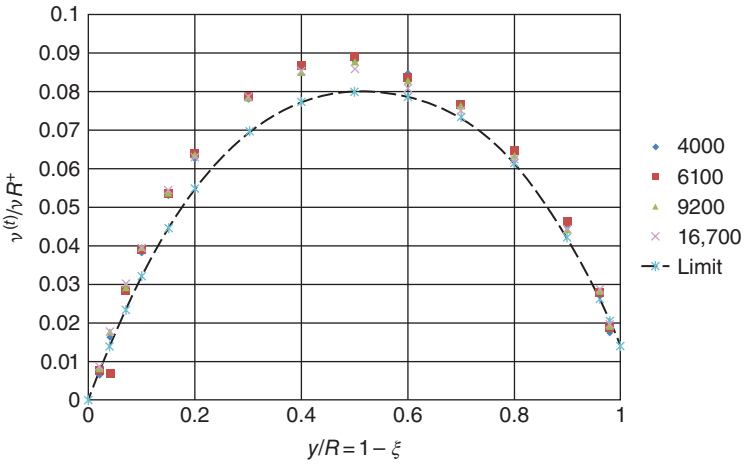

Figure 15.6 The eddy-viscosity profiles of Nikuradse for his lowest 4 Reynolds numbers. The dashed line is the limit curve for large Reynolds numbers. Points for the lower Reynolds numbers generally lie slightly higher than the limit curve. Here, the Reynolds numbers are 4000, 6100, 9200, and 16,700.

where

$$f = \frac{2\tau_o}{\rho\langle\overline{v}_z^2\rangle}, \quad \xi = r/R, \quad \text{and} \quad M = \frac{\nu^{(t)}}{\nu R^+}. \tag{15.78}$$

M is the quantity plotted in Figure 15.6.

The dissipation theorem equation 15.74 provide a means of recovering the eddy kinematic viscosity. Then, the limit curve in Figure 15.6 is reproduced if the Decay is modified to read

$$\text{decay} = \frac{\rho R^2}{\tau_0^2}\text{Decay} = \frac{\Lambda(D^2 + \epsilon D/R^+)}{\xi^2(R^+)^2}, \tag{15.79}$$

where $\Lambda = 0.17$, $\epsilon = 0.3$, and $D = \mu\mathcal{D}_V/\tau_0^2$.

Eisenberg[17] provides mass-transfer data at high Sc for systems of rotating cylinders with five different values of $\kappa = R_i/R_o$, the ratio of the inner rotating cylinder to that of the outer stationary cylinder. Mohr[18] provides additional mass-transfer data for four thinner gaps, with κ closer to 1. Some of Eisenberg's data are covered by equation 17.78. More information should be able to be extracted, but the results of Eisenberg and of Mohr are not in adequate harmony.[14, 19]

PROBLEM

15.1 Show that equation 15.6 implies that

$$\nabla \times \mathbf{g} = 0.$$

This condition is satisfied by most gravitational fields.

NOTATION

a	constant = 0.51023
A	constant
$\mathbf{B}$	magnetic induction, Wb/m^2
c	molar concentration of a single electrolyte, mol/cm^3
c_i	concentration of species i, mol/cm^3
D	diffusion coefficient of electrolyte, cm^2/s
D	dimensionless volumetric dissipation
$D^{(t)}$	eddy diffusivity, cm^2/s
D_i	diffusion coefficient of species i, cm^2/s
$\mathcal{D}_V$	volumetric dissipation, J/cm^3·s
$\mathbf{E}$	electric field, V/cm
f	friction factor
f	function for radial velocity, s^{-1}
$\mathbf{f}$	force per unit area, N/cm^2
F	dimensionless radial velocity
F	Faraday's constant, 96,487 C/mol
g	function for velocity in θ direction, s^{-1}
$\mathbf{g}$	acceleration of gravity, cm/s^2
G	dimensionless velocity in θ direction
h	axial velocity, cm/s
H	dimensionless axial velocity
i	uniform current density on disk electrode, A/cm^2
$\mathbf{i}$	current density, A/cm^2
$\mathbf{I}$	unit tensor
$\overline{\mathbf{J}}_i^{(t)}$	mean turbulent mass flux of species i, mol/cm^2·s
k	parameter in Decay, cm^3/J
M	$v^{(t)}/vR^+$
M_i	molar mass of species i, g/mol
$\mathbf{n}$	unit vector normal to surface
p	pressure, N/cm^2
P	dimensionless dynamic pressure
$\mathcal{P}$	dynamic pressure, N/cm^2
r	radial distance, cm
r_0	radius of disk electrode, cm
r_1, r_2	principal radii of curvature of surface, cm
R	universal gas constant, 8.3143 J/mol·K
R^+	stress parameter
Re	Reynolds number
Sc	Schmidt number
St	Stanton number
t	time, s
t_0	time over which quantities are averaged, s
t_i	transference number of species i
T	absolute temperature, K

$\mathbf{v}$	mass-average velocity, cm/s
$\mathbf{v}_i$	velocity of species i, cm/s
$\langle v_z \rangle$	average velocity in a pipe, cm/s
x	tangential distance, cm
y	distance from surface, cm
z	axial distance, cm
z_i	charge number of species i
$\Gamma(4/3)$	0.89298, the gamma function of 4/3
ϵ	permittivity, F/cm
ϵ	parameter in decay
ϵ	parameter in formula for decay of turbulence
ϵ_0	permittivity of free space, 8.8542×10^{-14} F/cm
ζ	dimensionless axial distance from disk
θ	angle in cylindrical coordinates, rad
κ	ratio of cylinder radii
κ	conductivity, S/cm
Λ	equivalent conductance of binary electrolyte, S·cm^2/mol
Λ	parameter in decay of turbulence
μ	viscosity, mPa·s
$\mu^{(t)}$	eddy viscosity, mPa·s
ν	kinematic viscosity, cm^2/s
$\nu^{(t)}$	eddy kinematic viscosity, cm^2/s
ν_+, ν_-	numbers of cations and anions into which a molecule of electrolyte dissociates
ξ	dimensionless axial distance from disk
ξ	r/R
ρ	density, g/cm^3
ρ_e	electric charge density, C/cm^3
σ	interfacial tension, mN/m
τ	stress, N/cm^2
Φ	electric potential, V
Ω	rotation speed of disk, rad/s

Subscripts

0	at electrode surface
∞	in bulk solution
s	surface

Superscripts

$'$	fluctuation or derivative
(l)	viscous
(t)	turbulent
$+$	related to universal velocity profile
overbar	time average

REFERENCES

1. Hermann Schlichting, *Boundary-Layer Theory* (New York: McGraw-Hill, 1979).
2. R. Byron Bird, Warren E Stewart, and Edwin N. Lightfoot, *Transport Phenomena*, 2nd edition (New York: Wiley, 2002).
3. J. Newman, "Transport Processes in Electrolytic Solutions," in C. W. Tobias, ed., *Advances in Electrochemistry and Electrochemical Engineering*, Vol. *5* (Wiley, 1967).
4. Th. v. Kármán, "Über laminare und turbulente Reibung," *Zeitschrift für angewandte Mathematik und Mechanik*, *1* (1921), 233–252.
5. A. C. Riddiford, "The Rotating Disk System," *Advances in Electrochemistry and Electrochemical Engineering*, *4* (1966), 47–116.
6. W. G. Cochran, "The Flow Due to a Rotating Disc," *Proceedings of the Cambridge Philosophical Society*, *30* (1934), 365–375.
7. M. H. Rogers and G. N. Lance, "The Rotationally Symmetric Flow of a Viscous Fluid in the Presence of an Infinite Rotating Disk," *Journal of Fluid Mechanics*, *7* (1960), 617–631.
8. B. Levich, "The Theory of Concentration Polarization, I," *Acta Physicochimica U.R.S.S.*, *17* (1942), 257–307.
9. B. Levich, "The Theory of Concentration Polarization, II," *Acta Physicochimica U.R.S.S.*, *19* (1944), 117–132.
10. E. V. Murphee, "Relation between Heat Transfer and Fluid Friction," *Industrial and Engineering Chemistry*, *24* (1932), 726–736.
11. T. K. Sherwood, "Mass, Heat, and Momentum Transfer between Phases," *Chemical Engineering Progress Symposium Series, no. 25*, 55 (1959), 71–85.
12. D. T. Wasan, C. L. Tien, and C. R. Wilke, "Theoretical Correlation of Velocity and Eddy Viscosity for Flow Close to a Pipe Wall," *AIChE Journal*, *9* (1963), 567–568.
13. B. T. Ellison and I. Comet, "Mass Transfer to a Rotating Disk," *Journal of the Electrochemical Society*, *118* (1971), 68–72.
14. John Newman, "Theoretical Analysis of Turbulent Mass Transfer with Rotating Cylinders," *Journal of the Electrochemical Society*, *163* (2016), E191–E198.
15. J. Nikuradse, "Gesetzmässigkeiten der turbulenten Strömung in glatten Rohren," *Forschungsheft 356, Beilage zu Forschung auf dem Gebiete des Ingenieurwesens*, Edition B, Volume 3, September/October, 1932 (Berlin NW7: VDI-Verlag GMBH, 1932)," *Laws of Turbulent Flow in Smooth Pipes, NASA TT F-10*, *359* (Washington: National Aeronautics and Space Administration, October 1966).
16. John Newman, "Further Thoughts on Turbulent Flow in a Pipe," *Russian Journal of Electrochemistry*, *55* (2019), 33–43.
17. Morris Eisenberg, *Studies of Rates of Solid Dissolution and of Electrode Reactions at Rotating Cylindrical Bodies*, dissertation, Berkeley: University of California, 1953.
18. Charles Milton Mohr, Jr., *Mass Transfer in Rotating Electrode Systems*, dissertation, Berkeley: University of California, 1975.
19. John Newman, *Turbulent Flow with the Inner Cylinder Rotating*, Russian Journal of Electrochemistry, *55* (2018), 44–51.

PART D

CURRENT DISTRIBUTION AND MASS TRANSFER IN ELECTROCHEMICAL SYSTEMS

Electrochemical systems find widespread technical application. Industrial electrolytic processes include electroplating and refining, electropolishing and machining, and the electrochemical production of chlorine, caustic soda, aluminum, and other products. Energy conversion in fuel cells and in primary and secondary batteries has received increasing attention. Electrochemical corrosion should not be neglected, and some systems for desalting water involve electrochemical processes. Electrochemical methods are used for qualitative and quantitative analysis. Idealized electrochemical systems are also of interest for studies of mass-transfer processes and the mechanisms of electrode reactions and for the determination of basic data on transport properties.

Engineering design procedures for electrochemical systems have not been developed as thoroughly as for mass-transfer operations such as distillation. Nevertheless, the fundamental laws governing electrochemical systems are known and have been developed in Parts A, B, and C of this book. The purpose of Part D is to review the analysis of certain electrochemical systems in relation to these fundamental laws. To a greater or lesser extent, one is concerned with fluid flow patterns, ohmic potential drop in solutions, restricted rates of mass transfer, and the kinetics of electrode reactions. The situation is complicated as well by the variety of specific chemical systems. These examples provide some of the main tools of the electrochemical engineer.

Application of the fundamental laws has followed two main courses. There are systems where the ohmic potential drop can be neglected. The current distribution is then determined by the same principles that apply to heat transfer and nonelectrolytic mass transfer. This usually involves systems operated at the limiting current with an excess of supporting electrolyte because, below the limiting current, neglecting the ohmic potential drop is usually not justified and because the presence of the supporting electrolyte allows the effect of ionic migration in the diffusion layer to be ignored. Furthermore, the concentration of the limiting reactant is zero at the electrode surface, and the treatment becomes simplified. Let us call these *convective-transport problems,* treated in Chapter 17.

Electrochemical Systems, Fourth Edition. John Newman and Nitash P. Balsara.

At currents much below the limiting current, it is possible to neglect concentration variations near the electrodes. The current distribution is then determined by the ohmic potential drop in the solution and by electrode overpotentials. Mathematically, this means that the potential satisfies Laplace's equation, and many results of potential theory, developed in electrostatics, the flow of inviscid fluids, and steady heat conduction in solids are directly applicable. Let us call these *potential-theory problems,* treated in Chapter 18. The electrode kinetics provides boundary conditions that are usually different from those encountered in other applications of potential theory.

Existing work on current distribution and mass transfer in electrochemical systems is reviewed here, with emphasis being placed on how each contribution is related to these limiting cases of convective-transport problems and applications of potential theory. This framework can be compared with Wagner's discussion[1] of the scope of electrochemical engineering. Much work either fits into the extreme cases or takes into account phenomena neglected in the extreme cases.

We also discuss problems that do not fall into either of these two classes. Some problems can be regarded as an extension of the convective-transport problems. At the limiting current, the ohmic potential drop in the bulk of the solution may still be negligible, but the electric field in the diffusion layer near electrodes may lead to an enhancement of the limiting current. The current density is then distributed along the electrode in the same manner as when migration is neglected, but the magnitude of the current density at all points is increased or diminished by a constant factor that depends upon the bulk composition of the solution (see Chapter 19). Free convection in a supported electrolytic solution also involves this migration effect. In addition, the nonuniform concentration of the added electrolyte affects the density distribution and hence the velocity profiles in the system. This effect, which does not disappear with a large excess of supporting electrolyte, is treated in the last section of Chapter 19.

At currents below, but at an appreciable fraction of, the limiting current, diffusion and convective transport are essential, but neither concentration variations near the electrode nor the ohmic potential drop in the bulk solution can generally be neglected. These problems are complex because all the factors are involved at once. They span the limiting cases of convective-transport problems and applications of potential theory and are treated in Chapter 21. Prior to this, the concept of the concentration overpotential is further developed in Chapter 20.

In technical electrochemical systems, the ohmic potential drop is of great importance, and potential-theory problems find applications here. Nevertheless, concentration variations near electrodes frequently provide limitations on reaction rates and current efficiencies in industrial operations. In view of the complexity of simultaneously treating concentration variations and ohmic potential drop, qualitative or semiquantitative application of these concepts may have to suffice for some time. Thus, only a limited number of systems can be discussed in Chapter 21.

Many electrodes found in fuel cells and primary and secondary batteries are porous in order to provide an extensive surface area for electrochemical reactions. In such electrodes, convection may not be present, but it is usually necessary to consider the ohmic potential drop, concentration variations, and electrode kinetics. Most treatments adopt a macroscopic model that does not take account of the detailed, random geometry of the porous structure. Results of potential theory are then not applicable since Laplace's equation does not hold. Porous-electrode problems thus do not fall within the framework of convective-transport problems and applications of potential theory. Flooded porous electrodes are treated in Chapter 22.

Chapter 23 deals with semiconductor electrodes, including solar energy conversion, in a manner that uses the fundamental principles as developed earlier in the book. Here we have macroscopic regions where electroneutrality is not obeyed.

Impedance involves the application of alternating current or potential to electrochemical systems and finds importance by providing a nondestructive diagnostic tool and an additional means to understand the physics and chemistry. Chapter 24 gives specific examples of electrochemical impedance modeled by application of the topics treated throughout the book, thereby going beyond equivalent circuits.

Earlier reviews of current distribution and mass transfer in electrochemical systems are given in Refs. [2–6]. Ref. [7] contains more mathematical development than is included here.

Significant parts of Chapter 22 are taken from Newman and Tiedemann,[8] reproduced by permission of the American Institute of Chemical Engineers.

REFERENCES

1. Carl Wagner, "The Scope of Electrochemical Engineering," in Charles W. Tobias, ed., *Advances in Electrochemistry and Electrochemical Engineering*, *2* (1962), 1–14.
2. John Newman, "Engineering Design of Electrochemical Systems," *Industrial and Engineering Chemistry*, *60* (1968), 12–27.
3. C. W. Tobias, M. Eisenberg, and C. R. Wilke, "Diffusion and Convection in Electrolysis: A Theoretical Review," *Journal of the Electrochemical Society*, *99* (1952), 359C–365C.
4. Wolf Vielstich, "Der Zusammenhang zwischen Nernstscher Diffusionsschicht und Prandtlscher Strömungsgrenzschicht," *Zeitschrift für Elektrochemie*, *57* (1953), 646–655.
5. N. Ibl, "Probleme des Stofftransportes in der angewandten Elektrochemie," *ChemieIngenieur-Technik*, *35* (1963), 353–361.
6. N. Ibl, "Current Distribution," in Ernest Yeager, J. O.'M. Bockris, Brian E. Conway, and S. Sarangapani, eds., *Comprehensive Treatise of Electrochemistry* (New York: Plenum, 1963), Vol. 6, pp. 239–315.
7. John Newman, "The Fundamental Principles of Current Distribution and Mass Transport in Electrochemical Cells," in Allen J. Bard, ed., *Electroanalytical Chemistry* (New York: Marcel Dekker 1973), Vol. 6, pp. 187–352.
8. John Newman and William Tiedemann, "Porous-electrode Theory with Battery Applications," *AIChE Journal*, *21* (1975), 25–41.

CHAPTER 16

FUNDAMENTAL EQUATIONS

16.1 TRANSPORT IN DILUTE SOLUTIONS

The laws of transport in dilute solutions have been known for many years and have been developed in Chapter 11. The four principal equations in dilute-solution theory are presented in Section 11.1. The flux of a solute species is due to migration in an electric field, diffusion in a concentration gradient, and convection with the fluid velocity.

$$\mathbf{N}_i = -z_i u_i F c_i \nabla\Phi - D_i \nabla c_i + \mathbf{v} c_i. \tag{16.1}$$

A material balance for a small-volume element leads to the differential conservation law:

$$\frac{\partial c_i}{\partial t} = -\nabla\cdot\mathbf{N}_i + R_i. \tag{16.2}$$

Since reactions are frequently restricted to the surfaces of electrodes, the bulk reaction term R_i is often zero in electrochemical systems. To a very good approximation, the solution is electrically neutral,

$$\sum_i z_i c_i = 0, \tag{16.3}$$

except in the diffuse part of the double layer very close to an interface. The current density in an electrolytic solution is due to the motion of charged species:

$$\mathbf{i} = F \sum_i z_i \mathbf{N}_i. \tag{16.4}$$

These laws provide the basis for the analysis of electrochemical systems. The flux relation, equation 16.1, defines transport coefficients—the mobility u_i and the diffusion coefficient D_i of an ion in a dilute solution. The dilute-solution theory has been applied fruitfully to many electrochemical

Electrochemical Systems, Fourth Edition. John Newman and Nitash P. Balsara.

systems. We furthermore assume that the physical properties are constant. The dominant factors are then revealed in the simplest manner, and the results have the widest range of applicability.

Many electrochemical systems involve flow of the electrolytic solution. For a fluid of constant density ρ and viscosity μ, the fluid velocity is to be determined from the Navier–Stokes equation (see Chapter 15):

$$\rho\left(\frac{\partial \mathbf{v}}{\partial t} + \mathbf{v}\cdot\nabla\mathbf{v}\right) = -\nabla p + \mu\nabla^2\mathbf{v} + \rho\mathbf{g} \tag{16.5}$$

and the continuity equation

$$\nabla\cdot\mathbf{v} = 0. \tag{16.6}$$

16.2 ELECTRODE KINETICS

The differential equations describing the electrolytic solution require boundary conditions for the behavior of an electrochemical system to be predicted. The most complex of these concerns the kinetics of electrode reactions, treated in Chapter 8. A single electrode reaction can be written in symbolic form as

$$\sum_i s_i M_i^{z_i} \rightarrow n\mathrm{e}^-. \tag{16.7}$$

Then the normal component of the flux of a species is related to the normal component of the current density, that which contributes to the external current to the electrode.

$$N_{in} = -\frac{s_i}{nF} i_n. \tag{16.8}$$

This equation is restricted not only to a single electrode reaction but also to the absence of an appreciable charging of the double layer, a process that does not follow Faraday's law.

Next, one needs an equation describing the kinetics of the electrode reaction, that is, an equation that relates the normal component of the current density to the surface overpotential at that point and the composition of the solution just outside the diffuse part of the double layer. The motivation of the electrochemical engineer in this regard is basically different from that of an electrochemist. The object is to predict the behavior of a complex electrochemical system rather than to elucidate the mechanism of an electrode reaction. To accomplish this objective, one needs an equation that describes accurately how the interface behaves during the passage of current, and, for this purpose, the interface includes the diffuse part of the double layer.

The surface overpotential η_s can be defined as the potential of the working electrode relative to a reference electrode of the same kind located just outside the double layer. Then one seeks a kinetic expression of the form

$$i_n = f(\eta_s, c_i), \tag{16.9}$$

where charging of the double layer is again ignored. The concentrations c_i here refer to the point just outside the double layer. Such an expression thus describes the interface since i_n, η_s, and c_i, are all local quantities. In particular, the concentration variation between the interface and the bulk solution and the ohmic potential drop in the solution have only an incidental bearing on events at the interface. At the same time, no attempt is made to give a separate account of the diffuse part of the double layer.

The function f in equation 16.9 is, in general, complicated. However, there is ample evidence that there is a large class of electrode reactions for which the current density depends exponentially on the surface overpotential in the following form:

$$i_n = i_0 \left[\exp\left(\frac{\alpha_a F}{RT} \eta_s \right) - \exp\left(-\frac{\alpha_c F}{RT} \eta_s \right) \right], \tag{16.10}$$

where i_0 is the exchange current density and depends on the concentrations c_i. This latter dependence can frequently be expressed as a product of powers of the concentrations (see Section 8.3). In this equation, i_n and η_s are positive for anodic processes, negative for cathodic processes. Both α_a and α_c are kinetic parameters and must be determined to agree with experimental data. A rereading of Section 1.3 may be useful at this point.

NOTATION

c_i	concentration of species i, mol/cm^3
D_i	diffusion coefficient of species i, cm^2/s
e^-	symbol for the electron
f	function in expression of electrode kinetics
F	Faraday's constant, 96,487 C/mol
$\mathbf{g}$	acceleration of gravity, cm/s^2
$\mathbf{i}$	current density, A/cm^2
i_0	exchange current density, A/cm^2
M_i	symbol for the chemical formula of species i
n	number of electrons transferred in electrode reaction
$\mathbf{N}_i$	flux density of species i, mol/cm^2·s
p	pressure, N/cm^2
R	universal gas constant, 8.3143 J/mol·K
R_i	rate of homogeneous production of species, mol/cm^3·s
s_i	stoichiometric coefficient of species i in electrode reaction
t	time, s
T	absolute temperature, K
u_i	mobility of species i, cm^2·mol/J·s
$\mathbf{v}$	fluid velocity, cm/s
z_i	charge number of species i
α_a, α_c	transfer coefficients
η_s	surface overpotential, V
μ	viscosity, mPa·s
ρ	density, g/cm^3
Φ	electric potential, V

CHAPTER 17

CONVECTIVE-TRANSPORT PROBLEMS

17.1 SIMPLIFICATIONS FOR CONVECTIVE TRANSPORT

For the reaction of minor ionic species in a solution containing excess supporting electrolyte, it should be permissible to neglect the contribution of ionic migration to the flux of the reacting ions (see Section 11.5), so that equation 16.1 becomes

$$\mathbf{N}_i = -D_i \nabla c_i + \mathbf{v} c_i, \tag{17.1}$$

and substitution into equation 16.2 yields

$$\frac{\partial c_i}{\partial t} + \mathbf{v} \cdot \nabla c_i = D_i \nabla^2 c_i. \tag{17.2}$$

This may be called the equation of *convective diffusion*. A similar equation applies to convective heat transfer and convective mass transfer in nonelectrolytic solutions. Since these fields have been studied in detail, it is possible to apply many results to electrochemical systems that obey equation 17.2. At the same time, electrochemical systems sometimes provide the most convenient experimental means of testing these results or of arriving at new results for systems too complex to analyze.

Essential to the understanding of convective-transport problems is the concept of the diffusion layer. Frequently, due to the small value of the diffusion coefficient, the concentrations differ significantly from their bulk values only in a thin region near the surface of an electrode. In this region, the velocity is small, and diffusion is of primary importance to the transport process. The thinness of this region permits a simplification in the analysis, but it is erroneous to treat the diffusion layer as a stagnant region. Figure 17.1 shows the concentration profile in the diffusion layer, with the electrode surface at the left. Far from the surface, convective transport dominates, while at the surface itself, there is only diffusion.

The systems typically studied in heat and mass transfer involve laminar and turbulent flow with various geometric arrangements. The flow may be due to some more or less well-characterized stirring (forced convection) or may be the result of density differences created in the solution as part of the transfer process (free convection). We discuss a few examples, although there is no need

Electrochemical Systems, Fourth Edition. John Newman and Nitash P. Balsara.

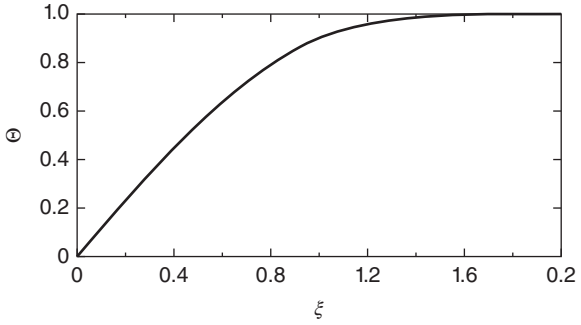

Figure 17.1 Concentration profile in the diffusion layer.

to be exhaustive since convective heat and mass transfer are thoroughly treated in many texts and monographs.[1–4] There are also several reviews of mass transfer in electrochemical systems.[5–7] The examples selected are primarily those that have been studied with electrochemical systems. In addition, certain theoretical results of general validity are included because they are particularly applicable to electrolytic solutions, where the Schmidt numbers are invariably large.

17.2 THE ROTATING DISK

Our first example of a convective-transport problem, the rotating-disk electrode, is well-known to electrochemists. Imagine a large, or infinite, disk rotating about its axis in an infinite fluid medium, so that wall and end effects may be ignored. Actually, these edge effects can be neglected for a suitable design of the disk. Thus, we consider the electrode shown in Figure 17.2, a disk electrode embedded in a larger insulating plane that also rotates. This system has been reviewed by Riddiford.[8]

The rotation of the disk provides the stirring of the fluid. The hydrodynamic aspects of the problem are presented in Section 15.4. The pertinent feature of those results is that the velocity normal to the disk, which brings fresh reactant to the surface, depends on z but not on r:

$$v_z = \sqrt{\nu\Omega}H\left(z\sqrt{\frac{\Omega}{\nu}}\right). \tag{17.3}$$

Consequently, there is no reason for the concentration to depend on anything besides the normal distance from the disk, and the equation of convective diffusion 17.2 reduces to

$$v_z\frac{dc_i}{dz} = D_i\frac{d^2c_i}{dz^2}, \tag{17.4}$$

with boundary conditions

$$c_i = c_0 \quad \text{at} \quad z = 0 \quad \text{and} \quad c_i = c_\infty \quad \text{at} \quad z = \infty. \tag{17.5}$$

At the limiting current, $c_0 = 0$. Thus, the fact that the convective velocity bringing fresh reactant to the electrode is the same over the entire surface of the disk has the mathematical advantage of reducing the equation of convective diffusion to an ordinary differential equation and the practical advantage that the reaction rate at the electrode will be everywhere the same, independent of the distance from the axis of rotation.

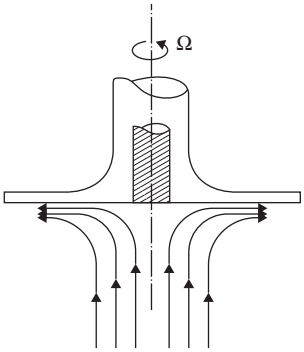

Figure 17.2 Rotating-disk electrode.

Levich[9] has analyzed the mass transfer to a rotating disk with the fluid motion described above. The analogous heat-transfer problem was not treated by Wagner[10] until 1948.

Equation 17.4 is a first-order differential equation for dc_i/dz and can be integrated to give

$$\ln \frac{dc_i}{dz} = \frac{1}{D_i} \int_0^z v_z dz + \ln K \tag{17.6}$$

or

$$\frac{dc_i}{dz} = K \exp\left(\frac{1}{D_i} \int_0^z v_z dz \right). \tag{17.7}$$

A second integration gives

$$c_i = c_0 + K \int_0^z \exp\left(\int_0^z \frac{v_z}{D_i} dz \right) dz. \tag{17.8}$$

The constant K is determined now from boundary condition 17.5:

$$\frac{c_\infty - c_0}{K} = \int_0^\infty \exp\left(\int_0^z \frac{v_z}{D_i} dz \right) dz$$

$$= \sqrt{\frac{\nu}{\Omega}} \int_0^\infty \exp\left[\mathrm{Sc} \int_0^\eta H(\zeta) d\zeta \right] d\eta, \tag{17.9}$$

where the last expression is obtained with the use of equation 17.3 and the definition of the Schmidt number $\mathrm{Sc} = \nu/D_i$. The solution thus can be expressed as

$$\Theta = \frac{\int_0^z \exp\left(\int_0^z \frac{v_z}{D_i} dz \right) dz}{\int_0^\infty \exp\left(\int_0^z \frac{v_z}{D_i} dz \right) dz}, \tag{17.10}$$

where

$$\Theta = \frac{c_i - c_0}{c_\infty - c_0} \tag{17.11}$$

is a dimensionless concentration.

The flux density from the disk surface is

$$N_{in} = -D_i \left.\frac{dc_i}{dz}\right|_{z=0} = -D_i K, \tag{17.12}$$

and by means of equation 16.8, the current density can be expressed as

$$\frac{i_n s_i}{nF(c_\infty - c_0)\sqrt{\nu\Omega}} = \frac{1}{\mathrm{Sc}}\Theta'(0), \tag{17.13}$$

where the prime denotes the derivative with respect to ζ and

$$\frac{1}{\mathrm{Sc}}\Theta'(0) = \frac{1}{\mathrm{Sc}\int_0^\infty \exp\left[\mathrm{Sc}\int_0^\eta H(\zeta)d\zeta\right]d\eta}. \tag{17.14}$$

The dimensionless mass-transfer rate in equation 17.14 is seen to depend only on the Schmidt number $\mathrm{Sc} = \nu/D_i$ and is plotted in Figure 17.3 (see Sparrow and Gregg[11]). If the mass flux or current density is known, then the ordinate is independent of the diffusion coefficient (see equation 17.13). Hence, this method of plotting is advantageous for the determination of diffusion coefficients by the rotating-disk method. From the limiting-current density, the ordinate can be calculated directly. The Schmidt number can then be obtained from the graph without a trial-and-error calculation, and the diffusion coefficient is then given by $D_i = \nu/\mathrm{Sc}$.

The asymptote for large Schmidt numbers was first derived by Levich in 1942. In this case, the diffusion coefficient D_i is very small, and the concentration variation occurs very close to the surface of the disk (at small values of ζ in Figure 15.2). Therefore, it is appropriate to use in equation 17.14, the first term of the velocity profile for small values of ζ as given in equation 15.29. The behavior for large Schmidt numbers is particularly important for diffusion in liquids since here the Schmidt number is on the order of 1000. Corrections to this asymptote can be obtained by expansion of the mass-transfer rate for large Schmidt numbers, with the result[12]

$$\frac{1}{\mathrm{Sc}}\Theta'(0) = \frac{0.62045\mathrm{Sc}^{-2/3}}{1 + 0.2980\mathrm{Sc}^{-1/3} + 0.14514\mathrm{Sc}^{-2/3} + O(\mathrm{Sc}^{-1})}. \tag{17.15}$$

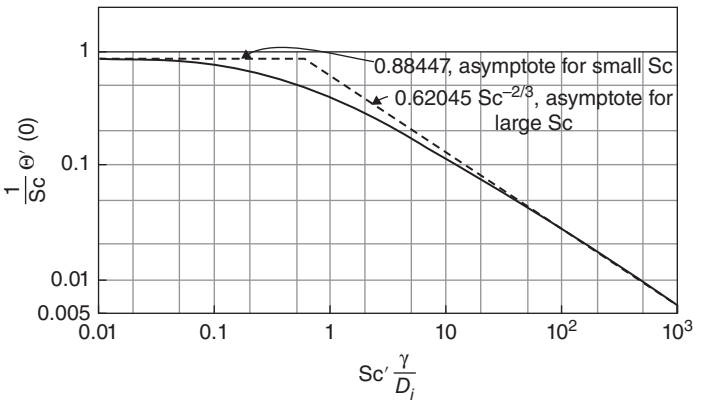

Figure 17.3 Dimensionless mass-transfer rates for a rotating disk. *Source*: Newman.[13] Copyright 1967. Reprinted with permission from John Wiley & Sons, Inc.

This expression adequately represents the curve in Figure 17.3 for $\mathrm{Sc} > 100$ (in this region, the maximum error is about 0.1%). See also Ref. [14].

On the other hand, for very low Schmidt numbers, the diffusion layer extends a large distance from the disk, and it is appropriate to use the velocity profile of equation 15.31. At very low Schmidt numbers, equation 17.14 becomes

$$\frac{1}{\mathrm{Sc}}\Theta'(0) = 0.88447e^{-1.611\mathrm{Sc}}[1 + 1.961\mathrm{Sc}^2 + O(\mathrm{Sc}^3)]. \tag{17.16}$$

The first term of equation 17.16 tells us that the maximum flux to the disk for very large diffusion coefficients is completely determined by the rate of convection of material from infinity:

$$N_{i\max} = -(c_\infty - c_0)\sqrt{\nu\Omega}H(\infty) = 0.88447(c_\infty - c_0)\sqrt{\nu\Omega}. \tag{17.17}$$

Because of the well-defined fluid motion, the rotating-disk electrode has been used extensively for the determination of diffusion coefficients and the parameters of electrode kinetics. It can also be used for quantitative analysis (polarography) in electrolytic solutions. The edge effect for the rotating disk is treated in Ref. [15].

The rotating ring–disk system is popular because active intermediates produced on the disk electrode can be detected with the ring electrode.[16, 17] The amount so detected can be compared with the theoretical collection efficiency[18, 19] for the system.

17.3 THE GRAETZ PROBLEM

An important problem that received early analytic treatment is that of mass transfer to the wall of a tube in which Poiseuille flow is presumed to prevail:

$$v_z = 2\langle v_z\rangle\left(1 - \frac{r^2}{R^2}\right), \tag{17.18}$$

$$v_r = v_\theta = 0. \tag{17.19}$$

Here r, θ, and z refer to cylindrical coordinates, with z measured along the tube and r being the radial distance from the center of the tube. Although the Reynolds number can attain values of 2000 before the flow becomes turbulent, this is not a boundary-layer flow.

The equation of convective diffusion is

$$v_z\frac{\partial c_i}{\partial z} = D_i\left[\frac{1}{r}\frac{\partial}{\partial r}\left(r\frac{\partial c_i}{\partial r}\right) + \frac{\partial^2 c_i}{\partial z^2}\right]. \tag{17.20}$$

We treat this for mass transfer to a section with a constant wall concentration,

$$c_i = c_0 \quad \text{at} \quad r = R, \tag{17.21}$$

beginning at $z = 0$ after the Poiseuille flow is fully developed. At the limiting current, $c_0 = 0$. For other boundary conditions, we may state

$$c_i = c_b \quad \text{at} \quad z = 0 \quad \text{and} \quad \frac{\partial c_i}{\partial r} = 0 \quad \text{at} \quad r = 0. \tag{17.22}$$

The inlet concentration is c_b, and symmetry dictates that the derivative should be zero at the center of the tube. The condition at $z = 0$ applies only after we have neglected axial diffusion when we reach equation 17.26.

Let us introduce dimensionless variables

$$\xi = \frac{r}{R}, \quad \Theta = \frac{c_i - c_0}{c_b - c_0}, \quad \zeta = \frac{zD_i}{2\langle v_z\rangle R^2}. \tag{17.23}$$

The equation of convective diffusion becomes

$$(1-\xi^2)\frac{\partial\Theta}{\partial\zeta} = \frac{1}{\xi}\frac{\partial}{\partial\xi}\left(\xi\frac{\partial\Theta}{\partial\xi}\right) + \frac{1}{\mathrm{Pe}^2}\frac{\partial^2\Theta}{\partial\zeta^2}, \tag{17.24}$$

where

$$\mathrm{Pe} = \mathrm{Re}\cdot\mathrm{Sc} = \frac{2R\langle v_z\rangle}{D_i} = \frac{2R\langle v_z\rangle}{\nu}\frac{\nu}{D_i} \tag{17.25}$$

is the Péclet number. On the assumption that the Péclet number is large, we discard the second derivative with respect to ζ:

$$\begin{gathered}(1-\xi^2)\frac{\partial\Theta}{\partial\zeta} = \frac{\partial^2\Theta}{\partial\xi^2} + \frac{1}{\xi}\frac{\partial\Theta}{\partial\xi},\\ \Theta = 1 \quad \text{at} \quad \zeta = 0\\ \Theta = 0 \quad \text{at} \quad \xi = 1\\ \frac{\partial\Theta}{\partial\xi} = 0 \quad \text{at} \quad \xi = 0.\end{gathered} \tag{17.26}$$

The total amount of material transferred to the wall in a length z is

$$J = -\int_0^z D_i\left.\frac{\partial c_i}{\partial r}\right|_{r=R} 2\pi R\, dz \tag{17.27}$$

or

$$\frac{J}{\pi R^2(c_b - c_0)\langle v_z\rangle} = 2\frac{\mathrm{Nu}_{\mathrm{avg}}}{\mathrm{Pe}}\frac{z}{R} = -4\int_0^\zeta \left.\frac{\partial\Theta}{\partial\xi}\right|_{\xi=1} d\zeta, \tag{17.28}$$

where $\mathrm{Nu}_{\mathrm{avg}}$ is the average Nusselt number based on the concentration difference at the inlet.

The Nusselt number is a dimensionless mass-transfer rate:

$$\mathrm{Nu} = -\frac{N_{in}2R}{D_i\Delta c_i}, \tag{17.29}$$

where the flux N_i is made dimensionless with a characteristic length, here $2R$, the diffusion coefficient D_i, and a concentration difference Δc_i, here equal to the value at the inlet, $c_b - c_0$. For the local Nusselt number, the local flux is used; for the average Nusselt number, the average flux is used. For convective-transport problems where the contribution of ionic migration is negligible, the flux is related to the concentration derivative at the wall. For a single electrode reaction following equation 16.7, equation 16.8 allows the local Nusselt number to be related to the current density:

$$\mathrm{Nu} = \frac{s_i 2R}{D_i\Delta c_i}\frac{i_n}{nF}. \tag{17.30}$$

Solution by Separation of Variables

Graetz,[20] followed by Nusselt,[21] treated this problem by the method of separation of variables:

$$\Theta = \sum_{k=1}^{\infty} C_k e^{-\lambda_k^2 \zeta} R_k(\xi), \tag{17.31}$$

in which the R_k satisfy the equation

$$\frac{1}{\xi}\frac{d}{d\xi}\left(\xi \frac{dR_k}{d\xi}\right) + \lambda_k^2(1-\xi^2)R_k = 0, \tag{17.32}$$

with the boundary conditions

$$\begin{gathered} R_k = 0 \quad \text{at} \quad \xi = 1. \\ R_k = 1, \quad \frac{dR_k}{d\xi} = 0 \quad \text{at} \quad \xi = 0. \end{gathered} \tag{17.33}$$

The solution of this Sturm–Liouville system has been calculated, and R_1, R_2 and R_3 are reproduced in Figure 17.4.

The total amount of material transferred to the wall can be calculated from the expression:

$$\begin{aligned} 1 - \frac{J}{\pi R^2 (c_b - c_0)\langle v_z \rangle} &= \sum_{k=1}^{\infty} 4C_k e^{-\lambda_k^2 \zeta} \int_0^1 \xi(1-\xi^2)R_k(\xi)\,d\xi \\ &= \sum_{k=1}^{\infty} M_k e^{-\lambda_k^2 \zeta}, \end{aligned} \tag{17.34}$$

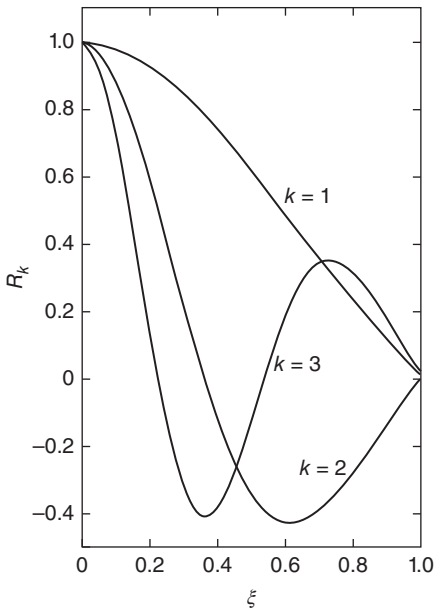

Figure 17.4 Graetz functions.

TABLE 17.1 Eigenvalues and coefficients for the Graetz series

k	λ_k	M_k
1	2.7043644	0.8190504
2	6.6790315	0.0975269
3	10.6733795	0.0325040
4	14.6710785	0.0154402
5	18.6698719	0.0087885
6	22.6691434	0.0055838
7	26.6686620	0.0038202
8	30.6683233	0.0027564
9	34.6680738	0.0020702
10	38.6678834	0.0016043

where the values of M_k and λ_k are given for 10 terms in Table 17.1 (see Brown[22]).

Solution for Very Short Distances

For small values of ζ, Lévêque[23] recognized that there is a diffusion layer near the wall, and derivatives with respect to ξ become large. Within the diffusion layer, the following approximations apply:

$$1 - \xi^2 = (1 - \xi)(1 + \xi) \approx 2(1 - \xi) \tag{17.35}$$

and

$$\frac{1}{\xi}\frac{\partial \Theta}{\partial \xi} \ll \frac{\partial^2 \Theta}{\partial \xi^2}, \tag{17.36}$$

and the diffusion equation becomes

$$2(1 - \xi)\frac{\partial \Theta}{\partial \zeta} = \frac{\partial^2 \Theta}{\partial \xi^2} \tag{17.37}$$

with boundary conditions

$$\Theta = 0 \quad \text{at} \quad \xi = 1 \quad \text{and} \quad \Theta = 1 \quad \text{at} \quad \zeta = 0. \tag{17.38}$$

In addition, Θ approaches 1 outside the diffusion layer.

The similarity transformation

$$\eta = (1 - \xi)(2/9\zeta)^{1/3} \tag{17.39}$$

reduces the diffusion equation to an ordinary differential equation

$$\Theta'' + 3\eta^2\Theta' = 0, \tag{17.40}$$

with the solution

$$\Theta = \frac{1}{\Gamma(4/3)}\int_0^{\eta} e^{-x^3}\,dx. \tag{17.41}$$

In terms of the physical variables, the similarity variable η is

$$\eta = y\left(\frac{4\langle v_z\rangle}{9zD_iR}\right)^{1/3}, \tag{17.42}$$

where

$$y = R - r \tag{17.43}$$

is the distance from the wall. The function given by equation 17.41 is plotted in Figure 17.1, where η is rendered as ξ on the abscissa.

The total amount of material transferred to the wall is given by

$$\frac{J}{\pi R^2(c_b - c_0)\langle v_z\rangle} = \frac{(48)^{1/3}}{\Gamma(4/3)}\zeta^{2/3} = 4.070\zeta^{2/3}. \tag{17.44}$$

This result shows more clearly than the Graetz series how the mass-transfer rate becomes infinite near the beginning of the mass-transfer section.

Extension of the Lévêque Solution

With an approximate solution for short distances, it should be possible[24] to obtain correction terms that account for approximations 17.35 and 17.36 and justify their validity. On this basis, the average Nusselt number referred to the concentration difference at the inlet can be expressed as

$$\begin{aligned}\mathrm{Nu}_{\mathrm{avg}} = 1.6151&\left(\frac{\mathrm{ScRe}}{z/2R}\right)^{1/3} - 1.2 \\ &- 0.28057\left(\frac{z/2R}{\mathrm{ScRe}}\right)^{1/3} + O\left(\frac{z/2R}{\mathrm{ScRe}}\right)^{2/3},\end{aligned} \tag{17.45}$$

and the local Nusselt number is

$$\begin{aligned}\mathrm{Nu}(\zeta) &= -2\left.\frac{\partial\Theta}{\partial\xi}\right|_{\xi=1} \\ &= 1.3566\zeta^{-1/3} - 1.2 - 0.296919\zeta^{1/3} + O(\zeta^{2/3}).\end{aligned} \tag{17.46}$$

In contrast to the Graetz series, the Lévêque series cannot be expected to converge for all values of z. It is useful for small values of z.

Figure 17.5 shows the local Nusselt number, divided by the first term of the Lévêque series so that this ratio approaches one as ζ approaches zero. The dashed lines indicate how well the Lévêque series approximates the exact solution. The dimensionless cup-mixing concentration difference Θ_m, related to the average Nusselt number by

$$\Theta_m = 1 - 2\frac{\mathrm{Nu}_{\mathrm{avg}}}{\mathrm{Pe}}\frac{z}{R}, \tag{17.47}$$

is also shown.

It is occasionally stated that the Lévêque solution should be good for $\zeta < 0.01$. At this value of ζ, where 16% of the possible mass transfer has already occurred, the Lévêque solution predicts an average rate of mass transfer that is too high by 15.4%, while the three-term Lévêque series is accurate to 0.1%.

For a more detailed discussion of the Graetz problem, see Ref. [25].

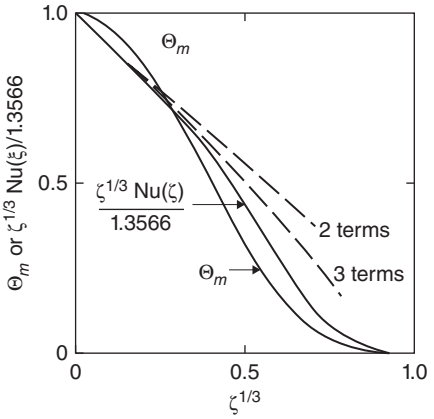

Figure 17.5 Dimensionless cup-mixing concentration difference Θ_m and the local Nusselt number (divided by Lévêque's solution). For comparison with the latter, the corresponding form of the Lévêque series is shown for two and three terms.

17.4 THE ANNULUS

Axial flow in the annular space between two concentric cylinders provides a convenient situation for experimental studies of mass transfer. In the work of Lin et al.,[26] the electrode of interest formed part of the inner cylinder, and the outer cylinder formed the counterelectrode. However, their experimental results and theoretical treatment have been severely criticized by Friend and Metzner.[27] Ross and Wragg[28] reviewed the problem and performed additional experiments with a similar arrangement. A circular tube with no inner cylinder is a limiting case of the annular geometry and has been studied by Van Shaw et al.[29] The theoretical treatment of this geometry in laminar flow constitutes the Graetz problem (see Section 17.3). Another limiting case investigated by Tobias and Hickman[30] is the flow between two plane electrodes.

Let the radius of the outer cylinder be R, and the radius of the inner cylinder be κR. The electrode of interest is of length L and is located far enough downstream in the annulus that the velocity distribution is fully developed before this electrode is reached. A limiting current is reached at this electrode when the concentration of the reactant drops to zero over the entire surface.

For laminar flow in the annulus, the local, limiting current density should follow the theoretical expression

$$i_n = 0.8546 \frac{nFD_i c_\infty}{s_i} \left[\frac{\langle v \rangle \phi}{(1-\kappa) R D_i x} \right]^{1/3}, \tag{17.48}$$

where c_∞ is the bulk concentration, $\langle v \rangle$ is the average velocity in the annulus, x is the distance from the upstream edge of the electrode, and $\phi^{1/3}$ is a function of the geometric parameter κ and is shown in Figure 17.6 for both the inner and the outer electrode.[27, 28]

Mass transfer in laminar flow in annuli is very similar to the classical Graetz problem, discussed in Section 17.3. Equation 17.48 is analogous to the Lévêque solution, being useful for electrode lengths such that $L/2R \ll \mathrm{Sc} \cdot \mathrm{Re}$. Frequently, this covers the entire range of interest, particularly for electrolytic solutions where the Schmidt number is large. It is straightforward to apply the method of Lévêque to mass transfer in annular spaces by using the velocity derivative at the walls of the annulus instead of

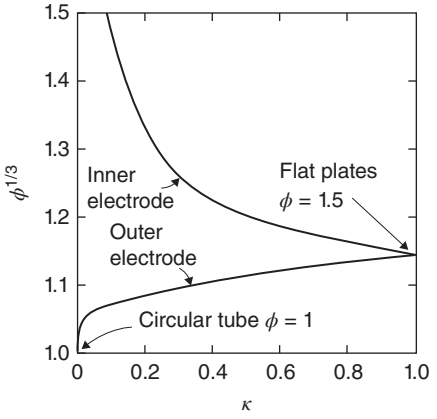

Figure 17.6 Coefficient for mass transfer in annuli.

that for the tube. Thus,

$$\phi_0 = \frac{1-\kappa}{2}\frac{1-\kappa^2-2\ln(1/\kappa)}{1-\kappa^2-(1+\kappa^2)\ln(1/\kappa)} \tag{17.49}$$

for the outer electrode, and

$$\phi_i = \frac{\kappa-1}{2\kappa}\frac{1-\kappa^2-2\kappa^2\ln(1/\kappa)}{1-\kappa^2-(1+\kappa^2)\ln(1/\kappa)} \tag{17.50}$$

for the inner electrode (see also Problem 17.1).

It might be estimated[28] that equation 17.48 is valid for

$$x < 0.005\mathrm{ReSc}d_e, \tag{17.51}$$

where $d_e = 2(1-\kappa)R$ is the equivalent diameter of the annulus, $\mathrm{Re} = d_e\langle v\rangle/\nu$ is the Reynolds number, and $\mathrm{Sc} = \nu/D_i$ is the Schmidt number (see the remark below equation 17.47). For Sc = 2000 and Re = 500, this condition yields

$$x < 5000d_e, \tag{17.52}$$

and is usually satisfied in experiments.

To facilitate comparison of results for different systems and with the standard correlations of heat and mass transfer, equation 17.48 is frequently written in dimensionless form:

$$\mathrm{Nu}(x) = 1.0767\left(\frac{\phi\mathrm{ReSc}d_e}{x}\right)^{1/3}, \tag{17.53}$$

where the Nusselt number is a dimensionless mass-transfer rate:

$$\mathrm{Nu}(x) = -\frac{N_i d_e}{c_\infty D_i}. \tag{17.54}$$

The average value of the Nusselt number, corresponding to the average mass-transfer rate over the length L, is

$$\mathrm{Nu}_{\mathrm{avg}} = 1.6151\left(\frac{\phi\mathrm{ReSc}d_e}{L}\right)^{1/3}. \tag{17.55}$$

As $\kappa \to 1$, these results apply to the flow between two flat plates, parts of which form plane electrodes. Then $\phi = 1.5$, and equations 17.48, 17.53, and 17.55 become

$$i_n = 0.9783 \frac{nFD_i c_\infty}{s_i} \left(\frac{\langle v \rangle}{hD_i x} \right)^{1/3}, \tag{17.56}$$

where $h = (1 - \kappa)R$ is the distance between the planes,

$$\mathrm{Nu}(x) = 1.2325 \left(\frac{\mathrm{ReSc}d_e}{x} \right)^{1/3}, \tag{17.57}$$

$$\mathrm{Nu}_{\mathrm{avg}} = 1.8488 \left(\frac{\mathrm{ReSc}d_e}{L} \right)^{1/3}. \tag{17.58}$$

In Figure 17.7, the curve denoted *limited by convection and diffusion* depicts the local current density as a function of position along the electrode. The geometric arrangement, the electrodes, and the diffusion layer near the cathode are shown in Figure 17.8. The mass-transfer rate is infinite at the upstream edge of the electrode where fresh solution is brought in contact with the electrode. The current decreases with increasing x, since the solution in the diffusion layer has already been depleted by the electrode reaction farther upstream. Later, it will be instructive to compare this current distribution with that which would be obtained when the ohmic potential drop in the solution is controlling.

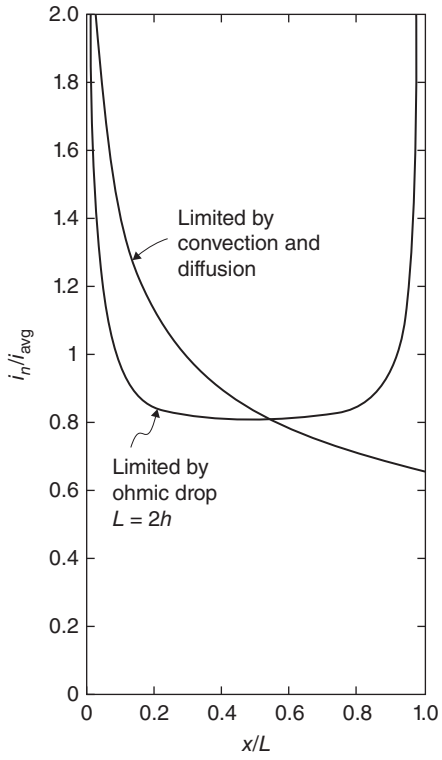

Figure 17.7 Current distribution on planar electrodes.

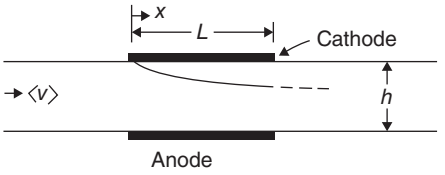

Figure 17.8 Plane electrodes in the walls of a flow channel.

The results of Lin et al. [26] for laminar flow fall roughly 17% below the values predicted by equation 17.55. Part of this discrepancy can be attributed to the fact that some of the diffusion coefficients were determined by fitting the experimental results to an erroneous equation. Ross and Wragg's[28] laminar results are 9 to 13% below those predicted, while those of Tobias and Hickman[30] scatter within 7% of the values predicted by equation 17.58.

Turbulent flow is characterized by rapid and apparently random fluctuations of the velocity and pressure about their average values. The turbulence is greater at a distance from solid walls, and the fluctuations gradually go to zero as the wall is approached. The fluctuations in velocity result in fluctuations in concentration and also in enhanced rates of mass transfer. Near the wall the fluctuations go to zero, and mass transfer at the wall is by diffusion. The details of the nature of the fluctuations are important in the region near the wall where diffusion and turbulent transport contribute roughly equally to the mass-transfer rate.

In the mass-transfer entry region in turbulent flow, Van Shaw et al. [29] expect the average Nusselt number in circular tubes to be given by

$$\mathrm{Nu}_{\mathrm{avg}} = 0.276\mathrm{Re}^{0.58}\mathrm{Sc}^{1/3}\left(\frac{d_e}{L}\right)^{1/3}. \tag{17.59}$$

The experimental results fall 7% below these values but exhibit the same dependence upon the Reynolds number and the electrode length. The data of Ross and Wragg[28] for the inner cylinder of an annulus with $\kappa = 0.5$ are correlated by equation 17.59. However, in this geometry, those authors expect the coefficient to be 9% higher.

The mass-transfer entry region where equation 17.59 applies is much shorter in turbulent flow than in laminar flow. The results of Van Shaw et al. [29] indicate that this length ranges from 2 diameters to 0.5 diameter as the Reynolds number ranges from 5000 to 75,000.

Beyond this short entry region, the Nusselt number rapidly approaches a constant value, corresponding to fully developed mass transfer. It is surprising that fully developed mass transfer has not been studied more extensively with electrochemical systems. The results of Lin et al.[26] agree well with the equation of Chilton and Colburn[31] for heat transfer:

$$\mathrm{Nu}_{\mathrm{avg}} = 0.023\mathrm{Re}^{0.8}\mathrm{Sc}^{1/3}. \tag{17.60}$$

Friend and Metzner[27] discuss critically the applicability of such an equation for Schmidt numbers as large as those encountered in electrochemical systems. However, Hubbard and Lightfoot[32] also obtained agreement with this equation. The concentration difference Δc_i (see equation 17.29 or 17.30) used for this average Nusselt number is the logarithmic average rather than the value at the inlet.

17.5 TWO-DIMENSIONAL DIFFUSION LAYERS IN LAMINAR FORCED CONVECTION

In 1942, Levich,[9] in treating electrolytic mass transfer to a rotating disk, remarked that in the case of diffusion, particularly the diffusion of ions, the Schmidt number reaches the value of several thousands. "Thus, in this case we deal with a peculiar limiting case of hydrodynamics, which may be called the hydrodynamics of Prandtl's (or Schmidt's) large numbers." Lighthill[33] developed a solution for the heat-transfer rate applicable when the region of temperature variation is thin compared to the region of velocity variation. Acrivos[34] realized that this method is applicable to a wide range of problems when the Schmidt number is large. Thus, for electrochemical systems where the Schmidt number is generally large, it is frequently possible to obtain the concentration distribution and the rate of mass transfer for steady problems when the velocity distribution near the electrode is known in advance. Many results for electrolytic mass transfer can be regarded as special cases of the application of this method.

The concentration distribution in a thin diffusion layer near an electrode is governed by the equation

$$v_x \frac{\partial c_i}{\partial x} + v_y \frac{\partial c_i}{\partial y} = D_i \frac{\partial^2 c_i}{\partial y^2}. \tag{17.61}$$

This equation applies to two-dimensional flow past an electrode, with x measured along the electrode from its upstream end and y measured perpendicularly from the surface into the solution.

Due to the thinness of the diffusion layer compared to the region of variation of the velocity, it is permissible to approximate the velocity components by their first terms in Taylor's expansions in the distance y from the wall:

$$v_x = y\beta(x) \quad \text{and} \quad v_y = -\frac{1}{2}y^2\beta'(x), \tag{17.62}$$

where $\beta(x)$ is the velocity derivative $\partial v_x/\partial y$ evaluated at the wall ($y = 0$). These expressions for the velocity, thus, satisfy the applicable form of equation 16.6:

$$\frac{\partial v_x}{\partial x} + \frac{\partial v_y}{\partial y} = 0, \tag{17.63}$$

as well as the boundary conditions $v_x = v_y = 0$ at $y = 0$. With this approximation, equation 17.61 becomes

$$y\beta \frac{\partial c_i}{\partial x} - \frac{1}{2}y^2\beta' \frac{\partial c_i}{\partial y} = D_i \frac{\partial^2 c_i}{\partial y^2}. \tag{17.64}$$

If the concentration at the surface is a constant c_0, then the concentration profiles at different values of x are similar and depend only on the combined variable

$$\xi = \frac{y\sqrt{\beta}}{\left(9D_i \int_0^x \sqrt{\beta}dx\right)^{1/3}}. \tag{17.65}$$

In terms of this similarity variable, the concentration profile is given by

$$\Theta = \frac{c_i - c_0}{c_\infty - c_0} = \frac{1}{\Gamma(4/3)} \int_0^\xi e^{-x^3} dx, \tag{17.66}$$

where $\Gamma(4/3) = 0.89298$. This function is plotted in Figure 17.1 and has been tabulated.[35]

The limiting current density (for $c_0 = 0$) is thus

$$i_n = \frac{nFD_i c_\infty \sqrt{\beta}/s_i \Gamma(4/3)}{\left(9D_i \int_0^x \sqrt{\beta} dx\right)^{1/3}}. \tag{17.67}$$

Equation 17.56 for flow between two plates is a special case of equation 17.67 for which β is independent of x and has the value $6\langle v\rangle/h$. Equation 17.67 gives the rate of mass transfer if β is already known.

17.6 AXISYMMETRIC DIFFUSION LAYERS IN LAMINAR FORCED CONVECTION

Equation 17.61 also applies to steady mass transfer in axisymmetric diffusion layers, that is, where the electrode forms part of a body of revolution. Examples would be the annulus and the disk electrode considered earlier and a sphere. The coordinates x and y have the same meaning; x is measured along the electrode from its upstream end, and y is measured perpendicularly from the surface into the solution. It is also necessary to specify the normal distance $\mathcal{R}(x)$ of the surface from the axis of symmetry. An axisymmetric body is sketched in Figure 17.9.

The applicable form of equation 16.6 now is[36]

$$\frac{\partial(\mathcal{R}v_x)}{\partial x} + \mathcal{R}\frac{\partial v_y}{\partial y} = 0. \tag{17.68}$$

Due to the thinness of the diffusion layer, it is still permissible to approximate the velocity components by their first terms in Taylor's expansions in y. However, in view of equation 17.68, these now take the form

$$v_x = y\beta(x) \quad \text{and} \quad v_y = -\frac{1}{2}y^2\frac{(\mathcal{R}\beta)'}{\mathcal{R}}, \tag{17.69}$$

and equation 17.61 becomes

$$y\beta\frac{\partial c_i}{\partial x} - \frac{1}{2}y^2\frac{(\mathcal{R}\beta)'}{\mathcal{R}}\frac{\partial c_i}{\partial y} = D_i\frac{\partial^2 c_i}{\partial y^2}. \tag{17.70}$$

The concentration profile is again given by equation 17.66, now in terms of the similarity variable

$$\xi = \frac{y\sqrt{\mathcal{R}\beta}}{\left(9D_i \int_0^x \sqrt{\mathcal{R}\beta} dx\right)^{1/3}}, \tag{17.71}$$

and the limiting current density is

$$i_n = \frac{\frac{nFD_i c_\infty \sqrt{\mathcal{R}\beta}}{s_i \Gamma(4/3)}}{\left(9D_i \int_0^x \mathcal{R}\sqrt{\mathcal{R}\beta}\, dx\right)^{1/3}}. \tag{17.72}$$

The Lévêque solution for a pipe in Section 17.3 is an example of the application of this similarity transformation, and equation 17.48 for the annulus is a special case of equation 17.72 in which $\mathcal{R}$ and β are independent of x and β is equal to $4\langle v\rangle\phi/(1-\kappa)R$. For the rotating disk in Section 17.2, $\mathcal{R} = r = x$,

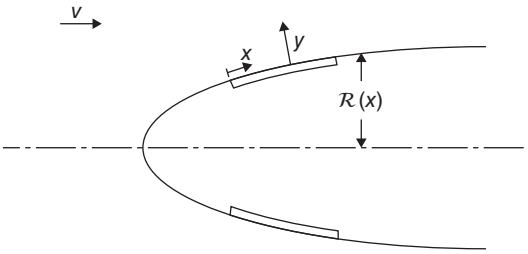

Figure 17.9 Electrode on an axisymmetric body with axisymmetric flow.

and the value of the velocity derivative at the surface is (see equation 15.29 and the first of equations 15.26)

$$\beta = a\Omega x\sqrt{\frac{\Omega}{\nu}}. \tag{17.73}$$

Substitution into equation 17.72 yields

$$i_n = 0.62045\frac{nFc_\infty}{s_i}\sqrt{\Omega\nu}\left(\frac{D_i}{\nu}\right)^{2/3}, \tag{17.74}$$

which is seen to be the high-Schmidt-number limit obtained from Figure 17.3 or equation 17.15.

17.7 A FLAT PLATE IN A FREE STREAM

The steady, laminar hydrodynamic flow parallel to a flat plate, beginning at $x = 0$ and extending along the positive x axis, has been treated extensively. The value of the velocity derivative at the surface is[37]

$$\beta = 0.33206v_\infty\sqrt{\frac{v_\infty}{\nu x}}, \tag{17.75}$$

where v_∞ is the value of v_x far from the plate. Substitution into equation 17.67 yields

$$i_n = 0.3387\frac{nFD_ic_\infty}{s_i}\left(\frac{v_\infty}{\nu x}\right)^{1/2}\left(\frac{\nu}{D_i}\right)^{1/3}. \tag{17.76}$$

The average Nusselt number for an electrode of length L is

$$\mathrm{Nu}_{\mathrm{avg}} = \frac{s_iLi_{\mathrm{avg}}}{nFD_ic_\infty} = 0.6774\mathrm{Re}_L^{1/2}\mathrm{Sc}^{1/3}, \tag{17.77}$$

where $\mathrm{Re}_L = Lv_\infty/\nu$. These results apply for laminar flow. The flow becomes turbulent at a Reynolds number of about 10^5.

Electrochemical systems for which these results are directly applicable are not frequently encountered. Unfortunately, the analysis for a flat plate in a free stream has been applied to annular geometries and the flow between two flat plates,[38–40] which should follow equations 17.48 and 17.56.

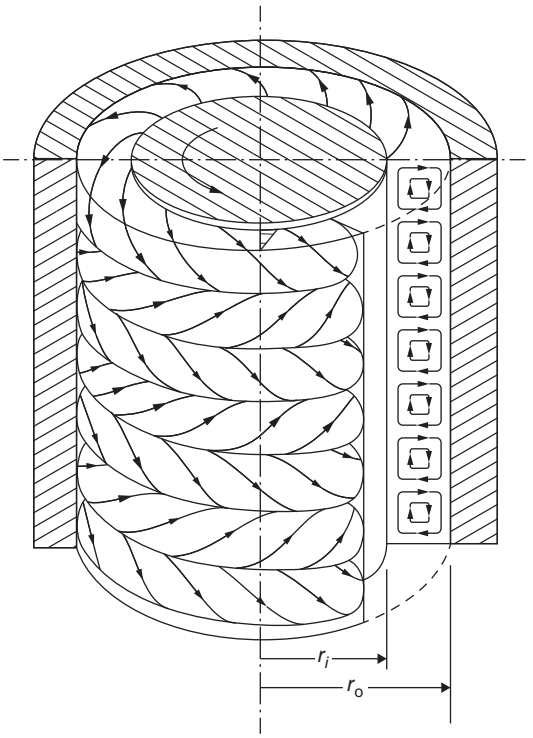

Figure 17.10 Sketch of Taylor vortices. *Source*: After H. Schlichting,[41] with permission of McGraw-Hill Book Company.

17.8 ROTATING CYLINDERS

Mass transfer between concentric cylinders, the inner of which is rotating with an angular speed Ω, has been studied by Eisenberg et al.[42] and by Arvia and Carrozza.[43] If the flow between the electrodes is tangential and laminar, it does not contribute to the rate of mass transfer since the flow velocity is perpendicular to the mass flux. At higher rotation speeds, the flow is still laminar but no longer tangential, and so-called *Taylor vortices* are formed. Superimposed on the tangential motion is a radial and axial motion, outward at one point and inward at a different axial position (see Figures 17.10 and 17.11). At still higher rotation speeds, the flow becomes turbulent. Mass transfer in this turbulent flow, which is achieved at lower rotation speeds if the inner cylinder rotates rather than the outer, has been studied and is reported in the above-mentioned works.

By the nature of the geometric arrangement, the current distribution is uniform. The results have been correlated by the equation

$$i_n = 0.0791 \frac{nFD_i c_\infty}{s_i d_R} \left(\frac{\Omega d_R^3}{2\nu d_L} \right)^{0.70} \left(\frac{\nu}{D_i} \right)^{0.356}, \tag{17.78}$$

or, in dimensionless form,

$$\mathrm{Nu} = 0.0791 \left(\frac{\mathrm{Re}\, d_R}{d_L} \right)^{0.70} \mathrm{Sc}^{0.356}, \tag{17.79}$$

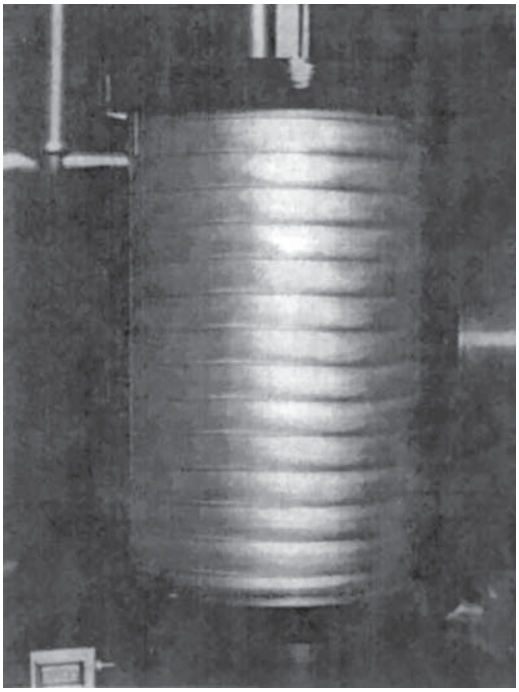

Figure 17.11 Photograph of Taylor vortices at a Reynolds number of 143 with $r_0/r_i = 1.144$. *Source*: From Donald Coles,[44] with permission of the author and of Cambridge University Press.

where d_R is the diameter of the inner, rotating cylinder, d_L is the diameter of the cylinder with the limiting current, $\mathrm{Nu} = i_n s_i d_R / nFD_i c_\infty$ is the Nusselt number, and $\mathrm{Re} = \Omega d_R^2 / 2\nu$ is the Reynolds number.

In the work of Eisenberg et al.,[42] the limiting electrode was the inner, rotating electrode, and $d_R = d_L$. The results, for which the Reynolds number ranged from 112 to 162,000 and the Schmidt number from 2230 to 3650, agree with equations 17.78 and 17.79 within 8.3%. Arvia and Carrozza[43] measured the limiting rates of mass transfer at the stationary, outer electrode.

Rotating cylinders were chosen to illustrate the behavior of electrochemical systems in Chapter 1.

The behavior of the interface, particularly the electrode kinetics, is important in determining the behavior of an electrochemical system. In selecting a system for the study of electrode kinetics, care should be used to avoid complications not essential to the electrode kinetics.

The rotating-disk electrode has been popular for the study of moderately fast electrode reactions because the hydrodynamic flow is well defined, concentration variations can be calculated, and the surface is uniformly accessible from the standpoint of diffusion and convection (see Sections 15.4 and 17.2). However, it should be realized that the primary current distribution is not uniform; and this problem becomes more serious for faster reactions, larger current densities, and larger disks (see Sections 18.2 and 18.3 and Chapter 21).

Perhaps more attention should be devoted to the possibility of using rotating cylindrical electrodes. Here, both the primary and mass-transfer-limited current distributions are uniform on the electrodes, and both the ohmic potential drop and the concentration change at the electrodes can be accurately calculated even though the flow is turbulent. It might be more difficult to maintain cleanliness in such a system than with a rotating-disk electrode.

Another way to avoid concentration variations in studies of the kinetics of moderately fast electrode reactions is to use a step change in current and follow the change in electrode potential in the time before the concentration can change significantly. For studies of the electrodeposition of copper by this method, Mattsson and Bockris[45] used small spherical electrodes, where the primary current distribution should be uniform and the ohmic potential drop can be calculated. Current-step methods should not be used if the primary current distribution is not uniform.

17.9 GROWING MERCURY DROPS

The limiting diffusion current to a dropping mercury electrode finds important applications in the quantitative analysis of electrolytic solutions. Let the mercury flow at a constant rate from the capillary tube to the drop growing at the tip, so that the radius increases as

$$r_0 = \gamma t^{1/3}. \tag{17.80}$$

The diffusion layer on the drop has a thickness proportional to $\sqrt{t}$. Ilkovič[46, 47] and also Mac Gillavry and Rideal[48] treated the problem with the assumption that the diffusion layer is thin compared to the radius of the drop.

For radial growth of the drop, without tangential surface motion, the limiting-current density is

$$i_n = \frac{nFc_\infty}{s_i}\left(\frac{7D_i}{3\pi t}\right)^{1/2}\left(1 + 1.0302\frac{D_i^{1/2}t^{1/6}}{\gamma}\right). \tag{17.81}$$

This equation, without the correction term, was first derived by Ilkovič. The correction term, which accounts for the greater thickness of the diffusion layer and for which at least three different values of the coefficient can be found in the literature, was first derived correctly by Koutecký.[49] We have carried this slightly further[50] to express the coefficient in terms of gamma functions:

$$1.0302 = \frac{16}{11}\left(\frac{3}{7}\right)^{1/2}\frac{\Gamma(15/14)}{\Gamma(11/7)}. \tag{17.82}$$

The total current to the drop, averaged over the lifetime T of the drop, then takes the form

$$I_{\text{avg}} = 3.5723\frac{nFc_\infty}{s_i}D_i^{1/2}m^{2/3}T^{1/6}\left[1 + 1.4530\left(\frac{D_i^3T}{m^2}\right)^{1/6}\right], \tag{17.83}$$

where m is the volumetric flow rate of the mercury (cm^3/s).

Since, in the absence of tangential surface motion, the convective flow is well defined, the dropping mercury electrode has frequently been used for the determination of diffusion coefficients.

17.10 FREE CONVECTION

Free convection is a hydrodynamic flow that results from density variations in the solutions produced, in the cases of interest here, by concentration variations near the electrode. Free convection at a vertical plate electrode has been studied extensively. For deposition of a metal, the solution density is lower near the electrode than in the bulk, and an upward flow near the electrode occurs. This upward flow

provides convective transport of the reactant to the electrode diffusion layer. Ibl[51] has reviewed the experimental work on this problem and reports the limiting current density to an electrode of length L.

$$i_{\text{avg}} = 0.66 \frac{nFD_i c_\infty}{s_i} \left[\frac{g(\rho_\infty - \rho_0)}{\rho_\infty D_i \upsilon L} \right]^{1/4} \tag{17.84}$$

or

$$\text{Nu}_{\text{avg}} = \frac{s_i L i_{\text{avg}}}{nFD_i c_\infty} = 0.66(\text{ScGr})^{1/4}, \tag{17.85}$$

where

$$\text{Gr} = \frac{g(\rho_\infty - \rho_0)L^3}{\rho_\infty \nu^2} \tag{17.86}$$

is the Grashof number. These results apply to values of ScGr between 10^4 and 10^{12}.

The problem of free convection in a binary solution for a vertical plate has been treated theoretically. The coefficient in equation 17.85 is expressed as a function of the Schmidt number in Table 17.2. Since the Schmidt number for electrolytic solutions is on the order of 1000, the agreement with equation 17.85 is good.

Free convection in solutions with an excess of supporting electrolyte is complicated by the fact that the concentration of the supporting electrolyte also varies in the diffusion layer and, therefore, contributes to the variation of the density. Approximate methods of estimating the interfacial density difference in the Grashof number consequently have been introduced, a popular method being that of Wilke et al.[52] This subject is considered further in Section 19.6.

For turbulent natural convection at a vertical plate, Fouad and Ibl[53] obtained the relation

$$\text{Nu}_{\text{avg}} = 0.31(\text{ScGr})^{0.28}, \tag{17.87}$$

applicable in the range $4 \times 10^{13} < \text{ScGr} < 10^{15}$.

Schütz[54] investigated experimentally free-convection mass transfer to spheres and horizontal cylinders and obtained for the average Nusselt number for spheres

$$\text{Nu}_{\text{avg}} = 2 + 0.59(\text{ScGr})^{1/4} \tag{17.88}$$

in the range $2 \times 10^8 < \text{ScGr} < 2 \times 10^{10}$ and for cylinders

$$\text{Nu}_{\text{avg}} = 0.53(\text{ScGr})^{1/4} \tag{17.89}$$

TABLE 17.2 Coefficient C expressing the rate of mass transfer for free convection at a vertical plate from a binary fluid with a uniform density difference between the vertical surface and the bulk solution

Sc	C	Sc	C	Sc	C
0.003	0.1816	0.72	0.5165	10	0.6200
0.01	0.2421	0.733	0.5176	100	0.6532
0.03	0.3049	1	0.5347	1000	0.6649
				∞	0.670327

Source: Refs. [55–57].

for $\mathrm{ScGr} < 10^9$. In forming these dimensionless groups, $L = d$, the diameter of the sphere or cylinder. Schütz also measured local Nusselt numbers using a sectioned-electrode technique.

Acrivos[58] has obtained a solution of the laminar free-convection boundary-layer equations for arbitrary two-dimensional and axisymmetric surfaces in the asymptotic limit $\mathrm{Sc} \to \infty$. These results should be of some interest here since the Schmidt number is large for electrolytic solutions. The local limiting current density for two-dimensional surfaces is predicted to be

$$i_n = 0.5029 \frac{nFD_i c_\infty}{s_i} \left[\frac{g(\rho_\infty - \rho_0)}{\rho_\infty D_i \nu} \right]^{1/4} \frac{(\sin \epsilon)^{1/3}}{\left[\int_0^x (\sin \epsilon^{1/3} dx) \right]^{1/4}}, \tag{17.90}$$

and the average limiting current density from $x = 0$ to $x = L$ is

$$i_{\mathrm{avg}} = 0.6705 \frac{nFD_i c_\infty}{L s_i} (\mathrm{ScGr})^{1/4} \left[\frac{1}{L} \int_0^L (\sin \epsilon)^{1/3} dx \right]^{3/4}, \tag{17.91}$$

where $\epsilon(x)$ is the angle between the normal to the surface and the vertical. For a vertical electrode, $\sin \epsilon = 1$, and the coefficient 0.6705 of equation 17.91 can be compared directly with the experimental coefficient of equation 17.84 (or with the theoretical value 0.670327 in Table 17.2).

For an axisymmetric surface, where $\mathcal{R}(x)$ is again the distance of the surface from the axis of symmetry, the local limiting current density is

$$i_n = 0.5029 \frac{nFD_i c_\infty}{s_i} \left[\frac{g(\rho_\infty - \rho_0)}{\rho_\infty D_i \nu} \right]^{1/4} \frac{(\mathcal{R} \sin \epsilon)^{1/3}}{\left[\int_0^x (\mathcal{R}^4 \sin \epsilon)^{1/3} dx \right]^{1/4}}. \tag{17.92}$$

The axis of symmetry should coincide with the direction of the gravitational acceleration in order to assure an axisymmetric velocity distribution.

From the results of Acrivos, the predicted coefficients of $(\mathrm{ScGr})^{1/4}$, in the expressions for the average Nusselt number for the sphere and the horizontal cylinder, are 0.58 and 0.50, respectively, which can be compared with the experimental coefficients in equations 17.88 and 17.89.

Free convection at a horizontal plate is essentially different from that discussed above since there is no chance for a laminar boundary layer to form and sweep fresh solution past the plate. At a horizontal electrode with a small density gradient, the solution at first remains stratified. With a higher density difference, a cellular flow pattern results; and for still higher density differences, the flow is turbulent. In the turbulent region, Fenech and Tobias[59] proposed the relation

$$i_n = 0.19 \frac{nFD_i c_\infty}{s_i} \left[\frac{g(\rho_\infty - \rho_0)}{\rho_\infty \nu D_i} \right]^{1/3}, \tag{17.93}$$

for electrodes with a minimum dimension greater than 2 cm.

17.11 COMBINED FREE AND FORCED CONVECTION

When there is the possibility of effects of free convection superimposed on forced convection, the situation becomes essentially more complicated. Fortunately, it appears that one effect or the other predominates in the mass-transfer process, depending upon the values of the Reynolds and Grashof

numbers. At horizontal electrodes, Tobias and Hickman[30] found that free convection predominates and the average rate of mass transfer is given by equation 17.93 if

$$\frac{Ld_e g(\rho_\infty - \rho_0)}{\langle v \rangle \nu \rho_\infty} > 923, \tag{17.94}$$

where L is the electrode length and d_e is the equivalent diameter of the channel. Otherwise, forced convection predominates, and the average rate of mass transfer is given by equation 17.58. These results apply to laminar flow ($\mathrm{Re} < 2100$). For turbulent flow, Tobias and Hickman found that forced convection predominates.

Acrivos[60] has analyzed the combined effect of free and forced convection for surfaces that are not horizontal and also found that the transition region between predominance of free convection and predominance of forced convection is usually narrow.

The rule to follow is to calculate the mass-transfer rate separately for free convection and again for forced convection and to assume that the higher value applies.

17.12 LIMITATIONS OF SURFACE REACTIONS

The work described above is restricted to processes at the limiting current where the concentration of the reactant at the surface has a constant value of zero. Most industrial processes are operated below the limiting current, and the kinetics of the surface reaction then influences the distribution of current. In this chapter on convective-transport problems, the ohmic potential drop is not considered. Thus, we must assume here that the ohmic potential drop is either negligible or constant for all parts of the electrode in question. The sum of the surface overpotential and the concentration overpotential is then constant, and the current distribution is determined by a balance of these overpotentials. The concentration and the current density at the surface vary with position on the electrode and must adjust themselves so that the total overpotential is constant. The more general problem involving the ohmic potential drop is discussed in Chapter 21.

Under these conditions, the reaction rate at the electrode can be expressed in terms of the concentration at the surface, and the problem is similar to nonelectrolytic catalytic problems.[61–64] The convective-transport problem can then be reduced to an integral equation relating the reaction rate to an integral over the surface concentration at points upstream in the diffusion layer. Other, approximate methods have also been developed for calculating the surface concentration and reaction rate as a function of position on the electrode. These methods, including the integral-equation method, should also provide a useful starting point for attacking the more general problem involving the ohmic potential drop.

On the basis of the Lighthill transformation (see Sections 17.5 and 17.6), one can express[19] the flux to the surface in terms of the (unknown) surface concentration

$$\left.\frac{\partial c_i}{\partial y}\right|_{y=0} = -\frac{\sqrt{\mathcal{R}\beta}}{\Gamma(4/3)} \int_0^x \left.\frac{dc_0}{dx}\right|_{x=x_0} \frac{dx_0}{\left(9D_i \int_{x_0}^x \mathcal{R}\sqrt{\mathcal{R}\beta}\, dx\right)^{1/3}} \tag{17.95}$$

$$c_0(x) - c_\infty = -\frac{(D_i/3)^{1/3}}{\Gamma(2/3)} \int_0^x \left.\frac{\partial c_i}{\partial y}\right|_{\substack{y=0 \\ x=x_0}} \frac{\mathcal{R}(x_0)\, dx_0}{\left(\int_{x_0}^x \mathcal{R}\sqrt{\mathcal{R}\,\beta}\, dx\right)^{2/3}}. \tag{17.96}$$

In these equations, one can set $\mathcal{R} = 1$ for a two-dimensional surface. These integrals contain the important part of the appropriate solutions of the diffusion-layer equations 17.64 and 17.70 since they

relate the reaction rate and the surface concentration. The solution of the integral equation resulting from the introduction of the rate expression can then be carried out without further reference to the original partial differential equation.

17.13 BINARY AND CONCENTRATED SOLUTIONS

It was shown in Section 11.4 that the concentration of a binary electrolyte also obeys the equation of convective diffusion, even during the passage of current. The diffusion coefficient D of the electrolyte then is to be used (see equations 11.21 and 11.22). This means that many of the results of this chapter should be applicable to binary electrolytes. Two differences must be kept in mind. The first is that D appears in the equation of convective diffusion, as noted above. The second is that migration makes a substantial contribution to the current density even at the limiting current. For deposition of the cation, this fact is reflected in the relationship 11.27 between the current density and the concentration derivative at the electrode (see also Problems 11.2 and 11.3).

Furthermore, the ohmic potential drop is much more important in a binary solution than in a solution with supporting electrolyte. This means that decomposition of the solvent may begin at one point on the electrode before a limiting current has been reached over all the remainder of the electrode. The limiting-current plateau on a current–potential plot is then difficult or impossible to discern.

Levich[9] originally treated the rotating disk for cation deposition from a binary electrolyte, his equation being

$$i_n = -0.62 \frac{z_+ \nu_+ F c_\infty}{1 - t_+} \frac{D^{2/3} \Omega^{1/2}}{\nu^{1/6}}. \tag{17.97}$$

The Ilkovič equation for a growing mercury drop has been extended to a binary electrolyte by Lingane and Kolthoff,[65] with the result

$$i_n = -\frac{z_+ \nu_+ F c_\infty}{1 - t_+} \left(\frac{7D}{3\pi t} \right)^{1/2}, \tag{17.98}$$

again for deposition of the cation.* For deposition of the cation from a binary electrolyte to a vertical electrode in free convection, the average limiting current density would be given by

$$i_{\text{avg}} = -C \frac{z_+ \nu_+ F D c_\infty}{1 - t_+} \left[\frac{g(\rho_\infty - \rho_0)}{\rho_\infty D \nu L} \right]^{1/4}, \tag{17.99}$$

where C is to be taken from Table 17.2 with $\text{Sc} = \nu/D$. In all these equations, c_∞ refers to the bulk concentration of the electrolyte, $\nu_+ c_\infty$ being the bulk concentration of the reacting cation.

Transport theory valid for dilute solutions has been applied fruitfully to electrochemical systems. It should be pointed out, however, that equations valid for concentrated solutions and multicomponent transport are available and have been developed in Chapter 12. Transport theory for solutions of a single salt is moderately simple and has been applied to electrodeposition on a rotating-disk electrode[66, 67]

*Note, however, that the formula given by Lingane and Kolthoff for anion reduction is not correct. For reduction of iodate ions from a solution of KIO_3 according to the reaction $IO_3^- + 3H_2O + 6e^- \rightarrow I^- + 6OH^-$, we calculate (by the methods in Chapter 19) the value $I_L/I_D = 0.6489$ for the ratio of the limiting current I_L to the value I_D prevailing in the absence of migration. This compares favorably with the experimental value of 0.65 reported by Lingane and Kolthoff. Neither their formula (yielding 0.84) nor one due to Heyrovsky (yielding 0.74) works nearly as well.

For anion reduction, there is never a binary solution of KIO_3 near the electrode since the product ions I^- and OH^- are always present. Consequently, the calculations are more complex and must be treated according to the development in Chapter 19.

and deposition from a stagnant solution.[68] Furthermore, transport properties for such solutions are frequently available in the literature (see Chapter 14).

Multicomponent transport theory could be applied to certain simple geometries that would involve numerical solution of ordinary differential equations for the concentration profiles. However, in most cases, data for all the necessary transport properties are incomplete,[69] and a rigorous treatment is precluded.

The properties of the solution (ρ, v, D_i, etc.) have been treated largely as constant in this chapter. This is not completely valid since they depend on the composition. However, there is something to be said for such constant-property solutions. As soon as one accounts for variations of properties, one is faced with numerical solutions for each particular case; this means each particular concentration difference and temperature for each electrolytic system. One could produce an encyclopedia of results that would be of little general interest. The constant-property solutions, on the other hand, are much simpler, have approximately the correct behavior, and show more clearly the consequences of the physical phenomena. They illustrate the analogy between heat and mass transfer and allow the results to be used in both fields. On the whole, the constant-property solutions are superior from a pedagogic point of view. Empirical or theoretical corrections to constant-property solutions will have to be fairly simple in order to have any permanent value. (Of course, the determination and explanation of how the properties vary with composition are important matters of great interest.)

One then uses the constant-property solutions with the best average properties available. Fortunately, there is reason to believe that integral diffusion coefficients measured, say, with a rotating-disk electrode at the limiting current, would also be applicable to other geometries even though there is migration in the diffusion layer[70] and the transport properties vary with composition in the diffusion layer.[34] Similarly, integral diffusion coefficients for polarography with growing mercury drops should be the same as those measured with an electrode at the limiting current at the end of a stagnant capillary. This possibility is discussed in Section 14.4.

PROBLEMS

17.1 The equation of convective diffusion for mass transfer in laminar flow in an annulus is given by equation 17.20. Neglect the axial diffusion term in the following analysis. The velocity profile is given by

$$v_z = Cr^2 + B\ln r + A.$$

The constants A and B can be selected so that the velocity vanishes at $r = \kappa R$ and $r = R$:

$$B = -CR^2\left(\frac{1-\kappa^2}{\ln(1/\kappa)}\right), \quad A = CR^2\left(-1 + \frac{1-\kappa^2}{\ln(1/\kappa)}\ln R\right).$$

The average velocity in the annulus is then given by

$$\langle v\rangle = \frac{CR^2}{2}\left(\frac{1-\kappa^2}{\ln(1/\kappa)} - 1 - \kappa^2\right).$$

(a) Show that the velocity profile near the outer wall $r = R$ can be expressed as

$$v_z = \beta_0 y\left[1 - \gamma_0\frac{y}{R} + O\left(\frac{y^2}{R^2}\right)\right]$$

where

$$y = R - r$$

is the distance from the wall, and

$$\beta_0 = \frac{4\langle v\rangle}{(1-\kappa)R}\phi_0, \quad \phi_0 = \frac{1-\kappa}{2}\frac{1-\kappa^2-2\ln(1/\kappa)}{1-\kappa^2-(1+\kappa^2)\ln(1/\kappa)},$$

$$2\gamma_0 = -\frac{1-\kappa^2+2\ln(1/\kappa)}{1-\kappa^2-2\ln(1/\kappa)}.$$

(b) Show that the velocity profile near the inner wall $r = \kappa R$ can be expressed as

$$v_z = \beta_i y\left[1 - \gamma_i\frac{y}{R} + O\left(\frac{y^2}{R^2}\right)\right]$$

where

$$y = r - \kappa R$$

is the distance from the wall, and

$$\beta_i = \frac{4\langle v\rangle}{(1-\kappa)R}\phi_i, \quad \phi_i = \frac{\kappa-1}{2\kappa}\frac{1-\kappa^2-2\kappa^2\ln(1/\kappa)}{1-\kappa^2-(1+\kappa^2)\ln(1/\kappa)},$$

$$2\kappa\gamma_i = \frac{1-\kappa^2+2\kappa^2\ln(1/\kappa)}{1-\kappa^2-2\kappa^2\ln(1/\kappa)}.$$

(c) By the substitution

$$\eta = y\left(\frac{\beta_i}{9D_i z}\right)^{1/3}, \quad Z = \left(\frac{9zD_i}{\beta_i R^3}\right)^{1/3}, \quad \Theta = \frac{c_i - c_0}{c_b - c_0},$$

transform the equation of convective diffusion for the diffusion layer near the inner electrode to

$$3\eta[1 - \gamma_i\eta Z + O(\eta^2 Z^2)]\left(Z\frac{\partial\Theta}{\partial Z} - \eta\frac{\partial\Theta}{\partial\eta}\right) = \frac{\partial^2\Theta}{\partial\eta^2} + \frac{Z}{\kappa+\eta Z}\frac{\partial\Theta}{\partial\eta}.$$

The boundary conditions for this equation are

$$\Theta = 0 \quad \text{at} \quad \eta = 0, \quad \Theta = 1 \quad \text{at} \quad \eta = \infty$$

(d) Assume a solution of the form

$$\Theta = \Theta_0(\eta) + Z\Theta_1(\eta) + O(Z^2).$$

By substituting this form into the equation of part (c), expanding for small values of Z, and setting the coefficient of each power of Z equal to zero, show that Θ_0 and Θ_1 satisfy the equations

$$\Theta_0'' + 3\eta^2\Theta_0' = 0.$$

$$\Theta_1'' + 3\eta^2\Theta_1' - 3\eta\Theta_1 = \left(3\gamma_i\eta^3 - \frac{1}{\kappa}\right)\Theta_0'.$$

(e) Show that the appropriate solutions of the equations of part (d) are

$$\Theta_0 = \frac{1}{\Gamma(4/3)} \int_0^\eta e^{-x^3}\, dx,$$

$$\Theta_1 = \frac{\gamma_i/5}{\Gamma(4/3)} \eta^2 e^{-\eta^3} - \frac{2\gamma_i - 5/\kappa}{10\Gamma(4/3)} \eta \int_\eta^\infty e^{-x^3}\, dx,$$

so that

$$\Theta_0'(0) = \frac{1}{\Gamma(4/3)} \quad \text{and} \quad \Theta_1'(0) = -\frac{2\gamma_i - 5/\kappa}{10}.$$

(f) Show that the average Nusselt number for the inner electrode is

$$\mathrm{Nu}_{\mathrm{avg}} = 1.6151\left(\frac{\phi_i \mathrm{ReSc} d_e}{L}\right)^{1/3} - (1-\kappa)\frac{2\gamma_i - 5/\kappa}{5} - O\left(\frac{L}{d_e \mathrm{ReSc}}\right)^{1/3}.$$

(g) In a similar manner, show that the average Nusselt number for the outer electrode is

$$\mathrm{Nu}_{\mathrm{avg}} = 1.6151\left(\frac{\phi_0 \mathrm{ReSc} d_e}{L}\right)^{1/3} - (1-\kappa)\frac{2\gamma_0 + 5}{5} + O\left(\frac{L}{d_e \mathrm{ReSc}}\right)^{1/3}.$$

(h) Show that as κ approaches 1, both γ_i, and γ_0 approach $1/(1-\kappa)$ and the average Nusselt number for flow between two plane electrodes can be expressed as

$$\mathrm{Nu}_{\mathrm{avg}} = 1.8488\left(\frac{\mathrm{ReSc} d_e}{L}\right)^{1/3} - 0.4 + O\left(\frac{L}{d_e \mathrm{ReSc}}\right)^{1/3}.$$

Estimate the error in equation 17.58 when $L = 0.005 \mathrm{ReSc} d_e$.

(i) Show that γ_0 approaches $\frac{1}{2}$ as κ approaches zero and that the average Nusselt number for a circular pipe can be expressed as

$$\mathrm{Nu}_{\mathrm{avg}} = 1.6151\left(\frac{\mathrm{ReSc} d_e}{L}\right)^{1/3} - 1.2 + O\left(\frac{L}{d_e \mathrm{ReSc}}\right)^{1/3}.$$

(Compare equation 17.45.)

(j) Show that as κ approaches zero, γ_i approaches $1/2\kappa$ and ϕ_i approaches $1/2\kappa \ln(1/\kappa)$. Discuss how the error in equation 17.55 behaves for small values of κ.

17.2 Derive equation 17.15 by means of the velocity profile for distances close to the disk. Note that $\Gamma(4/3) = 0.89298$ and $\Gamma(5/3) = 0.90275$.

17.3 Show that the concentration profile in the diffusion layer near a rotating disk is given, at high Schmidt numbers, by Figure 17.1 when the dimensionless variable ξ is given by

$$\xi = z\left(\frac{a\nu}{3D_i}\right)^{1/3} \sqrt{\frac{\Omega}{\nu}} = \zeta\left(\frac{a\mathrm{Sc}}{3}\right)^{1/3}.$$

Figure 17.1 is a plot of equation 17.66.

17.4 It is shown in Section 11.4 that a binary electrolyte also obeys the equation of convective diffusion with the diffusion coefficient D of the electrolyte. Show that Figure 17.3 applies to metal ion deposition on a rotating disk from such a solution (see equation 11.27), if the ordinate is taken to represent

$$\frac{-i_n t_-}{z_+ \nu_+ F(c_\infty - c_0)\sqrt{\nu\Omega}}$$

and the abscissa is taken to represent v/D. The concentration c of the electrolyte is taken to be c_0 at the electrode surface and c_∞, in the bulk solution.

17.5 Use the development in Section 17.6 to show that the limiting current density to a ring electrode, of inner radius r_1, embedded in a rotating, insulating disk is given by

$$i_n = 0.62045 \frac{nFc_\infty}{s_i}\sqrt{\Omega\nu}\left(\frac{D_i}{\nu}\right)^{2/3} \frac{r}{(r^3 - r_1^3)^{1/3}}.$$

17.6 **(a)** Show that the average current density to a two-dimensional electrode of length L and obeying equation 17.67 is

$$i_{avg} = \frac{nFc_\infty}{6Ls_i\Gamma(4/3)}\left[9D_i \int_0^L \sqrt{\beta}\,dx\right]^{2/3}.$$

Use this equation and $\beta = 6\langle v\rangle/h$ to obtain equation 17.58.

(b) Show that the total current to an axisymmetric electrode obeying equation 17.72 is

$$I = \frac{nFc_\infty}{s_i\Gamma(4/3)}\frac{\pi}{3}\left[9D_i \int_0^L \mathcal{R}\sqrt{\mathcal{R}\beta}\,dx\right]^{2/3}.$$

(c) Show that the total current to an axisymmetric electrode obeying equation 17.92 is

$$I = 1.341 \frac{nFD_i c_\infty}{s_i}\left[\frac{g(\rho_\infty - \rho_0)}{\rho_\infty D_i \upsilon}\right]^{1/4} \pi\left[\int_0^L (\mathcal{R}^4 \sin\epsilon)^{1/3} dx\right]^{3/4}.$$

17.7 One can derive limiting-current expressions for the binary electrolyte by writing $(1/c_\infty)\partial c_i/\partial y$ at $y = 0$ from the results given for solutions with supporting electrolyte. With D_i replaced by D, the same expression must apply to $(1/c_\infty)\partial c/\partial y$ at $y = 0$ for the binary electrolyte. Use this procedure to show that equation 17.99 is the correct expression for free convection from a binary electrolyte to a vertical electrode and to show that the limiting current density for cation deposition from a binary electrolyte in the rotating-cylinder system is

$$i_n = -\frac{z_+\nu_+ FDc_\infty}{1 - t_+}\frac{0.0791}{d_R}\left(\frac{\Omega d_R^3}{2\nu d_L}\right)^{0.70}\left(\frac{\nu}{D}\right)^{0.356}.$$

17.8 Equation 17.95 involves a Stieltjes integral and should perhaps be written as

$$\left.\frac{\partial c_i}{\partial y}\right|_{y=0} = -\frac{\sqrt{\mathcal{R}\beta}}{\Gamma(4/3)}\int_{x_0=0}^{x_0=x} \frac{dc_0}{\left(9D_i\int_{x_0}^{x}\mathcal{R}\sqrt{\mathcal{R}\beta}\,dx\right)^{1/3}}.$$

Derive the Levich formula for the rotating disk by pretending that c_0 changes discontinuously from c_∞, to 0 at $r = 0$. (For the rotating disk, $\mathcal{R} = r$ and $\beta = a\Omega r\sqrt{\Omega/\nu}$.) Derive the result of Problem 17.5 by assuming that c_0 changes discontinuously from c_∞ to 0 at $r = r_1$ and that $dc_0/dx = 0$ elsewhere.

17.9 A flat-blade impeller is used to stir the solution above a stationary plane and thereby creates a cyclone flow. This flow is rotating at a distance above the plane and therefore has a radial (centrifugal) pressure gradient, the pressure being lower in the center. Adjacent to the stationary plane, the fluid cannot rotate as fast. Consequently, the pressure gradient causes the fluid to flow inward near the plane. An axial flow, away from the stationary plane, is also generated by the radial flow. The velocity derivatives at the surface of the plane can be expressed as

$$\left.\frac{\partial v_r}{\partial z}\right|_{z=0} = -Ar, \quad \left.\frac{\partial v_\theta}{\partial z}\right|_{z=0} = Br,$$

where A is a positive constant, related to the kinematic viscosity and the rotation speed of the fluid above the plane. A disk electrode of radius r_0 is embedded in the plane and is centered with the centrifugal flow described above. The remainder of the stationary plane is insulating. We wish to investigate the limiting-current distribution for a species that reacts at the disk electrode.

(a) Write down the governing differential equation that we should wish to solve for the diffusion layer on the disk electrode in an electrolytic solution. Be sure to specify the coordinate system you are using, and make relevant substitutions for the velocity profiles.

(b) What boundary conditions should be applied to the differential equation of part (a)?

(c) Obtain a quantitative expression for the distribution of limiting current density on the disk electrode.

(d) Describe qualitatively the distribution of limiting current density on the disk electrode. Is it uniform or nonuniform?

17.10 In connection with Figure 17.3, it is stated that the diffusion coefficient can be obtained graphically from the limiting current density on a rotating-disk electrode without a trial-and-error calculation. Following Bruckenstein,[71] show how the diffusion coefficient can be obtained analytically from the limiting current density when equation 17.15 (valid for high Schmidt numbers) is applicable.

17.11 Small amounts of mercuric ions are to be removed from a sodium chloride solution by plating at the limiting current on the inside of tubes 0.05 cm in diameter. The mercury concentration is to be reduced from 5 to 0.002 ppm. The average velocity in each tube is 0.15 cm/s, and the counterelectrode is located upstream of the tubular electrode. The molar mass of mercury is 200.59 g/mol.

(a) Should fully developed, laminar flow within the tubes be expected in this particular situation?

(b) How long should the tubes be in order to meet the design specifications? The diffusion coefficient of mercuric ions can be taken to be 8.5×10^{-6} cm^2/s.

(c) How much current flows to each tube, assuming no side reactions, and what is the current density per unit of cross-sectional area of the tube? In principle, does one need to know the answer to part (b) in order to answer part (c)?

(d) Discuss the likelihood of side reactions in this electrode.

17.12 In a pulsed plating apparatus, the diffusion layer can be approximated as a stagnant region of thickness δ. The reactant moves in this region by diffusion alone (migration is negligible). Successive durations of time $\tau_1 = 1$ second with no current flow are interspersed with durations of time $\tau_2 = 0.1$ second, where plating is carried out at a limiting-current condition. Sketch the current density that you would expect as a function of time, and indicate also on the sketch the magnitude of the steady limiting current density that would result if the electrode were maintained at a limiting current all the time. Suggest a formula for this steady limiting current density. Under conditions of pulsed plating, compare the magnitude of the limiting current density averaged over all time with the steady limiting current density. Also compare the limiting current density averaged over the time of τ_2 of the pulse to the steady limiting current density. (Qualitative comparisons only.)

17.13 An aqueous solution contains 0.02 *M* potassium ferricyanide and 0.05 *M* potassium ferrocyanide, $K_4Fe(CN)_6$, and the supporting electrolyte is 1 *M* sodium hydroxide.

(a) Estimate the limiting current density for cathodic reduction of the ferricyanide ion on a disk electrode rotating in this solution at 600 rpm (10 Hz).

(b) Estimate the value of the concentration of ferrocyanide ion at the electrode surface under the limiting-current conditions of part (a).

For this problem, assume that dilute-solution theory applies, that the temperature is 25°C, and that the kinematic viscosity of the solution is 0.01 cm^2/s.

17.14 Describe the principles and methods by which you would estimate the rate of corrosion of a copper disk rotating in sea water that is saturated with oxygen.

NOTATION

a	0.51023
c_i	concentration of species i, mol/cm^3
d_e	equivalent diameter of annulus, cm
D	diffusion coefficient of electrolyte, cm^2/s
D_i	diffusion coefficient of species i, cm^2/s
F	Faraday's constant, 96,487 C/mol
g	acceleration of gravity, cm/s^2
Gr	Grashof number
h	distance between walls of a flow channel, cm
H	dimensionless normal velocity for rotating disk
i_n	normal component of current density at an electrode, A/cm^2
J	amount of material transferred to the wall, mol/s
L	length of electrode, cm
m	volumetric flow rate of mercury, cm^3/s
M_k	coefficient in Graetz series
n	number of electrons transferred in electrode reaction
N_i	flux density of species i, $mol/cm^2 \cdot s$
Nu	Nusselt number
O	of order
Pe	Péclet number
r	radial position coordinate, cm
r_0	radius of growing mercury drop, cm

R	radius of outer cylindrical electrode, cm
R_k	Graetz function
Re	Reynolds number
$\mathcal{R}$	defines position of surface for an axisymmetric body, cm
s_i	stoichiometric coefficient of species i in electrode reaction
Sc	Schmidt number
t	time, s
t_+	cation transference number
T	life time of drop, s
$\mathbf{v}$	fluid velocity, cm/s
$\langle v \rangle$	average velocity, cm/s
x	distance measured along an electrode surface, cm
y	normal distance from surface, cm
z	axial distance in cylindrical coordinates, cm
z_i	charge number of species i
β	velocity derivative at the solid electrode, s^{-1}
γ	constant in rate of growth of mercury drops, $cm/s^{1/3}$
$\Gamma(4/3)$	0.89298, the gamma function of 4/3
ϵ	angle between the normal to a surface and vertical, rad
ζ	dimensionless axial distance for rotating disk or Graetz problem (see equation 15.25 or 17.23)
η	similarity variable for Lévêque solution
Θ	dimensionless concentration
κ	ratio of radii of inner to outer cylinder
λ_k	eigenvalues for Graetz problem
ν	kinematic viscosity, cm^2/s
ν_+	number of cations produced by dissociation of one molecule of electrolyte
ξ	dimensionless radial distance
ξ	dimensionless similarity variable (see equations 17.65 and 17.71)
ρ	density, g/cm^3
ϕ	dimensionless velocity derivative at the surface
Ω	rotation speed, rad/s

Subscripts

avg	average
b	inlet
0	at the electrode surface
∞	in the bulk solution

REFERENCES

1. R. Byron Bird, Warren E Stewart, and Edwin N. Lightfoot, *Transport Phenomena*, 2nd edition (New York: John Wiley, 2002).
2. W. M. Kays, *Convective Heat and Mass Transfer* (New York: McGraw-Hill, 1966).
3. Veniamin G. Levich, *Physicochemical Hydrodynamics* (Englewood Cliffs, NJ: Prentice-Hall, 1962).
4. Hermann Schlichting, *Boundary-Layer Theory* (New York: McGraw-Hill, 1979).
5. C. W. Tobias, M. Eisenberg, and C. R. Wilke, "Diffusion and Convection in Electrolysis: a Theoretical Review," *Journal of the Electrochemical Society*, *99* (1952), 359C–365C.

6. Wolf Vielstich, "Der Zusammenhang zwischen Nernstscher Diffusionsschicht und Prandtischer Strömungsgrenzschicht," *Zeitschrift für Elektrochemie*, *57* (1953), 646–655.
7. N. Ibl, "Probleme des Stofftransportes in der angewandten Elektrochemie," *Chemieingenieur-Technik*, *35* (1963), 353–361.
8. A. C. Riddiford, "The Rotating Disk System," *Advances in Electrochemistry and Electrochemical Engineering*, *4* (1966), 47–116.
9. B. Levich "The Theory of Concentration Polarization," *Acta Physicochimica URSS*, *17* (1942), 257–307.
10. Carl Wagner, "Heat Transfer from a Rotating Disk to Ambient Air," *Journal of Applied Physics*, *19* (1948), 837–839.
11. E. M. Sparrow and J. L. Gregg, "Heat Transfer from a Rotating Disk to Fluids of Any Prandtl Number," *Journal of Heat Transfer*, *81C* (1959), 249–251.
12. John Newman, "Schmidt Number Correction for the Rotating Disk," *Journal of Physical Chemistry*, *70* (1966), 1327–1328.
13. J. Newman, "Transport Processes in Electrolytic Solutions," in C. W. Tobias, ed., *Advances in Electrochemistry and Electrochemical Engineering*, Vol. 5 (Wiley, 1967).
14. D. P. Gregory and A. C. Riddiford, "Transport to the Surface of a Rotating Disc," *Journal of the Chemical Society* (1956), 3756–3764.
15. William H. Smyrl and John Newman, "Limiting Current on a Rotating Disk with Radial Diffusion," *Journal of the Electrochemical Society*, *118* (1971), 1079–1081.
16. A. N. Frumkin and L. I. Nekrasov, "O kol'tsevom Diskovom Elektrode," *Doklady Akademii Nauk SSSR*, *126* (1959), 115–118.
17. Yu. B. Ivanov and V. G. Levich, "Izuchenie nestoĭkikh promezhutochnykh produktov elektrodnykh reaktsiĭ s pomoshch'yu vrashchayushchegosya diskovogo elektroda," *Doklady Akademii Nauk SSSR*, *726* (1959), 1029–1032.
18. W. J. Albery and S. Bruckenstein, "Ring–Disc Electrodes. Part 2. Theoretical and Experimental Collection Efficiences," *Transactions of the Faraday Society*, *62* (1966), 1920–1931.
19. William H. Smyrl and John Newman. "Ring–Disk and Sectioned Disk Electrodes," *Journal of the Electrochemical Society*, *119* (1972), 212–219.
20. L. Graetz, "Ueber die Wärmeleitungsfahigkeit von Flüssigkeiten," *Annalen der Physik und Chemie*, *18* (1883), 79–94, 25 (1885), 337–357.
21. Wilhelm Nusselt, "Die Abhängigkeit der Wärmeübergangszahl von der Rohrlänge," *Zeitschrift des Vereines deutscher Ingenieure*, *54* (1910), 1154–1158.
22. George Martin Brown, "Heat or Mass Transfer in a Fluid in Laminar Flow in a Circular or Flat Conduit," *AIChE Journal*, *6* (1960), 179–183.
23. M. A. Lévêque, "Les Lois de la Transmission de Chaleur par Convection," *Annales des Mines, Memoires, ser.* 12, *13* (1928), 201–299, 305–362, 381–415.
24. John Newman, "Extension of the Lévêque Solution," *Journal of Heat Transfer*, *91C* (1969), 177–178.
25. John Newman, "The Fundamental Principles of Current Distribution and Mass Transport in Electrochemical Cells," in Allen J. Bard, ed., *Electroanalytical Chemistry*, Vol. 6 (New York: Marcel Dekker, 1973), pp. 187–352.
26. C. S. Lin, E. B. Denton, H. S. Gaskill, and G. L. Putnam, "Diffusion-Controlled Electrode Reactions," *Industrial and Engineering Chemistry*, *43* (1951), 2136–2143.
27. W. L. Friend and A. B. Metzner, "Turbulent Heat Transfer Inside Tubes and the Analogy Among Heat, Mass, and Momentum Transfer," *AIChE Journal*, *4* (1958), 393–402.
28. T. K. Ross and A. A. Wragg, "Electrochemical Mass Transfer Studies in Annuli," *Electrochimica Acta*, *70* (1965), 1093–1106.
29. P. Van Shaw, L. Philip Reiss, and Thomas J. Hanratty, "Rates of Turbulent Transfer to a Pipe Wall in the Mass Transfer Entry Region," *AIChE Journal*, *9* (1963), 362–364.

30. Ch. W. Tobias and R. G. Hickman, "Ionic Mass Transport by Combined Free and Forced Convection," *Zeitschrift für physikalische Chemie (Leipzig)*, *229* (1965), 145–166.
31. T. H. Chilton and A. P. Colburn, "Mass Transfer (Absorption) Coefficients. Prediction from Data on Heat Transfer and Fluid Friction," *Industrial and Engineering Chemistry*, *26* (1934), 1183–1187.
32. Davis W. Hubbard and E. N. Lightfoot, "Correlation of Heat and Mass Transfer Data for High Schmidt and Reynolds Numbers," *Industrial and Engineering Chemistry Fundamentals*, *5* (1966), 370–379.
33. M. J. Lighthill, "Contributions to the Theory of Heat Transfer through a Laminar Boundary Layer," *Proceedings of the Royal Society*, *A202* (1950), 359–377.
34. Andreas Acrivos, "Solution of the Laminar Boundary Layer Energy Equation at High Prandtl Numbers," *Physics of Fluids*, *3* (1960), 657–658.
35. Milton Abramowitz and Irene A. Stegun, eds., *Handbook of Mathematical Functions*, (Washington, D.C.: National Bureau of Standards, 1964), p. 320.
36. Schlichting, op. cit., p. 235.
37. Ibid., p. 139.
38. J. C. Bazán and A. J. Arvía, "Ionic Mass Transfer in the Electrolysis of Flowing Solutions: the Electrodeposition of Copper under Mass-Transfer Control on Tubular Electrodes," *Electrochimica Acta*, *9* (1964), 17–30.
39. J. C. Bazán and A. J. Arvía, "Ionic Mass Transfer in Flowing Solutions: Electrochemical Reactions under Ionic Mass-Transfer Rate Control on Cylindrical Electrodes," *Electrochimica Acta*, *9* (1964), 667–684.
40. G. Wranglén and O. Nilsson, "Mass Transfer under Forced Laminar and Turbulent Convection at Horizontal Plane Plate Electrodes," *Electrochimica Acta*, *7* (1962), 121–137.
41. H. Schlichting, *Boundary-Layer Theory*, 1968, p. 501.
42. M. Eisenberg, C. W. Tobias, and C. R. Wilke, "Ionic Mass Transfer and Concentration Polarization at Rotating Electrodes," *Journal of the Electrochemical Society*, *101* (1954), 306–319.
43. A. J. Arvia and J. S. W. Carrozza, "Mass Transfer in the Electrolysis of $CuSO_4$-H_2SO_4 in Aqueous Solutions under Limiting Current and Forced Convection Employing a Cylindrical Cell with Rotating Electrodes," *Electrochimica Acta*, *7* (1962), 65–78.
44. Donald Coles, "Transition in Circular Couette Flow," *Journal of Fluid Mechanics*, *21* (1965), 385–425.
45. E. Mattsson and J. O'M Bockris, "Galvanostatic Studies of the Kinetics of Deposition and Dissolution in the Copper + Copper Sulphate System," *Transactions of the Faraday Society*, *55* (1959), 1586–1601.
46. D. Ilkovič, "Polarographie Studies with the Dropping Mercury Kathode. Part XLIV. The Dependence of Limiting Currents on the Diffusion Constant, on the Rate of Dropping and on the Size of Drops," *Collection of Czechoslovak Chemical Communications*, *6* (1934), 498–513.
47. D. Ilkovič, "Sur la valeur des courants de diffusion observés dans l'électrolyse à l'aide de l'électrode a gouttes des mercure: Étude polarographique," *Journal de Chimie Physique*, *55* (1938), 129–135.
48. D. Mac Gillavry and E. K. Rideal, "On the Theory of Limiting Currents. I. Polarographie Limiting Currents," *Recueil des Travaux Chimiques des Pays-Bas*, *56* (1937), 1013–1021.
49. Jaroslav Koutecký, "Correction for Spherical Diffusion to the Ilkovič Equation," *Czechoslovak Journal of Physics*, *2* (1953), 50–55.
50. John Newman, "The Koutecký Correction to the Ilkovič Equation," *Journal of Electroanalytical Chemistry and Interfacial Electrochemistry*, *15* (1967), 309–312.
51. N. Ibl, "The Use of Dimensionless Groups in Electrochemistry," *Electrochimica Acta*, *1* (1959), 117–129.
52. C. R. Wilke, M. Eisenberg, and C. W. Tobias, "Correlation of Limiting Currents under Free Convection Conditions ," *Journal of the Electrochemical Society*, *100* (1953), 513–523.
53. M. G. Fouad and N. Ibl, "Natural Convection Mass Transfer at Vertical Electrodes under Turbulent Flow Conditions," *Electrochimica Acta*, *3* (1960), 233–243.
54. G. Schütz, "Natural Convection Mass-transfer Measurements on Spheres and Horizontal Cylinders by an Electrochemical Method," *International Journal of Heat and Mass Transfer*, *6* (1963), 873–879.

55. Simon Ostrach, "An Analysis of Laminar Free-Convection Flow and Heat Transfer about a Flat Plate Parallel to the Direction of the Generating Body Force," , Report 1111. Thirty-Ninth Annual Report of the National Advisory Commitee for Aeronautics, 1953, including Technical Reports Nos. 1111 to 1157 (Washington, DC: US Government Printing Office, 1955).
56. E. M. Sparrow and J. L. Gregg, "Details of Exact Low Prandlt Number Boundary Layer Solutions for Forced and for Free Convection," *NASA Memo* 2-27-59E (1959).
57. E. J. LeFevre, "Laminar Free Convection from a Vertical Plane Surface," *Actes, IX Congrès International de Mécanique Appliquée (Brussels)*, *4* (1957), 168–174.
58. Andreas Acrivos, "A Theoretical Analysis of Laminar Natural Convection Heat Transfer to Non-Newtonian Fluids," *A.l.Ch.E. Journal*, *6* (1960), 584–590.
59. E. J. Fenech and C. W. Tobias, "Mass Transfer by Free Convection at Horizontal Electrodes," *Electrochimica Acta*, *2* (1960), 311–325.
60. Andreas Acrivos, "On the combined effect of forced and free convection heat transfer in laminar boundary layer flows," *Chemical Engineering Science*, *21* (1966), 343–352.
61. D. A. Frank-Kamenetskiĭ, *Diffusion and Heat Exchange in Chemical Kinetics*, translated by N. Thon (Princeton, NJ: Princeton University Press, 1955).
62. Andreas Acrivos and Paul L. Chambré, "Laminar Boundary Layer Flows with Surface Reactions," *Industrial and Engineering Chemistry*, *49* (1957), 1025–1029.
63. Daniel E. Rosner, "Reaction Rates on Partially Blocked Rotating Disks—Effect of Chemical Kinetic Limitations," *Journal of the Electrochemical Society*, *113* (1966), 624–625.
64. Daniel E. Rosner, "Effects of convective diffusion on the apparent kinetics of zeroth order surface-catalysed chemical reactions," *Chemical Engineering Science*, *21* (1966), 223–239.
65. James J. Lingane and I. M. Kolthoff, "Fundamental Studies with the Dropping Mercury Electrode. II. The Migration Current," *Journal of the American Chemical Society*, *61* (1939), 1045–1051.
66. J. Newman and L. Hsueh, "The Effect of Variable Transport Properties on Mass Transfer to a Rotating Disk," *Electrochimica Acta*, *12* (1967), 417–427.
67. L. Hsueh and J. Newman, "Mass Transfer and Polarization at a Rotating Disk Electrode," *Electrochimica Acta*, *12* (1967), 429–438.
68. L. Hsueh and J. Newman, "Concentration Profile at the Limiting Current in a Stagnant Diffusion Cell," *Electrochimica Acta*, *16* (1971), 479–485.
69. Donald G. Miller, "Application of Irreversible Thermodynamics to Electrolyte Solutions. II. Ionic Coefficients ℓ_{ij} for Isothermal Vector Transport Processes in Ternary Systems," *Journal of Physical Chemistry*, *71* (1967), 616–632.
70. John Newman, "The Effect of Migration in Laminar Diffusion Layers," *International Journal of Heat and Mass Transfer*, *10* (1967), 983–997.
71. S. Bruckenstein, "Calculation of Diffusion Coefficients from Rotating Disk Electrode Data," *Journal of the Electrochemical Society*, *122* (1975), 1215.

CHAPTER 18

APPLICATIONS OF POTENTIAL THEORY

The formulation of governing relations for electrochemical systems leads to complex coupled nonlinear problems that are not generally amenable to analytic solutions except with stringent restrictions and approximations and a loss of generality. The last chapter developed the situation when migration can be ignored and similar solutions and methodology can be adopted from heat transfer and nonionic mass transfer. Another classic approach is to consider current and potential distributions when concentration gradients can be ignored and the potential is governed by Laplace's equation. The motivation could be to achieve a uniform metal distribution in electrodeposition. Solutions of Laplace's equation are developed in the present chapter.

Intermediate cases between the extremes of Chapters 17 and 18 can be developed. Chapter 19 extends Chapter 17 by showing how the limiting current is modified when the solution is between a binary electrolyte and a well-supported solution, and Chapter 21 shows how to treat situations where it is not possible to assure either the lack of migration (as in Chapter 17) or the lack of concentration gradients (as in this chapter).

In this chapter on solutions of Laplace's equation, we first treat the approximation of neglecting the surface overpotential η_s. This leads to the so-called primary distribution (of current or potential) where the potential in solution adjacent to an electrode is uniform along the surface of the electrode. One becomes interested in the current distributions on electrodes and the resistances of electrochemical cells.

The primary current distribution is the most nonuniform approximation to an actual current distribution. One wants to relax this approximation by next considering the effects of electrode polarization. This requires us to adopt an explicit form of the electrode kinetics, and it leads to greater complexity, both in how to solve the problem and how to deal with a large number of physical parameters. However, it could still be regarded as simple in that the geometry and use of Laplace's equation remain. Some solution methods are still valid or can be extended to cover the modification of the boundary conditions. We should also realize that the concept of the potential remains well defined because the solution is of uniform composition.

Electrochemical Systems, Fourth Edition. John Newman and Nitash P. Balsara.

One last case deserves mention in this chapter, that of a uniform current density. This case focuses us on the maximum potential variation that can occur along the surface of an electrode. This can be expanded into an important principle of electrochemical engineering. Although the primary distribution focuses on nonuniform current density and cell resistance, the relative current density distribution is independent of the scale (size) of the system and of the conductivity of the solution. But at uniform current density, the maximum potential variation over the surface of an electrode is proportional to the size L of the system and inversely proportional to the conductivity κ of the solution.

18.1 SIMPLIFICATIONS FOR POTENTIAL-THEORY PROBLEMS

When concentration gradients in the solution can be ignored, substitution of equation 16.1 into equation 16.4 yields

$$\mathbf{i} = -\kappa \nabla \Phi, \tag{18.1}$$

where

$$\kappa = F^2 \sum_i z_i^2 u_i c_i \tag{18.2}$$

is the conductivity of the solution and where the convective transport terms sum to zero by the electroneutrality relation 16.3. Equation 16.2 when multiplied by z_i and summed over i yields

$$\nabla^2 \Phi = 0, \tag{18.3}$$

that is, the potential satisfies Laplace's equation.

The boundary conditions are determined with equation 18.1. On insulators

$$\frac{\partial \Phi}{\partial y} = 0, \tag{18.4}$$

where y is the normal distance from the surface. On electrodes, equation 18.1 relates this potential derivative to the surface overpotential through equation 16.9 or 16.10. If the potential Φ in the solution is measured with a reference electrode of the same kind as the working electrode,* then the surface overpotential is given by

$$\eta_s = V - \Phi \quad \text{at} \quad y = 0, \tag{18.5}$$

where V is the potential of the metal electrode. The resulting boundary condition is a nonlinear relationship between the potential and the potential derivative not commonly encountered in other applications of potential theory.

As formulated above, the potential-distribution problem is similar to the problem of the steady temperature distribution in solids, with the potential playing the role of the temperature, the current density that of the heat flux density, and the electrical conductivity that of the thermal conductivity. Consequently, it is useful to be familiar with treatises on heat conduction, such as that of Carslaw and Jaeger.[1] A knowledge of electrostatics[2] and of the flow of inviscid fluids[3] is helpful since they are also involved with the solution of Laplace's equation.

Rousselot[4] presents an interesting discussion of potential-distribution problems. Kronsbein[5] gives a historical account of the literature, and Fleck[6] reviews the available analytic solutions of such problems. Recent reviews include that of West and Newman.[7]

*Otherwise, an equilibrium potential difference must be included in equation 18.5. This difference is a constant here.

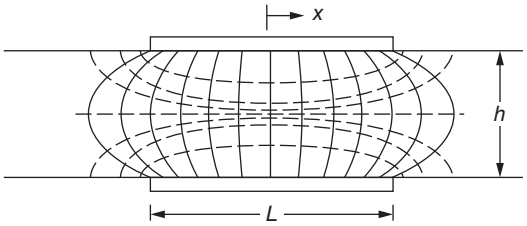

Figure 18.1 Two plane electrodes opposite each other in the walls of an insulating flow channel, showing equipotential surfaces (- - -) and current lines (—).

18.2 PRIMARY CURRENT DISTRIBUTION

The primary current and potential distributions are defined as the ideal situation in which the surface overpotential can be neglected altogether. The solution adjacent to an electrode is then taken to be an equipotential surface. Laplace's equation is not trivial to solve, even for relatively simple geometries.

Moulton[8] gives a classical solution for the primary current distribution for two electrodes placed arbitrarily on the boundary of a rectangle. This is an example of one way to solve Laplace's equation, that of conformal mapping,[9] using in this case the Schwarz–Christoffel transformation.

Consider a special case of this geometry, two plane electrodes placed opposite each other in the walls of a flow channel (see Figure 17.8). The potential distribution is sketched in Figure 18.1 for $L = 2h$. Here, current lines are represented by solid curves and equipotential surfaces by dashed curves. These two sets of curves are perpendicular to each other everywhere in the solution. The equipotential lines are close together near the edge of the electrode, and, at this point, the primary current density is infinite.

The primary current distribution on the electrode is shown in Figure 18.2 for $L = 2h$ and is given by the equation

$$\frac{i_n}{i_{\text{avg}}} = \frac{\epsilon \cosh \epsilon / K(\tanh^2 \epsilon)}{\sqrt{\sinh^2 \epsilon - \sinh^2(2x\epsilon/L)}}, \tag{18.6}$$

where $\epsilon = \pi L/2h$, x is measured from the center of the electrode, and $K(m)$ is the complete elliptic integral of the first kind, tabulated in Ref. [10]. From the complexity of this expression for the current density, one can perhaps appreciate the difficulty involved in obtaining the potential distribution. For contrast, the mass-transfer limiting current distribution for laminar flow is also shown in Figure 18.2 (see Section 17.4).

The primary current distribution shown in Figure 18.2 is independent of the flow rate since convection is great enough to eliminate concentration variations, and hence the distribution is symmetric. The current density is infinite at the ends of the electrodes since the current can flow through the solution beyond the ends of the electrodes (see Figure 18.1). This is a general characteristic of primary current distributions. The current density where an electrode meets an insulator is either infinite or zero unless they form a right angle (see Figure 18.3 and Problem 18.5). When the electrode and the insulator lie in the same plane, the primary current density is inversely proportional to the square root of the distance from the edge for positions sufficiently close to the edge. This behavior is exhibited by equation 18.6 for the current density. Generally, the primary current distribution shows that the more inaccessible parts of an electrode receive a lower current density.

The primary current distribution is determined by geometric factors alone. Thus, only the geometric ratios of the cell enter into the parameter ϵ, but the conductivity of the solution does not enter. The

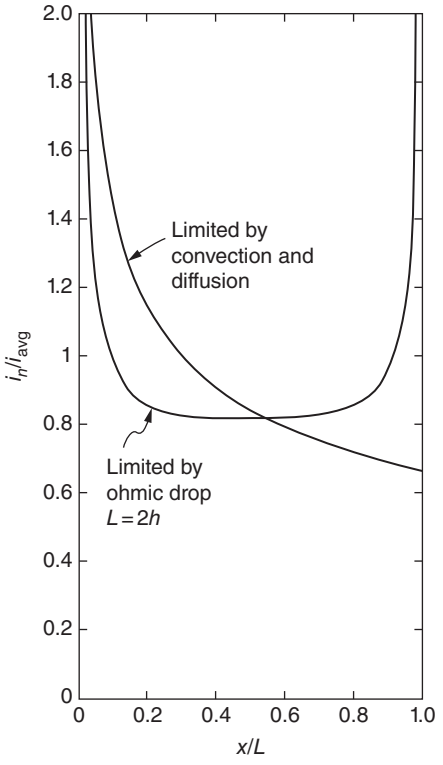

Figure 18.2 Current distribution on planar electrodes. Here x is measured from the edge of the electrode, not the center.

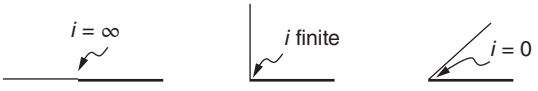

Figure 18.3 Behavior of the primary current distribution near the edge of an electrode.

resistance for this cell is

$$R = \frac{1}{\kappa W}\frac{K(1/\cosh^2\epsilon)}{K(\tanh^2\epsilon)}, \tag{18.7}$$

where W is the width of electrodes perpendicular to the length of the channel.

Kasper[11] gives the primary current distribution for a point electrode and a plane electrode, for line electrodes parallel to plane electrodes and plane insulators, and for cylindrical electrodes in various configurations. These systems illustrate the application of the method of images. Hine et al.[12] describe the primary current distribution for two plane electrodes of infinite length and finite width confined between two infinite, insulating planes perpendicular to, but not touching, the electrodes. Wagner[13] gives the primary current distribution for a two-dimensional slot in a plane electrode. These are further examples of the Schwarz–Christoffel transformation. Kojima[14] collected various expressions for the resistance between two electrodes in various configurations. The primary current distribution

is analogous to calculations of heat-transfer resistance with fixed temperatures at some boundaries[15] and to calculations of dielectric capacitance.

For a disk electrode of radius r_0 embedded in an infinite insulating plane and with the counterelectrode far away, the primary current distribution is given by[16]

$$\frac{i_n}{i_{\text{avg}}} = \frac{0.5}{\sqrt{1 - r^2/r_0^2}}, \tag{18.8}$$

and the equipotential and current lines in the solution are shown in Figure 18.4. Again, the equipotential lines are close together near the edge of the electrode; and, at this point, the current density is infinite, being proportional to the reciprocal of the square root of the distance from the edge near this point. Only geometric factors enter into the current distribution, and the resistance to a hemispherical counterelectrode at infinity is

$$R = \frac{1}{4\kappa r_0}. \tag{18.9}$$

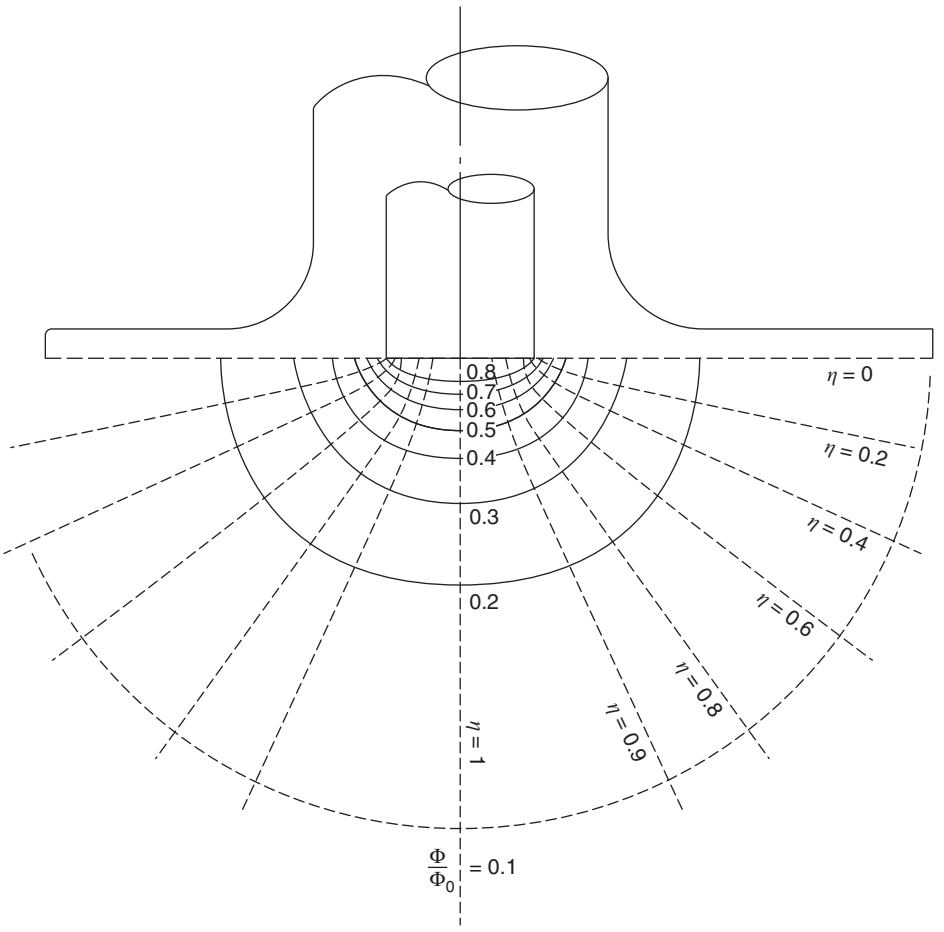

Figure 18.4 Current (- - -) and potential (—) lines for a disk electrode. *Source*: John Newman 1966.[16] Reproduced with permission of The Electrochemical Society, Inc.

This is a simple example of the application of the method of separation of variables leading to Fourier series and integrals.[17, 18]

For two electrodes embedded in an insulating plane, the inverse-square-root law applies near the edges of the electrodes. However, the coefficient becomes infinite, as the width of the separator approaches zero, in such a way that the total current flowing between the electrodes is infinite with no separation. Consequently, the solution for the primary distribution when two electrodes of different potentials meet has no physical meaning.

18.3 SECONDARY CURRENT DISTRIBUTION

When slow electrode kinetics is taken into account, the electrolytic solution near the electrode is no longer an equipotential surface, and the result of the calculations is the so-called *secondary current distribution*. The general effect of electrode polarization is to make the secondary current distribution more nearly uniform than the primary distribution and to restrict infinite current densities at electrode edges to finite values. This can be regarded as the result of imposing an additional resistance at the electrode interface. The mathematical problem now involves the solution of Laplace's equation, subject to a more complicated, perhaps even nonlinear, boundary condition.

A variety of expressions for the electrode polarization has been used, which reflects the variety of electrode kinetics as well as a variety of approximations. In practice, the electrode kinetic equation is frequently replaced by a linear or a logarithmic (Tafel) relation between the surface overpotential and the potential derivative at the electrode. In any case, additional parameters besides geometric ratios are required to specify the current distribution. The advantage of the linear and logarithmic approximations is that they add only one new parameter. Thus, fairly realistic cases can be treated without excessive complication.

For sufficiently small surface overpotentials, equation 16.10 can be linearized to read

$$i_n = \eta_s \frac{di_n}{d\eta_s}\bigg|_{\eta_s=0} = (\alpha_a + \alpha_c)\frac{i_0 F}{RT}\eta_s = -\kappa\frac{\partial \Phi}{\partial y} \quad \text{at} \quad y = 0. \tag{18.10}$$

This provides a linear boundary condition for Laplace's equation and has been popular in the literature since there is some hope of solving the resulting linear problem. Furthermore, if the range of current densities at the electrode is sufficiently narrow, as one wants to achieve in electroplating, it is, of course, justified to linearize the polarization equation about some other, nonzero value of the surface overpotential. Finally, with linear polarization, one achieves an economy of parameters needed to determine the current distribution, and the calculation of a family of curves representing the current distribution for a particular geometry is justified.

The secondary current distribution i_n/i_{avg} depends upon the same geometric ratios as the primary distribution and, in addition, for linear polarization, depends on the parameter $(L/\kappa)di_n/d\eta_s$, where L is a length characteristic of the system. This parameter has been identified by Hoar and Agar[19] for the characterization of the influence of electrolytic resistance, polarization, and cell size on current distribution. When both electrodes are polarized, there are two such parameters involving the slope of the polarization curve on both the anode and the cathode.

For a disk electrode, the additional parameter for linear polarization is[20]

$$J = (\alpha_a + \alpha_c)\frac{i_0 F r_0}{RT\kappa}. \tag{18.11}$$

The secondary current distribution for linear polarization on a disk electrode is shown in Figure 18.5, where $N = \infty$ means that the rotation speed is so high that concentration variations can be ignored.

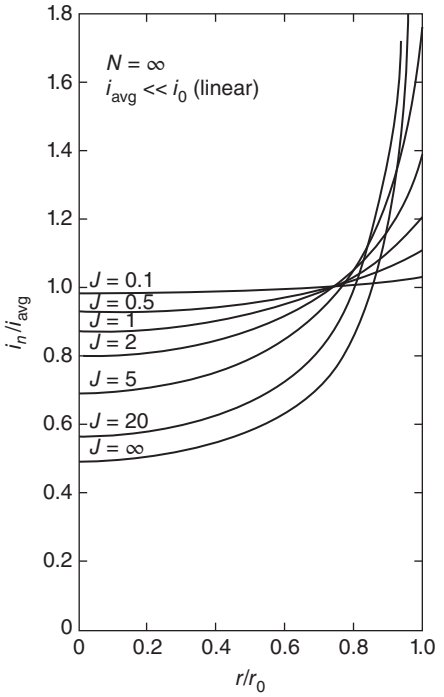

Figure 18.5 Secondary current distribution for linear polarization at a disk electrode. *Source*: John Newman 1966.[20] Reproduced with permission of The Electrochemical Society, Inc.

For $J \to \infty$, one obtains the primary current distribution. Then, the ohmic resistance dominates over the kinetic resistance at the interface. For any finite value of J, the distribution is more nearly uniform and is finite at the edge of the disk. For $J \to 0$, the distribution is uniform, but the average current must then be small for the linear law still to apply. Except for this, the current distribution i_n/i_{avg} is independent of the magnitude of the current.

The Tafel polarization law, where one of the exponential terms in equation 16.10 is negligible, is also popular in the literature. For a cathodic reaction, we have

$$\eta_s = -\frac{RT}{\alpha_c F}[\ln(-i_n) - \ln\, i_0]. \tag{18.12}$$

This is popular because, while being a fairly realistic polarization law, Tafel's equation introduces a minimum of additional parameters into the problem. In addition to depending on the same geometric ratios as the primary current distribution, the current distribution i_n/i_{avg} now depends on the parameter $|i_{\text{avg}}|\alpha_c FL/RT\kappa$. The current distribution now depends on the magnitude of the current, but it is independent of the value of the exchange current density i_0, insofar as Tafel polarization is applicable only for current densities appreciably above the exchange current density.

The secondary current distribution for Tafel polarization on a disk electrode[20] is shown in Figure 18.6. This is similar to the secondary current distribution with linear polarization, but the parameter $|i_{\text{avg}}|\alpha_c Fr_0/RT\kappa$ now plays the role of the parameter J (the characteristic length r_0 being appropriate for the disk electrode). In particular, the primary current distribution is still approached as this parameter approaches infinity.

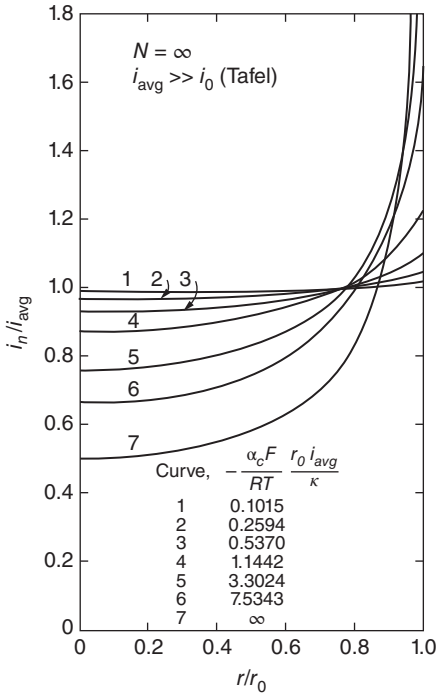

Figure 18.6 Secondary current distribution for Tafel polarization at a disk electrode. *Source*: John Newman 1966.[20] Reproduced with permission of The Electrochemical Society, Inc.

The parameter for polarization is always proportional to a characteristic length and inversely proportional to the conductivity κ and involves the nature of the polarization. Therefore, we may state as a general rule that for large systems and small conductivities the primary current distribution will be approached, independent of the nature of the polarization law.

If we are unwilling to make either the linear or the Tafel approximation to the full Butler–Volmer equations, then the secondary current distribution on a disk electrode depends on the parameters α_a/α_c, J (defined by equation 18.11), and

$$\delta = \frac{(\alpha_a + \alpha_c)Fr_0}{RT\kappa} i_{\text{avg}}. \tag{18.13}$$

General plots of the current distribution now become unwieldy. Consequently, we select as a measure of the nonuniformity the ratio of the current density at the center of the disk to the average current density. This ratio has the value 1 for the uniform distribution and the value 0.5 for the extremely nonuniform primary distribution.

To illustrate how J and δ jointly affect the nonuniformity,[20] we plot this ratio in Figure 18.7 for $\alpha_a = \alpha_c$. For large currents ($|\delta| \gg J$), the Tafel results apply. As the current is decreased, the distribution becomes more nearly uniform but approaches at low currents the linear results for the given value of J rather than a completely uniform current density. For larger values of J, the linear results apply to larger current densities.

The quantity $\kappa/(Ldi_n/d\eta_s)$, recognized to be important by Hoar and Agar,[19] has come to be called the Wagner number Wa as an honor to a researcher who has refined its use and understanding.[21]

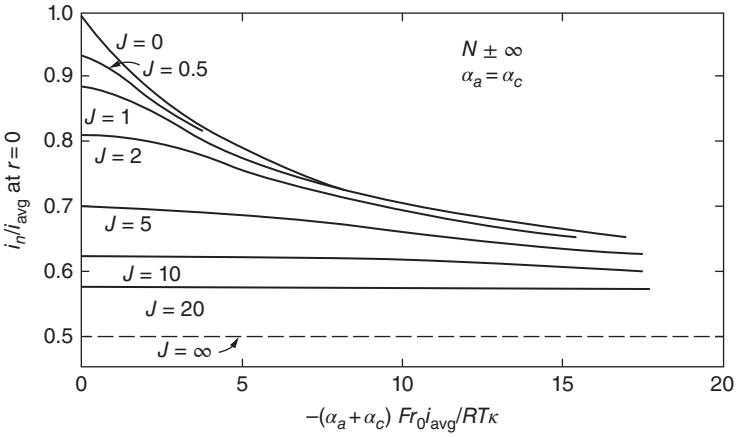

Figure 18.7 Current density at the center of the disk when concentration polarization is absent. *Source*: John Newman 1966.[20] Reproduced with permission of The Electrochemical Society, Inc.

Historically, its use may have been restricted to situations of linearization of the electrode kinetics (see remark below equation 18.10), but both J and $|i_{avg}|\alpha_c FL/RT\kappa$ can be regarded as reciprocals of Wagner numbers. As the Wagner number approaches zero, the primary distribution is approached.

Kasper[11] has treated the effect of linear polarization on some line-plane systems and for cylindrical electrodes. Wagner has treated the secondary current distribution for a plane electrode with a two-dimensional slot,[13] two cases of plane electrodes in the walls of an insulating channel, and a nonplanar electrode with a triangular profile.[21] One of the cases treated by Wagner for linear polarization, that of a plane electrode of finite width embedded in an insulating plane and with the counterelectrode at infinity, has been treated by Gnusin et al.[22] for Tafel polarization. Parrish and Newman[23, 24] discuss this case and the case of two plane electrodes opposite each other in the walls of a flow channel (see Figure 17.8).

Some of these cases illustrate the use of current sources distributed along the electrode surface as a method of reducing the problem to an integral equation. This integral equation, which may be linear or nonlinear depending on the polarization law used, frequently requires a numerical solution.

The primary current distribution for a disk electrode, shown again in Figure 18.8, can be contrasted with the uniform distribution found in Section 17.2 when convection and diffusion are governing. The nonuniform ohmic potential drop to the disk spoils the uniform accessibility from the mass-transfer standpoint. The polarization of the electrode promotes a uniform distribution to a degree determined by the parameters δ and J. How the resistive, diffusive, and convective factors interact is treated in Chapter 21. The potential distribution near the disk for a uniform current distribution[20] is also shown in Figure 18.8 (see also Nanis and Kesselman[25]). This curve is normalized in such a way that it can be compared conveniently with the value $\Phi_0 4\kappa r_0/I = 1$ for the primary current distribution. These extreme cases of uniform potential and uniform current density are clearly incompatible.

The uniform current density represents the extreme case of the variation of potential in the solution adjacent to the disk. The maximum potential difference between the center of the disk and the edge is

$$\Delta\Phi_0 = \frac{0.363 r_0 i_{avg}}{\kappa}. \tag{18.14}$$

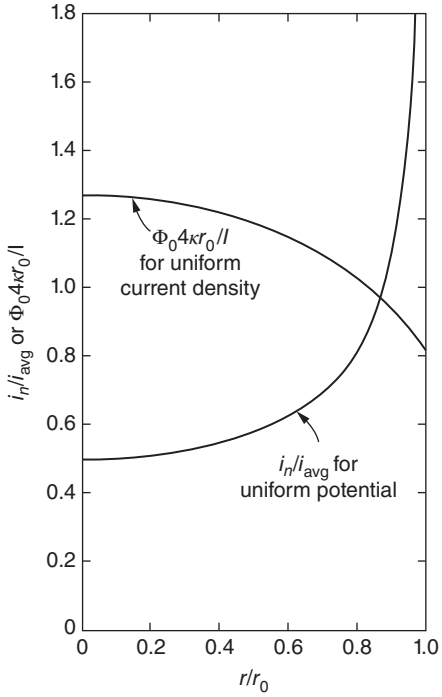

Figure 18.8 Primary current distribution and potential distribution for a uniform current density on a disk electrode. *Source*: John Newman 1966.[20] Reproduced with permission of The Electrochemical Society, Inc.

This formula has important implications in regard to the shape of limiting-current curves,[26] the sizes of disks that can be protected from corrosion anodically or cathodically,[27] the conditions for controlled-potential electrolysis,[28] and the determination of electrode kinetic parameters.[29] In each case, there is a maximum permissible variation of potential that governs the allowable values of r_0 and i_{avg} for a solution of given conductivity (see also equation 22.56). Cathodic protection of a metal surface, to keep it from corroding, is a useful application of the concept of a uniform current distribution and consequently is treated separately in Section 18.5.

18.4 NUMERICAL SOLUTION BY FINITE DIFFERENCES

Analytic solutions of current-distribution problems are usually restricted to simple geometric arrangements and to no polarization or linear polarization. The use of some analytic solutions is facilitated by computer evaluation of certain integrals and infinite series. Some methods, such as Wagner's integral-equation method or solutions in infinite series with undetermined coefficients, require numerical evaluation of the current distribution on the electrodes or of the coefficients. When such methods can be used, the labor is less and the results are more accurate than a numerical solution of Laplace's equation by finite-difference methods.

Finite-difference and finite-element methods have been developed for heat-conduction problems, for example, and extended to electrolytic cells. The widespread availability of commercial finite-element packages makes this technique convenient for analyzing the current distribution on complex geometries.

18.5 PRINCIPLES OF CATHODIC PROTECTION

Corrosion of iron occurs by electrochemical dissolution:

$$Fe \rightarrow Fe^{2+} + 2e^{-}. \tag{18.15}$$

The ferrous ions have a tendency to precipitate as ferrous hydroxide:

$$Fe^{2+} + 2H_2O \rightarrow Fe(OH)_2 + 2H^{+}. \tag{18.16}$$

Thus, the soil or medium near the corroding surface tends to become more acidic. Or the soil becomes less basic if hydroxyl ions are consumed:

$$Fe^{2+} + 2OH^{-} \rightarrow Fe(OH)_2. \tag{18.17}$$

The dissolution of iron is an anodic process. In corrosion, where the electrons do not flow to an external electrical circuit, the electrons must be consumed in another electrochemical process, frequently occurring on the same metal surface. A common oxidizing agent is oxygen, and we can write

$$O_2 + 4e^{-} + 2H_2O \rightarrow 4OH^{-} \tag{18.18}$$

or

$$O_2 + 4e^{-} + 4H^{+} \rightarrow 2H_2O. \tag{18.19}$$

In this process, the medium becomes more basic or less acidic. Thus, if the reactions 18.15, 18.16, and 18.19 or 18.15, 18.17, and 18.18 occur together on the same surface, the metal corrodes,

$$2Fe + O_2 + 2H_2O \rightarrow 2Fe(OH)_2, \tag{18.20}$$

without an imbalance in acid or base and without the external flow of an electric current.

For a metal as active as iron, acid can also appear as an oxidizing agent. The cathodic reaction can be written as

$$2H^{+} + 2e^{-} \rightarrow H_2. \tag{18.21}$$

The overall corrosion reaction could be written as

$$Fe + 2H^{+} \rightarrow Fe^{2+} + H_2 \tag{18.22}$$

or

$$Fe + 2H_2O \rightarrow Fe(OH)_2 + H_2. \tag{18.23}$$

The relationship of these reactions can be visualized with a Pourbaix diagram, or potential-pH diagram; see Figure 18.9. Such diagrams are also discussed in the text related to Figure 2.2. On such diagrams, it is convenient to indicate, by the dashed lines, the stability window for water.

At electrode potentials above the line labeled O_2, there is a tendency to evolve oxygen by the reverse of reaction 18.18 or 18.19. The potential depends on pH because H^{+} and OH^{-} ions are involved, but the two reactions merge into one line on the diagram. One thinks of reaction 18.18 occurring toward the right on the diagram where hydroxyl ions predominate, while reaction 18.19 is a natural way to write the reaction toward the left where hydrogen ions predominate. Below the line, oxygen tends to

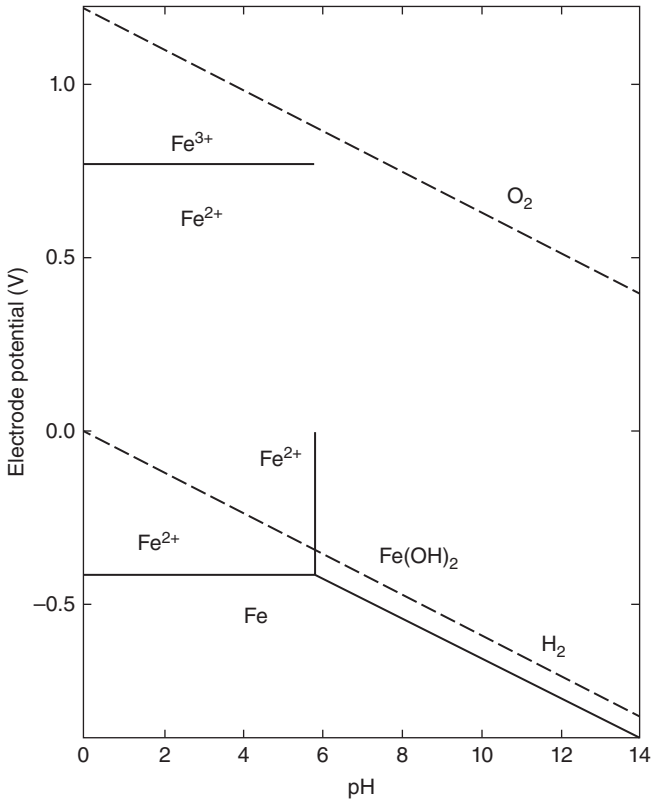

Figure 18.9 Simplified Pourbaix diagram for iron in water at 25°C. The oxide phases Fe_2O_3 and Fe_3O_4 are not shown.

be consumed by the electrochemical reactions 18.18 and 18.19 proceeding in the direction in which they are written. The potential line also depends on the partial pressure or fugacity of oxygen; it is customary to draw the curve for a value of 1 bar or 1 atm. Thus, bubbles of O_2 could not form unless the electrode potential is above this line (when the solution is maintained at a total pressure of 1 bar).

It may be necessary to hold the electrode potential substantially above the O_2 line before bubbles appear because a significant thermodynamic driving force then exists to drive the reaction. The vertical distance from the O_2 line is the overpotential for the reaction, a positive (or anodic) overpotential for points above the line and a negative (or cathodic) overpotential for points below the line. The relationship of the rate of the electrochemical reaction to the overpotential is the subject of electrochemical kinetics. The oxygen reaction is relatively slow, and its degree of slowness will be different on different metals and at different temperatures.

Similarly, the line labeled H_2 describes the equilibrium potentials for reaction 18.21. Hydrogen tends to be evolved at electrode potentials *below* this line and consumed at potentials above the line. Just like the oxygen reaction, there is a pH dependence and partial-pressure (of hydrogen) dependence of the equilibrium potential, and a nonzero overpotential is necessary to drive the reaction at appreciable rates.

Thus, one can say that water is stable between the O_2 and H_2 lines on the Pourbaix diagram. It is susceptible to O_2 evolution above the upper line and susceptible to H_2 evolution below the lower line.

The thermodynamic equilibrium potential for iron dissolution according to equation 18.15 is the horizontal line at about −0.409 V (for many years the standard electrode potential was taken to be −0.440 V). To the right of a pH of 5.84, the ferrous ions precipitate according to reaction 18.16. To the right of this value, we would logically write the reaction as

$$Fe + 2OH^- \rightarrow Fe(OH)_2 + 2e^-. \tag{18.24}$$

A separate equilibrium potential is shown on the diagram for this reaction; it has the same slope as the lines labeled O_2 and H_2 because these reactions all have one electron per OH^- or H^+ ion involved in the reaction. Thus, we can conclude that an electrode reaction, like equation 18.15, involving no H^+ or OH^- ions is a horizontal line on the diagram, whereas a reaction, like equation 18.16, involving no electrons is a vertical line. Other reactions will have a slope depending on the number of hydrogen or hydroxyl ions involved per electron transferred.

The oxidation of ferrous ions to ferric ions,

$$Fe^{2+} \rightarrow Fe^{3+} + e^-, \tag{18.25}$$

is represented on the diagram by a horizontal line at $U = 0.770$ V. This line depends also on the concentrations of the two ions; it is drawn for equal concentrations. The line moves up for an increase in the concentration of ferric ions and moves down for an increase in the concentration of ferrous ions. The line for reaction 18.15 also depends on the ferrous ion concentration; it is drawn for an "ideal 1 *m* solution."

The Pourbaix diagram indicates that iron is unstable with respect to oxidation by H^+ and that this is particularly true at the left side of the diagram. There is a strong driving force for oxygen to oxidize iron at any pH, and the reaction in aqueous medium is generally limited only by the rate of transport of O_2 to the iron surface. We also see that O_2 is strong enough to oxidize ferrous ions to ferric ions. A lot of chemistry is represented on this diagram.

The strategy for cathodic protection can now be stated very simply. We want to hold, by means of an external power supply, the electrode potential of iron low enough so that reactions 18.15 and 18.24 are suppressed. Then the iron will not corrode, but electrons will need to be supplied so that any oxygen transported to the surface will be reduced according to reaction 18.18 and any hydrogen ions will be reduced according to reaction 18.21. This leads to an interesting design problem for the placement of anodes to supply the ionic component of the current, while the negative terminal of the power supply is directly connected to the iron to be cathodically protected (see Figure 18.10).

Anions and cations migrate in the soil to balance the current flow required to reduce the O_2. This might at first appear to lower the pH near the protected cathode. However, the cathodic reactions 18.18 or 18.19 or 18.21 counteract this tendency and actually cause the pH to rise near the iron cathode. In fact, this change in chemical environment may be as important to the protection process as the direct flow of charge.

Figure 18.9 is drawn with the potentials referred to a hydrogen electrode in an ideal 1 *m* solution. For soil applications, the saturated $Cu/CuSO_4$ reference electrode, lying at a potential of 0.316 V relative to the hydrogen electrode, is generally used. Figure 18.11 shows some relevant potentials relative to the $Cu/CuSO_4$ electrode on a Pourbaix diagram. On this figure are some possible positions for the anode and the cathode of a cathodic-protection system, both shown at a nominal pH of 7. (The meaning of *near* and *far* sides will be explained shortly. The meaning of $x = 0$ and $x = L$ is explained in Figure 18.15; x is the axial distance from the power-supply lead along the pipe.)

A specific example is a long, cylindrical, buried pipeline, to be protected by means of a smaller, cylindrical anode that runs parallel to the pipe, sketched in Figure 18.12. The design problem involves determining how far away to place the anode. We might proceed as follows:

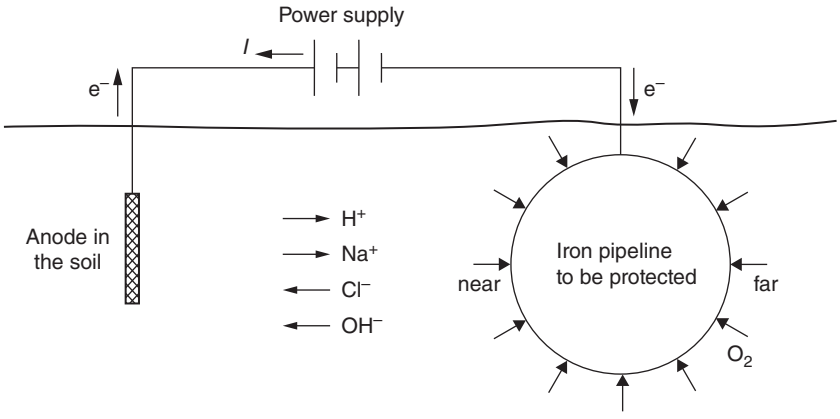

Figure 18.10 Cathodic protection system.

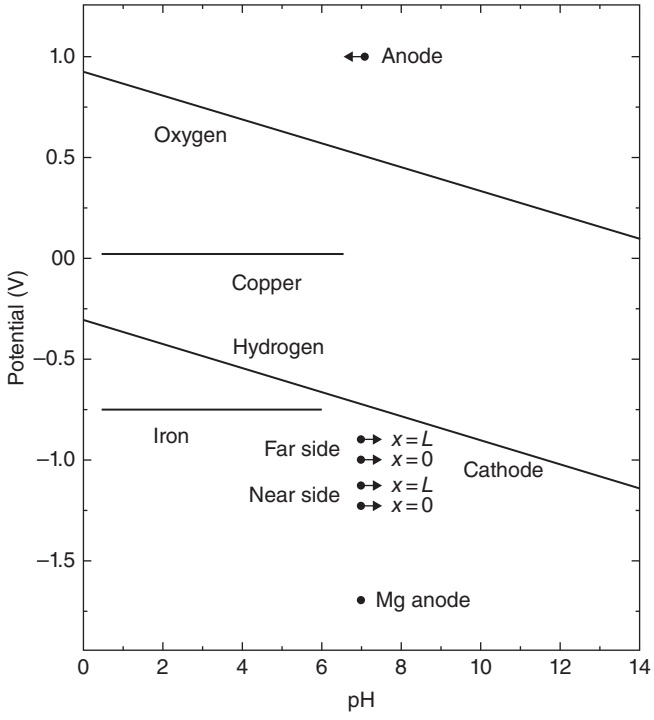

Figure 18.11 Potential relative to an adjacent saturated $Cu/CuSO_4$ reference electrode. Arrows indicate direction of pH shift induced by the expected electrochemical reactions.

1. Calculate or estimate the rate of transport of oxygen to the surface. Since oxygen is not ionic, only diffusion and convection through the soil are involved. Convert this mass-transfer rate, by Faraday's law, to a current density that must be supplied through the soil from the anode(s) to reduce the oxygen and prevent the dissolution of iron. We know that this can be stated as the current density flowing to a properly protected surface because

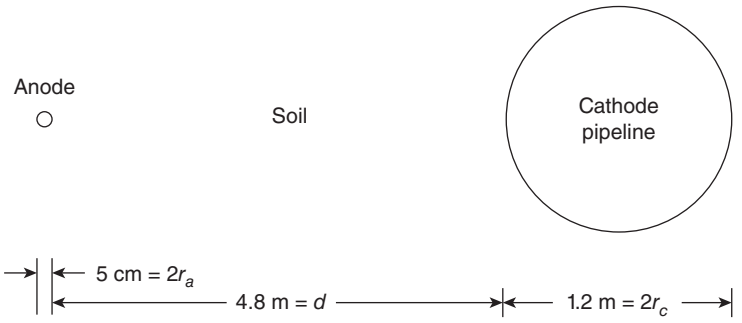

Figure 18.12 Protected pipeline and parallel, cylindrical anode that provides the required current. *Source*: Ref. 30. Reproduced with permission of The Electrochemical Society, Inc.

(a) Virtually all oxygen will be reduced (at the limiting current) at any potential near the iron potential. Figure 18.13 describes the current-potential characteristics for three possible electrode reactions and the sum of these currents.
(b) The current density for the iron dissolution reaction should be negligible because this is the purpose of the cathodic protection.
(c) The current density for hydrogen evolution should be maintained at a low value because any hydrogen evolution permitted is a waste of current, can lead to undesired hydrogen embrittlement of the steel, and distorts the current flow so that insufficient current flows to the more distant parts of the steel surface.

The required current density for oxygen reduction may frequently be stated as a uniform value i_{avg} for the entire surface, unless more detailed transport calculations have led to a specified distribution. The total current required is given by the analysis of oxygen transport.

2. Place one or more anodes in the soil to supply the total current without *overprotecting* the steel surface near the anode, resulting in hydrogen evolution there and necessarily leaving some more remote part of the surface *underprotected*. On the basis of Figure 18.13, one requires that the potential of any part of the cathode be maintained more negative than −0.850 V relative to an adjacent $Cu/CuSO_4$ reference electrode in order to provide adequate protection while at the same time maintaining all parts of the surface more positive than −1.20 V to prevent excessive hydrogen evolution. Consequently, the potential in the soil next to the cathode can vary by no more than 350 mV, and this becomes an important design criterion for the placement of the anodes and for determining how large a surface can be cathodically protected.
3. Determine the potential drop in the soil between the anode and the near part of the cathode, since it is an important component of the cell potential that must be provided by the rectifier. (A sacrificial anode such as Zn or Mg can also provide only a limited potential.)
4. Calculate the potential variation in the anode and the cathode and in lead wires connecting the electrodes to the power supply. These considerations have an impact on whether the cathode surface relative to the adjacent soil is maintained within the 350-mV window.

Figure 18.11 also shows some hypothetical electrode potentials (relative to the adjacent soil). The anode evolves oxygen and is shown with a 0.5 V overpotential. The electrochemical reaction tends to

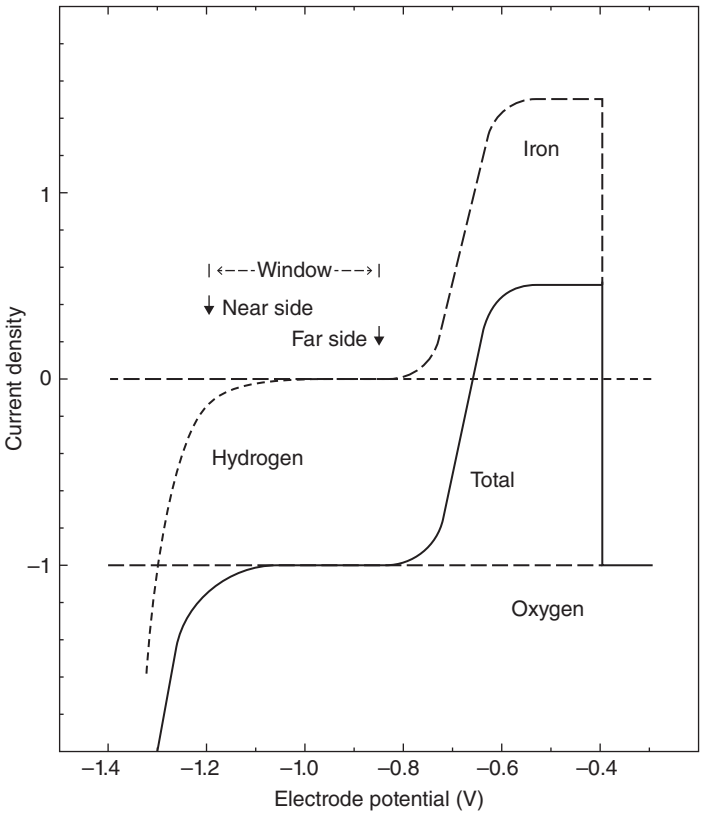

Figure 18.13 Current–potential curve for a local element. The electrode potential is the potential of the protected surface minus that of the adjacent soil, as assessed with a $Cu/CuSO_4$ reference electrode. The current density for oxygen is shown constant at -1, corresponding to the limiting current density in this range of potentials. *Source*: Ref. 30. Reproduced with permission of The Electrochemical Society, Inc.

lower the pH, as indicated by the horizontal arrow. The "near" side of the cathode at $x = 0$ (opposite a point where the power supply is connected to the anode) is shown at -1.20 V, as negative as possible subject to the limitation on hydrogen evolution. The "far" side at $x = 0$ is shown at -0.907 V. Thus, in this example, there are 293 mV of potential variation in the soil between the near side and the far side.

In Figure 18.12 one can see the near and far sides of the cathode pipeline. How do we get the required current density to the far side without overprotecting the near side? Qualitatively, placement of the anode at a great distance means that the current can flow out in all directions from the anode and eventually approach the cathode from all directions, producing only a small potential variation in the soil next to the cathode. However, a large value of d will require a high overall cell potential. Furthermore, it will produce an electric field in the soil at some distance from the cathode, and this can interfere with other steel structures and cathodic protection systems in the area. This can be quite detrimental because another structure can provide an alternative path so that current flows in the soil to a near part of the third structure, through the third structure to a point near the cathode, and thence through the soil to the cathode. However, when the current leaves the third structure, there will be an anodic reaction that will lead to augmented corrosion and eventually failure of the third structure.

Finally, there is a limited right-of-way for placement of the anode, and it would be desirable to have uniform conductivity everywhere the current flows in the soil.

We can also ask how the proper distance d depends on the parameters of the problem. As formulated in the preceding discussion, these parameters include the current density i_{avg} required for protection, the size of the structure to be protected (here r_c), and the soil conductivity κ. In addition, there is the allowed window for proper protection, $\Delta\Phi_{\max} = 350$ mV, and the radius r_a of the anode. Some results of dimensional analysis will emerge as we treat the problem.

When concentration variations and nonuniformity in the soil can be ignored, the potential in the soil satisfies Laplace's equation 18.3. This is a nice equation because it is homogeneous and introduces no characteristic length or potential, and there is a wealth of experience in solving it by both analytic and numerical methods. For boundary conditions, we can say that the potential approaches zero at infinity. More particularly, we should say that no current flows to infinity (or to distant ground) from the anode–cathode system. The reduction of oxygen on the cathode has led us to the uniform-current-density condition there,

$$\kappa \frac{\partial \Phi}{\partial n} = i_{\text{avg}} \text{ on the cathode,} \tag{18.26}$$

where n is the normal distance pointing from the protected surface into the soil and i_{avg} is taken to be a positive number (see step 1 above). If the anode is relatively small, the current density will be fairly uniform on it while at the same time the potential in the soil is little dependent on the angle. We shall take

$$\Phi = \text{constant on the anode,} \tag{18.27}$$

where the constant is a value we wish to find in order to determine the rectifier voltage.

We now have a well-defined problem. The values of r_c, r_a, and d enter through the specification of "on the cathode" and "on the anode." If we use $\kappa\Phi/i_{\text{avg}}\, r_c$ as a dimensionless potential, then κ and i_{avg} will disappear as separate parameters in the problem. If we make lengths and position coordinates dimensionless with the cathode radius r_c, then only geometric length ratios will remain in the problem. One of these is d/r_c, whose value we need to find so that the constraint $\Delta\Phi < 0.350$ V is satisfied, where $\Delta\Phi$ is the magnitude of the potential variation in the soil adjacent to the protected surface. This condition is, of course, applied with the potentials made dimensionless with κ, i_{avg}, and r_c as described above. The remaining length ratio is r_a/r_c. Since this quantity is small, it will have a barely noticeable effect on $\Delta\Phi$, but it will still have a significant effect on the potential drop in the soil between the anode and the near part of the cathode because the resistance becomes very large for a very small anode radius.

Figure 18.14 shows equipotential contours in the soil for the geometric lengths depicted in Figure 18.12. The anode is the small dot toward the left, the cathode is the smallest semicircle toward the right, and the contour for $\Phi = 0$ extends to infinity. Current is being driven through the soil from the anode to the cathode, and thus the potentials, which satisfy Laplace's equation, decrease in this direction. The dimensionless normal potential gradient on the cathode is unity.

Laplace's equation was solved[30] by separation of variables in a coordinate system of bipolar circles in which the anode and cathode surfaces form natural boundaries. We can see that the potential on the cathode is not uniform because the contour for $\kappa\Phi/i_{\text{avg}} r_c = -2$ does not coincide with the surface. The equipotential contours are approximately circles in this problem. The student can sketch in current lines going from the anode to the cathode by making them perpendicular to the potential contours. The current lines are approximately circles also.

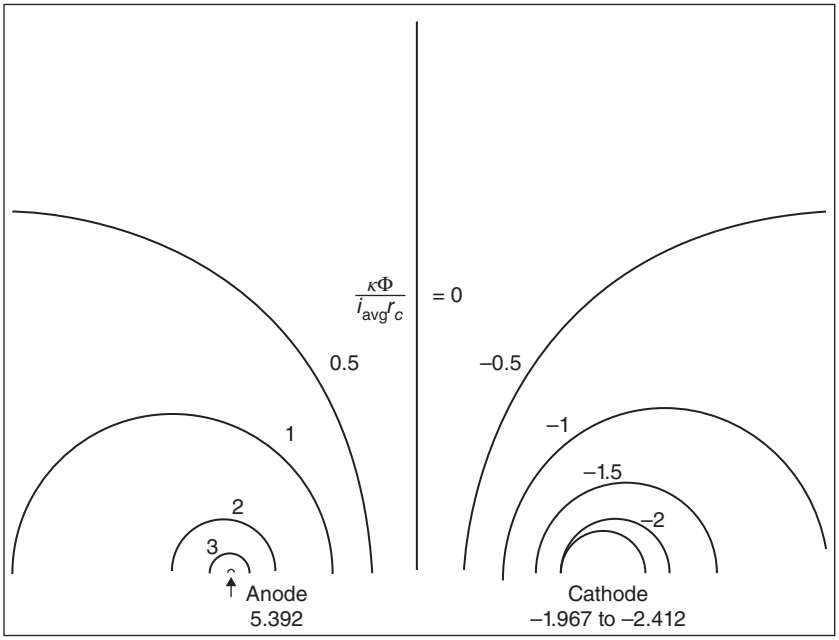

Figure 18.14 Equipotential contours (of the quantity $\kappa\Phi/i_{\text{avg}}r_c$) for the cathodic protection system with $r_c/r_a = 24$ and $d/r_c = 8$ and for a uniform current density on the cathode. *Source*: Ref. 30. Reproduced with permission of The Electrochemical Society, Inc.

In this problem, i_{avg} was set at 1.1 mA/m^2, and $\kappa = 10^{-3}$ S/m. Consequently, the dimensionless potentials depicted in Figure 18.14 must be multiplied by

$$i_{\text{avg}}r_c/\kappa = 1.1 \times 10^{-3} \times 0.6/10^{-3} = 0.66 \text{ V} \tag{18.28}$$

to obtain the actual potentials in the soil. This produces the potentials in the last column of Table 18.1 (with the exception of the value for the Mg anode). Thus, the potential variation in the soil between the near and far sides (from Figure 18.14) is $(2.412 - 1.967) \times 0.66 = 0.293$ V, and that between the anode and the near side of the cathode is $(5.392 + 1.967) \times 0.66 = 4.856$ V. Figure 18.11 explains the first two entries in column 2 of Table 18.1; based on other experiments, we add a 0.5 V kinetic overpotential to the anode, yielding a potential of 0.999 V, and the near part of the cathode is set at -1.2 V, the extreme limit defined earlier for proper cathodic protection. The values in the first column follow from those in columns 2 and 3. Thus, a potential difference of 7.056 V needs to be applied between the anode and the cathode at $x = 0$. About 2.2 V of "back EMF" (electromotive force) needs to be added to the potential difference in the soil between the anode and the near side of the cathode.

To understand the values at $x = L$, one needs to look at the method of powering the anode as shown in Figure 18.15. The anode has a resistance per unit length of $\rho' = 1.07$ mΩ/m, and the potential drop over a length L is

$$\Delta V = \rho' \pi r_c \, i_{\text{avg}} L^2. \tag{18.29}$$

Because the current is flowing from the anode to the cathode all along the length L, this value ΔV is half the value obtained if the total current flowed the entire length L along the anode. Figure 18.15

TABLE 18.1 Supplemental potential map for the base case

Location	Metal to ∞	Metal to soil	Soil to ∞
Anode	4.558	0.999	3.558
Cathode, near side, $x = 0$	−2.498	−1.2	−1.298
Cathode, far side, $x = 0$	−2.498	−0.907	−1.592
Cathode, near side, $x = L$	−2.448[a]	−1.15	−1.298
Cathode, far side, $x = L$	−2.448[a]	−0.857	−1.592
Mg anode (1.0 V overpotential)	−2.498	−1.686	−0.812

[a]The anode potential and the soil at the ∞ have changed by 50 mV from the value near the anode connector. The cathode itself is assumed to be of uniform potential.

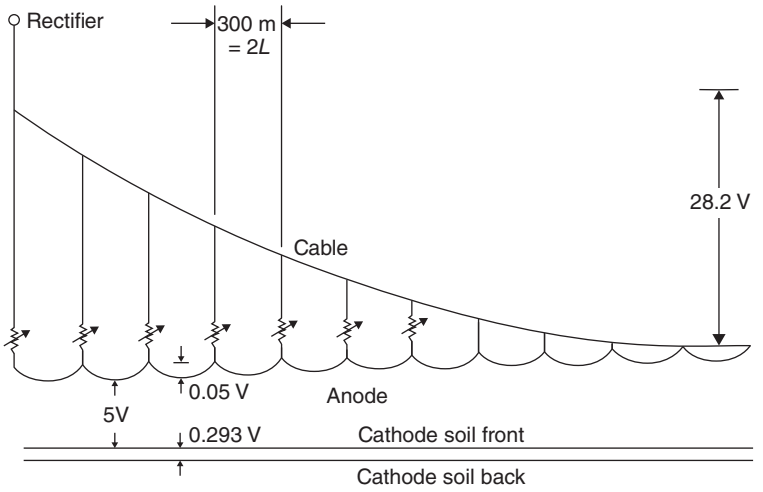

Figure 18.15 Potentials in the conductors of the system. Variable resistors are suggested between the anode and the power supply cable. *Source*: Ref. 30. Reproduced with permission of The Electrochemical Society, Inc.

calls for an anode connection every 300 m, selected so that the potential variation within the anode is about 50 mV. With $L = 150$ m and the values already given for the other parameters, $\Delta V = 0.050$ V. The consequence of the potential drop along the anode is that the cathode is less well protected at $x = L$ than at $x = 0$. Note that the 50 mV drop in the anode is not added to the rectifier requirement; that remains 7.056 V. The potential applied between the anode and the cathode at $x = L$ is reduced to 7.006 V, but the pipe is still adequately protected there because the cathode to far-side soil potential is still −0.857 V, less than the required −0.85 V. When designing the system, we must assure that the sum of the potential drop in the anode and the variation in the soil around the cathode remains less than 350 mV, the allowable potential window to prevent both iron dissolution and hydrogen evolution. This rule carries over to other geometries for cathodic protection.

Figure 18.16 presents the basis for design as a function of the geometric ratio d/r_c. The lower curve shows the dimensionless potential variation in the soil around the cathode. While shown for a particular value of r_c/r_a, this curve is not particularly sensitive to the value of the anode radius r_a. The upper curve for the dimensionless potential difference in the soil between the anode and the cathode is more sensitive to r_a because the current and potential lines are concentrated near a small anode.

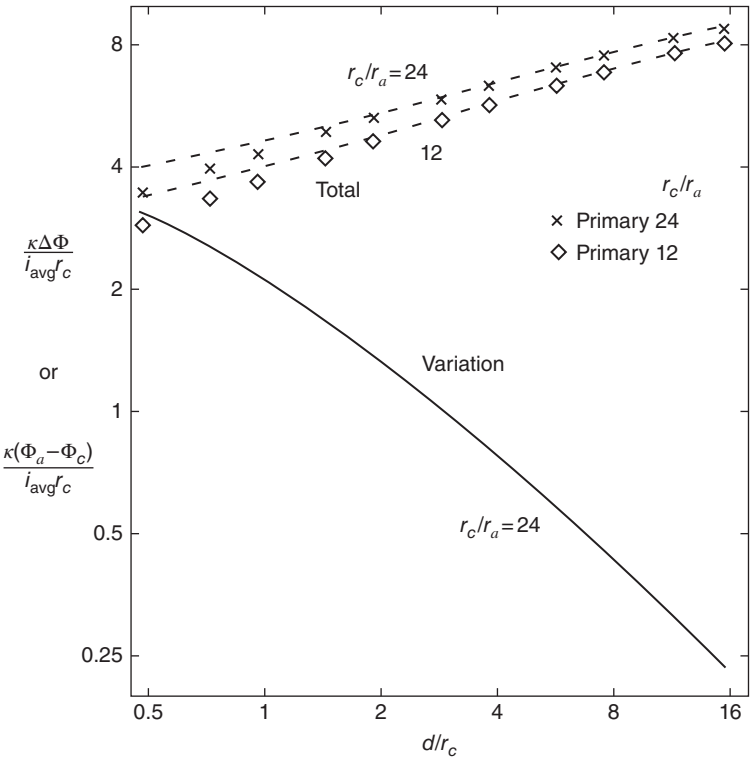

Figure 18.16 Variation of potential in the soil around the cathode and the average potential drop in the soil between the anode and the cathode. Note the logarithmic scales. For comparison, the points show the potential difference between the anode and the cathode when the soil potential near the cathode is uniform (corresponding to the primary current distribution in this system). *Source*: Ref. 30. Reproduced with permission of The Electrochemical Society, Inc.

(It would be somewhat more useful if the near point on the cathode were used instead of the average of the near and far points because then we could get the necessary applied potential by adding 2.2 V. See Figure 18.20.)

How do we use this design graph? First calculate $\kappa\Delta\Phi_{max}/i_{avg}r_c$ to find the allowed dimensionless potential variation around the cathode. You might want to use 300 mV for $\Delta\Phi_{max}$ instead of 350 mV to permit some potential variation within the anode itself. The calculated value constitutes the ordinate in Figure 18.16. Read across to the lower curve to find the distance d necessary to place the anode from the cathode. Then, read up to the appropriate upper curve to get the potential drop in the soil between the anode and the cathode as part of finding the required rectifier potential. A more difficult job, as governed by a larger value of the required current density i_{avg} or pipeline size r_c or soil resistivity $1/\kappa$ (or a smaller allowed potential variation $\Delta\Phi_{max}$), requires a greater distance of separation and correspondingly a larger rectifier potential. In the opposite extreme (of low soil resistivity, etc.), the anode could be placed very near the protected pipeline with little concern. There can be no rule of thumb for how many pipe diameters away to place the anode.

In some cases, it may be necessary or desirable to use two anodes instead of one. For example, the life of the anode may be longer if it carries less current. Or it may be desirable to reduce the rectifier

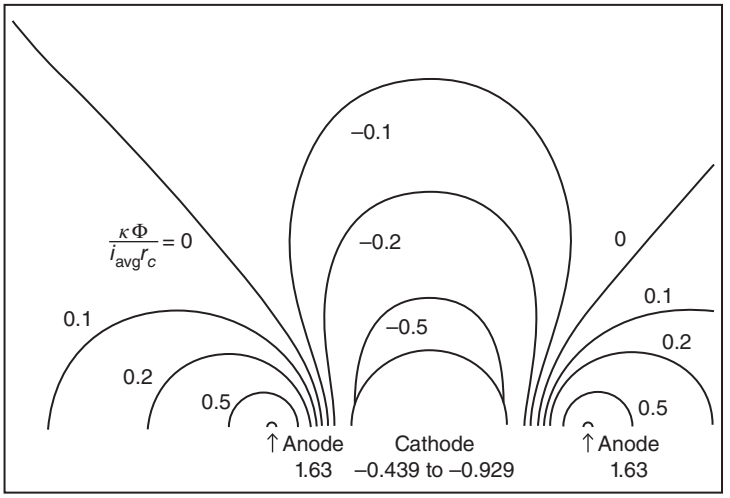

Figure 18.17 Equipotential contours for two symmetrically placed anodes, with $r_c/r_a = 24$ and $d/r_c = 1$. *Source*: Ref. 30. Reproduced with permission of The Electrochemical Society, Inc.

potential or reduce the spacing to confine the electric field to a region closer to the protected pipeline. If we ignore the interaction of the anodes, we can superpose the current and potential distributions due to single anodes placed at different positions.

Let us illustrate this with the two anodes placed symmetrically on opposite sides of the pipeline to be protected. Figure 18.17 shows potential contours for a spacing of $d/r_c = 1$. The potential distribution due to a single anode at this distance, shown in Figure 18.18, is reflected about a vertical plane through the center of the cathode to get the distribution due to the second anode placed to the right of the cathode. To get the distribution due to the two anodes, add the two distributions and divide by 2, since each anode now carries half the current of the cathode. The dimensionless potential at the near position of the cathode, thus, is $(0.6329 - 1.5109)/2 = -0.439$, as shown in Figure 18.17. The top of the pipeline now becomes the "far" point, with a dimensionless potential of -0.929.

With the same values of i_{avg}, r_c, and κ as before, the potential variation in the soil around the cathode at this anode spacing is $(0.929 - 0.439) \times 0.66 = 0.323$ V, still within the window for proper protection. At the same time, the potential difference in the soil from the anode to the near part of the cathode is $(1.629 + 0.439) \times 0.66 = 1.365$ V (and the required applied potential has dropped from 7.056 V for one anode to 3.564 V for two anodes).

In this manner, one can construct a design diagram for two anodes placed symmetrically on either side of the pipeline. This is shown in Figure 18.19 along with the potential variation for a single anode and asymptotic forms. For two anodes, the potential variation is less and decreases more rapidly with separation distance than for one anode. Similar plots could be developed for more anodes symmetrically, or perhaps even unsymmetrically, placed by paying more attention to the details of the potential distribution, for example, in Figure 18.18, for a single anode. The superposition method is approximate in the sense that the anodes do not remain equipotential surfaces, but the approximation is good for small anodes. The cathode does retain its uniform current density since two solutions are being superposed and each has a uniform current density on the cathode.

The potential difference in the soil between the anode and the near part of the cathode, which enters directly into the potential required of the rectifier, depends logarithmically on the anode radius.

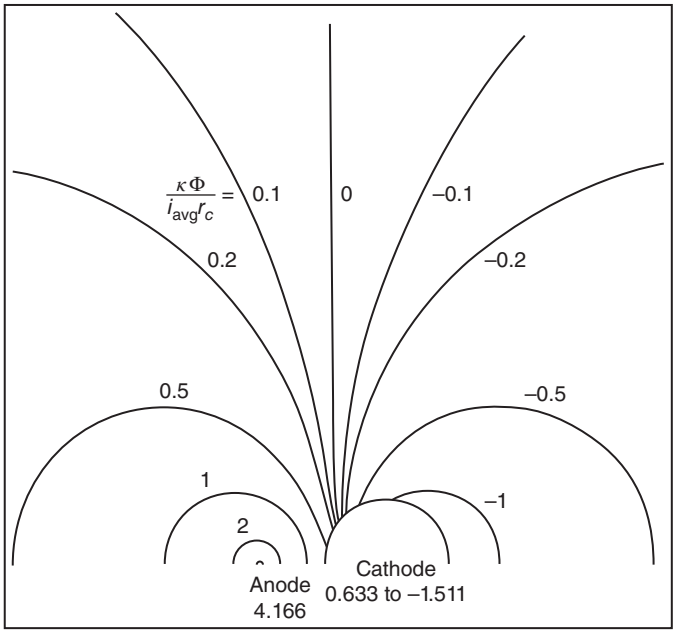

Figure 18.18 Equipotential contours for one anode, $r_c/r_a = 24$ and $d/r_c = 1$. *Source*: Ref. 30. Reproduced with permission of The Electrochemical Society, Inc.

By subtracting logarithmic terms, one can develop a method of plotting that shows predominantly a dependence on d/r_c. This is shown in Figure 18.20 for one anode and in Figure 18.21 for two anodes symmetrically placed. ($\kappa(\Phi_a - \Phi_{near})/i_{avg}r_c$ is the desired quantity and in Figure 18.20 is approximately equal to $\ln(D^2/r_a r_c)$. The correction to this approximation is what is actually plotted in the figure, and similarly for Figure 18.21.)

It is a simple matter to develop a design spreadsheet based on the asymptotes in Figures 18.19 to 18.21; see Table 18.2. The first column is supposed to emphasize the one-anode case shown in Figures 18.12, 18.14, and 18.16; column 2 treats the two-anode case illustrated in Figures 18.17, 18.19, and 18.21. The first block of rows shows the input design parameters for each case; the only difference here is the distance of the anode from the pipeline, d being 4.8 and 0.6 m in these two columns.

The second block of rows shows aspects of the one-anode design, including key potential differences in the soil. Column 1 is fine, but column 2 shows that the anode spacing of 0.6 m is too small and the potential window is exceeded (1320 mV), although the required anode-to-cathode potential is reduced (to 4.58 V).

The third block of rows has the same results but for the two-anode design. Here, the anode spacing of 0.6 m yields a potential variation near the cathode (330 mV) that is within the specification.

The bottom five rows summarize the rectifier requirements, showing that most of the ohmic potential drop occurs in the anode leads (see Figure 18.15). Fortunately, all of this drop does not appear as potential variation in the soil around the protected cathode.

The dashed lines in Figures 18.19 to 18.21 are used to obtain $\Phi_{near} - \Phi_{far}$ and $\Phi_{anode} - \Phi_{near}$. The potential drop in the anode comes from equation 18.29, and that in the anode leads comes from a similar equation.

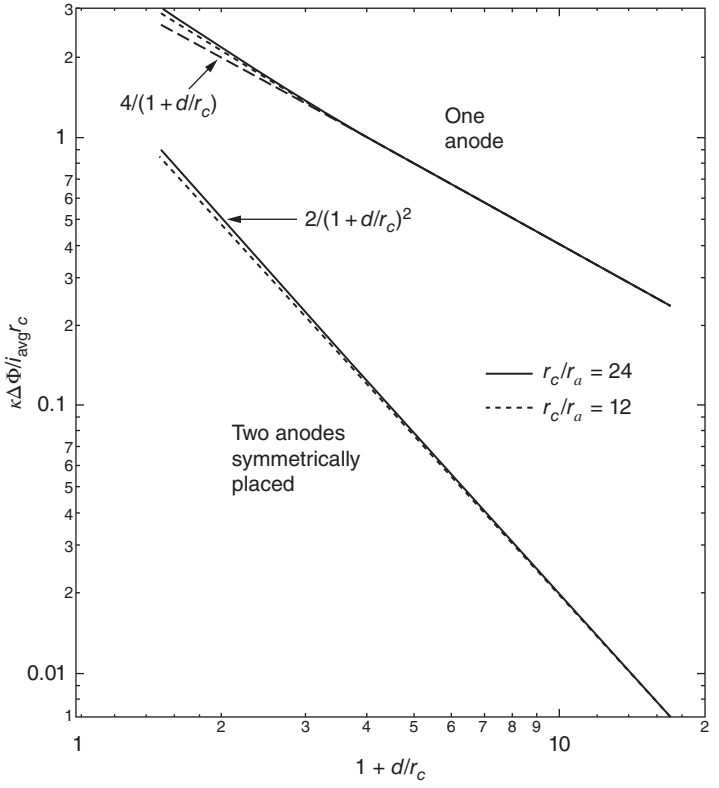

Figure 18.19 Variation of potential in the soil around the cathode for one or two anodes. Asymptotes of values of $\kappa\Delta\Phi/i_{avg}r_c$ for large d/r_c are also shown (dashed lines). *Source*: Ref. 30. Reproduced with permission of The Electrochemical Society, Inc.

Sacrificial Anodes

Instead of using an anode and an external power source, it is sometimes possible to use a metal that tends to be very negative by its own chemical nature. Zinc and magnesium are commonly used in this role.

Zinc finds itself at about −1.15 V relative to a $Cu/CuSO_4$ electrode in the adjacent soil. Directly connecting it electrically to a steel surface will protect the steel without any danger of overprotection. Hence, it is frequently used as a covering layer on the surface, for example by dipping in molten zinc, electroplating steel with zinc, or otherwise coating (*galvanized* steel). Even though there are small holes in the coating, the exposed steel is still cathodically protected. Zinc dissolves in preference to iron when electrons are required to reduce oxygen molecules arriving at the surface.

Because it is so negative, zinc would be expected to dissolve in water, with the liberation of hydrogen. However, the overpotential for H_2 evolution on pure Zn is quite high, and the intended application of zinc is practical.

Because zinc is only as negative as −1.15 V, it is limited in how large a surface can be protected by a remote zinc anode. It could not be used in the above pipeline example because there was required a 1.365 V potential drop in the soil between the anode and the near part of the pipe even in the two-anode system.

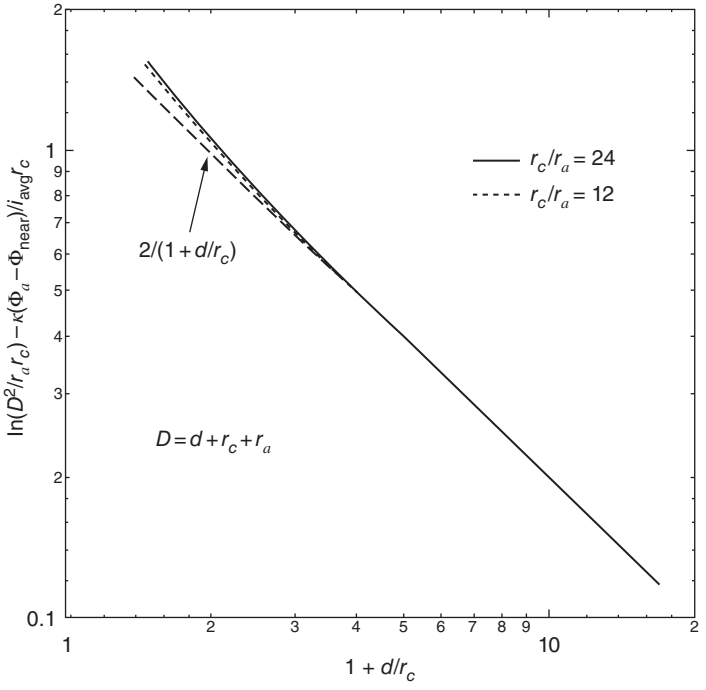

Figure 18.20 Correction for the potential difference in the soil between the anode and the near part of the cathode, for a cylindrical cathode with a single anode.

Magnesium has a theoretical open-circuit potential of about −2.7 V relative to a $Cu/CuSO_4$ reference electrode, but because of spontaneous reaction (producing hydrogen) it instead finds itself at about −1.7 V.[31] This means that the Mg has a limited life even if there is no additional current flow to protect a surface.

The more negative (than Zn) potential means that Mg could overprotect a surface. On the other hand, there is a greater possibility to place the anodes at a small distance in the soil from the surface to be protected. It is estimated[30] that the pipe treated above could be protected with 6 Mg anode wires (1.5 cm diameter) symmetrically placed around the pipe at a distance of 30 cm.

Passivation and Localized Corrosion

Figure 18.13 sketched the *passivation* of iron at a potential of about −0.4 V relative to a $Cu/CuSO_4$ reference electrode. The rate of dissolution drops to a negligible value because of the formation at this potential of a protective oxide film.

This passivation means that *anodic protection* could be used; apply a potential to the steel structure so that all parts stay within, say, −0.3 and +0.5 V relative to a $Cu/CuSO_4$ reference electrode by means of a power supply and an auxiliary cathode. In addition, the current density under passivation conditions may be small, for example, 1 mA/cm^2. These two factors combined yield a larger value of the design parameter $\kappa\Delta\Phi_{max}/i_{avg}r_c$. However, failure to achieve proper protection on all parts of the surface could lead to catastrophic failure.

The phenomenon of passivation also leads to localized corrosion, of which pitting corrosion is a good example to discuss. A tiny fracture of the protective oxide can occur on a stochastic basis. Subsequently,

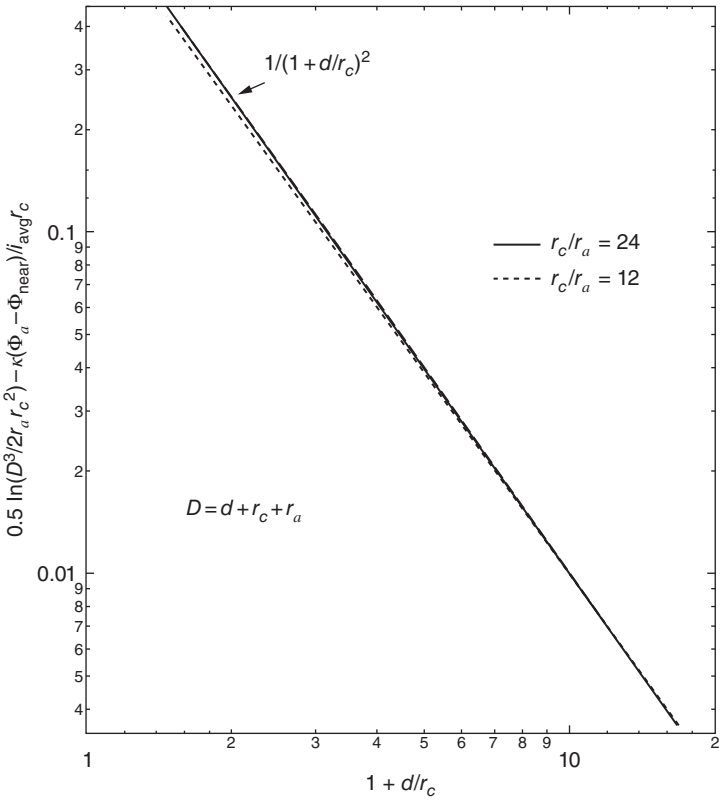

Figure 18.21 Correction for the potential difference in the soil between the anode and the near part of the cathode, for a cylindrical cathode with two anodes symmetrically placed.

an approximately hemispherical pit can form. Oxygen transport continues to the surrounding surface, which remains passivated. The anodic current required to balance this oxygen reduction is concentrated on the growing pit surface, and the resulting corrosion can be much more devastating than one might expect for conditions of uniform corrosion. Ionic migration into the anodic pit increases the chloride ion concentration, which enhances the instability of the passive oxide beyond that due to the lack of oxygen transport in this region.

Water-line corrosion and crevice corrosion are other forms of localized corrosion resulting from *differential aeration* of the surface.

Stainless steels achieve greater corrosion resistance by passivating more easily—that is, by being able to sustain only a small anodic current density before the passive oxide film appears.

PROBLEMS

18.1 The inner radius of a capillary tube is r_0, and its length is L. An electrode entirely fills the cross section at one end. The outer radius of the capillary tube can be taken to be very large, and the counterelectrode is placed a great distance from the open mouth of the capillary tube.

(a) Describe in words or with a sketch the primary distribution of current on the electrode at the end of the capillary. Consider explicitly the cases where L is very large or very small.

TABLE 18.2 Design spreadsheet

	Protection of one pipeline with parallel cylindrical anodes	
4.8	0.6	m, distance of anode from pipeline, d
100,000	100,000	Ω cm, soil resistivity
0.00107	0.00107	Ω/m, anode resistance per unit length
1.1	1.1	mA/m^2, pipe current density
26	26	mA/m, maximum allowed anode current per unit length
150	150	m, half the distance between anode connections, L
2.5	2.5	cm, anode radius, r_a
0.6	0.6	m, pipe radius, r_c
	One-anode design	
0.44444	2	dimensionless potential, near-far
7.35952	3.60559	dimensionless potential, anode-near
293.33	**1320**	mV, soil potential difference, near-far
4.86	**2.38**	V, soil potential difference, anode-near
4.15	4.15	mA/m, anode current per unit length
49.92	**49.92**	mV, ohmic drop in anode
1.24	1.24	A, required current per anode connection
7.06	4.58	V, applied potential at $x = 0$
	Two-anode design	
0.02469	0.5	dimensionless potential, near-far
4.53287	2.0631	dimensionless potential, anode-near
16.30	**330.00**	mV, soil potential difference, near-far
2.99	**1.36**	V, soil potential difference, anode-near
2.07	2.07	mA/m, anode current per unit length
24.96	**24.96**	mV, ohmic drop in anode
0.62	0.62	A, required current per anode connection
5.19	3.56	V, applied potential at $x = 0$
3600.00	3600.00	m, pipe length to be protected with one rectifier
0.0042	0.0042	Ω/m, lead wire resistance per unit length
28.22	28.22	V, lead wire potential drop
14.93	14.93	A, rectifier current
35.27	32.80	V, rectifier potential (one anode)

Bold numbers call attention to critical numbers in the design with respect to the allowed potential variation of 350 mV in the soil adjacent to the protected structure.

(b) Tell how the secondary current distribution on the electrode might be different from that described in part (a).

(c) For a capillary length several times the capillary diameter, the resistance of the system can be approximated by the value $L/\pi r_0^2\kappa$, where κ is the conductivity of the electrolytic solution. This expression does not include an end effect corresponding to the gathering together of the current lines as they enter the capillary tube from the bulk solution. To assess this end effect, what differential equation should be solved to determine the potential distribution in the region near the mouth of the capillary tube? Ignore concentration variations. Write out the equation and state its name. If you write out the equation in a particular coordinate system, be sure to define that coordinate system.

(d) Indicate carefully the boundary conditions to be satisfied by the solution of the differential equation of part (c). Phrase the problem so that the length L of the capillary tube will

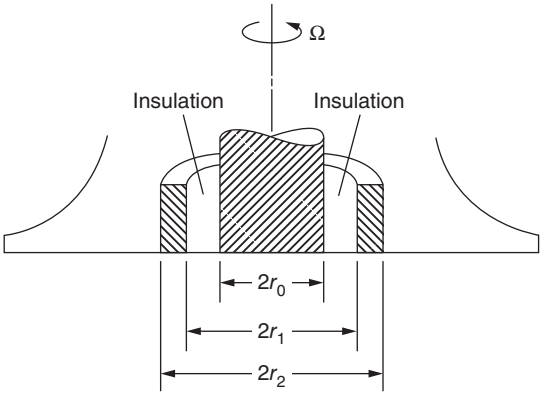

Figure 18.22 Ring–disk electrode, frequently rotated to provide a known hydrodynamic flow.

not be involved in the determination of the end-effect correction. That is, take L to be so large that its value does not affect the potential distribution in the region near the open mouth of the tube. Be sure to state enough boundary conditions to determine the potential distribution in this region, but do not state any extra boundary conditions.

(e) If you had before you the solution to the problem posed in parts (c) and (d), how would you evaluate the end-effect correction to the resistance?

(f) From dimensional considerations state the order of magnitude of the end-effect correction as a resistance to be added to the value stated in part (c).

18.2 A sectioned electrode is to be used to test the efficacy of plating baths. In an insulating plane, there is a disk electrode of radius r_0 surrounded by an insulated surface from $r = r_0$ to $r = r_1$, which in turn is surrounded by a *ring* electrode from $r = r_1$ to $r = r_2$ (see Figure 18.22). This device is rotated just like a conventional rotating-disk electrode. The ring and disk electrodes are maintained at the same potential (with a distant counterelectrode), but the current can be measured separately to each.

(a) Describe the limiting-current distribution on this two-electrode system. What happens as the gap distance $r_1 - r_0$ goes to zero?

(b) If the exchange current density is about 10^{-3} A/cm^2 and the solution conductivity is about 0.01 S/cm at 35°C, how large should the ring–disk system be for the ring electrode to have an average current density about 1.5 times that of the disk electrode? Assume that the areas of the ring and disk are about equal and that the gap is of negligible width. To measure approximately the exchange current density by this technique, it is desirable to operate under conditions such that linear electrode kinetics applies.

(c) What is the maximum current that should be passed to ensure that the system is operated in the linear range and not in the Tafel range? State *your* criterion clearly before calculating the result.

(d) At this current, estimate the difference in ohmic potential drop to the ring and disk electrodes. State clearly the assumptions you make as you arrive at a numerical value.

(e) At this current, it is desired to operate at 10% (or less) of limiting current. What minimum rotation speed does this imply if the gold reactant (in the form of $KAu(CN)_2$) is at a concentration of 0.02 mol/liter in the bulk? Assume values of any other physical properties you need.

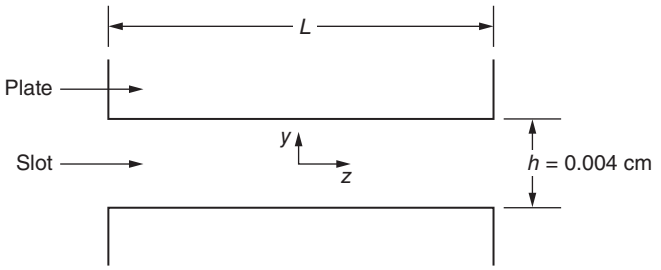

Figure 18.23 A section of a plate of thickness L with a two-dimensional slot of width h through its thickness.

18.3 It is desired to copper plate the faces of printed-circuit boards that are 20 cm long, 10 cm wide, and 0.02 cm thick. Not only are the faces to be plated, but also the holes, which are 0.004 cm in diameter, are to have a thin coating of copper. A circuit board is in a well-stirred plating bath between two counterelectrodes placed 3 cm from each face.

(a) Sketch the primary distribution of the current across the entire face of the circuit board. Sketch also the primary distribution within a hole and on the adjacent part of the face.

(b) Describe how the secondary current distribution would be expected to differ from the primary distribution.

(c) Set up, but do not solve, the equations and boundary conditions for the secondary distribution on the face of the circuit board. For this purpose, ignore the holes in the board. Polypropylene holders position the board in the middle of the tank, but at the same time they mask off 0.5 cm on two opposite edges of the board. Otherwise, the boards fill the entire cross section of the cell.

18.4 A plate of thickness L has a two-dimensional slot of width h through its thickness (see Figure 18.23). The origin of rectangular coordinates is at the centerline of the plate and the centerline of the slot. Two counterelectrodes are equally spaced on either side of the plate. We want to consider the possibility that deep within the slot the potential distribution is given by

$$\Phi = A \cosh \frac{\lambda z}{h} \cos \frac{\lambda y}{h},$$

where A is a constant.

(a) Does this potential distribution satisfy Laplace's equation?

(b) What boundary condition would be satisfied along the centerline of the plate ($z = 0$)? Is this reasonable from the point of view of the symmetry conditions prevailing for this system? Is this reasonable from the point of view of the suggested analytic form for the potential?

(c) What boundary condition would be satisfied along the centerline of the slot ($y = 0$)? Is this reasonable from the point of view of the symmetry conditions prevailing for this system? Is this reasonable from the point of view of the suggested analytic form for the potential?

(d) Is there a saddle point in the potential at the origin?

(e) Along the electrode surface (within the slot), what is the distribution of the current density that contributes to the overall electrode current?

(f) For a deep slot, what is the penetration depth according to the suggested analytic solution? (When quantities vary exponentially with distance, the penetration depth is the distance over which such quantities vary by a factor of e.)

(g) For the primary current and potential distribution, determine the parameter λ and a numerical value for the penetration depth. (The plate potential is zero.)

(h) For the secondary distribution, where linear electrode kinetics is obeyed with an exchange current density of $i_0 = 5 \times 10^{-4}$ A/cm^2, discuss how to determine the parameter λ and a numerical value for the penetration depth. A clear graphical method for determining λ and an indication of how its value depends on the magnitude of i_0 would be sufficient.

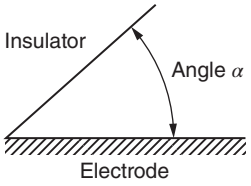

Figure 18.24 An electrode at angle $\theta = 0$ meets an insulator at angle $\theta = \alpha$.

18.5 An electrode at angle $\theta = 0$ meets an insulator at angle $\theta = \alpha$ (see Figure 18.24). Show how the primary current and potential distributions vary in this corner region by solving Laplace's equation in an appropriate coordinate system with appropriate boundary conditions. Assume that the potential shows a power dependence on the distance r from the corner itself.

18.6 Pitting corrosion involves the growth of a hemispherical pit in a ferrous alloy. The hemispherical surface dissolves in the active region at a current density of 5 A/cm^2, while the surrounding plane is passivated and can be approximated as an insulator (with the counterelectrode far away, at infinity). When the pit has grown to a diameter of 0.2 mm, estimate the potential in the solution at two positions—the lip of the pit and the base of the pit—both relative to the solution far away. Use an order-of-magnitude estimate. The electrolytic solution has a conductivity of 0.07 S/cm.

18.7 The Hull cell (see Figure 18.25) is used to test the "throwing power" of plating baths by assessing how nonuniform a deposit will form on an electrode, all parts of which are not equally accessible. There are two planar electrodes at opposite ends of the cell; one electrode is perpendicular to four insulating boundaries of the cell, but the other is at an angle α with one of the insulating walls, as shown. The cell also reveals the nature of the deposit that will form at the different current densities that occur along its surface.

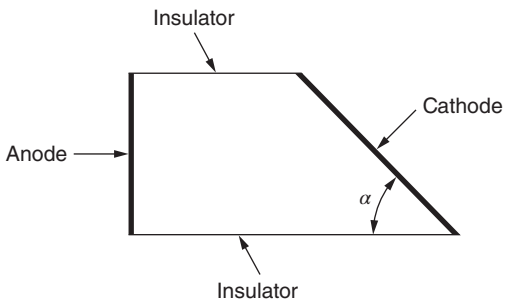

Figure 18.25 Top view of the Hull cell.

As an extreme case, it is desired to calculate the maximum potential variation that can occur in the solution adjacent to each electrode, and it is assumed that this occurs when there is a uniform current density on each electrode. Determine this distribution of potential in the solution under this condition and evaluate the maximum potential variation in the solution adjacent to each electrode. Further assume for this calculation that the solution is very well stirred and that the metal of each electrode is a very good electrical conductor.

Obtain numerical values for the case where the anode is 10 cm by 10 cm and is 10 cm from the cathode at the nearest point, the angle α is 45°, the current density on the anode is 20 mA/cm^2, and the solution conductivity is 0.06 S/cm.

18.8 The primary current distribution frequently represents the opposite extreme of being nonuniform on electrodes. Sketch the primary distributions on the two electrodes of the Hull cell and discuss any salient features shown on the sketch.

18.9 The solution placed in the Hull cell has 0.1 mol/liter of $AgNO_3$ with more or less supporting electrolyte of HNO_3, and the electrodes are both silver. In the absence of any overt stirring in the cell, which electrode would be expected to reach a limiting current first? Cite formulas, principles, and methods by which you would estimate the average limiting-current density on this electrode.

18.10 A copper disk rotated in seawater is observed to corrode preferentially near the periphery. An iron disk, on the other hand, is observed to corrode preferentially near the center. Discuss qualitatively these observations.

18.11 Two plane insulators meet at an angle α. It is desired to ascertain the distributions of current and potential near such a corner. In particular, how much current penetrates into an acute corner, and might current densities reach infinity for some large angles? Write down Laplace's equation in cylindrical coordinates, where the z axis is the line of intersection of the insulating planes. Seek the simplest, nontrivial solution for the potential Φ with no z dependence and satisfaction of the correct boundary conditions on the insulators.

18.12 In Problem 18.5, the primary potential distribution near an electrode edge was determined. This distribution is strictly valid only when the polarization parameter (J or δ) is infinite. For large, finite values of the polarization parameter, this distribution is a good approximation for large $\bar{r}$, where for linear kinetics $\bar{r} = r(\alpha_a + \alpha_c)Fi_0/RT\kappa$ and for Tafel kinetics $\bar{r} = r(\alpha_a FP_0/RT\kappa)^{2\beta/\pi}$ and where β is the angle between the insulator and the electrode (written as α in Problem 18.5). Near the corner, the primary current density on the electrode varies as $i_n \to P_0 r^{\beta}$, where P_0 is a parameter which depends on the overall geometry and current.

(a) Substitute $\bar{r}$ and a stretched potential,

$$\overline{\varphi} = \frac{\alpha_a F}{RT}(V - \Phi) - \frac{2\beta}{\pi} \ln \frac{\alpha_a FP_0}{RT\kappa} + \ln \frac{\alpha_a Fi_0}{RT\kappa},$$

into a Tafel kinetics boundary condition and a matching condition,

$$\Phi(\bar{r} \to \infty) = -\frac{2\beta}{\pi\kappa} P_0 r^{\pi/2\beta} \sin \frac{\pi\theta}{2\beta},$$

to show that the resulting problem statement, in terms of the stretched variables, is free of parameters. (Assume that $V = 0$.) Use the stretched variables to predict how the current density at the electrode edge depends on P_0 for large P_0.

(b) For linear kinetics, how must the potential be stretched for the problem statement to be free of parameters? How does i_{edge}/i_{avg} depend on i_0 for large exchange current densities? In both cases, the results should show that i_{edge}/i_{avg} approaches an infinite value for obtuse angles and a zero value for acute angles.

18.13 Calculate the potential and pH values in Figure 18.9 from the following thermodynamic data (at 25°C):

Substance	State	μ_i^0(kJ/mol)
Fe	Solid	0
Fe^{2+}	Dilute	−78.90
$Fe(OH)_2$	Solid	−486.5
OH^-	Dilute	−157.244
Fe^{3+}	Dilute	−4.7
H^+	Dilute	0
H_2	Gas	0
O_2	Gas	0
H_2	Liquid	−237.129

18.14 What is the p_{O_2} value at the position of the H_2 line on Figure 18.9?
Answer: $\exp(-1.229 \times 96487/2 \times 8.3143 \times 298.15) = 4.1 \times 10^{-11}$ bar.

18.15 Compare and contrast the parameter analysis below equation 18.27 with the dimensional analysis in Sections 18.2 and 18.3 for primary and secondary current distribution problems.

18.16 A large horizontal steel surface (the bottom of a storage tank) is to be cathodically protected by a series of horizontal anodes of radius r_a buried at a depth h below the protected surface and spaced (center to center) at a distance d from each other.

(a) Draw a clear sketch of the geometric situation. Emphasize a repeating section. Label clearly the "near" point and the "far" point on the protected surface.

(b) Define the dimensionless design correlation that should be put together to cover this situation, if the protected surface can be assumed to require a uniform cathodic protection current density i_{avg} (taken to be positive for convenience), the soil can be assumed to have a uniform conductivity κ, and the protected surface is required to be maintained between −0.85 and −1.20 V relative to an adjacent $Cu/CuSO_4$ reference electrode. What geometric ratios govern the problem?

(c) What differential equation and boundary conditions should govern the potential distribution in this problem? Make liberal use of the sketch developed in part (a).

(d) Discuss qualitatively how the design criteria would depend on a critical geometric ratio. Use a sketch to illustrate this result.

18.17 Discuss using $\kappa\Delta\Phi_{max}/i_{avg}$ as a length characteristic of how large a cathode can be protected cathodically.

18.18 Derive equation 18.29.

18.19 The cathode current density shown in Figure 18.13 is not strictly constant in the range from −0.85 to −1.20 V relative to a saturated $Cu/CuSO_4$ reference electrode. Discuss as quantitatively as possible whether the design procedure using the constant oxygen reduction

current density is conservative if the criterion for proper design remains as stated in terms of the cathode potential relative to the adjacent soil.

18.20 Develop Problem 18.19 more fully and discuss the greater complexity, not in terms of computation but in terms of expressing the results in simple design plots.

18.21 The criterion of potential range is frequently applied in a current-off or interruption method. Is this the same as looking at the potential with the current on? (See Ref. [32].) Do ohmic drops really disappear when the current is interrupted, or should the same care be exercised to extrapolate the soil potential to the surface of the cathode? Estimate a time constant, based on the double-layer capacity ($r_c C/\kappa$).

18.22 Interpret the Pourbaix diagram (Figure 18.9) to determine whether reaction 18.23 occurs spontaneously. Indicate your reasoning.

18.23 Sketch current lines on an equipotential diagram such as Figure 18.14 or 18.17.

NOTATION

c_i	concentration of species i, mol/cm^3
F	Faraday's constant, 96,487 C/mol
h	distance between walls of flow channel, cm
i_n	normal component of current density at an electrode, A/cm^2
i_0	exchange current density, A/cm^2
I	total current, A
J	dimensionless exchange current density
K	complete elliptic integral of the first kind
L	length of electrodes, cm
L	characteristic length, cm
r	radial position coordinate, cm
r_0	radius of disk electrode, cm
R	universal gas constant, 8.3143 J/mol·K
R	resistance, Ω
T	absolute temperature, K
u_i	mobility of species i, cm^2 mol/J·s
V	potential of an electrode, V
W	width of electrodes, cm
Wa	Wagner number
x	distance measured along an electrode surface, cm
y	normal distance from the surface, cm
z_i	charge number of species i
α_a, α_c	transfer coefficients
δ	dimensionless average current density
ϵ	$\pi L/2h$
η_s	surface overpotential, V
κ	conductivity, S/cm
Φ	electric potential, V

Subscripts

avg	average
0	at the electrode surface

REFERENCES

1. H. S. Carslaw and J. C. Jaeger, *Conduction of Heat in Solids* (Oxford: Clarendon Press, 1959).
2. John David Jackson, *Classical Electrodynamics* (New York: Wiley, 1975).
3. L. M. Milne-Thomson, *Theoretical Hydrodynamics* (New York: Macmillan, 1960).
4. Robert H. Rousselot, *Répartition du potentiel et du courant dans les électrolytes* (Paris: Dunod, 1959).
5. John Kronsbein, "Current and Metal Distribution in Electrodeposition. I Critical Review of the Literature," *Plating*, *37* (1950), 851–854.
6. R. N. Fleck, *Numerical Evaluation of Current Distribution in Electrochemical Systems*, MS thesis, University of California, Berkeley, September 1964 (UCRL-11612).
7. Alan C. West and John Newman, "Determining Current Distributions Governed by Laplace's Equation," *Modem Aspects of Electrochemistry*, *23* (1992), 101–147.
8. H. Fletcher Moulton, "Current Flow in Rectangular Conductors," *Proceedings of the London Mathematical Society* (ser. 2), *3* (1905), 104–110.
9. Ruel V. Churchill, *Complex Variables and Applications* (New York: McGraw-Hill, 1960).
10. Milton Abramowitz and Irene A. Stegun, eds., *Handbook of Mathematical Functions*, (Washington, DC: National Bureau of Standards, 1964), p. 608.
11. Charles Kasper, "The Theory of the Potential and the Technical Practice of Electrodeposition," *Transactions of the Electrochemical Society*, *77* (1940), 353–384; 78 (1940), 131–160; 82 (1942), 153–184.
12. Fumio Hine, Shiro Yoshizawa, and Shinzo Okada, "Effect of Walls of Electrolytic Cells on Current Distribution," *Journal of the Electrochemical Society*, *103* (1956), 186–193.
13. Carl Wagner, "Calculation of the Current Distributions at Electrodes Involving Slots," *Plating*, *48* (1961), 997–1002.
14. Kaoru Kojima, "Engineering Analysis of Electrolytic Cells: Electric Resistance between Electrodes," *Research Reports of the Faculty of Engineering. Niigata University*, No. 13 (1964).
15. Ulrich Grigull, *Die Grundgesetze der Wärmeübertragung* (Berlin: Springer, 1955), p. 117.
16. John Newman, "Resistance for Flow of Current to a Disk," *Journal of the Electrochemical Society*, *113* (1966), 501–502.
17. Ruel V Churchill, *Fourier Series and Boundary Value Problems* (New York: McGrawHill, 1963).
18. Parry Moon and Domina Eberle Spencer, *Field Theory Handbook* (Berlin: Springer, 1961).
19. T. P. Hoar and J. N. Agar, "Factors in Throwing Power Illustrated by Potential-Current Diagrams," *Discussions of the Faraday Society*, No. *1* (1947), 162–168.
20. John Newman, "Current Distribution on a Rotating Disk below the Limiting Current," *Journal of the Electrochemical Society*, *113* (1966), 1235–1241.
21. Carl Wagner, "Theoretical Analysis of the Current Density Distribution in Electrolytic Cells," *Journal of the Electrochemical Society*, *98* (1951), 116–128.
22. N. P. Gnusin, N. P. Poddubnyĭ, E. N. Rudenko, and A. G. Fomin, "Raspredelenie toka na katode v vide polosy v poluprostranstve elektrolita s polyarizatsionnoĭ krivoĭ vyrazhaemoĭ formulaĭ Tafelya," *Elektrokhimiya*, *1* (1965), 452–459.
23. W. R. Parrish and John Newman, "Current Distribution on a Plane Electrode below the Limiting Current," *Journal of the Electrochemical Society*, *116* (1969), 169–172.

24. W. R. Parrish and John Newman, "Current Distributions on Plane, Parallel Electrodes in Channel Flow," *Journal of the Electrochemical Society*, *117* (1970), 43–48.
25. Leonard Nanis and Wallace Kesselman, "Engineering Applications of Current and Potential Distributions in Disk Electrode Systems," *Journal of the Electrochemical Society*, *118* (1971), 454–461.
26. Ralph White and John Newman, "Simultaneous Reactions on a Rotating-Disk Electrode," *Journal of Electroanalytical Chemistry*, *82* (1977), 173–186.
27. Sonny Xiao-zhe Li and John Newman, "Cathodic Protection for Disks of Various Diameters," *Journal of the Electrochemical Society*, *148* (2001), B157–B162.
28. John Newman and J. E. Harrar, "Potential Distribution in Axisymmetric Mercury-Pool Electrolysis Cells at the Limiting Current," *Journal of the Electrochemical Society*, *120* (1973), 1041–1044.
29. William H. Smyrl and John Newman, "Detection of Nonuniform Current Distribution on a Disk Electrode," *Journal of the Electrochemical Society*, *119* (1972), 208–212.
30. John Newman, "Cathodic Protection with Parallel Cylinders," *Journal of the Electrochemical Society*, *138* (1991), 3554–3560.
31. Mars G. Fontana and Norbert D. Greene, *Corrosion Enginering* (New York: McGrawHill, 1978).
32. John Newman, "Ohmic Potential Measured by Interrupter Techniques," *Journal of the Electrochemical Society*, *117* (1970), 507–508.

CHAPTER 19

EFFECT OF MIGRATION ON LIMITING CURRENTS

Chapter 17 treated convective-transport problems, mostly at the limiting current and with an excess of supporting electrolyte. A relatively simple problem results if the current is maintained at a limiting value, but the concentration of supporting electrolyte is reduced relative to the concentration of the reacting ions. Since the current is at its limiting value, the ohmic potential drop in the bulk of the solution is still negligible,* and the current distribution is determined by mass transfer in the diffusion layer. However, the presence of an electric field in the diffusion layer can lead to an increase or a decrease in the limiting current due to migration of the reacting ions.

Let us regard Figure 17.1 as the concentration profile of $CuSO_4$ for deposition at the limiting current. Within the diffusion layer, migration and diffusion contribute to mass transfer. The electric field is then very high at the electrode surface because the concentration is zero there. If we now add an inert electrolyte, such as H_2SO_4, the electric field will be greatly diminished, particularly at the electrode surface. The contribution of migration decreases, and the limiting current is reduced.

Because of the electroneutrality condition 16.3, solutions of only two ions also satisfy the equation of convective diffusion 17.2 but with D_i, replaced by the diffusion coefficient D of the electrolyte (see Section 11.4). Consequently, it is relatively simple to solve convective-transport problems at the limiting current for these solutions (see Section 17.13). These results indicate an enhancement of the limiting current compared to the same discharging ions in a solution with excess inert electrolyte, and this can be attributed to the effect of migration in the diffusion layer.

There is some interest in calculating the limiting current for intermediate cases where there is some inert electrolyte but not a large excess. Eucken[1] gave the solution for three ion types in systems that could be represented by a stagnant Nernst diffusion layer (see also reference [2]). Because experimental data[3] for the discharge of hydrogen ions on growing mercury drops did not agree with Eucken's formula, Heyrovský[4] rejected his method and introduced a correction factor involving

*However, a nonuniform ohmic potential drop can lead to a secondary reaction, such as decomposition of the solvent, on one part of the electrode before the limiting current can be attained on another part of the same electrode.

Electrochemical Systems, Fourth Edition. John Newman and Nitash P. Balsara.

the transference number of the discharging ion. This transference-number correction is not based on quantitative arguments, but it has become entrenched in the electrochemical literature.

Okada et al.[5] have considered the effect of ionic migration on limiting currents for a growing mercury drop, and Gordon et al.[6] for a rotating-disk electrode. Newman[7] has treated the effect for four cases: the rotating disk, the growing mercury drop, penetration into a semi-infinite medium, and the stagnant Nernst diffusion layer. The ratio I_L/I_D of the limiting current to the limiting diffusion current, calculated as in Chapter 17 on convective-transport problems with excess supporting electrolyte, is a convenient measure of the effect of migration and depends on the ratios of concentrations in the bulk solution.

The effect of migration on limiting currents is a simple example of a phenomenon that does not occur in nonelectrolytic systems, in contrast to the convective-transport problems that have direct analogs in heat transfer and nonelectrolytic mass transfer.

19.1 ANALYSIS

For the rotating disk, the normal component of the velocity depends only on y, the distance from the disk (see Section 15.4). Consequently, c_i, and Φ also depend only on y in the diffusion layer, and the limiting-current density is uniform over the surface of the disk. Equations 16.1 and 16.2 can be combined to yield

$$D_i \frac{d^2 c_i}{dy^2} - v_y \frac{dc_i}{dy} + z_i u_i F \left(c_i \frac{d^2 \Phi}{dy^2} + \frac{dc_i}{dy} \frac{d\Phi}{dy} \right) = 0. \tag{19.1}$$

We further approximate the velocity by the first term of its power series expansion in y:

$$v_y = -a\Omega \sqrt{\frac{\Omega}{\nu}} y^2, \tag{19.2}$$

where $a = 0.51023$. This approximation should be valid within the diffusion layer at high Schmidt numbers. With the new variable

$$\xi = y \left(\frac{a\nu}{3D_R} \right)^{1/3} \sqrt{\frac{\Omega}{\nu}}, \tag{19.3}$$

where D_R is the diffusion coefficient of the limiting reactant, equation 19.1 becomes

$$\frac{D_i}{D_R} c_i'' + 3\xi^2 c_i' + \frac{z_i u_i F}{D_R} (c_i \Phi'' + c_i' \Phi') = 0, \tag{19.4}$$

where primes denote differentiation with respect to ξ.

There is one equation of the form of equation 19.4 for each solute species. These equations are to be solved in conjunction with the electroneutrality equation 16.3 for the solute concentrations c_i and the potential Φ.

For boundary conditions we can state

$$c_i = c_{i\infty} \quad \text{at } \xi = \infty, \quad \Phi = 0 \quad \text{at } \xi = \xi_{\max}, \tag{19.5}$$

where $\xi_{\max}$, the zero of potential, can be chosen arbitrarily. Let the electrode reaction be represented by equation 16.7. Then, the normal component of the flux density of a species at the electrode is related to the normal component of the current density by equation 16.8. Since we do not know the current density in advance, we instead relate the flux density of a species to the flux of the limiting reactant:

$$z_i u_i F c_i \frac{\partial \Phi}{\partial y} + D_i \frac{\partial c_i}{\partial y} = \frac{s_i}{s_R} \left(z_R u_R F c_R \frac{\partial \Phi}{\partial y} + D_R \frac{\partial c_R}{\partial y} \right) \tag{19.6}$$

at $y = 0$. In terms of the variable ξ, this becomes

$$z_i u_i F c_i \Phi' + D_i c_i' = \frac{s_i}{s_R}(z_R u_R F c_R \Phi' + D_R c_R') \quad \text{at } \xi = 0. \tag{19.7}$$

The boundary condition for the limiting reactant at the limiting current is

$$c_R = 0 \quad \text{at } \xi = 0. \tag{19.8}$$

These boundary conditions should be sufficient for the problem at hand. Equations 19.4 and 16.3 constitute a set of coupled, nonlinear, ordinary differential equations with boundary conditions at zero and infinity. These can be solved readily by the numerical method described in Appendix C. In fact, the computer program for this particular problem is reproduced there. The results are discussed in the next few sections. After the concentration and potential profiles are calculated, the limiting current density can be obtained from the flux of the limiting reactant. The ratio I_L/I_D of the limiting current to the limiting diffusion current is a convenient measure of the effect of migration.

The problem is similar for the effect of migration in other hydrodynamic situations. For a mercury drop growing in a solution that initially had a uniform composition, the transient transport equations can be reduced to

$$\frac{D_i}{D_R} c_i'' + 2\xi c_i' + \frac{z_i u_i F}{D_R}(c_i \Phi'' + c_i' \Phi') = 0, \tag{19.9}$$

if we make the same approximations as are used in the derivation of the Ilkovič equation 17.81 (without the correction term). Equation 19.9 replaces equation 19.4 for the disk. For a mercury drop growing at a constant volumetric rate, ξ has the meaning

$$\xi = y\left(\frac{7}{12 D_R t}\right)^{1/2}, \tag{19.10}$$

although the analysis is not restricted to this case.

For mass transfer to a plane electrode from an infinite, stagnant medium, the transient transport equations also reduce to equation 19.9, where ξ now has the meaning

$$\xi = \frac{y}{\sqrt{4 D_R t}}. \tag{19.11}$$

For steady mass transfer in a fictitious, stagnant, Nernst diffusion layer of thickness δ, the transport equations are

$$\frac{D_i}{D_R} c_i'' + \frac{z_i u_i F}{D_R}(c_i \Phi'' + c_i' \Phi') = 0, \tag{19.12}$$

where

$$\xi = \frac{y}{\delta}. \tag{19.13}$$

These several cases are very similar and can all be handled by the same computer program, particularly since the boundary conditions 19.5, 19.7, and 19.8 apply to all cases at the limiting current (except that condition 19.5 is applied at $\xi = 1$ for the Nernst diffusion layer).

Since the mathematical problems are identical for the growing mercury drops and penetration into an infinite stagnant medium, the correction factor I_L/I_D is exactly the same for these two transient processes. One can also use the Lighthill transformation (see Sections 17.5 and 17.6) to show[8] that the correction factor for steady transfer in arbitrary two-dimensional and axisymmetric diffusion layers is exactly the same as that calculated for the rotating disk. This means that the current density is distributed along the electrode in the same manner as when migration is neglected (see Chapter 17), but the magnitude of the current density at all points is increased or diminished by a constant factor, I_L/I_D, which depends upon the bulk composition of the solution.

19.2 CORRECTION FACTOR FOR LIMITING CURRENTS

Figure 19.1 shows[7] the ratio I_L/I_D for metal deposition on a rotating disk electrode. Consider the solid curve for the $CuSO_4$–H_2SO_4 system. The so-called *diffusion limiting current* is that which exists when there is a small amount of $CuSO_4$ in a great excess of H_2SO_4, since migration should then make no contribution. Hence, the abscissa is the square root of the ratio of the normality of the added ion to that of the counterion, and the ordinate shows how the limiting current is enhanced by the effect of migration. For $r = 0$, we have a solution of the single salt $CuSO_4$. We see that it makes little difference whether we add $MgSO_4$ or H_2SO_4. A curve for the deposition of silver from solutions of $AgNO_3$ and HNO_3 is also shown.

The square-root scale is used on the abscissa since the addition of only a small amount of supporting electrolyte to the solution of a single salt causes a considerable reduction of the limiting current because it strongly affects the electric field at the electrode surface where the reactant concentration goes to zero.

We have also been able to calculate this effect of migration for several other hydrodynamic situations; a growing mercury drop as encountered in polarography; a fictitious, stagnant, Nernst diffusion layer; and penetration into a semi-infinite stagnant medium. The differences in the effect of migration, among these situations, are pronounced only when the reactant ion has a diffusion coefficient considerably different from the other ions present, as shown in Figure 19.2 for hydrogen ion discharge from HCl–KCl solutions. Here, the polarographic data of Šlendyk[3] are shown for comparison. Theory and experiment agree well for the 0.001 *N* HCl solutions. The discrepancy for the 0.01 *N* HCl solutions can be attributed[9] to the fact that the solubility limit for the hydrogen produced in the electrode reaction is exceeded and the gas bubbles stir the solution in a way not accounted for in the theory.

The effect of migration does not always enhance the limiting current. For cathodic reduction of an anion, such as ferricyanide in KOH solutions, migration reduces the limiting current because the

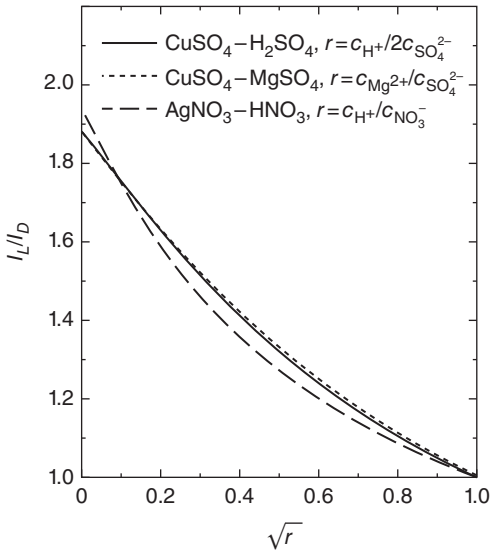

Figure 19.1 Effect of migration on limiting currents for metal deposition on a disk electrode. *Source*: Newman 1966.[7] Reproduced with permission of the American Chemical Society.

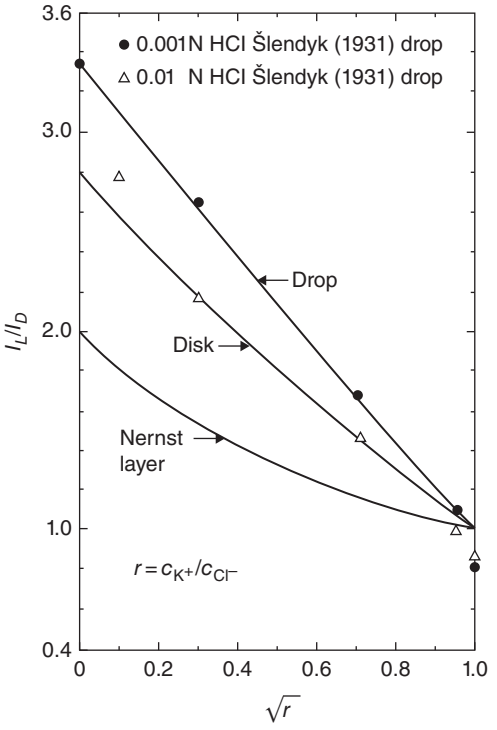

Figure 19.2 Effect of migration on limiting currents in discharge of hydrogen ions from KCl solutions. Lines represent values calculated with the present theory. *Source*: Newman 1966.[7] Reproduced with permission of the American Chemical Society.

direction of the electric field is then such as to tend to drive the anions away from the electrode. This is shown in Figure 19.3 for equimolar bulk concentrations of ferricyanide and ferrocyanide. The effect of ionic migration is always relatively small in redox systems because the product ion is always present at the electrode surface. Thus, in the absence of both the supporting electrolyte and the product ion in the bulk solution, $I_L/I_D = 0.866$ for the cathodic process,† and $I_L/I_D = 1.169$ for the anodic process on a rotating-disk electrode.

We find that the correction factor for the effect of migration on limiting currents for unsteady transfer from a stagnant, semi-infinite fluid to a plane electrode follows exactly the curve for unsteady transfer to a growing mercury drop. Also, the effect is exactly the same[8] for steady transfer in arbitrary two-dimensional and axisymmetric diffusion layers as that shown for the rotating disk. The quasi-potential transformation[10] permits many interesting problems with one electrode reaction and stagnant conditions to be treated like the Nernst stagnant diffusion layer. The geometry-dependent part of the problem reduces to Laplace's equation for the quasi-potential in the given geometry (solved by the methods described in Chapter 18), and the chemical part is identical to treating a Nernst diffusion layer, with even the possibility of variation of physical properties and any number of equilibrated homogeneous reactions.[11–13] Microelectrodes can also fall into this category.

† See also footnote on page 353

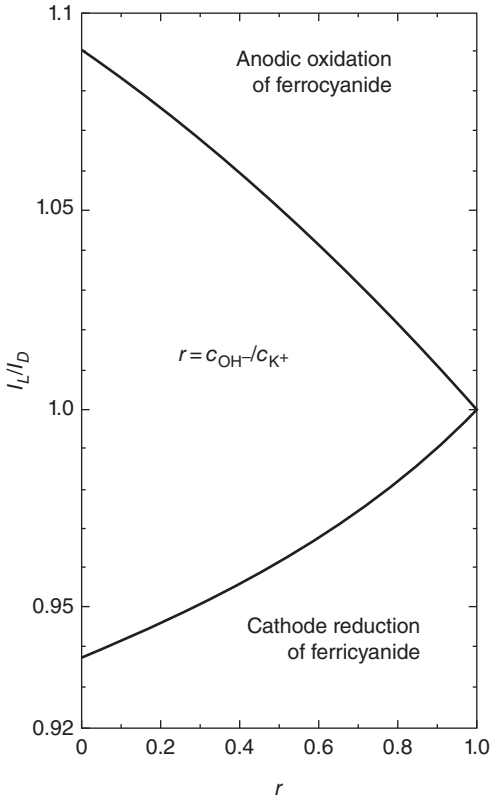

Figure 19.3 Effect of migration on limiting currents for a redox reaction. Equimolar potassium ferrocyanide and ferricyanide in KOH, for a disk electrode. *Source*: Newman 1966.[7] Reproduced with permission of the American Chemical Society.

19.3 CONCENTRATION VARIATION OF SUPPORTING ELECTROLYTE

For many of the discharge reactions, the concentration of supporting electrolyte is higher at the electrode surface than in the bulk solution. This difference is calculated as a by-product in the calculations of the effect of migration on limiting currents. The value, however, is of considerable interest in free-convection problems since the convective velocity is due to the density differences in the solution produced by the electrode reaction, and these density differences are affected by the concentration of the supporting electrolyte to roughly the same extent as by the concentration of the reactant (see Section 17.10).

Figure 19.4 shows some of these concentrations at the electrode surface for two systems (discharge of Ag^+ from $AgNO_3$–HNO_3 solutions and H^+ discharge from HCl–KCl solutions) and for several hydrodynamic situations. For these ions of valence 1, the concentration difference for the added ion is roughly half that of the reactant ion when an excess of supporting electrolyte is present. The difference, of course, goes to zero when there is no supporting electrolyte, but it rises rapidly for even small amounts of impurities (note the square-root scale on the abscissa).

For the redox systems, one must be concerned with both the added ion and the product ion. Figure 19.5 shows these concentration differences for the anodic oxidation of ferrocyanide ions,

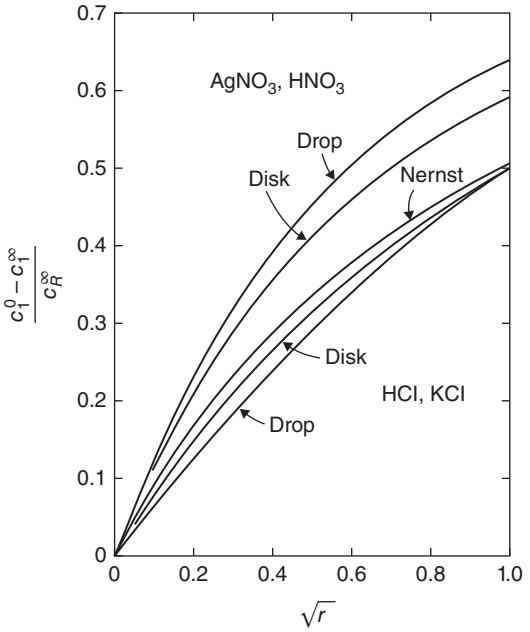

Figure 19.4 Concentration difference of the added ion divided by that of the reactant. The abscissa scale is defined in Figures 19.1 and 19.2.

and Figure 19.6 for the cathodic reduction of ferricyanide. In the latter case, the added hydroxide ion is depleted near the electrode. For these graphs, the ferrocyanide and ferricyanide ions have equal concentrations in the bulk solution, and the counterion is K^+. The abscissa scale is defined in Figure 19.3. Results for the copper sulfate–sulfuric acid system are reserved for the next section.

In Section 11.5 we treated systems with supporting electrolyte, showing how one can calculate the concentration profile of the supporting electrolyte as well as those of the minor species. Let us now use this method to calculate the surface concentration of the added ion and a product ion in the limit $r \to 1$, that is, with a large excess of supporting electrolyte. This procedure should yield the ordinate values in Figures 19.4 to 19.6 for $r = 1$.

With the use of the Nernst–Einstein relation 11.41, equation 19.4 for the rotating disk becomes

$$3\xi^2 \frac{dc_i}{d\xi} + \frac{D_i}{D_R}\left[\frac{d^2 c_i}{d\xi^2} + z_i \frac{d}{d\xi}\left(c_i \frac{d\phi}{d\xi}\right)\right] = 0, \tag{19.14}$$

where $\phi = F\Phi/RT$. Let the added ions and counterions be species 1 and 2, the reactant be $R = 3$, and the product be species 4, also present in small amount.

For the reactant, we can neglect ionic migration in the limit $r \to 1$, and the concentration profile is given by

$$c_R = \frac{c_R^\infty}{\Gamma(4/3)} \int_0^\xi e^{-x^3}\, dx. \tag{19.15}$$

For the product, migration can also be neglected, and equation 19.14 becomes

$$3\xi^2 \frac{dc_4}{d\xi} + \frac{D_4}{D_R} \frac{d^2 c_4}{d\xi^2} = 0, \tag{19.16}$$

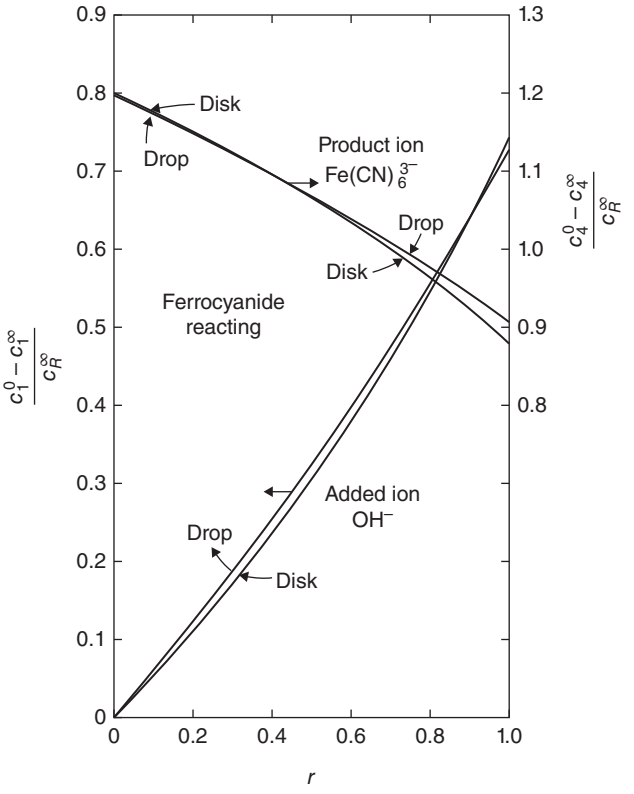

Figure 19.5 Surface concentrations for the anodic reaction in the $K_3Fe(CN)_6$–$K_4Fe(CN)_6$–KOH system.

and the boundary condition 19.7 at the electrode reduces to

$$D_4 \frac{dc_4}{d\xi} = \frac{s_4}{s_R} D_R \frac{dc_R}{d\xi} \quad \text{at } \xi = 0. \tag{19.17}$$

The solution therefore is

$$c_4 = c_4^\infty + \frac{s_4}{s_R} \frac{D_R}{D_4} \frac{c_R^\infty}{\Gamma(4/3)} \int_\infty^\xi e^{-x^3 D_R/D_4}\, dx, \tag{19.18}$$

from which we obtain

$$\frac{c_4^0 - c_4^\infty}{c_R^\infty} = -\frac{s_4}{s_R}\left(\frac{D_R}{D_4}\right)^{2/3}. \tag{19.19}$$

After linearization, the equations for the counterion and the added ion are

$$3\xi^2 \frac{dc_1}{d\xi} + \frac{D_1}{D_R}\left[\frac{d^2 c_1}{d\xi^2} + z_1 \frac{d}{d\xi}\left(c_1^0 \frac{d\phi}{d\xi}\right)\right] = 0, \tag{19.20}$$

$$3\xi^2 \frac{dc_2}{d\xi} + \frac{D_2}{D_R}\left[\frac{d^2 c_2}{d\xi^2} + z_2 \frac{d}{d\xi}\left(c_2^0 \frac{d\phi}{d\xi}\right)\right] = 0, \tag{19.21}$$

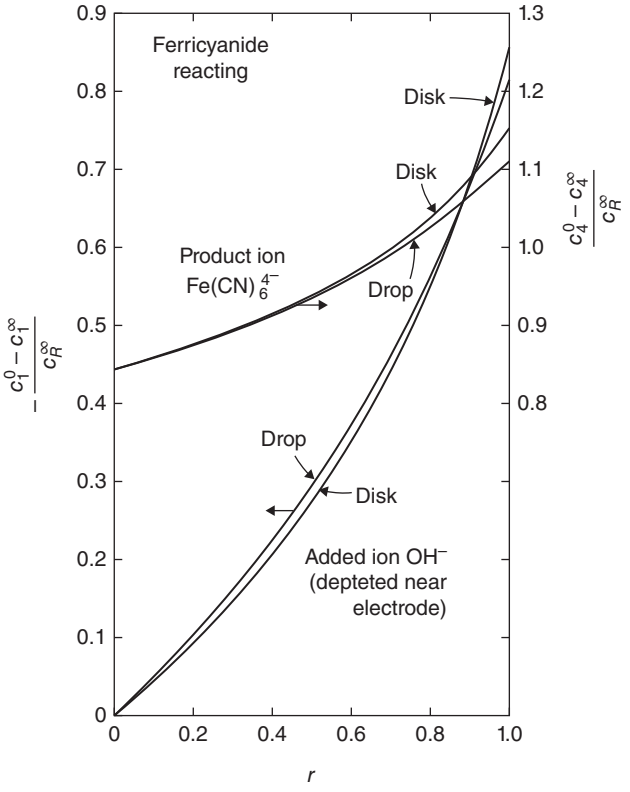

Figure 19.6 Surface concentrations for the cathodic reaction in the $K_3Fe(CN)_6$–K4Fe$(CN)_6$–KOH system.

where c_1^0 and c_2^0 are the uniform concentrations of these ions that prevail in the absence of the reactant and product species (see Section 11.5).

The concentrations satisfy the electroneutrality relation in the forms

$$z_1c_1 + z_2c_2 + z_3c_3 + z_4c_4 = 0, \tag{19.22}$$

$$z_1c_1^0 + z_2c_2^0 = 0. \tag{19.23}$$

Elimination of ϕ and c_2 from equations 19.20 and 19.21 therefore yields

$$\left(1 - \frac{z_1}{z_2}\right)\left(\frac{d^2c_1}{d\xi^2} + 3\xi^2\frac{D_R}{D_e}\frac{dc_1}{d\xi}\right) = \frac{z_3}{z_2}\left(1 - \frac{D_R}{D_2}\right)\frac{d^2c_3}{d\xi^2} + \frac{z_4}{z_2}\left(1 - \frac{D_4}{D_2}\right)\frac{d^2c_4}{d\xi^2}, \tag{19.24}$$

where

$$D_e = \frac{D_1D_2(z_1 - z_2)}{z_1D_1 - z_2D_2}. \tag{19.25}$$

This is a generalization of equation 11.34 for the case where there are two minor species. Substitution of equations 19.15 and 19.18 gives

$$\left(1-\frac{z_1}{z_2}\right)\left(\frac{d^2c_1}{d\xi^2}+3\xi^2\frac{D_R}{D_e}\frac{dc_1}{d\xi}\right)=3\xi^2\frac{z_R}{z_2}\left(\frac{D_R}{D_2}-1\right)\frac{c_R^\infty}{\Gamma(4/3)}e^{-\xi^3}$$
$$-3\xi^2\frac{z_4}{z_2}\frac{s_4}{s_R}\frac{D_R}{D_4}\left(\frac{D_R}{D_4}-\frac{D_R}{D_2}\right)\frac{c_R^\infty}{\Gamma(4/3)}e^{-\xi^3 D_R/D_4}. \tag{19.26}$$

The solution of this equation satisfying the boundary condition at infinity is

$$c_1=c_1^\infty+\frac{z_R}{z_2-z_1}\frac{(D_R/D_2)-1}{(D_R/D_e)-1}\frac{c_R^\infty}{\Gamma(4/3)}\int_\infty^\xi e^{-x^3}\,dx+B\int_\infty^\xi e^{-x^3 D_R/D_e}dx$$
$$+\frac{z_4}{z_2-z_1}\frac{s_4}{s_R}\frac{D_R}{D_4}\frac{(D_4/D_2)-1}{(D_4/D_e)-1}\frac{c_R^\infty}{\Gamma(4/3)}\int_\infty^\xi e^{-x^3 D_R/D_4}dx. \tag{19.27}$$

The boundary condition at the electrode is that the flux density of ions 1 and 2 is zero and takes the form

$$\frac{dc_1}{d\xi}+z_1c_1^0\frac{d\phi}{d\xi}=0 \quad \text{and} \quad \frac{dc_2}{d\xi}+z_2c_2^0\frac{d\phi}{d\xi}=0. \tag{19.28}$$

With equation 19.23 this becomes

$$\frac{dc_1}{d\xi}+\frac{dc_2}{d\xi}=0, \tag{19.29}$$

and with equation 19.22 we have

$$\frac{dc_1}{d\xi}\left(1-\frac{z_1}{z_2}\right)=\frac{z_3}{z_2}\frac{dc_3}{d\xi}+\frac{z_4}{z_2}\frac{dc_4}{d\xi}$$
$$=\frac{z_R}{z_2}\frac{c_R^\infty}{\Gamma(4/3)}+\frac{z_4}{z_2}\frac{s_4}{s_R}\frac{D_R}{D_4}\frac{c_R^\infty}{\Gamma(4/3)} \tag{19.30}$$

at $\xi=0$. This allows the determination of the constant B in equation 19.27:

$$B=\frac{c_R^\infty}{\Gamma(4/3)}\frac{(D_R/D_e)-(D_R/D_2)}{z_2-z_1}\left[\frac{z_R}{(D_R/D_e)-1}+\frac{s_4}{s_R}\frac{z_4}{(D_4/D_e)-1}\right]. \tag{19.31}$$

Finally, we can calculate the concentration change of species 1 between the bulk and the electrode surface:

$$\frac{c_1^0-c_1^\infty}{c_R^\infty}=\frac{-z_R}{z_2-z_1}\left\{\frac{(D_R/D_2)-1}{(D_R/D_e)-1}\left[1-\left(\frac{D_e}{D_R}\right)^{1/3}\right]+\left(\frac{D_e}{D_R}\right)^{1/3}\right\}$$
$$-\frac{z_4}{z_2-z_1}\frac{s_4}{s_R}\left\{\frac{(D_4/D_2)-1}{(D_4/D_e)-1}\left[1-\left(\frac{D_e}{D_4}\right)^{1/3}\right]+\left(\frac{D_e}{D_4}\right)^{1/3}\right\}\left(\frac{D_R}{D_4}\right)^{2/3}. \tag{19.32}$$

The case where there is no product ion can be treated by setting $s_4=0$ or $z_4=0$. The corresponding equation for c_2 can be obtained from equation 19.32 by reversing the subscripts 1 and 2.

For a growing mercury drop, the expressions for the concentration differences should become

$$\frac{c_1^0 - c_1^\infty}{c_R^\infty} = \frac{-z_R}{z_2 - z_1}\left\{\frac{(D_R/D_2) - 1}{(D_R/D_e) - 1}\left[1 - \left(\frac{D_e}{D_R}\right)^{1/2}\right] + \left(\frac{D_e}{D_R}\right)^{1/2}\right\}$$
$$- \frac{z_4}{z_2 - z_1}\frac{s_4}{s_R}\left\{\frac{(D_4/D_2) - 1}{(D_4/D_e) - 1}\left[1 - \left(\frac{D_e}{D_4}\right)^{1/2}\right] + \left(\frac{D_e}{D_4}\right)^{1/2}\right\}\left(\frac{D_R}{D_4}\right)^{1/2} \tag{19.33}$$

and

$$\frac{c_4^0 - c_4^\infty}{c_R^\infty} = -\frac{s_4}{s_R}\left(\frac{D_R}{D_4}\right)^{1/2}. \tag{19.34}$$

Hauser and Newman[14] extended this analysis to include the case where one ion of the supporting electrolyte is involved in the electrode reaction.

Over the years we have discovered a number of cases in which the potential gradient has the opposite sign at the electrode from what we should expect on the basis of the direction of current. It is a lot of fun to sketch concentration profiles of reactants, products, and supporting electrolyte, as called for in Problem 11.4. The reversal of the potential gradient leads to unexpected minima or maxima in the concentration profiles and can be traced to the diffusion potential term (see, e.g., equation 11.11). Hauser and Newman[14] have investigated this phenomenon in more detail and find that a prediction of reversal of potential gradient can be made solely on the basis of the stoichiometry of the reaction as well as the charge numbers, diffusion coefficients, and mobilities of the species present (see Problem 19.7). Reversal occurs only when more than one ionic species is involved in the reaction. Reversal occurs for reduction of $Zn(OH)_4^{2-}$ and $CuCl_2^-$ to the metal, but not for reduction of $AuCl_4^-$.

19.4 ROLE OF BISULFATE IONS

Bisulfate ions do not completely dissociate in sulfuric acid solutions (see Section 4.7). A simple, dramatic example is found in the conductivity of solutions of copper sulfate and sulfuric acid, as shown in Figure 19.7. When copper sulfate is added to a solution of sulfuric acid, the conductivity is found to decrease. If the conductivity is predicted from limiting ionic mobilities (see Table 11.1), the result is in accord with this observation if bisulfate ions are assumed to be undissociated. Predictions based on sulfate and hydrogen ions are, on the other hand, in qualitative and quantitative discord with the experimental values.

The incomplete dissociation of bisulfate ions should also have dramatic consequences for the effect of ionic migration on limiting currents. When copper sulfate is added to sulfuric acid solutions, the electric field increases not only because the current increases but also because hydrogen ions combine to form bisulfate ions and the conductivity decreases. This is shown in Figure 19.8. The parameter r in the abscissa is still based on the ratio of the stoichiometric concentrations of sulfuric acid and copper sulfate.

The partial dissociation of bisulfate ions can also be taken into account.[2] As in Section 19.1, material-balance equations are written for the hydrogen, sulfate, bisulfate, and copper ions, the equations including, where appropriate, the rate of production in the homogeneous reaction

$$HSO_4^- \rightleftharpoons H^+ + SO_4^{2-} \tag{19.35}$$

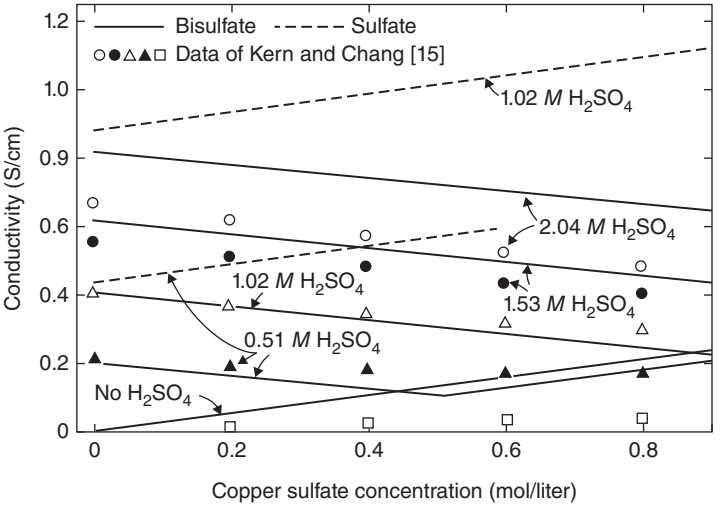

Figure 19.7 Conductivity of aqueous solutions of copper sulfate and sulfuric acid at 25°C. *Source*: Data from Kern and Chang 1923.[15]

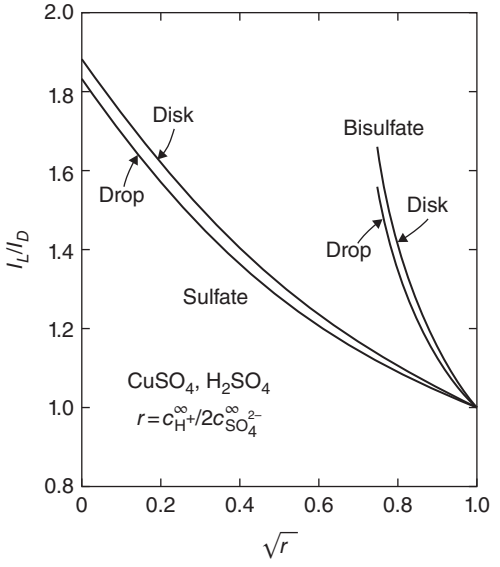

Figure 19.8 Effect of migration in the $CuSO_4$–H_2SO_4 system with no dissociation and with complete dissociation of bisulfate ions.

(see equation 16.2). The reaction is assumed to be fast, so that the concentrations also satisfy the relation (see equation 4.64)

$$K' = \frac{c^*_{H^+} c^*_{SO_4^{2-}}}{c^*_{HSO_4^-}}, \tag{19.36}$$

where K' is taken to be independent of position. Asterisks denote the fact that these quantities refer to a view of the solution as composed of water molecules and hydrogen, bisulfate, sulfate, and copper

ions. The material-balance equations are then added to obtain three equations that do not include the reaction rate. These three equations, equation 19.36, and the electroneutrality relation are then used to determine the concentration distributions of the four ions and the potential distribution by the numerical method described in Appendix C.

Let c_A^∞ and c_B^∞ be the bulk stoichiometric concentrations of copper sulfate and sulfuric acid, and let I be the bulk ionic strength based on a convention of complete dissociation:

$$I = 4c_A^\infty + 3c_B^\infty. \tag{19.37}$$

The two important parameters will then be the relative amounts of reactant and supporting electrolyte, expressed as

$$r = \frac{c_B^\infty}{c_A^\infty + c_B^\infty}, \tag{19.38}$$

and the ratio I/K' of the ionic strength to the dissociation constant.

The effect of migration on limiting current is shown in Figures 19.9 and 19.10 for the rotating-disk electrode and the growing mercury drop. The ordinate, I_L/I_D, is the ratio of the limiting current to the limiting diffusion current of a well-supported solution when the effect of viscosity variations is excluded. The abscissa is the ratio r of equation 19.38, and values of I/K' are given as a parameter. The two solid lines indicate the two extreme cases of complete ($I/K' = 0$) and no dissociation ($I/K' = \infty$) of bisulfate ions.

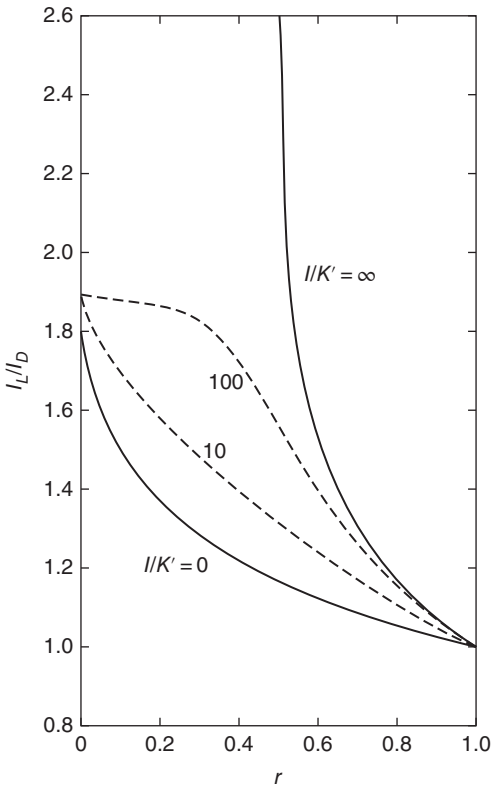

Figure 19.9 Effect of migration for a rotating-disk electrode. *Source*: Hsueh and Newman 1971.[2] Reproduced with permission of the American Chemical Society.

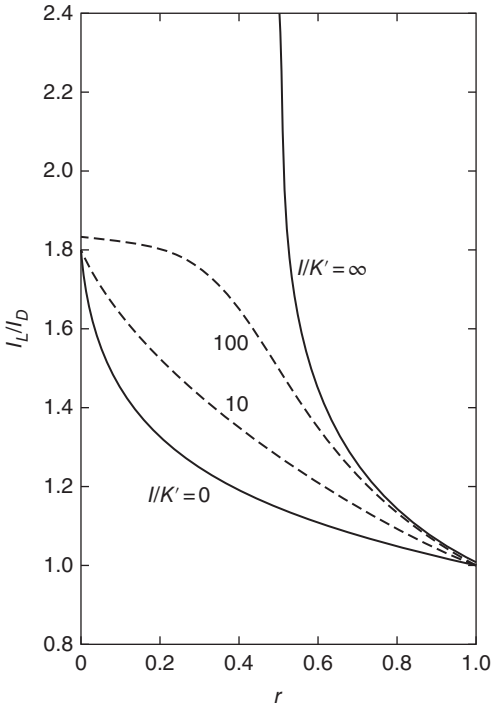

Figure 19.10 Effect of migration for a growing mercury drop or in a stagnant diffusion cell. *Source*: Hsueh and Newman 1971.[2] Reproduced with permission of the American Chemical Society.

The concentration difference of sulfuric acid between the electrode surface and the bulk solution is shown in Figures 19.11 and 19.12 for the two electrochemical systems. One may notice that the concentration of sulfuric acid would even decrease near the electrode surface for some values of r when bisulfate ions are not completely dissociated. Qualitatively speaking, the bisulfate ions, containing hydrogen, are driven away from the electrode because of their negative charge. For no dissociation, one should consider that $r = 0.5$ corresponds to a binary solution of copper bisulfate.

An analytic solution can be obtained for a stagnant Nernst diffusion layer, and the results shown in Figures 19.13 and 19.14 serve to complete the picture presented in Figures 19.9 to 19.12. The quasipotential extends the physical situation covered here to include microelectrodes and pitting corrosion under stagnant conditions.

In practical applications, the dissociation constant K' can be related to the true ionic strength I_r of the bulk solution

$$I_r = \frac{1}{2}\sum_i z_i^2 c_i^{*\infty}, \tag{19.39}$$

the correlation having been given in Figure 4.4 and equation 4.66.

Figure 19.15 shows the wide range of concentration differences that are conceivable in the copper sulfate, sulfuric acid system. Results for free convection, from Section 19.6, are shown in addition to the rotating disk, the growing mercury drop, and the stagnant Nernst diffusion layer. For comparison, the values calculated by Wilke et al.[16] and by Fenech and Tobias[17] are also shown. For the quantity plotted on Figure 19.15, the value 0.71 can be deduced from the results of one of Brenner's

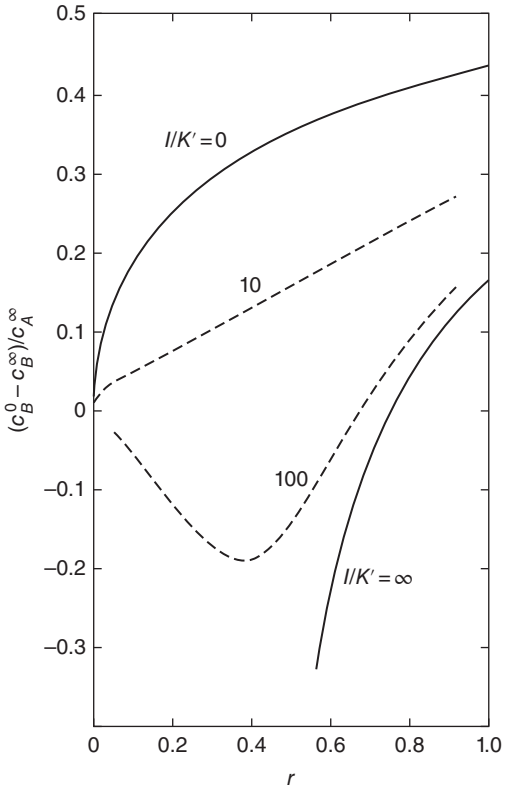

Figure 19.11 Surface concentration change for a rotating-disk electrode. *Source*: Hsueh and Newman 1971.[2] Reproduced with permission of the American Chemical Society.

experiments.[18] Hsueh and Newman[2] obtained four values in the range from 0.50 to 0.57 and one value of 0.75.

19.5 PARADOXES WITH SUPPORTING ELECTROLYTE

The use of a supporting electrolyte raises a number of questions, such as:

1. Which species is carrying the current?
2. If the reactant is carrying the current in the diffusion layer, how does the supporting electrolyte have an effect?
3. If the supporting electrolyte is motionless in the diffusion layer, is it also motionless in the bulk of the solution? Again, what species is carrying the current?

We shall endeavor to answer such questions in this section.

The nature of the problem can perhaps be seen more clearly from the fundamental transport relations. If there are no concentration gradients, then equation 18.1 applies:

$$\mathbf{i} = -\kappa \nabla \Phi, \tag{19.40}$$

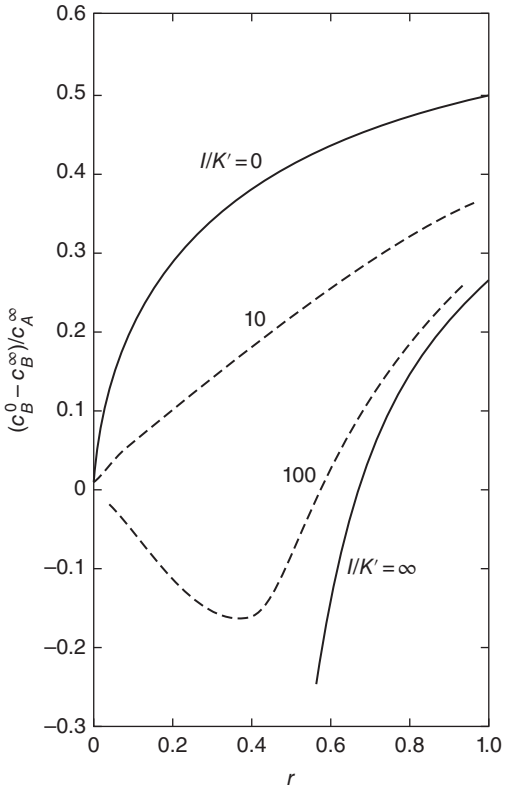

Figure 19.12 Surface concentration change for a growing mercury drop or in a stagnant diffusion cell. *Source*: Hsueh and Newman 1971.[2] Reproduced with permission of the American Chemical Society.

where

$$\kappa = F^2 \sum_i z_i^2 u_i c_i. \tag{19.41}$$

This is the conductivity we measure with a conductivity cell, using alternating current, and is the usual basis for defining transference numbers (equation 11.9) and deciding how the various species contribute to the current. These concepts sometimes clash with what we find on more detailed analysis of the effect of supporting electrolyte.

Consider an electrolytic cell with two electrodes and a solution between. Near each electrode there is a stagnant diffusion layer in which mass-transfer effects are important, and the bulk of the solution is well mixed.

At the electrode, the flux of all species is zero except for a reactant. In a stagnant diffusion layer, this implies that the added ions and the counterions are motionless, having adopted concentration distributions so that the forces of migration and diffusion cancel. How then can the supporting electrolyte act to reduce the electric field strength when it carries no current? In this regard, the effect of adding supporting electrolyte is essentially no different from adding more reacting electrolyte. This excess electrolyte is not moving either. Problem 19.7 may give additional insight into how addition of supporting electrolyte can reduce the potential gradient even though concentration gradients are

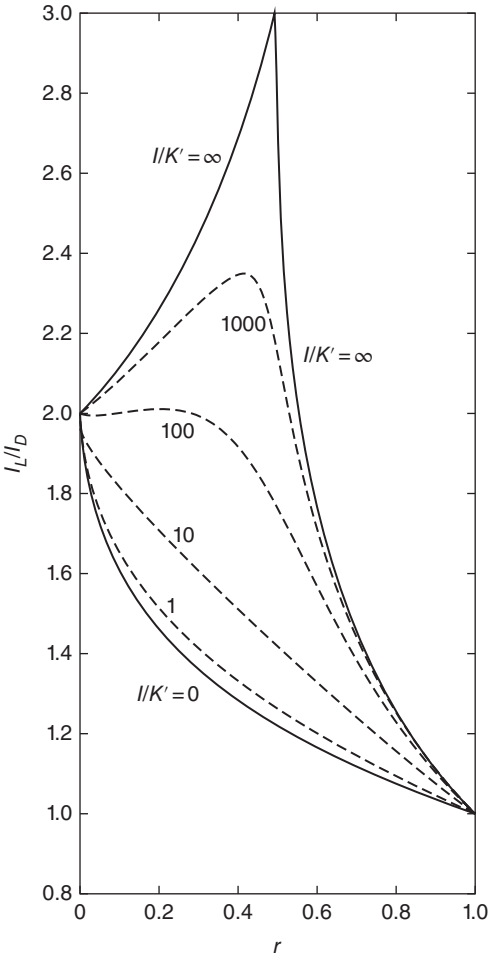

Figure 19.13 Effect of migration in a Nernst diffusion layer. *Source*: Hsueh and Newman 1971.[2] Reproduced with permission of the American Chemical Society.

present and equations 19.40 and 19.41 are not applicable unless we replace the conductivity κ with κ':

$$\kappa' = -F^2 \frac{\sum_i z_i^2 u_i c_i / D_i}{\sum_i z_i s_i / n D_i}.$$

There are several reasons why we might use a supporting electrolyte instead of adding more reacting electrolyte. Without the supporting electrolyte, the conductivity of the solution may be limited by the solubility of the reacting electrolyte. The current distribution is likely to be more uniform with a higher conductivity (see Section 18.3), and the ohmic potential drop will be smaller. We may want to keep the inventory of working material down and use a cheaper material that we can discard when it gets dirty. We may want to adjust the pH (see also Section 1.6).

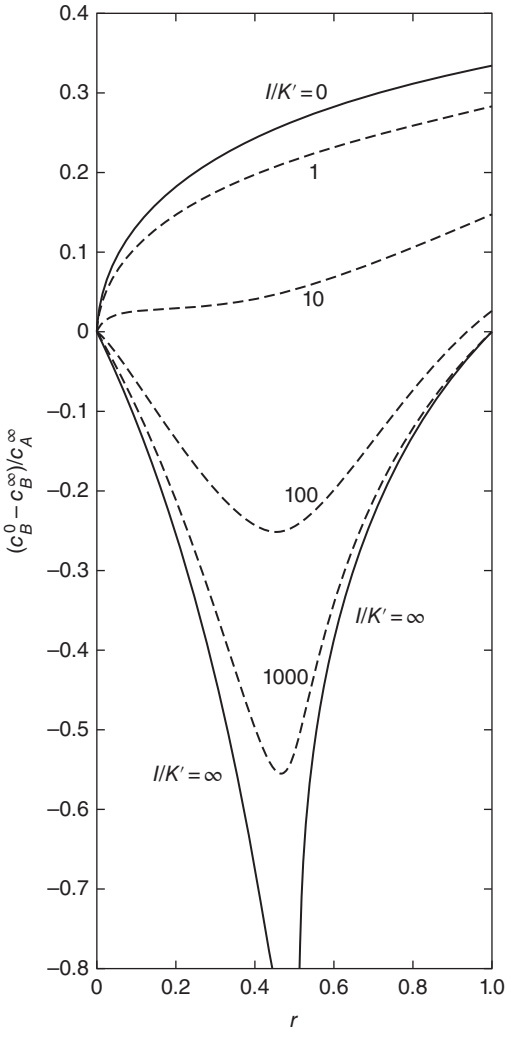

Figure 19.14 Surface concentration change in a Nernst diffusion layer. *Source*: Hsueh and Newman 1971.[2] Reproduced with permission of the American Chemical Society.

Now suppose that the region outside the stagnant diffusion layer is *well stirred* so that there are no concentration gradients. (It may be useful to consider the rotating-cylinder system treated in Chapter 1. A concentration profile was shown in Figures 1.7 and 1.10.) In this region, equation 19.40 should apply, so that the supporting electrolyte is apparently moving and carrying a current. How can we have a flux that suddenly becomes zero at the edge of the diffusion layer? Actually, the net flux of supporting electrolyte must be zero throughout the solution. The velocity of stirring cannot be one dimensional. A sufficient concentration gradient exists across the bulk solution so that convection cancels the migration flux of the supporting electrolyte and augments that of the reactant; this is the purpose of stirring in the first place. (Compare with the description of the turbulent transport mechanism and the eddy diffusivity in Section 15.7.) The faster the stirring, the lower the gradients; but the fluid motion carries no current since the solution is electrically neutral. However, the potential drop in the

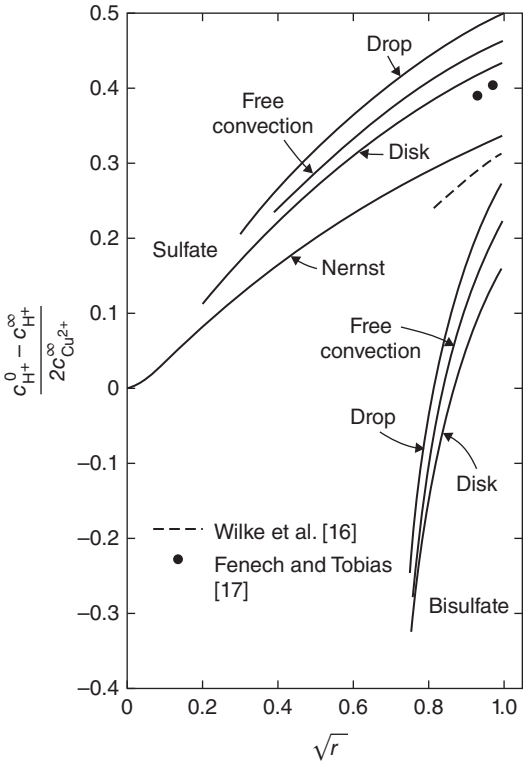

Figure 19.15 Concentration differences of sulfuric acid possible in the copper sulfate, sulfuric acid system with complete and with no dissociation of bisulfate ions and for several hydrodynamic situations.

bulk is still given by equation 19.40 and can be considerably reduced by the addition of supporting electrolyte.

A statement of how much current each ionic species is carrying thus depends upon one's reference frame. Some people base their answer on the net flux. Others prefer to ignore the convective flux, saying that it does not contribute to the current. Still others give an answer based only on migration fluxes and transference numbers.

Finally, one may be puzzled by the fact that the addition of a supporting electrolyte reduces the ohmic potential drop and yet can lead to a reduction of the limiting current by a factor of 2. The reason is that the potential drop in the bulk solution is not relevant at the limiting current. By lowering the electric field in the diffusion layer, so that migration makes no contribution to the flux of the reactant, the supporting electrolyte reduces the limiting current density. At this point one can contrast Figure 1.13 with Figure 1.12. To pass 5 A with no supporting electrolyte requires about 0.6 V, whereas with supporting electrolyte only about 0.26 V is required. At higher potentials, mass-transfer in the diffusion layer becomes a more severe restriction with the supporting electrolyte.

19.6 LIMITING CURRENTS FOR FREE CONVECTION

The addition of supporting electrolyte to a solution does not make the free-convection problem directly comparable to that of heat transfer and nonelectrolytic mass transfer in a binary fluid because, while

it does reduce the effect of ionic migration, the concentration variation of the supporting electrolyte affects the density variation to roughly the same extent as the reactant and thus influences the velocity profile. Since the mass-transfer rate depends upon the velocity profile, the limiting current density is also affected.

The quantities of practical interest are the mass transfer to the wall and the shear stress at the wall. For laminar free convection from a solution to a vertical electrode with a constant density difference $\Delta\rho$ between the surface and the bulk solution, the results can be expressed in dimensionless form as

$$\mathrm{Nu}_{\mathrm{avg}} = \frac{s_R i_{\mathrm{avg}} L}{nFD_R c_{R\infty}} = C(\mathrm{ScGr})^{1/4} \tag{19.42}$$

and

$$\frac{\tau_0}{Lg\Delta\rho} = B(\mathrm{ScGr})^{-1/4}, \tag{19.43}$$

where τ_0 is the shear stress at the wall averaged over the length L, g is the magnitude of the gravitational acceleration, $\mathrm{Sc} = \nu/D_R$ is the Schmidt number, Gr is the Grashof number

$$\mathrm{Gr} = \frac{gL^3\Delta\rho}{\rho_\infty \nu^2}, \tag{19.44}$$

and $\Delta\rho = |\rho_\infty - \rho_0|$ is the magnitude of the density difference between the bulk solution and the electrode surface. C and B are dimensionless coefficients that depend on the Schmidt number and the composition of the bulk solution. Values of C for a binary fluid were given in Table 17.2. For free convection to a vertical surface with a constant density difference $\Delta\rho$, the local rate of mass transfer is inversely proportional to $x^{1/4}$, and the local shear stress is proportional to $x^{1/4}$, where x is the vertical distance along the surface measured from the beginning of the boundary layer.

We treat[19] this problem in the limit of infinite Schmidt number and express the results in the form of C/C_b and B/B_b, where C_b and B_b are the values appropriate to a binary fluid and have the values $C_b = 0.670327$ and $B_b = 0.932835$.

The copper sulfate/sulfuric acid system was treated first. In view of the low value of the dissociation constant of bisulfate ions, the calculations were carried out for no dissociation of bisulfate ions as well as for complete dissociation to sulfate and hydrogen ions (see also Section 19.4). Results are shown in Figure 19.16 for B/B_b for complete dissociation of bisulfate ions and the ratio C/C_b for both no dissociation and complete dissociation. Dashed lines show the corresponding values of I_L/I_D for a rotating disk.

For metal deposition from a binary electrolytic solution, one can show that

$$C = \frac{(D/D_R)^{3/4}}{1 - t_R} C_b(\mathrm{Sc}_e) \tag{19.45}$$

and

$$B = \left(\frac{D}{D_R}\right)^{1/4} B_b(\mathrm{Sc}_e) \tag{19.46}$$

(see equation 17.99 and Problem 17.7), where $\mathrm{Sc}_e = \nu/D$ is based on the diffusion coefficient D of the salt and t_R is the transference number of the reacting cation (see equations 11.22 and 11.28).

As r approaches unity, one would expect C/C_b and B/B_b to approach unity if the appearance of $\Delta\rho$ in the Grashof number were sufficient to correlate the effect of the supporting electrolyte. The contrary

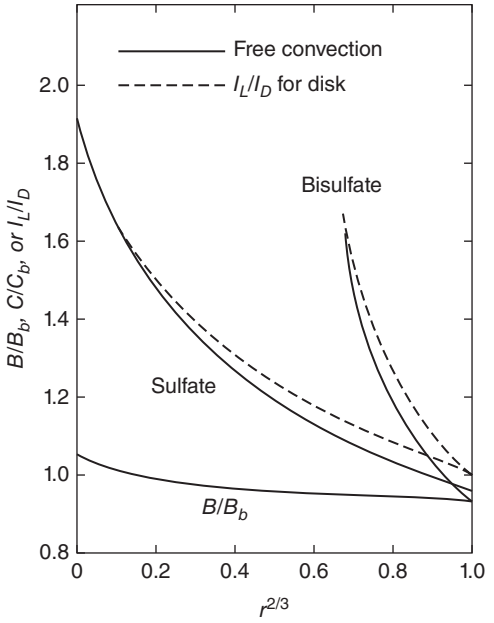

Figure 19.16 Coefficients for shear stress (complete dissociation only) and mass transfer in the $CuSO_4$–H_2SO_4 system. Dashed curves show for comparison values of I_L/I_D for the rotating disk. *Source*: [14]. Reproduced with permission of the American Chemical Society.

behavior emphasizes the fact that these ratios express not only the effect of ionic migration but also the effect of the density profile not being similar to that for a binary fluid.

To be specific, the diffusion layer thickness is greater for H_2SO_4 than for $CuSO_4$ because of the larger value of the diffusion coefficient of hydrogen ions. Thus, the density difference in the outer part of the diffusion layer is positive while it is negative near the electrode. Consequently, the value of $\Delta\rho$ does not, by itself, give sufficient information about the density profile. In fact, with added H_2SO_4, the velocity profile shows a maximum within the diffusion layer. This is shown for excess sulfuric acid in Figure 19.17. Since these phenomena occur in a more drastic fashion in some redox systems, we shall postpone their further discussion. In Figure 19.17, the abscissa is the similarity variable

$$\eta = y\left(\frac{3g\Delta\rho}{4\nu D_R \rho_\infty x}\right)^{1/4}, \tag{19.47}$$

and the velocity profile is related to $dF/d\eta$ by

$$\frac{dF}{d\eta} = \left(\frac{3\nu\rho_\infty}{4g\Delta\rho D_R x}\right)^{1/2} v_x. \tag{19.48}$$

The redox reaction

$$Fe(CN)_6^{3-} + e^- \rightleftharpoons Fe(CN)_6^{4-} \tag{19.49}$$

is popular in mass-transfer studies and has been used in free convection, although it is not common. The densification in this system is much weaker than in copper sulfate solutions since the excess of product ion largely compensates for the deficit of the reactant.

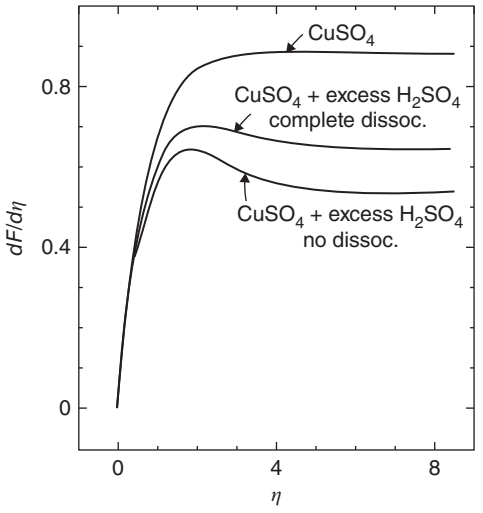

Figure 19.17 Velocity profiles for binary salt solution ($CuSO_4$) and for $CuSO_4$ with excess H_2SO_4 ($r = 0.99998$) completely dissociated and undissociated. *Source*: Hauser and Newman 1989.[14] Reproduced with permission of the American Chemical Society.

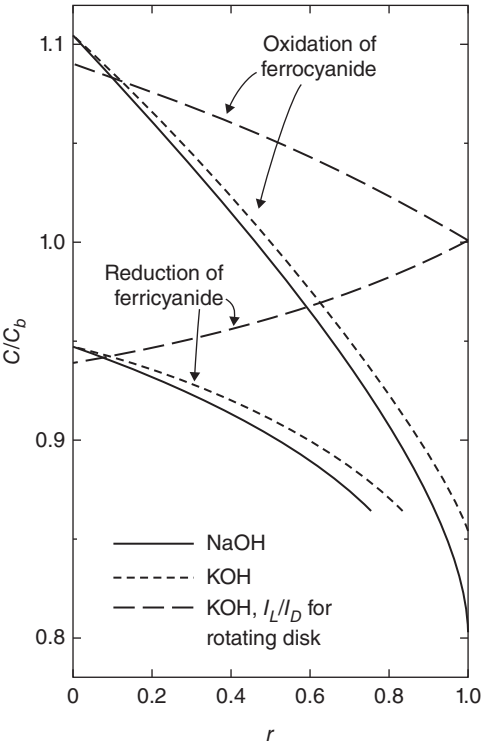

Figure 19.18 Coefficient for mass-transfer rate in the supported ferricyanide–ferrocyanide systems, for equal bulk concentrations of $K_3Fe(CN)_6$ and $K_4Fe(CN)_6$. *Source*: Hauser and Newman 1989.[14] Reproduced with permission of the American Chemical Society.

The ratio C/C_b is shown in Figure 19.18 as a function of

$$r = \frac{c^{\infty}_{OH^-}}{c^{\infty}_{K^+} + c^{\infty}_{Na^+}}. \tag{19.50}$$

The solutions have equal bulk concentrations of potassium ferrocyanide and potassium ferricyanide, with either sodium hydroxide or potassium hydroxide added as a supporting electrolyte. On Figure 19.18, values of I_L/I_D for the rotating disk with KOH supporting electrolyte are plotted for comparison.

Figure 19.18 shows a conspicuous deviation of the values of C/C_b from the values of I_L/I_D for the rotating disk. In contrast, the concentration ratios shown in Figure 19.19 are essentially independent of the hydrodynamic situation, almost coinciding with the results for the rotating disk (which are not shown). Figure 19.18 reflects the strong dissimilarity of the density profile in the supported solutions compared to that in a binary solution. A dramatic consequence of this is shown in the velocity profiles

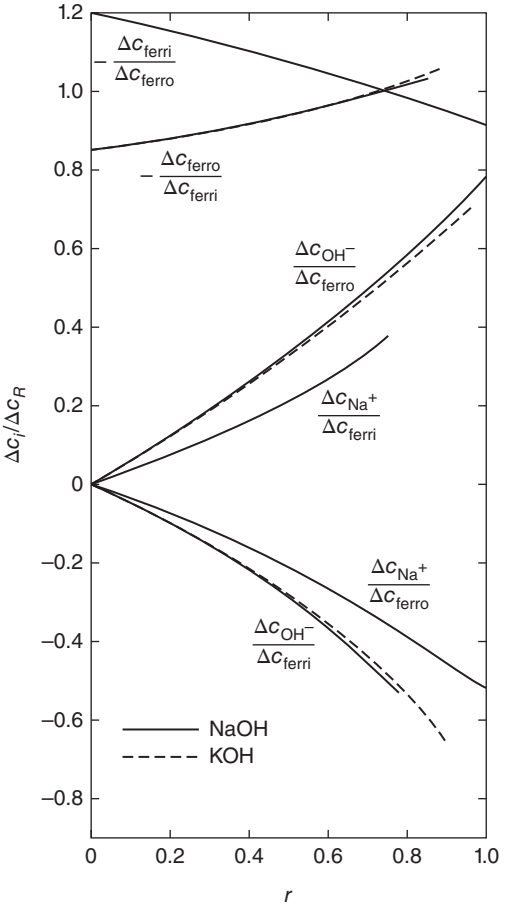

Figure 19.19 Surface concentrations in the supported ferricyanide–ferrocyanide systems, for equal bulk concentrations of $K_3Fe(CN)_6$ and $K_4Fe(CN)_6$. *Source*: Hauser and Newman 1989.[14] Reproduced with permission of the American Chemical Society.

in Figure 19.20. There is a velocity maximum that becomes more pronounced as KOH is added, and the magnitude of the velocities becomes smaller. The profile for $r = 0.95$ yields a converged but physically unreasonable solution since the velocity far from the electrode has reversed sign. Reasonable solutions were not obtained in the cathodic case for r greater than 0.85 for KOH, and 0.75 for NaOH, supporting electrolyte.

The situation is different only in degree from the one encountered in the case of supported $CuSO_4$. Normalized density profiles for the two cases are compared in Figure 19.21. The ferricyanide–ferrocyanide system has a weaker densification than $CuSO_4$, and, consequently, the addition of supporting electrolyte can have relatively a much greater effect on the density profile, as we see in Figure 19.21.

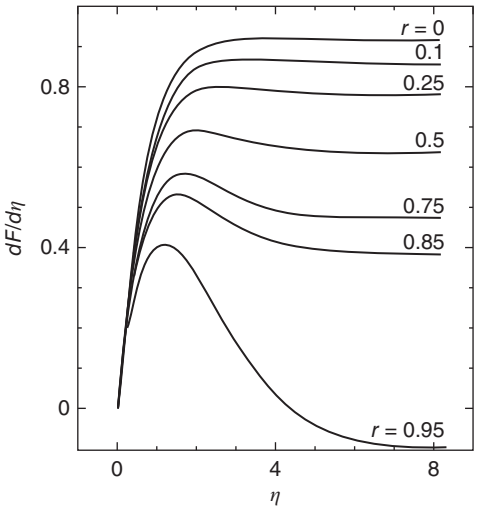

Figure 19.20 Velocity profiles for various values of r for cathodic reduction of ferricyanide ions with KOH supporting electrolyte. *Source*: Hauser and Newman 1989.[14] Reproduced with permission of the American Chemical Society.

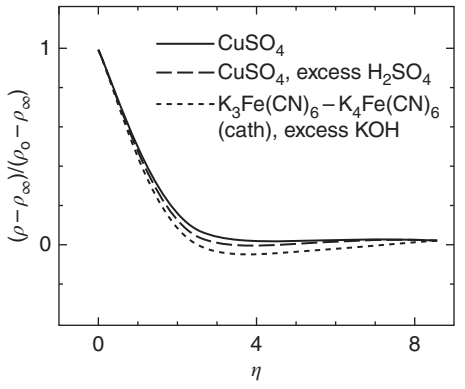

Figure 19.21 Normalized density profiles for binary salt solution ($CuSO_4$), for $CuSO_4$ with excess H_2SO_4 ($r = 0.99998$), and for equimolar ferricyanide–ferrocyanide with excess KOH (cathodic reaction, $c_{OH^-}/c_{K^+} = 0.95$). *Source*: Hauser and Newman 1989.[14] Reproduced with permission of the American Chemical Society.

Many of the phenomena reported here can be attributed to the large diffusion coefficient of the supporting electrolyte used. For a system where the diffusion coefficients of the solutes are roughly the same, one could estimate the value of I_L/I_D from calculations for other hydrodynamic situations and then assume that this is equal to the value of C/C_b, for free convection with little error.

The analysis applies to large Schmidt numbers. In this limit, the present results can be applied to other geometries by using the transformation of Acrivos (see Section 17.10). This means that the coefficient 0.6705 in equation 17.91 is replaced by C or that the coefficient 0.5029 in equations 17.90 and 17.92 is replaced by $3C/4$.

PROBLEMS

19.1 Use the results of Section 17.13 to show that the correction factor for migration for the discharge of cations from a binary salt solution is

$$\frac{I_L}{I_D} = \frac{(D/D_R)^{2/3}}{1 - t_R}$$

for a disk electrode and

$$\frac{I_L}{I_D} = \frac{(D/D_R)^{1/2}}{1 - t_R}$$

for a growing mercury drop. Show that the corresponding expression for a stagnant Nernst diffusion layer is

$$\frac{I_L}{I_D} = \frac{D/D_R}{1 - t_R}.$$

19.2 Verify equations 19.33 and 19.34.

19.3 Show that, for a stagnant Nernst diffusion layer, equations 19.33 and 19.34 should be replaced by

$$\frac{c_4^0 - c_4^\infty}{c_R^\infty} = -\frac{s_4}{s_R}\frac{D_R}{D_4}$$

and

$$\frac{c_1^0 - c_1^\infty}{c_R^\infty} = \frac{-z_R}{z_2 - z_1} - \frac{z_4}{z_2 - z_1}\frac{s_4}{s_R}\frac{D_R}{D_4}.$$

19.4 The latter part of Section 19.3 deals with concentration profiles at the limiting current with a large excess of supporting electrolyte. Use these results to reexamine the questions raised in Problem 11.4.

19.5 It is desired to obtain a numerical value for I_L/I_D for hydrogen ion discharge in turbulent flow. For this purpose, we shall use the rotating-cylinder system with the limiting current on the inner, rotating cylinder. Assume that no gas bubbles are formed on either electrode.

(a) State the electrochemical reaction occurring at the cathode.

(b) For a very dilute aqueous solution of hydrochloric acid with a large excess of potassium chloride as a supporting electrolyte, state a formula for the *total* limiting current at a rotating electrode.

(c) For the same very dilute aqueous solution of hydrochloric acid, but in the absence of potassium chloride (i.e., for a binary electrolyte), obtain an expression for the total limiting current at the rotating electrode.

(d) Obtain an expression and a numerical value for I_L/I_D for this particular turbulent-flow system. Use transport properties in Table 11.1.

19.6 Problem 2.18 dealt with a cell for producing chlorate ions. Sketch profiles of the ionic compositions as functions of distance from the anode (where chlorate is produced). Try to satisfy the electroneutrality condition and indicate how diffusion and migration contributions are to be reconciled with the net flux density of each ionic species.

19.7 Because of the diffusion potential, it is sometimes possible for the electric field in the solution to be reversed near an electrode, that is, for $\partial\Phi/\partial y$ at $y = 0$ to be positive for an anode or negative for a cathode. Here, Φ represents the electrostatic potential and y is the position measured from the electrode surface into the solution. Assume that a steady state prevails.

(a) Show that this reversal of electric field can never occur in the solution outside the diffusion layer where $\nabla c_i = 0$.

(b) For a single electrode reaction

$$\sum_i s_i M_i^{z_i} \rightarrow ne^-,$$

write Faraday's law so as to express the flux density N_{iy} at the electrode in terms of the normal component i_n of the current density.

(c) On the basis of part (b), express the normal component of the concentration gradient of species i in terms of the current density and the potential gradient.

(d) Sum over i the concentration gradients multiplied by charge number and, thus, relate the normal component of the potential gradient to the current density at an electrode in an expression not involving the concentration gradients.

(e) Test this expression for the reaction

$$\mathrm{Cu} + 2\mathrm{Cl}^- \rightarrow \mathrm{CuCl}_2^- + \mathrm{e}^-.$$

Use the Nernst–Einstein relation, and take the composition near the electrode to be $c_{\mathrm{KCl}} = 1\,M$, $c_{\mathrm{KCuCl_2}} = 0.001\,M$, and take the diffusion coefficient of CuCl_2^- to be 0.54×10^{-5} cm^2/s.

NOTATION

a	0.51023
B	coefficient for shear stress in free convection
B_b	0.932835
c_i	concentration of species i, mol/cm^3
C	coefficient for mass transfer in free convection
C_b	0.670327
D	diffusion coefficient for a binary electrolyte, cm^2/s
D_e	diffusion coefficient of supporting electrolyte, cm^2/s
D_i	diffusion coefficient of species i, cm^2/s

F	Faraday's constant, 96,487 C/mol
F	dimensionless stream function for free convection
g	magnitude of the gravitational acceleration, cm/s^2
Gr	Grashof number
i	current density, A/cm^2
I	ionic strength, mol/liter
I_D	limiting diffusion current
I_L	limiting current
I_r	*true* ionic strength, mol/liter
K'	dissociation constant, mol/liter
L	height of vertical electrode, cm
n	number of electrons transferred in electrode reaction
Nu	Nusselt number
r	ratio of supporting electrolyte to total electrolyte
R	universal gas constant, 8.3143 J/mol·K
s_i	stoichiometric coefficient of species i in electrode reaction
Sc	Schmidt number
t	time, s
t_i	transference number of species i
T	absolute temperature, K
u_i	mobility of species i, cm^2·mol/J·s
υ_x	velocity component parallel to the electrode, cm/s
υ_y	velocity component perpendicular to the electrode, cm/s
x	distance along the electrode measured from the beginning of the boundary layer, cm
y	normal distance from the electrode, cm
z_i	charge number of species i
$\Gamma(4/3)$	0.89298, the gamma function of 4/3
δ	thickness of Nernst stagnant diffusion layer, cm
η	similarity variable for free convection
κ	conductivity, S/cm
ν	kinematic viscosity, cm^2/s
ξ	dimensionless distance from the electrode
ρ	density, g/cm^3
$\Delta\rho$	$\lvert\rho_\infty - \rho_0\rvert$
τ_0	shear stress averaged over the electrode, N/cm^2
ϕ	$F\Phi/RT$
Φ	electric potential, V
Ω	rotation speed, rad/s

Subscripts and Superscripts

avg	average
R	limiting reactant
0	at the electrode surface
0	zero-order concentration of supporting ions
∞	in the bulk solution
*	see equation 19.36

REFERENCES

1. Arnold Eucken, "Über den stationären Zustand zwischen polarisierten Wasserstoffelektroden," *Zeitschrift für physikalische Chemie*, *59* (1907), 72–117.
2. Limin Hsueh and John Newman, "The Role of Bisulfate Ions in Ionic Migration Effects," *Industrial and Engineering Chemistry Fundamentals*, *10* (1971), 615–620.
3. I. Šlendyk, "Polarographic Studies with the Dropping Mercury Kathode. Part XXI. Limiting Currents of Electrodeposition of Metals and of Hydrogen," *Collection of Czechoslovak Chemical Communications*, *3* (1931), 385–395.
4. D Ilkovič, "Polarographic Studies with the Dropping Mercury Kathode. Part XLIV. The Dependence of Limiting Currents on the Diffusion Constant, on the Rate of Dropping and on the Size of Drops," *Collection of Czechoslovak Chemical Communications*, *6* (1934), 498–513.
5. Shinzo Okada, Shiro Yoshizawa, Fumio Hine, and Kameo Asada, "Effect of Migration on Polarographic Limiting Current," *Journal of the Electrochemical Society of Japan*, (Overseas Edition) *27* (1959), E51–E52.
6. Stanley L. Gordon, John S. Newman, and Charles W. Tobias, "The Role of Ionic Migration in Electrolytic Mass Transport; Diffusivities of $[Fe(CN)_6]^{3-}$ and $[Fe(CN)_6]^{4-}$ in KOH and NaOH Solutions," *Berichte der Bunsengesellschaft für physikalische Chemie*, *70* (1966), 414–420.
7. John Newman, "Effect of Ionic Migration on Limiting Currents," *Industrial and Engineering Chemistry Fundamentals*, *5* (1966), 525–529.
8. John Newman, "The Effect of Migration in Laminar Diffusion Layers," *International Journal of Heat and Mass Transfer*, *10* (1967), 983–997.
9. John Newman and Limin Hsueh, "Currents Limited by Gas Solubility," *Industrial and Engineering Chemistry Fundamentals*, *9* (1970), 677–679.
10. Daniel R. Baker, Mark W. Verbrugge, and John Newman, "A transformation for the treatment of diffusion and migration. Application to stationary disk and hemisphere electrodes," *Journal of Electroanalytical Chemistry*, *314* (1991), 23–44.
11. Bava Pillay and John Newman, "Modeling Diffusion and Migration in Dilute Electrochemical Systems Using the Quasi-Potential Transformation," *Journal of the Electrochemical Society*, *140* (1993), 414–420.
12. Mark W. Verbrugge, Daniel R. Baker, and John Newman, "Dependent-Variable Transformation for the Treatment of Diffusion, Migration, and Homogeneous Reactions. Application to a Corroding Pit," *Journal of the Electrochemical Society*, *140* (1993), 2530–2537.
13. Mark W. Verbrugge, Daniel R. Baker, and John Newman, "Reaction Distribution in a Corroding Pit," *Electrochimica Acta*, *38* (1993), 1649–1659.
14. Alan K. Hauser and John Newman, "Potential and Concentration Variations of a Reacting, Supporting Electrolyte," *Journal of the Electrochemical Society*, *136* (1989), 3319–3325.
15. Edward F. Kern and M. Y. Chang, "Conductivity of Copper Refining Electrolytes," *Transactions of the American Electrochemical Society*, *41* (1922), 181–196.
16. C. R. Wilke, M. Eisenberg, and C. W. Tobias, "Correlation of Limiting Currents under Free Convection Conditions," *Journal of the Electrochemical Society*, *100* (1953), 513–523.
17. E. J. Fenech and C. W. Tobias, "Mass Transfer by Free Convection at Horizontal Electrodes," *Electrochimica Acta*, *2* (1960), 311–325.
18. A. Brenner, "A Method for Studying Cathode Films by Freezing," *Proceedings of the American Electroplaters' Society*, (1940), 95–98.
19. Jan Robert Selman and John Newman, "Free-Convection Mass Transfer with a Supporting Electrolyte," *Journal of the Electrochemical Society*, *118* (1971), 1070–1078.

CHAPTER 20

CONCENTRATION OVERPOTENTIAL

20.1 DEFINITION

The concentration overpotential was defined in Section 1.5 as the potential difference between a reference electrode adjacent to the surface, just outside the diffuse double layer, and another reference electrode in the bulk of the solution, minus the potential difference that would exist between these reference electrodes if the current distribution were unchanged but there were no concentration variations between the electrode surface and the bulk solution. These reference electrodes were to involve the same electrode reaction as that under consideration at the working electrode.

This idealized definition is based on the concept of a diffusion layer near the electrode, where the concentration variations occur, and a bulk solution, where the composition is uniform. The ohmic potential is subtracted from the measurement, so that the resulting concentration overpotential is independent of the precise placement of the reference electrode in the bulk solution. The ohmic potential that is subtracted is not the actual ohmic potential drop but is that which would prevail in a solution of uniform composition (with the same current distribution). This has the advantage that this ohmic potential drop can be calculated by solving Laplace's equation, as in Chapter 18, without explicit consideration of the concentration variations near the electrode, which would destroy the validity of Laplace's equation in this region. We shall see how this works in the next chapter, where we want to treat the current distribution below, but at an appreciable fraction of, the limiting current.

In Section 1.5, we also considered another possible decomposition of the potential variation in the solution, in which the ohmic portion is that which would disappear immediately if the current density were to become zero everywhere. This decomposition has the practical disadvantage that in most geometries interruption of the external current to an electrode does not automatically ensure that the local current density is everywhere equal to zero,[1] even in the absence of concentration variations near electrodes. It has the theoretical disadvantage that the calculation of the ohmic potential drop would then include directly some of the effect of the variation of composition.

Electrochemical Systems, Fourth Edition. John Newman and Nitash P. Balsara.

According to the development in Chapter 2, the potential V_r of a movable reference electrode (relative to a fixed reference electrode) varies with position as

$$\nabla V_r = -\sum_i \frac{s_i}{nF} \nabla \mu_i, \tag{20.1}$$

where the electrode reaction for the reference electrode is given by equation 2.6. By selecting an ionic species n, we can write this as

$$\nabla V_r = \frac{1}{z_n F} \nabla \mu_n - \sum_i \frac{s_i}{nF} \left(\nabla \mu_i - \frac{z_i}{z_n} \nabla \mu_n \right), \tag{20.2}$$

since

$$\sum_i z_i s_i = -n. \tag{20.3}$$

Substitution of equation 2.68 yields

$$\nabla V_r = -\frac{\mathbf{i}}{\kappa} - \sum_i \frac{s_i}{nF} \left(\nabla \mu_i - \frac{z_i}{z_n} \nabla \mu_n \right) - \sum_j \frac{t_j^0}{z_j F} \left(\nabla \mu_j - \frac{z_j}{z_n} \nabla \mu_n \right). \tag{20.4}$$

The first two terms on the right are the ohmic potential drop and the terms relating to the specific electrode reaction. The last two terms are expressed in terms of the gradients of the electrochemical potentials of neutral combinations of ions and are zero in the absence of concentration variations, in which case κ is a constant.

Let us introduce the concentrations into equation 20.4 by means of equation 11.69. Then we have

$$\nabla V_r = -\frac{\mathbf{i}}{\kappa} - \frac{RT}{nF} \sum_i s_i \nabla \ln \, c_i f_{i,n} - \frac{RT}{F} \sum_j \frac{t_j^0}{z_j} \nabla \ln c_j f_{j,n}, \tag{20.5}$$

where $f_{i,n}$ is the molar activity coefficient of species i referred to the ionic species n (see equation 11.71). The last term represents the diffusion potential (see equation 11.11).

If we subtract the ohmic drop that would exist in the absence of concentration variations and integrate across the diffusion layer, we obtain the concentration overpotential as defined above

$$\eta_c = \int_0^\infty i_y \left(\frac{1}{\kappa} - \frac{1}{\kappa_\infty} \right) dy + \frac{RT}{nF} \sum_i s_i \ln \frac{(c_i f_{i,n})_\infty}{(c_i f_{i,n})_0} + \frac{RT}{F} \int_0^\infty \sum_j \frac{t_j^0}{z_j} \frac{\partial \ln \, c_j f_{j,n}}{\partial y} dy, \tag{20.6}$$

where ∞ denotes the bulk solution and 0 denotes the electrode surface (outside the diffuse double layer). The current density i_y is approximately constant in the diffusion layer and can be taken to be equal to i_n, the value at the electrode. For dilute solutions, we can neglect the activity coefficients and let the transference numbers be given by equation 11.9, with the result

$$\eta_c = i_n \int_0^\infty \left(\frac{1}{\kappa} - \frac{1}{\kappa_\infty} \right) dy + \frac{RT}{nF} \sum_i s_i \ln \frac{c_{i\infty}}{c_{i0}} + F \int_0^\infty \sum_j \frac{z_j D_j}{\kappa} \frac{\partial c_j}{\partial y} dy, \tag{20.7}$$

where the Nernst–Einstein relation 11.41 has been used. Equation 20.7 can be compared with equation 30 of Ref. [2].

Subtraction of i_y/κ_∞ in the integrals in equations 20.6 and 20.7 corresponds to subtracting the ohmic contribution that would exist in the absence of concentration variations. The concentration overpotential is, thus, the potential difference of a concentration cell plus an ohmic contribution due to the variation of conductivity within the diffusion layer, which can logically be associated with concentration variations near electrodes.

20.2 BINARY ELECTROLYTE

The potentials of concentration cells involving solutions of a single electrolyte were treated in Section 2.6. On the basis of equation 2.85, the concentration overpotential in this case can be expressed as

$$\eta_c = i_n \int_0^\infty \left(\frac{1}{\kappa} - \frac{1}{\kappa_\infty}\right) dy - \frac{\nu RT}{F} \int_0^\infty \left(\frac{t_-^0}{z_+\nu_+} - \frac{s_-}{n\nu_-} + \frac{s_0 c}{nc_0}\right) \frac{\partial \ln cf_{+-}}{\partial y} dy. \tag{20.8}$$

For dilute solutions, this reduces to

$$\eta_c = \frac{i_n}{z_+\nu_+F^2(z_+u_+ - z_-u_-)} \int_0^\infty \left(\frac{1}{c} - \frac{1}{c_\infty}\right) dy + \frac{z_+ - z_-}{z_+} \frac{RT}{F} \left(\frac{t_-^0}{z_-} + \frac{s_-}{n}\right) \ln \frac{c_\infty}{c_0}. \tag{20.9}$$

(In equation 20.8, c_0 is the solvent concentration; in equation 20.9, it is the value of c at the electrode.)

It is tempting to try to simplify this expression for the concentration overpotential even further. For the purpose of evaluating the integral in equation 20.9, the concentration profile could be approximated as (compare Figure 17.1)

$$\begin{aligned} c &= c_0 + (c_\infty - c_0)\frac{y}{\delta} \quad \text{for} \quad y < \delta \\ &= c_\infty \quad \text{for} \quad y > \delta, \end{aligned} \tag{20.10}$$

where δ is given by

$$\frac{\partial c}{\partial y} = \frac{c_\infty - c_0}{\delta} \text{ at } y = 0. \tag{20.11}$$

Then

$$\int_0^\infty \left(\frac{1}{c} - \frac{1}{c_\infty}\right) dy = \frac{\delta}{c_\infty - c_0} \ln \frac{c_\infty}{c_0} - \frac{\delta}{c_\infty} = \frac{\ln(c_\infty/c_0) - (c_\infty - c_0)/c_\infty}{\partial c/\partial y|_{y=0}}. \tag{20.12}$$

Now

$$\frac{i_n}{F}\left(\frac{s_-}{n} + \frac{t_-^0}{z_-}\right) = \nu_- D \left.\frac{\partial c}{\partial y}\right|_{y=0}. \tag{20.13}$$

Consequently, with the Nernst–Einstein relation 11.41, the concentration overpotential becomes

$$\eta_c = \frac{RT}{z_+z_-F} \frac{z_+ - z_-}{1 + (z_-s_-/nt_-^0)} \times \left\{\left[1 + \frac{z_-s_-}{n}\left(2 + \frac{z_-s_-}{nt_-^0}\right)\right] \ln \frac{c_\infty}{c_0} - t_+^0\left(1 - \frac{c_0}{c_\infty}\right)\right\}, \tag{20.14}$$

and, for a metal deposition reaction ($s_- = 0$), this reduces to

$$\eta_c = \frac{(z_+ - z_-)RT}{z_+ z_- F}\left[\ln\frac{c_\infty}{c_0} - t_+^0\left(1 - \frac{c_0}{c_\infty}\right)\right]. \tag{20.15}$$

This is the basis for Problem 1.1.

20.3 SUPPORTING ELECTROLYTE

For solutions with an excess of supporting electrolyte, it should be possible to neglect conductivity variations in the diffusion layer. Then equation 20.7 for the concentration overpotential becomes

$$\eta_c = \frac{RT}{nF}\sum_i s_i \ln\frac{c_{i\infty}}{c_{i0}} + \frac{F}{\kappa_\infty}\sum_j z_j D_j(c_{j\infty} - c_{j0}). \tag{20.16}$$

Now, the last term is also on the order of the reactant concentration divided by the supporting electrolyte concentration and can be neglected, with the result

$$\eta_c = \frac{RT}{nF}\sum_i s_i \ln\frac{c_{i\infty}}{c_{i0}}. \tag{20.17}$$

20.4 CALCULATED VALUES

The most salient feature of the concentration overpotential is that it becomes infinite when the concentration of one of the reactants becomes zero at the electrode, corresponding to the limiting current. The concentration overpotential also allows us to calculate the current–potential relationship for a complete cell, as presented in Figures 1.12 and 1.13. (There we see that the surface overpotential also becomes infinite at the limiting current because the exchange current density goes to zero.) For many cell geometries, the calculations are more difficult. This is treated in Chapter 21.

The nature of concentration overpotentials can be revealed by some examples. Figure 1.11 was calculated for a rotating disk electrode[3] by using equation 20.6 or 20.8, that is, without approximations for dilute solutions. The values of i and η_c are those for the center of the disk, in case the current distribution is nonuniform.

Tables 20.1 and 20.2 give values of η_c calculated according to equation 20.7 for a rotating-disk electrode. The concentration profiles were calculated with the computer program in Appendix C for the effect of migration on limiting currents, but with a nonzero value for the reactant concentration at the electrode. Thus, approximations for dilute solutions are already introduced: Variations of activity coefficients are neglected, equations 11.7 and 11.9 are used for the conductivity and transference numbers, and the Nernst–Einstein relation 11.41 is used.

In Table 20.1 for copper deposition, comparison with equations 20.15 and 20.17 is made, thus providing a check on the error involved in the additional approximations used to derive these equations. The presence of the diffusion potential shows up in this table. For example, the value −6.69 mV for $c_{R0}/c_{R\infty} = 0.7$ and $r = 0.25$ is greater in magnitude than the corresponding values for $r = 0$ and $r = 1$. In Table 20.2 for the reduction of ferricyanide ions, equation 20.17 works well throughout the range of the table, being exact for $r = 1$.

TABLE 20.1 Values of concentration overpotential η_c (in mV) for copper deposition on a rotating disk from solutions of copper sulfate and sulfuric acid, with complete dissociation of bisulfate ions

	$c_{R0}/c_{R\infty}$					
r^a	0.1	0.25	0.5	0.7	0.9	0.95
0[b]	−49.84	−27.85	−12.63	−6.06	−1.67	−0.800
0	−50.52	−28.27	−12.79	−6.10	−1.67	−0.798
0.25	−37.35	−23.94	−12.65	−6.69	−2.01	−0.984
0.5	−34.23	−21.62	−11.38	−6.04	−1.83	−0.897
0.7	−32.18	−19.96	−10.33	−5.43	−1.63	−0.799
0.9	−30.39	−18.48	−9.35	−4.85	−1.44	−0.704
0.99	−29.66	−17.87	−8.95	−4.61	−1.36	−0.663
1[c]	−29.58	−17.81	−8.90	−4.58	−1.35	−0.659

[a] $r = c^{\infty}_{H+}/2c^{\infty}_{SO_4^{2-}}$.
[b] Equation 20.15.
[c] Equation 20.17.

TABLE 20.2 Values of concentration overpotential η_c (in mV) for reduction of ferricyanide ions on a rotating disk from solutions equimolar in potassium ferricyanide and potassium ferrocyanide and with various amounts of added potassium hydroxide

	$c_{R0}/c_{R\infty}$					
r^a	0.1	0.25	0.5	0.7	0.9	0.95
0	−74.22	−48.67	−27.15	−15.14	−4.84	−2.41
0.25	−74.85	−49.22	−27.57	−15.42	−4.95	−2.46
0.5	−75.47	−49.79	−28.02	−15.73	−5.08	−2.53
0.7	−76.04	−50.32	−28.44	−16.03	−5.20	−2.59
0.9	−76.78	−51.01	−29.00	−16.44	−5.36	−2.68
0.99	−77.21	−51.41	−29.34	−16.68	−5.46	−2.73
1	−77.27	−51.47	−29.38	−16.71	−5.47	−2.74

[a] $r = c^{\infty}_{OH^-}/c^{\infty}_{K+}$.

PROBLEMS

20.1 For the electrode reaction

$$Pb(s) + SO_4^{2-} \rightleftharpoons PbSO_4(s) + 2e^-$$

in a sulfuric acid solution supposed to be dissociated into hydrogen and sulfate ions, show that the concentration overpotential can be approximated as

$$\eta_c = -\frac{(z_+ - z_-)RT}{z_+ z_- F}\left[\ln\frac{c_\infty}{c_0} - t^0_-\left(1 - \frac{c_0}{c_\infty}\right)\right].$$

20.2 For the electrode reaction

$$PbO_2(s) + SO_4^{2-} + 4H^+ + 2e^- \rightleftharpoons PbSO_4(s) + 2H_2O$$

in a sulfuric acid solution supposed to be dissociated into hydrogen and sulfate ions, show that the concentration overpotential can be approximated as

$$\eta_c = \frac{(z_+ - z_-)RT}{z_+ z_- F}\left[\frac{1 + 3t_-^0}{1 + t_-^0}\ln\frac{c_\infty}{c_0} - \frac{t_+^0 t_-^0}{1 + t_-^0}\left(1 - \frac{c_0}{c_\infty}\right)\right].$$

20.3 For an anode, equation 20.15 can give negative values for η_c. Explain how this situation arises and discuss whether any basic physical laws are violated by having a negative overpotential at an anode.

20.4 Using the ferrous–ferric redox reaction

$$Fe^{2+} \rightleftharpoons Fe^{3+} + e^-$$

in an excess of supporting electrolyte as an example, show that equations 8.23 and 8.24 can be rearranged to yield the rate equation

$$i = i_0^\infty\left\{\frac{c_{10}}{c_{1\infty}}\exp\left[\frac{(1-\beta)nF}{RT}\eta\right] - \frac{c_{20}}{c_{2\infty}}\exp\left[-\frac{\beta nF}{RT}\eta\right]\right\},$$

where species 1 is the ferrous ion, species 2 is the ferric ion, η is the total overpotential $\eta_s + \eta_c$, and i_0^∞ is the exchange current density at the bulk composition, having the composition dependence

$$i_0^\infty = nFk_c^{1-\beta}k_a^\beta c_{1\infty}^\beta c_{2\infty}^{1-\beta}$$

if the rules for reaction orders after equation 8.28 are followed.

NOTATION

c	concentration of binary electrolyte, mol/cm^3
c_i	concentration of species i, mol/cm^3
D	diffusion coefficient of binary electrolyte, cm^2/s
D_i	diffusion coefficient of species i, cm^2/s
$f_{i,n}$	molar activity coefficient of species i referred to species n
f_{+-}	mean molar activity coefficient of binary electrolyte
F	Faraday's constant, 96,487 C/mol
i	current density, A/cm^2
n	number of electrons involved in the electrode reaction
R	universal gas constant, 8.3143 J/mol·K
s_i	stoichiometric coefficient of species i in electrode reaction
t_i^0	transference number of species i with respect to the velocity of species 0
T	absolute temperature, K
u_i	mobility of species i, cm^2 mol/J·s
V_r	potential of a reference electrode, V

y	normal distance from an electrode, cm
z_i	charge number of species i
δ	equivalent diffusion-layer thickness, cm
η_c	concentration overpotential, V
κ	conductivity, S/cm
μ_i	electrochemical potential of species i, J/mol
ν	$\nu_+ + \nu_-$
ν_+, ν_-	numbers of cations and anions produced by dissociation of one molecule of electrolyte

Subscripts

0	at the electrode surface
∞	in the bulk solution

REFERENCES

1. John Newman, "Ohmic Potential Measured by Interrupter Techniques," *Journal of the Electrochemical Society*, *117* (1970), 507–508.
2. John Newman, "The Effect of Migration in Laminar Diffusion Layers," *International Journal of Heat and Mass Transfer*, *10* (1967), 983–997.
3. J. Newman and L. Hsueh, "The Effect of Variable Transport Properties on Mass Transfer to a Rotating Disk," *Electrochimica Acta*, *12* (1967), 417–427.

CHAPTER 21

CURRENTS BELOW THE LIMITING CURRENT

At currents below, but at an appreciable fraction of, the limiting current, it is necessary to consider concentration variations near electrodes, the surface overpotential associated with the electrode reaction, and the ohmic potential drop in the bulk of the solution. These problems are inherently of greater complexity than either the convective-transport problems or the potential-theory problems, treated in Chapters 17 and 18, in which one or more of these factors could be ignored.

In many electrolytic cells, the concentration variations are still restricted to thin diffusion layers near the electrodes, and Laplace's equation still applies to the bulk of the solution outside these diffusion layers. This means that one can devote separate attention to these different regions. Since the diffusion layers are thin, the bulk region essentially fills the region of the electrolytic solution bounded by the walls of the cell and the electrodes. In this region, the potential is determined so as to satisfy Laplace's equation and agree with the current density distribution on the boundaries of the region. In the diffusion layers, the concentrations are determined so as to satisfy the appropriate form of the transport equations, with a mass flux at the wall appropriate to the current density distribution on the electrodes and with the concentration approaching the bulk concentrations far from the electrode. The current distribution and concentrations at the electrode surface must adjust themselves so as to agree with the overpotential variation determined from the calculation of the potential in the bulk region. We are thus faced with a singular-perturbation problem, and the treatment of the two regions is coupled through the boundary conditions.

The thinness of the diffusion layers also allows one to separate the irreversible part of the cell potential into the sum of the surface overpotentials, the concentration overpotentials, and the ohmic potential drop in the solution (see Section 1.6). The surface overpotential has been defined and discussed in Sections 1.3 and 16.2 and Chapter 8. It is related to the concentrations and current density at the electrode surface by the polarization equation 16.9. The surface overpotential varies with position on the electrode unless the concentrations and current density are uniform on the electrode. The concentration overpotential was discussed in Section 1.5 and Chapter 20. In general, the concentration overpotential also depends upon position along the electrode surface.

Electrochemical Systems, Fourth Edition. John Newman and Nitash P. Balsara.

Asada et al.[1] have used a separate treatment of the diffusion layers and the bulk solution to treat free convection in a rectangular cell with a vertical electrode at each end for currents below the limiting current. Newman has given a detailed justification for such a procedure for systems with laminar, forced convection[2] and has applied the method to the rotating-disk electrode.[3–5] References [6–12] reflect on the experimental verification of the results. The problem for two electrodes of length L placed opposite each other at a distance h, embedded in the walls of a flow channel with steady, laminar flow, is formulated in Ref. [13] and has been worked out by Parrish and Newman.[5, 14] Alkire and Mirarefi[15] treated an interior, tubular electrode with a downstream or upstream counterelectrode. Simultaneous reactions have been treated for the rotating disk by White and Newman[16] and for the channel flow geometry by Edwards and Newman[17] and by White et al.[18] Pierini and Newman applied these methods to a ring-disk geometry,[19] and Pierini et al. applied them to a redox reaction on a disk electrode,[20] while Nişancioğlu and Newman dealt with a rotating spherical electrode.[21]

21.1 THE BULK MEDIUM

We deal here with forced-convection systems where the hydrodynamic velocity distribution can be assumed to be known. When the Péclet number $\mathrm{Pe} = UL/D_R$ (where U is a characteristic velocity and L is a characteristic length) is large, mass transfer by convection predominates over diffusion except in a thin diffusion layer near an electrode surface. Outside these diffusion layers, in the bulk solution, the concentrations are uniform; and the potential satisfies Laplace's equation (see Section 18.1). We use a tilde to denote the potential and current distributions in this region. Thus, we have

$$\nabla^2 \tilde{\Phi} = 0. \tag{21.1}$$

In the bulk medium, the current density is related to the potential gradient by Ohm's law

$$\tilde{\mathbf{i}} = -\kappa_\infty \nabla \tilde{\Phi}. \tag{21.2}$$

In this singular-perturbation problem, the diffusion layers approach zero thickness as the Péclet number approaches infinity. Consequently, we solve Laplace's equation in the region confined by the electrodes and the insulating walls of the cell, as though the diffusion layers were not present. At the walls, the current density in the bulk region must match with the current density in the outer limit of the diffusion layer. In Section 21.3, we argue that the normal component of the current density changes very little in the thin diffusion layer and is essentially equal to the value at the wall. Therefore, the boundary condition for Laplace's equation is

$$\frac{\partial \tilde{\Phi}}{\partial y} = -\frac{i_n}{\kappa_\infty} \quad \text{at} \quad y = 0, \tag{21.3}$$

where y is the distance from the wall and i_n is the y component of $\mathbf{i}$ at the wall. Thus, i_n represents the contribution to the external current flowing to an electrode and is zero on insulating surfaces. On electrodes, i_n is not known until we have solved simultaneously for the bulk medium and the diffusion layers.

Laplace's equation is to be solved for the bulk medium in much the same way as in Chapter 18, where there were no concentration variations; the same methods can be used, and geometric arrangements that proved intractable there would be equally difficult to treat here. For plane electrodes in the walls of a flow channel,[5, 13, 14] an integral equation can be used to relate the potential and the normal component of the potential gradient at the wall, for the solution of Laplace's equation. For the

disk electrode, the same thing can be accomplished by using the coefficients of an infinite series[3] obtained by the method of separation of variables, although an integral equation could also be used.[22] Where these methods can be used, they are superior, in terms of computational effort and accuracy, to a numerical solution of Laplace's equation in the bulk medium by finite differences.

If V_{met} is the potential of the electrode metal and $\tilde{\Phi}$ in the bulk solution is that measured by a reference electrode of the same kind as the working electrode, then the total overpotential at the electrode is

$$\eta = V_{\text{met}}(x) - \tilde{\Phi}_0(x), \tag{21.4}$$

where x is distance measured along the electrode and $\tilde{\Phi}_0$ is the value of $\tilde{\Phi}$ evaluated at $y = 0$. This is the sum of the concentration overpotential η_c, associated with concentration changes in the diffusion layer, and the surface overpotential η_s, associated with the heterogeneous electrode reaction,

$$\eta = \eta_c + \eta_s. \tag{21.5}$$

We can see that this conforms to our previous definitions of η_c and η_s in terms of reference electrodes located outside the diffuse double layer and in the bulk solution. Since $\tilde{\Phi}_0$ is the value of $\tilde{\Phi}$ at $y = 0$, subtracting it from V_{met} in equation 21.4 corresponds to subtracting the ohmic potential drop in the bulk solution, calculated with the actual current distribution but extrapolated to the electrode surface with a constant conductivity κ_∞, as though there were no concentration variations in the diffusion layer. Hence η, and η_c in particular, includes only the ohmic potential drop associated with concentration variations in the diffusion layer.

21.2 THE DIFFUSION LAYERS

Because of the thinness of the diffusion layer, effects of curvature can be neglected, and we adopt the usual boundary layer coordinates: x, measured along the electrode from its upstream end, and y, the normal distance from the surface. In the diffusion layer, the transport equation simplifies to

$$\frac{\partial c_i}{\partial t} + v_x \frac{\partial c_i}{\partial x} + v_y \frac{\partial c_i}{\partial y} = D_i \frac{\partial^2 c_i}{\partial y^2} + z_i u_i F \left(c_i \frac{\partial^2 \Phi}{\partial y^2} + \frac{\partial c_i}{\partial y} \frac{\partial \Phi}{\partial y} \right). \tag{21.6}$$

On the right side, derivatives with respect to x have been ignored compared to the derivatives with respect to y.

We also assume that the Schmidt number $\text{Sc} = \nu/D_R$ is large. This means that the diffusion layer is thin even when compared with any hydrodynamic boundary layer that may be present, and, within the diffusion layer, the velocity components can be represented as (see equations 17.62 and 17.69)

$$v_x = y\beta(x) \quad \text{and} \quad v_y = -\frac{1}{2} y^2 \frac{(\mathcal{R}\beta)'}{\mathcal{R}}, \tag{21.7}$$

where $\beta(x)$ is the velocity derivative at the solid wall, $\beta = \partial v_x/\partial y$ at $y = 0$, and the prime denotes the derivative with respect to x. These equations apply to two-dimensional and axisymmetric diffusion layers; for a two-dimensional diffusion layer, $\mathcal{R}(x)$ is to be set equal to 1.

In equations 21.6 for mass transfer in the diffusion layer, only derivatives of potential with respect to y appear and not Φ itself or the x derivative of Φ. Consequently, we can introduce a new potential ϕ in the diffusion layer, defined as

$$\phi = \Phi(x, y) - \tilde{\Phi}_0(x), \tag{21.8}$$

or we can even assign the zero of ϕ arbitrarily at each value of x. Then, $\tilde{\Phi}_0(x)$ is important only in the determination of the total overpotential η.

Matters are simplified considerably if we are further willing to neglect migration in the diffusion layer, so that equation 21.6 becomes

$$\frac{\partial c_i}{\partial t} + y\beta\frac{\partial c_i}{\partial x} - \frac{y^2(\mathcal{R}\beta)'}{2\mathcal{R}}\frac{\partial c_i}{\partial y} = D_i\frac{\partial^2 c_i}{\partial y^2}. \tag{21.9}$$

Even though the ohmic potential drop in the bulk solution has an important effect on the variation of the total overpotential along the electrode surface, migration within the diffusion layer does not have a crucial effect on the current distribution. We have seen that, at the limiting current, the effect of migration is to change the magnitude but not the distribution of the current.

Equation 21.9 applies if there is an excess of supporting electrolyte (see Section 11.5). However, the importance of the ohmic drop in the bulk solution depends on the ratio of a characteristic length to the conductivity κ_∞, as brought out in Chapter 18, and this ratio can be large even in the presence of supporting electrolyte. Equation 21.9 also applies to the other extreme case, solutions of a binary electrolyte (see Section 11.4), where D_i is to be replaced by D, the diffusion coefficient of the electrolyte.

Equations 21.6, one for each species, are to be solved along with the electroneutrality equation 16.3 for the concentrations and the potential. For the simplified case, equation 21.9 need be solved only for those species that participate in the electrode reaction.

The concentrations approach their bulk values as y approaches infinity. At the electrode surface, the fluxes are related to the current density by equation 16.8:

$$N_{in} = -\frac{s_i}{nF}i_n \quad \text{at} \quad y = 0. \tag{21.10}$$

When migration can be ignored, this becomes

$$\frac{\partial c_i}{\partial y} = \frac{s_i i_n}{nFD_i} \quad \text{at} \quad y = 0. \tag{21.11}$$

The equations of Section 17.12 then allow us to solve the diffusion-layer equations 21.9 (in the steady state) and to relate the surface concentration to the concentration derivative at the surface. Further reference to the diffusion-layer equations is then unnecessary. Substitution of equation 21.11 into equation 17.95 gives

$$\frac{s_i i_n(x)}{nFD_i} = -\frac{\sqrt{\mathcal{R}\beta}}{\Gamma(4/3)}\int_0^x \left.\frac{dc_{i0}}{dx}\right|_{x=x_0} \frac{dx_0}{\left(9D_i\int_{x_0}^x \mathcal{R}\sqrt{\mathcal{R}\beta}dx\right)^{1/3}}, \tag{21.12}$$

where $c_{i0}(x)$ is the surface concentration of species i. In applications, the fact that this is a Stieltjes integral should be borne in mind (see Problem 17.8).

21.3 BOUNDARY CONDITIONS AND METHOD OF SOLUTION

Certain boundary conditions have already been discussed in connection with the diffusion layers and the bulk medium. The solution for the potential $\tilde{\Phi}$ in the bulk solution must satisfy the condition 21.3, relating the potential derivative to the external current density. It also provides the total overpotential

through equation 21.4. The solution in the diffusion layer requires matching the fluxes and the current density through equation 21.10. This is already incorporated into equation 21.12.

The current densities for the diffusion layer and the bulk medium must match. The current density satisfies equation 11.14:

$$\nabla \cdot \mathbf{i} = 0. \tag{21.13}$$

In a two-dimensional diffusion layer, this can be written as

$$\frac{\partial i_x}{\partial x} + \frac{\partial i_y}{\partial y} = 0 \tag{21.14}$$

or

$$i_y = i_n - \int_0^y \frac{\partial i_x}{\partial x} dy. \tag{21.15}$$

Since the diffusion layer is thin, i_y is approximately constant throughout the thickness of the diffusion layer, and, therefore, the value at the wall is appropriate to use in the boundary condition 21.3 for the solution of Laplace's equation in the bulk medium.

It remains to adopt expressions for the concentration overpotential η_c and the surface overpotential η_s. The former can be calculated from equation 20.7. However, equations 20.15 and 20.17 have the advantage of involving only the concentrations at the surface and not the concentration profiles in the diffusion layer. They are therefore appropriate to use if equation 21.12 has been adopted. For many electrodes, the surface overpotential can be related to the current density through equation 16.10:

$$i_n = i_0 \left[\exp\left(\frac{\alpha_a F}{RT} \eta_s \right) - \exp\left(-\frac{\alpha_c F}{RT} \eta_s \right) \right], \tag{21.16}$$

where the exchange current density i_0 depends on the composition of the solution adjacent to the electrode.

The situation at this point may be confusing, particularly with regard to the diffusion layer, because we have presented several alternative equations. Let us suppose that we have only one reactant species and that we have adopted equation 21.12 as the diffusion-layer equation and either equation 20.15 or 20.17 for the concentration overpotential. The principal unknowns then are the current density and the concentration at the electrode surface. These must adjust themselves so as to agree with the total overpotential η available after subtracting the ohmic potential drop from the electrode potential.

Suppose we know the distribution of η along the electrode. Then η_s in equation 21.16 can be replaced by $\eta - \eta_c$, where η_c is related to the surface concentration by equation 20.15 or 20.17. Substitution of equation 21.16 into equation 21.12 then gives an integral equation for the surface concentration. The numerical solution of this integral equation is actually fairly simple since there is no upstream propagation of effects in the diffusion layer, and a nonlinear equation for c_{i0} need be solved only once at each value of x.

The following procedure might be suggested for solving the problem:

1. Assume a distribution of $i_n(x)$ along the surfaces of the electrodes.
2. Calculate the potential in the bulk medium from Laplace's equation and boundary condition 21.3. There is an arbitrary, additive constant in the solution.
3. Calculate the distribution of total overpotential η along an electrode.
4. Solve the integral equation for the surface concentration along this electrode. This integral equation is formed as described above from equations 21.12, 21.16, 20.15 or 20.17, and 21.5. In

addition to the surface concentration, this calculation also yields the current distribution i_n and the split of the total overpotential into η_c and η_s.

5. In calculating the total overpotential in step 3, there is an uncertainty in the additive constant that is removed by specifying the electrode potential and the additive constant in step 2. In the case of a single electrode whose behavior is not influenced by the placement of the counterelectrode, a trial-and-error calculation can be avoided at this point by specifying the electrode potential relative to a suitably placed reference electrode, or the current density or total overpotential at the beginning of the diffusion layer. However, if the total current to the electrode is specified, it is now necessary to adjust the constant in step 3 until this current is reached. Thus, steps 3 and 4 must be repeated until this condition is satisfied. If there are two electrodes that directly influence each other, it is necessary to specify the total current (so that it will be the same on both electrodes), and repetition of steps 3 and 4 is necessary.
6. If there are two electrodes, steps 3 to 5 must now be carried out for the second electrode.
7. Steps 3 to 6 yield a new current distribution i_n on the electrodes, which may be different from that used in step 2. Steps 2 to 6 must be repeated with a new current density distribution, and this must be continued until the distribution obtained from steps 3 to 6 agrees sufficiently well with that used in step 2. Convergence of this procedure can usually be accomplished if the new current distribution chosen is some average of the previous distribution used in step 2 and that produced by steps 3 to 6.

Other convergence methods have proved useful, including a multidimensional Newton–Raphson.

21.4 RESULTS FOR THE ROTATING DISK

Let us look at the current distribution on a rotating disk electrode[3, 5] (see Figure 17.2) embedded in a larger insulating disk, both of which rotate about their axis in an electrolytic solution. The counterelectrode is supposed to be far enough away that it does not affect the current distribution on the disk electrode. The limiting current was treated in Sections 17.2, 17.13, and 19.2 and is distributed uniformly over the surface of the electrode. The primary and secondary current distributions were discussed in Sections 18.2 and 18.3.

It is assumed that there is one reactant whose concentration is important, and this concentration in the diffusion layer obeys the equation

$$ay\Omega\sqrt{\frac{\Omega}{\nu}}\left(r\frac{\partial c_R}{\partial r}-y\frac{\partial c_R}{\partial y}\right)=D\frac{\partial^2 c_R}{\partial y^2}, \tag{21.17}$$

a form of equation 21.9. For a solution of a single salt, D is the diffusion coefficient of the salt. For reaction of a minor component in a solution with excess supporting electrolyte, D denotes the diffusion coefficient of the reactant. In both cases, the normal current density at the electrode surface is given by

$$\frac{s_R i_n}{nF}=\frac{D}{1-t}\frac{\partial c_R}{\partial y}\quad \text{at}\quad y=0, \tag{21.18}$$

where t is the transference number of the reactant.

For the concentration overpotential we used the expression

$$\eta_c=-\frac{RT}{ZF}\left[\ln\left(\frac{c_\infty}{c_0}\right)-t\left(1-\frac{c_0}{c_\infty}\right)\right]. \tag{21.19}$$

This corresponds to metal deposition from a solution of a single salt (see equation 20.15) if we take t to be the transference number of the reacting cation and set

$$Z = -\frac{z_+ z_-}{z_+ - z_-}. \tag{21.20}$$

Equation 21.19 applies approximately to the reaction of a minor component from a solution with excess indifferent electrolyte (see equation 20.17) if we set $t = 0$ and $Z = -n/s_R$.

The electrode kinetics is expressed by equation 16.10 where we have set $\alpha_a = \alpha Z$ and $\alpha_c = \beta Z$ and have given the concentration dependence of the exchange current density the form

$$i_0(c_0) = \left(\frac{c_0}{c_\infty}\right)^\gamma i_0(c_\infty). \tag{21.21}$$

The current distribution is then determined by seven dimensionless parameters. These are a dimensionless exchange current density J, a dimensionless average current density δ, a dimensionless limiting current density N, the transference number t, the exponent γ in the concentration dependence of the exchange current density, and α and β in the kinetic equation. J, δ, and N are given by

$$J = \frac{ZFr_0}{RT\kappa_\infty} i_0(c_\infty), \quad \delta = \frac{ZFr_0}{RT\kappa_\infty} i_{\text{avg}}, \tag{21.22}$$

and

$$N = -\left(\frac{r_0^2\Omega}{\nu}\right)^{1/2} \left(\frac{a\nu}{3D}\right)^{1/3} \frac{nZF^2Dc_\infty}{s_R RT(1-t)\kappa_\infty}, \tag{21.23}$$

where r_0 is the radius of the disk electrode.

Figure 21.1 shows the distribution of the reactant concentration at the electrode surface. Due to the ohmic potential drop, there tends to be a higher current density near the edge of the disk, and this produces a decrease in the concentration. The distribution is more nonuniform for higher rotation speeds N^2, but the concentration cannot become negative. The disk becomes mass-transfer limited first near the edge. Figure 21.2 shows the corresponding current distribution, expressed as i_n/i_{lim}. The local current density can rise above the average limiting current density because of the nonuniform potential drop, but it is likely to decrease again toward the edge due to the limited rate of mass transfer by convection and diffusion. Higher values of N lead again to a more nonuniform distribution.

The corresponding curves in Figures 21.1 and 21.2 can be identified by the fact that

$$\frac{i_n}{i_{\text{lim}}} = 1 - \frac{c_0}{c_\infty} \tag{21.24}$$

at the center of the disk.

Figure 21.3 shows how the parameters of the system affect the nonuniformity of the current distribution (compare Figure 18.7), but this time the effect of concentration variations is included (N) along with the current level (δ), while J is restricted to the reversible and Tafel cases. Notice that the mass-transfer limitations do not ensure a uniform current density except very close to the limiting current.

Figure 21.4 shows the polarization curve for copper deposition from a 0.1 M cupric sulfate solution.[23] The concentration and surface overpotentials at the center of the disk contribute relatively little compared to the ohmic potential drop in this solution of low conductivity. The ohmic potential

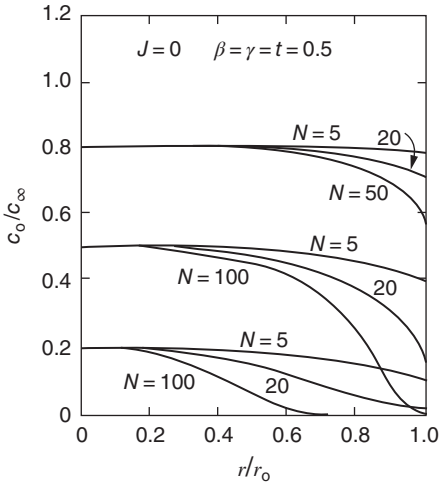

Figure 21.1 Surface concentration for Tafel kinetics. *Source*: John Newman 1966.[3] Reproduced with permission of The Electrochemical Society, Inc.

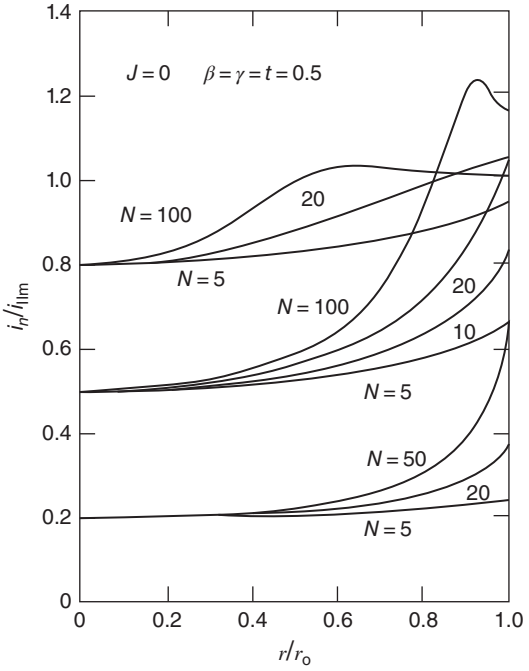

Figure 21.2 Current distribution for Tafel kinetics with an appreciable fraction of the limiting current. *Source*: W. R. Parrish and John Newman 1969.[5] Reproduced with permission of The Electrochemical Society, Inc.

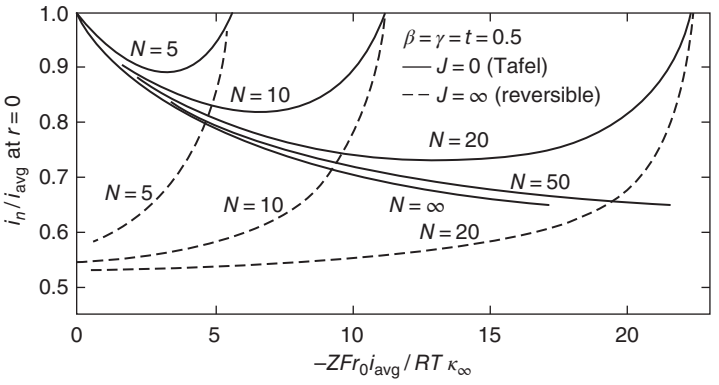

Figure 21.3 Current density at the center of the disk. *Source*: John Newman 1966.[3] Reproduced with permission of The Electrochemical Society, Inc.

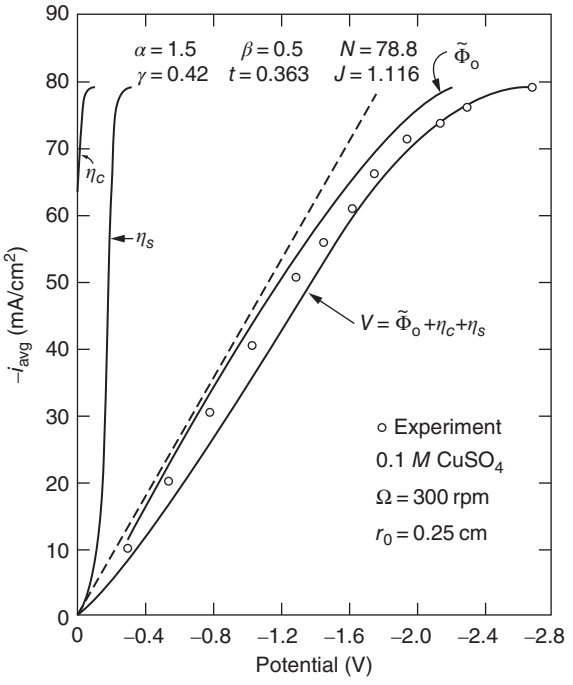

Figure 21.4 Overpotentials for copper deposition on a rotating disk. Dashed line is ohmic drop for the primary current distribution; $\tilde{\Phi}_0, \eta_c$, and η_s are evaluated at the center of the disk. *Source*: John Newman 1966.[3] Reproduced with permission of The Electrochemical Society, Inc.

is not linear since the current distribution changes near the limiting current. Additional parameters for this system are $i_0 = 1$ mA/cm^2 and $\kappa_\infty = 0.00872$ S/cm for a 0.1 M $CuSO_4$ solution at 25°C.

Figure 21.5 shows the total overpotential η at the center of the disk, at the edge of the disk, and at $r = 0.898 r_0$. The ohmic drop $\tilde{\Phi}_0$ also depends on radial position in such a way that the electrode potential $V = \tilde{\Phi}_0 + \eta$ is uniform. Figure 21.5 shows that the overpotential at the edge can be 0.8 V,

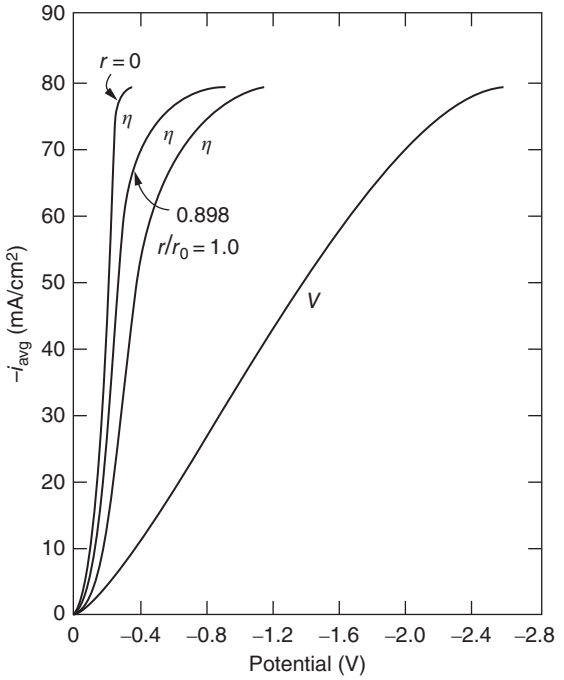

Figure 21.5 Total overpotential at several positions on the disk.

while that at the center is only 0.25 V. Thus, hydrogen may begin to be evolved at the edge before the center has reached the limiting current.

PROBLEMS

21.1 Suppose that we wish to treat the current distribution in an electrochemical system involving a redox reaction and an excess of supporting electrolyte. Use equation 17.96 to show that the product concentration at the surface can be related to that of the reactant according to

$$\frac{c_{40} - c_{4\infty}}{c_{R0} - c_{R\infty}} = \frac{s_4}{s_R}\left(\frac{D_R}{D_4}\right)^{2/3}$$

(compare equation 19.19), where the product of the reaction is labeled as species 4. Use this result to show that the concentration overpotential according to equation 20.17 can be expressed, for ferricyanide reduction from a solution equimolar in ferricyanide and ferrocyanide, as

$$\eta_c = -\frac{RT}{F}\ln\left[\frac{c_{R\infty}}{c_{R0}} + \left(\frac{D_R}{D_4}\right)^{2/3}\left(\frac{c_{R\infty}}{c_{R0}} - 1\right)\right].$$

These results mean that only one diffusion-layer equation of the form 21.12 need be solved for each diffusion layer.

21.2 For the rotating-disk electrode, show that the parameter N can be given as

$$N = -\Gamma\left(\frac{4}{3}\right)\frac{ZFr_0}{RT\kappa_\infty}i_{\lim},$$

thus substantiating that it is a dimensionless limiting-current density.

21.3 Consider here in more detail the plating of the inside of the holes of the circuit board of Problem 18.3. The convection in the bath is such that the flow through the holes is well approximated by Poiseuille flow:

$$v_z = 2\langle v_z\rangle\left(1 - \frac{r^2}{R^2}\right), \quad v_r = v_\theta = 0,$$

with an average velocity of 5 cm/s. The solution contains 0.5 M $CuSO_4$ and 1.5 M H_2SO_4.

(a) Ignoring the effect of migration, calculate a numerical value for the limiting current for a single hole.

(b) Obtain a numerical correction to the limiting-current result in part (a) to account for the effect of migration.

(c) For the problem at an appreciable fraction of, but still below, the limiting current, set up but do not solve the governing equations for the current and potential distribution within a hole. For this purpose, assume that the concentration of copper has not been diminished by the reaction on the face.

21.4 An electrochemical reactor is to be designed to oxidize A to B at the anode while reducing A to C at the cathode. C is insoluble, but B is soluble and can eventually be transported from the anode, where it is produced, to the cathode surface where it would be reduced and thereby decrease the current efficiency and possibly the yield of the reactor. To be specific, you can think of A as ferrous ions, B as ferric ions, and C as metallic iron plated on the cathode—although examples in organic electrosynthesis may be equally important.

The reactor involves two plane electrodes embedded in the walls of a flow channel with fully developed laminar flow (see Figure 21.6). For this geometry and velocity profile, a student in a transport phenomena course suggests that it would be relatively easy to obtain the solution to

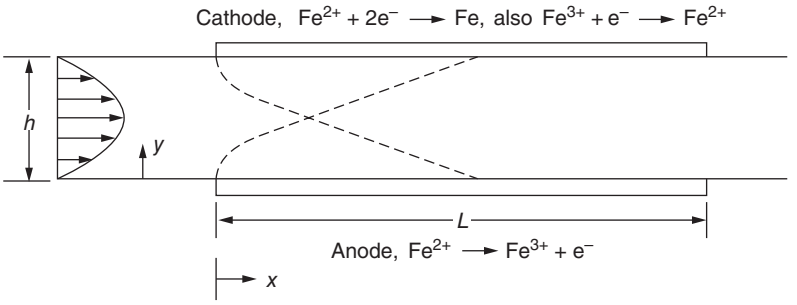

Figure 21.6 Channel flow cell, with diffusion layers shown for the two electrodes.

the following problem:

$$v_x \frac{\partial c_i}{\partial x} = D_i \frac{\partial^2 c_i}{\partial y^2},$$

$$c_i = 0 \quad \text{at} \quad x = 0,$$

$$= 1 \quad \text{at} \quad y = 0, \quad x > 0.$$

$$= 0 \quad \text{at} \quad y = h, \quad x > 0.$$

Discuss how this mathematical solution might be useful in the design of the electrochemical reactor, including the assessment of how much of the product is reacted back to A at the cathode.

NOTATION

a	0.51023
c_i	concentration of species i, mol/cm^3
D	diffusion coefficient of reactant or of binary electrolyte, cm^2/s
D_i	diffusion coefficient of species i, cm^2/s
F	Faraday's constant, 96,487 C/mol
h	distance between walls of a flow channel, cm
i	current density, A/cm^2
i_n	normal current density at electrode surface, A/cm^2
i_0	exchange current density, A/cm^2
J	dimensionless exchange current density
L	electrode length, cm
L	characteristic length, cm
n	number of electrons transferred in electrode reaction
N	dimensionless limiting current density
N_{in}	normal component of the flux of species i, mol/cm^2·s
Pe	Péclet number
r	radial distance, cm
r_0	radius of disk electrode, cm
R	universal gas constant, 8.3143 J/mol·K
$\mathcal{R}$	distance of axisymmetric surface from axis of symmetry, cm
s_i	stoichiometric coefficient of species i in electrode reaction
Sc	Schmidt number
t	time, s
t	transference number of reactant
T	absolute temperature, K
u_i,	mobility of species i, cm^2·mol/J·s
U	characteristic velocity, cm/s
v	fluid velocity, cm/s
V, V_{met}	electrode potential, V
x	distance along electrode from its upstream edge, cm
y	distance from electrode surface, cm
z_i	charge number of species i
Z	$-z_+z_-/(z_+ - z_-)$ for binary electrolyte

Z	$-n/s_R$ for excess supporting electrolyte
α_a, α_c	transfer coefficients
α, β	transfer coefficients
$\beta(x)$	velocity derivative $\partial v_x/\partial y$ at the wall, s^{-1}
γ	exponent in concentration dependence of i_0
$\Gamma(4/3)$	0.89298, the gamma function of 4/3
δ	dimensionless average current density
η	total overpotential, V
η_c	concentration overpotential, V
η_s	surface overpotential, V
κ	conductivity, S/cm
ν	kinematic viscosity, cm^2/s
ϕ	potential (see equation 21.8), V
Φ	electric potential, V
Ω	rotation speed, rad/s

Subscripts and Superscripts

$\sim$	in the bulk medium
0	at the electrode surface
∞	in the bulk solution
R	reactant

REFERENCES

1. Kameo Asada, Fumio Hine, Shiro Yoshizawa, and Shinzo Okada, "Mass Transfer and Current Distribution under Free Convection Conditions," *Journal of the Electrochemical Society*, *107* (1960), 242–246.
2. John Newman, "The Effect of Migration in Laminar Diffusion Layers," *International Journal of Heat and Mass Transfer*, *10* (1967), 983–997.
3. John Newman, "Current Distribution on a Rotating Disk below the Limiting Current," *Journal of the Electrochemical Society*, *113* (1966), 1235–1241.
4. John Newman, "The Diffusion Layer on a Rotating Disk Electrode," *Journal of the Electrochemical Society*, *114* (1967), 239.
5. W. R. Parrish and John Newman, "Current Distribution on a Plane Electrode below the Limiting Current," *Journal of the Electrochemical Society*, *116* (1969), 169–172.
6. D. H. Angell, T. Dickinson, and R. Greef, "The Potential Distribution near a Rotating-Disk Electrode," *Electrochimica Acta*, *13* (1968), 120–123.
7. W. J. Albery and J. Ulstrup, "The Current Distribution on a Rotating Disk Electrode," *Electrochimica Acta*, *13* (1968), 281–284.
8. Vinay Marathe and John Newman, "Current Distribution on a Rotating Disk Electrode," *Journal of the Electrochemical Society*, *116* (1969), 1704–1707.
9. Stanley Bruckenstein and Barry Miller, "An Experimental Study of Nonuniform Current Distribution at Rotating Disk Electrodes," *Journal of the Electrochemical Society*, *117* (1970), 1044–1048.
10. William H. Smyrl and John Newman, "Ring-Disk and Sectioned Disk Electrodes," *Journal of the Electrochemical Society*, *119* (1972), 212–219.
11. William H. Smyrl and John Newman, "Detection of Nonuniform Current Distribution on a Disk Electrode," *Journal of the Electrochemical Society*, *119* (1972), 208–212.

12. Barry Miller and Maria I. Bellavance, "Measurement of Current and Potential Distribution at Rotating-Disk Electrodes," *Journal of the Electrochemical Society*, *120* (1973), 42–53.
13. John Newman, "Engineering Design of Electrochemical Systems," *Industrial and Engineering Chemistry*, *60*(4) (April 1968), 12–27.
14. W. R. Parrish and John Newman, "Current Distributions on Plane, Parallel Electrodes in Channel Flow," *Journal of the Electrochemical Society*, *117* (1970), 43–48.
15. Richard Alkire and Ali Asghar Mirarefi, "The Current Distribution within Tubular Electrodes under Laminar Flow," *Journal of the Electrochemical Society*, *120* (1973), 1507–1515.
16. Ralph White and John Newman, "Simultaneous Reactions on a Rotating Disk Electrode," *Journal of Electroanalytical Chemistry and Interfacial Electrochemistry*, *82* (1977), 173–186.
17. Victoria Edwards and John Newman, "Design of Thin-Gap Channel Flow Cells," *Journal of the Electrochemical Society*, *134* (1987), 1181–1186.
18. R. E. White, Mike Bain, and Mike Raible, "Parallel Plate Electrochemical Reactor Model," *Journal of the Electrochemical Society*, *130* (1983), 1037–1042.
19. Peter Pierini and John Newman, "Current Distribution on a Rotating Ring-Disk Electrode below the Limiting Current," *Journal of the Electrochemical Society*, *124* (1977), 701–706.
20. Peter Pierini, Peter Appel, and John Newman, "Current Distribution on a Disk Electrode for Redox Reactions," *Journal of the Electrochemical Society*, *123* (1976), 366–369.
21. Kemal Nişancioğlu and John Newman, "Current Distribution on a Rotating Sphere below the Limiting Current," *Journal of the Electrochemical Society*, *121* (1974), 241–246.
22. John Newman, "The Fundamental Principles of Current Distribution and Mass Transport in Electrochemical Cells," in Allen J. Bard, ed., *Electroanalytical Chemistry* (New York: Marcel Dekker, 1973), Vol. *6*, pp. 187–352.
23. L. Hsueh and J. Newman, "Mass Transfer and Polarization at a Rotating Disk Electrode," *Electrochimica Acta*, *12* (1967), 429–438.

CHAPTER 22

POROUS ELECTRODES

Porous electrodes have numerous industrial applications primarily because they promote intimate contact of the electrode material with the solution and possibly a gaseous phase. Advantages are:

1. The intrinsic rate of the heterogeneous electrochemical reaction may be slow. A porous electrode can compensate for this by providing a large interfacial area per unit volume (e.g., $10^4\ \text{cm}^{-1}$).
2. Double-layer adsorption constitutes the basis for novel separation processes involving cycling of the electrode potential. Just as in conventional fluid–solid adsorption, a high specific interfacial area is desirable.
3. Important reactants may be stored in the solution in close proximity to the electrode surface. This permits sustained high-rate discharge of the lead–acid cell.
4. A dilute contaminant can be removed effectively with a flow-through porous electrode. The proximity of the flowing stream to the electrode surface is again important.
5. Nonconducting reactants of low solubility can also be stored close to the electrode surface. For example, another solid phase (as in batteries) or a gas phase (as in fuel cells) may be incorporated into the system, or the reactants may be dissolved and forced through a porous electrode.
6. The compactness of porous electrodes can reduce the ohmic potential drop by reducing the distance through which current must flow. This has obvious advantages in reducing the losses in batteries and fuel cells. It may also permit operation without side reactions by providing potential control for the desired process.

If porous electrodes were trivially different from plane electrodes, there would be no motivation for their separate study. But here inherent complications arise because of the intimate contact between electrode and solution—the ohmic potential drop and the mass transfer occur both in series and in parallel with the electrode processes, with no way to separate them. One needs to develop an intuitive feeling for how and why the electrode processes occur nonuniformly through the depth of the electrode. Finally, we seek methods for designing a porous electrode for a particular application in such a way as to maximize the efficiency.

Electrochemical Systems, Fourth Edition. John Newman and Nitash P. Balsara.

Even if we restrict ourselves to flooded porous electrodes (without a separate gaseous phase), a broad subject area remains. Battery electrodes illustrate an industrially important application of porous-electrode theory. Flow-through porous electrodes can be used for recovery and removal of electropositive metals (Ag, Au, Cu, Hg) from dilute solutions, for electro-organic synthesis, and for oxidation of unwanted organic pollutants and surfactants. Transient double-layer charging and adsorption are of interest in the determination of the internal area of porous electrodes, in some separation processes, and in the interpretation of impedance measurements on porous electrodes.

This chapter draws heavily on the reviews of Newman and Tiedemann.[1, 2] These sources contain additional details and historical information.

22.1 MACROSCOPIC DESCRIPTION OF POROUS ELECTRODES

Porous electrodes consist of porous matrices of a single reactive electronic conductor or mixtures of solids that include essentially nonconducting, reactive materials in addition to electronic conductors. An electrolytic solution fills the void spaces of the porous matrix. At a given time, there may be a large range of reaction rates within the pores. The distribution of these rates will depend on physical structure, conductivity of the matrix and of the electrolyte, and on parameters characterizing the electrode processes themselves.

To perform a theoretical analysis of such a complex problem, it is necessary to establish a model that accounts for the essential features of an actual electrode without going into exact geometric detail. Furthermore, the model should be described by parameters that can be obtained by suitably simple physical measurements. For example, a porous material of arbitrary, random structure can be characterized by its porosity (void volume fraction), average surface area per unit volume, volume-average resistivity, and so forth. Similarly, one can use a volume-average resistivity to describe the electrolytic phase in the voids. A suitable model would involve averages of various variables over a region of the electrode small with respect to the overall dimensions but large compared to the pore structure. In such a model, rates of reactions and double-layer charging in the pores will have to be defined in terms of transferred current per unit volume.

Some authors represent the structure with straight pores, perpendicular to the external face of the electrode, and a one-dimensional approximation is introduced and justified on the basis of the small diameter of the pore compared to its length. As de Levie[3] points out, the mathematical equations are then essentially identical with those of the macroscopic model, although a parameter such as the diffusion coefficient has a different interpretation. We prefer to speak in terms of the macroscopic model.

Average Quantities

In this macroscopic treatment, we disregard the actual geometric detail of the pores. Thus, we can define a potential Φ_1 in the solid, conducting matrix material and another potential Φ_2 in the pore-filling electrolyte. These quantities, and others to be defined shortly, are assumed to be continuous functions of time and space coordinates. In effect, the electrode is treated as the superposition of two continua, one representing the solution and another representing the matrix. In the model, both are present at any point in space.

Averaging is to be performed in a volume element within the electrode. The *porosity* is the void volume fraction ϵ within the element, and this is taken here to be filled with electrolytic solution. The element also contains representative volumes of the several solid phases that may be present. Let c_i be the solution-phase concentration of species i, averaged over the pores. The superficial concentration is thus ϵc_i. For flow-through electrodes, c_i is the preferred average concentration because it is continuous

as the stream leaves the electrode. Furthermore, c_i, rather than ϵc_i, is likely to be used to correlate the composition dependence of diffusion coefficients, activity coefficients, and the conductivity of the solution phase.

The specific interfacial area a is the surface area of the pore walls per unit volume of the total electrode. Let j_{in} be the pore-wall flux density of species i averaged over this same interfacial area. The pore-wall flux density to be averaged is the normal component of the flux density of species i at the pore wall, relative to the velocity of the pore wall, and in the direction pointing into the solution. The pore wall may be moving slightly because of a dissolution process. Thus, aj_{in} represents the rate of transfer of the species from the solid phases to the pore solution (per unit volume of the total electrode).

Next, let $\mathbf{N}_i$ be the average flux density of species i in the pore solution when averaged over the cross-sectional area of the electrode. Thus, for a plane surface, of normal unit vector $\mathbf{n}$, cutting the porous solid, $\mathbf{n}\cdot\mathbf{N}_i$ represents the amount of species i crossing this plane in the solution phase, but referred to the projected area of the whole plane rather than to the area of an individual phase.

The superficial current density $\mathbf{i}_2$ in the pore phase is due to the movement of charged species (compare equation 16.4):

$$\mathbf{i}_2 = F\sum_i z_i\mathbf{N}_i. \tag{22.1}$$

Similarly, the current density $\mathbf{i}_1$ in the matrix phase is defined to refer to the superficial area and not to the area of an individual phase.

Material Balance for Solutes

Within a pore, in the absence of homogeneous chemical reactions, a differential material balance can be written for a species i. This equation can be integrated over the volume of the pores in an element of the electrode, and surface integrals can be introduced by means of the divergence theorem. Careful use of the definitions of average quantities yields[4] the material balance for species i:

$$\frac{\partial \epsilon c_i}{\partial t} = aj_{in} - \nabla\cdot\mathbf{N}_i. \tag{22.2}$$

This result applies to the solvent as well as the solutes.

Three different averages are represented in equation 22.2: c_i is an average over the volume of the solution in the pores; j_{in} is an average over the interfacial area between the matrix and the pore solution; and $\mathbf{N}_i$ is an average over a cross section through the electrode, cutting matrix and pore. It should be borne in mind that the averages ideally involve a volume that is large compared to the pore structure and small compared to the regions over which considerable macroscopic variations occur.

Equation 22.2 states that the concentration can change at a point within the porous electrode because the species moves away from the point (divergence of the flux density $\mathbf{N}_i$) or because the species is involved in electrode processes (faradaic electrochemical reactions or double-layer charging) or simple dissolution of a solid material. This latter term, aj_{in} resembles the term that would describe the bulk production of a species by homogeneous chemical reactions. In the macroscopic model, the transfer or creation from the matrix phases appears to occur throughout the bulk of the electrode because of the averaging process.

Material Balance for Insertion Electrodes

A significant class of electrodes involves insertion or intercalation in which an ion from the solution enters into the crystal lattice of a solid. At the same time, electrons enter or leave the crystal to maintain electroneutrality. This process represents an oxidation or reduction of the crystal. The open-circuit

potential of the crystal, relative to a reference electrode, will depend on the concentration c_s of intercalating ions. The nickel (NiOOH)/metal hydride (MH) battery is an example of a system with two insertion electrodes, whose reactions can be written as

$$\mathrm{NiOOHH}_{y+\delta} + \delta\mathrm{OH}^- \rightarrow \mathrm{NiOOHH}_y + \delta\mathrm{H_2O} + \delta\mathrm{e}^-$$

and

$$\mathrm{MH}_{x+\delta} + \delta\mathrm{OH}^- \rightarrow \mathrm{MH}_x + \delta\mathrm{H_2O} + \delta\mathrm{e}^-.$$

As written, an inserted proton (H) and a hydroxyl ion (OH^-) react to yield water.

With no volume changes in the insertion material and constant transference number, a mass balance on the inserted species is

$$\frac{\partial c_s}{\partial t} = \nabla\cdot D\nabla c_s \tag{22.3}$$

with a boundary condition that the flux density at the surface is equal to the rate of the electrochemical reaction.

The material (MH_x or $NiOOHH_y$) has a well-defined potential relative to a reference electrode, such as mercury/mercuric oxide (Hg/HgO) in an aqueous KOH solution. This potential increases continuously as more protons are extracted from the solid. There are many more examples in lithium batteries.

Electroneutrality and Conservation of Charge

A volume element within the porous electrode will be, in essence, electrically neutral because it requires a large electric force to create an appreciable separation of charge over an appreciable distance. We shall also take each phase separately to be electrically neutral. For the solution phase, this takes the form of equation 16.3. Our assumption here means that the interfacial region that comprises the electric double layer (where departures from electroneutrality are significant) constitutes only a small volume compared to any of the phases or the electrode itself. This will not be true for finely porous media and very dilute solutions, where the diffuse layer may be more than 10 nm thick. Furthermore, we make no attempt here to treat electrokinetic effects like electro-osmosis and the streaming potential (see Chapter 9).

It is a consequence of the assumption of electroneutrality that the divergence of the total current density is zero. For the macroscopic model, this is expressed as (compare equation 11.14)

$$\nabla\cdot\mathbf{i}_1 + \nabla\cdot\mathbf{i}_2 = 0; \tag{22.4}$$

charge that leaves the matrix phases must enter the pore solution. In fact, combination of equations 22.1, 22.2, and 16.3 gives

$$\nabla\cdot\mathbf{i}_2 = aF\sum_i z_i j_{in} = ai_n, \tag{22.5}$$

where i_n is the average transfer current density (positive in the direction from the matrix phase into the solution phase); $\nabla\cdot\mathbf{i}_2$ is the transfer current per unit volume of the electrode (A/cm^3) and is positive for an anodic current.

Faradaic Processes

For a single electrode reaction, as represented in equation 16.7, Faraday's law is expressed as (compare equation 16.8)

$$aj_{in} = -\frac{as_i}{nF} i_n = -\frac{s_i}{nF} \nabla \cdot \mathbf{i}_2 \tag{22.6}$$

if the electrode is operating in a steady state or a pseudo-steady-state where double-layer charging can be ignored. Equation 22.2 becomes

$$\frac{\partial \epsilon c_i}{\partial t} = -\nabla \cdot \mathbf{N}_i - \frac{s_i}{nF} \nabla \cdot \mathbf{i}_2. \tag{22.7}$$

The polarization equation describes the faradaic transfer of charge from the matrix to the solution. This can be written in the general Butler–Volmer form (compare equation 16.10):

$$\nabla \cdot \mathbf{i}_2 = a i_0 \left[\exp\left(\frac{\alpha_a F \eta_s}{RT} \right) - \exp\left(-\frac{\alpha_c F \eta_s}{RT} \right) \right], \tag{22.8}$$

with the surface overpotential $\eta_s = \Phi_1 - \Phi_2 - U$, where U is the open-circuit value of $\Phi_1 - \Phi_2$ at the prevailing composition at the surface of the pores. The open-circuit cell potential U can be taken to be zero if Φ_2 is assessed with a reference electrode of the same kind as the working electrode, which we shall assume to be the case in Section 22.2. However, for insertion electrodes, U is also a function of the amount of intercalation that has occurred, that is, it is a function of the concentration c_s in the solid material.

Capacitive Processes

In addition to faradaic reactions, electrode processes can involve charging of the electric double layer at the interface between the pore solution and the conducting phases of the matrix. For dependent variables we may choose q, the surface charge density on the electrode side of the double layer, and Γ_i, the surface excess or surface concentration of a solute species i. Here, we mean averages over the surface of the pores. These surface quantities can be taken to depend on the solution-phase composition, as represented by c_i and on the electrode potential $\Phi_1 - \Phi_2$, where Φ_2 is measured with a given reference electrode. Since the interface as a whole is electrically neutral and the charge on the solution side of the double layer is comprised of the contributions of adsorbed solute species, the surface charge is related to the species surface excesses:

$$q = -F \sum_i z_i \Gamma_i. \tag{22.9}$$

A separate material balance can be written for a solute species at the interface (see Problem 9.5). In the absence of electrokinetic effects, that is, ignoring translation of the solution side of the double layer in a direction parallel to the surface, this becomes

$$\frac{\partial a\Gamma_i}{\partial t} = aj_{in,\text{faradaic}} - aj_{in} = -\frac{as_i}{nF} i_{n,\text{faradaic}} - aj_{in}, \tag{22.10}$$

where the subscript faradaic refers to charge or mass that is actually transported through the interface or is involved in a charge-transfer reaction. It is assumed in the last form that only a single electrode reaction is involved.

Addition of equation 22.10 according to equation 22.5 gives

$$\nabla \cdot \mathbf{i}_2 = a i_{n,\text{faradaic}} + \frac{\partial aq}{\partial t}; \tag{22.11}$$

the current transferred from the matrix to the solution is involved either in double-layer charging or in faradaic electrode reactions. One can use equation 7.27 to introduce the double-layer capacitance C into this equation.

Treatment of the concentration dependence of the surface excesses is just as complicated as it was for a nonporous electrode, and fundamental data are just as incomplete. The differential double-layer capacity is relatively easy to measure, and data are available over a wider range of concentrations than for Γ_i.

Transport Processes

In the matrix phase, the movement of electrons is governed by Ohm's law:

$$\mathbf{i}_1 = -\sigma \nabla \Phi_1, \tag{22.12}$$

where σ is the effective conductivity of the matrix. This quantity will be affected by the volume fraction of the conducting phase or phases, the inherent conductivity of each conducting solid phase, and the manner in which granules of conducting phases are connected together.

In a dilute electrolytic solution within the pores, the flux density of mobile solutes can be attributed to diffusion, dispersion, migration, and convection (compare equation 16.1):

$$\frac{\mathbf{N}_i}{\epsilon} = -(D_i + D_a)\nabla c_i - z_i u_i F c_i \nabla \Phi_2 + \frac{\mathbf{v} c_i}{\epsilon}. \tag{22.13}$$

Since $\mathbf{N}_i$ is the superficial flux density based on the area of both matrix and pore, one can think of $\mathbf{N}_i/\epsilon$ as the flux density in the solution phase. Similarly, $\mathbf{v}/\epsilon$ will be roughly the velocity in the solution phase if we take $\mathbf{v}$ to be the superficial bulk fluid velocity, for example, the volumetric flow rate entering the electrode divided by its superficial area.

The ionic diffusion coefficient and mobility of a free solution require a correction for the tortuosity of the pores in order to yield D_i and u_i. A porosity factor has already been taken out; that is, ϵD_i might logically be regarded to be the effective diffusion coefficient of the species in the pore solution in the same way that σ is the effective conductivity of the matrix. The effective conductivity κ of the pore solution, introduced later in equations 22.20 and 22.21, is frequently expressed as

$$\kappa = \kappa_0 \epsilon^{1.5}, \tag{22.14}$$

where κ_0 is the conductivity the solution would have outside any porous structure. In a similar manner, the bulk values of diffusion coefficients and mobilities would be multiplied (in the whole chapter) by $\epsilon^{0.5}$ to yield D_i and u_i values corrected for tortuosity. Equation 22.14 is simple and reasonably accurate; it is generally credited to Bruggeman.[5] Efforts to treat this dependence can be traced back to Maxwell.[6]

The dispersion coefficient D_a represents the effect of axial dispersion—the attenuation of concentration gradients as a fluid flows through a porous medium. Plug flow does not prevail in the pores; fluid near the wall moves more slowly than fluid toward the center of the void space. The compensation for this convective nonideality appears as a diffusive phenomenon. However, the dispersion coefficient

is not a fundamental transport property—it depends on the fluid mixing and vanishes in the absence of convective fluid motion. A correlation is referred to in Section 22.6 on flow-through porous electrodes.

When equation 22.13 is substituted into equation 22.1, an equation similar to equation 11.11 is obtained—Ohm's law for solutions is modified by the presence of concentration gradients.

Limiting cases of transport laws are likely to receive special treatment. For example, migration can be neglected for the reaction of a minor component from a solution with excess supporting electrolyte (see Chapter 19). On the other hand, the more sophisticated concentrated-solution theory (see Chapter 12 and below) can replace the dilute-solution approximation.

Concentrated Binary Electrolyte

Many battery systems involve solutions of a single electrolyte. Consequently, it is desirable to develop the theory with all possible exactness, particularly since the equations to use are not overly complicated and thermodynamic and transport data are frequently available for binary solutions. Flux densities relative to the mass-average, molar-average, and solvent velocities are stated in Chapter 12. Newman and Chapman[7] showed how the volume-average velocity $\mathbf{v}^{\square}$ can be used.

For the binary system, there are three material balances, equation 22.2, one for each species. These three material balances can be rearranged to yield three equivalent expressions that emphasize one physical feature or another. The simplest form is the charge-conservation equation, which takes the form of equation 22.4 for porous electrodes. The second and third forms are

$$\begin{aligned}\epsilon\frac{\partial c}{\partial t}+\mathbf{v}^{\square}\cdot\nabla c=\nabla\cdot[\epsilon(D+D_a)\nabla c]\\ +ac_0\overline{V}_0\left(\frac{t_-^0}{\nu_+}j_{+n}+\frac{t_+^0}{\nu_-}j_{-n}\right)-ac\overline{V}_0j_{0n}\\ -c_0\overline{V}_0\frac{\mathbf{i}_2\cdot\nabla t_+^0}{z_+\nu_+F}+\frac{c\epsilon(D+D_a)}{c_0\overline{V}_0}(\nabla c)\cdot\nabla\overline{V}_e\end{aligned}\tag{22.15}$$

and

$$\begin{aligned}\frac{\partial\epsilon}{\partial t}+\nabla\cdot\mathbf{v}^{\square}=a\left[\overline{V}_0j_{0n}+\frac{\overline{V}_et_-^0}{\nu_+}j_{+n}+\frac{\overline{V}_et_+^0}{\nu_-}j_{-n}\right]\\ -\overline{V}_e\frac{\mathbf{i}_2\cdot\nabla t_+^0}{z_+\nu_+F}-\epsilon\frac{D+D_a}{c_0\overline{V}_0}(\nabla c)\cdot\nabla\overline{V}_e.\end{aligned}\tag{22.16}$$

Remember that these three equations have been manipulated substantially from the original material balances. Equation 22.15 can be regarded as an equation for the concentration of the electrolyte, a variant of equation 12.14. It is complicated because no approximations have been made. Note that, if the partial molar volume $\overline{V}_e$ of the electrolyte and the transference number t_+^0 are constant, this reduces to

$$\begin{aligned}\epsilon\frac{\partial c}{\partial t}+\mathbf{v}^{\square}\cdot\nabla c=\nabla\cdot[\epsilon(D+D_a)\nabla c]+ac_0\overline{V}_0\left(\frac{t_-^0}{\nu_+}j_{+n}+\frac{t_+^0}{\nu_-}j_{-n}\right)\\ -ac\overline{V}_0j_{0n},\end{aligned}\tag{22.17}$$

a form very similar to the idealized equation 17.2 of convective diffusion. Equation 22.16 similarly simplifies to

$$\frac{\partial \epsilon}{\partial t} + \nabla \cdot \mathbf{v}^{\square} = a\left[\overline{V}_0 j_{0n} + \frac{\overline{V}_e t_-^0}{\nu_+} j_{+n} + \frac{\overline{V}_e t_+^0}{\nu_-} j_{-n}\right]. \tag{22.18}$$

This can be regarded as an idealized equation of continuity (cf. equation 15.3). The reason for mentioning these equations is that we may wish frequently to approximate $\overline{V}_e$ and t_+^0 as constant while still retaining the composition dependence of D and κ. The volume-average velocity $\mathbf{v}^{\square}$ has the advantage that its divergence becomes close to zero if $\overline{V}_e$ is constant. From these equations one can see explicitly how production or consumption of species +, −, and 0 as well as porosity changes and volume changes on mixing influence the concentration of the solution and the fluid velocity. Equation 22.32 (see Section 22.4) can be used to eliminate $\partial\epsilon/\partial t$ from equations 22.16 or 22.18.

Equation 12.27 is used to describe the potential variation in a concentrated binary electrolyte as measured by a reference electrode directly immersed in the solution. ($\nabla\mu_e$ can be replaced by a concentration gradient according to equation 2.32.) There is a problem keeping straight what potential is being used. See the discussion in the latter part of Section 12.4. Is the potential measured with an electrode of the same kind as the working electrode, immersed in the same solution, or is it assessed with a reference electrode of a given kind? See Section 5.7. In the former case, the stoichiometric coefficients of the reference electrode should appear in the modified Ohm's law equation (see equation 12.27); in the latter case, the potential is more like an electrostatic or quasi-electrostatic potential or the potential relative to a given reference electrode. We want to follow the first approach so that liquid junction potentials do not need to be introduced into a discussion where they are otherwise absent. Such questions are raised in Problem 7.4 and answered in Section 5.7.

Thermal Behavior

An electrochemical cell frequently changes temperature during operation. As a first approximation, the central part of the cell, containing the electrodes and separator, can be taken to be at a uniform temperature, but one that changes with time. A simple energy balance yields

$$C_p \frac{dT}{dt} = \left(U - V - T\frac{\partial U}{\partial T}\right) I + h_0(T_a - T). \tag{22.19}$$

The irreversible heat generation term (per unit of separator area) is $(U-V)I$, where V is the cell potential, U is the open-circuit value of V, and I is the current density; $U-V$ can be regarded as the potential loss due to overpotentials and ohmic potential drop, although they may result from complicated processes in both series and parallel connection. The product $(U-V)I$ is always positive because $U-V$ changes sign when I changes sign. The reversible heat-generation term is $-TI\,(\partial U/\partial T)$ and is directly related to the entropy change due to the electrochemical reaction. It changes sign when the current density I changes sign. The heat entering the cell (W/cm^2) is described by the heat-transfer coefficient h_0 (based on a unit area of the separator) and the temperature difference $T_a - T$, where T_a is the ambient temperature. The energy related to the temperature rise is given by $C_p(dT/dt)$, where C_p is the heat capacity of the cell per unit of separator area. This heat balance and the resulting temperature rise are necessarily simplified, and one may wish to calculate detailed temperature distributions. Bernardi et al.[8] discuss a more general energy balance. The simplified balance ignores heat-of-mixing effects, but these are estimated by Thomas and Newman[9] to be quite modest. See also Chapter 13. Rao and Newman[10] include the local generation of heat in insertion electrodes.

Summary

The equations governing porous electrodes are diverse, but they build upon the material in the earlier chapters of the text. Transport in the matrix phase (equation 22.12) and in the solution phase (equation 22.13) enters into material balances (equation 22.2 or 22.17) and involves coupling through polarization relations (equation 22.8) and capacitative effects in such a way that the electrolytic processes may look like a homogeneous term in the material balances (compare equation 16.3). There are several unknowns, such as concentration, potentials, flux densities, and temperature, that are closely coupled and are likely to satisfy nonlinear partial differential equations. Succeeding sections show how some of this works in terms of specific systems, approximations, and boundary conditions.

22.2 NONUNIFORM REACTION RATES

This section is designed to illustrate, by means of examples that can be solved analytically, how transport and electrode processes interact to produce nonuniform reaction rates and to set the stage for later developments where many processes are still coupled and where computer solutions may be required to reveal the essential behavior of systems.

Many special cases are treated in the literature. The simplest assume that the solution phase is uniform in composition—either because the current has just been switched on and the concentrations have not had time to change or because there is forced convection through the electrode so as to maintain the composition uniform. Double-layer charging is also to be ignored. One can still vary the relative electric conductivities of the two phases, the thickness of the electrode, and the form of the polarization equation expressing the electrochemical kinetics.

Consider a porous electrode in the form of a slab of thickness L, as sketched in Figure 22.1. The electrode is in contact with an equipotential metal surface (a so-called current collector) on one side at $x = L$ and in contact with an electrolytic solution on the other at $x = 0$. In such problems, it is convenient to specify the superficial current density I flowing through the electrode rather than the potential difference across it. Positive values of I will correspond to anodic currents. The structure of the electrode will be taken to be uniform.

The four governing differential equations take on a one-dimensional form. Equation 22.4 expresses conservation of charge. Equation 22.13 can be added over species according to equation 22.1 to yield Ohm's law for the pore solution

$$\mathbf{i}_2 = -\kappa \nabla \Phi_2, \tag{22.20}$$

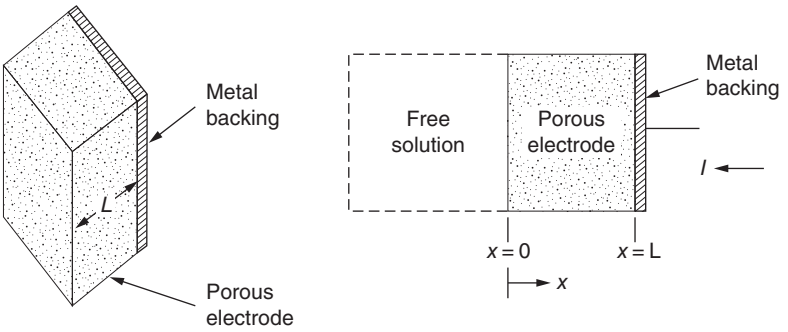

Figure 22.1 Schematic of a one-dimensional porous electrode. *Source:* Newman and Tobias 1962.[11] Reproduced with permission of The Electrochemical Society, Inc.

where

$$\kappa = \epsilon F^2 \sum_i z_i^2 u_i c_i, \tag{22.21}$$

and equation 22.12 is the same law for the matrix. The polarization equation 22.8 describes the transfer of charge from the matrix to the solution.

Sufficient boundary conditions include

$$i_2 = -I, \quad i_1 = 0, \quad \Phi_2 = 0 \text{ at } x = 0, \tag{22.22}$$

$$i_2 = 0 \text{ at } x = L. \tag{22.23}$$

These say that at the electrode–solution interface ($x = 0$) the current is carried entirely by the pore electrolyte, while at the metal backing the current is carried entirely by the matrix. As an arbitrary reference of potential, we choose $\Phi_2 = 0$ at $x = 0$. Somewhere within the electrode, between $x = 0$ and $x = L$, the current is transferred from the solution to the matrix, and the rate of reaction is proportional to di_2/dx.

The reaction distribution is generally nonuniform within the electrode. To minimize the ohmic potential drop, the current tends to divide between the solution and the matrix in proportion to their effective conductivities. However, this requires high reaction rates near $x = 0$ and/or $x = L$. Slow electrode reaction kinetics forces the reaction to be more uniformly distributed in order to reduce the transfer current density. These competing effects of ohmic potential drop and slow reaction kinetics determine the resulting distribution. Figure 22.2 shows an equivalent circuit of the porous electrode (under conditions of a linear polarization equation) illustrating the current flowing through the matrix and solution resistances and the transfer from one phase to the other.

For the problem as formulated above, four dimensionless ratios govern the current distribution. These can be stated as a dimensionless current density (compare equation 18.13)

$$\delta = \frac{\alpha_a FIL}{RT}\left(\frac{1}{\kappa} + \frac{1}{\sigma}\right), \tag{22.24}$$

a dimensionless exchange current for the electrode (compare equation 18.11)

$$\nu^2 = (\alpha_a + \alpha_c)\frac{Fai_0L^2}{RT}\left(\frac{1}{\kappa} + \frac{1}{\sigma}\right), \tag{22.25}$$

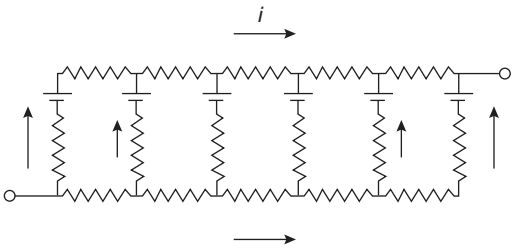

Figure 22.2 Electric analog of a porous electrode with ohmic resistances representing matrix and pore solution (upper and lower horizontal resistors) and kinetic resistance (vertical elements). The vertical branches also have elements representing a cell of potential U.

the ratio α_a/α_c of the transfer coefficients in the polarization equation 22.8, and the ratio κ/σ of the effective conductivities of the solution and matrix phases.

The first two, δ and ν^2, are ratios of the competing effects of ohmic potential drop and slow electrode kinetics. For large values of either δ or ν^2, the ohmic effect dominates, and the reaction distribution is nonuniform. The ratio α_a/α_c seems to be unavoidable, but its role is more difficult to discern. For small values of κ/σ, the reaction occurs preferentially near the electrode–solution boundary at the expense of the region near the backing plate.

The description of a porous electrode in the absence of concentration variations is similar to that of the secondary current distribution at a disk electrode, discussed in Section 18.3. It is customary to introduce one of two approximations to the polarization equation 22.8. For very low overpotentials, this can be linearized to read

$$\frac{di_2}{dx} = (\alpha_a + \alpha_c)\frac{ai_0F}{RT}(\Phi_1 - \Phi_2). \tag{22.26}$$

On the other hand, at very high overpotentials, one or the other of the terms on the right in equation 22.8 can be neglected. The first term is neglected for a cathode, the last term for an anode. This is the Tafel approximation.

For systems with a finite conductivity of each phase, the solution of these equations with the linear electrode kinetics has been given by Euler and Nonnenmacher[12] and restated by Newman and Tobias.[11] These last workers also obtained the solution for Tafel polarization.

Reference [1] reviews in more detail the many special cases that were treated in the early years.

One feature of the results is the nonuniformity of the reaction rate within the electrode. Figure 22.3 shows the distribution of reaction rate for Tafel kinetics and for $\sigma = \kappa$. As in the classical

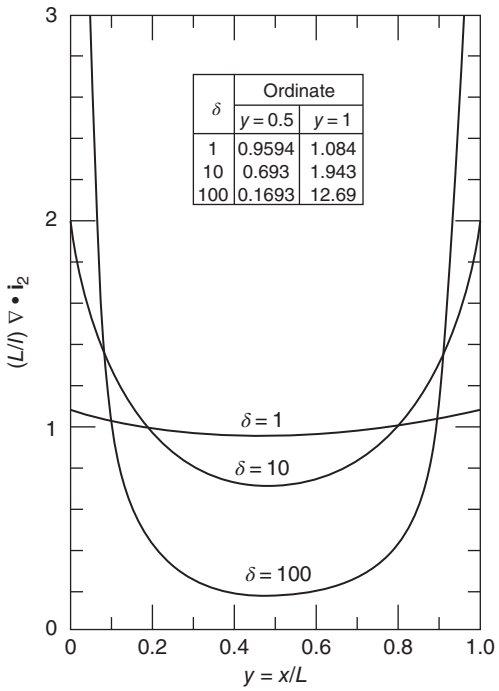

Figure 22.3 Reduced current distribution for Tafel polarization with $\sigma = \kappa$. *Source:* Newman and Tobias 1962.[11] Reproduced with permission of The Electrochemical Society, Inc.

secondary-current-distribution problem, the value of ai_0 is unimportant as long as the backward reaction can truly be neglected. In the Tafel case, the current distribution depends only on the parameter δ and on the ratio κ/σ. (For cathodic polarization in the Tafel range, replace α_a by $-\alpha_c$ in equation 22.24 in order to use these results.) For a small value of δ, the reaction is uniform; but for large values of δ, the reaction takes place mainly at the electrode interfaces. The ratio κ/σ serves to shift the reaction from one face to the other so that the reaction is somewhat more uniform as κ approaches σ at constant δ.

Curves for the linear-polarization equation would have the same general appearance as Figure 22.3. In analogy with the classical problem of the secondary current distribution, the reduced distribution depends only on the parameter ν and on the ratio κ/σ and is independent of the magnitude of the current. The distribution becomes nonuniform for large values of ν, that is, for large values of the exchange current density, the specific interfacial area, or the electrode thickness or for small values of the conductivities. The ratio κ/σ still shifts the reaction from one face to the other.

Potential distributions for Tafel kinetics are illustrated in Figure 22.4 for

$$\alpha_a \frac{Fai_0L^2}{RT}\left(\frac{1}{\kappa}+\frac{1}{\sigma}\right)=0.1. \tag{22.27}$$

(For Tafel kinetics, with a given value of I, changes in ai_0 merely add a constant to $\Phi_1-\Phi_2$ without affecting the current or potential distributions in any other way. Remember also that U, taken here

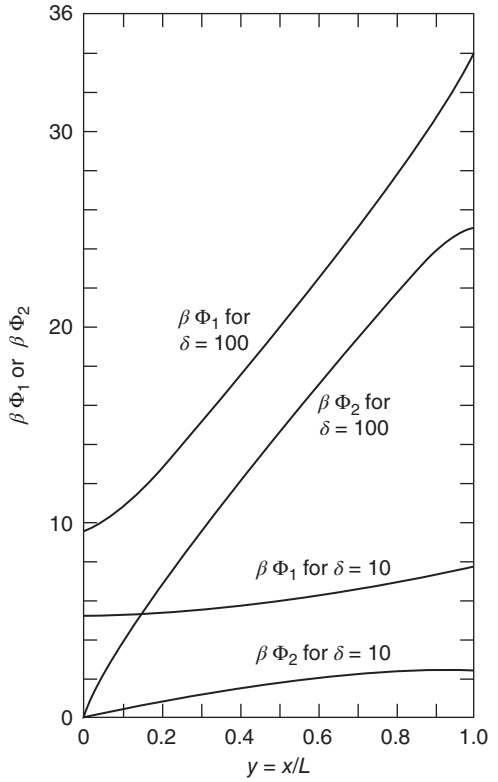

Figure 22.4 Potential distributions for Tafel polarization with $\sigma=\kappa$. Here $\beta=\alpha_aF/RT$ (or $-\alpha_cF/RT$ for cathodic currents). *Source:* Newman and Tiedemann 1975.[1] Reproduced with permission of the American Institute of Chemical Engineers.

to be zero, would also add a constant to $\Phi_1 - \Phi_2$.) The slope of the curves gives the current density flowing in either the matrix or the pore solution, according to Ohm's law. Consequently, the second derivative of either Φ_1 or Φ_2 is related to the local reaction rate, that is, the rate at which current is transferred from one phase to the other. The difference $\Phi_1 - \Phi_2$ also gives this reaction rate through the polarization equation.

The total potential loss in the electrode, a combination of kinetic or surface overpotential and ohmic potential drop, is given by the difference between the potential Φ_1 in the matrix at the current collector and the potential Φ_2 in the pore solution at the pore mouth (where Φ_2 was actually taken to be zero in equation 22.22). For linear polarization, this loss can be expressed as

$$\frac{\Phi_1(L) - \Phi_2(0)}{I} = \frac{L}{\kappa + \sigma}\left[1 + \frac{2 + (\sigma/\kappa + \kappa/\sigma)\cosh\nu}{\nu \sinh\nu}\right]. \tag{22.28}$$

This formula can be broadened in applicability to include capacitive,[13] intercalation, and impedance[14] effects if one is still willing to ignore concentration changes in the pore electrolyte.

The potential loss for Tafel polarization is plotted in Figure 22.5 under the condition of equation 22.27. This Tafel plot has a slope of 2.303 for low values of δ. As δ increases, the potential drop due to resistance becomes important. For a high conductivity of one phase, a double Tafel slope results, as pointed out by Ksenzhek and Stender[15] and by Winsel[16] among others. Thus, the lower curve in Figure 22.5 attains a slope of 4.605 for large δ. If both conductivities are nonzero, the ohmic contribution to the potential loss will eventually dominate. Thus, the upper curve in Figure 22.5 becomes linear in δ, not linear in the logarithm of δ. The behavior of both curves for large δ illustrates the general rule that the ohmic potential drop becomes more important at large currents.

The Tafel approximation becomes poor at low currents. One cannot extrapolate Figure 22.5 since $\beta\Phi_1(L)$ should approach zero as δ approaches zero. The backward reaction should be accounted for, and eventually the linear approximation becomes applicable at very low values of δ. With the restrictions of a semi-infinite electrode and a high conductivity of one phase, the current–potential relation for an electrode with the general electrode kinetics (equation 22.8) is

$$I^2 \frac{2ai_0\kappa RT}{\alpha_a\alpha_c F}\left[\alpha_c \exp\left(\frac{\alpha_a FV}{RT}\right) + \alpha_a \exp\left(-\frac{\alpha_c FV}{RT}\right) - \alpha_a - \alpha_c\right], \tag{22.29}$$

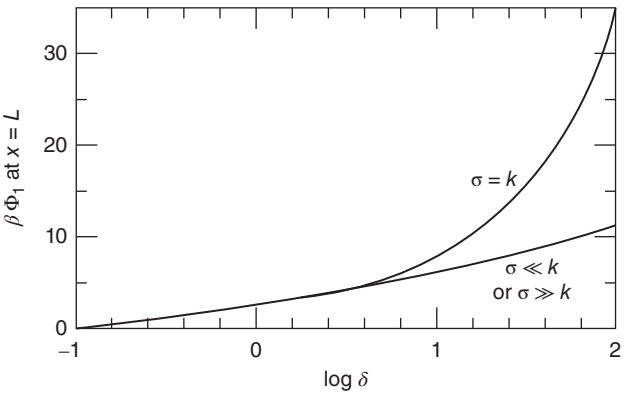

Figure 22.5 Potential of the metal backing plate as it depends on δ. Here $\beta = \alpha_a F/RT$ (or $-\alpha_c F/RT$ for cathodic currents). *Source:* Newman and Tobias 1962.[11] Reproduced with permission of The Electrochemical Society, Inc.

where $V = \Phi_1 - \Phi_2 - U$ with Φ_1 measured in the metal at the backing plate and Φ_2 measured at $x = 0$, the solution side of the electrode. On the other hand, equation 22.28 is the result without these restrictions but instead restricted to the linear approximation.

22.3 MASS TRANSFER

Steady Mass Transfer

A solution-phase reactant will be depleted during the operation of a porous electrode, and diffusion of this species from a reservoir at the face of the electrode represents a loss, in addition to the ohmic potential drop and surface overpotential considered in the previous section.

Two special problems might be defined in this area. The first involves a redox reaction obeying the equation (compare Problem 20.4)

$$\nabla \cdot \mathbf{i}_2 = a i_0 \left[\frac{c_1}{c_1^0} \exp\left(\frac{\alpha_a F \eta}{RT}\right) - \frac{c_2}{c_2^0} \exp\left(-\frac{\alpha_c F \eta}{RT}\right) \right], \tag{22.30}$$

where $\eta = \Phi_1 - \Phi_2 - U'$; U' is the open-circuit value of $\Phi_1 - \Phi_2$ when the concentrations of the reactant and product are c_1^0 and c_2^0 and i_0 is a constant representing the corresponding exchange current density at the composition c_1^0, c_2^0, which might conveniently be taken to be the initial concentrations of the reactants or the concentrations prevailing external to the electrode. (The prime is put on U' to emphasize that here we are dealing with potentials relative to a given reference electrode, as defined in Section 5.7.) The reaction is taken to be first order with respect to the reactant and product, at a given electrode potential. Alternatively, Φ_2 could be measured with a reference electrode of the same kind as the working electrode, with the local composition. Then equation 22.8 could be used, with the exchange current density depending on the composition as given in equation 8.23. Thus, in equation 22.8 we have $\eta_s = \Phi_1 - \Phi_2 - U$ with U evaluated at the local composition, but in equation 22.30 we have $\eta = \eta_s + \eta_c = \Phi_1 - \Phi_2 - U'$ with U' evaluated relative to a given reference electrode. See also Chapter 21.

The reactant and product species, whose stoichiometric coefficients are taken to be $+1$ and -1, move by molecular diffusion alone, since convection is assumed to be absent and migration is negligible if an excess of supporting electrolyte is presumed to be present. This excess of supporting electrolyte is also used to justify the approximation of a constant solution-phase conductivity κ and neglect of the diffusion potential,* so that Ohm's law (equation 22.20) can still be used for the solution phase.

The second special case involves a binary electrolyte, where the solution-phase conductivity can be taken to be proportional to the concentration.*

For the first special case, for each species two new parameters are introduced—a diffusion coefficient and a bulk or characteristic concentration c_i^0. These can be combined into the dimensionless group $\gamma_i = s_i I L / n F \epsilon D_i c_i^0$.

Early analytic and computer solutions for steady mass transfer are reviewed in reference [1]. Noteworthy among them is the occurrence of a double Tafel slope at high polarization. This

*In the steady state, the diffusion potential can be included, without a separate term, by using a modified conductivity:

$$\kappa' = -n\epsilon F^2 \frac{\sum_i z_i^2 u_i c_i / D_i}{\sum_i z_i s_i / D_i}.$$

phenomenon is due to a mass-transfer effect and can be contrasted with the double Tafel slope, mentioned below equation 22.28, due to an ohmic effect. Also of interest is the concept of the penetration depth, characterizing the region in which reaction rates are appreciable, and thereby related directly to the nonuniform reaction rate that characterizes porous electrodes. In Section 22.2 for the case with no concentration gradients and with linear kinetics, this penetration depth is of the magnitude

$$\frac{L}{\nu} = \left(\frac{RT\kappa\sigma}{(\alpha_a + \alpha_c) a i_0 F (\kappa + \sigma)} \right)^{1/2}. \tag{22.31}$$

At high current levels (with Tafel kinetics), L/δ is a length that is more characteristic of the penetration of the reaction.

For diffusive transport of reactants or consumption of reactants stored in the matrix or the pore solution, other factors will enter into the optimization of the electrode thickness. For large anodic polarization the penetration depth becomes equal to L/γ_i. The distance to which the reaction can penetrate the electrode determines how thick an electrode can be effectively utilized. Electrodes much thinner than the penetration depth behave like plane electrodes with an enhanced surface area. Electrodes much thicker are not fully utilized.

Transient Mass Transfer

To follow the course of the discharge of a porous electrode, beginning with a uniform solution composition and following the development toward a steady state, requires a consideration of the time derivative in equation 22.7. The difficulty and complexity of analytic solutions to the coupled governing equations lead us toward computer solutions where drastic assumptions can be avoided and there can be fidelity with the physically based governing equations.

Stein[17] treated the change of sulfuric acid concentration in the pores of a lead–acid battery. The performance during a very-high-rate discharge is limited by a severe depletion of acid directly at the mouth of the pores of the positive plate. To study this effect, Stein was able to avoid consideration of structural changes, and he assumed that the electrode reaction itself occurred reversibly. Doyle and Newman have reviewed some other analytic solutions for transient mass transfer.[18]

A characteristic time for diffusion processes is L^2/D_i. For an electrode thickness of 1 mm and an effective diffusion coefficient of 10^{-5} cm^2/s, this leads to diffusion times of the order of 1000 s. However, for thick electrodes, the presence of a reservoir of unreacted species in the depth has little effect on the dominant processes occurring near the solution side of the electrode. The penetration depth (e.g., L/γ_i) can then be used rather than L in forming the characteristic time for diffusion. Thus, 90% of the electrode potential change can occur in a time as short as 30 s. (The characteristic time for charging the double-layer capacity is usually much less. The ratio of the double-layer charging time to the diffusion time is $D_i a C/\kappa$. This ratio is greater than one only for very high interfacial areas and low conductivities.)

22.4 BATTERY SIMULATION

Porous electrodes used in primary and secondary batteries frequently involve solid reactants and products, and the matrix is changed during discharge. Consequently, no steady-state operation is strictly possible. Such systems are complex, and their simulation on the computer will continue to be refined.

For the purposes of modeling, batteries can be grouped under the following types of reaction mechanisms:

1. **Solution, Precipitation Electrodes** Products (or reactants) can end up in the solution phase and subsequently precipitate on crystals. If these materials are reasonably soluble, they may precipitate at some distance from their original location and such shape change can constitute a failure mechanism.[19] Sparingly soluble products (or reactants) may end up closer to where they started and may be able to be cycled more times. The lead sulfate in a lead–acid system is more benign in this regard, but prolonged standing in a partially discharged state can lead to the growth of larger particles of $PbSO_4$, thereby making recharge difficult or impossible on a reasonable time scale.
2. **Electrodes with Films** The idea is that product species would form a coherent film on the electrode surface, and subsequent reaction might require species involved in the reaction to move or migrate through this film. The *solid electrolyte interphase* (SEI) on lithium metal in many organic solvents (or even polymers) is an example of this situation. The Li^+ ions are supposed to migrate through this film and thereby permit charge and discharge of the system and protect the underlying Li. A nonzero transference number for electrons (or holes) may permit reduction of solvent or anion species on the outer surface of the film, thereby constituting a side reaction. On the other hand, the film probably is never perfectly compact and bonded to the Li. Then some buckling and cracking is likely, and there will be a more or less continuous and steady discharge of Li by means of new cracks on the surface. Variations in the compactness and durability of this film would lead to variabilities in the usefulness of different solvents and anions in Li batteries.
3. **Intercalation Electrodes** Next, there are intercalation materials in which an ion from the solution enters the crystal structure of the active materials, its charge being counterbalanced by electrons (or holes) from the current collector. Examples in the aqueous arena include nickel hydroxide and metal hydride, mentioned in Section 22.1. Lithium-ion batteries rely on having positive and negative electrodes both operating on this principle.[20] Ideally, this insertion of ions is not supposed to change the lattice spacing of the crystal, so that there are no stresses to cause fragmentation and no changes in volume of each phase. In these systems, in contrast to a two-phase electrode like $PbO_2/PbSO_4$, the open-circuit potential depends on the state of charge or degree of filling of the lattice by ions. Palladium is a metal particularly known for taking H^+ ions into its lattice (along with counterbalancing electrons). Some of these materials (like NiOOH) show an interesting hysteresis of potential as they are cycled.
4. **Alloy Electrodes** Alloying the reactive metal can lower its chemical potential and promote the deposition of metal more in the depth of the electrode, in an attempt to avoid dendrites and consequent shorting of the cell. Pollard[21] modeled LiAl porous electrodes.

Structural Changes

For a single electrode reaction, a material balance on the solid phases shows how the porosity changes with the extent of reaction at each location within the electrode:

$$\frac{\partial \epsilon}{\partial t} = -A_0 \nabla \cdot \mathbf{i}_2, \tag{22.32}$$

where

$$A_0 = -\sum_{\text{solid phases}} \frac{s_i M_i}{\rho_i n F}, \tag{22.33}$$

M_i being the molar mass and ρ_i the density of the solid phase (taken here to be a pure substance). This formula does not allow for expansion and compression of individual electrodes. Rigorous treatment of volume change of electrodes requires knowledge of the mechanical properties of the battery materials, including the container.

Winsel[16] allowed for the consumption of a solid reactant by setting the transfer current equal to zero at any point in the electrode where the charge passed was equal to that which this fuel could supply. Because of the nonuniform current distribution, the solid fuel is exhausted first at the side of the electrode adjacent to the solution. Cutting off the reaction in this region forces a higher average reaction rate in the remainder of the porous structure (for a constant-current discharge), yielding a higher electrode overpotential. The ohmic potential drop in the solution in the depleted part of the electrode also contributes significantly to the overpotential. This can be compared with the reaction-zone model in the next section.

Alkire et al.[22] treated the change in pore size and solution composition and the attendant fluid flow for dissolution of porous copper in sulfuric acid solution. The treatment of a straight-pore system is particularly appropriate here since they were able to wind copper wire carefully and sinter the coil to produce a uniform pore structure.[23]

Dunning and Bennion[24] developed a battery-electrode model that described mass transfer of sparingly soluble fuel from nonconducting crystallites to electrochemical reaction sites. They obtained an analytic solution exhibiting a limiting current due to internal mass-transfer limitations, and they discussed acceptable limits of the solubility of the sparingly soluble reactant. Self-discharge can impose an upper limit, and adequate power density, a lower limit. The movement of species during the cycling of a secondary cell can impose a perhaps more stringent upper limit to reactant solubility.

Later, Dunning et al.[25] analyzed discharge and cycling, with the internal mass-transfer coefficient dependent on the local state of charge. Their next work[26] included discharge and cycling of silver–silver chloride and cadmium–cadmium hydroxide electrodes in binary electrolytes of NaCl and KOH, respectively. The mechanism of discharge included, in series, the kinetics of dissolution or precipitation of the sparingly soluble fuel, the diffusion to the reaction site, and the electrochemical kinetics of the reaction—with regard for the changes in the areas available for these processes. Also accounted for were porosity changes according to equations 22.32 and 22.33, fluid flow due to the volume changes associated with the electrochemical reaction, concentrated-solution transport theory, and variations in physical properties of the solution.

Thus, a number of factors can affect the extent of utilization of a battery as a function of rate of discharge:

1. Higher current densities yield higher overpotentials, and thus a given cutoff potential is reached sooner.
2. Electrolyte depletion at the pore mouth[17] hastens the end of discharge, particularly at high current densities.
3. Concentration changes in the solid insertion materials lead to higher overpotentials.
4. The pores may become constricted or even plugged with solid reaction products. A nonuniform reaction distribution will accentuate this problem at the mouth of the pores.
5. The reaction surface can become covered with reaction products.
6. Rates of mass transfer between crystallites and the reaction surface may become more limiting as the discharge exhausts the front part of the electrode. This could account for changes in the apparent limit of utilization with current density.

Optimization of Electrode Thickness and Porosity

We want to design a battery for optimum cost and energy efficiency. To do this, we could take a battery model that handles consumption of active material, ohmic potential drop, and concentration variations and vary the design, including variation of electrode thickness and porosity, until we obtain the best result. To illustrate the principles we seek to use a very simple model, and leave the actual

battery design to more sophisticated programs, which, however, still might follow the methodology illustrated here.

An important characteristic of batteries is that their potential declines through discharge and eventually reaches a voltage cutoff, and the battery is discharged. To simulate this behavior in a simple system, we ignore concentration variations, take the electrode kinetics to be very fast, and take the matrix conductivity to be very high. These conditions create a very nonuniform reaction rate, as demonstrated in Section 22.2, and the sharp reaction zone moves through the electrode, leaving behind a reacted region.[27] This moving reaction zone is depicted in Figure 22.6.

The equivalent circuit shown in Figure 22.7 shows a separator resistance, a pore-electrolyte resistance inside the porous electrode, and a series of exhausted battery elements in the region behind the reaction zone.

Before we can optimize anything, we need to have a mathematical description of the discharge. With a uniform discharge current density, the reaction zone moves at a uniform velocity away from the separator. When it reaches the distant end, at the current collector, the active material is fully exhausted. This is the end of discharge unless the cell potential has already dropped below the cutoff potential. At the cutoff potential, determined by the application, the battery is deemed unable to perform its mission. With a constant-current discharge, it is a valid design point for the cell to run out of active material exactly when the potential hits the cutoff.

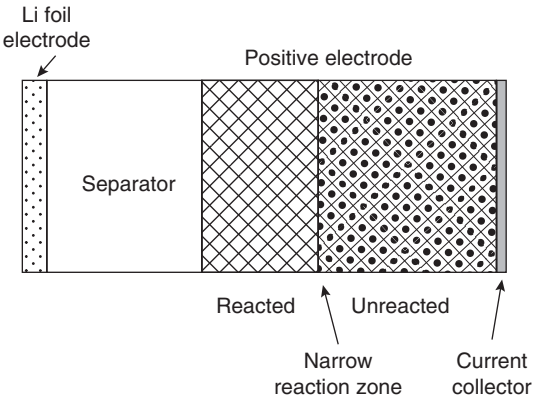

Figure 22.6 Pictorial of the battery system. *Source:* Newman 1995.[27] Reproduced with permission of The Electrochemical Society, Inc.

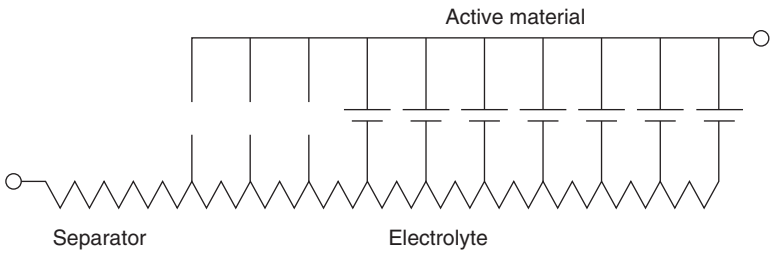

Figure 22.7 Equivalent-circuit representation for the reaction-zone model. *Source:* Newman 1995.[27] Reproduced with permission of The Electrochemical Society, Inc.

But how do we determine the current density, as well as the electrode thickness and porosity, the time of discharge, and the separator thickness? The time of discharge t_d is taken to be specified by the battery's mission. We also take the separator thickness L_s to be specified on the basis that it should be as thin as possible consistent with its purpose of preventing shorts. Thus, it cannot be optimized simply to maximize the specific energy (J or W·h per unit mass of the battery). This conclusion may not apply to the lead–acid cells or sodium/sulfur cells, where an important reactant is contained in the electrolytic solution. However, it does apply to many alkaline cells and lithium batteries where the main reacting ion, OH^-or Li^+, is produced at one electrode at the same rate that it is consumed at the other, leaving the average concentration of the solution unchanged.

Optimizing the current density is equivalent to optimizing the size of the cell (i.e., separator area) to perform a given duty. To optimize the current density, and eventually the electrode thickness and porosity, we need expressions for the cell potential and energy delivered during discharge. The reaction zone at a position x_r moves through the electrode; a material balance shows that

$$x_r = \frac{It}{(1-\epsilon)q_+}, \tag{22.34}$$

where I is the current density (taken to be constant with time), t is the time since the beginning of the discharge, ϵ is the porosity of the positive electrode, and q_+ is the capacity per unit volume of solid material (active material, conductive additives, and binder). The cell potential V at any given time is the open-circuit potential U minus the ohmic drop required for the ionic current to flow across the separator and through the pores in the positive electrode up to the region x_r where the reaction is taking place:

$$V = U - I\left(\frac{L_s}{\kappa_s} + \frac{x_r}{\kappa}\right) = U - \frac{L_s}{\kappa_s}I - \frac{I^2 t}{\kappa(1-\epsilon)q_+}. \tag{22.35}$$

The energy E (per unit of separator area) delivered is the integral of the instantaneous power;

$$E = \int_0^{t_d} VI\,dt = \left(U - \frac{L_s}{\kappa_s}I\right)It_d - \frac{I^3 t_d^2}{2k(1-\epsilon)q_+}. \tag{22.36}$$

Finally, the mass M per unit of separator area can be expressed as

$$M = \rho_r L_r + \rho_s L_s + [\rho_- q_+(1-\epsilon)/q_- + \epsilon\rho_s + (1-\epsilon)\rho_+]L_+. \tag{22.37}$$

The first term on the right represents the remainder of the system, such as any current collector or other sheets between the cells. The second term is the mass of the separator. Here, it is assumed that the negative electrode, with density ρ_- and capacity density q_-, is proportional to the positive electrode in thickness and capacity. If this is not the case, the mass of the negative electrode should be lumped in with the residual mass $\rho_r L_r$, taken to be constant. The remaining terms are the mass of the positive electrode, including the electrolyte within the pores.

The effective conductivity κ of the electrolytic phase in the positive electrode is assumed to be given by the Bruggeman equation 22.14.[5] Here we can take $\epsilon_s = 1$, and hence $\kappa_s = \kappa_0$.

We wish to maximize the value of the energy per unit mass, E/M, for a given discharge time t_d, open-circuit potential U, separator thickness L_s, positive-electrode capacity density q_+, and separator conductivity κ_s. The other parameters, such as ρ_r, L_r, ρ_s, and ρ_+, are supposed to be fixed. The parameters that are free to be varied to attain the maximum are the discharge current density I, the thickness L_+ of the positive electrode, and the porosity ϵ, representing the volume fraction of the electrolyte in the positive electrode.

It is easiest to maximize first with respect to the discharge current for given L_+ and ϵ because the value obtained is then independent of the mass parameters. This yields

$$I_{\text{opt}} = \frac{\kappa_s U/L_s}{1 + \left(1 + \dfrac{3Ut_d\kappa_s^2}{2\kappa(1-\epsilon)q_+L_s^3}\right)^{1/2}}. \tag{22.38}$$

However, there are two constraints to consider. At the end of discharge, the cell potential V must be greater than the cutoff potential V_c. This requires that

$$I_{\text{opt}} \le \frac{\kappa_s U}{L_s} \frac{2(1 - V_c/U)}{1 + (1 + 4(U - V_c)t_d\kappa_s^2/\kappa(1-\epsilon)q_+L_s^2)^{1/2}}. \tag{22.39}$$

Furthermore, the capacity of the positive electrode must not be exhausted, and this is expressed as

$$I_{\text{opt}} \le \frac{\kappa_s U}{L_s} \frac{L_+L_s(1-\epsilon)q_+}{Ut_d\kappa_s}. \tag{22.40}$$

The smallest of these three values must be used. The last condition can be replaced by an equality, since otherwise there would remain unused capacity and the situation could be improved by reducing L_+ until the equality held.

The dimensionless specific energy to be maximized now takes the form

$$\frac{E\rho_s}{MUq_+} = \frac{(1-U)I_0T - I_0^3T^2/2\epsilon^{1.5}(1-\epsilon)}{\rho_rL_r/\rho_sL_s + 1 + (L_+/L_s)[\epsilon + (1-\epsilon)(\rho_+/\rho_s)]}, \tag{22.41}$$

where I_0 is the minimum value of $I_{\text{opt}}L_s/\kappa_sU$ governed by equations 22.38 to 22.40 and

$$T = \frac{U\kappa_s t_d}{q_+L_s^2}. \tag{22.42}$$

This can be regarded as a discharge time t_d made dimensionless with the other parameters, which thereby achieve increased importance in the design.

Figure 22.8 shows how the dimensionless specific energy depends on electrode thickness and porosity for $T = 100$. The mass in the denominator of equation 22.41 contributes an additional penalty for increasing the thickness of the electrode. At the optimum, $\epsilon = 0.227$ and $L_+/L_s = 1.95$ (at this value of $T = 100$).

Figure 22.9 shows the optimum electrode thickness, and Figure 22.10 shows the optimum positive-electrode porosity, both as functions of the dimensionless discharge time T. For these calculations, the ratio of the cutoff potential to the open-circuit potential is taken to be $\frac{2}{3}$. Also, $\rho_+ = \rho_s$, and $\rho_rL_r = 0$.

Toward the left on these figures (for high-rate discharges), the ohmic potential drop is important, and the inequality in equation 22.39 becomes an equality. That is, the cell reaches the voltage cutoff at the end of discharge. Above about $T = 50$, the voltage cutoff is no longer reached (for $\rho_+ = \rho_s$ and $\rho_rL_r = 0$); weight considerations become more important.

Other values of ρ_+/ρ_s, and ρ_rL_r/ρ_sL_s are explored by Newman.[27] A larger value of residual mass pushes the optimum porosity up toward the value of 0.6 corresponding to the capacity maximization.[27, 28] At the same time, this permits an increase in the optimum electrode thickness because of the more open electrode.

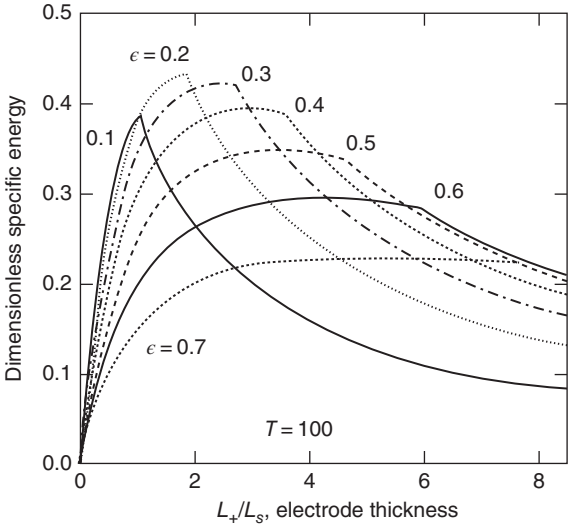

Figure 22.8 Specific energy for various electrode thicknesses and porosities. The optimum is $\epsilon = 0.227$ and $L_+/L_s = 1.95$. *Source:* Newman 1995.[27] Reproduced with permission of The Electrochemical Society, Inc.

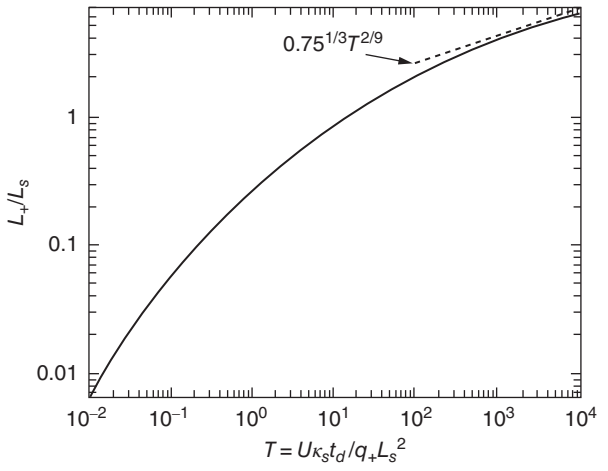

Figure 22.9 Optimum electrode thickness as it depends on the parameter determined by discharge time, electrode capacity density, open-circuit potential, and separator parameters. *Source:* Newman 1995.[27] Reproduced with permission of The Electrochemical Society, Inc.

On the other hand, an increase in the density of the positive electrode material increases the optimum porosity but reduces the optimum electrode thickness since these changes can compensate for the increased mass.

The approximations invoked of fast reactions and no concentration variations are more restrictive than we would like. More complicated computer models, such as those described in the next section, can be used, with the simpler reaction-zone model serving to illustrate the nature of the results and the

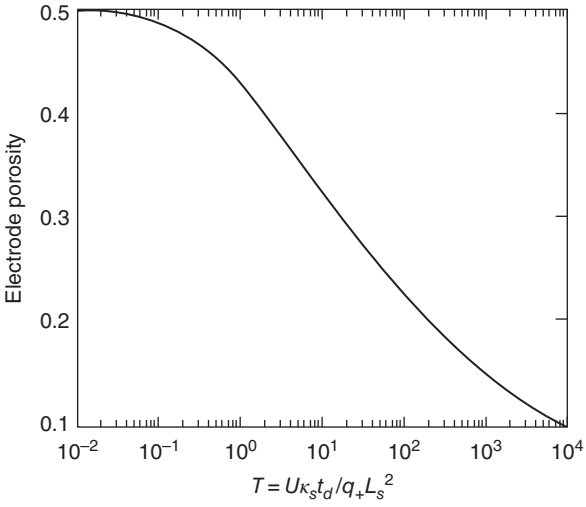

Figure 22.10 Optimum porosity as it depends on the parameter determined by discharge time, electrode capacity density, open-circuit potential, and separator parameters. *Source:* Newman 1995.[27] Reproduced with permission of The Electrochemical Society, Inc.

method of optimizing over first current density and then battery design parameters such as porosity and electrode thickness.

Another caveat relates to the difficulty of manufacturing electrodes with the porosity specified by the optimization procedures. One then should wish to optimize current density and electrode thickness with the porosity constrained by manufacturability. One can also explore the breadth of the optimization maxima to ascertain the consequences of manufacturing variability as well as those of the inability to produce the optimum porosity.

Figure 22.11 shows a *Ragone plot* of specific energy versus average specific power; the ratio of these two quantities is the parameter t_d or, in dimensionless form, T. The three lower curves are calculated with fixed values of electrode thickness and porosity, those selected as optimum values from Figures 22.9 and 22.10 for the three values of $T = 2$, 100, and 5000. These curves illustrate how the compromise between energy and power shifts as one optimizes for different discharge times.

Also shown in Figure 22.11 is a curve where the electrode thickness and porosity are optimized for each point (which corresponds to a given value of T). This curve provides an envelope of the best performance attainable and gives some perspective to the compromises represented in the other curves. The system will have a natural minimum practical discharge time corresponding to a T of about 2 or 5. That is to say, selection of a value of T significantly less than 2 makes it impossible to use very much of the capability of the battery to store energy.

In conclusion, the most significant factor affecting the design of a battery is its discharge time. (The next most important is its capacity.) It is shown here how the electrode thickness and porosity are determined by this discharge time for a particularly simple battery model. Shorter discharge times (high-power applications) require thinner electrodes because of the significant ohmic potential drop within the electrode. Longer discharge times permit thicker electrodes. They also allow smaller porosities to get more capacity into a given volume without incurring a large ohmic penalty.

Further examples of optimization are given by Fuller et al.,[29] Thomas et al.,[30] and Fellner and Newman.[31]

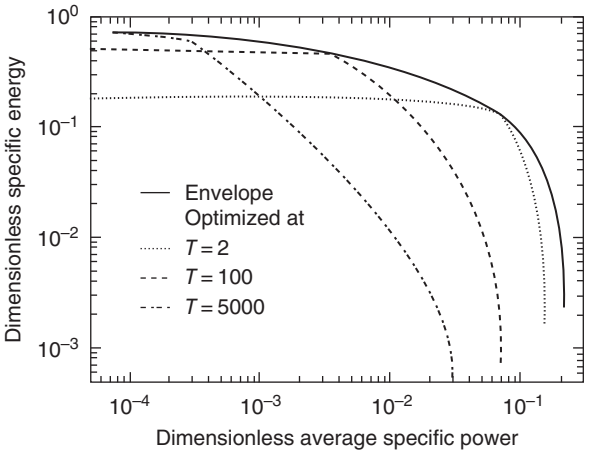

Figure 22.11 Specific energy versus average specific power. For three of the curves, the electrode thickness and porosity are optimized at the values of T given. For the envelope curve, the electrode thickness and porosity are optimized for each point on the curve. Here $\rho_+/\rho_s = b = 1$. *Source:* Newman 1995.[27] Reproduced with permission of The Electrochemical Society, Inc.

Cell-Sandwich Model

The complexity of the factors involved in the analysis of the behavior of porous electrodes leads to the use of a computer. The models of single battery electrodes discussed in the previous sections can be extended to treat both electrodes of a cell simultaneously and thereby give a more realistic treatment without artificial boundary conditions where the other electrode is supposed to be. In the next section, we illustrate the cell-sandwich model with the example of lithium alloy, iron sulfide cells used with a molten electrolyte, but in general we are interested in the spatial distributions of potentials and composition and the overall transient behavior of cell potential and temperature. Figure 22.12 shows a picture of the cell sandwich, with the negative electrode on the left, the separator in the middle, and the positive on the right.

This model was developed first for the lead–acid cell.[32] However, it is much more general and has been applied, with changes in details, to the molten-salt cells (to the FeS electrode with a straightforward reaction sequence[33] or with a more complicated set of reactions[34] or to the FeS_2 electrode[35]) and to other systems. We mention in particular lithium and lithium-ion batteries with one or two insertion electrodes.[36]

The modeling of porous electrodes involves establishing a number of unknowns which one needs to determine and a set of governing equations. In this application, these equations are likely to include transport processes, such as Ohm's law in the matrix and the description of migration, diffusion, and convection in the solution, material balances on liquid and solid phases, and kinetics for electrochemical reactions.

For unknowns, as functions of time and position in Figure 22.12, we may cite the following: composition as given by the mole fraction of LiCl in the electrolyte, the potential Φ_1 and Φ_2 in the matrix of each electrode and in the electrolyte, the superficial current densities in the same phases, the porosity, and the velocity of the electrolyte. There are also the volume fractions of each of the solid phases and the local composition of the alloy in the negative. For overall variables that are functions of time, one may mention the cell potential and the average temperature of the cell sandwich.

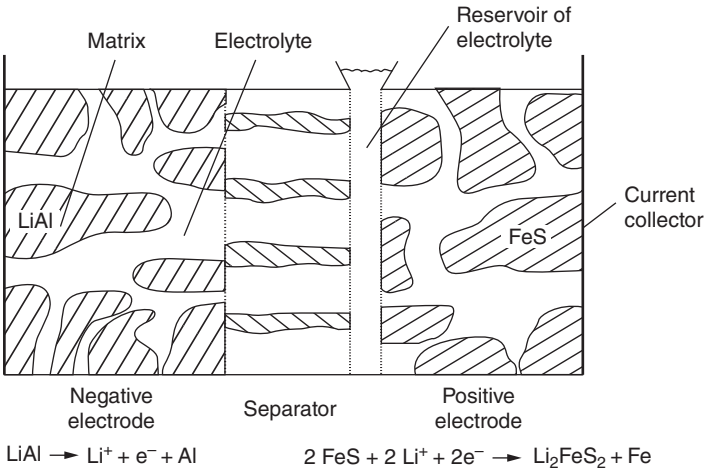

Figure 22.12 Schematic diagram of the LiAl–FeS cell, as an example of the cell-sandwich model. *Source:* Pollard and Newman 1981.[33] Reproduced with permission of The Electrochemical Society, Inc.

In many battery systems, the electrolyte can be considered to be a binary mixture, and this makes it possible to apply concentrated-solution transport theory as developed in Chapter 12 (Sections 12.2 through 12.6) or more general equations for a binary molten electrolyte.[37] A single composition variable is sufficient for the electrolyte. For example, a lead–acid battery has an aqueous solution of sulfuric acid, and the concentration of $PbSO_4$ can be ignored. The three relevant transport properties are the conductivity, diffusion coefficient, and one transference number, and these are known reasonably well as functions of composition and temperature. A number of batteries use an aqueous KOH solution. Hydrogen, cadmium, iron, and zinc are used for negative electrodes, and the positive can be Ag/Ag_2O, Ag/AgO, NiOOH, MnO_2, or air. The solubility of ZnO is high enough in concentrated KOH that one might not want to treat the solution as binary in that case. The sodium/sulfur battery uses sodium polysulfides in the positive electrode compartment, and these can probably be treated as a binary system because the polysulfides are in equilibrium with each other (compare Section 4.7).

Overall, one may then program four to six equations for simultaneous solution as coupled, ordinary, nonlinear, differential equations at each time step, with boundary conditions at two values of x (see Appendix C for some discussion of numerical methods for coupled differential equations). The velocity may be able to be eliminated because of its similarity to the current density i_2, and the porosity is related to the transfer current density and the time step by equation 22.32 (and the solid-phase volume fractions by similar equations). The polarization equation, relating the transfer current $\nabla \cdot \mathbf{i}_2$ to the concentration and overpotential, can include complexing and mass transfer of a sparingly soluble reactant and electrochemical kinetics on a surface area that changes with the local state of charge.

The polarization equation is the principal point where the macroscopic theory of porous electrodes will be subject to further refinement, as one tries to account not only for the mechanism of the charge-transfer process but also for the morphology of the electrode, the formation of covering layers or of crystallites of sparingly soluble species, and the transport from such sparingly soluble phases to the site of the charge-transfer process.

The boundary conditions can be made to include a limited reservoir of solution adjacent to the electrode and perhaps even a remote reservoir, connected to the adjacent reservoir by a mass-transfer coefficient. This will allow simulation of the recovery of the electrode potential with time as the electrolyte concentration is restored.

The cell-sandwich model or a summary of its results can be incorporated into a model of grid resistances for battery plates where the current from the reaction sites must be gathered into one conductor for transmission to a subsequent cell in series connection.[38, 39] This can be used to optimize current collector thickness and shape.

Lithium Alloy, Iron Sulfide Cells

Figure 22.12 shows the cell sandwich that represents a molten-salt cell designed to form part of a high-power battery. The current flows as in the single-electrode system in Figure 22.1, but it now continues through the separator in ionic form and reacts in the counterelectrode. Electrode reactions are indicated for a negative made of LiAl and for one of the reactions of an iron sulfide positive electrode. At the temperatures of molten salts, the electrode kinetics tends to be relatively fast. As an alternative to the reaction of FeS to Li_2FeS_2 (also called *X* phase), the reaction can go through a complex compound called *J* phase (which is $LiK_6Fe_{24}S_{26}Cl$) according to the following scheme:

$$26FeS + Li^+ + Cl^- + 6K^+ + 6e^- \rightarrow LiK_6Fe_{24}S_{26}Cl + 2Fe \tag{22.43}$$

followed by the reaction of *J* phase to other compounds, such as

$$J + 25Li^+ + 20e^- \rightarrow 13Li_2FeS_2 + 11Fe + 6K^+ + Cl^-. \tag{22.44}$$

Figure 22.13 shows concentration profiles of LiCl in the LiCl/KCl molten electrolyte for a LiAl/FeS cell discharging through the Li_2FeS_2 (*X* phase) mechanism. At short times, the concentration profiles reflect the stoichiometry of the electrode reactions. In the negative, Li^+ ions are injected into the electrolyte, thus raising the mole fraction of LiCl; while in the positive, Li^+ ions are extracted from the

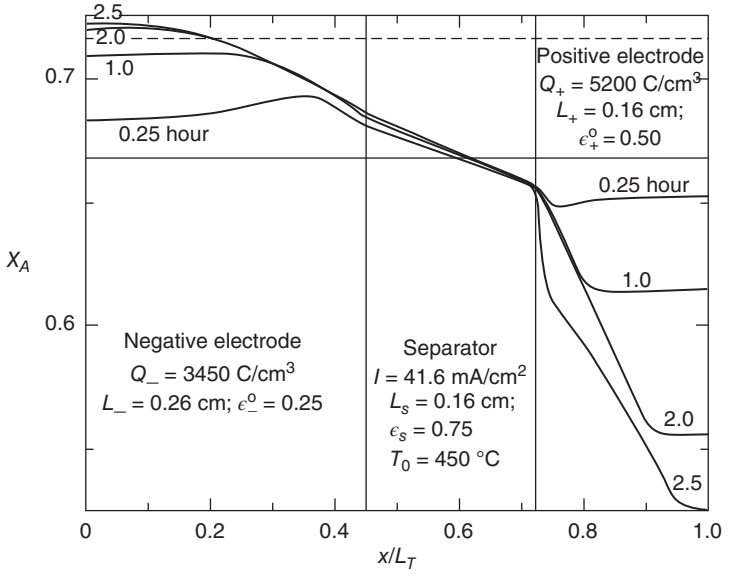

Figure 22.13 Position dependence of mole fraction of LiCl at different discharge times, for *X*-phase mechanism. Dashed line represents saturation limit for LiCl at 450°C. *Source:* Bernardi et al. 1981.[34] Reproduced with permission of The Electrochemical Society, Inc.

melt, thus lowering the mole fraction of LiCl. The figure shows that the reactions occur relatively close to the separator since the locations of injection and extraction occur close to the separator, and one can see the regions moving into the depth of the electrodes as time progresses. The negative electrode is opening up as the reaction occurs, and the concentration profiles are not very sharp there, while in the positive electrode, the porosity is small after the first reaction, and the progress of the reaction front through the electrode is clearly visible. The reaction zone is also less distinct in the negative electrode because this is an alloy electrode, and changes in the composition of the LiAl alloy result in concentration overpotentials that tend to spread the reaction region over the depth of the electrode. After 2.5 hours, a second reaction front is visible in the positive, before the first reaction front has reached the back of the electrode. The second reaction of Li_2FeS_2 to Fe and Li_2S reduces the porosity further, and concentration gradients become even more pronounced in the positive. This eventually leads to precipitation of KCl in the positive, and in the model this causes the cell potential to drop drastically if the precipitate blocks the pore cross section.

Figure 22.14 shows contrasting concentration profiles predicted for the reaction through the *J* phase. Here, the mole fraction rises in the positive as well as the negative in the early stages of discharge because K^+ ions are extracted in greater numbers than the Li^+ ions. However, the subsequent reaction in the positive brings the mole fraction down again, and more drastically than in the *X*-phase mechanism, because no Li^+ ions were transferred during the early stages of the discharge.

Figure 22.15 shows predicted discharge curves (for the *X*-phase mechanism) contrasted with experimental cell-potential data. The model results follow the experimental results reasonably well in the latter part of the discharge if precipitation of KCl is precluded in the model. The curves labeled *A* and *B* indicate the early termination of the discharge if precipitation is allowed to occur. The discharge curve calculated for the *J*-phase mechanism is shown in Figure 22.16. The first reaction (equation 22.43) occurs during the first 11% of utilization of the positive electrode, according to this mechanism, and comparison with Figure 22.15 suggests that the high potentials during the early part of discharge may be due to discharge by the *J*-phase mechanism.

Figure 22.17 shows predicted and experimental results for the discharge of the LiAl/FeS_2 cell. The top curve, with several line segments, corresponds to a reversible discharge and is based on thermodynamic cell potentials. The model calculations lie slightly below the reversible curve, and the experimental results lie below that. All three curves reflect the reaction sequence believed to apply to the FeS_2 electrode. In the early stages of discharge, the model results do not show as much polarization as the experimental curve, indicating that the resistances within the electrodes are not properly accounted for. Also, the model results show an end of discharge, due to precipitation, much

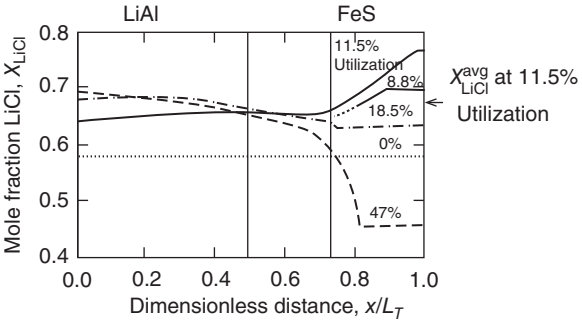

Figure 22.14 Composition profile through the cell sandwich, with *J*-phase mechanism. *Source:* Pollard and Newman 1988.[33] Reproduced with permission of The Electrochemical Society, Inc.

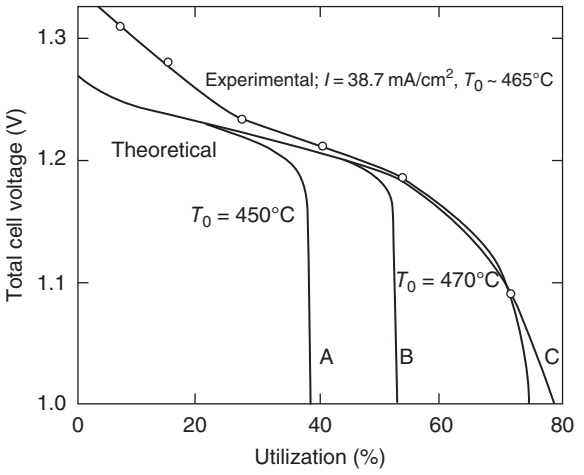

Figure 22.15 Comparison of theoretical and experimental discharge curves for the *X*-phase mechanism. *Source:* Bernardi et al. 1981.[34] Reproduced with permission of The Electrochemical Society, Inc.

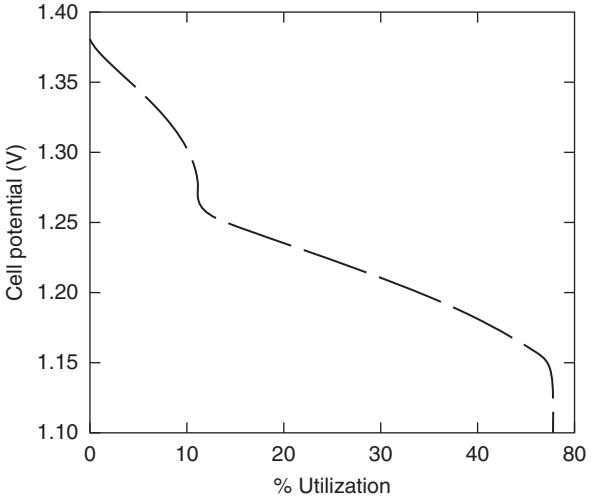

Figure 22.16 Discharge curve with *J*-phase mechanism.

earlier than the experimental curve. This illustrates the two major discrepancies between the model and the experiment: there is too little voltage loss and too much precipitation.

Figure 22.18 shows volume fractions of various phases at a point in the discharge of the FeS electrode by means of the *X*-phase mechanism. Here both reaction fronts can be seen; the front for the first reaction is at about 0.077 cm, and that for the second reaction is at about 0.01 cm. The initial porosity is about 0.5, and this is reduced to about 0.29 after the first reaction and to about 0.06 after the second reaction. However, at the reaction front for the first reaction, the porosity drops sharply to a small value over a very small distance. This is due to the calculated precipitation of KCl in the positive electrode, and this causes the discharge potential to drop considerably, eventually leading to the prediction of the end of discharge.

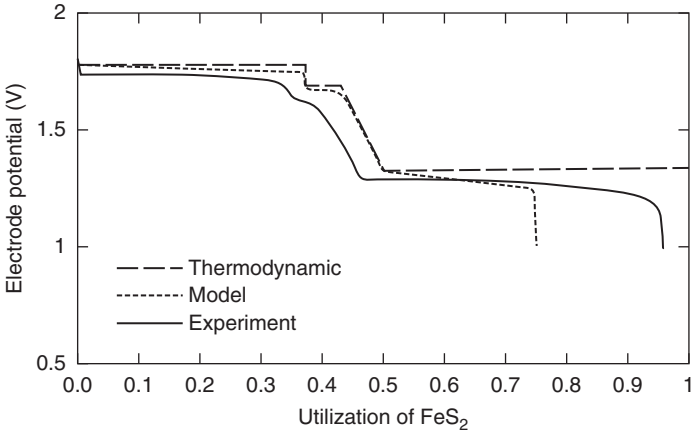

Figure 22.17 Comparison of model and experimental results for the potential of the FeS_2 electrode in a LiAl–FeS_2 cell, relative to a LiAl ($\alpha - \beta$) reference electrode (450°C, 50 mA/cm^2, $x^0_{LiCl} = 0.68$). The reversible, thermodynamic potential is also shown in order to display more clearly the losses of the system. *Source:* Bernardi and Newman 1987.[35] Reproduced with permission of The Electrochemical Society, Inc.

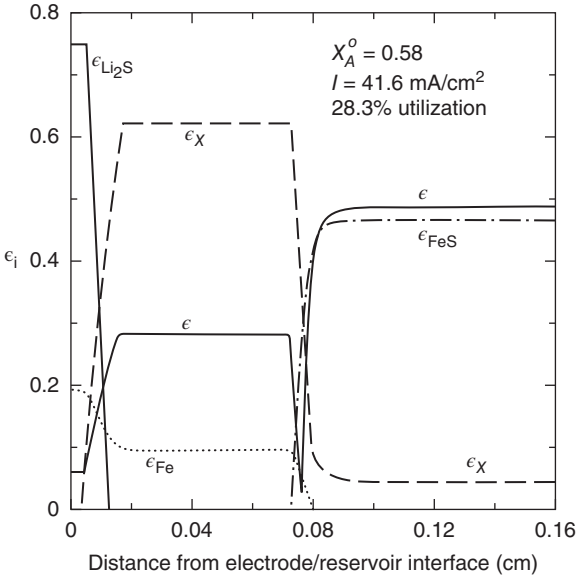

Figure 22.18 Volume fraction of solid phases and electrolyte in the positive electrode of LiAl–FeS cell discharging by the *X*-phase mechanism. *Source:* Bernardi et al. 1981.[33] Reproduced with permission of The Electrochemical Society, Inc.

In summary, let us emphasize that models of batteries with porous electrodes can predict polarization characteristics, as well as temperature changes. They can also give details of what is going on inside, such as composition profiles, precipitation of electrolyte, and reaction and porosity distributions, which would be difficult to determine experimentally. These details, as well as attempts to reconcile results with experiments, can enhance our understanding of how such systems operate.

22.5 DOUBLE-LAYER CHARGING AND ADSORPTION

A measurement of the double-layer capacity of a porous electrode most directly reflects the active surface area coherently connected electrically and therefore accessible for electrochemical reactions. Changes in the nature of the solid-phase composition, surface crystal structure, adsorbed materials, solution composition, temperature, and electrode potential also influence the measured value. Such results should be useful for the characterization of battery electrodes and may be especially valuable since the electrode is not destroyed, and indeed need not be removed from the cell in which it is being studied.

Johnson and Newman[40] have shown that the current response of a porous electrode to a step change in the potential yields, under certain circumstances, a nearly constant value of $i\sqrt{t}$, the product of the current density and the square root of time (also indicated by Ksenzhek and Stender[41] and Posey and Morozumi[42]). A value of the double-layer capacity can be inferred from this constant value of $i\sqrt{t}$. However, most porous electrodes have nonzero resistances that prevent the attainment of a constant value of $i\sqrt{t}$ at short times, and the capacity begins to saturate at long times. Tiedemann and Newman[43] used the same technique to study the PbO_2 and Pb electrodes in H_2SO_4 solution. A plot of $i\sqrt{t}$ versus $\sqrt{t}$ yields a maximum in $i\sqrt{t}$, and this value was used to obtain a value for the double-layer capacity. Figure 22.19 shows the comparison between theory and experiment for the charging curve of PbO_2 in H_2SO_4 solution. Emphasis on the maximum of this charging curve minimizes the ohmic effects at short times as well as the faradaic effects at long times. As faradaic reactions become more important, a positive displacement of the experimental curve from the theoretical curve is observed at long times. However, the shape of the curve near the maximum remains relatively unchanged.

Johnson and Newman also demonstrated that specific adsorption of ions on a porous high-surface-area carbon electrode can be used to bring about a separation or concentration of soluble

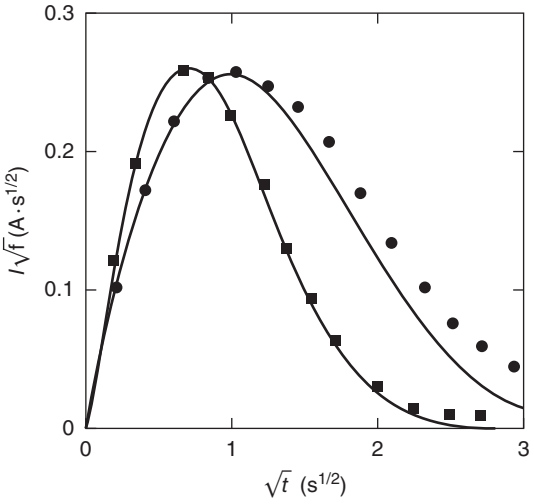

Figure 22.19 Comparison of experimental and theoretical results for potentiostatic double layer charging of porous PbO_2 electrodes. Area = 241 cm^2, $L = 0.095$ cm, temperature = 28°C. ■: freshly prepared PbO_2 electrode, $\Delta V = 2.51$ mV, $\lambda = 1.33$, $aC = 23.33$ F/cm^3; •: cycled PbO_2 electrode, $\Delta V = 1.52$ mV, $\lambda = 0.768$, $aC = 26$ F/cm^3. (λ is a ratio of the external resistance, Ω cm^2, to L/κ.) Solid curves are theoretical. *Source:* Tiedemann and Newman 1975.[43] Reproduced with permission of The Electrochemical Society, Inc.

species. By alternating the applied potential at specified time intervals, a NaCl solution could be desalted during the adsorption cycle and concentrated during the desorption cycle. This technique constitutes a novel means of separation. It can also be used with hard-to-plate ions such as Zn^{2+} and Pb^{2+}.

Double-layer capacitors are also used for energy storage. They have a fast response time and are not degraded much by the adsorption process, but the energy-storage capability is limited compared to many batteries.

22.6 FLOW-THROUGH ELECTROCHEMICAL REACTORS

Flow-through porous electrodes possess inherent advantages over nonporous electrodes with flowing solutions or porous electrodes without flow. This has been well demonstrated by Kalnoki-Kis and Brodd,[44] who showed increases in current by factors of 10^2 to 10^4 at a given overpotential. High specific interfacial area allows the attainment of relatively high volumetric rates of reaction, and the flowing solution eliminates or reduces mass-transport problems. Thick electrodes and low flow rates produce relatively long contact times for treatment of very dilute solutions.

Liebenow[45] showed how mass-transport limitations could be diminished by flowing a solution through an electrode. Heise[46] discussed in great detail the usefulness of flow-through porous electrodes for a number of processes of industrial interest: (i) conversion of manganate to permanganate, ferrous to ferric, nitrate to nitrite, and arsenite to arsenate; (ii) electrowinning of copper; and (iii) electro-organic oxidation and reduction. The advantages and limitations of such electrode systems are also discussed.

In modeling of the system for design purposes, a number of factors might be included in the analysis. Many of these are already relevant for porous electrodes without flow and can be reviewed here:

1. Should a straight-pore model or a homogeneous macroscopic model be used?
2. Should transport processes be described by dilute or concentrated electrolyte theory? How are conductivities and other transport properties to be estimated for porous media? Should ohmic losses in the solid matrix be included?
3. What are the kinetics of the reactions and the effects of side reactions?
4. Is the system isothermal?
5. Is operation steady or transient?

New factors are also introduced specifically for flow-through electrodes. These include:

1. Is the flow uniform through the electrode, or is there channeling?
2. What is the direction of flowing solution with respect to the counterelectrode? The counterelectrode can be upstream or downstream (a flow-through electrode), or it can be beside the working electrode (a so-called flow-by system). Two, rather than one, dimensional consideration of the distributions of concentration, current, and potential may be necessary.
3. How fast can reactants be transported from the flowing solution to the solid surface? Chemical-engineering correlations of mass-transfer coefficients in packed beds (Bird et al.,[47] Wilson and Geankoplis[48]) have been extended to electrochemical situations by Yip,[49] Gracon,[50] and Appel.[51]
4. Do the flow patterns promote significant axial mixing? This dispersion effect is mathematically similar to diffusion and can be characterized by a dispersion coefficient D_a. Sherwood et al.[52] correlated available data on dispersion in packed beds and expressed their results in a figure by

plotting a Péclet number proportional to $v/a(D + D_a)$ against a Reynolds number proportional to $v/a\nu$, with the Schmidt number† ν/D as a parameter. At low flow rates, axial mixing becomes less important than molecular diffusion, but the Reynolds number at which this occurs decreases as the Schmidt number becomes larger.

5. What is the approach to limiting current and the degree of conversion?

The extent to which any or all of the above are incorporated into the analysis is dependent on the specific system and given design and optimization requirements. Equations 22.7 (Faraday's law), 22.30 (the polarization equation), 22.12 (Ohm's law in the matrix), and 22.13 (the flux density in the solution) facilitate the formulation of the problem, but to effect a solution may require various assumptions.

Design and optimization are specific to the given system and have been discussed by Bennion and Newman[53] and by Gurevich et al.[54] To illustrate the design principles outlined by Bennion and Newman, we examine the removal of Cu^{2+} and Pb^{2+}, for example, from a waste stream. The Pb^{2+} turns out to be difficult to remove in a porous electrode[55] and is included in order to show how the design is influenced by the concentration of the feed.

1. We want to promote intimate contact between the electrode and the solution in order to carry out reactions to a high degree of completion. This calls for small flow channels (pores) and hence for a flow-through (or flow-by) porous electrode.
2. Carrying reactions to a high degree of completion also calls for operation at the limiting current, so that the concentration at the walls of the pores is close to zero. This also brings about considerable simplification in the design calculations since it decouples the potential distribution from the mass-transfer rates and current distribution.
3. We want to avoid side reactions. These could range from unwanted evolution of hydrogen or oxygen to competing reactions or subsequent reactions in electro-organic synthesis. Consequently, the potential variation in the solution phase should not exceed a certain limit, one or two tenths of a volt in moderately sensitive cases. This is an application of the principle of electrochemical engineering discussed in Chapter 18 that potentials need to be maintained in certain bounds, a principle that applies in a number of situations ranging from cathodic protection to controlled-potential electrolysis.

To effect this simple design, we begin with the concentration distribution along the length of the pores. With assumptions of negligible migration, appropriate to a dilute solution of Cu^{2+} ions in H_2SO_4 or Na_2SO_4 solution or Hg^{2+} ions in NaCl solution, equation 22.13 becomes

$$\frac{\mathbf{N}_{ix}}{\epsilon} = -(D_i + D_a)\frac{\partial c_i}{\partial x} + \frac{v_x c_i}{\epsilon}. \tag{22.45}$$

We take D_i, D_a, ϵ, and v_x to be constants, independent of x. Equation 22.2 gives the material balance. For a steady process, the time derivative vanishes, and j_{in}, the flux density from the wall to the pore solution, is described by a mass-transfer coefficient[2, 53] k_m as

$$j_{in} = k_m(c_{i,0} - c_i), \tag{22.46}$$

where $c_{i,0}$ is the concentration at the surface and c_i is the average concentration in the pores.

† The Schmidt number being based on the true molecular diffusion coefficient without any tortuosity factor.

How k_m depends on velocity v_x and diffusion coefficient D_i is reviewed by Newman and Tiedemann.[2] When equations 22.45 and 22.46 are substituted into the material-balance equation 22.2, we obtain

$$v_x \frac{\partial c_i}{\partial x} = (D_i + D_a)\frac{\partial^2 c_i}{\partial x^2} + ak_m(c_{i,0} - c_i). \tag{22.47}$$

In a flow-through electrode with significant flow, the diffusion term can be neglected with respect to the convective term on the left. This is discussed more extensively by Newman and Tiedemann.[2] The mass transfer is decoupled from the electrode kinetics by assuming that limiting-current conditions prevail. (Relaxation of this assumption is discussed more extensively by Trainham and Newman.[56]) The equation reduces to

$$v_x \frac{\partial c_i}{\partial x} = -ak_m c_i \tag{22.48}$$

with the solution

$$c_i = c_f \exp\left(-\frac{ak_m x}{v_x}\right) = c_f\, e^{-ax}, \tag{22.49}$$

where $\alpha = ak_m/v_x$ and c_f is the feed concentration to the porous electrode.

If we specify also the effluent concentration c_L, this yields a design equation

$$L = \frac{v_x}{ak_m} \ln \frac{c_f}{c_L} \tag{22.50}$$

showing how thick the electrode should be made or how slow the fluid velocity v_x should be made in order to achieve a specified removal of the solute. One can see that tightening this specification by an additional factor of 10 does not increase the electrode thickness by very much.

Generally one would want to use as high a velocity as possible in order to reduce the capital costs. How large can we make v_x? This is determined by the ohmic potential drop in the x direction; we want to maintain the limiting-current condition ($c_{i,0} \approx 0$) along the length without generating too much side reaction at one end or the other. We express this, approximately, as a certain allowed variation of potential drop $\Delta(\Phi_1 - \Phi_2)$ along x. Figure 22.4 shows potential profiles for one porous-electrode model, where the minimum value of $(\Phi_1 - \Phi_2)$ occurs in the interior of the porous electrode. The maximum value usually occurs at one end or the other. (This assumption of a given value of $\Delta|\Phi_1 - \Phi_2|$ is relaxed by Trainham and Newman,[56] but then one needs to account for the side reaction, necessarily encountered as one approaches the limiting current, solve coupled equations for the potential, current density, and concentration, and state an optimization criterion to permit one to decide how much side reaction is permissible.) From a current–potential curve for copper deposition, like that in Figure 1.13, we make the subjective judgment that $\Delta\Phi_{\max}$ might be about 0.2 V to assure that we are close enough to the limiting current but not permitting much side reaction. One should appreciate that this value depends on the chemical system involved. We use 0.1 V for Pb deposition because it is a less noble metal than Cu, but even this value may be too large. By assuming that $\sigma \gg \kappa$, we can apply $\Delta\Phi_{\max}$ as a limit for $\Delta\Phi_2$ within the electrode.

Equations 22.7 and 22.45 form the basis for writing Faraday's law

$$\frac{di_2}{dx} = -\frac{nF}{s_i} v_x \frac{dc_i}{dx}, \tag{22.51}$$

where axial diffusion is again neglected. For the configuration in Figure 22.20a, the boundary conditions are

$$i_2 = I \quad \text{at} \quad x = 0, \quad i_2 = 0 \quad \text{at} \quad x = L. \tag{22.52}$$

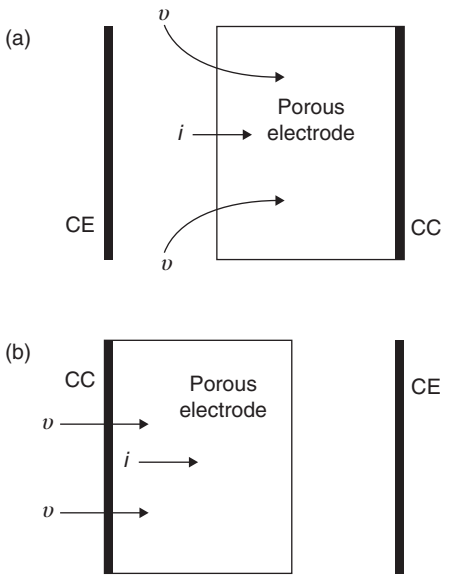

Figure 22.20 Two configurations of a flow-through porous electrode showing the placement of the counterelectrode (CE) and the current collector (CC). A desirable configuration is to have the CE upstream, as in (a), but the downstream CE in (b) may keep reaction products from the CE out of the working electrode. A third possibility (not shown) is to place the CE along the working electrode.

Integration with these boundary conditions gives

$$i_2 = nFv_x c_f(e^{-ax} - c_L/c_f), \tag{22.53}$$

where we have also chosen s_i to be -1, so that n is the number of electrons transferred when one molecule or ion reacts. The integration constant implies an *upstream* counterelectrode; this would be modified substantially for a downstream counterelectrode, where $i_2 = 0$ at $x = 0$. (See Problem 22.7.)

We use equation 22.20 for Ohm's law because we assume the presence of supporting electrolyte. Integration of i_2 according to this equation gives the potential distribution

$$\Phi_2 = \beta\left[e^{-\alpha x} - 1 - \alpha x\frac{c_L}{c_f}\right], \tag{22.54}$$

where $\beta = nFv_x^2 c_f/ak_m\kappa$ and we have taken $\Phi_2 = 0$ at $x = 0$. Then

$$\Delta\Phi_2 = \beta[1 - (\alpha L - 1)e^{-\alpha L}]. \tag{22.55}$$

In the common case where $\sigma \gg \kappa$, $\Delta\Phi_2$ is essentially the same as $\Delta\Phi_{\max}$ because the potential drop in the matrix is negligible. See also Problem 22.7.

When we carry a reaction (or separation) to a high degree of completion, $e^{-\alpha L}$ is very small, and $\Delta\Phi_2 \approx \beta$. This yields our second design equation

$$|\Delta\Phi_{\max}| = \frac{nFv_x c_f}{\kappa}\frac{v_x}{ak_m}, \tag{22.56}$$

TABLE 22.1 Operating conditions, design results, and costs for removal of lead and copper ions from given solutions

	Pb system		Cu system	
Feed concentration, mg/liter	1.45		667	
Product concentration, mg/liter	0.05		1	
Solution conductivity, S/cm	0.8		0.17	
Allowable potential variation, V	0.1		0.2	
Specific electrode area, cm^{-1}	25		25	
Superficial velocity, cm/s	0.64		0.0036	
Electrode thickness, cm	60		5	
Time to plug, days	377		5	
	$/m^3	$/kg	$/m^3	$/kg
Electrode capital cost	0.2133	1.472	25.4	0.424
Operating labor	0.0173	0.144	4.0	0.067
Electrical energy	0.0020	0.014	3.2	0.053
Pumping energy	0.1267	0.87	0.013	0.0002
Total	0.36	2.49	33	0.544

which can be regarded as the product of a superficial current density ($nFv_x c_f$) with the reciprocal of the effective conductivity ($1/\kappa$) and an effective depth of penetration of the reaction into the electrode (v_x/ak_m). The mass-transfer coefficient k_m itself depends on the velocity, so that $|\Delta\Phi_{\max}|$ is proportional to the velocity to about the 1.5 power.

In practice, we would use this equation to determine the maximum permissible velocity or throughput that can be achieved while avoiding side reactions and yet operating near limiting current. Note how the difficulty of the problem (or separation process) is governed by the ratio c_f/κ of the reactant concentration to the conductivity and by the specific interfacial area a of the electrode. (After allowance for the dependence of k_m on a, $|\Delta\Phi_{\max}|$ is proportional to a to about the -1.5 power.)

The thickness of the electrode is now determined by the required degree of reaction, given by equation 22.50.

Costs, of course, depend on how c_0, c_b^L, κ, and a affect v and L. Comparisons are given in Table 22.1 for the lead and copper systems. As the feed concentration is increased by a factor of 415, the cost per unit volume of solution goes up by a factor of 90 while the cost per unit mass of dissolved metal goes down by a factor of 4.6. (Costs are in 2002 dollars, approximately.) The pumping power makes a dramatic increase in importance for dilute solutions.

PROBLEMS

22.1 A porous electrode system with an open-circuit potential U of 2.0 V is to be designed to produce electric power of 25 kW. The porous electrode is separated from a highly reversible plane electrode by a porous fiber material of thickness L_s and effective electrolytic conductivity κ_s. The porous electrode of thickness L can be attributed an infinite matrix conductivity σ, linear polarization characteristics, an absence of concentration gradients, and an inexhaustable supply of fuel. Under these conditions, the cell potential can be expressed as

$$V = U - IR, \tag{22.57}$$

where I is the superficial current density and R ($\Omega\,\text{cm}^2$) is the internal resistance of the system, including the porous electrode and the separator. You are to design the system to minimize the capital cost, which is given by

$$\text{Capital cost} = A(a + bL), \tag{22.58}$$

where A is the superficial area of the electrode system, $a = \$8/\text{m}^2$ and $b = \$0.2/\text{m}^3$.

(a) Show that the optimum superficial current density is given by

$$I_{\text{opt}} = U/2R. \tag{22.59}$$

(b) Show how to optimize the electrode thickness L with the system always operated at the optimum current density of part (a).

(c) Obtain a numerical value for the optimum electrode thickness when the following design data apply:

$$\begin{aligned} L_s &= 0.02\,\text{cm}, & \kappa_s &= 0.1\,\text{S/cm}, \\ \alpha_a + \alpha_c &= 1, & \kappa &= 0.1\,\text{S/cm}, \\ a &= 10^5\,\text{cm}^{-1}, & i_0 &= 10^{-5}\,\text{A/cm}^2, \\ F/RT &= 40\,\text{V}^{-1}. \end{aligned}$$

22.2 A flow-through, porous-electrode, electrochemical reactor is to be used for the recovery of silver from a photographic fixing solution where the silver is present at low concentrations as the complex ion $\text{Ag}(\text{S}_2\text{O}_3)_2^{3-}$, that is, it is complexed with thiosulfate. The solution is well supported, and one of the principal ions, the thiosulfate, undergoes a side reaction:

$$\text{S}_2\text{O}_3^{2-} + 8\text{e}^- + 8\text{H}^+ \rightleftharpoons 2\text{HS}^- + 3\text{H}_2\text{O}. \tag{22.60}$$

To design this reactor to operate below the limiting current, you are asked to develop the equations for subsequent computer modeling. The desired computer program is to involve only two unknown functions that are determined simultaneously throughout the thickness of the porous electrode. You should assume that the reactor operates in a steady state with an excess of supporting electrolyte and with no gas phase present. The counterelectrode is upstream. Derive and state the differential equations and boundary conditions that should be programmed for the computer.

22.3 A cylindrical configuration is fairly common for porous battery electrodes, particularly those in Leclanché cells and in alkaline–manganese dioxide cells. You are assigned to set up a simple model of such an electrode. Use a macrohomogeneous model with no concentration variations, uniform properties, and linear electrode kinetics. Double-layer charging can also be ignored. Formulate an ordinary differential equation for a single variable of your choice and specify appropriate boundary conditions for one of the following situations (specify clearly which):

(a) Counterelectrode is outside the electrode of interest, and the current collector is a carbon core at the center of the electrode of interest.

(b) Counterelectrode is inside the electrode of interest, and the current collector is outside.

(c) Counterelectrode is inside the electrode of interest, and the current collector is a perforated, highly conducting, inert sheet at the inner side of the electrode of interest.

The inner radius of the porous electrode is r_i, and the outer radius is r_o. Assuming that you have the results of the model you developed above, specify how one is to obtain the following quantities:

i. Distribution of Φ_1, the potential in the solid matrix, as a function of radial position.

ii. Distribution of Φ_2, the potential in the pore solution.

iii. Distribution of i_2, the superficial current density for the pore solution.

iv. Distribution of i_1, the superficial current density for the solid matrix.

v. Distribution of the reaction rate (A/cm^3).

vi. Overall potential difference across the porous electrode (minus any open-circuit value).

22.4 A porous electrode is claimed to show a *double Tafel slope* under two disparate conditions. The condition of uniform composition and Tafel kinetics is *not* of interest here. Instead look at the situation where ohmic drop is negligible in both the matrix and solution phases and there is a large excess of supporting electrolyte and a small concentration of the critical reactant, which is maintained at a concentration c_b at the electrode face at $x = 0$. Formulate a problem (differential equation with complete boundary conditions) for the concentration distribution of this reactant. The geometry is one dimensional, not cylindrical. The diffusion potential is negligible, and the composition dependence of the exchange current density is given by the rules formulated in Section 8.3. This means that the electrode reaction turns out to be first order (in the forward rate for the critical reactant) at a fixed value of the electrode potential $\Phi_1 - \Phi_2$ (compare Problem 20.4).

Solve this problem for the concentration distribution $c_i(x)$. You may assume the electrode to be infinitely thick if you wish. Determine whether this solution corresponds to a double Tafel slope at large electrode potentials.

22.5 Discuss what type of reference electrode is imagined to ascertain the solution-phase potential Φ_2 in Problem 22.4.

22.6 Derive the "general" porous-electrode equation $\nabla^2\eta_s = a(1/\kappa + 1/\sigma)f(\eta_s)$, where $f(\eta_s)$ represents the rate function, as in equation 8.5, and $\eta_s = \Phi_1 - \Phi_2 - U$. In this problem, take the composition to be uniform, as in Section 22.2.

22.7 For flow-through porous electrodes, there are several combinations of placement of the counterelectrode and of the current collector, relative to the porous electrode itself. The text treats an upstream counterelectrode. For a system with a downstream counterelectrode and an upstream current collector, but still with the approximation of a limiting-current distribution, derive equations for c_i, i_2, Φ_2, and Φ_1 as functions of x, the distance through the porous electrode. Sketch the results, or use a spreadsheet to obtain more quantitative results. Include the cases of $\sigma \gg \kappa$ and $\sigma = 2\kappa$. See Figure 22.20b.

NOTATION

a	specific interfacial area, cm^{-1}
A_0	constant defined by equation 22.33
c_i	concentration of species i per unit volume of solution, mol/cm^3
c_i^0	reference or bulk concentration, mol/cm^3
C	differential double-layer capacity, F/cm^2
C_p	cell heat capacity per unit of separator area, J/cm^2·K
D_a	dispersion coefficient, cm^2/s
D_i	diffusion coefficient of species i, cm^2/s

F	Faraday's constant, 96,487 C/mol
h_0	heat-transfer coefficient, based on separator area, W/cm^2·K
i_0	exchange current density, A/cm^2
$\mathbf{i}_1$	superficial current density in the matrix, A/cm^2
$\mathbf{i}_2$	superficial current density in pore phase, A/cm^2
i_n	transfer current per unit of interfacial area, A/cm^2
I	superficial current density to an electrode, A/cm^2
j_{in}	pore-wall flux density of species i, mol/cm^2·s
k_m	coefficient of mass transfer between flowing solution and electrode surface, cm/s
L	thickness of porous electrode, cm
M_i	molar mass of species i, g/mol
n	number of electrons transferred in electrode reaction
$\mathbf{n}$	normal unit vector
$\mathbf{N}_i$	superficial flux density of species i, mol/cm^2·s
q	surface charge density on solid side of double layer, C/cm^2
R	universal gas constant, 8.3143 J/mol·K
s_i	stoichiometric coefficient of species i in electrode reaction
Sc	Schmidt number, ν/D
t	time, s
T	absolute temperature, K
T_0	initial temperature, K
T_a	ambient temperature, K
u_i	mobility of species i, cm^2·mol/J·s
U	open-circuit cell potential, V
U'	open-circuit value of $\Phi_1 - \Phi_2$, V
υ	superficial fluid velocity, cm/s
V	electrode or cell potential, V
x	distance through porous electrode, cm
z_i	valence or charge number of species i
α_a, α_c	transfer coefficients
β	$\alpha_a F/RT$ or $-\alpha_c F/RT$
γ_i	dimensionless diffusion parameter
Γ_i	surface concentration of species i, mol/cm^2
δ	dimensionless current density defined in equation 22.24
ϵ	porosity or void volume fraction
η	overpotential, V
η_s	surface overpotential, V
κ	effective conductivity of solution, S/cm
κ_0	free solution conductivity, S/cm
κ'	modified solution conductivity, S/cm
λ	resistance ratio (see Figure 22.19)
ν	square root of dimensionless exchange current (see equation 22.25) or kinematic viscosity, cm^2/s
ρ_i	density of a solid phase of species i, g/cm^3
σ	effective conductivity of the solid matrix, S/cm
Φ_1	electric potential in the matrix, V
Φ_2	electric potential in the solution, V

REFERENCES

1. John Newman and William Tiedemann, "Porous-Electrode Theory with Battery Applications," *AIChE Journal*, *21* (1975), 25–41.
2. John S. Newman and William Tiedemann, "Flow-through Porous Electrodes," *Advances in Electrochemistry and Electrochemical Engineering*, *11* (1978), 353–438.
3. Robert de Levie, "Electrochemical Response of Porous and Rough Electrodes," *Advances in Electrochemistry and Electrochemical Engineering*, *6* (1967), 329–397.
4. John Stephen Dunning, *Analysis of Porous Electrodes with Sparingly Soluble Reactants*, Dissertation, University of California, Los Angeles, 1971.
5. D. A. G. Bruggeman, "Berechnung verschiedener physikalischer Konstanten von heterogenen Substanzen. I. Dielektrizitätskonstanten und Leitfähigkeiten der Mischkörper aus isotropen Substanzen," *Annalen der Physik, ser.* 5, *24* (1935), 636–664.
6. James Clerk Maxwell, *A Treatise on Electricity and Magnetism*, 3rd ed., vol. 1 (Oxford: Clarendon, 1904), pp. 435–449.
7. John Newman and Thomas W. Chapman, "Restricted Diffusion in Binary Solutions," *AIChE Journal*, *79* (1973), 343–348.
8. D. Bernardi, E. Pawlikowski, and J. Newman, "A General Energy Balance for Battery Systems," *Journal of the Electrochemical Society*, *132* (1985), 5–12.
9. Karen E. Thomas and John Newman, "Thermal Modeling of Porous Insertion Electrodes," *Journal of the Electrochemical Society*, *150* (2003), A176–A192.
10. Lin Rao and John Newman, "Heat Generation Rate and General Energy Balance for Insertion Battery Systems," *Journal of the Electrochemical Society 144* (1997), 2697–2704.
11. John S. Newman and Charles W. Tobias, "Theoretical Analysis of Current Distribution in Porous Electrodes," *Journal of the Electrochemical Society*, *109* (1962), 1183–1191.
12. J. Euler and W. Nonnenmacher, "Stromverteilung in porösen Elektroden," *Electrochimica Acta*, *2* (1960), 268–286.
13. Irene J. Ong and John Newman, "Double-Layer Capacitance in a Dual Lithium Ion Insertion Cell," *Journal of the Electrochemical Society*, *146* (1999), 4360–4365.
14. Jeremy P. Meyers, Marc Doyle, Robert M. Darling, and John Newman, "Impedance Response of a Porous Electrode Composed of Intercalation Particles," *Journal of the Electrochemical Society*, *147* (2000), 2930–2940.
15. O. S. Ksenzhek and V. V. Stender, "Raspredelenie toka v poristom elektrode," *Doklady Akademii Nauk SSSR*, *107* (1956), 280–283.
16. A. Winsel, "Beiträge zur Kenntnis der Stromverteilung in porösen Elektroden," *Zeitschrift für Elektrochemie*, *66* (1962), 287–304.
17. Werner Stein, *The Physical Processes in the Pores of Plates During the Discharge of a Lead Storage Battery with Large Current Densities*, PhD thesis, RheinischWestfalischen Technischen Hochschule Aachen, 1959.
18. M. Doyle and J. Newman, "Analysis of capacity-rate data for lithium batteries using simplified models of the discharge process," *Journal of Applied Electrochemistry*, *27*(7) (1997), 846–856.
19. King Wah Choi, Drannan Hamby, Douglas N. Bennion, and John Newman, "Engineering Analysis of Shape Change in Zinc Secondary Electrodes. II. Experimental," *Journal of the Electrochemical Society*, *123* (1976), 1628–1636.
20. Karen E. Thomas, John Newman, and Robert M. Darling, "Mathematical Modeling of Lithium Batteries," in Walter A. van Schalkwijk and Bruno Scrosati, eds., *Advances in Lithium-Ion Batteries* (New York: Kluwer Academic/Plenum, 2002).
21. Richard Pollard, *Mathematical Modeling of the Lithium-Aluminum Iron Sulfide Battery*, Dissertation, University of California, Berkeley, 1979.

22. Richard C. Alkire, Edward A. Grens II, and Charles W. Tobias, "A Theory for Porous Electrodes Undergoing Structural Change by Anodic Dissolution," *Journal of the Electrochemical Society*, *116* (1969), 1328–1333.
23. Richard C. Alkire, Edward A. Grens II, and Charles W. Tobias, "Preparation of Uniform Pore Structures for Porous Electrode Studies," *Journal of the Electrochemical Society*, *116* (1969), 809–810.
24. J. S. Dunning and D. N. Bennion, "A Model for Secondary Battery Electrodes," *Proceedings, Advances in Battery Technology Symposium, 5*, 135–152 (Southern California–Nevada Section of the Electrochemical Society, December, 1969).
25. John S. Dunning, Douglas N. Bennion, and John Newman, "Analysis of Porous Electrodes with Sparingly Soluble Reactants," *Journal of the Electrochemical Society*, *118* (1971), 1251–1256.
26. John S. Dunning, Douglas N. Bennion, and John Newman, "Analysis of Porous Electrodes with Sparingly Soluble Reactants II. Variable Solution Properties, Convection, and Complexing," *Journal of the Electrochemical Society*, *120* (1973), 906–913.
27. John Newman, "Optimization of Porosity and Thickness of a Battery Electrode by Means of a Reaction-Zone Model," *Journal of the Electrochemical Society*, *142* (1995), 97–101.
28. William Tiedemann and John Newman, "Maximum Effective Capacity in an Ohmically Limited Porous Electrode," *Journal of the Electrochemical Society*, *122* (1975), 1482–1485.
29. Thomas F. Fuller, Marc Doyle, and John Newman, "Simulation and Optimization of the Dual Lithium Ion Insertion Cell," *Journal of the Electrochemical Society*, *141* (1994), 1–10.
30. Karen E. Thomas, Steve E. Sloop, John B. Kerr, and John Newman, "Comparison of Lithium-Polymer Cell Performance with Unity and Nonunity Transference Numbers," *Journal of Power Sources*, *89* (2000), 132-138.
31. Christian Fellner and John Newman, "High-power Batteries for Use in Hybrid Vehicles," *Journal of Power Sources*, *85* (2000), 229–236.
32. William H. Tiedemann and John Newman, "Mathematical Modeling of the Lead-Acid Cell," in Sidney Gross, ed., *Proceedings of the Symposium on Battery Design and Optimization* (Princeton: The Electrochemical Society, 1979), pp. 23–38.
33. Richard Pollard and John Newman, "Mathematical Modeling of the Lithium-Aluminum, Iron Sulfide Battery I. Galvanostatic Discharge Behavior," *Journal of the Electrochemical Society*, *128* (1981), 491–502.
34. Dawn Bernardi, Ellen M. Pawlikowski, and John Newman, "Mathematical Modeling of LiAl/LiCl,KCl/FeS Cells," *Journal of the Electrochemical Society*, *135* (1988), 2922–2931.
35. Dawn Bernardi and John Newman, "Mathematical Modeling of Lithium(alloy), Iron Disulfide Cells," *Journal of the Electrochemical Society*, *134* (1987), 1309–1318.
36. Marc Doyle, Thomas F. Fuller, and John Newman, "Modeling of Galvanostatic Charge and Discharge of the Lithium/Polymer/Insertion Cell," *Journal of the Electrochemical Society*, *140* {1993), 1526–1533.
37. Richard Pollard and John Newman, "Transport Equations for a Mixture of Two Binary Molten Salts in a Porous Electrode," *Journal of the Electrochemical Society*, *126* (1979), 1713–1717.
38. William H. Tiedemann and John Newman, "Current and Potential Distribution in Lead-Acid Battery Plates," Sidney Gross, ed., *Proceedings of the Symposium on Battery Design and Optimization*, vol. *79-1* (Princeton: The Electrochemical Society, 1979), pp. 39–49.
39. Gary G. Trost, Victoria Edwards, and John S. Newman, "Electrochemical Reaction Engineering," in James J. Carberry and Arvind Varma, eds., *Chemical Reaction and Reactor Engineering* (New York: Marcel Dekker, 1987), pp. 923-972.
40. A. M. Johnson and John Newman, "Desalting by Means of Porous Carbon Electrodes," *Journal of the Electrochemical Society*, *118* (1971), 510–517.
41. O. S. Ksenzhek and V. V. Stender, "Opredelenie udel'noĭ Poverkhnosti Poristykh Elektrodov Metodami Izmereniya Emkosti," *Doklady Akademii Nauk SSSR*, *106* (1956), 487–490.
42. F. A. Posey and T. Morozumi, "Theory of Potentiostatic and Galvanostatic Charging of the Double Layer in Porous Electrodes," *Journal of the Electrochemical Society*, *113* (1966), 176–184.
43. William Tiedemann and John Newman, "Double-Layer Capacity Determination of Porous Electrodes," *Journal of the Electrochemical Society*, *122* (1975), 70–74.

44. T. Kalnoki-Kis and R. J. Brodd, "Characterization of Porous Flow Through Electrodes," Abstract No. 237, Chicago meeting, *Journal of the Electrochemical Society*, *120* (1973), 109C.
45. Liebenow, "Über die Berechnung der Kapazität eines Bleiakkumulators bei variabelor Stromstärke," *Zeitschrift für Elektrochemie*, *4* (1897), 58–63 (particularly p. 63).
46. George W. Heise, "Porous Carbon Electrodes," *Transactions of the Electrochemical Society*, *75* (1939), 147–166.
47. R. Byron Bird, Warren E. Stewart, and Edwin N. Lightfoot, *Transport Phenomena*, 2nd edition (New York: Wiley, 2002), p. 441.
48. E. J. Wilson and C. J. Geankoplis, "Liquid Mass Transfer at Very Low Reynolds Numbers in Packed Beds," *Industrial and Engineering Chemistry Fundamentals*, *5* (1966), 9–14.
49. Harry Hung-Kwan Yip, *Mass Transfer Coefficient in Packed Beds at low Reynolds Numbers*, MS thesis, University of California, Berkeley, 1973, LBL-1831.
50. Brian Eugene Gracon, *Experimental Studies of Flow-through Porous Electrodes*, MS thesis, University of Illinois, Urbana, 1974.
51. Peter Willem Appel, *Electrochemical Systems: Impedance of a Rotating Disk and Mass Transfer in Packed Beds*, Dissertation, University of California, Berkeley, 1976, LBL-5132.
52. Thomas K. Sherwood, Robert L. Pigford, and Charles R. Wilke, *Mass Transfer* (New York: McGraw-Hill, 1975), p. 136.
53. Douglas N. Bennion and John Newman, "Electrochemical removal of copper ions from very dilute solutions," *Journal of Applied Electrochemistry*, *2* (1972), 113-122.
54. G. Gurevich, Yu. F. Budeka, and V. S. Bagotskiĭ, "Zavisimost' Raboty Zhidkostnykh Poristykh Elektrodov s Prinuditel'noĭ Podachei Reagenta ot Koeffitsienta Ego ispol'zovaniya," *Elektrokhimiya*, *4* (1968), 1251–1252.
55. Gary George Trost, *Applications of Porous Electrodes to Metal-Ion Removal and the Design of Battery Systems*, Dissertation, University of California, Berkeley, 1983, LBL-16852.
56. James A. Trainham and John Newman, "A Flow-Through Porous Electrode Model: Application to Metal-Ion Removal from Dilute Streams," *Journal of the Electrochemical Society 124* (1977), 1528–1540.

CHAPTER 23

SEMICONDUCTOR ELECTRODES

Solid-state semiconductors have very low concentrations of mobile charge carriers, and the use of a semiconductor electrode can move the region with limitations of diffusion and migration from the solution side of the interface to the electrode side, with the creation of spatially large double-layer or space-charge regions. Illumination of such semiconductor electrodes can create additional charge carriers in the very region where interesting things are happening and provides an additional way to investigate the system.

Semiconductor electrodes can also have practical applications in sensors or perhaps solar energy conversion to:

1. Decompose water and provide a fuel for later use.
2. Operate on redox couples and store chemical energy within the cell or in auxiliary tanks.
3. Produce electrical energy directly.

At one time there was hope that a liquid, solid interface with a polycrystalline semiconductor would provide an inexpensive junction. Formation of a solid junction by diffusion of a dopant gave best results with single crystals because diffusion rates are much higher along grain boundaries. However, newer technologies of vapor or plasma deposition of thin films allow construction of solar cells with polycrystalline materials and remove this disadvantage of solid-state devices. At the same time, additional research with liquid-junction solar cells showed that corrosion is hard to avoid because of the necessity of matching band gaps to the energy of redox couples and the stability limitations of available materials.

Semiconductor electrodes are developed here as an extension of conventional systems governed by thermodynamic, transport, and kinetic considerations. Included is a tutorial on the mechanism of cell operation, including descriptions of band bending and straightening, interfacial phenomena, and current flow. Electrons and holes can be treated as chemical species, with activity-coefficient corrections if necessary. The semiconductor is then similar to a dilute electrolytic solution, but with homogeneous

Electrochemical Systems, Fourth Edition. John Newman and Nitash P. Balsara.

reactions involving generation and recombination of electrons and holes and with a fixed background charge due to the dopant atoms (in analogy to ion-exchange membranes).

Recent reviews include those of Uosaki and Kita[1] and Orazem and Newman.[2]

23.1 NATURE OF SEMICONDUCTORS

Conduction and Valence Bands in Solids

The inner shells of electrons in an atom are associated with the corresponding nucleus and are not free to move in a solid. The outer shell of electrons may be involved in covalent bonding with adjacent atoms, or they may be associated with the crystal structure as a whole.

The quantum mechanical energy states associated with isolated atoms become merged in a solid. The states of a given energy in the isolated atoms then form, in the solid, a *band* of energies closely spaced within a narrow range. If an energy band is full, that is, the number of electrons matches the number of energy states available, then the electrons are not free to move within the solid because there are no adjacent sites of equal or nearly equal energy. This situation would correspond to a pure insulator at low temperatures, but it can be modified by one of three situations.

1. At low temperatures the electrons occupy the lowest available energy states. The highest-energy occupied band is called the valence band, and the lowest-energy unoccupied band is called the conduction band. As the temperature is increased, a larger proportion of electrons will have the energy to occupy states in the conduction band, and this will leave unoccupied states in the valence band. If the *energy gap* between the bands is modest, this effect will occur at modest temperatures, and the material is called a *semiconductor* rather than an insulator.
2. Impurity atoms in the lattice may have a different number of outer-shell electrons from the rest of the atoms. An extra electron will occupy a state in the conduction band, while a deficiency of an electron will create an unoccupied state in the valence band. Again, the situation will depend on temperature with the excess or deficient electron being localized with the impurity atom at very low temperatures. Such an impurity atom is said to be nonionized.
3. Two bands at the margin of occupied and unoccupied states may overlap in energies to form what is, in essence, a half-filled band. Here the electrons are free to move because there are always adjacent sites of nearly equal energy, and metallic conduction prevails, even down to very low temperatures.

Defects in the lattice structure of the solid can lead to electron energy states that do not match with energies of the bands. These are called *trap states* or simply *traps* and are of greater interest if the energy level lies between the valence and conduction bands. More nearly perfect crystals will have a lower density of trap states. Surfaces involve a discontinuity in the lattice structure and therefore a higher concentration of trap states, which are commonly called *surface states*. Again, more nearly perfect surfaces, perhaps those formed by etching, will have fewer surface states than less perfect surfaces such as those formed by machining. Trap states, both in the bulk and at a surface, can have a significant role in facilitating transfer of electrons between the conduction and valence bands.

Electrons have a spin of $\frac{1}{2}$ and therefore obey Fermi–Dirac statistics. This means that the probability of occupancy of a state of energy E is

$$f(E) = \frac{1}{1 + \exp\left(\frac{E - E_f}{kT}\right)}, \tag{23.1}$$

where E_f, called the *Fermi energy* (or *Fermi level*), is the energy level at which a state has a 50% probability of being occupied. For a semiconductor, the Fermi level is generally in the gap between the bands, and therefore the state with a 50% probability of being occupied would have to be a trap.

Electrons and Holes as Species

The number of electrons in the conduction band can be expressed as an integral over the occupied states:

$$n = \int_{E_c}^{\infty} f(E)N(E)dE, \tag{23.2}$$

where n is the concentration, in moles per unit volume, or the number density of electrons per unit volume of solid; $N(E)$ is the density of states, per unit volume and per unit of energy, or by dividing by Avogadro's number it is in moles per unit volume and per unit energy. The upper limit of integration could be taken as the upper energy of the conduction band since $N(E)$ would become zero at the band edge.

Figure 23.1 illustrates the density of states in the relevant regions near the band edges, where $N(E)$ is proportional to the square root of the distance from the band edge (see Problem 23.1). Also indicated are the lower edge E_c of the conduction band, the upper edge E_v of the valence band, the band gap E_g, and the Fermi energy E_f.

We restrict ourselves to temperatures such that all the electrons in the conduction band have energies very close to the lower edge E_c of the band. Then all these occupied electronic states have nearly identical properties, and these electrons can be treated as one *species*. Integration of equation 23.2 allows the Fermi level to be related to the concentration of conduction band electrons, leading to the definition of the activity coefficient f_{e^-} of electrons according to

$$\exp\left(\frac{E_f - E_c}{kT}\right) = \frac{n}{N_c} f_{e^-}, \tag{23.3}$$

where N_c is the *effective* density of states for the bottom of the conduction band. Because of the way in which the integration is carried out, N_c depends on the temperature. Higher energies can effectively

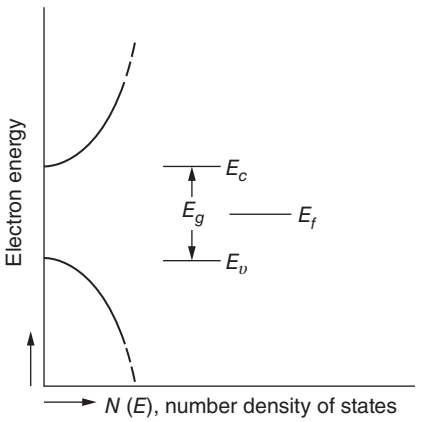

Figure 23.1 Density of states $N(E)$ versus energy level near the band edges. More, unfilled bands would lie above the energies shown, and more, filled bands would lie below.

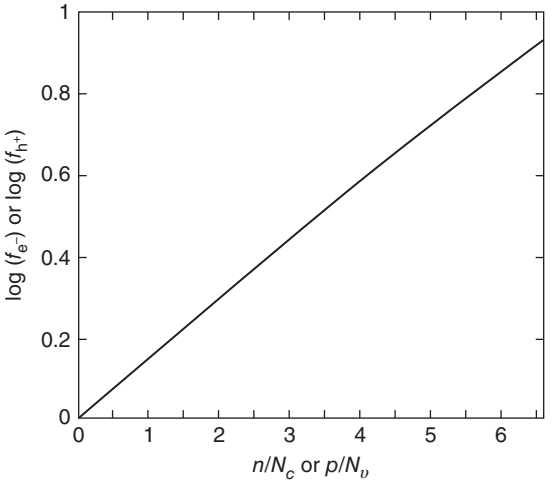

Figure 23.2 Activity coefficients of holes and electrons.

be occupied at higher temperatures, and N_c increases with T (see Problem 23.1). The integration gives the composition dependence of f_{e^-} shown in Figure 23.2 or approximately by

$$\ln f_{e^-} = 0.334 \frac{n}{N_c}. \tag{23.4}$$

See also Problem 23.5.

On the other hand, the valence band is mostly occupied, and it is convenient to place emphasis on the unoccupied states, which are termed *holes* since an electron can be put into them and they become occupied. The unoccupied states, at ordinary temperatures, are concentrated near the top of the valence band, and they can be treated collectively as the species, *holes*. Integration over unoccupied states in the valence band is similar to integration over occupied states in the conduction band and leads to

$$\exp\left(\frac{E_v - E_f}{kT}\right) = \frac{p}{N_v} f_{h^+}, \tag{23.5}$$

where p is the concentration of holes, N_v is the *effective* density of states for the top of the valence band, E_v is the energy of the top of the valence band, and the activity coefficient f_{h^+} is also given by Figure 23.2. It follows that the gap energy mentioned earlier is related to E_c and E_v:

$$E_g = E_c - E_v. \tag{23.6}$$

The Fermi–Dirac distribution has some interesting properties. We can see that $f(E)$, the probability of occupancy, and $1 - f(E)$, the probability of vacancy, have symmetric forms. The distribution goes properly from 1 at low energies to 0 at high energies, is sharp at low temperatures and more diffuse at high temperatures, and forces, even at low temperatures, occupancy of successively higher energy states until all the electrons have been accounted for.

When the Fermi energy is not close to the band edges, it frequently becomes convenient to adopt the *Boltzmann approximation*, whereby the 1 in the denominator is neglected and we have

$$n \approx N_c \exp\left(\frac{E_f - E_c}{kT}\right) \tag{23.7}$$

and

$$p \approx N_v \exp\left(\frac{E_v - E_f}{kT}\right). \tag{23.8}$$

The product of the electron and hole concentrations then becomes independent of the Fermi level:

$$np \approx N_c N_v \exp\left(\frac{-E_g}{kT}\right), \tag{23.9}$$

a formula that reminds us of the mass-action law of chemical thermodynamics. We should keep in mind, however, that replacement of the original Fermi–Dirac distribution in equation 23.1 by a Boltzmann distribution could imply probabilities of occupancy greater than 1 or accumulation of electrons into low energy states.

Doping

Values of N_c and N_v can be quite low at least in comparison with aqueous electrolytic solutions. For a gallium arsenide semiconductor at 300 K, we use the values $N_c = 7.80 \times 10^{-7}$ mol/cm^3 or 4.7×10^{17}/cm^3 and $N_v = 1.16 \times 10^{-5}$ mol/cm^3 or 7×10^{18}/cm^3. Furthermore, with $E_g = 1.4$ J/C, one can estimate a further reduction in the concentration of mobile charges according to equation 23.9:

$$\sqrt{np} \approx (N_c N_v)^{1/2} \exp\left(\frac{-E_g}{2kT}\right) = 5.228 \times 10^{-18} \text{ mol/cm}^3. \tag{23.10}$$

An important characteristic of semiconductors is that their properties can be modified greatly by adding small concentrations of *dopant* atoms to the intrinsic semiconductor. Atoms that can ionize to yield an additional electron are called *donors*, and their use produces *n*-doped semiconductors. Atoms that ionize by consuming or localizing an electron are called *acceptors,* and their use produces *p*-doped semiconductors. In the case of a compound semiconductor like CdS, a slight deficiency of S atoms constitutes *n*-doping. For a group IV semiconductor such as germanium or silicon, an element such as arsenic will be a donor while indium will be an acceptor.

In reality, the ionization level of acceptors and donors will depend on the temperature and the local Fermi level. We shall simplify the situation by assuming complete ionization under the conditions of interest. Thus, the concentrations N_a and N_d of acceptors and donors will imply a level of *fixed charge* in the semiconductor, positive if $N_d > N_a$, and vice versa. The charge is fixed because the acceptor and donor atoms are assumed to be immobile. Thus the electric charge density within the semiconductor is taken to be

$$\rho_e = F(p - n + N_d - N_a). \tag{23.11}$$

An appropriate level of doping would be between the intrinsic carrier concentration given by equation 23.10 and a value on the order of N_c or N_v. Smaller values would have negligible effect, and larger values would promote metallic properties. In the given range, the conductivity of the semiconductor can be varied by many orders of magnitude. The dopant level can vary with position. Furthermore, at different positions within the semiconductor with a given dopant level, the carrier concentrations can be reduced below $|N_d - N_a|$ and toward the value given by equation 23.10 (a situation called *depletion*) or increased toward a value of N_c or N_v (a situation called *degeneracy,* where the Fermi–Dirac distribution is not well approximated by the Boltzmann distribution). For GaAs we shall consider dopant levels in the range from 10^{13} to 10^{18}/cm^3.

Electrical State Variable

The numerical values given above for intrinsic concentrations of holes and electrons and for common dopant levels emphasize the fact that we are dealing with a very dilute solution, in fact, a very good approximation to the *ideal-dilute* solution mentioned in the last part of Section 3.5. Consequently, although the conductivity and the concentrations of charge carriers can change by many orders of magnitude, the basic character and composition remain fixed, and other properties such as mobilities or the band-gap energy are largely independent of dopant and charge carrier concentrations. Of course, extremely large dopant concentrations would change the basic character of the semiconductor, giving a variation of band-gap energy and perhaps a change of crystal structure. The environment of individual electrons and holes would change, much as the environment of individual ions changes in concentrated electrolytic solutions.

But let us stress the dilute nature of the semiconductor. Different regions of the semiconductor have nearly identical chemical composition, and the concept of the electrostatic potential loses some of the ambiguity associated with it in more concentrated solutions. To be specific, we can think of Φ as the cavity potential in this chapter. Figure 23.3 sketches the energy levels in the junction between two metals. The *work function* is the energy required to be imparted to electrons in order to free them from the metal. As the sketch suggests, the electron when free of the metal is at the cavity potential, and this is pictured as an electron in a cavity near the surface of the metal so that stray, external electric fields will not act on the electron or cause charge to accumulate at the metal–vacuum interface (see Figure 3.5). The Fermi level characterizes the energy of electrons in the metal, and as the sketch suggests, the work function is the difference between $-e\Phi$ and E_f.

The Fermi level itself can be associated with the electrochemical potential of electrons in the metals. In fact, the relationship is

$$\mu_{e^-} = LE_f + \text{constant}, \tag{23.12}$$

where L is Avogadro's number. The Fermi level is the same in the two metals in Figure 23.3, so that the electrons can be equilibrated between them. Since the work functions are different, the cavity potential must vary across the metal junction, as sketched in the figure. Consideration of Poisson's equation 3.8 or Gauss's law 3.11 suggests that there must be a double layer of charge at the junction between the two metals. Because of the high concentrations of electrons in the metals, the charge layer is very narrow.

The situation at a metal junction can be contrasted with the semiconductor junction in Figure 23.4. Here the junction is formed in one material by doping the left region with an excess of acceptor atoms

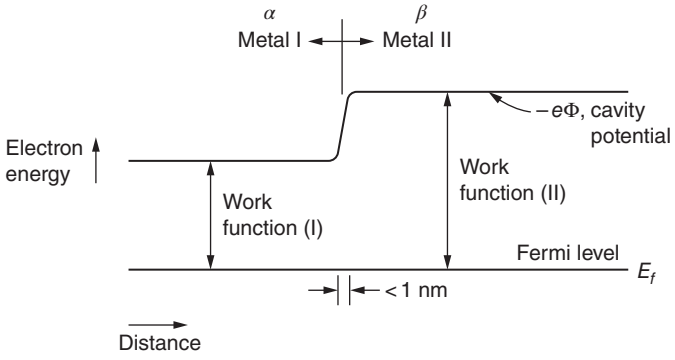

Figure 23.3 Junction between two metals.

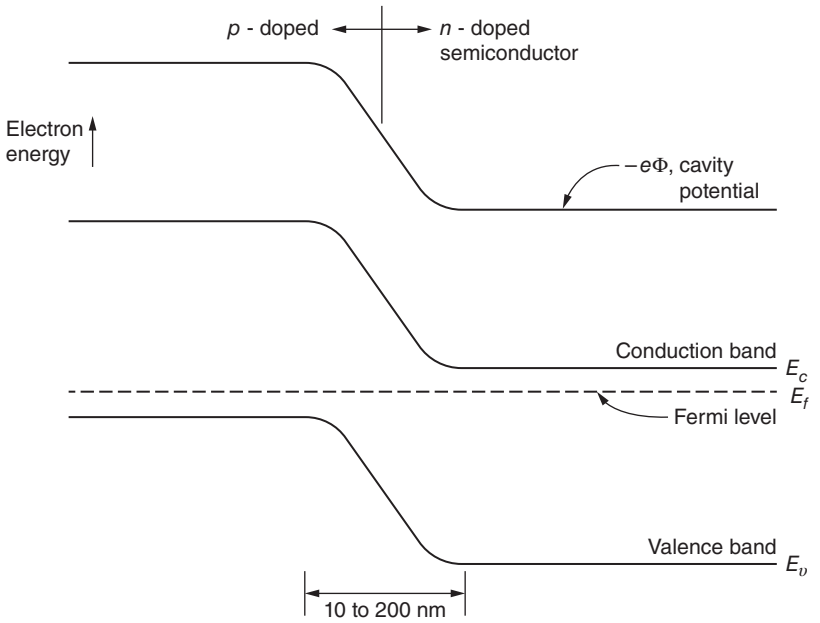

Figure 23.4 Junction between semiconductors of different doping levels.

and the right region with an excess of donor atoms. The Fermi level lies closer to the conduction band in the *n*-doped region. Since the Fermi level or electrochemical potential is uniform at equilibrium, the bands must bend from one region to the other. The work function is seen to depend upon the doping level. Because the concentration of charge carriers is much less than in the metals, the double charge layer is much thicker, perhaps 10 to 200 nm. The energies E_v, E_c, and $-e\Phi$ all bend together, and it is convenient to use a single variable to characterize the electrical state. Thus, we can write

$$E_v = E_v^* - e\Phi \tag{23.13}$$

and

$$E_c = E_v^* + E_g - e\Phi, \tag{23.14}$$

where E_v^* is a fixed value, independent of the electrical state, and equal to the valence band energy *relative to vacuum*. The relationship of band bending to the concentrations of holes and electrons is given by Poisson's equation 3.8, which takes the form

$$\frac{d^2\Phi}{dx^2} = -\frac{F}{\epsilon}(p - n + N_d - N_a). \tag{23.15}$$

In the bulk of the *n*-doped region, electroneutrality prevails, and the electron concentration is higher than in the *p*-doped region. The converse statement is true for holes. While the dopant concentration might change somewhat abruptly at the junction, the concentrations of holes and electrons change gradually, while preserving the equilibrium relationship given by equation 23.9. The fixed dopant charges are not balanced by the carrier concentrations in the junction region, and a net charge distribution or double charge layer results. One can visualize this by taking the second derivative of the potential distribution in Figure 23.4 (see Figure 23.5).

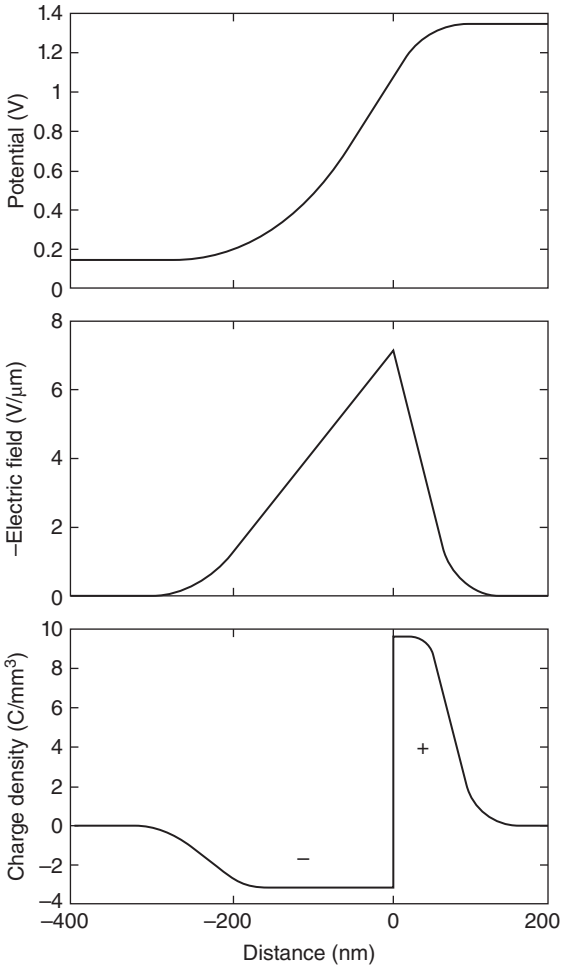

Figure 23.5 Potential, field, and charge density. Dopant levels are 2×10^{16} and $6 \times 10^{16}/\text{cm}^3$ in the p- and n-doped regions, respectively. $T = 300\,\text{K}$, and $E_g = 1.4\,\text{J/C}$.

The nature of the semiconductor in the region of band bending is similar to that of the diffuse layer in an electrolytic solution at an electrode (Section 7.4). The approximations of ideal-dilute solutions hold better because of the lower concentrations, and the greater thickness of the region permits a greater opportunity to probe it. (Recall that the Debye length for electrolytic solutions is typically 0.1 to 1 nm.) One way to probe this region is to shine light on it and to study the behavior of holes and electrons generated by the illumination. This also provides the concept for direct conversion of solar energy into electrical energy. The greater thickness allows substantial variation in the potential across the region of band bending (such as that depicted in Figure 23.4), even though the electric field is smaller than that in the electrolytic double layer. The fixed charge associated with the dopant atoms is also important because it can force an even greater thickness to the region of space charge or departure from electroneutrality. The depletion region can be thicker than the Debye length for the semiconductor.

Band bending in semiconductors can also occur near the boundary of the semiconductor with a metal, a gas, or an electrolytic solution. Such a boundary can be expected to have a higher density

of defects than the junction depicted in Figure 23.4, where the dopant level varies from left to right. These surface states or surface traps, alluded to earlier, are analogous to specifically adsorbed ions in the inner Helmholtz plane on the solution side of an interface. These states can number from 10^{10} to 10^{16} /cm^2 (corresponding to 0.0016 to 1600 μC/cm^2) and are most important when their energy levels lie between E_v and E_c. Attraction or repulsion of electrons by these surface states can also lead to a space-charge region within the semiconductor near the surface, like specific adsorption at an electrode–solution interface. The magnitude of the space charge can also be modified by polarizing the interface, like an ideally polarizable electrode. Similarly, electrode reactions, including corrosion of the semiconductor, can spoil the ideally polarizable nature of an interface.

Electrochemical Potentials

It is particularly auspicious to treat the electrochemical potentials of electrons and holes by relating them to the concentrations and the electrostatic potential (see equation 3.16)

$$\mu_i = \mu_i^\theta + RT \ln(c_i f_i) + z_i F \Phi. \tag{23.16}$$

The very low concentrations would suggest that the activity coefficients could be taken to be unity (see Figure 23.2 and equation 23.4). The condition where $f_i = 1$ (infinite dilution) basically determines the value of the secondary-reference-state quantity μ_i^θ.

The use of the Boltzmann approximation to the Fermi–Dirac statistics is equivalent to setting the activity coefficients to unity, and both approximations break down together when the concentration of holes or electrons approaches the effective density of states in the appropriate electron band.

In the semiconductor, the combination of holes and electrons is a possible homogeneous reaction

$$e^- + h^+ \rightleftharpoons 0. \tag{23.17}$$

If this reaction is equilibrated, then

$$\mu_{e^-} + \mu_{h^+} = 0, \tag{23.18}$$

and a single Fermi level is adequate. In nonequilibrium situations, perhaps produced by electrochemical reaction or by illumination, this relationship does not hold, and one should use separate values for the electrochemical potentials. This is equivalent to using separate *quasi-Fermi levels* for the holes and electrons. The departure from equation 23.18 provides the driving force for the reaction of holes and electrons—perhaps thermal generation in a depletion region or recombination of excess holes and electrons created by illumination.

Within the semiconductor there are three unknowns or variables, n, p, and Φ, whose values need to be determined as functions of position and time, a situation comparable to the binary electrolyte (see Section 11.4). Additional variables, such as the electrochemical potentials, are to be expressed in terms of n, p, and Φ. Material balances on electrons and holes constitute two governing equations. Since the semiconductor is not electrically neutral, Poisson's equation 23.15 prevails instead of the electroneutrality relation (see Section 11.8). The semiconductor material, including any dopants, plays the role of a solvent. The presence of the immobile dopant charges leads to behavior different from the binary electrolyte studied earlier.

The "nearly identical composition" of the semiconductor allows us to avoid certain philosophical questions that arise in somewhat more concentrated solutions. We have not heretofore inquired into the meaning of activity coefficients in a region of nonzero electric charge density nor have we sought to measure physical properties like diffusion coefficients in such regions. Notice that a theoretical model is used here to provide numerical values of activity coefficients, and there is no treatment of effects like

variations of the composition of the medium. Any composition dependence of diffusion coefficients is also likely to be ignored.

Diffusion, Migration, and Homogeneous Reaction

Equation 11.64 describes the flux densities of electrons and holes in terms of the gradient of the electrochemical potential. Within the solid semiconductor, the convective velocity can be taken to be zero, and with equation 23.16 for the chemical potential, we have

$$\mathbf{N}_i = -D_i \nabla c_i - D_i c_i \nabla \ln f_i - \frac{z_i D_i F}{RT} c_i \nabla \Phi. \tag{23.19}$$

The activity-coefficient term can frequently be neglected.

The diffusion coefficients themselves are much larger than we might expect from values for aqueous solutions, and this can compensate partially for the small charge carrier concentrations when the conductivity is computed. For GaAs at 300 K, we shall use the values 220 and 6.46 cm^2/s for the diffusion coefficients of electrons and holes, respectively.

Electrons and holes can recombine according to equation 23.17 and thereby annihilate each other. Physically, an electron is transferred from the conduction band to the valence band. The reverse reaction is the *thermal generation* of electrons and holes, whereby electrons are transferred from the valence band to the conduction band. At equilibrium, the rates of these two processes are equal, and equation 23.18 relates the electrochemical potentials of the species. This leads, in turn, to a relationship between the concentrations of holes and electrons (see equation 23.10)

$$np = \frac{n_i^2}{f_{\mathrm{e}^-} f_{\mathrm{h}^+}} = \frac{N_c N_v \exp(-E_g/kT)}{f_{\mathrm{e}^-} f_{\mathrm{h}^+}}. \tag{23.20}$$

Let us take the activity coefficients to be unity. When the electron is transferred directly from band to band, the net rate of the thermal generation–recombination reaction can be written

$$r = k_{\mathrm{th}} - k_{\mathrm{rec}} np = k_{\mathrm{rec}}(n_i^2 - np), \tag{23.21}$$

whereby the recombination partial reaction is taken to be first order in both electrons and holes and the thermal generation to be independent of these concentrations. More complicated mechanisms have also been envisioned. Specifically, the processes can occur through intermediate trap states whose energy level lies within the band gap. Analysis of this mechanism can lead to the rate expression

$$r = \frac{N_t k_2 k_4 (n_i^2 - np)}{k_1 + k_2 p + k_3 + k_4 n}, \tag{23.22}$$

where N_t is the density of traps (mol/cm^3) and k_1, k_2, k_3, and k_4 are rate constants for processes of transfer of an electron between the valence band and the trap states, the trap states and the valence band, the trap states and the conduction band, and the conduction band and the trap states, respectively. The latter rate expression shows how the kinetics of the process is facilitated by an increase in the density of traps, which we can equate to a lack of perfection of the crystal structure. In principle, the band-to-band process and the trap-facilitated process can proceed in parallel.

For a doped semiconductor it is convenient to use the term *minority carrier* to refer to the species, electrons or holes, inherently reduced to a low level by the doping process. Departures from equilibrium concentrations would be more noticeable for the minority carrier. If excess minority carriers are injected

into an electrically neutral, bulk semiconductor, they will recombine with pseudo-first-order kinetics. The *lifetime* τ of such minority carriers (the time required for decay by a factor of $1/e$) would be

$$\tau = \frac{1}{k_{\text{rec}}|N_d - N_a|} \tag{23.23}$$

for the band-to-band kinetic mechanism and

$$\tau = \frac{k_1 + k_2 p + k_3 + k_4 n}{N_t k_2 k_4 |N_d - N_a|} \tag{23.24}$$

for the trap-intermediate mechanism. In the latter expression, the majority concentration, n or p, would be replaced by $|N_d - N_a|$ and the minority concentration by zero. The *diffusion length* L_i of minority carriers, characteristic of the distances over which an excess over the equilibrium concentration can exist, is then given by

$$L_i = (D_i \tau)^{1/2}. \tag{23.25}$$

The photoresponse is an important aspect of semiconductor electrodes. Light, with photons having energy greater than the band-gap energy E_g, shining on the material generates electrons and holes independently of the thermal generation–recombination process described above. The rate is proportional to the light intensity, and the semiconductor is more or less transparent to the light. Consequently, we shall express the rate of generation of holes and electrons as

$$r = \eta m q_0 e^{-my}, \tag{23.26}$$

where q_0 is the incident flux density (mol/cm^2·s), η is the fraction of the incident photons with energy greater than the band-gap energy, m is the absorption coefficient (cm^{-1}), and y is the distance in the direction of the light in the semiconductor. A photon must have an energy of E_g in order to transfer an electron from the valence band to the conduction band. It is a challenge to recover as large a fraction of the energy E_g as possible in the form of electrical or chemical energy. We investigate this in more detail in Section 23.3.

23.2 ELECTRIC CAPACITANCE AT THE SEMICONDUCTOR–SOLUTION INTERFACE

Let the system now consist of a doped semiconductor in contact with an electrolytic solution. We can think in terms of Figures 23.4 and 23.5 with the p-doped semiconductor region replaced by an electrolytic solution, and at first let us imagine that no electrochemical reactions occur at the interface and we have the analogue of the ideally polarizable electrode of Chapter 7. The profiles of potential, electric field, and charge density depicted in Figure 23.5 for distances greater than zero could still apply to the semiconductor region, at least under certain external conditions. If the potential of the semiconductor is changed relative to a reference electrode in the solution and the electrode remains ideally polarizable, the potential and charge distributions within the semiconductor will also change. The analysis of these changes leads to the electric capacitance of the semiconductor in a manner similar to that in Section 7.4 for the electrolytic solution. In fact, in the situation discussed here, there will also be a double layer in the solution since the charge must balance between the semiconductor and the solution in such a way that the interface as a whole remains electrically neutral—where the interface is defined to include any region of nonzero charge density even though this may extend 1000 nm into the semiconductor.

At steady-state, equilibrium conditions, the charge density will depend on the local value of the electric potential. Let

$$\phi = \frac{e\Phi - E_v^* + E_f}{kT}. \tag{23.27}$$

The Fermi level will be uniform within the semiconductor at equilibrium, and one can solve for the value of ϕ in the bulk of the semiconductor by the requirement that the charge density be zero. Let this value be denoted ϕ_{fb}, where "fb" denotes "flat band," the condition where the potential is uniform.

The charge density of equation 23.11 becomes

$$\rho_e(\phi) = F(N_v e^{-\phi} - N_c e^{\phi - E_g/kT} + N_d - N_a) \tag{23.28}$$

with the use of the Boltzmann approximation of equations 23.7 and 23.8. When the activity coefficients are included, the expression is more complicated, but ρ_e is still a function of ϕ. The electric field, $E = -d\Phi/dy$, also becomes a function of ϕ, and Poisson's equation 3.8 takes the form

$$\frac{d^2\Phi}{dy^2} = -\frac{dE}{dy} = -\frac{dE}{d\Phi}\frac{d\Phi}{dy} = E\frac{dE}{d\phi}\frac{e}{kT} = -\frac{\rho_e}{\epsilon} \tag{23.29}$$

or

$$\frac{dE^2}{d\phi} = -\frac{2kT}{\epsilon e}\rho_e(\phi) \tag{23.30}$$

(compare equation 7.35). Integration gives

$$E^2 = -\frac{2kT}{\epsilon e}\int_{\phi_{\text{fb}}}^{\phi} \rho_e(\phi)d\phi. \tag{23.31}$$

The surface charge density in the space-charge region of the semiconductor is given by

$$q_{\text{sc}} = \int_0^\infty \rho_e dy = -\int_0^\infty \epsilon\frac{d^2\Phi}{dy^2}dy = \epsilon\frac{d\Phi}{dy}\Big|_{y=0} = -\epsilon E(\phi_0), \tag{23.32}$$

where ϕ_0 is the value of ϕ at $y = 0$ (compare equation 7.33). One could go on to get the spatial distribution of ρ_e, ϕ, and E by means of an equation like 7.39; in fact, this was done to construct Figure 23.5. However, this is not necessary in order to obtain the capacitance C_{sc} of the space-charge region in the semiconductor since C_{sc} is related to q_{sc}:

$$C_{\text{sc}} = -\frac{dq_{\text{sc}}}{d\Phi_0} = \frac{\epsilon F}{RT}\frac{dE(\phi_0)}{d\phi_0}. \tag{23.33}$$

Since E is given by equation 23.31, the differentiation can be carried out to yield

$$C_{\text{sc}} = -\frac{\rho_e(\phi_0)}{E(\phi_0)}. \tag{23.34}$$

Figure 23.6 shows the semiconductor capacitance. (This is plotted versus $\Phi_{\text{fb}} - \Phi_0$ because of the custom in electrochemistry to use the potential of the electrode relative to the solution, rather than the reverse.) In contrast to the capacitance given by equation 7.48 or 7.49 for the diffuse double layer in an electrolytic solution, the minimum in C_{sc} does not occur at the flat-band potential. The presence of the dopant and the immobile charge has made the capacitance asymmetric with respect to ϕ_{fb}. Already

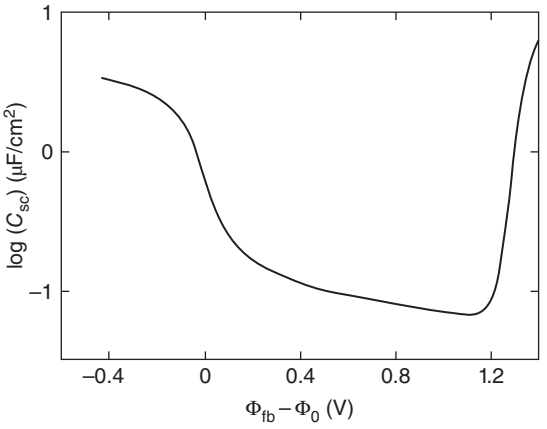

Figure 23.6 Capacity of the space-charge region.

at ϕ_{fb} there are very few holes in the *n*-doped material, and this situation prevails for most of the potential range. Displacement of the potential such that $\phi_{fb} < \phi_0$ draws even more electrons toward the interface, and the excess charge is relatively closer to the interface because of the exponential nature of the Boltzmann relation. Consequently, C_{sc} increases, just as in the case of C_d, because the effective distance of separation in the capacitor decreases. Eventually, C_{sc} levels off somewhat because f_{e^-} increases, reflecting some saturation of the occupancy of states near the interface.

Displacement of the potential such that $\phi_{fb} > \phi_0$ drives the electrons away from the interface, so that the excess charge is due to the immobile dopant atoms. Increasing $\phi_{fb} - \phi_0$ causes more immobile charge to be exposed, thereby increasing the effective separation distance of the capacitor and decreasing the value of C_{sc}. Eventually, the polarization becomes so extreme that the hole concentration becomes significant near the interface. Now the increase in charge occurs at a small effective separation distance, and C_{sc} increases. When the inherent minority carrier concentration (p in this case) rises and becomes significant compared to $|N_d - N_a|$, *inversion* is said to have occurred.

The Mott–Schottky plot in Figure 23.7 produces a straight line of $1/C_{sc}^2$ versus potential over a significant range of potential. This can be understood by a rearrangement of equation 23.34:

$$\frac{1}{C_{sc}^2} = \frac{E^2(\phi_0)}{\rho_e^2(\phi_0)} = \frac{-2RT}{\epsilon F \rho_e^2(\phi_0)} \int_{\phi_{fb}}^{\phi_0} \rho_e(\phi) d\phi. \tag{23.35}$$

For ϕ_0 somewhat below ϕ_{fb}, $\rho_e(\phi_0)$ becomes essentially equal to $F(N_d - N_a)$, due to the dopant atoms, and the slope of the Mott–Schottky plot becomes

$$\frac{d(1/C_{sc}^2)}{d(\Phi_{fb} - \Phi_0)} = \frac{2}{\epsilon F(N_d - N_a)}. \tag{23.36}$$

The straight-line plot fails in the vicinity of $\phi_{fb} \leq \phi_0$ because the majority carriers are now accumulating at the interface. C_{sc} increases (or $1/C_{sc}^2$ decreases) as $\phi_{fb} - \phi_0$ decreases, but not as fast as required by equation 23.36. The straight-line plot also fails for significantly large values of $\phi_{fb} - \phi_0$, where inversion eventually occurs, the effective separation distance of the capacitor decreases, and C_{sc} increases (or $1/C_{sc}^2$ decreases). Reference to Figure 23.6 suggests that the straight-line behavior in Figure 23.7 would extend out to about $\phi_{fb} - \phi_0 = 1.1$ V.

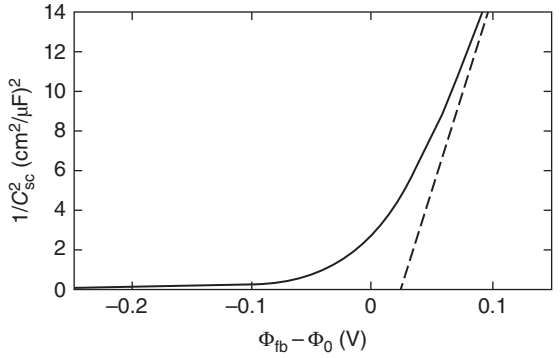

Figure 23.7 Capacity in a Mott–Schottky plot.

The Mott–Schottky plot has a significant place in the study of semiconductor electrodes and yields information on the flat-band potential (from the intercept at $1/C_{sc}^2 = 0$) and the effective dopant level near the interface (from the slope). The intercept is displaced from the flat-band potential by an amount RT/F for n-doping and $-RT/F$ for p-doping if the Boltzmann approximation can be applied. Of course, significant potentials can lead to decomposition of the semiconductor or to electrochemical reaction of species in the solution, and the condition of an ideally polarizable electrode is violated.

Other parts of the interface, such as the inner region and the diffuse layer in the solution, have their own capacitances that can be regarded as being in series with the capacitance of the space-charge region (see, e.g., equation 7.53).

23.3 LIQUID-JUNCTION SOLAR CELL

Let us now add explicitly the possibility of an electrochemical reaction and of generation of electrons and holes by means of illumination (see Figure 23.8). Figure 23.9 shows potential profiles under three conditions: (a) at open circuit in the dark, (b) at open circuit with illumination at an intensity that approximates solar radiation that, because of the angle of the sun, has passed through twice as much air as when the sun is directly overhead (atmospheric mass 2, or AM-2), and (c) with illumination and passing current in the anodic direction such that the semiconductor electrode potential, relative to a reference electrode, is almost the same as it was in case (a). These examples are taken from the work of Orazem.[3, 4]

More details need to be specified. The semiconductor is n-GaAs doped to a level of $6 \times 10^{16}/\text{cm}^3$. The electrolytic solution concentrations are 1 M KOH, 0.8 M K_2Se, and 0.1 M K_2Se_2, and the electrode reaction is

$$2Se^{2-} \rightarrow Se_2^{2-} + 2e^- . \tag{23.37}$$

The Debye length is about 17 nm for the semiconductor and 0.2 nm for the solution. With a band gap of 1.4 J/C, the band bending for curve (a) is substantial. In fact, the electron and hole concentrations, as shown in Figure 23.10, vary so that electrons are the major charge carriers at the right while holes are in excess at the semiconductor–solution interface (inversion), and the intervening region is largely depleted.

Curves (a) in Figures 23.9 and 23.10 show band bending in the dark. This must result from an equilibrium distribution of charge among the space-charge region, the diffuse layer, the inner Helmholtz

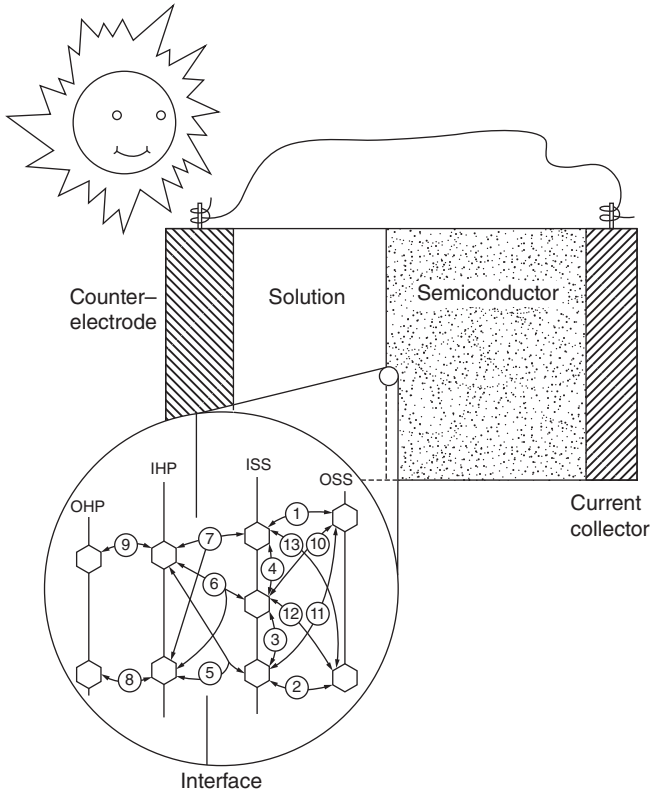

Figure 23.8 Sketch of the liquid-junction photovoltaic cell, showing assumed interfacial reactions. *Source*: Mark E. Orazem and John Newman 1984.[5] Reproduced with permission of The Electrochemical Society, Inc.

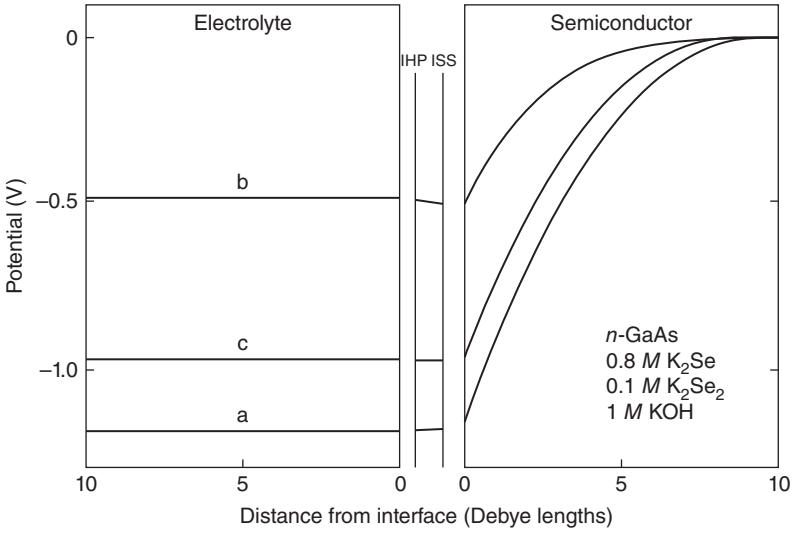

Figure 23.9 Potential distribution for the photoelectrochemical cell with no interfacial kinetic limitations. Curve (a), open circuit in the dark; curve (b), open circuit under 882 W/m^2 illumination; and curve (c), near short circuit ($i = -23.1$ mA/cm^2) under illumination. The semiconductor is n-GaAs, and the solution contains 0.8 M K_2Se, 0.1 M K_2Se_2, and 1 M KOH.

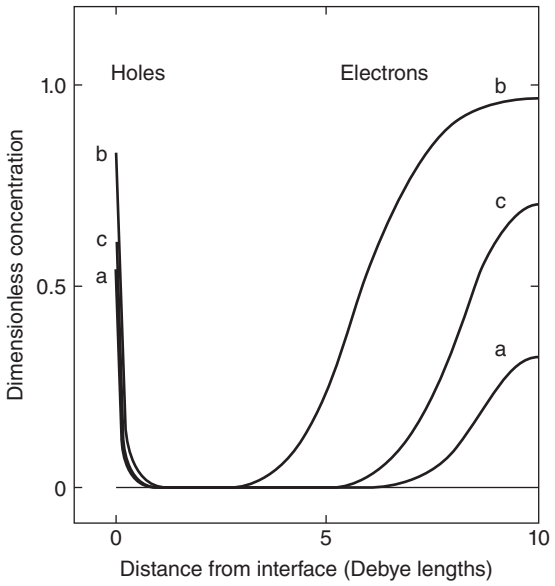

Figure 23.10 Concentration distributions for the photoelectrochemical cell with no interfacial kinetic limitations. Curves and conditions are as in Figure 23.9. Concentrations are made dimensionless with the net dopant concentration $N_d - N_a$. *Source*: Mark E. Orazem and John Newman 1984.[4] Reproduced with permission of The Electrochemical Society, Inc.

plane, and the inner surface states. The affinity of different regions for the various species is built into the system model through various equilibrium constants associated with possible chemical reactions. The 13 interfacial reactions depicted in Figure 23.8 include three major classes:

1. Reactions of electrons (reactions 1, 10, and 11) or holes (reactions 2, 12, and 13) with surface states or the transfer (reactions 3 and 4) of electrons between surface states of different energy. These are all reactions involving transfer of an electron from one energy level to another and are similar to the thermal generation–recombination reactions that can occur within the bulk of the semiconductor, although the densities of states and inherent rate constants can be quite different in the interfacial region.
2. Adsorption–desorption reactions (8 and 9) of Se^{2-} and Se_2^{2-} ions between the outer and inner Helmholtz planes.
3. The charge-transfer process (reactions 5, 6, and 7) where an adsorbed ion reacts with electrons from the surface states to produce the other ion of the redox couple.

While the values could be different from those built into this model, it is the parameters of the interfacial reactions that determine the amount of band bending. Even with current flowing and with illumination, the overall behavior of the system must be the composite result of the interaction of factors that we should understand and describe separately. A somewhat more general discussion of interfacial reactions is included in the next section.

Illumination of the semiconductor generates electrons and holes, generally tending to increase their concentrations relative to those prevailing at equilibrium. The potential gradient already established tends to drive the holes toward the semiconductor–solution interface and the electrons in the opposite direction.

In the absence of current flow, the electrons and holes accumulate in different regions and establish an electric field opposing that originally present in the dark. Thereby, the band bending in Figure 23.9 is decreased. If the counterelectrode is equilibrated with the same redox reaction, then the open-circuit cell potential was zero in the dark, and the decreased band bending under illumination causes the semiconductor electrode to become negative relative to the counterelectrode (or a redox reference electrode). Equilibrium no longer prevails; charge carriers are being generated by the photons and are recombining with a dissipation of energy. When the illuminated cell is shorted, this situation causes current to flow in the external circuit from the counterelectrode to the semiconductor electrode, thereby making the latter carry out an anodic reaction, such as that expressed in equation 23.37. Since the holes are regarded as a separate species and have accumulated near the interface, the anodic reaction could also be written as

$$2Se^{2-} + 2h^{+} \rightarrow Se_2^{2-}. \tag{23.38}$$

Mechanistically, this is regarded as different from equation 23.37. The occurrence of the anodic reaction or reactions allows the generated holes and electrons to pass out of the semiconductor, permitting their concentrations to drop and the band bending to increase toward that which had prevailed at equilibrium in the dark.

Figure 23.11 shows several current–potential curves for the system, with the doping level as a parameter. The curve labeled 0.896×10^{-7} equiv/cm^3 corresponds most closely to the parameters of Figures 23.9 and 23.10. The curves show an open-circuit potential and a limiting current. The former

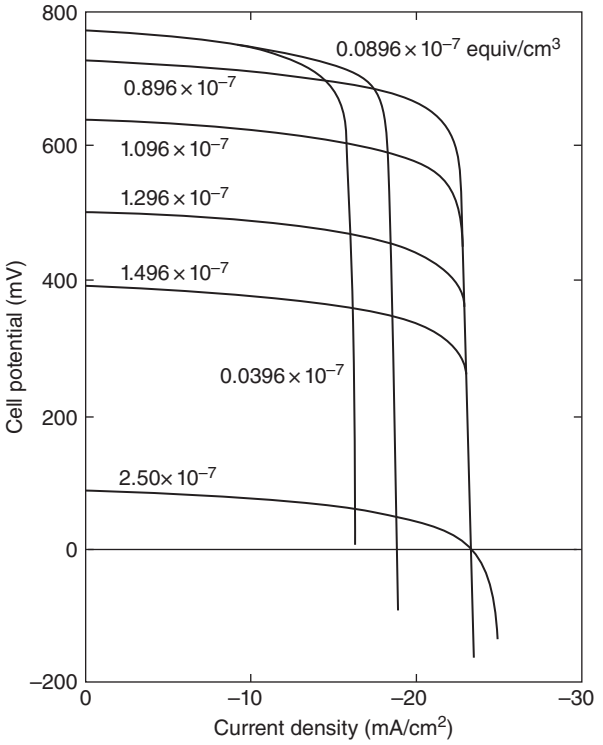

Figure 23.11 Computed current–potential curves for an *n*-type GaAs anode with dopant concentration as a parameter. The semiconductor is 10 Debye lengths thick in each case. *Source*: Mark E. Orazem and John Newman 1984.[4] Reproduced with permission of The Electrochemical Society, Inc.

is determined by the degree of band bending in the dark and unbending under illumination (see Figure 23.9). This is affected, in turn, by the generation of holes and electrons by the light and by the rate of recombination, which occurs primarily at the boundary of the semiconductor and is affected by the rate constants for reactions of electrons. Thus, a semiconductor material with fewer defects at the surface will exhibit a higher open-circuit potential.

The observed limiting current is due to limitations of mass transfer and generation of holes in the semiconductor. An increase in the rate constants for reactions of electrons also decreases the limiting current by encouraging recombination at the interface rather than reaction with ions of the solution. The strength of the illumination, after correction for reflection losses, has a major effect on the limiting current since the illumination produces the charge carriers.

Other losses in the system, such as low rate constants for the ion-adsorption or charge-transfer reactions or the solution resistance, lower the cell potential in the range of intermediate currents, between open circuit and the limiting value, producing current–potential curves with a point of inflection.[4] This adversely affects the power performance of the cell.

Figure 23.11 emphasizes the effect of dopant level, a parameter subject to control in design and manufacture. One should like to optimize the dopant level, semiconductor thickness, and solar absorption coefficient in relation to each other so that the light is absorbed in the region of band bending and the generated charge carriers can be driven to the surface and the current collector. In Figure 23.11 a high open-circuit potential is observed with a low dopant concentration because the semiconductor is thicker and the band bending occurs over a greater distance. At higher dopant levels, the band bending is confined to a smaller region near the surface and is not matched with the absorption coefficient. Very low doping levels require the holes to diffuse farther to the interface, and recombination can occur leading to lower limiting currents.

The effect of varying the semiconductor thickness at constant doping level is described in Ref. [4], where other factors are also explored. Optimization of cell design with respect to shadowing and cell resistance due to placement of the counterelectrode has been investigated.[6]

23.4 GENERALIZED INTERFACIAL KINETICS

Often we wish to treat the kinetics of interfacial reactions. Sometimes we wish to recognize the overall reaction, which represents a boundary condition on adjacent phases; sometimes we wish to treat a detailed and complex reaction mechanism in which there may be both consecutive and parallel reactions and a number of intermediate species that do not appear in the overall reaction. Sometimes the interface is broken down to include at least one surface phase, or adsorbed layer, and perhaps several regions, as in Figure 23.8, where one sees an inner Helmholtz plane and a plane of inner surface states, as well as a diffuse layer in the solution and a space-charge region within the semiconductor. At times, these diffuse regions are treated like the adjacent bulk phases, having spatial extent but not being electrically neutral, and at other times one seeks a treatment that lumps these regions into a simpler, overall treatment. The purpose of the detailed treatment of complex mechanisms is to show the processes involved and to yield a suitable mathematical approximation to kinetic behavior, but it is also necessary to ensure that the kinetic treatment yields the correct thermodynamic behavior under equilibrium conditions.

Let us treat a reaction involving species at two planes, α and δ (see Figure 23.12). Electrons should have no special role; they constitute just one of several species—in fact, they may be a species present at both planes α and δ. In order to have a defined direction, let α be closer to the "electrode terminal" and δ be closer to the "electrolytic solution" so that there is a specific direction for anodic charge

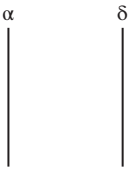

Figure 23.12 Planes in the interfacial region between an electrode and a solution. Species at plane α, which is closer to the electrode terminal, can react with species at plane δ, which is closer to the solution. Reaction can include transfer of an ion or molecule from plane δ to plane α.

transfer. In some examples the distinction may be arbitrary. Some examples of possible meanings for α and δ are:

1. $\alpha = m$ and $\delta = 0$ for the overall reaction between metal and solution, where 0 denotes the solution "just outside the diffuse part of the double layer."
2. $\alpha = m$ and $\delta = 1$ for charge transfer between a metal and the inner Helmholtz plane.
3. $\alpha = 1$ and $\delta = 2$ for ion adsorption between the inner Helmholtz plane (α) and the outer Helmholtz plane (δ).
4. Examples with the semiconductor electrode, for example, α representing the inner surface states and δ representing the inner Helmholtz plane (see Figure 23.8).

With no explicit mention of electrons, the electrode reaction is written as

$$\sum_i s_i M_i^{z_i} \rightarrow 0. \tag{23.39}$$

The amount of charge transferred still allows n to be defined:

$$n = -\sum_\delta s_i z_i = \sum_\alpha s_i z_i, \tag{23.40}$$

and we shall write the reaction so that n is positive. This means that $s_i > 0$ for anodic reactants and $s_i < 0$ for cathodic reactants, just as in Section 8.3.

The condition for equilibrium is (compare equation 2.7)

$$\sum_i s_i \mu_i = 0, \tag{23.41}$$

and departures from this relationship provide the driving force for the reaction. Consequently the surface overpotential η_s can be defined by a reinterpretation of equation 8.2:

$$nF\eta_s = \sum_i s_i \mu_i. \tag{23.42}$$

We probably should reserve the term *surface overpotential* for an overall electrode reaction; here η_s is the overpotential of a partial reaction or elementary step. Eventually, one needs to add a subscript, such as l, to all quantities referring to a particular reaction. This would include η_s, n, and s_i, as well as β, k_f, k_b, and K, introduced later, and the rate r_l of the reaction itself.

Following the general dictates of Section 8.2, we should express the kinetics of the rate of reaction as

$$r_l = \frac{i_l}{nF} = \frac{i_0}{nF}\left[\exp\left(\frac{\alpha_a F}{RT}\eta_s\right) - \exp\left(-\frac{\alpha_c F}{RT}\eta_s\right)\right]. \tag{23.43}$$

According to the *model construction* of Section 8.3, we should write

$$r_l = k_f\left(\prod_{s_i>0} a_i^{s_i}\right)\exp\left[\frac{(1-\beta)nF}{RT}(\Phi^\alpha - \Phi^\delta)\right] - k_b\left(\prod_{s_i<0} a_i^{-s_i}\right)\exp\left[\frac{-\beta nF}{RT}(\Phi^\alpha - \Phi^\delta)\right]. \tag{23.44}$$

(The subscripts f and b for *forward* and *backward* may be more general than a and c for *anodic* and *cathodic*.)

The concentration c_i in equation 8.26 has been replaced by the activity a_i here so that it can be expressed as either c_i or Γ_i as appropriate to the treatment of the phases or planes α and δ. For a metal electrode, a_i for electrons may be taken to be unity and then not appear explicitly in the equation. For a plane or for surface trap states, it is appropriate to treat vacant *sites* explicitly as a species, with a stoichiometric coefficient and a place as one of the reactants or products in equation 23.44. This is the basis of the kinetic derivation of the Langmuir adsorption isotherm.

With the electrochemical potentials in phases α and δ written as

$$\mu_i^\alpha = \mu_i^A + RT\ln a_i^\alpha + z_i F\Phi^\alpha \tag{23.45}$$

and

$$\mu_i^\delta = \mu_i^\Delta + RT\ln a_i^\delta + z_i F\Phi^\delta, \tag{23.46}$$

where μ_i^A and μ_i^Δ represent secondary-reference-state quantities for the two regions, substitution into equation 23.41 yields a Nernst relation

$$\Phi^\alpha - \Phi^\delta = -\frac{RT}{nF}\ln\left(K\prod_i a_i^{s_i}\right), \tag{23.47}$$

where

$$K = e^{-\Delta G^\circ/RT} \tag{23.48}$$

and

$$\Delta G^\circ = -\sum_\delta s_i\mu_i^\Delta - \sum_\alpha s_i\mu_i^A. \tag{23.49}$$

Comparison with the rate equation 23.44 at equilibrium shows that

$$K = \frac{k_f}{k_b}. \tag{23.50}$$

Equations 23.48 and 23.50 show that forward and backward rate constants for a complex reaction sequence cannot both be selected arbitrarily; they must be in harmony with the requirements of thermodynamics. Even if chemical thermodynamic data are not available for all the secondary-reference-state

quantities for all species in all phases, particularly adsorption planes, calculation of equilibrium constants by means of equation 23.48 provides a convenient way of assuring thermodynamic consistency. It is equivalent to the determination of a set of independent chemical reactions and relating equilibrium constants of dependent reactions to those for the chosen set of independent reactions. Examples of dependent reactions can be found in the text associated with equations 2.129 through 2.137.

In establishing a table of chemical thermodynamic data (secondary-reference-state quantities) one is free to choose arbitrarily the values of the molar enthalpy and entropy of each element in a standard state (primary reference state)—usually the stable form of the element at 298.15 K. One is also free to choose the values for one charged species, due to the arbitrary zero of potential used in defining the electrical state. If one has no interest in relating the definitions of electrical state in phases of different composition, one can choose a charged species in each phase for an arbitrary reference. However, if one wishes the potential difference in equation 23.47 to have some clear meaning, the arbitrary choice is limited to one charged species in one phase. This would be the case if equation 23.47 were to represent the difference of cavity potentials between two phases, but then such cavity-potential measurements would have had to form part of the database used in establishing the secondary-reference-state quantities for charged species in one phase in harmony with those for another phase.

We have emphasized in Chapters 2 and 6 how one can avoid such difficult measurements if one sought the usual thermodynamic and kinetic quantities, such as the open-circuit potentials of cells or overall kinetic relationships. The quasi-electrostatic potential allowed one to do detailed computations accounting for the composition dependence of activity coefficients and transport properties. However, the microscopic model of kinetics among interfacial planes, and in particular the use of Gauss's law, implies that one would like to use cavity potentials and perhaps be able to discover the seat of the electromotive force of an electrochemical power source.

For (empty) sites in an adsorption plane, the secondary-reference-state quantity μ_i^A can also be taken to be zero. Notice that activity coefficients are not generally used when a_i in equation 23.44 is replaced by c_i or Γ_i, but activity coefficients are implied to belong in equations 23.45 through 23.47, which are more strict, thermodynamically. This is consistent with the way the problem was approached in Chapter 8. In the macroscopic approach, the exchange current density i_0 depends in an unspecified way on the composition at planes α and β. This takes care of any thermodynamic requirements but provides no clues about this composition dependence itself. The microscopic model predicts such a dependence in a nonrigorous way and provides a basis for testing the applicability of alternative reaction mechanisms. The formal procedure described here applies also to nonelectrochemical reactions, where $n = 0$.

In the electrochemical case, it should be emphasized that Gauss's law may need to be included in the set of governing equations in order to relate the potential distribution to the charge distribution that develops at the reaction planes. The use of Gauss's law here is analogous to the use of Poisson's equation 23.15 in the semiconductor, together with material balances and transport relations. In the diffuse charge layer in the solution another form of Poisson's equation is needed, and, in the solution outside the diffuse layer, this reduces to the electroneutrality relation as an additional equation that permits the potential distribution to be determined.

23.5 ADDITIONAL ASPECTS

Semiconductor Electrode Kinetics

Gerischer[7] has developed a quantum mechanical theory of electrode kinetics and applied it to redox reactions at semiconductor electrodes. Summaries of this work have been given by Vetter,[8] Erdey-Grúz,[9] and Hamnett.[10]

The theory shows:

1. Reaction of redox species in solution with holes is distinguished from that with electrons; that is, reaction 23.38 is different from reaction 23.37.
2. For redox couples with a positive potential, the exchange rate (i_0) at equilibrium will be higher for the reaction with holes (e.g., reaction 23.38). Conversely, for redox couples with a more negative potential, i_0 will be higher for the electron reaction.
3. Exponential or Tafel expressions are adequate approximations to the potential dependence of the four partial reactions defined above.
4. Other things being equal, the hole reactions are more favored in the anodic direction while electrons dominate in the cathodic direction. This can be related to the tendency to increase the appropriate charge-carrier concentration at the interface under the direction of polarization indicated. It also means that the symmetry factor β is apparently closer to 1 (smaller anodic transfer coefficient) for the electron reactions and closer to zero (large anodic transfer coefficient) for the hole reactions. This can be stated equivalently in terms of Tafel slopes. These conclusions apparently describe the interaction of the semiconductor space-charge region with the interface and not just the kinetics of the interfacial reactions.
5. It is necessary to deal with the space-charge region separately, as discussed in the preceding sections, so that the electron and hole concentrations used are those near the interface (see Figure 23.10) and the potential difference applied to interfacial reactions is not just the applied (or easily measured) potential but is corrected for the potential variation within the space-charge region of the semiconductor, similar to the Frumkin correction in Section 8.4.

Fermi Level in the Solution

Gerischer[7] regarded a redox species in solution, such as a $Fe(CN)_6^{3-}$ ion, as a possible site for an electron. The occupied site becomes $Fe(CN)_6^{4-}$, which we know and regard as a separate ionic species. Gerischer introduced the term *Fermi level in the solution* to denote a quantity perceived to relate to the electrochemical potential of electrons in the solution. Thus, one might write

$$\mu_{e^-} = \mu_{Fe(CN)_6^{4-}} - \mu_{Fe(CN)_6^{3-}}. \tag{23.51}$$

Uosaki and Kita[1] summarized criticisms of this approach.

The Fermi level in solution really represents a definition for a redox couple. One excludes reactions that involve either dissolution of the semiconductor or plating of some material on the semiconductor, both to preserve the structure of the electrode and to allow the Fermi level to refer only to the charge transfer of an electron. Plating and dissolution involve other species in or on the solid surface. If several redox couples are involved, different results would be obtained unless the several species (say, Fe^{3+}, Fe^{2+}, Cu^{2+}, Cu^{+}) were equilibrated. Rapid redox equilibration in the bulk can be expected with many couples, but there may be slow couples, and *in principle* one should go back to a general formulation where an η_s value can be assigned to each reaction at the surface (see equation 23.42). This nonequilibrium concept should be extended to the semiconductor as well, where the holes and electrons are not in general in equilibrium with each other. Thus, the more general approach, outlined in the preceding sections, ascribes separate electrochemical potentials to each species—electrons and holes in the semiconductor and ionic species in the solution—and describes transport in bulk phases according to the gradient of the electrochemical potential (equation 23.19) and describes reactions between phases or planes by the departures from equilibrium as represented by η_s (equation 23.42).

A motivation for using the Fermi level in the solution may come from a need to relate energy states in adjacent planes in an absolute manner, a procedure that would aid in the a priori estimation of rate constants for heterogeneous reactions.

In computations, the diffusion and migration terms in equation 23.19 may each be large but nearly cancel to produce a modest flux density $\mathbf{N}_i$. Under the equilibrium circumstances discussed in Sections 23.2 and 23.3, the canceling is exact, and $\mathbf{N}_i = 0$. Numerical accuracy can be enhanced by using the defined quantity

$$A_i = c_i \exp\left(\frac{z_i F}{RT}\Phi\right), \tag{23.52}$$

which has many of the properties of the absolute activity (see λ_i in Section 2.3). Equation 23.19 then becomes

$$\mathbf{N}_i = -D_i c_i \nabla \ln A_i. \tag{23.53}$$

Potential Distribution across Phases

In earlier chapters, potential distributions are described only within a given phase, and potential differences between phases are understood to have an unspecified additive constant included because of the difficulty of defining and ascertaining the difference in electrical state between phases or regions of different composition. Thus the macroscopically defined surface overpotential η_s is quickly introduced, and otherwise one focuses on the overall potential of complete cells, with both leads made of the same material. The quasi-electrostatic potential and the potentials of reference electrodes are introduced to probe the potential variation within a solution in a manner that can be related to the customary experimental measurements, which rely on a reference electrode.

This general approach leaves the student unclear about the seat, or exact location, of the electromotive force in a lead–acid battery or a hydrogen, oxygen fuel cell, where the positive electrode is the cathode on discharge. It is appropriate to retain this uncertainty because the equilibrium, open-circuit potential of the cell is determined largely by thermodynamic principles, and thus it involves reactions at both electrodes.

In idealized models one uses an electrostatic potential that is usually defined more vaguely. This occurs notably in Debye–Hückel theory of the distribution of ions around a central ion (Section 4.1), in the diffuse-layer structure (Section 7.4), and in models of electrode kinetics (Section 8.3). The semiconductors studied in this chapter conform well to the conditions of ideal-dilute solutions and prompt us to regard the potential being discussed to be the cavity potential. Another factor favoring this approach is the spatial extent of the charge region in the semiconductor, which allows us to imagine a macroscopic cavity being placed in the region. Such a cavity is too large to place at the inner Helmholtz plane or other planes directly at an interface. The general difficulty of making a cavity potential measurement and the eventual cancellation of the numerical value in most experiments governed by thermodynamics, interfacial kinetics, and transport phenomena discourage us from using the cavity potential extensively as an aid in treating electrochemical systems. The semiconductor system, with the important effects of light absorption in the region of band bending, prompts us to make more extensive use of the cavity potential in this application.

Figure 23.13 is a sketch of the variation of the cavity potential across the cell

$$\mathrm{Pt}\left|\begin{matrix}\mathrm{K_2Se}, & \mathrm{K_2Se_2}, \\ \mathrm{KOH}, & \mathrm{H_2O}\end{matrix}\right| n\text{-GaAs}\,\Big|\,\mathrm{Pt} \tag{23.54}$$

at equilibrium in the dark. We should obtain zero for the overall open-circuit potential independently of whether the electrode is Pt, C, or *n*-GaAs (in the absence of side reactions) and independent of whether we write the electrode reaction according to equation 23.37 or 23.38.

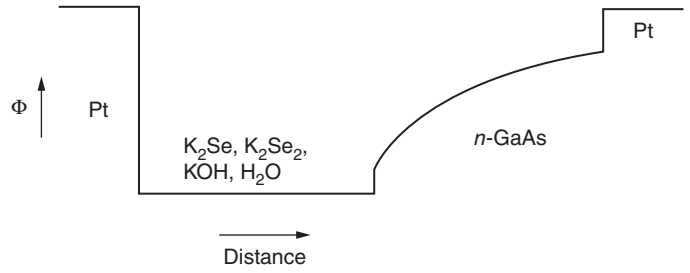

Figure 23.13 Variation of cavity potential Φ from a platinum counterelectrode, through an electrolytic solution and a semiconductor electrode, and into a platinum current collector. Potential jumps occur at the phase boundaries, but the overall cell potential is zero at open circuit in the dark.

With reference to Figure 23.9 one should be able to redraw Figure 23.13 to show the potential distribution with illumination. Unbending of the bands produces a nonzero open-circuit potential, and this is the source of the electromotive force of the cell. With passage of current in the illuminated cell, the bands bend again, and the cell potential decreases toward zero, but now with a current produced by the illumination.

Corrosion

A semiconductor corrodes if it becomes unstable and decomposes under the operating conditions. At any electrode, oxidation or reduction reactions can be expected to occur, and consideration must be given to finding a stable electrode material and a compatible electrolytic environment without compromising the original purpose of the system. For example, GaAs could react anodically:

$$\mathrm{GaAs} + 6\mathrm{h}^+ + 2\mathrm{H_2O} \rightarrow \mathrm{Ga}^{3+} + \mathrm{AsO_2^-} + 4\mathrm{H}^+. \tag{23.55}$$

According to the methods of Section 2.9, and with the help of tables of chemical thermodynamic data, $U^\theta = 0.057$ V for this reaction. Thus, GaAs would be expected to be unstable in the presence of a more positive redox couple, such as $\mathrm{Fe(CN)_6^{4-}/Fe(CN)_6^{3-}}$ for which $U^\theta = 0.36$ V. Similarly, a ferrous–ferric couple will corrode iron and many other metals.

Some semiconductors, such as CdS, will be subject to both anodic decomposition, such as

$$\mathrm{CdS} + 2\mathrm{h}^+ \rightarrow \mathrm{Cd}^{2+} + \mathrm{S}, \tag{23.56}$$

or cathodic decomposition, such as

$$\mathrm{CdS} + 2\mathrm{e}^- \rightarrow \mathrm{Cd} + \mathrm{S}^{2-}. \tag{23.57}$$

A semiconductor stable at open-circuit in the dark may decompose under illumination or upon passage of current. In this case one must be able to evaluate η_s for a decomposition reaction like equation 23.55, but this evaluation must be made under conditions prevailing at the interface. In particular, one must keep track of the variation of μ_{h^+} (or, equivalently, the quasi-Fermi level for holes or $\ln A_{\mathrm{h}^+}$) through the semiconductor, perhaps with a detailed model such as that used to obtain Figures 23.9 and 23.10. For assessing whether a given reaction can occur, one needs a combination of the potential and the hole concentration, which may be varying in an offsetting manner. (See the discussion preceding equation 23.52.) As a challenge, the student can try to sketch the variation of $\ln A_i$ for holes and electrons under conditions of open-circuit illumination [curves (b) on Figures 23.9 and 23.10].

PROBLEMS

23.1 If $N(E) = A_c(E - E_c)^{1/2}$ near the band edge and if this form can be used effectively for all states with a significant probability of being occupied and if $E_c - E_f$ is large compared to kT, show that

$$N_c = \frac{\sqrt{\pi}}{2}(kT)^{3/2}A_c.$$

This value of N_c corresponds to filling the conduction band to what level, expressed in units of kT, above the bottom of the band?

23.2 **(a)** What value of the activity coefficient would be obtained from Debye–Hückel theory (equation 4.21) for the intrinsic GaAs semiconductor? What value would be obtained with a doping level of $6 \times 10^{16}/\text{cm}^3$? Assume that the permittivity of the material is 1.06×10^{-12} C/V·cm.

(b) Calculate also the Debye length for these two cases, using equation 4.9. Remember to include the dopant in the sums over ionic species, even though they are not mobile.

23.3 **(a)** Estimate the Fermi-level position within the gap of GaAs for an n-doping level of $6 \times 10^{16}/\text{cm}^3$ and for a p-doping level of 2×10^{16}. How much is the work function changed by doping? Use the Boltzmann approximations for hole and electron concentrations, and set the electric charge density to zero in the bulk of the semiconductor.

(b) Calculate n and p for the two doping levels. If these two doping levels correspond to the regions in Figure 23.4, relate the overall band bending to a formula such as

$$\Delta\Phi = \frac{RT}{F}\ln\frac{n_{\text{right}}}{n_{\text{left}}} = \frac{RT}{F}\ln\frac{p_{\text{left}}}{p_{\text{right}}}.$$

23.4 Analyze the kinetics of the ferricyanide reduction if it is assumed to occur in the following three steps:

1. Adsorption of ferricyanide ion (from the outer Helmholtz plane to the inner Helmholtz plane):
$$\text{Fe(CN)}_6^{3-} \rightleftharpoons [\text{Fe(CN)}_6^{3-}]_{\text{ads}}.$$
2. Transfer of an electron from the metal to the adsorbed ion:
$$\text{e}^- + [\text{Fe(CN)}_6^{3-}]_{\text{ads}} \rightleftharpoons [\text{Fe(CN)}_6^{4-}]_{\text{ads}}.$$
3. Desorption of ferrocyanide ion (from the inner Helmholtz plane to the outer Helmholtz plane):
$$[\text{Fe(CN)}_6^{4-}]_{\text{ads}} \rightleftharpoons [\text{Fe(CN)}_6^{4-}].$$

You need not treat the diffuse part of the double layer or the diffusion layer. Three potentials are involved: Φ_m of the metal, Φ_1 of the inner Helmholtz plane, and Φ_2 of the outer Helmholtz plane. Two volume concentrations, c_3 and c_4 of the ferricyanide and ferrocyanide ions at the outer Helmholtz plane, are involved. Surface concentrations Γ_3 and Γ_4 of the adsorbed species at the inner Helmholtz plane will eventually need to be eliminated from an overall kinetic expression. The potential Φ_{I} should also be eliminated. The total concentration of sites in the inner Helmholtz plane can be represented as $\boldsymbol{\Gamma}_{\max}$. Ferricyanide ions and ferrocyanide ions are the only charged adsorbed species.

You will need to formulate Butler–Volmer kinetic rate expressions for each of the three processes. You will need to formulate additional applications of Gauss's law. Assume steady state, and take the current density to be specified.

Obtain a clear statement of the governing equations and independent variables before undertaking to eliminate the dependent variables. You are seeking an overall kinetic relation showing how the current density depends on the potential difference $\Phi_m - \Phi_2$ and the concentrations at the outer Helmholtz plane:

$$i = f(\Phi_m - \Phi_2, c_3, c_4).$$

23.5 **(a)** By substitution of $N(E)$ and N_c from Problem 23.1 and $f(E)$ from equation 23.1 into equation 23.2, show that the electron concentration can be expressed as

$$\frac{n}{N_c} = \frac{2}{\sqrt{\pi}} \int_0^\infty \frac{\sqrt{x}\, dx}{1 + Be^x},$$

where $B = \exp[(E_c - E_f)/kT]$ and hence (from the definition 23.3 of f_{e^-}) that[11]

$$f_{e^-} = \frac{N_c}{nB} = \frac{\sqrt{\pi}}{2B \int_0^\infty \frac{\sqrt{x}\, dx}{1+Be^x}}.$$

(b) Show that $f_{e^-} \to 1$ as $B \to \infty$. Discuss whether this is the limit of infinite dilution of electrons in the semiconductor.

Note that evaluation of the above integral[12] gives n/N_c as a function of $E_c - E_f$ and hence gives f_{e^-} as a function of either n/N_c (plotted in Figure 23.2) or as a function of $(E_c - E_f)/kT$. Some curve fitting leads to the approximate equation 23.4 or to

$$f_{e^-} = \frac{0.75\sqrt{\pi} + B^{-1}[\ln(B + 25)]^{1.5}}{B[\ln(B + 25)]^{1.5}}$$

for f_{e^-} as a function of $(E_c - E_f)/kT$. The latter expression is convenient to use when computing the capacity of the space-charge region, leading to Figure 23.6.

NOTATION

a_i	c_i or $\mathbf{\Gamma}_i$
A_c	parameter related to N_c (see Problem 23.1)
A_i	electrically dependent activity, mol/cm^3
c_i	concentration of species i, mol/cm^3
C_{sc}	capacity of space-charge region, F/cm^2
D_i	diffusion coefficient of species i, cm^2/s
e	magnitude of electronic charge, 1.602×10^{-19} C
E	energy, J
E	electric field, V/cm
E_c	energy at lower edge of conduction band, J
E_f	Fermi energy, J
E_g	band-gap energy, J
E_v	energy at upper edge of valence band, J

E_v^*	value independent of electrical state, J
f	probability of occupancy of a state
f_i	activity coefficient of species i
F	Faraday's constant, 96,487 C/mol
ΔG°	"standard" Gibbs energy change for a reaction, J/mol
i_0	exchange current density, A/cm^2
i_l	current density for reaction l, A/cm^2
k	Boltzmann constant, 1.38×10^{-23} J/K
k_b	rate constant in the backward direction
k_f	rate constant in the forward direction
k_{rec}	recombination rate constant
k_{th}	thermal-generation rate constant
k_1, k_2, k_3, k_4	rate constants for trap processes
K	equilibrium constant $= k_f/k_b$
L	Avogadro's number, 6.0225×10^{23}/mol
L_i	diffusion length, cm
m	absorption coefficient, cm^{-1}
M_i	symbol for the chemical formula of species i
n	concentration of electrons, mol/cm^3
n	number of electronic charges transferred in reaction
n_i	intrinsic concentration, mol/cm^3
N_a	acceptor concentration, mol/cm^3
N_c	effective density of states for the bottom of the conduction band, mol/cm^3
N_d	donor concentration, mol/cm^3
$N(E)$	density of states, mol/cm^3·J
$\mathbf{N}_i$	flux density of species i, mol/cm^2·s
N_t	density of trap states, mol/cm^3
N_v	effective density of states for the top of the valence band, mol/cm^3
p	concentration of holes, mol/cm^3
q_0	incident photon flux density, mol/cm^2·s
q_{sc}	charge in space-charge region, C/cm^2
r	rate of generation of holes and electrons, mol/cm^3·s
r_l	net rate of reaction l, mol/cm^2·s
R	universal gas constant, 8.3143 J/mol·K
s_i	stoichiometric coefficient
T	absolute temperature, K
U^θ	standard electrode or cell potential, V
x	distance, cm
y	distance in direction of light path, cm
z_i	charge number of species i
α_a, α_c	transfer coefficients
β	symmetry factor
Γ_i	surface concentration of species i, mol/cm^2
ϵ	permittivity, F/cm
η	fraction of incident light with energy $> E_g$
η_s	surface overpotential, V
μ_i	electrochemical potential of species i, J/mol
$\mu_i^A, \mu_i^\Delta, \mu_i^\theta$	secondary-reference-state quantities, J/mol
ρ_e	electric charge density, C/cm^3

τ	lifetime of minority carriers, s
ϕ	dimensionless potential
ϕ_0	value of ϕ at interface of electrode with solution
ϕ_{fb}	flat-band value of ϕ
Φ	cavity potential, V

REFERENCES

1. Kohei Uosaki and Hideaki Kita, "Theoretical Aspects of Semiconductor Electrochemistry," *Modern Aspects of Electrochemistry*, No. *18* (New York: Plenum, 1986), pp. 1–60.
2. Mark E. Orazem and John Newman, "Photoelectrochemical Devices for Solar Energy Conversion," *Modern Aspects of Electrochemistry*, No. *18* (New York: Plenum, 1986), pp. 61–112.
3. Mark Edward Orazem, *Mathematical Modeling and Optimization of Liquid-Junction Photovoltaic Cells*, Dissertation, University of California, Berkeley, 1983.
4. Mark E. Orazem and John Newman, "Mathematical Modeling of Liquid-Junction Photovoltaic Cells. I. Governing Equations," *Journal of the Electrochemical Society*, *131* (1984), 2569–2574.
5. Mark E. Orazem and John Newman, "Mathematical Modeling of Liquid-Junction Photovoltaic Cells. II. Effect of System Parameters on Current–Potential Curves," *Journal of the Electrochemical Society*, *131* (1984), 2574–2582.
6. Mark E. Orazem and John Newman, "Mathematical Modeling of Liquid-Junction Photovoltaic Cells. III. Optimization of Cell Configurations," *Journal of the Electrochemical Society*, *131* (1984), 2582–2589.
7. H. Gerischer, "Über den Ablauf von Redoxreaktionen an Metallen und an Halbleitern. III. Halbleiterelektroden," *Zeitschrift für physikalische Chemie N.F.*, *27* (1961), 48–79.
8. Klaus J Vetter. *Electrochemical Kinetics* (New York: Academic, 1967), pp. 121–128.
9. Tibor Erdey-Grúz, *Kinetics of Electrode Processes* (New York: Wiley-Interscience, 1972), pp 379–383.
10. Andrew Hamnett, "Semiconductor Electrochemistry," in R. G. Compton, ed., *Comprehensive Chemical Kinetics, Vol. 27, Electrode Kinetics: Reactions* (Amsterdam: Elsevier, 1987), pp. 61–246, particularly pp. 124–128.
11. Arthur J. Rosenberg, "Activity Coefficients of Electrons and Holes at High Concentrations," *Journal of Chemical Physics*, *33* (1960), 665–667.
12. J. McDougall and Edmund C. Stoner, "The computation of fermi–dirac functions," *Philosophical Transactions of the Royal Society of London, A 237* (1938), 67–104.

CHAPTER 24

IMPEDANCE

One can learn a lot about a system at equilibrium by perturbing it slightly from equilibrium and studying how it returns to equilibrium. The analysis becomes much simpler for a disturbance applied steadily at a single frequency, with the experiment repeated at different frequencies ranging from very low to very high. Different phenomena become important at different frequencies. Electrochemical systems are easy to study because it is easy to vary the electrode potential in a sinusoidal manner and electronic equipment is readily available to apply the signal and to analyze the system response.

The amplitude of the sine wave determines the smallness of the disturbance. At small amplitudes, the system behaves linearly, and one frequency does not interfere with another.

One way to proceed is with equivalent circuits, studied in electronics. The principal elements are resistors, capacitors, and inductors, although power sources can be added. Figure 24.1 is a rectifier designed to convert an alternating power source into a direct-current source. The rectifier allows current to flow only in the direction of the arrow. For the full-wave rectifier shown, the current flows in one direction, but it has a ripple, made up of many frequencies, as shown in Figure 24.2.

Better filtering can be obtained by making a more complicated network of inductors, capacitors, and resistors. However, the object here is not to design rectifier systems, but rather to introduce these current elements and the concept of the equivalent circuit.

The imagination of the investigator can be applied to create an equivalent circuit which represents the physical attributes of the system being studied. However, a better way to proceed is to write down complicated governing physical and chemical laws which describe what is going on. These are basically the laws of thermodynamics, electrochemical and chemical kinetics, and transport phenomena which constitute Parts A, B, and C of this book. This is the way to construct a system model for steady or transient processes based on physical principles. It is a straightforward process to construct an impedance model by linearizing the more complete model. There is probably no limit to the complexity of the physical model which can be treated. This chapter covers several systems, including:

1. A disk electrode like that shown in Figure 18.4 with an insulating plane surrounding the disk electrode and with a counterelectrode far away. For the first example, it is assumed that the electrolytic solution is so well stirred that it has no concentration gradients. This solution acts like a resistor, but constitutes a distributed-parameter system–all parts of the electrode are not

Electrochemical Systems, Fourth Edition. John Newman and Nitash P. Balsara.

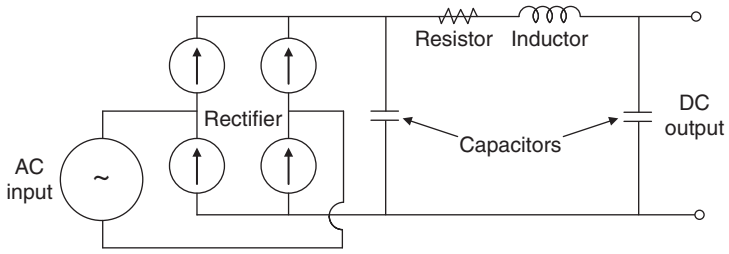

Figure 24.1 Equivalent circuit with, from left to right, a power source, a rectifier, a capacitor, a resistor, an inductor, another capacitor, and a DC output.

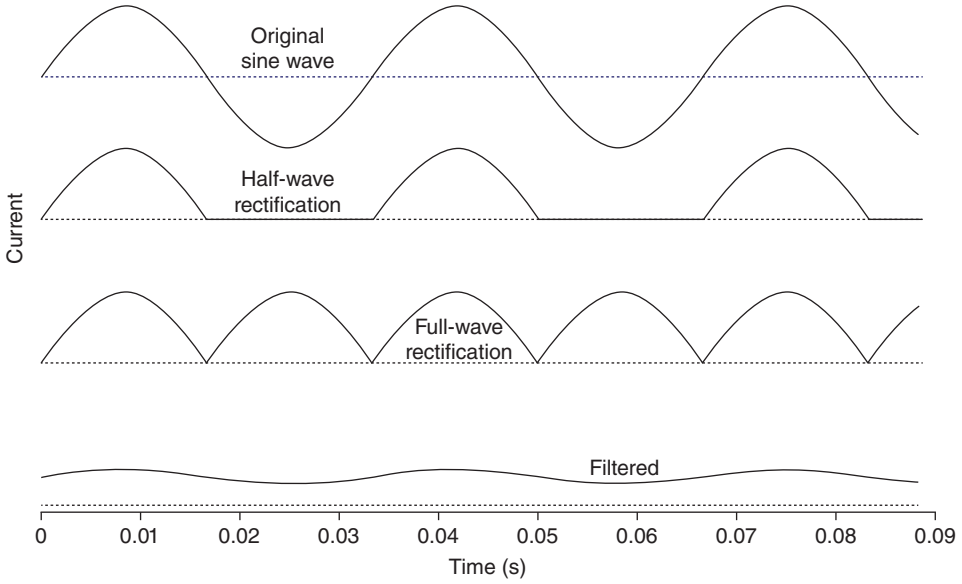

Figure 24.2 Wave forms, with, from top to bottom, a 60-Hz sinusoidal alternating current (AC), direct current (DC) after half-wave rectification, DC after full-wave rectification, and DC at the outlet after some filtering.

equivalent because some parts can send current more easily to the distant counterelectrode. The surface phenomena (covered in Chapters 7 and 8) are simplified to linear kinetics with a double-layer capacitance. An equivalent circuit for the interface is represented in Figure 24.3. The resistor represents the electrode kinetics (by means of linear kinetics, see equation 8.7), and the capacitor represents the double layer, with a constant capacitance. For very fast kinetics, the resistance would be zero. The system is already linear, but the elements are not simply connected. Current flows from all parts of the electrode, through the electrolytic solution, and to the counterelectrode.[1]

2. A second example has a rotating disk electrode, but now with fluid flow and concentration gradients added. Steady behavior is treated in Chapter 21. However, this example also treats the situation where the rotation speed can vary sinusoidally, but with a small amplitude of variation. There are three levels of complexity, treatment of the hydrodynamic velocity profile with AC

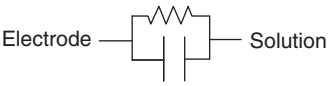

Figure 24.3 Equivalent circuit of the interface, showing a resistor for electrochemical kinetics in parallel with a capacitor for the double-layer capacity.

oscillation, treatment of the concentration profile(s) in this hydrodynamic flow, and treatment of the interface with its kinetics and double-layer capacitance.[2]

3. Chapter 22 treats porous electrodes with various levels of complexity. This has major applications in electrochemical energy storage (batteries). A complicated computer program (called dualfoil on the website http://www.cchem.berkeley.edu/jsngrp/) is available to treat discharge and cycling of lithium and lithium-ion and nickel/metal-hydride batteries. Again, it is straightforward to convert this program (based on detailed physical laws) to an impedance program.[3] (This has already been done, on the same website.)

To meet the requirements of starting with a steady state, the AC disturbance should be applied to the battery at open-circuit. However, it is evident that the impedance results are meaningful at frequencies where the battery, through its discharge process, does not change significantly during a single AC cycle. Such limitations also apply to impedance modeling of corroding systems or any system which eventually degrades.

The general procedure, or the key, for this form of impedance modeling is to represent all physical quantities (appearing in the physical model) as a sum of a steady part and a sinusoidally varying part. For the rotation speed Ω of the disk

$$\Omega = \overline{\Omega} + \Delta\Omega \,\mathrm{Re}\{\exp(j\omega t)\}, \tag{24.1}$$

where ω is the angular frequency of the variation which is superposed on the steady rotation speed $\overline{\Omega}$ and j is the square root of -1. Thus, there is a frequency of rotation and a frequency of the superposed variation. Because the system is linear due to the small amplitude $\Delta\Omega$ of the disturbance, all parts of the system will vary with the same frequency ω. Thus, for example, the potential at any point in the solution is

$$\Phi = \overline{\Phi}(r, z) + \mathrm{Re}\{\widetilde{\Phi}(r, z)\exp(j\omega t)\}. \tag{24.2}$$

$\widetilde{\Phi}$ is in general a complex quantity depending on position. This complex formulation is easier to handle than an equally valid but more cumbersome treatment where the amplitude and phase angle for any quantity are calculated as functions of position. A quantity like Φ remains real even though $\widetilde{\Phi}$ is complex; that is the reason for taking the real part in equation 24.1.

Because the system is linear, only one frequency ω need be handled at a time. The amplitude $\Delta\Omega$ of the disturbance is kept small so that the system can be linearized around a steady state. In some cases, one can have an applied potential that varies as well as a variation in the rotation speed. When both disturbances are kept small, they do not interfere with each other.

24.1 FREQUENCY DISPERSION AT A DISK ELECTRODE

The physical model for the disk electrode embedded in an insulating plane is based on Chapters 7, 8, and 18. The potential in the solution satisfies Laplace's equation

$$\nabla^2\Phi = 0. \tag{24.3}$$

Far from the disk electrode, the potential is taken to be zero.

$$\Phi \to 0 \quad \text{as} \quad r^2 + z^2 \to \infty, \tag{24.4}$$

where r and z are cylindrical coordinates. On the insulating plane, the normal component of the potential gradient is zero.

$$\frac{\partial \Phi}{\partial z} = 0 \quad \text{at} \quad z = 0, \ \ r > r_0. \tag{24.5}$$

On the electrode itself, the normal component of the current density relates to the potential, with kinetic and capacitive components.

$$i_n = -\kappa \frac{\partial \Phi}{\partial z} = C \frac{d(V - \Phi_0)}{dt} + (\alpha_a + \alpha_c) \frac{i_0 F}{RT} (V - \Phi_0) \quad \text{at} \quad z = 0, \ \ r < r_0. \tag{24.6}$$

The kinetic part is already linearized from a more general Butler–Volmer equation.

As stated in the preceding section, all variables, such as i_n, Φ, and V need to be regarded as the real parts of complex variables, such as

$$V = \overline{V} + \text{Re}\{\tilde{V} \ \exp(j\omega t)\}. \tag{24.7}$$

To obtain the AC problem, substitute equation 24.2 into equations 24.3 through 24.6. Thus t is replaced by ω, and ω has only one value at a time. Each equation in the physical model produces three equations in the impedance model, one for the steady problem (exemplified by $\overline{\Phi}$ and treated in Section 18.3) and one each for the real and imaginary parts of the transient equations. Cancel $\exp(j\omega t)$ from the latter.

For example, substitution into equation 24.6 gives (all at $z = 0$ and $r < r_0$)

$$\bar{i}_n = -\kappa \frac{\partial \overline{\Phi}}{\partial z} = (\alpha_a + \alpha_c) \frac{i_0 F}{RT} (\overline{V} - \overline{\Phi}_0), \tag{24.8}$$

and

$$\tilde{i}_n = -\kappa \frac{\partial \tilde{\Phi}}{\partial z} = j\omega C(\tilde{V} - \tilde{\Phi}_0) + (\alpha_a + \alpha_c) \frac{i_0 F}{RT} (\tilde{V} - \tilde{\Phi}_0). \tag{24.9}$$

Time derivatives in the physical problem are replaced by $j\omega$ times the complex parts of the variables. The real and imaginary parts of the last equation show that the real part of $C(\tilde{V} - \tilde{\Phi}_0)$ appears in the imaginary equation, and the imaginary part of $C(\tilde{V} - \tilde{\Phi}_0)$ appears in the real equation. Thus, these two equations are coupled.

The steady part is just like the steady part solved already in Section 18.3, and the current distribution on the disk is shown in Figure 18.5. With the original Butler–Volmer equation 16.10, the steady problem would be nonlinear, and the current distributions on the disk electrode for Tafel kinetics are in Figure 18.6. As an exercise for the student, formulate the impedance problem for Butler–Volmer kinetics (but keeping equations 24.3 through 24.5), develop the treatment of Section 18.3 for the steady part of the problem, but also linearize equation 24.6 or its generalization around the steady solution and arrive at an AC problem that is still linear. (See Problem 24.1.)

Solving the AC problem is still relatively straightforward. The governing differential equation comes from equation 24.3. For this geometry of the disk electrode there are three mathematical techniques which apply.[4] Separation of variables is generally used. Hankel transforms and a superposition integral are two other methods. Impedance problems usually yield to the same solution methods used

in solving the steady part of the problem. Although the impedance problem is linear, it requires the solution for the steady part of the problem.

The main result from this analysis is the impedance of the system comprising the disk electrode and the solution. The problem does not usually require the detailed profiles of the real and imaginary parts of the potential in the solution, and probably not even the complex distribution of $\tilde{i}_n$ on the electrode. The complex impedance of the system can be defined as

$$Z = \tilde{V}/\tilde{I} = R_{\text{eff}} + \frac{1}{j\omega\pi r_0^2 C_{\text{eff}}}, \tag{24.10}$$

which can be thought of as a series connection of the resistance R_{eff} and a capacitance of $\pi r_0^2 C_{\text{eff}}$. R_{eff} includes the solution resistance and also any contribution from the kinetics at the interface. C_{eff} has the units (F/m^2) of a double-layer capacitance. However, R_{eff} and C_{eff} are best thought of as effective values which reflect what is happening due to the kinetics, double-layer capacitance, and the solution resistance, but taking into account the complex geometric relationship of the interface and the electrolytic solution. To get the result requires the analysis. R_{eff} and C_{eff} generally depend on the frequency ω. Therefore, they do not represent simple resistive and capacitive elements.

Dimensionless groups can express how $4\kappa r_0 R_{\text{eff}}$ and C/C_{eff} depend on $\Omega = \omega C r_0/\kappa$ and $J = (\alpha_a + \alpha_c) i_0 F r_0/RT\kappa$. The first is the resistance of the system divided by the resistance $1/4\kappa r_0$ for the primary current distribution (see equation 18.9). The second is the double-layer capacity C divided by the effective value. These depend, for linear kinetics, on the parameter J defined in Section 18.3 and the dimensionless frequency $\Omega = \omega C r_0/\kappa$.

When J is zero, there is no electrochemical reaction. Then, at low frequency the double-layer capacity is the main impediment to current flow, there is a uniform, but capacitive current density, $C/C_{\text{eff}} = 1$, and $4\kappa r_0 R_{\text{eff}}$ is 1.081, the value corresponding to resistance with a uniform current density. At high frequency, the current density on the disk approaches a primary distribution, $4\kappa r_0 R_{\text{eff}}$ becomes 1, and C/C_{eff} approaches infinity. With a primary distribution, any impediment to current flow lies entirely within the solution.

When J is nonzero, the low-frequency behavior approaches that of the secondary current distribution discussed in Section 18.3. The current distribution becomes that given in Figure 18.5. C/C_{eff} becomes zero, and $4\kappa r_0 R_{\text{eff}}$ approaches the value given by the appropriate value of J. At high frequencies, the capacitive current density again approaches the primary distribution, $4\kappa r_0 R_{\text{eff}}$ approaches 1, and C/C_{eff} goes to infinity, much as it did when J was zero.

When the primary current distribution is approached, the current density becomes very large in a small region near the edge of the disk, as given by equation 18.8 and shown as the limit on Figure 18.5 as J becomes infinite. Reference [1] carries out a singular-perturbation analysis for large values of $\omega C r_0/\kappa$, treating separately the edge region of the disk and the region away from the edge. Thereby it arrives at the asymptotic behavior

$$C/C_{\text{eff}} \to 0.563 + 0.25\ \ln(\Omega) \quad \text{as} \quad \Omega \to \infty. \tag{24.11}$$

This asymptote and some calculated values for finite values of $\omega C r_0/\kappa$ are shown in Figure 24.4.

A similar system is treated by Nişancioğlu and Newman[5] where a constant current or potential is applied to the disk electrode. They show how the distributions change from a primary distribution, particularly at short times. They also treat the steady problem at large exchange current densities. Smyrl and Newman[6] look at high current densities where Tafel kinetics is a valid approximation to the Butler–Volmer equation. Tribollet et al.[8] describe a method for measuring the diffusion coefficient of a reacting species from impedance data in the low-frequency range.

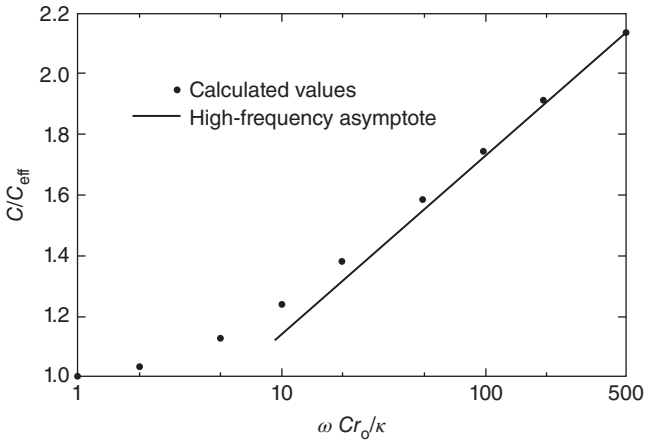

Figure 24.4 Frequency dependence of apparent capacity on a smooth disk in the absence of faradaic reactions.

24.2 MODULATED FLOW WITH A DISK ELECTRODE

Fluid flow to a rotating disk is treated in Section 15.4. It is a complex flow, having a swirling motion somewhat like a tornado. The rotating disk drags adjacent layers of fluid with it, in an angular direction. The centripetal force of this flow creates a radial flow away from the axis. An axial flow toward the disk arises to replace the fluid flowing radially outward. This flow is of interest in many applications because it can be calculated accurately and the flow toward the disk depends only on the distance from the disk and is independent of the radial and angular directions. This provides a means for measuring diffusion coefficients and for studying the kinetics of heterogeneous reactions.

Tokuda et al.[7] propose a then new impedance technique whereby the rotation speed of the disk is driven with a small perturbation, as in equation 24.1. The variation in the angular velocity can cause variations of the current or potential, which are also periodic and can be measured easily. The original theory treats the flow as quasisteady at the instantaneous rotation speed, a procedure which gives good results at low values of $p = \omega/\overline{\Omega}$, but at higher values discrepancies between theory and experiment become apparent. This problem can be addressed by the method describes so far in this chapter.

Fluid flow.–Section 15.4 describes how the von Kármán transformation permits the governing hydrodynamic equations to be reduced to four ordinary differential equations in the distance z from the disk. It turns out that the transient flow with a sinusoidal variation of the rotation speed Ω can still be reduced to ordinary differential equations by the von Kármán transformation, but now with inclusion of appropriate derivatives of the velocities with respect to time. Treatment of all variables, such as v_r, v_θ, v_z, and the dynamic pressure $\mathcal{P}$, demonstrates the power of the impedance approach. Expansion in the parameter $\Delta\Omega/\overline{\Omega}$ gives, in addition to the four steady equations 15.26, four complex equations for the perturbations in the velocity and the dynamic pressure. The latter equations yield eight equations for the real and imaginary parts.

The boundary conditions 15.17 are treated the same way, with the replacement of Ω by equation 24.1. The resulting ordinary differential equations for the perturbation quantities are linear and coupled and are solved by the technique detailed in Appendix C of this book. These equations also involve the functions for the steady velocity which were obtained by solving the nonlinear equations 15.26 (with the boundary conditions 15.27) as discussed in Section 15.4. See also Figure 15.2 and Problem 24.2.

For the subsequent parts of the problem, it is most useful to have the velocity profiles, or particularly that for v_z, close to the disk, since the diffusion layer is generally thin for the systems at high Schmidt numbers, Sc, encountered in electrochemical systems (see Sections 17.5 and 17.6). The necessary information can be found in the original reference.[2]

Mass-transport application.–The concentration of the critical species in the diffusion layer is governed by the unsteady equation of convective diffusion 17.2.

$$\frac{\partial c_i}{\partial t} + v_z \frac{\partial c_i}{\partial z} = D_i \frac{\partial^2 c_i}{\partial z^2}. \tag{24.12}$$

This is appropriate for a solution with a lot of supporting electrolyte. It could also apply to a binary electrolyte (see equation 11.21). v_z is assumed to be known and given by the preceding analysis. It is assumed that the disk is uniformly accessible, since v_z is independent of r, and therefore i_n is uniform and c_i depends only on z. Thus the radial dependence of the potential Φ is ignored. See Chapter 21.

Equation 24.12 is linear in c_i, but it is nonlinear in the amplitude of the perturbation since both v_z and c_i have AC parts. Therefore, after linearization, the AC part of the problem reads

$$j\omega\tilde{c}_i + \overline{v}_z \frac{\partial \tilde{c}_i}{\partial z} + \tilde{v}_z \frac{\partial \overline{c}_i}{\partial z} = D_i \frac{\partial^2 \tilde{c}_i}{\partial z^2}. \tag{24.13}$$

$\overline{c}_i$ is determined as in Chapter 17. $\overline{i}_n$ can be between zero and the limiting current density. The boundary conditions for $\tilde{c}_i$ are taken to be

$$\tilde{c}_i = \tilde{c}_{i,0} \quad \text{at} \quad z = 0 \quad \text{and} \quad \tilde{c}_i \to 0 \quad \text{as} \quad z \to \infty. \tag{24.14}$$

The objective of this subsection is to relate $\tilde{c}_{i,0}$ to $\partial\tilde{c}_i/\partial z|_{z=0}$, so that the next subsection can address the interface and the hydrodynamic impedance.

The parameters involved have already been reduced by using the variable $\varsigma = z\sqrt{\overline{\Omega}/\nu}$, which is essentially the axial distance z divided by the thickness of the hydrodynamic boundary layer. The differential equation introduces the diffusion coefficient, and therefore the Schmidt number $\mathrm{Sc} = \nu/D_i$ becomes a parameter. For the mass-transfer problem, it is convenient to replace ζ with

$$\xi = \varsigma\left(\frac{a\nu}{3D_i}\right)^{1/3}, \tag{24.15}$$

which is in essence the ratio of z to the diffusion-layer thickness (compare Problem 17.3). Thus $\overline{c}_i$ depends on $c_{i,\infty} - \overline{c}_{i,0}$, Sc, and ξ.

Since equation 24.13 is linear in $\tilde{c}_i$, one can determine first the solution of the homogeneous equation (i.e., without the term with $\overline{c}_i$). This is termed the convective Warburg problem, which has been addressed in the literature. One homogeneous solution is called $\theta(\xi, \mathrm{Sc})$. Then one can obtain a particular solution of the nonhomogeneous equation by reduction in order.

Reference [2] deals with these issues by expressing the result as

$$\left.\frac{d\tilde{c}_i}{d\xi}\right|_{\xi=0} = \tilde{c}_{i,0}\theta'(0) + \frac{\Delta\Omega}{\overline{\Omega}} \left.\frac{d\overline{c}_i}{d\xi}\right|_{\xi=0} W, \tag{24.16}$$

where $\theta'(\xi) = d\theta/d\xi$ and W is a defined quantity. Both $\theta'(0)$ and W depend on Sc and $p = \omega/\overline{\Omega}$ and are tabulated in Ref. [2]. This relationship between $\tilde{c}_{i,0}$ and $d\tilde{c}_i/d\xi|_{\xi=0}$ is necessary for unravelling the interfacial behavior, in the third part of the problem.

Electrochemical application.–The specifics of the behavior at the interface have not yet been introduced. Reference [2] utilizes an electrochemical redox reaction of ferricyanide and ferrocyanide

$$\mathrm{Fe(CN)}_6^{-3} + e^- \rightarrow \mathrm{Fe(CN)}_6^{-4} \tag{24.17}$$

as well as a double-layer capacity. The reaction itself is reasonably facile, and the system is well studied, including transport properties of the solution. The steady part of the current density could be anywhere between the anodic and cathodic limiting currents.

To do the problem right at this point would require solving first for the steady concentration profiles with the assumption of a large excess of supporting electrolyte. The concentration of the two minor ions at the surface ($z = 0$) as well as the double-layer capacitance C would be determined for the steady current.

These steady results provide the background for the hydrodynamic modulation. The boundary condition on the surface could be written as

$$i_n = i_f + i_c, \tag{24.18}$$

where

$$i_f = i_0 \left[\frac{c_{4,0}}{c_{4,\infty}} \exp\left(\frac{\alpha_a F \eta}{RT}\right) - \frac{c_{3,0}}{c_{3,\infty}} \exp\left(\frac{-\alpha_c F \eta}{RT}\right) \right] \tag{24.19}$$

and

$$i_c = C \frac{d(V - \Phi_0)}{dt} \tag{24.20}$$

are the faradaic and capacitive parts of the total current density at the electrode surface. The total overpotential η is the sum of the surface and concentration overpotentials; see Problem 20.4 and equation 21.4.

$$\eta = V - \Phi_0 - U_\infty, \tag{24.21}$$

where U_∞ is the open-circuit potential for the reaction at the bulk conditions and Φ_0 is the potential in the bulk of the solution extrapolated to the surface as though there were no concentration variations. (Φ_0 would have got a tilde over it, as in Chapter 21, but this would have caused confusion with the tilde denoting AC quantities disturbed from steady values.) Equation 24.19 permits reaction orders of the product and reactant ions to be shown explicitly and permits i_0 and U_∞ to be constants, because they are evaluated at the (steady) bulk concentrations. Its use should be restricted to solutions with an excess of supporting electrolyte. The authors of Ref. [2] include an $i_n R$ term, in case there is some solution resistance included in the measurement of V relative to Φ_0.

The ability to distinguish between faradaic and capacitive current, as in equation 24.18, has been questioned. See the discussion of Refs. [8 to 11] of Chapter 8, two paragraphs below equation 8.70. This problem needs to be ignored here.

Also among the boundary conditions at the electrode surface is the relationship of the flux densities of the reactant and product ions to the faradaic current density:

$$-D_i \left.\frac{\partial c_i}{\partial z}\right|_{z=0} = -\frac{s_i i_f}{nF}, \tag{24.22}$$

where s_i and n are the stoichiometric coefficients and number of electrons involved in the single electrode reaction (see equation 16.8).

It is further assumed that Φ_0 and i_n are uniform over the disk surface. Treating their variation, as in Chapter 21, would be quite complicated. The migration contribution to the flux density in equation 24.22 is also neglected, in harmony with the assumption that there is excess supporting electrolyte, and double-layer adsorption of reactant and product is ignored.

Now that one has stated the boundary condition on the electrode surface and its assumptions, one is ready to proceed in the manner of this chapter, namely to substitute equation 24.2 for any variables, linearize all relevant equations, and identify the steady and AC parts of these equations. This involves $\tilde{c}_{i,0}$ and $d\tilde{c}_i/dz|_{z=0}$; the relationship of these two quantities to each other and the hydrodynamic and convective diffusion was developed in the preceding subsection (see equation 24.16).

There have been some essential approximations here, such as ignoring radial variation of Φ_0. Some other approximations have been adopted for experimental verification of the theory of hydrodynamic modulation. These include use of a supporting electrolyte and adoption of a single electrochemical reaction. A high level of complexity can still be included. To verify the theory and bring out some of the essence, one can treat a facile reaction like the ferricyanide/ferrocyanide reaction so that the surface overpotential is negligible compared to the concentration overpotential.

In this section, it is the disk rotation speed that is modulated. One could also modulate either the electrode potential or the current (even at a different frequency). Here potentiostatic control is taken to mean that $\tilde{V} = 0$ and one measures the response with $\tilde{i}_n$. Galvanostatic control is taken to mean that $\tilde{i}_n = 0$ and one measures the response with $\tilde{V}$. Here, there are two species involved in the electrochemical reaction. One can focus on one of these by operating with the steady electrode potential set very positive or very negative. Figure 24.5 shows the measured response in galvanostatic control at half the limiting current. Part A shows the phase angle of the response, and Part B shows the amplitude of the response divided by that at a very low frequency. It is remarkable that the theory

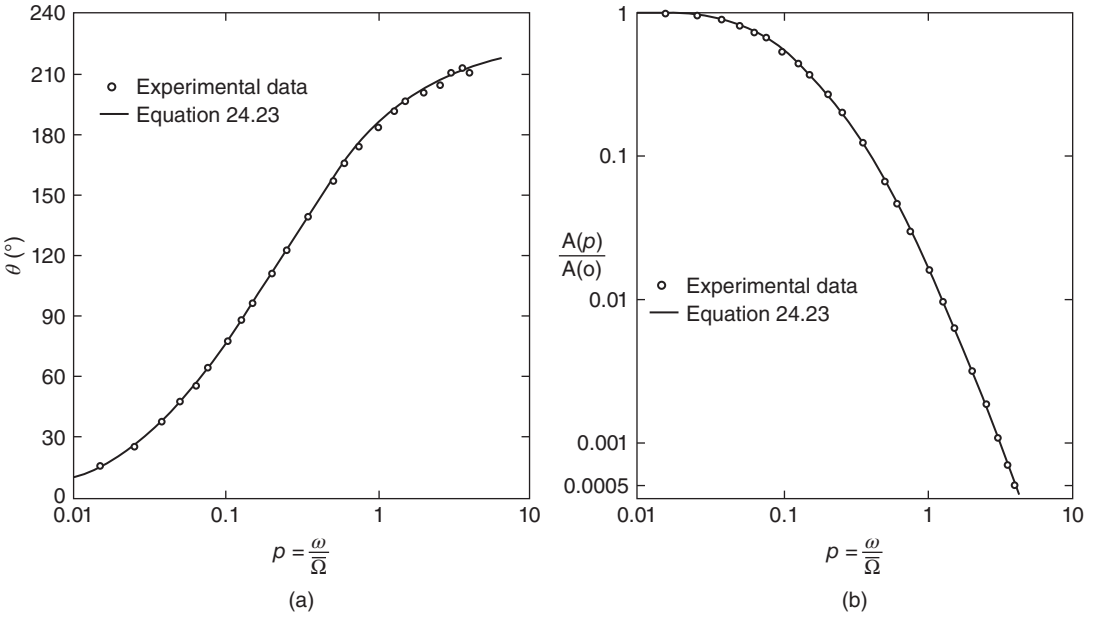

Figure 24.5 Comparison between the theoretical curve from equation 24.23 and the experimental data in galvanostatic mode. The data were obtained with the $Fe(CN)_6^{-3}/Fe(CN)_6^{-4}$ system at $\bar{i}_n = 0.5\ i_{lim}$. Supporting electrolyte is 1 *M* KCl, Sc = 1200, $\overline{\Omega} = 120$ rpm. (a) phase shift versus dimensionless frequency, (b) normalized amplitude versus dimensionless frequency.

and the experiment can follow each other through a decrease of the amplitude by a factor of 2000. The equation used to represent the theory is

$$\frac{\tilde{V}}{\Delta\Omega} = -\frac{\bar{i}}{\Omega} Z_D W, \tag{24.23}$$

where

$$Z_D = \frac{-RT}{(nF)^2} \sum_{i=3}^{4} \frac{s_i^2 \delta_i}{\bar{c}_{i,0} D_i \theta_i'(0)} \tag{24.24}$$

is the diffusion or convective Warburg impedance approximated for fast kinetics and W and Z_D are evaluated as though the two diffusion coefficients were equal.

$$\delta_i = \sqrt{\frac{\nu}{\Omega}} \left(\frac{3D_i}{a\nu} \right)^{1/3}. \tag{24.25}$$

24.3 POROUS ELECTRODES FOR BATTERIES

Battery systems typically utilize porous electrodes to facilitate contact between the solid phase and the electrolytic solution (see Chapter 22). Electrochemical reactions provide the energy for battery discharge but result in changes in the composition and possibly morphology. In addition, there can be double-layer charging and temperature changes and heat transfer. Models of batteries range from simple equivalent circuits to descriptions of the chemical and physical processes, including thermal effects. The message of this chapter is that almost any model designed to describe battery discharge and degradation can be modified slightly to handle impedance phenomena. (The impedance is frequently done with a disturbance around open-circuit in order to avoid problems with the conditions for the Kramers–Kronig relation, as developed in the next section.)

Impedance testing is relatively nonintrusive and can reveal a lot about the battery and its properties without destroying the battery. Such data are best interpreted with a fairly complete physical and chemical model because the changes in the response can be related to specific factors in the model. Another use of impedance measurements is to detect and interpret changes in the battery with age, and this applies to corroding and degrading systems in general. The changes can be detected from the measurements themselves over time, but their interpretation is compromised by using a model of resistors and capacitors which reflects poorly (or in an undefined manner) the actual system.

Models of lithium-ion, nickel/metal hydride, and lead/acid batteries have been developed in some detail, and many features can be incorporated to describe diffusion in solid and solution phases, the stoichiometry of the reactions, simultaneous reactions, etc. By these means the discharge behavior can be reproduced more accurately, understanding is enhanced, and impedance methods can be used. The steps for incorporating the impedance analysis into the model are straightforward. Express all quantities in terms of a steady part and a small AC perturbation as in equation 24.2. Substitute these into the model equations, including any transient terms which could reflect concentration changes, consumption of active material, double-layer charging, and heat generation. Linearize the equations so that they are expressed in terms of a (possibly nonlinear) steady part and a linear AC part. If the nonlinear problem for discharge is solved by iteration over the nonlinearities by a properly quadratically convergent method (see Appendix C), the matrix for the AC part is easily obtainable from the matrix used for solving the discharge behavior. The matrix is made up of four submatrices because there are now real and imaginary parts for each physical quantity treated. The upper left and lower right submatrices are

identical to that used in iterating over the nonlinearities and can be thought of as describing how all the real parts affect all the other real parts (the upper left submatrix) and how the imaginary parts affect all the other imaginary parts. The time derivatives generate terms with $j\omega$ as in going from equations 24.6 to 24.9 and populate the other two submatrices and describe how the imaginary parts affect all the real parts, and vice versa.

In running the computer program, one would first solve for the steady part, iterating over nonlinearities as necessary. This steady part is independent of the frequency ω, but if the problem is nonlinear, it will be necessary to use this steady part to solve the linear equations for the AC part. Problem 24.1 should help you understand how this works. Then, always with the same steady part, run through the entire desired frequency range with one frequency after another.

Reference [3] discusses this process in more detail, with examples from lithium-ion batteries. The model treats a binary electrolyte with concentrated-solution theory (see Chapter 12), ohmic potential drop, charge-transfer processes including double-layer charging, surface films, diffusion within spherical particles of active material including multiple diameters and different materials (like Li_yCoO_2 mixed with $Li_yMn_2O_4$), conservation of charge, and radial diffusion in the pores. (It may be that the impedance analysis has not been updated with respect to some of these features because program modifications are made as the need arises and impedance may not be the focus.)

Figure 22.6 is a complex-impedance plot of the impedance response of a $Li/PEO_{18}LiCF_3SO_3/Li_yTiS_2$ system (see Ref. [3] for details) for a number of different values of the solid-phase diffusion coefficient for the Li_yTiS_2 material. The base case uses circles for symbols. Low frequencies start at the upper right and increase toward the lower left, ending up on the real axis. Note the units (Ω-cm^2) reflecting the fact that the unit area of the system is what is important in modeling and scale up. Think of this as the potential $\tilde{V}$ divided by the current density $\tilde{i}_n$.

There is a characteristic semicircle in the high-frequency region, related to the kinetics and the capacitance of the interface (see Figure 24.3 and Problem 24.3). Toward the low frequencies, the curves go off to the upper right, reflecting diffusion effects and also the limited capacity of the active material over the potential range of the AC perturbation.

Impedance people learn to recognize certain features on such a complex-impedance plot. However, the plot does not make clear what the frequency is as one follows along a curve. Some information is lost. The alternative is the Bode plot, where the magnitude of the impedance is plotted against the frequency ω, both on a logarithmic scale. On an accompanying plot, the phase angle of the complex number is plotted against the logarithm of the frequency. Figure 24.5 is an example of a Bode plot. All information is clearly shown, but it should be remembered that the angle is the angle on the complex plane of a line drawn from a point to the origin. It is not a tangent to the curve on a complex-impedance plot (Figure 24.6).

Time constants, or characteristic frequencies for different processes (like double-layer capacity versus diffusion), may occur at widely different frequencies; for this reason they may show up in different parts of the diagram. Effects for the two electrodes may show up on top of each other, and it may be difficult to put a reference electrode into a practical cell. The model can help greatly in this regard because one can vary parameters to see where different effects show up on the plots.

Reference [3] looks in more detail at the interesting question of how well one can detect the value of a solid-state diffusion coefficient by looking at the computed impedance spectrum. A specific value is put into the model. Can it be recovered from the results? The paper examines three techniques developed in the literature to test the accuracy one can expect from an experiment. As D_s increases, it ceases to be a limiting factor and cannot be recovered accurately from impedance data. However, even at lower values of D_s other factors like the finite capacity of the system may obscure the results.

Reference [9] examines how far one can go in representing complicated phenomena by analytic models. The approach is to treat transient diffusion in a single spherical particle and then to add a surface film. The impedance response of a single such particle can be regarded as a building block

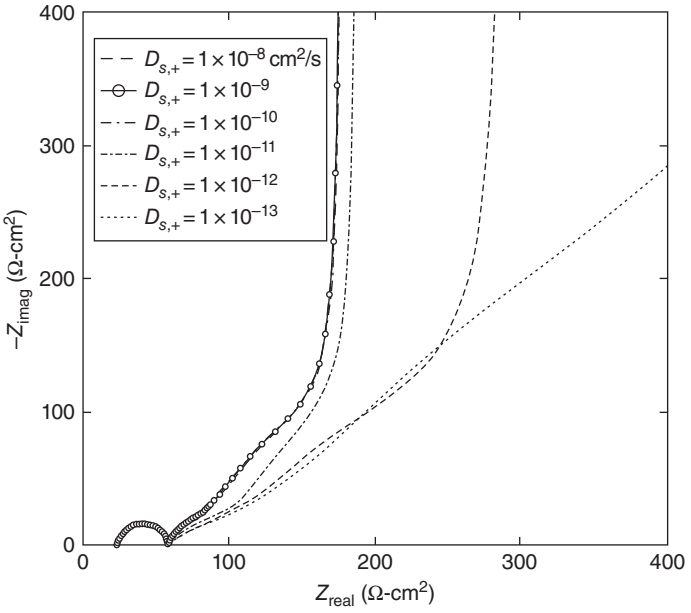

Figure 24.6 Dependence of the impedance response on the diffusion coefficient D_s in the positive-electrode material Li_yTiS_2.

which is used to construct a porous electrode and eventually a system with two porous electrodes and a separator. The authors find that they can build the complete system and include ohmic potential drop within the pore solution and still retain an analytic solution, but they could not include transient diffusion in the pore solution (a feature which was included in the computer analysis of Ref. [3]).

de Levie[10] presents an early and complete treatment of dispersion effects at rough and porous electrodes. One feature noted is that a porous electrode tends to cut the phase angle by a factor of 2. Reference [3] observes that the computer model did not necessarily show this halving of the phase angle because that model, while including axial diffusion, did not include diffusion in the radial direction or in a direction perpendicular to the pores.

24.4 KRAMERS–KRONIG RELATION

Jakšić and Newman[11] aim to show the applicability of the Kramers–Kronig (K–K) relations for describing the behavior of impedance, to use these relations for calculating both the effective resistance (R_{eff}) and the effective double-layer capacity (C_{eff}) in Section 24.1 as functions of frequency, and thus to show the consistency of that theory and results with the K–K relations. The causality principle in physics leads to the result that the impedance of an electrode system is analytic in the lower half of the frequency plane. Consequently, if the simple pole point $\omega_0 = \omega$ is excluded from the region of integration, the function $(Z(\omega_0) - Z_\infty)/(\omega_0 - \omega)$ is analytic everywhere within any closed contour C, and the contour integral along C is thereby zero. When part of the contour is a semicircle at infinity, the integral along this semicircle is also zero. These basic features are the main prerequisite for the application of the Kramers–Kronig (K–K) relation.[12–14]

Thus, the effective double-layer capacity can be evaluated from the effective resistance, and vice versa, by means of the K–K relations while avoiding difficulties due to the singularity in the integrand.

Integration around the entire contour C leads to[14]

$$\int_{-\infty}^{\infty} \frac{Z(\omega_0) - Z_\infty - j\sigma/\omega_0}{\omega_0 - \omega} d\omega_0 + \pi j[Z(\omega) - Z_\infty - j\sigma/\omega] = 0, \tag{24.26}$$

where the integral is the Cauchy principal value of the integral. The second term results from the Cauchy integral formula for $\omega = \omega_0$. The terms in Z_∞ and σ are included so that the integrand will be well behaved at both zero and infinity. This is necessary even with simple elements like a resistor and a capacitor.

The above equation splits into two Kramers–Kronig relations for the electrode impedance:

$$Z_r(\omega) - Z_\infty = \frac{-1}{\pi} \int_{-\infty}^{\infty} \frac{Z_i(\omega_0) - \sigma/\omega_0}{\omega_0 - \omega} d\omega_0, \tag{24.27}$$

and

$$Z_i(\omega) = \frac{1}{\pi} \int_{-\infty}^{\infty} \frac{Z_r(\omega_0) - Z_\infty}{\omega_0 - \omega} d\omega_0 + \frac{\sigma}{\omega}, \tag{24.28}$$

and recognition that the real and imaginary parts of the impedance are even and odd in the frequency, respectively, allows expressions with integration over positive frequencies.

$$Z_r(\omega) - Z_\infty = \frac{-2}{\pi} \int_{0}^{\infty} \frac{\omega_0 Z_i(\omega_0)}{\omega_0^2 - \omega^2} d\omega_0, \tag{24.29}$$

and

$$Z_i(\omega) = \frac{2\omega}{\pi} \int_{0}^{\infty} \frac{Z_r(\omega_0) - Z_\infty}{\omega_0^2 - \omega^2} d\omega_0 + \frac{\sigma}{\omega}. \tag{24.30}$$

Since the real part of the impedance appears on the left and the imaginary part under the integral in the first equation, this formula permits the real part at a given frequency ω to be calculated from the imaginary part of the impedance over the entire frequency range. The reverse is true in the second equation. This ability to calculate one quantity from knowledge of another is somewhat analogous to the Gibbs–Duhem equation (see equation 2.36), where the osmotic coefficient can be calculated from data on the activity coefficient (of a single solute), and vice versa. A difference is that the K–K relation is inherently an integral relation, whereas the Gibbs–Duhem relation is a differential relation applying at a point. The K–K relation can act as a consistency check on experimental impedance data, just as the Gibbs–Duhem equation can act as a consistency check on the chemical potentials of two components of a binary system. Similarly, from knowledge of just one of the quantities, you can calculate the other. Both procedures find application in scientific work.

The K–K relation is quite general; it applies to any physical system as long as there is a steady state. It can apply to a fuel cell when operated at a steady state, but a battery under discharge conditions has no steady state. The K–K relation will automatically apply to any physically valid model perturbed around a steady state. Therefore, the analysis in Section 24.1 is valid since it is based on a physical model.

One of the main, hidden, reasons for using equivalent-circuit models may be that they assure that the resulting impedance will satisfy the K–K relation. On the other hand, separate empirical fits of the real and imaginary parts of the impedance would not generally be expected to obey the K–K relation.

There are times, as in the original work of Kramers and Kramer (who worked independently), when one part of the impedance function is easier to measure than the other. Then the K–K relation provides a means of calculating the missing function. The electrical conductivity and the dielectric constant relate to the real and imaginary parts of the same quantity. One is easier to measure than the other.

The general conclusion is that impedance data should satisfy the K–K relation, and the latter can be used as a check on consistency of data.

The remainder of Ref. [11] treats how to deal with the singularity in the integral in a straightforward way. Since

$$\int_0^\infty \frac{d\omega_0}{\omega_0^2 - \omega^2} = 0, \tag{24.31}$$

the relations can be rewritten to avoid the singularities at $\omega_0 = \omega$.

$$Z_r(\omega) - Z_\infty = \frac{-2}{\pi} \int_0^\infty \frac{\omega_0 Z_i(\omega_0) - \omega Z_i(\omega)}{\omega_0^2 - \omega^2} d\omega_0, \tag{24.32}$$

and

$$Z_i(\omega) = \frac{2\omega}{\pi} \int_0^\infty \frac{Z_r(\omega_0) - Z_r(\omega)}{\omega_0^2 - \omega^2} d\omega_0 + \frac{\sigma}{\omega}. \tag{24.33}$$

PROBLEMS

24.1 Formulate the impedance problem for the system of Section 24.1 but with the linear kinetics in boundary condition 24.6 replaced by the Butler–Volmer equation 8.6. Discuss how this leads to the steady nonlinear problem treated in Section 18.3 for the steady part of the problem but still leads to a linear problem for the AC problem. How does the solution of the steady problem enter into the AC problem?

24.2 Obtain a complete and well defined problem statement for the fluid flow to a rotating disk with a modulated rotation speed as given by equation 24.1.

(a) What equations should you start with?

Answer: Equations 15.18 for the material balance and 15.19 through 15.21 for the momentum balance.

(b) What coordinate system should you use? (Answer: cylindrical coordinates as used in Section 15.4.)

(c) What boundary conditions are appropriate? (Answer: Equation 15.17.)

(d) Outline the subsequent procedure. (Answer: Substitute equations 24.2 for all variables into the equations and the boundary conditions. Expand these equations for small values of the parameter $\Delta\Omega/\overline{\Omega}$ and linearize by dropping quadratic and higher terms. Separate these equations into those for the steady part of the problem and those for the transient part of the problem. You should have both differential equations and boundary conditions. It is suggested to use the notation $p = \omega/\overline{\Omega}$ and

$$v_r = r\overline{\Omega}F(\zeta) + r\Delta\Omega \mathrm{Re}\{\tilde{f}(\zeta)\exp(j\omega t)\},$$

$$v_\theta = r\overline{\Omega}G(\zeta) + r\Delta\Omega \mathrm{Re}\{\tilde{g}(\zeta)\exp(j\omega t)\},$$

$$v_z = \sqrt{\nu\overline{\Omega}}\left(H(\zeta) + \frac{\Delta\Omega}{\overline{\Omega}}\mathrm{Re}\{\tilde{h}(\zeta)\exp(j\omega t)\}\right),$$

and

$$\mathcal{P} = \mu\overline{\Omega}\left(P(\varsigma) + \frac{\Delta\Omega}{\overline{\Omega}}\mathrm{Re}\{\tilde{p}(\varsigma)\exp(j\omega t)\}\right),$$

where $\varsigma = z\sqrt{\overline{\Omega}/\nu}$. If you get into trouble, consult the original reference.[2])

(e) Propose a BAND map (see Appendix C) to indicate how all these equations and boundary conditions are to be fitted into the BAND(j) computer program. Since the steady problem can be solved, with iteration over nonlinearities, prior to addressing the AC problem, you may want to make two BAND maps. You can choose to do only one of these, that for the steady problem or that for the transient problem where the steady solution is already available and where one or a number of values of ω (or $p = \omega/\overline{\Omega}$) are to be chosen and run sequentially.

24.3 Consider Figure 24.3 to be the entire system you want to analyze; that is, you want to place emphasis on the impedance $[(\tilde{V} - \tilde{\Phi}_0)/\tilde{i}_n]$ of the interface. Equations 24.6 through 24.9 provide you all you need. Obtain an expression for the complex impedance and show that it would plot as a semicircle on a complex-impedance plot. What is the diameter of the semicircle, and what is the (characteristic) frequency at the top of the semicircle? In addition to expressions, give numerical values for this diameter and frequency when $C = 10\,\mu\mathrm{F/cm^2}$, $i_0 = 10^{-3}\,\mathrm{A/cm^2}$, and $T = 298.15\,\mathrm{K}$. Assume that $\alpha_a + \alpha_c = 1$, $r_0 = 5\,\mathrm{mm}$, and $\kappa = 0.2\,\mathrm{S/cm}$.

24.4 Use equations 24.32 and 24.33 to show that a resistor has no imaginary part of the impedance and that a capacitor has no real part of the impedance. Are the terms Z_∞ and σ important in the analysis?

(a) Take the real part of the impedance of the resistor to be R_{eff}. Use equation 24.32 to calculate the imaginary part of the impedance.

(b) Take the imaginary part of the impedance of the capacitor to be $1/j\omega\pi r_0^2 C_{\mathrm{eff}}$. Use equation 24.33 to calculate the real part of the impedance.

NOTATION

c_i	concentration of species i, mol/cm^3
C	double-layer capacitance, F/m^2
C_{eff}	double-layer capacitance (effective), F
D_i	diffusion coefficient of species i, cm^2/s
D_s	diffusion coefficient in solid battery material, cm^2/s
F	Faraday's constant, 96487 C/mol
F, G, H	dimensionless velocity components
i	current density, A/cm^2
i_c	capacitive current density, A/cm^2
i_f	faradaic current density, A/cm^2
i_{lim}	limiting current density, A/cm^2
i_n	normal current density, A/cm^2
i_0	exchange current density, A/cm^2
I	current or current density
j	square root of -1
J	$(\alpha_a + \alpha_c)i_0 F r_0/RT\kappa$, dimensionless exchange current density
n	number of electrons involved in single electrode reaction
p	$\omega/\overline{\Omega}$

$\mathcal{P}$	dynamic pressure, N/cm^2
r	radial distance, cm
r_0	disk radius, cm
R	universal gas constant, 8.3143 J/mol·K
R_{eff}	effective resistance, ohm
s_i	stoichiometric coefficient of species i
Sc	$= \nu/D_i$, Schmidt number
t	time, s
U_∞	open-circuit potential at bulk composition, V
V	potential of electrode, V
v_r, v_θ, v_z	velocity components, cm/s
z	axial distance, cm
Z	impedance, ohm
α_a, α_c	transfer coefficients
δ	dimensionless average current density
δ_i	diffusion layer thickness, cm
η	total overpotential, V
θ	dimensionless concentration
κ	conductivity, S/cm
μ	viscosity, mPa s
ν	kinematic viscosity, cm^2/s
ξ, ζ	dimensionless distance from electrode, see Eq. 24.15
σ	resistance term
Φ	potential, V
Φ_0	potential in the bulk extrapolated to surface, V
ω	frequency of superposed variation, rad/s
Ω	rotation speed, rad/s

Subscripts, Superscripts, and Special symbols

AC	alternating current
DC	direct current
Re	real
Im	imaginary
overbar	steady component
tilde	oscillating component

REFERENCES

1. John Newman, "Frequency Dispersion in Capacity Measurements at a Disk Electrode," *Journal of the Electrochemical Society*, *117* (1970), 198–203.
2. Bernard Tribollet and John Newman, "The Modulated Flow at a Rotating Disk Electrode," *Journal of the Electrochemical Society*, *130* (1983), 2016–2026.
3. Marc Doyle, Jeremy P. Meyers, and John Newman, "Computer Simulations of the Impedance Response of Lithium Rechargeable Batteries," *Journal of the Electrochemical Society*, *147* (2000), 99–110.
4. John Newman, "The Fundamental Principles of Current Distribution and Mass Transport in Electrochemical Cells." Allen J. Bard, ed., *Electroanalytical Chemistry* (New York: Marcel Dekker, Inc., 1973), *6*, 187–352.

5. Kemal Nişancioğlu and John Newman, "The Short-Time Response of a Disk Electrode," *Journal of the Electrochemical Society*, *121* (1974), 523–527.
6. William H. Smyrl and John Newman, "Current Distribution at Electrode Edges at High Current Densities," *Journal of the Electrochemical Society*, *136* (1989), 132–139.
7. Bernard Tribollet, John Newman, and William H. Smyrl, "Determination of the Diffusion Coefficient from Impedance Data in the Low Frequency Range," *Journal of the Electrochemical Society*, *135* (1988), 134–138.
8. Koichi Tokuda, Stanley Bruckenstein, and Barry Miller, "The Frequency Response of Limiting Currents to Sinusoidal Speed Modulation at a Rotating Disk Electrode," *Journal of the Electrochemical Society*, *122* (1975), 1316–1322.
9. Jeremy P. Meyers, Marc Doyle, Robert M. Darling, and John Newman, "The Impedance Response of a Porous Electrode Composed of Intercalation Particles," *Journal of the Electrochemical Society*, *147* (2000), 2930–2940.
10. Robert de Levie, "Electrochemical Response of Porous and Rough Electrodes," in Paul Delahay, ed., *Advances in Electrochemistry and Electrochemical Engineering* (New York: Interscience Publishers), *6* (1967), pp. 329–397.
11. Milan M. Jakšić and John Newman, "The Kramers-Kronig Relations and Evaluation of Impedance for a Disk Electrode," *Journal of the Electrochemical Society*, *133* (1986), 1097–1101.
12. H. A. Kramers, *Physikalische Zeitschrift*, 30 (1929), 522. Also *Collected Scientific Papers* (Amsterdam: North-Holland Publishing Co., 1956), p. 347.
13. R. de L. Kronig, "On the Theory of the Dispersion of X-Rays," *Journal of the Optical Society of America Review of Scientific Instruments*, *12* (1926), 547–557.
14. L. D. Landau and E. M. Lifshitz, *Electrodynamics of Continuous Media, Vol. 8, Course of Theoretical Physics* (New York: Pergamon Press, 1960), pp. 256–284.

APPENDIX A

PARTIAL MOLAR VOLUMES

Partial molar volumes are occasionally used as properties of solutions. However, the density of the solution is the quantity that is measured experimentally. For n components, the density is a function of $n-1$ independent concentrations c_i at a given temperature and pressure. Let us suppose that the density ρ of the solution is given by the experimental correlation in terms of these $n-1$ concentrations:

$$\rho = \rho(c_1, c_2, \ldots, c_{n-1}). \tag{A.1}$$

We want to show here how to calculate the partial molar volumes of the components from the experimental density data. However, we are not concerned here with the partial molar volumes of individual ions, only with those of the neutral components of the solution. The method is thus equally applicable to nonelectrolytic solutions.

The partial molar volume of component j is given by

$$\overline{V}_j = \left(\frac{\partial V}{\partial n_j}\right)_{\substack{T,p,n_i \\ i\neq j}}, \tag{A.2}$$

where V is the volume of the solution and n_i is the number of moles of component i in the solution. The density of the solution is also given by

$$\rho = \sum_{i=1}^{n} c_i M_i = \frac{1}{V}\sum_{i=1}^{n} n_i M_i, \tag{A.3}$$

where M_i is the molar mass of component i and $n_i = c_i V$.

Electrochemical Systems, Fourth Edition. John Newman and Nitash P. Balsara.

From equations A.2 and A.3, the partial molar volume of component j is

$$\begin{aligned}\overline{V}_j &= \frac{1}{\rho}\frac{\partial}{\partial n_j}\sum_{i=1}^{n} n_i M_i + \left(\sum_{i=1}^{n} n_i M_i\right)\frac{\partial(1/\rho)}{\partial n_j} \\ &= \frac{M_j}{\rho} - \frac{V}{\rho}\frac{\partial \rho}{\partial n_j}.\end{aligned} \tag{A.4}$$

From the density correlation A.1 we obtain

$$\begin{aligned}\frac{\partial \rho}{\partial n_j} &= \sum_{k=1}^{n-1}\frac{\partial \rho}{\partial c_k}\frac{\partial c_k}{\partial n_j} = \sum_{k=1}^{n-1}\frac{\partial \rho}{\partial c_k}\frac{\partial (n_k/V)}{\partial n_j} \\ &= \sum_{k=1}^{n-1}\frac{\partial \rho}{\partial c_k}\left(\frac{1}{V}\frac{\partial n_k}{\partial n_j} - \frac{n_k}{V^2}\frac{\partial V}{\partial n_j}\right) = \sum_{k=1}^{n-1}\frac{\partial \rho}{\partial c_k}\left(\frac{\delta_{jk}}{V} - \frac{c_k}{V}\overline{V}_j\right),\end{aligned} \tag{A.5}$$

where δ_{jk} is the Kronecker delta, $\delta_{jk} = 1$ for $j = k$, and $\delta_{jk} = 0$ for $j \neq k$.

Substitution of equation A.5 into equation A.4 yields

$$\overline{V}_j = \frac{M_j}{\rho} - \frac{1}{\rho}\sum_{k=1}^{n-1}\frac{\partial \rho}{\partial c_k}\delta_{jk} + \frac{\overline{V}_j}{\rho}\sum_{k=1}^{n-1} c_k\frac{\partial \rho}{\partial c_k}. \tag{A.6}$$

Solving for $\overline{V}_j$, we obtain

$$\overline{V}_j = \frac{M_j - \sum_{k=1}^{n-1}\frac{\partial \rho}{\partial c_k}\delta_{jk}}{\rho - \sum_{k=1}^{n-1} c_k\frac{\partial \rho}{\partial c_k}} = \frac{M_j - \frac{\partial \rho}{\partial c_j}(1-\delta_{jn})}{\rho - \sum_{k=1}^{n-1} c_k\frac{\partial \rho}{\partial c_k}}. \tag{A.7}$$

In particular, for a single salt solution where the density is given by $\rho = \rho(c)$, c being the concentration of the salt, the partial molar volume of the electrolyte is

$$\overline{V}_e = \frac{M_e - \frac{d\rho}{dc}}{\rho - c\frac{d\rho}{dc}}, \tag{A.8}$$

and the partial molar volume of the solvent is

$$\overline{V}_0 = \frac{M_0}{\rho - c\frac{d\rho}{dc}}. \tag{A.9}$$

If the density is a linear function of the concentration, the partial molar volumes of the electrolyte and the solvent are constant. Conversely, if the partial molar volume of one component is constant, the partial molar volume of the other component is also constant, and the density is a linear function of concentration.

APPENDIX B

VECTORS AND TENSORS

Transport equations can become quite lengthy, and this frequently leads one to introduce vector notation, which has several advantages:

1. The equations become considerably more compact when written in vector notation.
2. The equations have significance independent of any particular coordinate system.
3. It is easier to grasp the meaning of an equation (after the vector notation becomes familiar).

You may regard vector notation as a form of shorthand writing, but it would be a good idea for you to develop an intuitive feel for the significance of some of the more common vector operations.

A vector has both magnitude and direction and can be decomposed into components in three rectangular directions:

$$\mathbf{v} = \mathbf{e}_x v_x + \mathbf{e}_y v_y + \mathbf{e}_z v_z. \tag{B.1}$$

Here, $\mathbf{e}_x$, $\mathbf{e}_y$, and $\mathbf{e}_z$ denote unit vectors in the x, y, and z directions, respectively.

The *divergence* of a vector field is

$$\nabla \cdot \mathbf{v} = \frac{\partial v_x}{\partial x} + \frac{\partial v_y}{\partial y} + \frac{\partial v_z}{\partial z}. \tag{B.2}$$

(These operations have different forms in other coordinate systems; see Ref. [1], pp. 832–837). This quantity is a scalar whose physical significance can be seen most easily from the continuity equation 15.2:

$$\frac{\partial \rho}{\partial t} = -\nabla \cdot (\rho \mathbf{v}). \tag{B.3}$$

Electrochemical Systems, Fourth Edition. John Newman and Nitash P. Balsara.

The mass flux is $\rho\mathbf{v}$, showing the direction and magnitude of mass transfer per unit area, and $\nabla \cdot (\rho\mathbf{v})$ represents the *rate of mass flowing away from a point*—hence the name *divergence*. We might call $-\nabla \cdot (\rho\mathbf{v})$ the *convergence* of the mass flux $\rho\mathbf{v}$. Then, the equation of continuity says

$$\frac{\partial \rho}{\partial t} = -\nabla \cdot (\rho\mathbf{v})$$

rate of accumulation = rate of convergence or net input.

Similar conservation or continuity equations have appeared in other places, for example, in equations 11.3 and 11.13.

The *curl* of a vector field yields another vector defined as

$$\boldsymbol{\Omega} = \nabla \times \mathbf{v} = \begin{vmatrix} \mathbf{e}_x & \mathbf{e}_y & \mathbf{e}_z \\ \partial/\partial x & \partial/\partial y & \partial/\partial z \\ v_x & v_y & v_z \end{vmatrix}$$

$$= \mathbf{e}_x \left(\frac{\partial v_z}{\partial y} - \frac{\partial v_y}{\partial z} \right) + \mathbf{e}_y \left(\frac{\partial v_x}{\partial z} - \frac{\partial v_z}{\partial x} \right) + \mathbf{e}_z \left(\frac{\partial v_y}{\partial x} - \frac{\partial v_x}{\partial y} \right). \tag{B.4}$$

When $\mathbf{v}$ is the fluid velocity, $\boldsymbol{\Omega}$ is known as the *vorticity*, which can be regarded as proportional to the angular velocity (rad/s) of a fluid element. This vector operation is encountered in fluid mechanics and in electromagnetic theory (see equation 3.3), but electrochemists may find little use for it.

The *gradient* of a scalar field is a vector:

$$\nabla\Phi = \mathbf{e}_x \frac{\partial \Phi}{\partial x} + \mathbf{e}_y \frac{\partial \Phi}{\partial y} + \mathbf{e}_z \frac{\partial \Phi}{\partial z}. \tag{B.5}$$

The gradient of Φ shows the change of electric potential with position and is the negative of the electric field. The direction of the gradient shows the direction of the greatest change, and the magnitude is the rate of change in this direction. The gradient of a vector field, on the other hand, is a *tensor*. It has nine components because it is necessary to describe the rate of change of each component of the vector in each of three directions:

$$\nabla\mathbf{v} = \begin{pmatrix} \frac{\partial v_x}{\partial x} & \frac{\partial v_y}{\partial y} & \frac{\partial v_z}{\partial z} \\ \frac{\partial v_x}{\partial y} & \frac{\partial v_y}{\partial y} & \frac{\partial v_z}{\partial y} \\ \frac{\partial v_x}{\partial z} & \frac{\partial v_y}{\partial z} & \frac{\partial v_z}{\partial z} \end{pmatrix}. \tag{B.6}$$

A tensor is an operator for vectors. The result of a tensor operating on a vector is another vector:

$$\begin{aligned} \boldsymbol{\tau} \cdot \mathbf{a} = {} & \mathbf{e}_x(\tau_{xx}a_x + \tau_{xy}a_y + \tau_{xz}a_z) \\ & + \mathbf{e}_y(\tau_{yx}a_x + \tau_{yy}a_y + \tau_{yz}a_z) \\ & + \mathbf{e}_z(\tau_{zx}a_x + \tau_{zy}a_y + \tau_{zz}a_z). \end{aligned} \tag{B.7}$$

(The result of a tensor operating on a vector can also be written $\mathbf{a}\cdot\boldsymbol{\tau}$, but this is not the same as $\boldsymbol{\tau}\cdot\mathbf{a}$; see entry 1(d) of Table B.1.)

TABLE B.1 Vector and tensor algebra and calculus

1. *Definitions*
   (a) Dyadic product. $(\mathbf{ac})_{ij} = a_i c_j$. (**ac** is a tensor.)
   (b) Double dot product.
   $$\boldsymbol{\sigma} : \boldsymbol{\tau} = \sum_i \sum_j \sigma_{ij}\tau_{ij}.$$
   (c) A tensor operating on a vector from the right yields a vector.
   $$\mathbf{a} \cdot \boldsymbol{\tau} = \sum_i \sum_j \mathbf{e}_i a_j \tau_{ji}.$$
   (d) Transpose of a tensor.
   $$(\boldsymbol{\tau}^*)_{ij} = \tau_{ij} \text{ or } \boldsymbol{\tau} \cdot \mathbf{a} = \mathbf{a} \cdot \boldsymbol{\tau}^*.$$
   (e) Product of two tensors.
   $$(\boldsymbol{\tau} \cdot \boldsymbol{\sigma}) \cdot \mathbf{v} = \boldsymbol{\tau} \cdot (\boldsymbol{\sigma} \cdot \mathbf{v}) \quad \text{or} \quad (\boldsymbol{\tau} \cdot \boldsymbol{\sigma})_{ij} = \sum_k \tau_{ik}\sigma_{kj}.$$
   (f) The divergence of a tensor is a vector.
   $$\nabla \cdot \boldsymbol{\tau} = \sum_i \sum_j \mathbf{e}_i \left(\frac{\partial \tau_{ji}}{\partial x_j} \right).$$
   (g) Laplacian of a scalar.
   $$\nabla^2 \Phi = \nabla \cdot \nabla \Phi = \sum_i \left(\frac{\partial^2 \Phi}{\partial x_i^2} \right).$$
   (h) Gradient of a vector. $(\nabla \mathbf{v})_{ij} = \partial v_j / \partial x_i$.
   (i) Laplacian of a vector. $\nabla^2 \mathbf{v} = \nabla \cdot \nabla \mathbf{v} = \nabla (\nabla \cdot \mathbf{v}) - \nabla \times \nabla \times \mathbf{v}$.
2. *Algebra*
   (a) $\boldsymbol{\tau} : (\mathbf{ab}) = \mathbf{b} \cdot (\boldsymbol{\tau} \cdot \mathbf{a})$.
   (b) $(\mathbf{uv}) : (\mathbf{wz}) = (\mathbf{uw}) : (\mathbf{vz}) = (\mathbf{u} \cdot \mathbf{z})(\mathbf{v} \cdot \mathbf{w})$.
   (c) $\mathbf{a} \cdot (\mathbf{bc}) = (\mathbf{a} \cdot \mathbf{b})\mathbf{c}$.
   (d) $(\mathbf{ab}) \cdot \mathbf{c} = \mathbf{a}(\mathbf{b} \cdot \mathbf{c})$.
   (e) $\mathbf{a} \times (\mathbf{b} \times \mathbf{c}) = \mathbf{b}(\mathbf{a} \cdot \mathbf{c}) - \mathbf{c}(\mathbf{a} \cdot \mathbf{b})$.
   (f) $\mathbf{u} \cdot (\mathbf{v} \times \mathbf{w}) = \mathbf{v} \cdot (\mathbf{w} \times \mathbf{u})$.
   (g) $(\mathbf{u} \times \mathbf{v}) \cdot (\mathbf{w} \times \mathbf{z}) = (\mathbf{u} \cdot \mathbf{w})(\mathbf{v} \cdot \mathbf{z}) - (\mathbf{u} \cdot \mathbf{z})(\mathbf{v} \cdot \mathbf{w})$.
   (h) $\mathbf{v} \cdot (\boldsymbol{\tau}^* \cdot \mathbf{w}) = \mathbf{w} \cdot (\boldsymbol{\tau} \cdot \mathbf{v})$.

(*continued*)

TABLE B.1 (*continued*)

3. *Differentiation of products*
   (a) $\nabla\phi\psi = \phi\,\nabla\psi + \psi\,\nabla\phi$ (a vector).
   (b) $\nabla\phi\mathbf{v} = \phi\,\nabla\mathbf{v} + (\nabla\phi)\mathbf{v}$ (a tensor).
   (c) $\nabla(\mathbf{a}\cdot\mathbf{c}) = \mathbf{a}\cdot\nabla\mathbf{c} + \mathbf{c}\cdot\nabla\mathbf{a} + \mathbf{a}\times\nabla\times\mathbf{c} + \mathbf{c}\times\nabla\times\mathbf{a}$
   $= (\nabla c)\cdot\mathbf{a} + (\nabla a)\cdot\mathbf{c}$ (a vector).
   (d) $\nabla\cdot(\phi\mathbf{v}) = \phi\,\nabla\cdot\mathbf{v} + \mathbf{v}\cdot\nabla\phi$ (a scalar).
   (e) $\nabla\cdot(\mathbf{v}\times\mathbf{w}) = \mathbf{w}\cdot(\nabla\times\mathbf{v}) - \mathbf{v}\cdot(\nabla\times\mathbf{w})$ (a scalar).
   (f) $\nabla\times(\phi\mathbf{v}) = \phi\,\nabla\times\mathbf{v} + (\nabla\phi)\times\mathbf{v}$ (a vector).
   (g) $\nabla\times(\mathbf{b}\times\mathbf{c}) = \mathbf{b}(\nabla\cdot\mathbf{c}) - \mathbf{c}(\nabla\cdot\mathbf{b}) + \mathbf{c}\cdot\nabla\mathbf{b} - \mathbf{b}\cdot\nabla\mathbf{c}$ (a vector).
   (h) $\nabla\cdot(\mathbf{ab}) = (\nabla\cdot\mathbf{a})\mathbf{b} + \mathbf{a}\cdot\nabla\mathbf{b}$ (a vector).
   (i) $\nabla\cdot(\phi\boldsymbol{\tau}) = \phi\,\nabla\cdot\boldsymbol{\tau} + (\nabla\phi)\cdot\boldsymbol{\tau}$ (a vector).
   (j) $\nabla\cdot(\mathbf{u}\cdot\boldsymbol{\tau}) = \boldsymbol{\tau}:\nabla\mathbf{u} + \mathbf{u}\cdot\nabla\cdot\boldsymbol{\tau}^{*}$ (a scalar).
4. *Various forms of Gauss's law (divergence theorem) and Stokes's law* ($\mathbf{dS}$ = area element, $\mathbf{d}\boldsymbol{\ell}$ = line element, dv = volume element. Integration over a closed surface or a closed curve is denoted by a circle through the integral sign. In the first case, $\mathbf{dS}$ is normally outward from the surface; in the second case, $\mathbf{d}\boldsymbol{\ell}$ and $\mathbf{dS}$ are related by a right-hand screw rule, that is, a right-hand screw turned in the direction of $\mathbf{d}\boldsymbol{\ell}$ advances in the direction of $\mathbf{dS}$.)
   (a) $\oint \mathbf{dS}\cdot\mathbf{F} = \int dv\,\nabla\cdot\mathbf{F}$.
   (b) $\oint \mathbf{dS}\phi = \int dv\,\nabla\phi$.
   (c) $\oint(\mathbf{dS}\cdot\mathbf{G})\cdot\mathbf{F} = \int dv\,\mathbf{F}\nabla\cdot\mathbf{G} + \int dv\,\mathbf{G}\cdot\nabla\mathbf{F}$.
   (d) $\oint \mathbf{dS}\times\mathbf{F} = \int dv\,\nabla\times\mathbf{F}$.
   (e) $\oint \mathbf{dS}\cdot\tau = \int dv\,\nabla\cdot\tau$.
   (f) $\oint \mathbf{dS}\cdot(\Psi\nabla\phi - \phi\nabla\Psi) = \int dv(\Psi\nabla^2\phi - \phi\nabla^2\Psi)$.
   (g) $\oint \mathbf{d}\boldsymbol{\ell}\cdot\mathbf{F} = \int \mathbf{dS}\cdot\nabla\times\mathbf{F}$.
   (h) $\oint \mathbf{d}\boldsymbol{\ell}\phi = \int \mathbf{dS}\times\nabla\phi$.
5. *Miscellaneous*
   (a) $\nabla\cdot\nabla\times\mathbf{E} = 0$.
   (b) $\nabla\times\nabla\phi = 0$.
   (c) $\mathbf{w}\cdot\nabla\mathbf{v} = \sum_i\sum_j \mathbf{e}_i w_j \dfrac{\partial v_i}{\partial x_j}$.
   (d) $D/Dt = \partial/\partial t + \mathbf{v}\cdot\nabla$.
   (e) $D\mathbf{v}/Dt = \partial\mathbf{v}/\partial t + \dfrac{1}{2}\nabla v^2 - \mathbf{v}\times\nabla\times\mathbf{v}$.
   } where $\mathbf{v}$ is the mass-average velocity.

The stress $\boldsymbol{\tau}$ due to viscous forces is a tensor (see Section 15.2). Its nine components tell us the force acting on surfaces with various orientations:

$$\mathbf{f} = \mathbf{n} \cdot \boldsymbol{\tau}, \tag{B.8}$$

where $\mathbf{n}$ is a unit vector normal to a surface and $\mathbf{f}$ is the stress on the surface. The equation of motion for a Newtonian fluid of constant density and viscosity (equation 15.10) is a vector equation involving the tensor $\nabla\mathbf{v}$. The components of this equation in rectangular coordinates are

$$\begin{aligned}
\frac{\partial v_x}{\partial t} + v_x\frac{\partial v_x}{\partial x} + v_y\frac{\partial v_x}{\partial y} + v_z\frac{\partial v_x}{\partial z} &= -\frac{1}{\rho}\frac{\partial p}{\partial x} + \nu\left(\frac{\partial^2 v_x}{\partial x^2} + \frac{\partial^2 v_x}{\partial y^2} + \frac{\partial^2 v_x}{\partial z^2}\right) + g_x. \\
\frac{\partial v_y}{\partial t} + v_x\frac{\partial v_y}{\partial x} + v_y\frac{\partial v_y}{\partial y} + v_z\frac{\partial v_y}{\partial z} &= -\frac{1}{\rho}\frac{\partial p}{\partial y} + \nu\left(\frac{\partial^2 v_y}{\partial x^2} + \frac{\partial^2 v_y}{\partial y^2} + \frac{\partial^2 v_y}{\partial z^2}\right) + g_y. \\
\frac{\partial v_z}{\partial t} + v_x\frac{\partial v_z}{\partial x} + v_y\frac{\partial v_z}{\partial y} + v_z\frac{\partial v_z}{\partial z} &= -\frac{1}{\rho}\frac{\partial p}{\partial z} + \nu\left(\frac{\partial^2 v_z}{\partial x^2} + \frac{\partial^2 v_z}{\partial y^2} + \frac{\partial^2 v_z}{\partial z^2}\right) + g_z.
\end{aligned} \tag{B.9}$$

This equation and others of frequent use to us can be found written out in several coordinate systems in Ref. [1].

A few definitions and identities are given in Table B.1. Vectors are denoted by boldface; Latin characters and tensors by boldface Greek characters. The directions *x, y,* and *z* in rectangular coordinates are denoted 1, 2, and 3, so that $x_2 = y$, $\mathbf{e}_2 = \mathbf{e}_y$, and so on, and sums extend over the indices 1, 2, and 3.

REFERENCE

1. R.B. Bird, W.E. Stewart, and E.N. Lightfoot, *Transport Phenomena*, second edition (New York: Wiley, 2002).

APPENDIX C

NUMERICAL SOLUTION OF COUPLED, ORDINARY DIFFERENTIAL EQUATIONS

The mathematical modeling of physical phenomena usually finds expression in partial differential equations. Often these reduce to ordinary differential equations, either because only one independent variable is pertinent or because of the applicability of a special technique such as a similarity transformation or the method of separation of variables. The availability of digital computers and a generalized method of solution allows such problems to be treated without the drastic approximations frequently needed to obtain analytic solutions. The original problems are often nonlinear and involve several dependent variables, but by a proper linearization of such problems a convergent iteration scheme usually results, although convergence cannot generally be assured. We discuss here the errors involved in the finite-difference calculations, the linearization of nonlinear problems, the method of solving the linearized equations, and an example by two different methods.

Since other, very different techniques (such as the Runge–Kutta method) work well with initial-value problems, attention is restricted here to boundary-value problems—that is, with boundary conditions at $x = 0$ and $x = L$ or $x = \infty$. The procedure used here has been found to be quite useful in a variety of problems, and it seems appropriate to report it[1, 2] so that other workers can implement it with ease.

Boundary-value problems of interest in the present context arise, for example, in the following situations:

1. Mass transfer into a semi-infinite, stagnant medium (*penetration* model).
2. Mass transfer in a stagnant film or a porous solid, as encountered with heterogeneous catalysis or porous electrode.
3. Mass transfer in boundary layers possessing profiles similar in the distance along a surface. This can include both free and forced convection, and for large Schmidt numbers the similarity of the hydrodynamics ceases to be essential (see Sections 17.5 and 17.6).
4. Velocity distributions in self-similar boundary layers. (See, for example, the hydrodynamics of a rotating disk in Section 15.4.)

Electrochemical Systems, Fourth Edition. John Newman and Nitash P. Balsara.

5. Distribution of charge and mass in diffuse, electric double layers.
6. Distributions of potential and of hole and electron concentrations in semiconductor electrodes.

The concentration distributions of several species may be coupled among themselves or with the velocity and temperature fields for a number of reasons.

1. The diffusion coefficients, viscosity, and other physical properties depend upon the composition, temperature, and pressure.
2. The interfacial velocity at the surface is related to the rate of mass transfer.
3. The species may be charged and interact with each other through the electric potential.
4. The components may be involved in heterogeneous or homogeneous reactions described by equilibrium or rate expressions.
5. For free convection, the fluid motion results from density differences created by nonuniform composition and temperature.

The calculation procedure was first generalized to an arbitrary number of coupled equations for treating the effect of ionic migration on limiting currents (see Chapter 19), where an arbitrary number of species may be involved.

C.1 ERRORS IN FINITE-DIFFERENCE CALCULATIONS

In simulation, we frequently use finite-difference approximations to the governing differential equations. This necessarily involves an error, which, however, can be made smaller by using more mesh nodes, characterized by the mesh interval h between nodes. For example, we can write, for a first derivative,

$$\left.\frac{dc_i}{dx}\right|_j = \frac{c_i(j+1) - c_i(j-1)}{2h} + O(h^2). \tag{C.1}$$

Here the mesh points are at x_j, where $x_{j+1} - x_j = h$. By using a central difference, the error is of order h^2. This can be a test of our computer program; a calculated overall or local answer should yield a straight line when plotted against h^2 on linear scales. Using successively smaller values of h permits us to extrapolate to the correct answer.

To obtain the error order, expand the unknown, c_i, in a Taylor series around the mesh point j. Express $c_i(j+1)$ and $c_i(j-1)$ in terms of this series. Eliminate the value of $c_i(j)$ between the two equations and divide by $2h$.

For a first-order differential equation, jagged results are obtained when a central difference is used because, in a sense, adjacent points are not connected to each other; in the calculation the point $j-1$ is connected to the point at $j+1$. However, the use of a backward (or forward) difference yields an error of order h:

$$\left.\frac{dc_i}{dx}\right|_j = \frac{c_i(j) - c_i(j-1)}{h} + O(h). \tag{C.2}$$

At small values of h, this error is larger than an error of $O(h^2)$.

The situation can be redeemed by instead writing the equation half-way between mesh points:

$$\left.\frac{dc_i}{dx}\right|_{j-1/2} = \frac{c_i(j) - c_i(j-1)}{h} + O(h^2). \tag{C.3}$$

Practically, this means that any other terms in the equation must also be evaluated at this half-mesh point. For example, since $D_i(j-1/2) \approx [D_i(j) + D_i(j-1)]/2$,

$$D_i \left.\frac{dc_i}{dx}\right|_{j-1/2} = \frac{D_i(j) + D_i(j-1)}{2} \frac{c_i(j) - c_i(j-1)}{h} + O(h^2). \tag{C.4}$$

For second-order differential equations, central differences are appropriate:

$$\left.\frac{d^2c_i}{dx^2}\right|_j = \frac{c_i(j+1) + c_i(j-1) - 2c_i(j)}{h^2} + O(h^2). \tag{C.5}$$

Remember that these equations and their error orders can be verified by expanding quantities in Taylor series about the appropriate point.

There is another forward-difference formula for first derivatives:

$$\left.\frac{dc_i}{dx}\right|_j = -\frac{c_i(j+2) - 4c_i(j+1) + 3c_i(j)}{2h} + O(h^2). \tag{C.6}$$

This is useful for expressing boundary conditions involving a derivative while still fitting it into the BAND structure. A similar backward-difference formula is useful when the derivative occurs at the right side of the domain:

$$\left.\frac{dc_i}{dx}\right|_j = \frac{c_i(j-2) - 4c_i(j-1) + 3c_i(j)}{2h} + O(h^2). \tag{C.7}$$

Internal boundaries between different regions, such as between a negative porous electrode and a separator, can also be handled with the usual tridiagonal BAND structure by writing a material balance for the half-element on each side of the boundary and then adding them together. Accuracy to order h^2 can still be achieved by this *control-volume* approach.

Another approach to handling boundary conditions at the left or right side of a region is to use an *image point*, which is outside the region by a distance h. Accuracy to order h^2 is achieved by programming the governing equations at the real boundary point, as at interior points, and programming the derivative boundary condition with a central difference, using the image point and the point just inside the region. This equation is stored at the image point and requires use of the X or Y array (see equation C.16 or C.26). In effect, the unknown at the imaginary point is eliminated between these two equations.

For third- and fourth-order differential equations, it is usually convenient to define an auxiliary variable, such as $c_k = c_i''$, and treat instead coupled first- or second-order equations.

A computer carries a limited number of significant figures, leading to a so-called *round-off* (truncation) error. Taking derivatives leads to a loss of significant figures, and this is aggravated by using a smaller mesh interval h and more mesh points. Consequently, finite-difference and round-off errors work in opposite directions, one being larger at large h and the other at small h. The user should be aware of the limitations of the computer and not push the calculations to too small a value of h in a quest for very accurate results.

Another possible source of errors is convergence over nonlinearities, where the finite-difference equations are not completely satisfied. Such errors can be made as small as wished, particularly by using a method with quadratic convergence characteristics. Here, the error on the kth iteration is proportional to the square of that at the $(k-1)$th iteration (after these errors become small). This means that the number of correct significant figures doubles with each iteration. See the next section for more detailed discussion of how to achieve quadratic convergence.

A final source of error may be time stepping. This can have similar principles to finite-difference errors, with the time step Δt playing the role of the mesh interval h. For example, one can regard battery simulation to involve coupled differential equations in distance, where what is to be solved at time t looks like ordinary differential equations except that there is a dependence on the (now known) answers at $t - \Delta t$.

C.2 CONVERGENCE OVER NONLINEARITIES

The Newton–Raphson method is frequently applied to a nonlinear governing equation with one unknown, c. Seek the solution of

$$g(c) = 0. \tag{C.8}$$

Let c° be an initial guess, and expand the function in a Taylor series about this point:

$$g(c) = g(c^\circ) + \left.\frac{dg}{dc}\right|_\circ (c - c^\circ) + \cdots. \tag{C.9}$$

Let $\Delta c = c - c^\circ$, and call this a *change variable*. As an approximation, neglect higher (quadratic, cubic, etc.) terms and set the result to zero:

$$\Delta c = -\frac{g(c^\circ)}{dg/dc|_\circ}. \tag{C.10}$$

Successive approximation, by setting c° to the old value of c° plus Δc, yields quadratic convergence.

This method can be extended to several unknowns. A multidimensional Taylor series is now used, and a matrix inversion is needed to obtain values of Δc_k. In finite-difference calculations, we are likely to be concerned with a more general problem of the form

$$g_i(C_{k,j}, C_{k,j+1}, C_{k,j-1}) = 0, \quad i = 1 \text{ to } n, \quad j = 1 \text{ to } nj, \quad k = 1 \text{ to } n. \tag{C.11}$$

We consider a number n of unknowns C_k designated by the subscript k and defined at the mesh points j by means of n governing equations $g_i = 0$, each of which can contain all the unknowns and is defined at all the mesh points.

Again, each equation is expanded in a multidimensional Taylor series around $C^\circ_{k,j}$, terms beyond the linear are dropped, and the result is set equal to zero:

$$0 = g^\circ_{i,j} + \sum_k \left.\frac{\partial g_{i,j}}{\partial C_{k,j-1}}\right|_\circ \Delta C_{k,j-1} + \sum_k \left.\frac{\partial g_{i,j}}{\partial C_{k,j}}\right|_\circ \Delta C_{k,j} + \sum_k \left.\frac{\partial g_{i,j}}{\partial C_{k,j-1}}\right|_\circ \Delta C_{k,j+1}. \tag{C.12}$$

This can be written in the general form

$$\sum_k A^\circ_{i,k} \Delta C_{k,j-1} + B^\circ_{i,k} \Delta C_{k,j} + D^\circ_{i,k} \Delta C_{k,j+1} = g^\circ_{i,j}, \tag{C.13}$$

where

$$A^\circ_{i,k} = -\left.\frac{\partial g^\circ_{i,j}}{\partial C_{k,j-1}}\right|_\circ, \quad B^\circ_{i,k} = -\left.\frac{\partial g^\circ_{i,j}}{\partial C_{k,j}}\right|_\circ, \quad D^\circ_{i,k} = -\left.\frac{\partial g^\circ_{i,j}}{\partial C_{k,j-1}}\right|_\circ. \tag{C.14}$$

Equation C.13 is still a matrix equation to solve for $\Delta C_{k,j}$, but all j must be considered at once. This is a tridiagonal matrix with respect to j:

$$\begin{pmatrix} \underline{\frac{B(1)}{A(2)}} & \underline{\frac{D(1)}{B(2)}} & & & & \\ & \underline{\frac{D(2)}{A(3)}} & \underline{\frac{D(2)}{B(3)}} & \underline{\frac{D(3)}{\cdot}} & 0 & \\ & & & \cdot & & \\ & & & & \cdot & \\ & 0 & & \underline{A(nj-1)} & \underline{\frac{B(nj-1)}{A(nj)}} & \underline{\frac{D(nj-1)}{B(nj)}} \end{pmatrix} \Delta\underline{C} = \underline{G},$$

where $G_i = g^{\circ}{}_{i,j}$; $\underline{A}$, $\underline{B}$, and $\underline{D}$ represent $(n \times n)$ submatrices embedded in an otherwise zero matrix; $\underline{G}$ and $\underline{\Delta C}$ are $n \times nj$ matrices. The $\underline{A}, \underline{B}, \underline{C}$ tridiagonal matrix shown above is $(n \times nj) \times (n \times nj)$ if we count all the subarrays as $n \times n$. One wants to use an efficient matrix-inversion routine that takes advantage of the many zero elements. This routine, BAND(j), is described in more detail in the next section. One has here a convenient tool for handling coupled nonlinear differential equations, covering a variety of interesting problems.

To get a little more generality, terms at $j+2$ and $j-2$ are added at the ends to facilitate handling boundary conditions with derivatives.

$$\begin{pmatrix} \underline{\frac{B}{A}} & \underline{\frac{D}{B}} & \underline{\frac{X}{D}} & & & \\ & \underline{\frac{A}{A}} & \underline{\frac{B}{B}} & \underline{\frac{D}{\cdot}} & 0 & \\ & & & \cdot & & \\ & & & & \cdot & \\ & 0 & & & \underline{\frac{A}{Y}} & \underline{\frac{B}{A}} & \underline{\frac{D}{B}} \end{pmatrix} \Delta\underline{C} = \underline{G},$$

where

$$X^{\circ}_{i,k} = -\left.\frac{\partial g^{\circ}_{i,j}}{\partial C_{k,j+2}}\right|_{\circ} \quad \text{and} \quad Y^{\circ}_{i,k} = -\left.\frac{\partial g^{\circ}_{i,j}}{\partial C_{k,j-2}}\right|_{\circ}. \tag{C.15}$$

C.3 SOLUTION OF COUPLED, LINEAR, DIFFERENCE EQUATIONS

This section details the algorithm for solving for the unknowns. Because change variables ΔC_k do not need to be used, the program was written to solve a matrix equation where G_i need not be zero when the program converges. Hence, the notation here uses C_k instead of ΔC_k as the unknown.

The method is to start solving for the unknowns from left to right, but doing this requires a more complicated system because the values at $j+1$ are not yet known. To handle this difficulty, the unknowns are expressed in terms of trial values $\xi_k(j)$ and a matrix E that will allow later back substitution. This form is contained in equations (C.17, C.22), although the former requires an additional x array to handle the X array. When reaching the right (nj) mesh point, there is enough information to calculate the unknowns $C_k(nj)$. Finally, one goes back through the system, from right to left, making back substitutions according to equation C.22 and lastly equation C.17. This procedure is elaborated upon below.

At $j = 1$, the equations are

$$\sum_{k=1}^{n} B_{i,k}(1)C_k(1) + D_{i,k}(1)C_k(2) + X_{i,k}C_k(3) = G_i(1). \tag{C.16}$$

There is no point for $j = 0$, so $A_{i,k}$ does not appear. However, in order to allow for the treatment of complex boundary conditions, the third term involving the unknowns at $j = 3$ has been added. For $j = 1$, let $C_k(j)$ take the form

$$C_k(1) = \xi_k(1) + \sum_{l=1}^{n} E_{k,l}(1)C_l(2) + x_{k,l}C_l(3). \tag{C.17}$$

The term in x permits the term in X in equation C.16 to be handled. Substitution into equation C.16 shows that ξ_k, $E_{k,l}$, and $x_{k,l}$ satisfy the equations

$$\sum_{k=1}^{n} B_{i,k}(1)\xi_k(1) = G_i(1), \tag{C.18}$$

$$\sum_{k=1}^{n} B_{i,k}(1)E_{k,l}(1) = -D_{i,l}(1), \tag{C.19}$$

$$\sum_{k=1}^{n} B_{i,k}(1)x_{k,l}(1) = -X_{i,l}, \tag{C.20}$$

which all have the same matrix of coefficients $B_{i,k}$ and which can be readily solved.

For the intermediate points, the governing equations are

$$\sum_{k=1}^{n} A_{i,k}(j)C_k(j-1) + B_{i,k}(j)C_k(j) + D_{i,k}(j)C_k(j+1) = G_i(j). \tag{C.21}$$

For the intermediate points, except $j = nj$, the unknowns C_k assume the form

$$C_k(j) = \xi_k(j) + \sum_{l=1}^{n} E_{k,l}(j)C_l(j+1), \tag{C.22}$$

a little simpler than equation C.17. Substitution of equation C.22 into equation C.21 to eliminate first $C_k(j-1)$ and then $C_k(j)$ and setting the remaining coefficient of each $C_k(j+1)$ equal to zero yield a set of equations for the determination of ξ_k and $E_{k,l}$:

$$\sum_{k=1}^{n} b_{i,k}(j)\xi_k(j) = G_i(j) - \sum_{l=1}^{n} A_{i,l}(j)\xi_l(j-1), \tag{C.23}$$

$$\sum_{k=1}^{n} b_{i,k}(j)E_{k,m}(j) = -D_{i,m}(j), \tag{C.24}$$

where

$$b_{i,k}(j) = B_{i,k}(j) + \sum_{l=1}^{n} A_{i,l}(j)E_{l,k}(j-1). \tag{C.25}$$

The solution of these linear equations at each point j is again straightforward, but the point at $j-1$ must be calculated first, since $\xi_k(j-1)$ appears on the right side of equation C.23 and $E_{k,l}(j-1)$ appears in the matrix of coefficients $b_{i,k}$. The equations for $j = 2$ actually take a slightly different form since equation C.17 should be used instead of equation C.22 to eliminate $C_k(1)$ from equation C.21.

Finally, for $j = nj$, one has

$$\sum_{k=1}^{n} Y_{i,k}C_k(j-2) + A_{i,k}(j)C_k(j-1) + B_{i,k}(j)C_k(j) = G_i(j), \tag{C.26}$$

where the coefficients $Y_{i,k}$ again allow the introduction of derivative boundary conditions at the upper limit ($x = L$) of the domain of interest, in the same way that the coefficients $X_{i,k}$ do at $x = 0$. If $C_k(j-2)$ and $C_k(j-1)$ are eliminated by means of equation C.22, then the values of $C_k(nj)$ can be determined from the resulting equations:

$$\sum_{k=1}^{n} b_{i,k}(j)C_k(j) = G_i(j) - \sum_{l=1}^{n} Y_{i,l}\xi_l(j-2) - \sum_{l=1}^{n} a_{i,l}(j)\xi_l(j-1), \tag{C.27}$$

where

$$a_{i,l}(j) = A_{i,l}(j) + \sum_{m=1}^{n} Y_{i,m}E_{m,l}(j-2)$$

$$b_{i,k}(j) = B_{i,k}(j) + \sum_{l=1}^{n} a_{i,l}(j)E_{l,k}(j-1). \tag{C.28}$$

Having in hand values for $C_k(j)$ for $j = nj$, one is now in a position to determine $C_k(j)$ in reverse order in j from equation C.22 and finally to determine $C_k(1)$ from equation C.17. Such repetitive calculations are, of course, intended to be carried out with a digital computer.

Because the boundary-value problem involves boundary conditions at both $x = 0$ and $x = L$, it is not possible to start at either end and obtain final values of the unknowns; this is possible only for initial-value problems. Instead, BAND makes two passes through the domain of interest, in opposite directions. In equation C.22, $E_{k,l}$ allows the effects of the boundary conditions at $x = L$ to be propagated back through the domain, the effect not being realized until the back substitution is complete.

C.4 PROGRAM FOR COUPLED, LINEAR DIFFERENCE EQUATIONS

All the steps for solving coupled, linear difference equations have been given above. However, to program these complicated steps is a bit tricky, and it is easy to make a mistake. Consequently, we give here subroutines, written in Fortran 77, for implementing the solution method. To solve a problem, one then only needs to write a main program that supplies values of $\underline{A}$, $\underline{B}$, $\underline{D}$, and $\underline{G}$ appropriate to that problem. Remember that $\underline{G}$ represents the governing equations and $\underline{A}$, $\underline{B}$, and $\underline{D}$ are derivatives according to equations C.14. An example of a main program that uses these subroutines is given in the next section.

To save storage space, the arrays $\underline{A}$, $\underline{B}$, $\underline{D}$, and $\underline{G}$ are to be supplied by the main program for each value of j, and the subroutine BAND(J) is to be called for each value of j. The values of $\underline{X}$ are to be supplied for $j = 1$, and the values of $\underline{Y}$ are to be supplied for $j = nj$. The values of $\underline{X}$ are not to be disturbed for any intermediate calculations between $j = 1$ and $j = nj$. The dimensions have been selected for $n = 6$, the number of unknown variables at each mesh point, and $nj = 402$, the number of mesh points including image points, if any. These can be changed appropriately for a particular problem. The second dimension of the D array is to be $2n + 1$, to accommodate the $2n + 1$ unknowns represented in equations C.18, C.19, and C.20, although values need to be supplied only for the original n by n array. The second dimension of the E array is $n + 1$ since ξ_k is stored there.

```
      SUBROUTINE BAND(J)
      IMPLICIT REAL*8(A-H,O-Z)
      DIMENSION E(6,7,402)
      COMMON A(6,6),B(6,6),C(6,402),D(6,13),G(6),X(6,6),Y(6,6),N,NJ
      SAVE E,NP1
  101 FORMAT (/15H DETERM=0 AT J=,I4)
      IF (J.GT.1)  GO TO 6
      NP1= N + 1
      DO 2 I=1,N
      D(I,2*N+1)= G(I)
      DO 2 L=1,N
      LPN= L + N
    2 D(I,LPN)= X(I,L)
      CALL MATINV (N,2*N+1,DETERM)
      IF (DETERM.EQ.0.0)  PRINT 101, J
      DO 5 K=1,N
      E(K,NP1,1)= D(K,2*N+1)
      DO 5 L=1,N
      E(K,L,1)= - D(K,L)
      LPN= L + N
    5 X(K,L)= - D(K,LPN)
      RETURN
    6 IF(J.GT.2) GO TO 8
      DO 7 I=1,N
      DO 7 K=1,N
      DO 7 L=1,N
    7 D(I,K)= D(I,K) + A(I,L)*X(L,K)
    8 IF (J.LT.NJ)  GO TO 11
      DO 10 I=1,N
      DO 10 L=1,N
      G(I)= G(I) - Y(I,L)*E(L,NP1,J-2)
      DO 10 M=1,N
   10 A(I,L)= A(I,L) + Y(I,M)*E(M,L,J-2)
   11 DO 12 I=1,N
      D(I,NP1)= - G(I)
      DO 12 L=1,N
      D(I,NP1)= D(I,NP1) + A(I,L)*E(L,NP1,J-1)
      DO 12 K=1,N
   12 B(I,K)= B(I,K) + A(I,L)*E(L,K,J-1)
      CALL MATINV (N,NP1,DETERM)
      IF (DETERM.EQ.0.0) PRINT 101, J
      DO 15 K=1,N
      DO 15 M=1,NP1
   15 E(K,M,J)= - D(K,M)
      IF (J.LT.NJ)  RETURN
      DO 17 K=1,N
```

```
17 C(K,J)= E(K,NP1,J)
   DO 18 JJ=2,NJ
   M= NJ - JJ + 1
   DO 18 K=1,N
   C(K,M)= E(K,NP1,M)
   DO 18 L=1,N
18 C(K,M)= C(K,M) + E(K,L,M)*C(L,M+1)
   DO 19 L=1,N
   DO 19 K=1,N
19 C(K,1)= C(K,1) + X(K,L)*C(L,3)
   RETURN
   END
```

The subroutine MATINV is used to solve the linear equations C.19, C.23, C.24, and C.27, which arise at each value of j. If, at any value of j, the determinant of the matrix of these equations is found to be zero, this fact is reported in the output. This usually indicates that all the equations have not been programmed or that they are not all independent. It can also indicate that the equations for $j = 1$ are not sufficient to determine the image points, although the equations for $j = 1$ and $j = 2$ would be sufficient to determine both the boundary point and the image point. In rare instances, it may indicate that the trial solution is inadequate and gives a zero determinant.

```
   SUBROUTINE MATINV (N,M,DETERM)
   IMPLICIT REAL*8(A-H,O-Z)
   COMMON A(6,6),B(6,6),C(6,402),D(6,13)
   DIMENSION ID(6)
   DETERM=1.0
   DO 1 I=1,N
1  ID(I)=0
   DO 18 NN=1,N
   BMAX=1.1
   DO 6 1=1,N
   IF(ID(I).NE.0) GO TO 6
   BNEXT=0.0
   BTRY=0.0
   DO 5 J=1,N
   IF(ID(J).NE.0) GO TO 5
   IF(DABS(B(I,J)).LE.BNEXT) GO TO 5
   BNEXT=DABS(B(I,J))
   IF(BNEXT.LE.BTRY) GO TO 5
   BNEXT=BTRY
   BTRY=DABS(B(I,J))
   JC=J
5  CONTINUE
   IF(BNEXT.GE.BMAX*BTRY) GO TO 6
   BMAX=BNEXT/BTRY
   IROW=I
   JCOL=JC
6  CONTINUE
   IF(ID(JC).EQ.O) GO TO 8
   DETERM=0.0
   RETURN
8  ID(JCOL)=1
```

```
      IF(JCOL.EQ.IROW) GO TO 12
      DO 10 J=1,N
      SAVE=B(IROW, J)
      B(IROW,J)=B(JCOL,J)
10    B(JCOL,J)=SAVE
      DO 11 K=1,M
      SAVE=D(IROW,K)
      D(IROW,K)=D(JCOL,K)
11    D(JCOL,K)=SAVE
12    F=1.0/B(JCOL,JCOL)
      DO 13 J=1,N
13    B(JCOL,J)=B(JCOL,J)*F
      DO 14 K=1,M
14    D(JCOL,K)=D(JCOL,K)*F
      DO 18 I=1,N
      IF(I.EQ.JCOL) GO TO 18
      F=B(I,JCOL)
      DO 16 J=1,N
16    B(I,J)=B(I,J)-F*B(JCOL,J)
      DO 17 K=1,M
17    D(I,K)=D(I,K)-F*D(JCOL,K)
18    CONTINUE
      RETURN
      END
```

Experience suggests that there are distinct advantages in solving for the change variables Δc_k, as developed in Section C.2. Some advantages of this procedure are:

1. The right side of the equation, which becomes $G_i(j)$, has a simple relationship to the original equation, thereby facilitating the checking of the computer program.
2. $G_i(j)$ will vanish when the iteration process converges. This provides a clear convergence criterion and ensures that if an answer is obtained it is correct, if $G_i(j)$ has been programmed correctly, even if $A_{i,k}$, $B_{i,k}$, and $D_{i,k}$ are in error. This iteration procedure might even help with the inversion of certain linear equations.
3. $A_{i,k}$, $B_{i,k}$, and $D_{i,k}$ can be calculated with greater ease because of the relationships represented by equation C.14. This can help obtain an analytic form for the coefficients because they are derivatives of $G_i(j)$, which is itself related back to the original equation. Furthermore, one can develop an AUTOBAND program in which the coefficients are calculated by numerical derivatives. This greatly speeds the programming, but there are two difficulties. The increment used for the numerical derivatives can lead to errors if it is too small, because of round-off error, or if it is too large, because it yields a poor approximation to the derivative. (See, however, item 2.) The numerical derivative must also be evaluated many times, and this significantly increases the computation time.

A sample of such an AUTOBAND program is given below. This is stated as a subroutine that would be called by a main program, and it succeeds in providing the information necessary for BAND by repeatedly calling the subroutine EQN(J,EQ,JP,K,DC), which in turn evaluates the governing equations (EQ(I)), written so as to equal zero when the correct answer has been obtained, with unknown C(K,JP) incremented by an amount DC.

```
      SUBROUTINE AUTOBAND
      IMPLICIT REAL*8 (A-H,O-Z)
      DIMENSION CC(6,402),DC(6),EQ(6)
      COMMON A(6,6),B(6,6),C(6,402),D(6,13),G(6),X(6,6),Y(6,6),N,NJ
      JCOUNT=0
      DC(1)=2.E-7
      DC(2)=0.00002
      DC(4)=0.01*DABS(AMP)
      IF(DC(4).LT.1.d-5) DC(4)=1.d-5
      DC(3)=DC(4)/0.1
      DC(5)=0.00001
      DC(6)=0.00002
    7 JCOUNT=JCOUNT+1
      DO 8 J=1,NJ
      DO 8 I=1,N
    8 CC(I,J)=C(I,J)
      J=0
      DO 9 I=1,N
      DO 9 K=1,N
      Y(I,K)=0.0D0
    9 X(I,K)=0.0D0
   10 J=J+1
      DO 11 I=1,N
      G(I)=0.0D0
      DO 11 K=1,N
      A(I,K)=0.0D0
      B(I,K)=0.0D0
   11 D(I,K)=0.0D0
      CALL EQN(J,EQ,1,1,0.0D0)
      G(1)=EQ(1)
      G(2)=EQ(2)
      G(3)=EQ(3)
      G(4)=EQ(4)
      G(5)=EQ(5)
      G(6)=EQ(6)
      DO 20 K=1,N
      CALL EQN(J,EQ,J,K,DC(K))
      DO 12 I=1,N
   12 B(I,K)=-(EQ(I)-G(I))/DC(K)
      IF(J.EQ.1) GO TO 14
      CALL EQN(J,EQ,J-1,K,DC(K))
      DO 13 I=1,N
   13 A(I,K)=-(EQ(I)-G(I))/DC(K)
   14 IF(J.EQ.NJ) GO TO 16
      CALL EQN(J,EQ,J+1,K,DC(K))
      DO 15 I=1,N
   15 D(I,K)=-(EQ(I)-G(I))/DC(K)
```

```
  16 IF(J.NE.1) GO TO 18
     CALL EQN(J,EQ,J+2,K,DC(K))
     DO 17 I=1,N
  17 X(I,K)=-(EQ(I)-G(I))/DC(K)
  18 IF(J.NE.NJ) GO TO 20
     CALL EQN(J,EQ,J-2,K,DC(K))
     DO 19 I=1,N
  19 Y(I,K)=-(EQ(I)-G(I))/DC(K)
  20 CONTINUE
     CALL BAND(J)
     IF(J.LT.NJ) GO TO 10
     DO 21 J=1,NJ
     IF(C(1,J).LT.-0.99*CC(1,J)) C(1,J)=-0.99*CC(1,J)
     IF(C(N,J).GT.0.05) C(N,J)=0.05
     IF(C(N,J).LT.-0.05) C(N,J)=-0.05
     DO 21 1=1,N
  21 C(I,J)=CC(I,J)+C(I,J)
     IF(JCOUNT.GT.1l) GO TO 22
     IF(DABS(C(N,NJ)-CC(N,NJ)).GT.1.0D-11*DABS(CC(N,NJ))) GO TO 7
     IF(DABS(C(1,NJ)-CC(1,NJ)).GT.1.OD-11*DABS(CC(1,NJ))) GO TO 7
  22 RETURN
     END

     SUBROUTINE EQN(J,EQ,JP,K,DC)
     IMPLICIT REAL*8 (A-H.O-Z)
     COMMON A(6,6),B(6,6),C(6,402),D(6,13),G(6),X(6,6),Y(6,6),N,NJ
     DIMENSION EQ(6)
     CSAVE=C(K,JP)
     C(K,JP)=C(K,JP)+DC
C    EQUATION 1 . . .
   1 EQ(1)=0.0  ! insert appropriate equation here
C    EQUATION 2 . . .
   2 EQ(2)=0.0  ! insert appropriate equation here
C    EQUATION 3 . . .
   3 EQ(3)=0.0  ! insert appropriate equation here
C    EQUATION 4 . . .
   4 EQ(4)=0.0  ! insert appropriate equation here
C    and similarly for the other equations.
     C(K,JP)=CSAVE
     RETURN
     END
```

C.5 PROGRAM FOR THE EFFECT OF IONIC MIGRATION ON LIMITING CURRENTS

This program gives an example of the use of the subroutines presented earlier to solve a particular problem, that of the effect of ionic migration on limiting currents (see Chapter 19). Each iteration begins at statement 5 and involves setting up the coefficients A, B, D, and G for each value of j

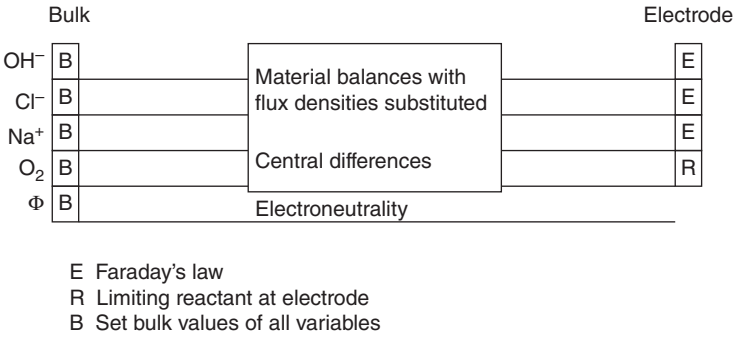

Figure C.1 BANDmap for migration program set up for oxygen reduction from a solution of NaCl. An alternative would be to use bulk boundary conditions only for the first four equations (for the potential and three concentrations) and to let one ion concentration in the bulk, say Cl^-, to be determined by electroneutrality.

followed by calling subroutine BAND(J) for each value of j. In the program, $U(I)$ is proportional to $z_i u_i$, and the electric potential is the nth unknown variable, the other unknowns being the $n-1$ species concentrations. MODE is 1 for a Nernst stagnant diffusion layer, 2 for a growing mercury drop or unsteady diffusion into a stagnant fluid, and 3 for a rotating disk. The mesh size is H, and CR0 is the concentration of the reactant at the electrode (equal to zero at the limiting current). For cases below the limiting current, the concentration overpotential is also calculated according to the dilute solution development in Section 20.1 (see equation 20.7).

The heart and core of the program lies between the dashed lines, and the really important statements, which define values of G, are underlined. This program is written with change variables ΔC_k. You can follow the various values of j and equation numbers i which determine which equations or boundary conditions are specified.

Figure C.1 gives a BANDmap. This is an aid that shows explicitly what equations are being solved and how they fit in with the boundary equations. Here there is a material-balance equation for each solute species (equation 19.4 for the rotating disk and other boundary-layer flows, 19.9 for the growing mercury drop and other transient or penetration-type problems, or 19.12 for the Nernst stagnant diffusion layer and other quasi-potential problems), and electroneutrality (equation 16.3) constitutes the last equation so that the number of equations agrees with the number of unknowns. Equation 19.5 states the boundary conditions in the bulk solution. Equation 19.8 sets the concentration of the limiting reactant at the electrode, and equation 19.7 relates the flux densities at the electrode of the other species to that of the limiting reactant.

```
C      PROGRAM MIGR
       IMPLICIT REAL*8 (A-H,O-Z)
       COMMON A(6,6),B(6,6),C(6,402),D(6,13),G(6),X(6,6),Y(6,6),N,NJ
C      Program for effect of migration on limiting current
       DIMENSION U(6),V(402),DIF(6),Z(6),S(6),CIN(6),REF(6),cold(6,402)
  102  FORMAT (4F8.4.A6)
  103  FORMAT (/4H NJ=,I4,5H, H=,F6.4//34H SPECIES     U    DIF    Z
     1   S/(1X,A6,2X,F8.3,F8.5,2F5.1))
  106  FORMAT (28H ROTATING DISK, Sc**(-1/3)=,F7.4)
  109  FORMAT (27X.F10.6/(1X,A6,2X, 2E12.5))
  110  FORMAT (/35H SPECIES     CINF     CZERO     AMP)
```

```
  111 FORMAT (8X,'ETA=',F9.4,' mV,  ETA0=',F9.4,' mV')
  112 FORMAT (5f12.8)
  113 FORMAT ( 6H AMP2=,F10.6,5X,2HV=,F10.6,2X,7HJC0UNT=,I4)
      F = 0.96487
      FRT=96487.0/8.3143/298.15
      AA=0.51023262  ! constant a for flow to a rotating disk
      BB=-0.61592201 ! constant b for flow to a rotating disk
C     N is the number of unknowns = number of species + 1
C   CR0 is thev concentration of the limiting reactant at the electrode.
   99 READ *, N,CR0
      IF(N.LE.0) STOP
C     IR is the number of the limiting reactant.
      IR=N-1
      NM1=N-1
C     D(I) is multiplied by 1.E5 before reading as DIF(I).
C     Equivalent ionic conductances (with a sign) are read as
C     U(I). These must be divided by F to get z(i)u(i)F.
C     We divide by F/1.E5 so that the correct ratio of U(I)/DIF(I)
C     will be maintained. Then C(N,J) = PHI will be in volts.
      READ 102, (U(I),DIF(I),Z(I),S(I),REF(I),I=1,NM1)
      DIFMAX=0.0
      DO 98 1=1,NM1
      IF(DIF(I).GT.DIFMAX) DIFMAX=DIF(I)
   98 U(I) = U(I)/F
C     Scm3 is the Schmidt number to the -1/3 power. A zero value
C       corresponds to the infinite-Schmidt-number approximation.
      READ *, MODE,NJ,Scm3
      if(mode.eq.1) then
      CONST=0.0
      PRINT *, ' Nernst stagnant diffusion layer'
      AMPD=1.0
      XIMAX=1.0
      elseif(mode.eq.2) then
      CONST= 2.0
      PRINT *, ' growing drop or plane electrode'
      AMPD=1.128379167
      XIMAX=3.3*(DIFMAX/DIF(IR))**0.5
      elseif(mode.eq.3) then
      CONST= 3.0
      PRINT 106, Scm3  ! rotating disk
      AMPD=1.119846522 ! 1/GAMMA(4/3)
      XIMAX=2.0*(DIFMAX/DIF(IR))**(1.0/3.0)
      endif
      H= XIMAX/dble(NJ-1)
      PRINT 103, NJ,H,(REF(I),U(I)*F,DIF(I),2(1),S(I),I=1,NM1)
      PRINT 110
```

```
   96 READ *, (CIN(I),I=1,NM1) ! concentrations in the bulk
      CIN(N)=0.0               ! potential in the bulk
      IF(CIN(1).LT.0.0) GO TO 99
      DO 4 J=1,NJ
      V(J)=CONST*H*dble(NJ-J)*DIF(IR)
C     ZE is zeta in the Von Karman transformation for the
C     rotating disk, see section 15.4.
      ZE=H*dble(NJ-J)*(3./AA)**(1./3.)*Scm3
      IF(MODE.EQ.3) V(J)=V(J)*H*dble(NJ-J)
     1*(1.0-ZE/AA*(1./3.+BB/6.*ZE+(BB*ZE)**2/30.
     1+AA*ZE**3/180.-(1.-4.*AA*BB)*ZE**4/1260.))
      C(IR,J)= CR0 + (CIN(IR) -CR0)*dble(NJ-J)/dble(NJ-1)
      C(N,J)= 0.0  ! initialization
      DO 4 I=1,NM1
    4 IF(I.NE.IR) C(I,J)= CIN(I)
      JCOUNT=0
      AMP=0.0
    5 JCOUNT=JCOUNT+1
      J=0
      DO 6 I=1,N
      DO 6 K=1,N
      Y(I,K)=0.0
    6 X(I,K)=0.0
    7 J=J+1
      DO 8 1=1,N
      G(I)=0.0
      cold(i,j)=c(i,j)
      DO 8 K=1,N
      A(I,K)=0.0
      B(I,K)=0.0
    8 D(I,K)=0.0
-----------------------------------------------------------------------
      if(j.eq.1) then
C     Boundary condition away from electrode
      DO 9 I=1,N
      G(I)= CIN(I)-c(i,j)
    9 B(I,I)=1.0
      else
C     Electroneutrality
      DO 11 K=1,NM1
      g(n)=g(n)-z(k)*c(k,j)
   11 B(N,K)= Z(K)
      if(j.lt.nj) then
C     Material balance at an interior point
      DO 12 I=1,NM1
      PP= U(I)/DIF(I)*(C(N,J+1)-C(N,J-1))/2.0
      PPP= U(I)/DIF(I)*(C(N,J+1)+C(N,J-1)-2.0*C(N,J))
      CP= (C(I,J+1) - C(I,J-1))/2.0
      G(I)= PPP*C(I,J) + PP*CP - H*V(J)/DIF(I)*CP
```

```
     %+c(i,i+1)+c(i,i-1)-2.0*c(i,j)
      A(I,I)= - 1.0 + PP/2.0 - H*V(J)/2.0/DIF(I)
      B(I,I)= 2.0 - PPP
      D(I,I)= - 1.0 - PP/2.0 + H*V(J)/2.0/DIF(I)
      A(I,N)= U(I)/DIF(I)*(CP/2.0 - C(I,J))
      B(I,N)= 2.0*U(I)/DIF(I)*C(I,J)
   12 D(I,N)= - U(I)/DIF(I)*(CP/2.0 + C(I,J))
      elseif(j.eq.nj) then
C     Boundary condition at electrode.
C     Each flux is related to the flux of the principal reactant
C     for a single electrode reaction.
      DO 14 I=1,NM1
      IF(I.EQ.IR) GO TO 14
      Q=S(I)*DIF(IR)/S(IR)/DIF(I)
      Q2=(S(I)/S(IR)*U(IR)*CR0-U(I)*C(I,NJ))/DIF(I)
      PP=U(I)/DIF(I)*(3.0*C(N,J)-4.0*C(N,J-1)+C(N,J-2))
      G(I)=Q*(3.0*c(ir,j)-4.0*c(ir,j-1)+c(ir,j-2))
     %+Q2*(3.0*c(n,j)-4.0*c(n,j-1)+c(n,j-2))
     %-(3.0*c(i,j)-4.0*c(i,j-l)+c(i,j-2))
      Y(I,IR)=-Q
      A(I,IR)=4.0*Q
      B(I,IR)=-3.0*Q
      Y(I,N)=-Q2
      A(I,N)=4.0*Q2
      B(I,N)=-3.0*Q2
      Y(I,I)=1.0
      A(I,I)=-4.0
      B(I,I)=3.0+PP
   14 continue
      G(IR)=CR0-c(ir,j)  ! Set concentration of principal reactant.
      B(IR,IR)=1.0
      endif
      endif
      CALL BAND(J)
      if(j.lt.nj) go to 7
      do i=1,n
      do j=1,nj
      c(i,j)=cold(i,j)+c(i,j) ! add corrections
      enddo
      enddo
-----------------------------------------------------------------------
      AMPO=AMP
      I=IR
      j=nj
      CP=(2.5*C(I,J)-4.8*C(I,J-1)+3.6*C(I,J-2)-1.6*C(I,J-3)+0.3*C(I,J-4)
     1)/1.2/H
      PP=(2.5*C(N,J)-4.8*C(N,J-1)+3.6*C(N,J-2)-1.6*C(N,J-3)+0.3*C(N,J-4)
     1)/1.2/H
```

```
      AMP=-H*(U(I)*CR0*PP/DIF(I)+CP)/(CIN(I)-CR0)/AMPD
      if(dabs(amp-ampo).gt.1.e-5*dabs(amp). and. JCOUNT.le.10) go to 5
      if(dabs(amp-ampo).gt.1.e-5*dabs(amp))
     :PRINT *, ' The next run did not converge'
      PRINT 109, AMP,(REF(I),C(I,1),C(I,NJ),I=1,NM1)
c     print 112, (h*(nj-j),(c(i,j),i=1,nm1),j=nj,1,-1)
      IF(CR0.EQ.0.0) GO TO 96
C     Calculation of concentration overpotential.
      AN=0.0
      ETAO=0.0
      CAPINF=0.0
      DO 16 I=1,NM1
      AN=AN-S(I)*Z(I)
      IF(S(I).EQ.0.0 .OR. CIN(I).EQ.0.0) GO TO 16
      ETA0=ETA0+S(I)*DLOG(CIN(I)/C(I,NJ))
   16 CAPINF=CAPINF+Z(I)*U(I)*CIN(I)
      ETA0=ETA0/AN/FRT*1000.0
      ETA=-AN/S(IR)*AMP/CAPINF*DIF(IR)*(CIN(IR)-CR0)*XIMAX*AMPD
      ETA=(ETA+C(N,NJ)-C(N,1))*1000.0 + ETA0
      PRINT 111, ETA,ETA0
      GO TO 96
      END
```

A sample data file follows:

```
  5 0                                    ! N, CR0
-197.600 5.26000 -1.00000-4.00000 OH- !U(I), DIF(I), Z(I), REF(I)
-76.340 2.03200 -1.00000 0.00000 Cl-
  50.110 1.33400 1.00000 0.00000 Na+
   0.000 2.00000 0.00000 1.00000 O2
  3 101 0.032                     ! MODE, NJ, Scm3
  0.0 1.0 1.0 2.E-4                ! CIN (I) for I = 1 to NM1
-1.0 0.0 0.0 0.0     ! another set of bulk composition (or not)
  -5 0 0.0          ! another problem (or not)
```

C.6 SECOND EXAMPLE: MULTICOMPONENT DIFFUSION

Programming for concentrated solutions is recorded in the study by Tribollet and Newman.[3] However, that procedure is rather complicated. The process is made much more simple by programming directly the ordinary differential equations, setting forth separately the material balances and the multicomponent diffusion equations.

We choose an example very similar to the preceding one—the effect of migration on limiting currents. The basic problem is the same as that developed in Chapter 19, and it is still possible to identify three subcases: (i) a stagnant Nernst diffusion layer, (ii) a similarity transformation for transient problems such as the growing mercury drop and diffusion into a semi-infinite stagnant medium, and (iii) boundary-layer problems, as exemplified by the rotating-disk electrode.

The transport problem for case 2 is developed explicitly here. The material balance

$$\frac{\partial c_i}{\partial t} = -\nabla \cdot \mathbf{N}_i, \tag{C.29}$$

without any homogeneous chemical reactions, transforms to

$$\frac{d\mathcal{N}_i}{d\eta} = \frac{2\eta}{c_T^0}\frac{dc_i}{d\eta}, \tag{C.30}$$

where

$$\eta = \frac{y}{2\sqrt{\mathscr{D}_{0R}t}} \tag{C.31}$$

and

$$\mathcal{N}_i = \frac{2}{c_T^0}\sqrt{\frac{t}{\mathscr{D}_{0R}}}N_i. \tag{C.32}$$

The term c_T^0 is the bulk (constant) value of c_T, which equals $\sum c_i$ and $\mathscr{D}_{0R}$ is the value of the diffusion coefficient for interaction between the limiting reactant R and the solvent.

To put a specific problem in our minds, let us treat reduction of O_2 in a NaCl solution at the limiting current; see Problem 11.4. The species are H_2O, OH^-, Cl^-, Na^+, and O_2. The first 5 (or nm) variables are the values of $\mathcal{N}_k$. The next five variables are the particle fractions c_k/c_T, numbered from $k = nm + 1$ to $k = 2nm$ (or $k = 6$ to 10). The last variable is Φ, which becomes C_n or C_{11}.

Only $nm - 1$ (or 4) multicomponent diffusion equations are independent. Equation 12.1 becomes

$$c_i\nabla\mu_i = RT\sum_k \frac{1}{c_T\mathscr{D}_{ik}}(c_i\mathbf{N}_k - c_k\mathbf{N}_i). \tag{C.33}$$

We approximate the electrochemical potential term according to

$$\nabla\mu_k = RT\nabla\ln\left(\frac{c_k}{c_T}\right) + z_kF\nabla\Phi. \tag{C.34}$$

Activity coefficients can be introduced if desired and if data are available.

After transformation, the multicomponent diffusion equation becomes

$$\frac{dc_i}{d\eta} + \frac{z_iFc_i}{RT}\frac{d\Phi}{d\eta} = \sum_k \frac{\mathscr{D}_{0R}}{\mathscr{D}_{ik}}(c_i\mathcal{N}_k - c_k\mathcal{N}_i). \tag{C.35}$$

The multicomponent diffusion coefficients can also be dependent on composition if data are available. But in the sample program we take $\mathscr{D}_{i0} = \mathscr{D}_{0i} = \mathscr{D}_i$ for solutes where $\mathscr{D}_{0i}$ refers to the solute/solvent interaction and D_i is the dilute solution diffusion coefficient (see, e.g., Table 11.1), and $\mathscr{D}_{ij}$ = a large number otherwise, so that these solute/solute interactions are negligible (recall the reciprocal relationship between K_{ij} and $\mathscr{D}_{ij}$).

How these fit into the BAND(J) program is shown in the BANDmap in Figure C.2. Before looking at boundary conditions, note that equation 10 (or $2nm$) relates to the fact that all concentrations add to c_T or

$$\sum_k x_i = 1, \tag{C.36}$$

and equation C.11 (or $2nm + 1$) is the electroneutrality equation.

The first-order equations each provide room for one boundary condition. For some equations, backward differences are used to leave room for a boundary condition at the left. In the BANDmap this is done for the material balances. The last of these, labeled R, calls for setting the concentration of the limiting reactant (O_2 in this example) at the electrode. (Here the electrode is at the left, and the bulk solution is at the right. This is the reverse of that in the preceding example and Figure C.1.) E represents a flux boundary condition for the other species, wherein this flux density is related by Faraday's law to that of the limiting reactant (which is still unknown at the beginning of the problem):

$$N_i = \frac{s_i}{s_R}N_R \quad \text{at} \quad x = 0. \tag{C.37}$$

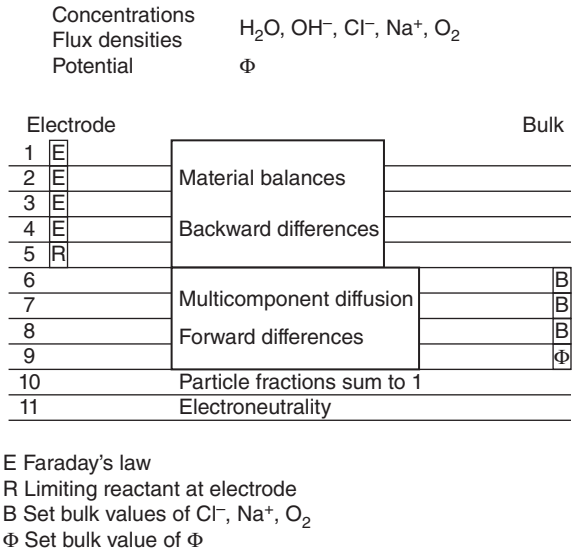

Figure C.2 BANDmap for the effect of migration, using multicomponent diffusion equations. Reduction of O_2 from a solution of NaCl.

The next four (or $nm - 1$) equations are written with forward differences. This provides room for conditions of the concentrations of three species and the potential in the bulk. The other two bulk values can be regarded as being set by the last two equations. (This could be a problem if one tries to set the bulk concentration of a neutral species by electroneutrality. An alternative, like that used in the preceding example, would be to specify all six values with the last six equations. This requires care to make sure that the set values do actually satisfy equation C.36 and electroneutrality.)

The following computer program shows the heart of the program between the dashed lines, and the really important equations, those which define values for *G*, are underlined. You can follow the various values of *j* and equation numbers *i*, which determine which equations or boundary conditions are specified.

```
c      Transient, multicomponent migration and diffusion.
       IMPLICIT REAL*8 (A-H,O-Z)
       COMMON A(11,11),B(11,11),C(11,402),D(11,23),G(11),X(11,11)
      :,Y(11,11),N,NJ
       dimension cold(11,402),dif(7,7),z(7),s(7),ref(7),u(7),cin(7)
   101 format (i4,a6,2el5.5,2f6.1)
   102 format (4f8.4,A6)
    99 READ *, n,cr0
       if(n.le.0) stop
       read 102, (U(i),dif(1,i),z(i),s(i),ref(i),i=2,n)
       read *, mode,nj,Scm3
    96 read *, (cin(i),i=2,n)
       IF(CIN(2).LT.0.0) STOP
       cin(n+1)=0.0
       nm=n      ! number of species, including the solvent
       n=2*n+1   ! number of unknowns, including the potential
       ctot=55.5d-3 ! mol/cm3
```

```
      cin(1)=ctot*1000.
      do i=2,nm
      Dif(1,i)=dif(1,i)*ctot ! mol/cm-s, Dli times total
        concentration
      Dif(i,1)=Dif(1,i)
      cin(1)=cin(1)-cin(i) ! solvent concentration
      enddo
      do i=1,nm
      do k=1,nm
      if(dif(i,k).eq.0.0) dif(i,k)=1.d6 ! large value for solutes
      enddo
      enddo
      h=6.0/dble(nj-1)
      do j=1,nj  ! initial values
      do i=1,nm
        c(i,j)=0.0 ! flux densities
        c(nm+i,j)=cin(i)/ctot/1000. ! mole fractions
      enddo
        c(n,j)=0.0 ! potential
      enddo
c     ref(1)=' H20'
      z(1)=0.0
      s(1)=0.0
      do i=1,nm
      print 101, i,ref(i),dif(1,i)/ctot,cin(i),z(i),s(i)
      enddo

    5 jcount=0
      jcount=jcount+1
      j=0
      do i=1,n
        do k=1,n
          x(i,k)=0.0
          y(i,k)=0.0
        enddo
      enddo
    7 j=j+l
      do i=1,n
        g(i)=0.0
        cold(i,j)=c(i,j)
        do k=1,n
          a(i,k)=0.0
          b(i,k)=0.0
          d(i,k)=0.0
        enddo
      enddo
-----------------------------------------------------------------------
      g(n-1)=1.0     ! sum of mole fractions = 1
      g(n)=0.0       ! electroneutrality
```

```
 do i=1,nm
   g(n-1)=g(n-1)-c(nm+i,j)
   b(n-1,nm+i)=1.0
   g(n)=g(n)-z(i)*c(nm+i,j)
   b(n,nm+i)=z (i)
 enddo
 if(j.gt.1) then ! material balances
   do i=1,nm
     g(i)=c(i,j)-c(i,j-1)
:    -2.0*h*dble(j-1+j-2)/2.0*(c(nm+i,j)-c(nm+i,j-1))
     b(i,i)=-1.0
     a(i,i)= 1.0
     b(i,nm+i)= 2.0*h*dble(j-1+j-2)/2.0
     a(i,nm+i)= -2.0*h*dble(j-1+j-2)/2.0
    enddo
  else ! boundary conditions at electrode
    g(nm)=0.0-c(nm+nm,j) ! zero concentration of limiting reactant
    b(nm,nm+nm)=1.0
  do i=1,nm-1
    g(i)=s(i)/s(nm)*c(nm,j) -c(i,j)  ! relate flux density
    b(i,i)=1.0                       ! to that of limiting reactant
    b(i,nm)=-s(i)/s(nm)
  enddo
  endif

  if(j.lt.nj) then ! multicomponent-diffusion equations
    do i=1,nm-1
      g(nm+i)=-(c(nm+i,j+1)-c(nm+i,j))/h
:     -z(i)*(c(nm+i,j+1)+c(nm+i,j))/2.0*(c(n,j+1)-c(n,j))/h
      d(nm+i,nm+i)= 1.0/h+z(i)/2.0*(c(n,j+1)-c(n,j))/h
      b(nm+i,nm+i)=-1.0/h+z(i)/2.0*(c(n,j+1)-c(n,j))/h
      b(nm+i,n)=-z(i)*(c(nm+i,j+1)+c(nm+i,j))/2.0/h
      d(nm+i,n)= z(i)*(c(nm+i,j+1)+c(nm+i,j))/2.0/h
      do k=1,nm
      if (k.ne.i) then
        g(nm+i)=q(nm+i)+(c(nm+i,j)*c(k,j)+c(nm+i,j+1)*c(k,j+1)
:       -c(nm+k,j)*c(i,j)-c(nm+k,j+1)*c(i,j+1))*dif(1,3)/dif(i,k)/2.
        b(nm+i,nm+i)=b(nm+i,nm+i)-c(k,j  )*dif(1,3)/dif(i,k)/2.0
        d(nm+i,nm+i)=d(nm+i,nm+i)-c(k,j+1)*dif(1,3)/dif(i,k)/2.0
        b(nm+i,nm+k)=b(nm+i,nm+k)+c(i,j  )*dif(1,3)/dif(i,k)/2.0
        d(nm+i,nm+k)=d(nm+i,nm+k)+c(i,j+1)*dif(1,3)/dif(i,k)/2.0
        b(nm+i,k)=-c(nm+i,j  )*dif(1,3)/dif(i,k)/2.0
        d(nm+i,k)=-c(nm+i,j+1)*dif(1,3)/dif(i,k)/2.0
        b(nm+i,i)= b(nm+i,i)+c(nm+k,j  )*dif(1,3)/dif(i,k)/2.0
        d(nm+i,i)= d(nm+i,i)+c(nm+k,j+1)*dif(l,3)/dif(i,k)/2.0
      endif
      enddo
    enddo
  else ! boundary conditions at bulk
   do i=3,nm+1
     g(nm+i-2)=c(nm+i,j)-c(nm+i,j) ! set concentration or potential
     b(nm+i-2,nm+i)=1.0
  enddo
  endif
```

```
c
       call band(j)
       if(j.lt.nj) go to 7
       nerr=0
       do j=l,nj
         do i=1,n
           if(dabs(c(i,j)).gt.1.d-10*dabs(cold(i,j))
      :.and. dabs(c(i,j)).gt.1.d-18) nerr=nerr+1
           c(i,j)=cold(i,j)+c(i,j)
         enddo
       enddo
------------------------------------------------------------------------------
       print *, nerr,'fluxes ',(c(i,1),i=1,nm)
       if(nerr.gt.0 .and. jcount.lt.30) go to 5
       print *, '            z           OH-          Cl-          '
      :,' Na+                    O2'
       print 999, (h*dble(j-1),ctot*1000.*c(7,j),ctot*1000.*c (8,j)
      :,ctot*1000.*c(9,j),Ctot*1000.*c(10,j), j=1,nj
       print *, 'solution number ',jcount

999    format (fl0.3, 4fl5.6)
997    format (fl0.3, Ip3el5.7)
       end
```

Figure C.2 gives a BANDmap showing how the governing equations and boundary conditions fit into a BAND structure. This can be contrasted with that in Figure C.1. Here first-order equations are programmed directly, with forward or backward differences being used so that the boundary conditions can be fit in where appropriate.

Figure C.3 gives concentration profiles calculated by the program. This can be considered a solution to Problem 11.4(b), and the student can see how the profiles relate to electroneutrality, migration and diffusion of each species, and production or consumption, if any, in the electrode reaction.

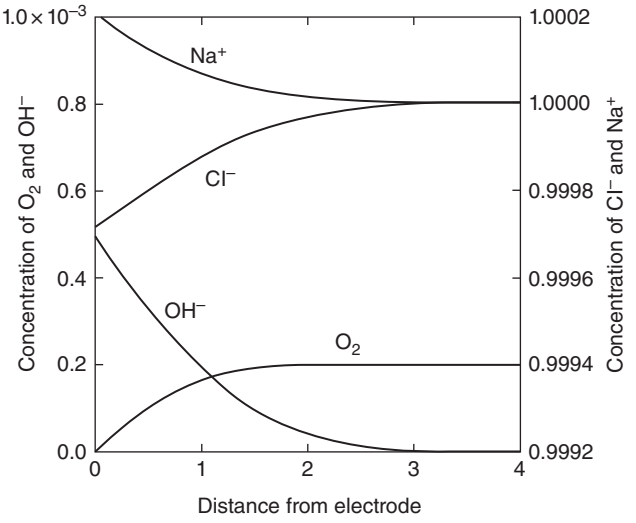

Figure C.3 Concentration profiles for reduction of O_2 from a solution of NaCl, as calculated by the transient multicomponent-diffusion program.

C.7 DISCUSSION AND CONCLUSIONS

The procedure outlined here for solving coupled, nonlinear, difference equations by linearization and subsequent iteration is quite general and flexible and has proved useful for a number of problems. For special problems it may be possible to devise more efficient methods, but with a loss of generality and an expense of effort.

Two other methods might occur to one faced with a problem of the type treated here. One is to linearize and decouple the equations by taking the coefficients of the derivatives to be given by a trial solution, for example, approximate $c_1 dc_2/dx$ by $c_1^{\circ} dc_2/dx$. Then, the decoupled equations are solved one after another in a cyclic process, producing new functions to be used as a trial solution. In general, the convergence behavior is poorer than for the present method, although there are special problems where the coupling is not strong and the method works.

A second method would be to treat the problem as an initial-value problem and to fabricate the needed initial conditions. This method requires little storage space, but the adjustment of the added initial conditions so as to satisfy the boundary conditions at $x = L$ can be tricky or impossible.

The errors in the present method arise from three sources, as discussed earlier: convergence errors for the nonlinear problem (which can be made negligibly small here), errors in the difference approximations to the differential equations (which decrease with the mesh interval h), and round-off errors in the computer (which increase as the mesh distance is decreased). Convergence may not be possible if there are sharp variations of the unknowns in some region of x; in such a case a singular-perturbation method may be appropriate.

REFERENCES

1. John Newman , "Numerical Solution of Coupled, Ordinary Differential Equations," *Industrial and Engineering Chemistry Fundamentals*, *7* (1968), 514–517.
2. John Newman, "Numerical Solution of Coupled, Ordinary Differential Equations," Lawrence Radiation Laboratory, University of California, Berkeley, August, 1967 (UCRL-17739).
3. Bernard Tribollet and John Newman, (1984). "Impedance Model for a Concentrated Solution. Application to the Electrodissolution of Copper in Chloride Solutions," *Journal of the Electrochemical Society*, *131* (1984), 2780–2785.

INDEX

Italicized page numbers indicate pages that contain a relevant figure.

Electrochemical Systems, Fourth Edition. John Newman and Nitash P. Balsara.

WILEY END USER LICENSE AGREEMENT

Go to www.wiley.com/go/eula to access Wiley’s ebook EULA.